Proceedings

5th International Conference on Intelligent Communication, Control and Devices - 2022

11th-12th November 2022

Dehradun, India

Editors

Dr. Adesh Kumar
Dr. Piyush Kuchhal
Dr. Abhinav Sharma
Dr. Rupendra Kumar Pachauri

Organized By
University of Petroleum and Energy Studies
Dehradun, Uttrakhand-248007, India

Table of Contents

15	4322	Sanjay Chouhan, Aditi Soni, Ganesh Mukati, Kishor Kumbhare, Jitendra Yadav, Santosh Kurre	Design and Analysis of 2x2 MIMO Antenna Using Reshape Hexagonal Geometry for Wideband Wireless Application	
16	4572	M.D. Sharique, Kavita Kushwah, Ashish Kumar Singhal	Application of 7-Level NPC Converter for Low Voltage Wind Energy Conversion System	
17	4773	Rohit Sharma, Iqbal Singh, Ajay Vasishth, Sourbh Thakur	Overview of Hydrogels and Hydrogels based Actuators for Biomedical Applications	
18	5017	Deepak Bharadwaj, Roushan Kumar	Simulink Computed Torque Control of a Novel 15-DOF Anthropomorphic Robotic Fingers	
19	5088	Devendra Rawat, Mukul Kumar Gupta and Abhinav Sharma	Optimum Point Trajectory Tracking of a Robotic Manipulator System using Extremum Seeking Control	
20	5601	Jitendra Yadav, Santosh Kumar Kurre, Shubham Thakur	Design and Development of Alcohol Detection Sensor Mechanism for Safe Driving in Automobile	
21	5628	Ajay Prasad Nautiyal, Sapna Bisht, Kapil Rajput	The Impact & Usage of Digital Payment System in India during the Covid-19 Pandemic	
22	6225	Ritika Raturi, Deval Verma	Palm Print Recognition based on Correlation features	
23	6243	Shruti Sharma, Deval Verma	Breast Cancer Prediction using Statistical Features	
24	6470	Kumar Abhinandan Patial, Simran Dogra, Ankush Kapoor	An Insight on the Swastika Shaped Antenna Design	
25	6504	Prashant Kumar, Paramjeet Singh Paliyal , Surajit Mondal	Designing of Smart Grid System in Indian Scenario	
26	6526	Mohd Nazim, Faizan A Khan, Ahmad F Minai, Mohammed Asim, M. A. Mallick, Mahfooz Ahmad	IoT Enabled Solar PV Maximum Power Tracking System	
27	6681	Shivmanmeet Singh, Harmandeep Kaur, Lakhveer Singh, Rehan Dhir, Ajay Vasishth	Survey on Optical Technologies used for Communication	
28	6837	Sanjay Chouhan, Khelta Ram Jadhaw, Ganesh Mukati, Kishor Kumbhare, Jitendra Yadav, Santosh Kumar Kurre	Four Element Modified Rectangular Slotted Antenna for Wireless Application	
29	6995	Avtar Singh, Deval Verma	Face Recognition using Shape Invariant Features	
30	6999	Reshampal Kaur	Efficiency Evaluation and Ranking of Indian PSBs: An Application of Data Envelopment Analysis	
31	7025	Sulekha Singh Marko, Suneel Kanojiya, Aayush Shrivastava, Ashish Singhal	Solar Power Integration Impact on Power Grid Performance	
32	7305	Shivmanmeet Singh, Harmandeep Kaur, Lakhveer Singh, Rehan Dhir, Ajay Vasishth	Overview and Design of Mecanum Wheel	
33	7395	Ruchi, Suniti Dutt, Mitali Sinha, Aditay Kalia, Saksham Kanwar, Sanchit Khatkar, Ayush Srivastav,	ELEKX - Adding Mental Health Perspective to a Chatbot	

		Ajay Vasishth		
34	7499	Dhruv Sharma, R K Chaurasia	Role of Linear Algebra in Image Compression	
35	7710	Parth Sethi, Deval Verma	Vectorization of Text in Natural Language Processing	
36	8597	Akash Goel, Amit Kumar Goel, Adesh Kumar	Miscellaneous Artificial Intelligence and Machine Learning Models for Multimedia and Medical Applications	
37	8916	Geetanjali Raghav	Analysis of Various Factors Affecting the Life of Concentrated Solar Power Systems in Real Environmental Condition	
38	9092	Madhukant Patel, Suhani Patel	Coastal Surveillance and Detection of Intruder – A Mechanism using Antenna Arrays	
39	9127	Deepak Bhardwaj, Roushan Kumar	Computation of Singular Posture of New 15-DOF Anthropomorphic Robotic Fingers	
40	9264	Parth Vyas, R. K. Chaurasia and A.K Saini	Predicting Coma Patient Emotions based on a Real-World Study using Machine Learning and Deep Learning Techniques	
41	9417	Harshita Prashar and Deval Verma	Extraction of Features in Number Plate using Contour Spotting	
42	9534	Mocherla Chakradhar Abhinay, Seetharam Reddy Ramireddy, Vamsiram Gandham, Vaegae Naveen Kumar	Real Time Cloud Enabled Water Quality Supervising and Aerator Actuation in Shrimp Farming	
43	9713	Kapil Joshi, Adarsh Kumar, Minakshi Memoria, Rajiv Kumar	Research Trends of Network Security in IoT: A Generic Review	
44	9868	Praful Ranjan, Vaibhav Saini, N. Prasanth Kumari	Concept and Design of a Deep-Functioning Robotic Arm Driven by an Android App to Transport Hazardous Goods	

Preface

The Electrical Cluster, School of Engineering, University of Petroleum and Energy Studies, Dehradun, takes immense pleasure in announcing Fifth International Conference on Intelligent Communication, Control and Devices (ICICCD-2020) to be held on 11th November to 12h November 2022. ICICCD focus on the integration of intelligent communication systems, control systems, & devices related to all aspects of engineering and sciences. ICICCD-2022 aims to provide an opportune forum and vibrant platform for Researchers, Academicians, Scientists and Industrial Practitioners to share their original research work, findings and practical development experiences. The proceedings will be submitted to be reviewed for inclusion in relevant indexing database such as SCOPUS, CPCI, Crossref (by assigning doi), Google scholar etc.

The general aim of the conference is to promote international collaboration in Education and Research in all fields and disciplines of engineering. ICICCD-2022 will be an International Forum for those who wish to present their projects and innovations, having also the opportunity to discuss the main aspects and the latest results in the field of Education and Research.

The Organizing committee is extremely grateful to the authors from India and abroad who had shown tremendous response to the call for papers. Close to Eighty papers were submitted from the researchers, academicians and students on the research areas divided into three parallel tracks of Intelligent Communication, Intelligent Control and Intelligent Devices, out of which a total of forty papers were selected for oral presentations.

We are obliged to our Honorable Chancellor Dr. S. J. Chopra, Vice Chancellor Dr. Sunil Rai, Pro- Vice Chancellor, Dr. Ram Sharma, Dean Research & Development Dr. D. K. Avasthi, Dean (SoE) Dr. Gurvinder Virk for providing full support and guidance to us in organizing this international conference ICICCD-2022.

We extend our thanks to all faculty members and staff in different sub committees for organizing the conference and make it a grand success.

Editors
Dr. Adesh Kumar
Dr. Piyush Kuchhal
Dr. Abhinav Sharma
Dr. Rupendra Kumar Pachauri

Acknowledgments

The Editor acknowledges River publishers for this opportunity and professional support. My special thanks to Mr. Rajeev Prasad, River publishers for the excellent support, he provided us to complete this book.

Thanks to the manuscript authors and reviewers for their availability for this work.

Adesh Kumar, University of Petroleum and Energy Studies, India

Piyush Kuchhal, University of Petroleum and Energy Studies, India

Abhinav Sharma, University of Petroleum and Energy Studies, India

Rupendra Kumar Pachauri, University of Petroleum and Energy Studies, India

Editors Biographies

Dr. Adesh Kumar is working as ***Senior Associate Professor*** in the Department of Electrical & Electronics, Engineering ‘‘University of Petroleum and Energy Studies, Dehradun, India. He is B.Tech in Electronics & Communication Engineering from Uttar Pradesh Technical University Lucknow, India in 2006. M.Tech (Hons) in Embedded Systems Technology, from SRM University, Chennai in 2008. **Ph.D. (Electronics Engineering) from the University of Petroleum and Energy Studies (UPES), Dehradun India in 2014.** He has also worked as Senior Engineer in TATA ELXSI LIMITED Bangalore and a faculty member at ICFAI University, Dehradun. His areas of interest are VLSI Design, Embedded Systems Design, Telecommunications, and Signal Processing, He has published more than **100**+ research papers in international peer-reviewed journals (SCI/Scopus) and conferences. He has supervised 7 Ph.D. scholars and 5 candidates are doing research under his supervision. He has chaired more than 10 sessions at international conferences and is involved in the Ph.D. evaluation committee in UPES and UTU, and India.

Guest Editor: Special Issue-**"Intelligent Devices & Computing Applications"** *in Computer Systems Science & Engineering,* Journal, Tech Science, 2022 **(SCI Indexed).**
Guest Editor: Special Issue-**"Intelligent Communication and Smart Grid Automation Applications"** *in Intelligent Automation & Soft Computing,* Journal, Tech Science, 2021 **(SCI Indexed).**
Editor: Proceedings of Intelligent Communication, Control and Devices in Advances in Intelligent system and Computing (AISC), Book Series, Springer, Vol.989, 2020. **(Scopus Indexed).**

Dr. Adesh Kumar
Senior Associate Professor
Department of Electrical & Electronics Engineering
University of Petroleum and Energy Studies, Dehradun, India
Contact: **+91-9410542870, +91 -7017150991 (What’s up)**
E-mail: **adeshmanav@gmail.com**; **adeshkumar@ddn.upes.ac.in**
URL: **https://upes.irins.org/profile/91847**
Research Gate: https://www.researchgate.net/profile/Adesh-Kumar-3
Google Scholar ID: PRYDRikAAAAJ
Vidwan ID-91847
Orchid Id: 0000-0002-0209-9206
Scopus Id: 57221101879
Total Citations: 1000+
Research Papers:100+
H-index-16
i-10 Index-23

Dr. Piyush Kuchhal is working as *Professor* in the Department of Electrical & Electronics, Engineering ‘‘University of Petroleum and Energy Studies’, Dehradun, India. He is M.Sc and Ph.D from the Indian Institute of Technology (IIT), Roorkee, India in 1995 and 2001 respectively. He has also worked with Mody University, Rajasthan, India He has published more than 80+ research papers, in international peer-reviewed journals (SCI/Scopus) and conferences, 4 patents, and 2 grated projects. His areas of interest are Wireless Analog Electronics. Microwave Engineering, Solar Electromagnetic Field Theory, Engineering, Physics, Solar PV technology, He has supervised 12 Ph.D. scholars and 4 candidates are doing research under his supervision. He has chaired more than 15 sessions in international conferences and is involved in the Ph.D. evaluation committee in UPES India.

Dr. Piyush Kuchhal
Professor
Electrical & Electronics Engineering
University of Petroleum and Energy Studies, Dehradun, India
Contact: **+91-9997422104**
E-mail: pkuchhal@ddn.upes.ac.in
URL: **https://upes.irins.org/profile/77133**
Google Scholar ID: ZSFK6oIAAAAJ
Vidwan ID-77133
Orchid Id: 0000-0002-6326-9440
Scopus Id: 6602725859
Total Citations: 600+
Research Papers:90+
H-index-13
i-10 Index-17

Dr. Abhinav Sharma received his B. Tech. from H. N. B. Garhwal University, Srinagar, India, in 2009 and the M. Tech. and Ph. D. from Govind Ballabh Pant University of Agriculture and Technology, Pantnagar, India, in 2011 and 2016. He is working as an Assistant Professor (Selection Grade) in the Department of Electrical and Electronics Engineering, School of Engineering at the University of Petroleum and Energy Studies, Dehradun. He has taught subjects such as data communication networks, microprocessors, and embedded systems, artificial intelligence and machine learning, and communication systems. He has publications in IEEE, Taylor & Francis, Elsevier, Springer, Emerald, and many other national and international journals and conferences. His field of interest includes adaptive array signal processing, artificial intelligence and machine learning, optimization techniques, and smart antennas. He has authored/edited 5 books, one of them in River Publication (Use of AI, Robotics, and Modern Tools to Fight Covid-19 in series, Automation, Control and Robotics ;
https://www.riverpublishers.com/book_details.php?book_id=918)

Dr. Abhinav Sharma
Assistant Professor-SG
Electrical & Electronics Engineering Department
University of Petroleum and Energy Studies, Dehradun, India
Contact: **+91-9897636885**
E-MAIL: abhinav.sharma@ddn.upes.ac.in
URL: **https://upes.irins.org/profile/79349**
Google Scholar ID: faesEY8AAAAJ
Scopus Id: 57192423909
Total Citations: 500+
Research Papers:40+
H- index: 12
i-10 index: 13

Dr. Rupendra Kumar Pachauri received his Ph. D degree in Renewable energy from G. B. University, Gautam Buddha Nagar, India in 2016. M. Tech degree from EED, Zakir Husain College of Engineering and Technology, Aligarh Muslim University (AMU), Aligarh, India in 2009. He is currently working as an Assistant Professor in the Electrical and Electronics Engineering Department at the University of Petroleum and Energy Studies (UPES), Dehradun, India. He has published more than 100 research papers in International repute Science citation/Scopus-indexed journals along with IEEE/Springer conferences. He has published/granted patents also. His fields of research are Solar Energy, Fuel cell technology, and Smart grid operations. He is associated as Editorial board member of Scopus indexed journal and served as guest editor Techscience publication. Also, edited one book with CRC press "Applied Soft Computing and Embedded System Applications in Solar Energy" ISBN 9780367625122

Dr. Rupendra Kumar Pachauri
Assistant Professor-SG
Electrical & Electronics Engineering Department
University of Petroleum and Energy Studies, Dehradun, India
Contact: **+91-7455077626**
E-mail: rpachauri@ddn.upes.ac.in
URL: **https://upes.irins.org/profile/96379**
Google Scholar ID: KGAYVMsAAAAJ&hl
Scopus Id: 6602725859
Total Citations: 1457+
Research Papers:110+
H- index:21
i-10 index: 36

Performance Evaluation of Non-Dominated Sorting Genetic Algorithm III in Wireless Sensor Network

Kantveer[1], Dr. Navdeep Singh[2], Dr. Harminder Singh Bindra[3], Ajay Vasishth[4]

[1]*Research Scholar, I.K Gujral, Punjab Technical University, Jalandhar, kantveer1@gmail.com*
[2]*AssociateProfessor, Amritar Group of Colleges, Amritsar, arora_navdeep@rediffmail.com*
[3]*Professor and Head of Department (IT), Malout Institute of Management and Information Technology, Malout. bindra.harminder@gmail.com*
[4]*Department of Physics, Chandigarh University, Mohali, Punjab, India*

Abstract.

Wireless Sensor network plays an vital role in developing robust, affordable and convenient network. The Wireless Sensor Network methods are effectively used to implement Time division Multiplexing (TDM). In WSN sensor nodes are connecting to one another wirelessly and one of the main characteristics of the WSN is that they are cost effective and efficient. Due to the vibrant nature of Wireless Sensor network the links in the network changes consequently. The proposed method uses NSGA-iii for data aggregation. The proposed algorithm is power efficient. It has been visualized that the proposed protocol considerably improves the life span of the network over the other traditional techniques. The proposed work is done in two phases in the first phase Tree based clustering is done for WSN. Clustering schemes in the WSN has certain drawbacks as it leads to data redundancy. Hence, to reduce the limitations of the clustering scheme inter cluster data aggregation is used. It will improve the lifeline of the network and power efficient.

Keywords. Wireless Sensor Network (WSN), Time Division Multiplexing (TDM), Non-dominated sorting genetic algorithm (NSGA-III).

1. INTRODUCTION

WSN is a collection of nodes in which all node is connected to other Senor. Every node as different parts. A Radio transceiver, microcontroller, source of energy. Multiple sensor nodes are included in the Wireless Sensor Network and each node is power-efficient, Multi-function, and equipped with wireless communication. The architecture of wireless Sensor network contains 3 units.

- Sensing Unit
- Processing Unit
- Transmitter
- Power unit

- Position Finding System
- Mobilizer

1.1. Sensing Unit

The sensor nodes in the WSN have power limitations and can be able to handle low-data rate.

1.2. Processing unit

Processing unit comprised of 2 Sub-units. Processor and the storage processor which is used to compute both the local information as well as the information from another computing node and the storage unit are used to store data. This can be in the form of RAM and ROM.

1.3. Transmission Unit

The communication between the nodes in WSN is radio waves. The topology which is used for the WSN can be Star Network, Mesh Network, and Hybrid Network etc.

WSNis the kind of ad-hoc network which is very effective in nature. The topology in the Wireless Sensor Network changes when the new node enters the network or left the network

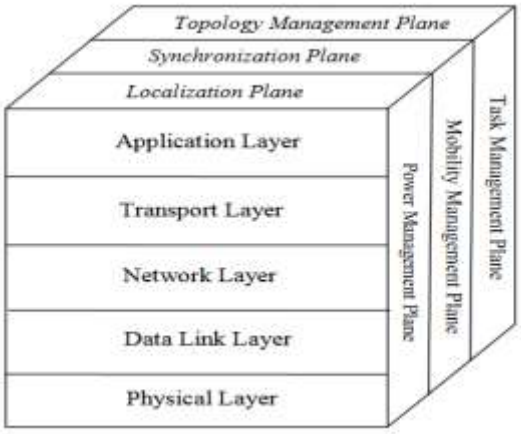

Figure 1.1. Layered Architecture of WSN [2, 3]

2. LAYERS OF WIRELESS SENSOR NETWORK

- ***Physical Layer:*** The Physical Layer Transfer the data in the form of stream of bits.

- ***Data Link Layer:*** The Data Link Layer accept the data in the form of bits and convert it into the form of frames and the layer is also accountable for flow control and error control.

- ***Network Layer:*** The main function of the layer is to perform Routing. There are many routing algorithms available to perform routing. These routing protocols adjust themselves according to the path available.

- ***Transport Layer:*** The transport layer is accountable for the host to host delivery. The main function of transport layer is to avoid congestion. It uses two protocols:
  - Transmission control protocol.
  - User Datagram protocol.

- ***Application Layer:*** The layer provides services to the user. The Application layer can be used to provide services such as Military, Environment, Health Monitoring and Agriculture.

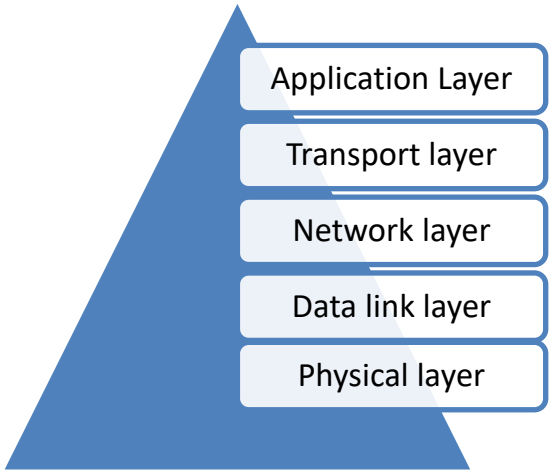

Figure 2.1. Layers of Wireless sensor Network [5, 6]

3. APPLICATIONS OF WIRELESS SENSOR NETWORK

3.1. Environment Monitoring

WSN is used to collect the data sample from the various geographical locations, such as oceanography, land, forest etc.

3.2. Security

Security is one of the major challenges in this dynamic work. WSN is used to provide security for Public Infrastructure as well as for home network. Public infrastructures include Nuclear power plant, Data centers, warehouses etc.

3.3. Military

In Military sector Wireless Sensor Network is widely used to track the location of enemy's vehicle, or to provide communication between tanks and the fighter plans.

3.4. Medical Sector

Wireless Sensor Network is used to diagnostic investigation, drug administration, Patients Psychological information.

3.5. Industries

One of the major advantages of Wireless Sensor Network is it hiding the complexity and provides services to the user. As the Wired network is highly complex as it comprised of complex set of wires.

4. RELATED WORK

Reham et al. states that the Wireless Sensor Network has diverse applications in the field of military, automations, health, and transportation. Residual energy, topology and data routing protocol are very significant. The author proposed a dynamic routing protocol. The simulation results states the network life span of the network has increased by 13 percent.

Parshant et al. States that the Wireless Sensor Network communicate through a single channel. The channel has a behavior of broadcasting a message at one time. WSNitself organizing network. The nodes in the wireless sensor network adjust them according to the incoming traffic. Routing protocols are used to provide communication within the network. Numerous routing protocol are used to provide communication. However, security is the major concern of the network. The purpose of this work is to enhance the security of the network.

Kemal Akkaya et al. states that every routing protocol should be examined on the basis of the network flow and Quality of service.

A.P. Chandrakasanet et al. States to improve the lifespan, minimize delay and improve overall quality LEACH protocol is used. The finding has suggested that the LEACH protocol has significantly improve the life span of the network.

Ming Liu et al. States that one of the major concern in the wireless sensor network is to conserve energy. The energy is conserved by optimizing the load across all the nodes EAP adds a new clusters in the network that can handle energy levels better.

Meghna et al. uses a tree which is self replicating tree to minimize the utilization of energy. The simulation results are performed using NS-2 simulator. The nodes in the network has different densities such as 20ms, 40ms, 60ms. The proposed method conserves energy and the life span of the network also improved.

Syed Umar et al. Wireless sensor network has diverse applications in the field of military, medical, and communication. The Proposed work use tree based energy protocol which conserves the energy and hence improves the life span of the network.

Shiksha Chabra et al. States that the wireless sensor network has limited battery capacity and it is very difficult to conserve the energy in the wireless sensor network. The author used GSTEB technique for improving the efficiency of the network.

Alain Bertrand Bomgni et al. states that the wireless sensor network is comprised of small devices which are known as stations. These stations are having less energy which significantly reduces network life time. The objective of each node is to deliver each item to its intended recipient. The proposed technique conserves sensor energy and thus the life span of the network improved significantly.

5. ROUTING PROTOCOL IN THE WIRELESS SENSOR NETWORK.

Routing protocol in the sensor network is categorized in the following parts:

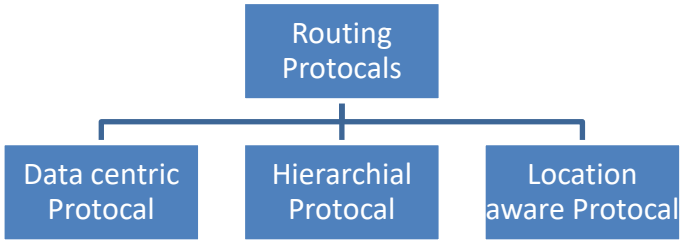

Figure: 5.1. Types of Routing Protocal [1]

5.1. Data Centric Protocal

WSNis collection of Multiple nodes and it is not possible that each node in the network is provided with an identifier. The Data-centric protocal do not use identifier and instead of this naming of these nodes are based on the attributes.

5.2. Hieraricahal Protocal

WSNis a set of complex nodes and hence scalability is one of the major issue. In case of single node design the problem of conjection arises and this result in overloading of the network. The hierarichal protocal are highly scalable network and one such example of hierarchial network is LEACH.

5.3. Location Aware Protocal

These protocals are used to find the distance between the noses. Most important location aware protocal are CBGR, TTDD, and MECN.

5.4. Quality Based Protocal

When the broadcast of the data is done from the source to destination it must satisfy parameters like Bandwidth, Latency, energy consumption and data quality.

6. PROPOSED WORK

6.1. Inter clustring techniques

In the clustering techniques nodes are organised in the hierarchial fashion and effectively used to the resources such as electricity, frequency and Bandwidith. In order to decrease the data redundancy in the network certain kind of the inter clustring is done. This not only focus on the data redundacy by also manages the traffcing in the network.

6.2. Objectives of the Interclustring

- *Load Balancing:* Inter clustering algo is use certain kind of aggeration which balance the load in the network and hence congestion can be controlled.

- *Fault tolerance:* Fault tolerence is the ability of the network to work in the even when any of the sensor node failuare occurs.

- *Network lifetime:* The life time of the network can be imporved by distributing the load over the CHS, selecting particular path for the data delivery.

7. PARAMETERS TO EVALUATE THE PERFORMANCE OF THE SYSTEM

7.1. Network Life time

The network life span is calculated on the basis of different charging schemes, effect of different areas, effect of different moving speeds of Wireless sensor network.
The network life time is shown in the figure 6.1. The number of nodes selected from 40 to 70. And the area size is taken in the dimenssions of 50*50, 100*100, 150*150, 200*200.

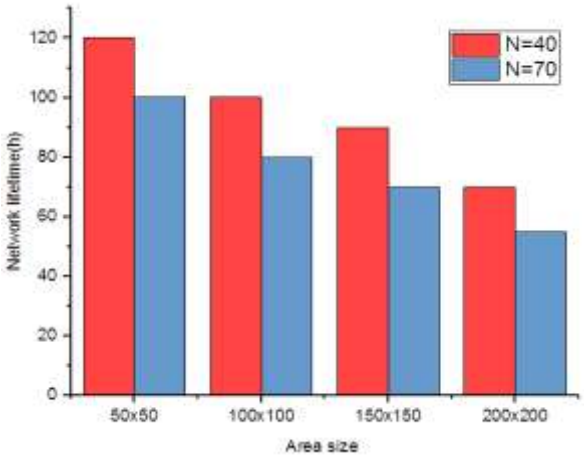

Figure:6.1. Network lifetime

7.2. Energy consumption

Energy utilization is the total energy used by the sensor nodes while transmitting the data from the source station to destination station. When the propesed method is compared with the traditional method it result in 20% energy consumption.

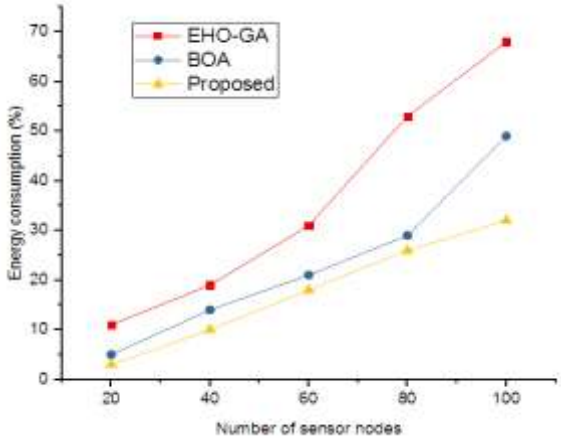

Figure:6.2 Energy consumption

7.3. Throughput

The following draft shows that the troughput of the propsed method is highly efficient when compared with the traditional system.

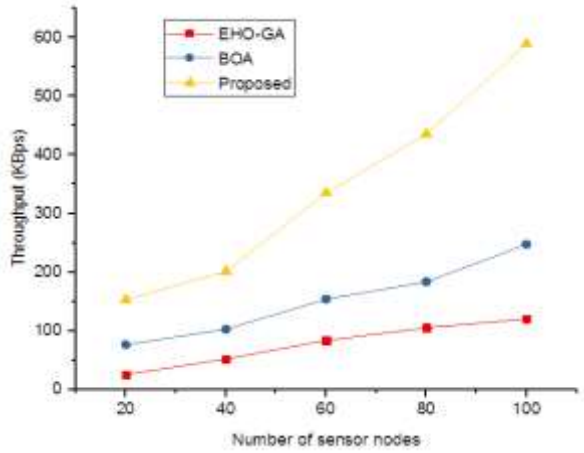

Figure:6.3 Throughput

7.4. End to End delay

End to End delay may be define as the total time required to send the packet to the reciver to the number of packets recived by the reciver.

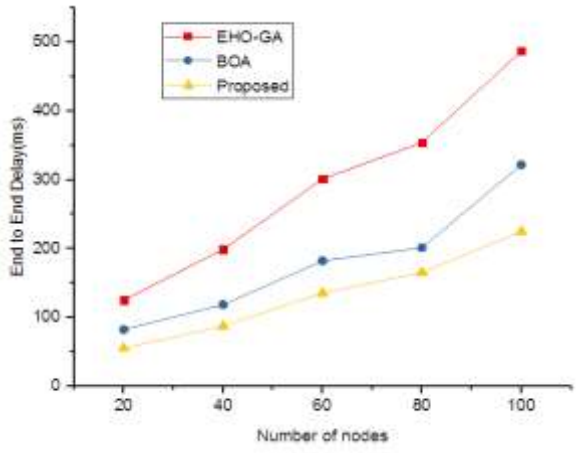

Figure6.4 End to End delay

8. CONCLUSION

The energy conservation is one othe maindare in WSNand it effects the lifetime of the network. The porposed work designed an energy efficiancy routing protocal. It may be possible that the number of phases in the porposed system increases and the network life time significantly impove the proposed work. The proposed algorithm used in the study will enhance the network life time and also use better optimized path. The performance of the parameters such as energy consumption, end to end delay, throughput imporved significantly when compared with traditional methods. For performing the whole work MATLAB is used. The proposed work is performed using clustring approach. While considering the performance of the whole network the physical factors such as temprature, pressure and sound are all real time.

9. FUTURE WORK

The proposed research work is performed using static nodes. In near future we wil further work on dynamic nodes and evaluate the performance of the system. We will futher investigates various routing protocal which improved the life span of the network. In the proposed work to evaluate the performance of the network simulator is used in near future we will use real network test bed to evaluate network performance. When we use wireless sensor network in the typical environemtn the security threats may occur. Therefore, we will also focus on improving the security of the network.

10. REFERENCES:

[1] Garcia-Sanchez, A.-J., Garcia-Sanchez, F., Losilla, F., and Palomares, F., (2010), "Wireless Sensor Network Deployment for Monitoring Wildlife Passages," Sensors, 10(8), pp. 7236–7262.

[2] Heinzelman, WB, Chandrakasan, AP, and Balakrishnan, H, (2002), "An application-specific protocol architecture for wireless micro sensor networks," IEEE Transactions on Wireless Communications, 1(4), pp. 660-670.

[3] Olariu, S., and Xu, Q., (2005), "Information Assurance in Wireless Sensor Networks," In 19th IEEE International Parallel and Distributed Processing Symposium, pp.1-5.

[4] Matin, M. A., and Islam, M. M.,(2012), "Overview of Wireless Sensor Network', In Wireless Sensor Networks-Technology and Protocols. In Tech open Book," pp. 3-24.

[5] Akkaya, K., and Younis, M.,(2005), "A survey on routing protocols for wireless sensor networks," Ad Hoc Networks, 3(3),pp. 325–349.

[6] Akyildiz, I.F., and Kasimoglu, I.H., (2004), "Wireless Sensor and Actor Networks: Research Challenges," Ad hoc Networks Journal-Elsevier, 2(4), pp.351-367.

[7] Al-Karaki, J.N., and Kamal, A.E., (2004), "Routing Techniques in Wireless Sensor Networks: A Survey," IEEE wireless communications Journal, 11(6), pp.6-28.

[8] Krishnamachari, B., Estrin, D., and Wicker, S.,(2002), "Modeling Data Centric Routing in Wireless Sensor Networks," USC Computer Engineering Technical Report CENG 02-14.

[9] Bakr, B.A., and Lilien, L.T., (2014), "Extending Lifetime of Wireless Sensor Networks by Management of Spare Nodes," Procedia Computer Science- Elsevier, 34, pp. 493-498.

[10] Bandyopadhyay, S., and Coyle, E.J., (2003), 'An Energy Efficient Hierarchical Clustering Algorithm for Wireless Sensor Networks," Proceedings of IEEE INFOCOM, 3 , pp. 1713-1723.

[11] Attea, B. A., and Khalil, E. A., (2012), "A New Evolutionary Based Routing Protocol for Clustered Heterogeneous Wireless Sensor Networks," Applied Soft Computing Journal-Elsevier, 12(7), pp.1950-1957.

[12] Li, G., andZnati, T., (2007), "RECA: A ring-structured energy-efficient clustering architecture for robust communication in wireless sensor networks," International Journal Sensor Networks, 2(1/2), pp.34–43.

[13] Martirosyan, A., Boukerche, A., andPazzi, R., (2008),"A Taxonomy of Cluster-Based Routing Protocols for Wireless Sensor Networks," 2008 International Symposium on Parallel Architectures, Algorithms, and Networks (i-Span 2008), pp. 247-253.

[14] Yi, C., Wang, L., and Li, Y., (2015),"Energy Efficient Transmission Approach for WBAN Based on Threshold Distance," IEEE Sensors, 15(9), pp. 5133–5141.

[15] Liaw, J.-J., Dai, C.-Y., and Wang, Y.-J., (2009),"The Steady Clustering Scheme for Heterogeneous Wireless Sensor Networks," 2009 Symposia and Workshops on Ubiquitous, Autonomic and Trusted Computing, pp. 336-341.

[16] Rezvani, M., Ignjatovic, A., Bertino, E., &Jha, S., (2015),"Secure Data Aggregation Technique for Wireless Sensor Networks in the Presence of Collusion Attacks," IEEE Transactions on Dependable and Secure Computing, 12(1), pp. 98–110.

[17] Tiwari, T., and Roy, N.R., (2015), "Modified DEEC: A Varying Power Level Based Clustering Technique for WSNs," International Conference on Computer and Computational Sciences (ICCCS-2015)-IEEE, pp. 170-176.

[18] Bsoul, M., Al-Khasawneh, A., Abdallah, A. E., and Abdallah, E. E., (2012),"An Energy-Efficient Threshold-Based Clustering Protocol for Wireless Sensor Networks," Wireless Personal Communications, 70(1), pp, 99–112.

[19] Ramachandran, C., Misra, S., and Obaidat, M.S., (2008), "A Probabilistic Zonal Approach for Swarm-Inspired Wildfire Detection Using Sensor Networks," International Journal of Communication Systems, 21(10), pp.1047-1073.

[20] Ramesh and Somasundaram,(2011), "A Comparative Study of Cluster Head Selection Algorithms in Wireless Sensor Networks," International Journal of Computer Science &Engineering Survey(IJCSES), 2(4), pp. 153-164.

Design and cost study of a 25kW SPV system based on real performance in an Indian environment

Ahmad Faiz Minai[1], Akhlaque Ahmad Khan[2], Mohammad Atif Siddiqui[3], Rupendra Kumar Pachauri[4] Shashikant[5] Akshay Raj[6]

[1,2,3]*Electrical Engineering Department, Integral University, Lucknow, Uttar Pradesh, India*

[4]*Electrical and Electronics Engineering Department, School of Engineering, University of Petroleum and Energy Studies, Dehradun, Uttarakhand, India*

[5]*Electrical Engineering Department, Babu Banarasi Das University, Uttar Pradesh, Lucknow, India*

[6]*Research and Development Department, IIMT University, Meerut, Uttar Pradesh*

fzminai@gmail.com[1], akhlaq.ee@gmail.com[2], atifsiddiqui@iul.ac.in[3] rupendrapachauri@gamil.com[4] shashikant52@gmail.com[5] akshay.raj@iimtindia.net[6]

Abstract.

The present paper focuses on solar PV system design and includes a cost analysis based study of a 25kW off-grid photovoltaic (PV) system at Integral University, Lucknow, India (28.5616N, 77.2802E). The cost of the electricity generated by the 25kW PV system has been calculated on a weekly and monthly basis. Additionally, the 25kW PV systems offer an internal rate of return of about 1.714%. With no outside financial support, a solar 25kW PV system with a cost of INR 0.9724/kWh is anticipated for a project with a 25-year profitable life based on the assumptions used in this analysis. This translates into an additional payment of 14.06 Lacks INR over the more expensive rate of power generated by the system at 25kWh. An additional cost charge is not required to maintain this type of PV system, though, if financial support is greater than 50% of the initial investment cost. In essence, this system was developed for a small town in a region with a limited supply of grid electricity. In rural India, a 25kW PV solar system is also quite advantageous.

Keywords- PVsyst Simulation, Si-Poly PV Module, Grid-connected photovoltaic system, Performance ratio, Renewable energy.

1. INTRODUCTION

Traditional energy sources are running out, which is bad for the environment and makes it even more important to find other ways to get power. Solar energy is the most abundant, clean, and promising nonconventional energy source. As the worldwide growth of renewable energy (RE) investment becomes more prominent. Economic and technological research is required to determine the viability of these resources. This study looks at how solar PV systems are designed and how well they work based on data collected in the field. As a limitation of solar PV system technology, the environmental conditions such as temperature and sun irradiation variations are major concerns about the performance degradation [1]. Moreover, when it comes to power quality, these discrepancies provide considerable challenges also [2]. An equally difficult procedure is the incorporation of renewable energy [3]. Isolated solar PV systems deliver better power quality in contrast to grid-integrated systems. Batteries in isolated systems connected to maximum power point technique (MPPT) charge regulators can endure any radiation exposure and temperature variations [4]. In this article, a small Indian community's concept for a 25kW off-grid PV system, primarily for rural areas, is presented. Also, PVsyst software has been used to

evaluate this rooftop system's performance based on a cost analysis [5]. Using the PVsyst application, it is possible to determine the amount of power that is generated, used, and wasted [6-7]. The gathered data is then used to perform the system's economical costing. Most of the study's data is annual, and the programme creates solar radiation data depending on the site's latitude and longitudinal data [8-11]. Then, for the given load, a variety of solar energy generation values are offered. An overview of PV system design is given in the second part, and the third section presents the results of the simulation. The paper's findings are then summarised in the concluding section.

2. DESIGN AND SPECIFICATIONS OF PV SYSTEM

The essential component of a PV system's design is the PV modules, which are linked together in a PV array in both parallel and series configurations. The size of the PV array is determined by the system's power rating. Vikram Solar PV modules (VSPV-CAAP-BC, 400Wp, Si-Poly) are used in the 25kW solar plant installation. Under ideal circumstances, each PV module can withstand a maximum voltage (42.5V) and current (9.72A) respectively. The combined maximum voltage and current for all PV modules is 42.5V and 43.6A, respectively [12-13]. This system also includes MPPT which is essential to extract the maximum power to the load. This system uses a generic universal MPPT controller with a maximum input current range of 30–45A and an output constant current of 14A. The entire setup is shown in Fig. 1 and Table-1 provides a list of every component. Fig. 2 displays the configuration of a 25kW stand-alone SPV system.

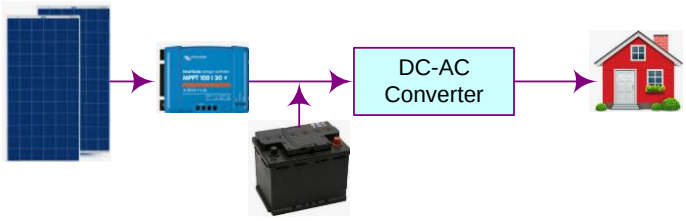

Fig.1: Schematic diagram of SPV system

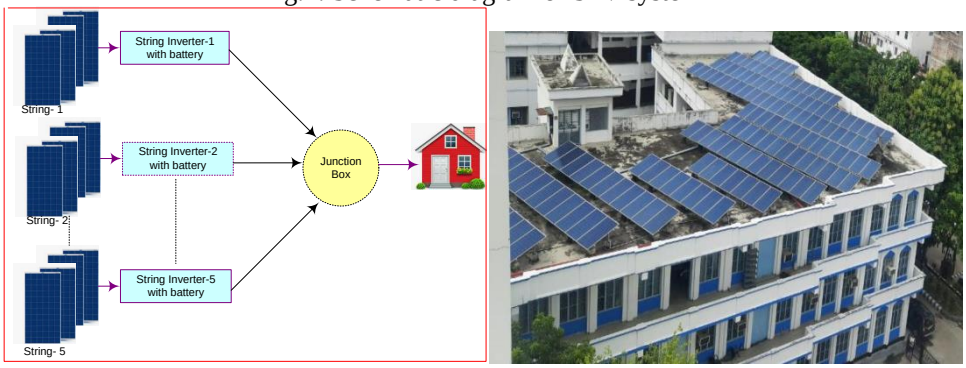

(a) (b)

Fig. 2: (a) Layout (b) On site PV system of a 25 kW power capacity

Table 1: Specification of 25kW Off-Grid Solar System (Calculated for 6 hour backup)

Particular	Company	Qty	Type	Efficiency	Lifespan	Price/ Qty	Investment cost
Solar Panels 25kW, 400W/ panel	Vikram Solar	63	Mono/ Poly	Up to 19%	25 Years	INR 12-15K/Panel	INR 7.56- 9.45L
5kVA String Inverter	Luminous	5	Off-Grid Solar Inverter	97%	5 Years	INR 45-50K /Inverter	INR 2.25-2.50L
150Ah, 12 Solar Power Battery	Exide	25	Tubular Solar Battery (C10)	-	3-5 Years	INR 13-15K/Battery	INR 3.25-3.75L
Other Accessories and Structure	Fasteners, cable ties, crimping tools, Earthing supplies, lighting interrupters, solar panels, 150 square metres space, 1 junction box, 220 metres of cable, and 150 metres of AC cable are needed.					INR 4-5K/kW: Thumb rule	INR 100-125L
						Total:	**INR 14.06-16.95L**

3. SIMULATION AND RESULTS

The installation and performance analysis of a 25kW PV system is carried out using the PVsyst tool. The beginning cost of the system under consideration ranges from 14.06-16.95 Lacks INR (Table-1). Specifically for household use, this investment will pay for a PV module, an MPPT controller, batteries, and an inverter. Table 2 provides data on the load and daily energy usage. The dedicated system's load required 110 kWh of electricity per day. PVsyst software is used to estimate the PV system's monthly energy output. As shown in Fig. 3 and Table 3, due to the influence of temperature on PV modules, the maximum global irradiation was only achieved in May month. May has the most solar energy compared to other months, and PVsyst simulates the highest generation in May month. The lowest insolation was received in the months of January and December, but because of temperature change, it is at its minimum in the month of December. Same thing happened with the simulated results using PVsyst. The minimum energy was recorded in the month of December, which validates the accuracy of the installed system. It's possible that the 3.67 MWhr of energy was generated throughout the year, which can also be use for the charging of batteries. Increases in battery storage capacity or higher consumption levels during the generating phase are two ways to utilise the unused energy. Fig. 3 shows the comparison of power generation, and it is compared with the simulation software PVsyst, for the validation of the installed system.

Table 2: Energy usage per day and load

S. no.	Load type	Quantity	Power Consumption	Uses	Energy (kWh/day)
1.	AC	4	2 Tons (2100 Watt)	6	50.4
2.	Fridge	1	2kW	6	12
3.	TV	1	80 W (Max.)	6	0.48
4.	Lights	1	2kW	6	12
5.	Pumps	1	5.5kW	6	33
				Total:	**110 (Approx.)**

Table 3:Performance ratio evolution of SCADA and PVsyst

Months	Temp. (ºC)	Insolation (kW/Hr)	SCADA		PVsyst	
			Energy (MWhr)	%PR	Energy (MWhr)	%PR
Jan	13.53	3.55	2.64	70.53	3.15	93.14
Feb	20.72	4.29	3.63	98.38	3.67	98.38
Mar	27.73	5.89	4.82	81.83	4.92	82.38
Apr	33.31	6.37	4.75	72.33	4.89	73.33
May	38.15	6.5	4.94	76.58	5.27	77.44
Jun	38.75	6.08	4.13	70.82	4.32	79.18
Jul	31.96	3.95	3.05	85.23	3.62	85.23
Aug	28.19	3.73	3.13	85.00	3.86	87.37
Sep	26.82	4.51	3.54	82.89	3.65	83.74
Oct	23.37	5.01	3.85	81.43	3.93	83.25
Nov	18.59	3.94	3.15	86.44	3.26	90.35
Dec	13.47	3.55	2.52	92.03	2.89	92.6
Average	**26.21**	**4.78**	**3.67**	**81.95**	**3.95**	**85.5325**
Total	**-**	**-**	**44.15**	**-**	**47.43**	**-**

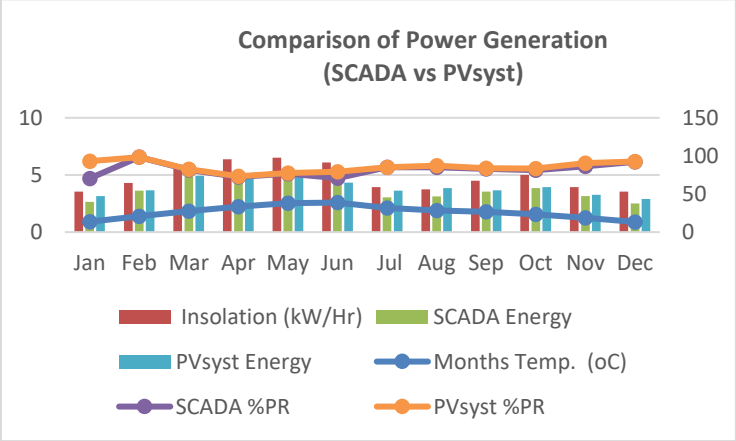

Fig. 3: Comparison of Power Generation (SCADA vs PVsyst)

4. CONCLUSION

In this study, a 25kW PV system for small communities in rural India is evaluated. The performance and cost analysis of the intended system have been evaluated using the PVsyst program. Due to the influence of temperature on PV modules, the maximum global irradiation was only achieved in May. The biggest amount of solar energy is also available in May compared to other months, and the generation is also maximum during the month of May, which is simulated using PVsyst. The lowest insolation was received in the months of January and December, but because of temperature change, it is at its minimum

in the month of December. The same thing happened with the simulated results using PVsyst. The minimum energy was recorded in the month of December, which validates the accuracy of the installed system. It's possible that the 44.15 MWHr of energy was generated throughout the year, which can also be used for the charging of batteries. A monthly estimate of the PV system's energy output is also provided and demonstrates how radiation from the sun affects solar energy generation. It is also computed to compare the energy generation results with PVsyst that was produced by the solar PV system.

REFERENCES

[1] Parlak, K.S.,"PV array reconfiguration method under partial shading conditions", Electr. Power Energy Syst, vol.63, pp.713-721, 2014.

[2] Patra, S., Kishor, N., Mohanty, S.R., Ray, P.K., "Power quality assessment in 3-U grid connected PV system with single and dual stage circuits", Electr. Power Energy Syst., vol.75, pp.275-288, 2015.

[3] Minai, Ahmad Faiz, Husain, Mohammed Aslam, Naseem, Mohammad and Khan, Akhlaque Ahmad. "Electricity demand modeling techniques for hybrid solar PV system" International Journal of Emerging Electric Power Systems, vol. 22, no. 5, 2021, pp. 607-615. https://doi.org/10.1515/ijeeps-2021-0085

[4] Pinto, S.J., Panda, G., "Performance evaluation of WPT based islanding detection for grid-connected PV systems", Electr. Power Energy Syst., vol.78, pp.537-546, 2014.

[5] Wu, Y.C., Chen, M.J., Huang, S.H., Tsai, M.T., Li, C.H., "Maximum power point tracking on stand-alone solar power system, three-point-weighting method incorporating mid-point tracking", Electr. Power Energy Syst., vol.52, pp.14-24, 2013.

[6] Fatima, K., Minai, A.F., Malik, H. (2022). Intelligent Approach-Based Maximum Power Point Tracking for Renewable Energy System: A Review. In: Malik, H., Ahmad, M.W., Kothari, D. (eds) Intelligent Data Analytics for Power and Energy Systems. Lecture Notes in Electrical Engineering, vol 802. Springer, Singapore.

[7] Minai, A.F., Usmani, T., Uz Zaman, S., Minai, A.K. (2022). Intelligent Tools and Techniques for Data Analytics of SPV Systems: An Experimental Case Study. In: Malik, H., Ahmad, M.W., Kothari, D. (eds) Intelligent Data Analytics for Power and Energy Systems. Lecture Notes in Electrical Engineering, vol 802. Springer, Singapore.

[8] Mermoud, A., "PVSyst: Software for the Study and Simulation of Photovoltaic Systems", ISE, University of Geneva, 2012.www.pvsyst.com.

[9] Irwan, Y.M., Amelia, A.R., Irwanto, M., Fareq, M., Leow, W.Z., Gomesh, N., Safwati, I., "Stand-alone photovoltaic (SAPV) system assessment using PVSyst software", in International Conference on Alternative Energy in Developing Countries and Emerging Economies, vol. 79. Elsevier, pp. 596-603, 2015.

[10] Minai, A.F., Usmani, T., Iqbal, A. (2021). Performance Evaluation of a 500 kWp Rooftop Grid-Interactive SPV System at Integral University, Lucknow: A Feasible Study Under Adverse Weather Condition. In: Malik, H., Fatema, N., Alzubi, J.A. (eds) AI and Machine Learning Paradigms for Health Monitoring System. Studies in Big Data, vol 86. Springer, Singapore. https://doi.org/10.1007/978-981-33-4412-9_24

[11] Metwally, H.M.B., Farahat, M.A., “Performance analysis of 3.6 kW rooftop grid connected photovoltaic system in Egypt”, in International Conference on Energy Systems and Technologies (ICEST2011), Cairo, Egypt, 11-14 March, 2011.

[12] Minai, A.F.; Usmani, T.; Alotaibi, M.A.; Malik, H.; Nassar, M.E. Performance Analysis and Comparative Study of a 467.2 kWp Grid-Interactive SPV System: A Case Study. Energies 2022, 15(3), 1107.

[13] A. A. Khan, A. F. Minai, L. Devi, Q. Alam and R. K. Pachauri, "Energy Demand Modelling and ANN Based Forecasting using MATLAB/Simulink," 2021 International Conference on Control, Automation, Power and Signal Processing (CAPS), 2021, pp. 1-6, doi: 10.1109/CAPS52117.2021.9730746.

Harmonics & Energy Saving Analysis of VFDs used for HVAC System: A Case Study in Oman

[1]Parmal Singh Solanki, [2]Sasidharan Sreedharan, [3]Piyush Dua

[1,2,3]University of technology and Applied Sciences-Suhar, Sultanate of Oman

solanki.soh@cas.edu.om; sasi.soh@cas.edu.om; piyushd.soh@cas.edu.om

Abstract

In this paper the methodology for harmonic and energy saving analysis for a laboratory building at the university campus in Oman have been proposed. The harmonics generated by the two variable frequency drives used for heating, ventilating and air conditioning of the building was modelled and simulated using SOLV and ETAP simulation software. The current and voltage distortion levels were measured under different loading scenarios. It is observed that lower order odd harmonics are dominating and can be mitigated using advanced universal harmonic filter to compliance the IEEE519 standard. The simulated results have revealed that about 10% of total energy consumed by induction motors can be saved by using VFDs along with extenuating all prevailing harmonics of the HVAC system.

Keywords Energy Saving, HVAC System, Harmonic Analysis, Harmonic Filters and VFDs

1. INTRODUCTION

Oman is one of middle-east country spread over 309500 square kilometres at Arabian Peninsula. Its climate is hot and dry while costal are hot and humid. To combat with long summer observed in Oman (about 9 months), Heating, and Ventilating and Air Conditioning (HVAC) system is extensively used across the country. The HVAC system alone is consuming about 52% of the total energy consumed by the residential sector [1]. It is also the major source of electricity consumption at the academic organizations and commercial sector. To increase the energy savings, HVAC unit are using the static converter based Variable Frequency Drives (VFDs). These drives act as non-linear loads to supply system.

The VFDs are equipped with solid state converters which control the operation of HVAC system. The VFDs are adjusting the speed of chilled water pump to meet the required comfort cooling. The static converters are consisting of power semiconductor devices which are source of harmonics [2]. The harmonic distortion is measure of the amount of deviation of voltage and current from their pure sinusoidal waveforms, caused by solid state converters in VFDs. The harmonic distortion is eventually polluting the quality of electrical power that adversely affects the power distribution system and connected equipment, if it exceeds certain limits [3]. Therefore, it essential to measure, analysed and limit harmonics in electrical system. There are various national and international standards governing the limits of total harmonic distortion (TDH) like IEEE 519, IEC 61000, EN 50160 and NRS 048-02 [4,5] etc. The recommended practices and harmonic limits prescribed by IEEE519-2014 and IEC 61000-3-4 are widely used by the commercial simulation programs to calculate and analysed the harmonic current, voltage and Total Demand Distortion (TDD). The commercial HVAC market in USA, Canada and other North American counties has adopted the IEEE519 standard.

The most common rectifier circuit in 3-phase VFD is 6-pulse diode rectifiers. It is robust, cost effective and extensively used in HVAC system to reduce its capital cost [6]. The shortcoming of 6-pulse rectifier is, it contains low order odd harmonics. There are various practices available to mitigate the harmonics problem in various applications [7, 8]. Also, VFDs analysis using machine learning tools seems to be more fruitful for extended operation in a complex industrial environment for high computational dependency [9-10]. For instance, based on the configuration of the input rectifier bridge, a 3-phase VFDs can use higher pulse techniques. Other than that, various types of passive filters can be used to alleviate the harmonics [11, 12]. The latter option is expensive and increases the installation cost of HVAC system.

At academic organization several nonlinear loads are connected to the supply system and many scholars had conducted the harmonic studies [13, 14]. In this paper, a case study to analyse the harmonics and energy savings of VFDs based HVAC system at university laboratory building have been proposed. Three scenarios are taken

into consideration to simulate each situation. Simulations are carried using SOLV and Electrical Transient Analyser Program (ETAP) software and results are compared to compliance with IEEE519 standard.

The paper has organised in 6 sections. The section 1 describes the introductory part while data collected for the case study is presented in section 2. The simulations carried out by simulator program under three scenarios are described in section 3. The results and conclusions are presented in section 4 &5 respectively. The references are listed in section 6.

2. HVAC AND POWER DISTRIBUTION SYSTEM

This study has carried out to analyse the harmonic analysis of the VFDs used for the HVAC system. This is providing the comfort cooling to engineering laboratories building at university campus. A segment of the schematic diagram of HVAC system where VFDs are driving to Chilled Water Pump (CWP) associated with Air Handling Unit (AHU) is shown in figure 2.1.

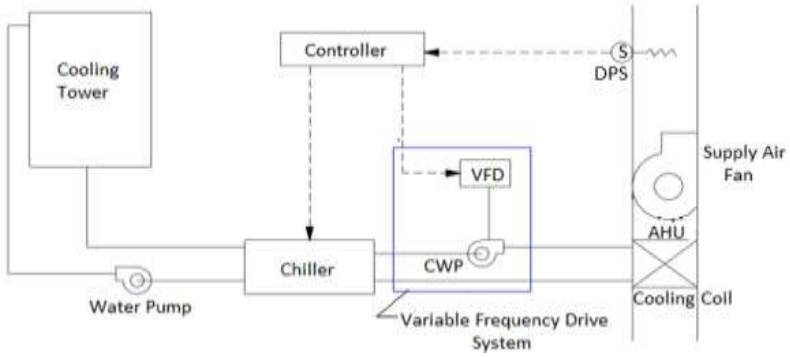

Figure 2.1.Schematic diagram of a segment of HVAC system and location of CWP [15]

Three induction motors, each 15 kW ratings are installed out of them two motors are operating the pumps to circulate the chilled water according to desired cooling. One motor is kept spare to meet any emergency. The discharge of the CWP is controlled by VFD system through Differential Pressure Sensors (DPS) connected to valves. A single line diagram of the electrical power distribution is shown in figure 2.2

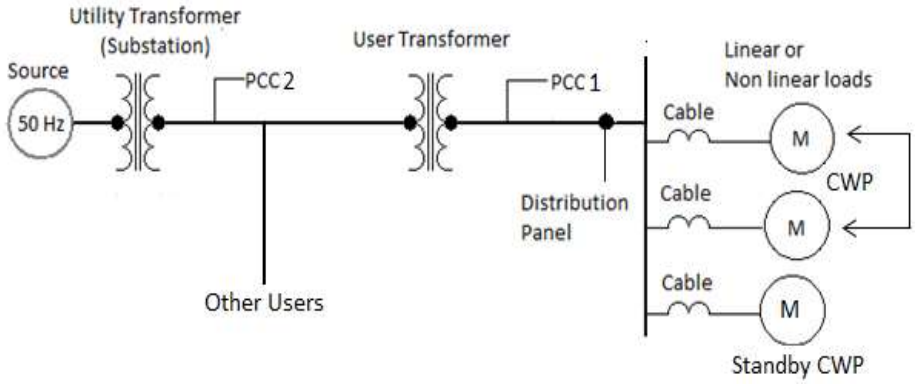

Figure 2.2.Single line diagram showing power distribution system

Point of Common Coupling (PCC) is the important location where power quality parameters are measured for harmonic analysis. As per IEEE 519 standard, it is preferred to be in the secondary side of utility and user's transformer. The specifications of other major components of distribution system are given below in table 2.1.

Table 2.1: Major components and their specifications

Components	Specifications
Utility Transformer	33/11 kV, 15 MVA, 50 Hz, %Z 5.5
User Transformer	11/0.440 kV, 1 MVA, 50 Hz, %Z 5.0
VFD: Induction Motors	3-phase, 0.440 kV, 15 kW, 50 Hz
Operating Information of HVAC System	Tariff: US$0.06 per kWh, Operating hour/day: 9 hrs, Operating days per year: 221 days

3. SIMULATION OF VFDS

Computer simulation program is used to simulate the existing VFDs. The simulator uses nodal analysis by expressing nodal matrix and evaluating the set of differential equations. The backward Euler and Fourier series are the major mathematical tools used by computer to analyse the periodic waveform like sinusoidal wave of integer multiple of 50 Hz frequency. The nonlinear loads are substituted by equivalent linear circuit models to get converge to final solution. To analyse the VFDs application following three scenarios are taken into consideration.

3.1. Scenario 1: CWP operated by 6-pulse VFDs

In this scenario, two induction motors of 20 hp each are coupled to chilled water pumps are operating. The speed of the motor is controlled by VFD which is using 6-pulse rectifier circuit to convert AC in to DC and Pulse Width Modulation (PWM) technique to convert DC into AC at desire voltage and frequency. The single line diagram of this scenario is shown in figure 3.1

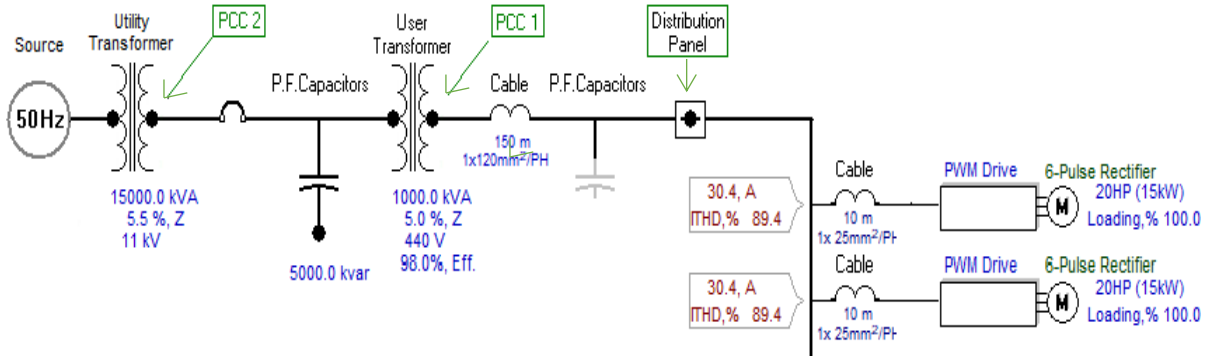

Figure 3.1.Single line configuration for simulating scenario-1

3.2. Scenario 2: CWP operated by 12-pulse VFDs

In this scenario, the speed of the chilled water pump is controlled by VFD. The 12-pulse rectifier circuit and inverter is supplied through a phase shifting transformer. To prevent the harmonics flow into upstream line, 2% reactor impedance at AC input reactor and 3% reactor impedance at DC link reactor are considered to simulate the scenario. The voltage to frequency ratio in all scenarios is kept constant to maintain the rated torque of the motor. The single line diagram of this scenario is shown in figure 3.2

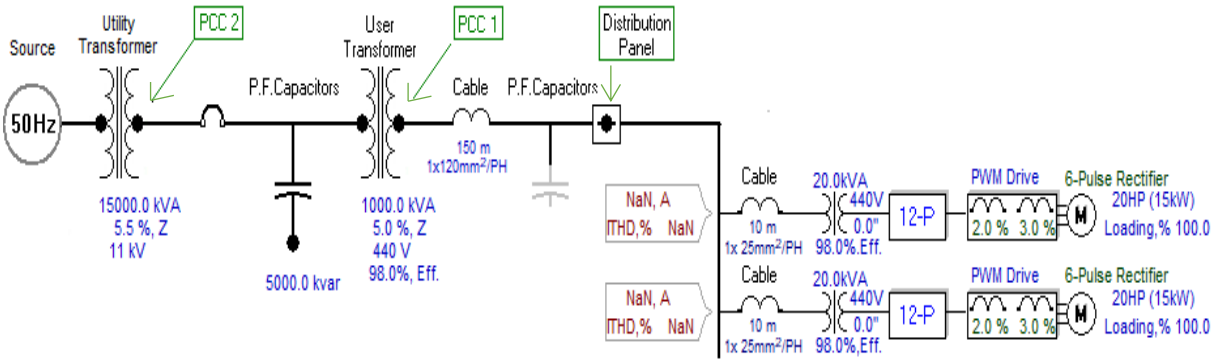

Figure 3.2.Single line configuration for simulating scenario 2

3.3. Scenario 3: CWP operated by VFDs along with Passive Filter

This topology is similar to scenario1. To reduce the impact of harmonics, the passive harmonic filters like Advanced Universal Harmonic Filter (AUHF) are considered to simulate the scenario. The single line diagram of this scenario is shown in figure 3.3

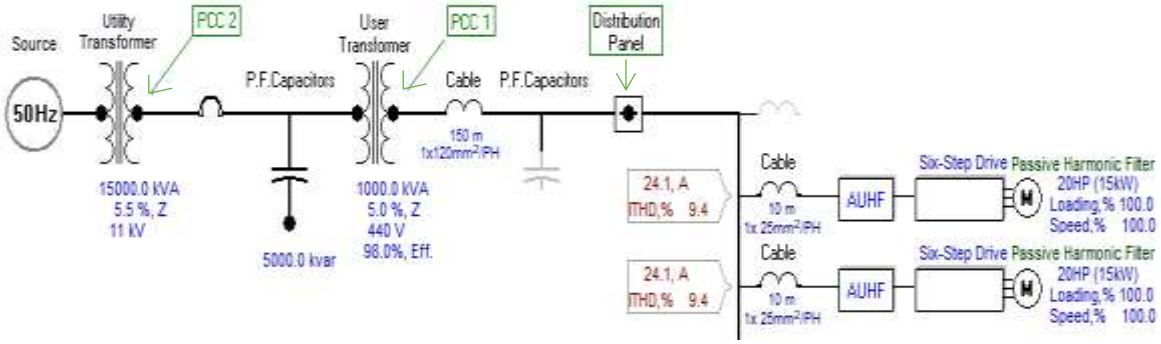

Figure 3.3.Single line configuration for simulating scenario 3

4. RESULTS

4.1 Voltage and Current Harmonics

It can be depicted from the figure 4.1 that, the VFDs consist of 6-pulse bridge rectifier along with PWM inverter generate the highest total harmonic distortion at PCC1. The waveform distortion reduces by using a 12-pulse bridge rectifier. More effectively the current wave and becomes near to sinusoidal in 3rd scenario which is using advanced universal harmonic filter.

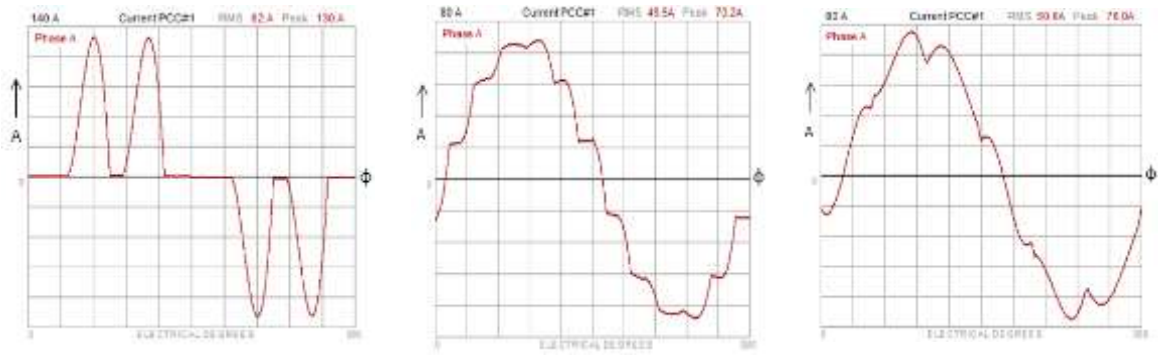

Figure 4.1.Total harmonic current waveforms of scenarios1, 2 &3 respectively

It can be seen from table 4.1, the total harmonic distortion and maximum individual harmonics of voltage in all scenarios have not exceeded the level of 1.1 and 0.7 % respectively. This is well below the recommended values of IEEE519-2014 standard.

Table 4.1: Total harmonic distortion of voltage at PCC1 under different scenarios

Total Harmonic Distortion under Different scenarios	**Calculated Value%{h}**	**IEEE-519:2014 Limits**	**Remarks**
Scenario 1			
Voltage Total Harmonic Distortion (THD_v)	1.1	8.0	Pass
Max Individual Voltage Harmonic	0.7{5th}	5.0	Pass
Scenario 2			
Voltage Total Harmonic Distortion (THD_v)	0.2	8.0	Pass
Max Individual Voltage Harmonic	0.2{11th}	5.0	Pass
Scenario 3			
Voltage Total Harmonic Distortion (THD_v)	0.2{7th}	8.0	Pass
Max Individual Voltage Harmonic	0.1	5.0	Pass

The current harmonics are more concern for any distribution system and are shown in table 4.2. It can be observed from table 4.2, the total harmonic distortion and low order harmonics except 17th are higher than the prescribed limits of international standard. Therefore, it is vital to mitigate harmonics to avoid their adverse effects on distribution system and connected devices. In scenario 2, a 12-pulse converter has used to operate the

VFD which is able to mitigate most of current harmonics except 11th order. To optimally mitigate all low order current harmonic, scenario 3 is more effective where an advanced universal passive harmonic filter has used to keep the total distortion less than IEEE519-2014 limit.

Table 4.2: Total harmonic distortion of current at PCC1 under different scenarios

Total Harmonic Distortion under Different scenarios	**Calculated Value%{h}**	**IEEE-519:2014 Limits**	**Remarks**
Scenario 1			
Current Total Demand Distortion (THD_i)	86.8	12.0	*Fail*
Max Individual Current Harmonic<11	70{5th}	10.0	*Fail*
11 to 16	12.6{11th}	4.5	*Fail*
17 to 22	0.1{17th}	4.0	Pass
23 to 34	3{23rd}	1.5	*Fail*
>35	1.1{35th}	0.7	*Fail*
Scenario 2			
Current Total Demand Distortion (THD_i)	9.1	12.0	Pass
Max Individual Current Harmonic<11	2.2{5th}	10.0	Pass
11 to 16	7.1{11th}	4.5	*Fail*
17 to 22	0.0{17th}	4.0	Pass
23 to 34	1.1{23rd}	1.5	Pass
>35	0.5{35th}	0.7	Pass
Scenario 3			
Current Total Demand Distortion (THD_i)	8.9	12.0	Pass
Max Individual Current Harmonic<11	8.1{7th}	10.0	Pass
11 to 16	2.5{11th}	4.5	Pass
17 to 22	0.0{17th}	4.0	Pass
23 to 34	0.8{23rd}	1.5	Pass
>35	0.4{35th}	0.7	Pass

4.2 Energy Saving

The energy consumed by motors at rated load have simulated by considering two situations, one when motors are operating without any control and second when these are controlled by the VFD system. It is observed that VFD system is able to reduce about 10% of total energy consumed by the motors. Further it is noted VFDs consist of higher pulse converters and harmonic filters are used, the energy consumption is slightly increases. For instance, the use of harmonic filters, compared to 6-pulse converter will increase about 0.75% energy consumption of the motors.

Though VFDs are responsible to generate the harmonics and theses harmonics flowing through the power system increase losses and energy consumption, but the total energy consumption of the motors equipped with VFDs consuming lesser power compared to operating the motors without control.

5. CONCLUSION

Following are the conclusions based on the harmonic analysis and energy savings of this study:

- The use VFDs for CWP in the HVAC system is useful. It is able to reduce about 10% energy consumption. It is beneficial to increase the system efficiency and to diminish the electricity bills.
- The advanced universal passive harmonic filters are capable to mitigate lower order prevailing harmonics to the compliance level of IEEE 519-2014 standard.
- The VFDs are generating the harmonics but these can be reduced by using phase shifting transformer, higher order bridge converters and harmonic filters.

ACKNOWLEDGEMENTS

Authors are thankful to the University of Technology and Applied Sciences-Suhar and its scientific research department for facilitating opportunity of internal research grant (IRG) project. Authors are also thankful to maintenance department and local utility for providing necessary data and support.

6. REFERENCES

[1]. T. Sweetnam, “Residential Energy Use in Oman: A Scoping Study”, Project Report, Authority for Electricity Regulation, Oman, Ver. 8, January 2014.

[2]. Y. Y. Garud, S. R. Gole, R. T. Jadhav, and S. U. Deoghare, “A Study on Variable frequency Drive and its Applications,” Int. J. Innov. Res. Sci. Eng. Technol. An ISO, vol. 3297, pp. 3079–3084, 2007.

[3]. C. L. Collocott, K. O. Awodele, and A. V. Adebayo, “Harmonic emission of non-linear loads in distribution systems - A computer laboratory case study,” 2020 Int. SAUPEC/RobMech/PRASA Conf. SAUPEC/RobMech/PRASA 2020, no. August, 2020.

[4]. T. M. Blooming, N. Carolina, and D. J. Carnovale, “Application of IEEE Standard 519-1992 Harmonic Limits” Eaton Electrical, pp. 1–9, 1992.

[5]. A. E. Legarreta, J. H. Figueroa and J. A. Bortolin, "An IEC 61000-4-30 class a — Power quality monitor: Development and performance analysis," 11th International Conference on Electrical Power Quality and Utilisation, 2011, pp. 1-6, doi: 10.1109/EPQU.2011.6128813.

[6]. Y. Siregar, W. K. Al-Azzawi, Z. Pane, U. E. Parhusip, and Suherman, “Study of harmonic distortion from variable speed drive and energy saving lamps,” Indonesian. J. Electrical. Eng. Computer. Sci., vol. 27, no. 2, pp. 667–677, 2022.

[7]. D. He, Q. Xiong, X. Zhang, Y. Dai, and Z. Jiang, “A Decentralized, Flat-Structured Control System for Chiller Plants.” MDPI applied sciences, 9, 4811 2019.

[8]. Poonam Kaur1, “Harmonic Analysis of VFD’s,” Ijmer, vol. 4, no. 5, pp. 55–57, 2014.

[9]. Ł. Michalec, M. Jasiński, T. Sikorski, Z. Leonowicz, Ł. Jasiński, and V. Suresh, “Impact of harmonic currents of nonlinear loads on power quality of a low voltage network—review and case study,” Energies, vol. 14, no. 12, 2021.

[10]. B. Krishnasamy and K. Ashok, “Assessment of Harmonic Mitigation in V/f Drive of Induction Motor Using an ANN-Based Hybrid Power Filter for a Wheat Flour Mill,” Processes, vol. 10, no. 6, 2022.

[11]. I. A. Adejumobi, O. I. Adebisi, and J. E. Amatu, “Harmonics mitigation on industrial loads using series and parallel resonant filters,” Niger. J. Technol., vol. 36, no. 2, p. 611, 2017.

[12]. T. Taufik, M. Muscarella, and D. Sawitri, “Power quality analysis of variable frequency drives connected to a reactively compensated mixed load system,” Proc. - 2016 Int. Semin. Appl. Technol. Inf. Commun. ISEMANTIC 2016, no. March 2018, pp. 261–266, 2017.

[13]. T. A. Papadopoulos, G. C. Christoforidis, K. C. Chatzisavvas, and G. K. Papagiannis, “Harmonic level measurements and analysis at higher education buildings,” IET Conf. Publ., vol. 2012, no. 613 CP, 2012.

[14]. M. N. Patil, R. M. Holmukhe, and S. Munde, “Power quality study of electrical installation in academic institute - Case study,” Int. J. Appl. Eng. Res., vol. 12, no. 11, pp. 2868–2875, 2017.

[15]. I. Joo, M. Liu, J. Wang and K. Hansen, “Application of Innovative Technologies during Continuous Commissioning,” Proceedings of the 3rd International Conference for Enhanced Building Operations, Berkeley, California, pp. 3–8, 2003.

Wireless Power Transmission of electricity for utilization of fused bulbs in rural India

Surajit Mondal[1], Arya Verma[1],Vikas Thapa[2, a]

[1]Department of Electrical and Electronics, University of Petroleum and Energy Studies, Dehradun, India, 248001

[2]School of Design, University of Petroleum and Energy Studies, Dehradun, India, 248001

[a]vikas08thapa@gmail.com

Abstract- Wireless power transfer of energy is used to transmit the electrical energy to an electrical load by giving a small amount of input current without any physical instrumental connection. The main problem which arises in wireless power transmission is the propagation loss. Over the long distances the transmission losses are very high. Tesla coil is the alternative solution to electrical energy transmission. The main advantage of using the tesla coil is that it uses the Electromagnetic field to transfer the energy. Our method provides a mobility solution for charging station for various electronic devices and novelty of our approach is to reuse the fused bulb which reduces the e-waste. We performed three experiments in which we change the Length of Secondary coil, Number of Turns in primary coil and the Diameter of the Secondary coil. The maximum electric and magnetic field observed were found to be 1400(V/m) and 99.9μT respectively. The primary focus of our research is to optimize tesla coil for the reusability of the fused or unused bulbs to reduce the e-waste in rural India.

Keywords: Wireless power transfer, Tesla coil, resonant coupling.

I. INTRODUCTION

During the last decade wireless transmission of electricity has been an essential requirement in many applications [1]. Wireless mobile charging station has become very popular during last few years. It is an economical approach in which efficiency is a substantial parameter. The proposed model provides a unique way to utilize the outdated (fused) fluorescent bulb. Cost has always been a challenge when using renewable energy resource like solar PV, biomass, biogas [2]. Near field Wireless power transfer topology can be categorize as electric induction and Magnetic induction of Wireless Power Transfer topology (WPTT) [3]. .

Our method utilizes the magnetic resonant coupling method in order to transmit the power wirelessly [4-8]. This method is based on electromagnetic field in which the waves doesn't propagates but creates an field around the transmitter [9-10]. The main advantage of such system is that the propagation loss is reduced, but the limitation to such system is that it has very low transmission distance [11-12].

II. WORKING PRINCIPLE

A. Concept of Electromagnetism

An oscillating magnetic field is induced inside the coil when an oscillating current travels across it. As a result, the voltage across the coil induces and tends to oppose the driving current [13][14]. According to Faraday's law, the EMF is the rate of change in magnetic flux:

$$\varepsilon = -N\ (d\phi_B/dt)$$

Where ,

N = number of turns of wire

ϕ_B= magnetic flux through a single loop

The Magneto-motive force (MMF) is the energy of magnetic fields. When a current flows, it creates an electromagnetic flux in thecase of a conductor material.

$$Fm = N \times I$$

When the N/I ratio reaches a saturation point, raising it no longer increases the flux(ϕ). Electrical energy will be generated in the model because of matching inductive and capacitive reactance. Resonance occurs at specific frequency for specific value of capacitance and inductance. It is used to filter and regulate the circuit. Electric field of capacitor and magnetic field of inductor will beperpendicular to each other.

B. LC circuit

Resonance is used to filter the circuit because it occurs at a particular frequency and y also depends on the exact value of inductance and capacitance [15][16]. LC circuit is designed to operate at high frequencies and for providing control of resonant frequency, the value of inductor and Capacitor can be adjusted [17]. The circuit diagram of LC circuit shown in figure 1 The inductive and capacitive reactance must be identical magnitude to reach resonance, as shown by,

$$\omega L = 1/(\omega C)$$

$$f = \frac{1}{2(LC)^{1/2}}$$

$$\omega = 2Mf$$

Where,

f = Resonance frequency in Hertz,L = Inductance in HenryC = Capacitance in farads.

When the same frequency is applied, resonant energy transfer, also known as resonant inductive coupling, based on near-field wireless transmission of energy in the form of electromagnetic radiation between two coils that reaches a highly resonant level [7].

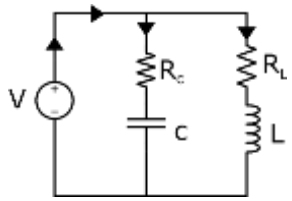

Figure.1 Schematic representation of LC circuit

Our research observed that the coupling in the Tesla coil work efficiently to provide electricity to supply a load wirelessly. Our work promises that in electrical appliances, there might be an elimination of wires in between power sources with the use of wireless power transfer.

While reviewing other research papers, most of the cases of Wireless Power Transfer (WPT) determines that the maximum transfer distance can be occupied when the alignment between the coil is coaxial [12]. But the efficiency will be reduced because of less coupling factor. Our work is different from this methodology. In our experiments, the coil alignment is in spiral so that the coupling factor will high for high power generation process and with the help of propagation of Magnetic(M-field) and Electric field(E-field) made by Toroidal propagation. This energy which generated as Electromagnetism form will be received by receiver circuit.

III. METHODOLOGY

If conducting matter is introduced in surrounding of a model, a potential difference can be produced via induced electric field that can cause charge separation. A coil of copper or another alloy material can effectively use to generate magnetic field. When the AC power is turned ON It generates an oscillating magnetic field in a conductive loop. With the help of coupling of coils, a pulsating magnetic field will be form in surrounding and that cause electric current flow through the second coil. Current will be generated by the second coil to energize the devices via Electromagnetism. Figure 2 shows the complete process of our experiment from generation to transmission.

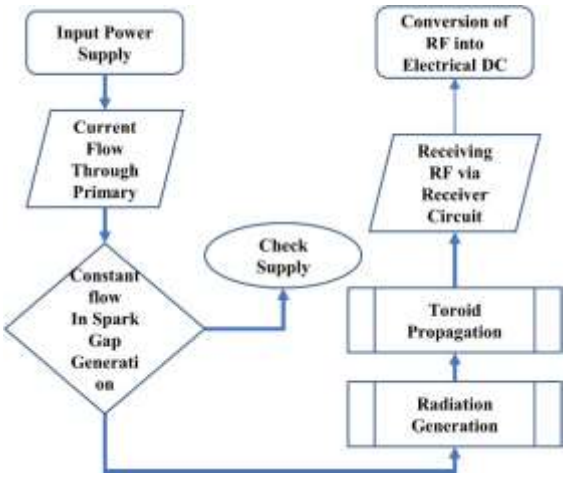

Figure.2 Methodology Diagram for the performed experiment

IV. RESULTS & DISCUSSUION

The output has based on the effect of electromagnetism and the distance between the bulb and the prototype. When the distance of a bulb from the prototype will increase, the intensity will decrease. As the frequency and the distance is indirectly proportional to each other.

Experiment:1

The first model is shown in figure 3, Bipolar N-P-N Transistor has used to protect the circuit. As it required small amount of current up to 0.5A and voltage up to 30 V. So the capacitor has no role in this circuit. If we use capacitor for the continuous flow of current that cause overheating or burning of Transistor. The coil parameters are shown in Table 1 and the desired output of frequency, Voltage and E-Field, M-field with respect to the distance has been shown in figure 4 and figure 5 the quantity of E-field and M-field radiation has shown in Table 2

Table 1. Parameter of experiment 1

Parameter	Value
Primary coil Turns	5
Secondary coil Turn	~450
Length of Secondarycoil	150mm
Diameter of SecondaryCoil	20mm
Primary wire width	2.2mm
Secondary wire width	0.96mm

Figure 3. Experimental setup for Prototype 1.

Table 2. Radiation and Frequency in experiment 1

Distance (cm)	E-field radiations(V/m)	M-field radiations(uT)	Frequency(MHz)
1	350-200	5-5.50	5.217MHz

2	220-150	4-5.5	4.876MHz.
3	200-175	2.5-3.5	4.24MHz
4	100-75	2.0-3.0	3.178MHz
5	90-35	1.5-2.2	2.69MHz
6	<60	<1.0	1.59MHz

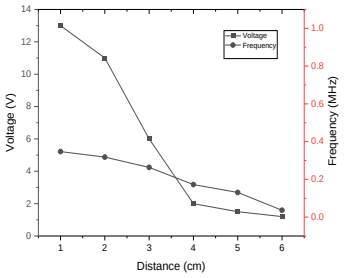

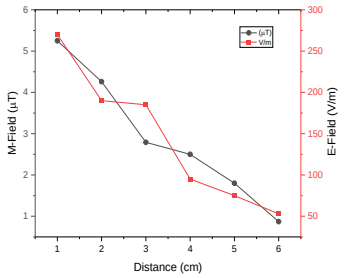

Figure 4. Graph of Frequency and voltage with respect to distance. Figure 5. Graph of E-field and M-field with respect to the distance.

Experiment 2:

Second prototype is shown in figure 6. Here the structure is approximately the same as first prototype. The difference is the size, number of turns and width of the coil. The output will be correspondingly high as compared with the previous circuit shown in Table 3 and the parameter for this experiment has shown below in Table 4. Here's Graph of frequency, Electric field and Magnetic field shown in figure 7.

Where, d is the distance perpendicular to the coil in cm and f is the frequency which can vary in kHz/MHz/GHz.

Table 3. Parameter of experiment 2

Parameter	**Value**
Primary coil Turns	7
Secondary coil Turn	650
Length of Secondary coil	300mm
Diameter of Secondary Coil	20mm
Primary wire width	2.9mm
Secondary wire width	0.96mm

.

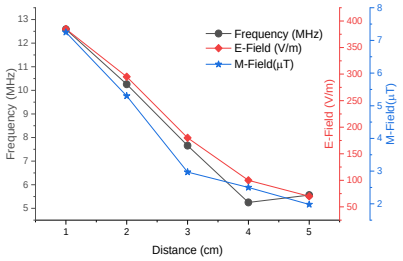

Figure 6. Experimental setup for experiment 2, Figure 7. Graph of frequency, E-field and M-field w.r.t the distance

Table 4. Radiation and frequency in experiment 2.

Distanc e (cm)	**E-field radiations(v/m)**	**M-field radiation**	**Frequency(MHz)**

		(μT)	
1	350-400	6-7.50	12.586MHz
2	220-300	4-5.5	10.256MHz
3	150-200	2.5-3.5	7.658MHz
4	70-120	2.0-3.0	5.249MHz
5	50-100	1.5-2.2	5.560MHz

Experiment 3:

In this experiment, different methodology has introduced in which spark gap have installed and to maintain the constant flow of current, capacitor band has used as shown in figure 8. The difference in this prototype is in the input circuit and the Toroid material to maintain its reasonable output. Now, the rechargeable batteries have been used for this prototype as it required continuous flow of current. As, the capacitor band has connected in parallel by which it maintains the spark gap so that the intensity in the bulb will be consistent. In this prototype, only three capacitors have been used. Number of capacitors can be calculated by RMS voltage divided DC Voltage of capacitor as capacitor is of Cornell-Dubliell so its capacitance and DC voltage is 0.15μf, 2000V DC. Since the methodology is different from the previous ones, The output will be high as compared to the previous circuit shown in Table 6 and the parameter for this experiment has shown in the Table 5.

Table 5. Parameter of experiment 3

Parameter	**Value**
Primary coil Turns	8
Secondary coil Turn	~800
Length of Secondary coil	150mm
Diameter of Secondary Coil	20mm
Primary wire width	3.0mm
Secondary wire width	0.96mm

Figure 8. Experimental setup for prototype 3..

Table 6, Radiations and frequency in experiment 3

Distance(cm)	E-field radiations (V/m)	M-field radiations(μT)	frequency
1	1300-1400	99.99	35MHz
2	1100-1200	77-89	31MHz
3	600-700	75-85	26MHz
4	200-250	65-70	18MHz
5	150-200	40-55	11MHz

V. CONCLUSION:

This system gives a way to have a mobile glowing bulb through an electromagnetic induction method without any

direct contact with a power source. We have tested different prototypes based on change in distance and turning of coils. It leads thesystem to give higher output with high radiations. This technology can be very helpful in hilly and rural areas where there areplenty of power issues. Our proposed structures have been installed in few nearby villages for test run also. The future of this technology focuses mainly the remote areas of India as well as State such as Uttarakhand.

Acknowledgement

This research was supported by the Department Sciences and Technology (DST) India, [grant number- SP-YO-058-2017].

References

[1] G.R. Chandra Mouli, P. van Duijsen, F. Grazian, A. Jamodkar, P. Bauer, O. Isabella, Sustainable E-bike chargingstation that enables AC, DC and wireless charging from solar energy, Energies (Basel). 13 (2020) 3549.

[2] E. Oró, V. Depoorter, A. Garcia, J. Salom, Energy efficiency and renewable energy integration in data centres.Strategies and modelling review, Renewable and Sustainable Energy Reviews. 42 (2015) 429–445.

[3] G. Bouattour, X. Chen, H.B.J. Derbel, O. Kanoun, Investigation on Flexible Coils Geometries for Inductive PowerTransmission Systems, in: 2019 5th International Conference on Nanotechnology for Instrumentation and Measurement (NanofIM), IEEE, 2019: pp. 1–7.

[4] J. Premalatha, U. Anitha, V. Manonmani, P. Ganesan, Survey on energy saving methods for green communication network, Indian J Sci Technol. 8 (2015) 1–5.

[5] G. de Freitas Lima, R.B. Godoy, Modeling and prototype of a dynamic wireless charging system using LSPScompensation topology, IEEE Trans Ind Appl. 55 (2018) 786–793.

[6] J. Ashok, P. Thirumoorthy, Design considerations for implementing an optimal battery management system of awireless sensor node, Indian J Sci Technol. 7 (2014) 1255.

[7] J.P.K. Sampath, D.M. Vilathgamuwa, A. Alphones, Efficiency enhancement for dynamic wireless power transfer system with segmented transmitter array, IEEE Transactions on Transportation Electrification. 2 (2015) 76–85.

[8] S. Bae, J.-J. Yun, Economic and energy efficient design method for a green wireless telecommunication power system, Indian J Sci Technol. 8 (2015) 1–6.

[9] W. Xifan, C. Chengjun, Z. Zhichao, Experiment on fractional frequency transmission system, IEEE Transactions onPower Systems. 21 (2006) 372–377.

[10] X. Wang, X. Wang, Feasibility study of fractional frequency transmission system, IEEE Transactions on PowerSystems. 11 (1996) 962–967.

[11] N. Tesla, Apparatus for transmitting electrical energy., (1914).

[12] R. Shadid, S. Noghanian, A. Nejadpak, A literature survey of wireless power transfer, in: 2016 IEEE InternationalConference on Electro Information Technology (EIT), IEEE, 2016: pp. 782–787.

[13] P.D. Abd Aziz, A.L. Abd Razak, M.I.A. Bakar, N.A. Aziz, A Study on wireless power transfer using tesla coil technique, in: 2016 International Conference on Sustainable Energy Engineering and Application (ICSEEA), IEEE,2016: pp. 34–40.

[14] E.J. Rothwell, M.J. Cloud, Electromagnetics, CRC press, 2018.

[15] Z. Shuai, D. Liu, J. Shen, C. Tu, Y. Cheng, A. Luo, Series and parallel resonance problem of wideband frequencyharmonic and its elimination strategy, IEEE Trans Power Electron. 29 (2013) 1941–1952.

[16] Y.W. Li, Control and resonance damping of voltage-source and current-source converters with $ LC $ filters, IEEETransactions on Industrial Electronics. 56 (2008) 1511–1521.

[17] A.S. Marincic, Nikola tesla and the wireless transmission of energy, IEEE Transactions on Power Apparatus andSystems. (1982) 4064–4068.

Co-estimation of state of charge, state of health, remaining useful life and state of function prediction for lithium ion battery in electrified vehicle using machine learning methods: A comprehensive review

Kaushik Das, Roushan Kumar #

Department of Mechanical Engineering, School of Engineering, University of Petroleum and Energy Studies, Dehradun, India
#***Corresponding Author:*** *Roushan Kumar, E-mail: rkumar@ddn.upes.ac.in*

Abstract

A novel machine learning based co-estimation approach of Lithium ion battery (LIB) co-estimation of State of Charge (SOC), State of Health (SOH), Remaining Useful Life (RUL)and State of Function (SOF), which provides comprehensive capabilities like range knowledge, battery diagnostics and prognostics need in electrified vehicle is proposed in this work. The review introduced a methodology for state co estimation for battery health management and monitoring, challenges, benefits, and key findings. It is considered as game changing technology that can push the boundary of electric vehicle applications. Recent breakthroughs in model-based, data-driven, and hybrid techniques are highlighted to provide one point solution by introducing the first comprehensive vision of battery's health management system. A flowchart illustrates the different techniques for co-estimation process and highlight its experimental conditions. Together, it provides a powerful guide to designing experiments or models for investigating battery health management system for electric vehicles.

Keywords. Electric vehicle, co estimation, lithium ion battery, machine learning, state of battery

1. INTRODUCTION

With widespread deployment of rechargeable lithium ion batteries (LIB) because of its high energy and power densities, aging and degradation prediction for safety, diagnostics and prognostics need has emerged a challenging issue [1],[2]. This nonlinear degradation by way of various thermo- electric- chemical- mechanical factors dependents on operating and environmental conditions [3],[4]. On electrochemical side, this is due to irreversibility in following recession reasons -phase changes in electrode materials, electrode dynamics during recession, electrolyte breakdown, and production of SEI films resulting into capacity and power fade [5],[6]. This fade necessitates quantization of various states like SOC, SOH, SOF, SOT, SOP, SOL, RUL, SOL [7],[8]etc. forms part of modern day requirement. All these state parameters are intertwined in some way as a battery can have low SOC (defined as ratio of available capacity and the maximum possible capacity) at high SOH (a figure of merit of present condition and is a ratio of present capacity to capacity at fresh) or high SOC at low SOH, but is not sufficient to guarantee performance of a certain duty, The peak output power of the battery [9], which is constrained by thresholds like voltage restrictions, current constraints, and SOC limits, may be used to illustrate how the battery performs in relation to actual load demands [10]. This is referred to as SOF and considered as a functionality derived from LIB transient behaviour and RUL, an asset at a particular time of operation. All these four state fulfil the aspects of safety, diagnostics, prognostics and performance of LIB and this review is centred on prospecting and proposing a novel co-estimation methodology for these four major indirect measurable indices.

Different state estimation approach focus on single or dual parameters, whereas very few work on over two states. The strong links between the four stages make it difficult for an isolated assessment of one or even two states to accurately reflect the true status of the battery. In actuality, the battery might adapt and optimise itself to its use case and hence requires significantly less calculations provided these estimated states are made available on the battery itself [11]. The main challenge for accurate prediction of actual state and the complexities in estimation has leads towards different methodologies like electrochemical methods, electrical equivalent circuit methods, mathematical methods and data driven methods, which requires different level of domain knowledge and expertise. These parameters are fundamental to the future development of electric vehicles, energy storage devises etc. which are large-scale deployment and complex in applications.

Complexities of real LIB is much more than a single cell, which houses hundreds to few thousands of identical capacity(but often slightly different behaviour) cells with battery management system (BMS), connectors, thermal management systems, packing materials, housings [12],[13]. where each and every components are responsible for its performance. The real battery works with huge fluctuation in vital and direct measurable parameters, voltage (V), current (I), temperature (T), internal impedance (IR) on time scale, which generates huge data for further development of secondary indices like state parameters. This data leads towards development of states understanding by way of employing suitable methods which can handle voluminous data and give suitable analysis and prediction in a timely manner with least resources used. Here comes different data driven machine learning (ML) methods, which comes handy in this application. In ML methods also, selection of an appropriate method is a multidimensional problem, depending on the extent of data available, quality of results looked for and physical interpretability of model required, which itself is a need for how accurate state estimation of some battery properties is needed or life predictions[14]-[16]. In addition, all these ML methods only provide point estimation of states (which serves as a “best guess” or “best estimation” of an unknown parameter). Especially for the data-driven method, state estimation result a non-smooth curve due to the measure noise and outliers of direct measurable indices. Hence, quantifying estimation uncertainty is to enable reliability assessment of state estimate, which not only keeps away from over-conservative estimations. The steps commonly employed are data pre-processing, training and estimation.

Table 1. State co estimation by different researchers

Reference	Battery	Cell	CAP	SOC	SOH	SOF	SOE	SOT	SOP	RUL	SOB/SOS
[1]	✓			✓				✓			
[2]	✓			✓	✓	✓					
[6][7]		✓	✓	✓							
[9]		✓		✓							
[10]		✓		✓	✓						
[11][12]	✓			✓					✓		
[15]		✓		✓	✓						
[5]		✓	✓	✓							
[18]		✓	✓	✓							
[19]		✓	✓	✓							
[20]		✓	✓	✓							
[21]		✓		✓	✓				✓		
[4][9]		✓		✓	✓						
[5][21]		✓		✓	✓						
[6][24]		✓		✓	✓						
[7][15]		✓	✓	✓							
[18][23]		✓		✓							

[[1][14]		✓		✓					
[20][24]		✓	✓	✓					
[5][10]	✓			✓	✓			✓	
[6][22]		✓		✓					
[9][24]		✓	✓			✓			
[7][13]		✓			✓				✓
[16][21]	✓	✓	✓	✓					

ML based different state estimation are available in literature, however very few studies are carried out for co estimation of different states using ML methods. [17] carried out SOC, SOH, RUL co estimation using DL method, [18],[19] used multi-stage model fusion method for estimating capacity-SOC. [20] used forgetting factor dual particle filter algorithm for estimation of SOC- SOH. Similar exercise and research is been carried out selectively [21]. To the best of our knowledge, there is, however, a lack of studies on ML based co-estimation of SOC, SOH, SOF and RUL prediction, Hence, it is a clear advantages of ML based estimation were insufficiently harnessed in the area of battery state monitoring, where handling the coupling of different states is a key challenge. Considering this research gap, we are strongly innervate to devise an innovative data-driven DL based co- estimation scheme of different states for improving battery monitoring and BMS accuracy and robustness. Figure 1 represents the interlinking relationship of SOC, SOH, RUL and SOF.

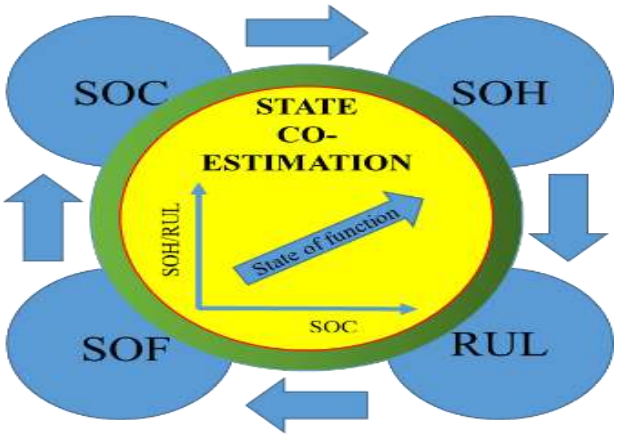

Figure 1. Interlinking relationship of SOC-SOH-RUL-SOF in LIB

The motivation of the review work covers state co estimation of lithium ion battery used in electric vehicle technology covers, Most of the research work for LIB state co-estimation is still in laboratory stage with predefined duty cycle and at controlled environment where as in reality operating and environmental condition in real world scenario is totally different, where actual battery works with several inconsistent cells. Limited works has focused on effective state co-estimation where accuracy of one state prediction is associated with the variation of another, which influences the result of other. Simultaneously, computational competency shall also increase to BMS in this scenario. Poor generality of model among family of LIB with different operating and environmental conditions.

2. PROPOSED METHODOLOGY

It is established that SOC and SOH are fully coupled in a nonlinear fashion; RUL has a linear relationship with SOH, SOF is dependence on discharge load on SOC and SOH at a given temperature. In model-based method the prediction results are universal and estimation accuracy does not depend on historical data, however it requires higher domain knowledge and is not practically applicable to the applications of EV[19]. In the proposed methodologies, we proposed ML based methodology which don't requires much domain knowledge, fast, capable of unified co estimation of different states and can be integral part of BMS[12],[13],[20],[21].

SOH is a metric to appraise the aging level, which includes capacity fade and/or power fade on time scale and the common used indicators are capacity decrease, DC resistance increase and AC impedance increase. The non-empirical lab data is handy to test and validate the result and trend can be conserved for a specific cell electrochemistry. The decrease in SOH has an impact on SOC and hence it is proposed that continuous SOH status shall be used as input for SOC estimation even it is a slowly time-varying state, which is also supported by research conducted earlier[9],[16]. The actual vehicle status data is continuously fetched and analyzed through BMS, which in conjunction to online SOH data is used for estimation of SOC. RUL is directly related to SOH data and is predicted from the results of SOH. The whole input of lab data & actual EV battery data is been processed for prediction in a suitable ML method based framework for determine the degradation physiognomies of batteries. This SOC & SOH data is proposed to be used for determining SOF with cell level temperature data using limiting algorithm, as SOF is the ability estimation and is dependent on SOC, SOH with temperature.

The main contributions of this study are as follows. Initially the authors proposed a suitable method for online co-estimation for SOC, SOH, RUL & SOF using machine learning. Second, SOH estimation is done through ML model and used as additional input for estimation of SOC with continuous updation. Third, SOC and SOH parameters are estimated simultaneously, and the proposed method can yield accurate SOC estimation results using the current state information of SOH. RUL is directly derivable from online SOH as being a linear functionality. Fourth, SOF is online estimated using the online input of SOC, SOF along with cell temperature data. Finally, a ML model bank is proposed to be developed to study degradation and nonlinear characteristics [22]-[26]. This study proposes the following improvements over previous studies. SOH estimation method is considerably different as it uses joint online input of EV LIB data and complete non-empirical cell level data to analysis and updation and not a single discharge cycle was used to estimate SOH, and SOH was estimated after one discharge cycle was complete.

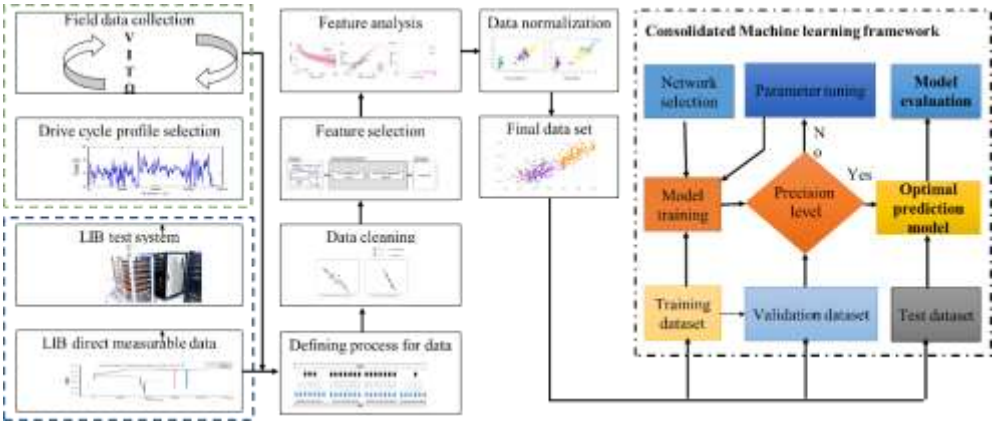

Figure 2. Online and offline data processing and consolidated machine learning framework

3. EVALUATION AND PROPOSAL OF SUITABLE ML METHOD

Existing literature has studied extensively different ML methods singularly or in hybridization with other ML methods or filter based methods. State estimation are defined as time- series processing problem [9]and it is well established that LSTM NN are effective and scalable models for handling time sequential data[4]. Other researchers had used different methods like supervised, semi supervised, unsupervised & reinforcement learning methods with different error estimation like MAE, RSME, R^2 etc [4],[16]. Temporal convolutional network (TCN), rather new concept, is found to have higher performance accuracy and thus improves considerably with increase in quantum of data where as other

simple statistical learning, traditional ML, shallow ML degrades and is found suitable in typical LIB datasets which are aperiodic and nonlinearity among variables, which is incapable by models to capture and have self-adaption of the complex data features. The need for co-estimation via TCN is actually a framework employing casual convolutions and dilations so that it is adaptive for sequential data with its temporality and large receptive fields. The strong robustness and high accuracy of TCN for high fidelity and multivariate voluminous data needed to be handled for co-estimation is highly attractive and is already used selectively for individual RUL, SOH, SOC estimation.

4. CONCLUSION & FUTURE WORK

Co-estimation algorithm utilizes the relationships among these four states appropriately, and is thus more prudent and precise than traditional discrete state estimation methodology with the following advantages:

1) Impact of aging and degradation on state estimation is taken into account. The capacity used in SOC estimation is updated online for SOH estimation & RUL prediction; therefore, accuracy of SOC estimation after battery aging is improved.

2) Impact of SOC on available energy and power is taken into account for the first time, which shall give accurate SOF. As battery OCV varies with SOC, and consequently maximum available energy and power is influenced by SOC, the SOC estimation result is used to obtain OCV in SOF estimation. Therefore, with an updated on SOC and correlated OCV, the accuracy of SOF estimation can be significantly improved.

3) TCN improves the prediction accuracy and minimize multivariate time series data dependence for aperiodic data and thus eliminates extra filters and estimate methods like KFs used in previous studies, TCN can support in readily transfer necessary data from BMS, such as cell temperature, I, V, Ω etc. flowing straight to SOH/SOC estimation.

4) Using learning methods like as gradient descent, the TCN may self-learn. This is in stark contrast to existing researches such as lumped parameter models and analogous electrochemical models, which take a long time with low accuracy and tough to implement.

5) It will be demonstrated that a single TCN can learn to state estimate at various environmental temperatures. This is advantageous since typical estimating procedures require separate models or look up tables for varied atmospheric temperatures.

In future the authors intended to test and validate the proposed TCN methods with the help of publically available LIB degradation datasets (NASA, Sandia National Laboratories, Oxford Battery Degradation Dataset etc) with actual EV LIB data at different operating(both actual and standard drive cycle like DST, UDDS etc) and with different environmental conditions.

REFERENCES

[1] J. Li, M. Ye, K. Gao, X. Xu, M. Wei, and S. Jiao, "Joint estimation of state of charge and state of health for lithium-ion battery based on dual adaptive extended Kalman filter," *Int. J. Energy Res.*, vol. 45, no. 9, pp. 13307–13322, 2021, doi: 10.1002/er.6658.

[2] P. Li *et al.*, "State-of-health estimation and remaining useful life prediction for the lithium-ion battery based on a variant long short term memory neural network," *J. Power Sources*, vol. 459, no. March 2022, 2020.

[3] R. Kumar, N. J. Ahuja, M. Saxena, and A. Kumar, "Automotive Power Window Communication with DTC Algorithm and Hardware-in-the Loop Testing," *Wirel. Pers. Commun.*, 2020.

[4] R. Kumar, A. Kumar, M. K. Gupta, J. Yadav, and A. Jain, "Solar tree-based water pumping for assured irrigation in sustainable Indian agriculture environment," *Sustain. Prod. Consum.*, vol. 33, pp. 15–27, 2022.

[5] Y. Shi *et al.*, "The optimization of state of charge and state of health estimation for lithium-ions battery using combined deep learning and Kalman filter methods," *Int. J. Energy Res.*, vol. 45, no. 7, pp. 11206–11230, 2021, doi: 10.1002/er.6601.

[6] Z. Li *et al.*, "Dual time-scale co-estimation of state-of-charge and state-of-health for lithium-ion battery pack

with passive balance control over whole lifespan based on particle filter," *J. Phys. Conf. Ser.*, vol. 1617, no. 1, 2020, doi: 10.1088/1742-6596/1617/1/012067.
[7] K. Li, K. J. Tseng, F. Wei, and B. H. Soong, "A Pragmatic SOH and SOC Co-Estimator for Lithium-ion Batteries in Smart Grid Applications," *2018 Int. Power Electron. Conf. IPEC-Niigata - ECCE Asia 2018*, no. Cc, pp. 1517–1523, 2018, doi: 10.23919/IPEC.2018.8507818.
[8] C. S. Meera, S. Sunny, R. Singh, P. S. Sairam, R. Kumar, and J. Emannuel, "Automated precise liquid transferring system," *India Int. Conf. Power Electron. IICPE*, vol. 2015-May, 2015.
[9] Z. Lyu, R. Gao, and L. Chen, "Li-Ion Battery State of Health Estimation and Remaining Useful Life Prediction through a Model-Data-Fusion Method," *IEEE Trans. Power Electron.*, vol. 36, no. 6, pp. 6228–6240, 2021, doi: 10.1109/TPEL.2020.3033297.
[10] X. Li, Z. Wang, and L. Zhang, "Co-estimation of capacity and state-of-charge for lithium-ion batteries in electric vehicles," *Energy*, vol. 174, pp. 33–44, 2019, doi: 10.1016/j.energy.2019.02.147.
[11] X. Lai *et al.*, "Co-Estimation of State-of-Charge and State-of-Health for Lithium-Ion Batteries Considering Temperature and Ageing," 2022.
[12] R. Kumar, K. Bansal, A. Kumar, J. Yadav, M. K. Gupta, and V. K. Singh, "Renewable energy adoption: Design, development, and assessment of solar tree for the mountainous region," *Int. J. Energy Res.*, no. May, pp. 1–17, 2021, doi: 10.1002/er.7197.
[13] R. Kumar, M. Kumar Gupta, A. Kumar, P. Sharma, and R. Deorari, "Analysis of electronic clutch control unit for manual transmission vehicle oriented toward safety," *Mater. Today Proc.*, no. xxxx, 2022.
[14] R. Kumar, P. K. Dwivedi, D. Praveen Reddy, and A. S. Das, "Design and implementation of hydraulic motor based elevator system," 2015, doi: 10.1109/IICPE.2014.7115821.
[15] M. S. Hossain Lipu *et al.*, "Deep learning enabled state of charge, state of health and remaining useful life estimation for smart battery management system: Methods, implementations, issues and prospects," *J. Energy Storage*, vol. 55, no. September, 2022, doi: 10.1016/j.est.2022.105752.
[16] R. Xiong, J. Wang, W. Shen, J. Tian, and H. Mu, "Co-Estimation of State of Charge and Capacity for Lithium-Ion Batteries with Multi-Stage Model Fusion Method," *Engineering*, vol. 7, no. 10, pp. 1469–1482, 2021, doi: 10.1016/j.eng.2020.10.022.
[17] R. Kumar, R. K. Pachauri, P. Badoni, D. Bharadwaj, U. Mittal, and A. Bisht, "Investigation on parallel hybrid electric bicycle along with issuer management system for mountainous region," *J. Clean. Prod.*, vol. 362, no. June, p. 132430, 2022, doi: 10.1016/j.jclepro.2022.132430.
[18] P. Ren, S. Wang, J. Huang, X. Chen, M. He, and W. Cao, "Novel co-estimation strategy based on forgetting factor dual particle filter algorithm for the state of charge and state of health of the lithium-ion battery," *Int. J. Energy Res.*, vol. 46, no. 2, pp. 1094–1107, 2022, doi: 10.1002/er.7230.
[19] R. Kumar, Divyanshu, and A. Kumar, "Nature Based Self-Learning Mechanism and Simulation of Automatic Control Smart Hybrid Antilock Braking System," *Wirel. Pers. Commun.*, vol. 116, no. 4, pp. 3291–3308.
[20] L. Xia, S. Wang, C. Yu, C. G. Jiang, Y. Fan, and W. Cao, "A Novel Prior Noise Correction - Adaptive Extended Kalman Filtering Method for the Full Parameter and State-of-energy co-estimation of the Lithium-ion Batteries," *Int. J. Electrochem. Sci.*, vol. 16, no. 7, pp. 1–15, 2021, doi: 10.20964/2021.07.30.
[21] X. Lai *et al.*, "Co-estimation of state of charge and state of power for lithium-ion batteries based on fractional variable-order model," *J. Clean. Prod.*, vol. 255, p. 120203, May 2020.
[22] Jitendra Yadav & G. Agnihotri, "Proposed Critical Damping for a Spring Mass System to Avoid Stick Slip" ,Springer Journal of the institution of engineers (India): Series C Volume 96, Number 3, PP 331-335.
[23] Yadav, Jitendra, et al. "Nonlinear dynamics of controlled release mechanism under boundary friction." Results in Engineering 11 (2021): https://doi.org/10.1016/j.rineng.2021.100265
[24] Jitendra Yadav and Geeta Agnihotri (2017), "Modeling and Simulation of the Dynamic Response of a Generic Mechanical Linkage for Control Application Under the Consideration of Nonlinearities Imposed by Friction", In Springer Proceedings of the International Conference on Nano-electronics, Circuits & Communication Systems, Lecture Notes in Electrical Engineering 403, DOI 10.1007/978-981-10-2999-8_26
[25] Maan A., Pitta P., Yadav J. (2018) Performance Evaluation of Rectangular Fins by Modeling and Simulations. In: Siddiqui N., Tauseef S., Abbasi S., Rangwala A. (eds) Advances in Fire and Process Safety. Springer Transactions in Civil and Environmental Engineering. Springer, Singapore 10.1007/978-981-10-7281-9_26
[26] Yadav J., Agnihotri G. (2018) Circumvention of Friction-Induced Stick-Slip Vibration by Modeling and Simulation. In: Singh R., Choudhury S., Gehlot A. (eds) Intelligent Communication, Control and Devices. Advances in Intelligent Systems and Computing, vol 624. Springer, Singapore https://doi.org/10.1007/978-981-10-5903-2_174

Heat transfer analysis of electrically conductive Blasius flow of Casson nanofluid in a porous medium

Ravinder Kumar
Department of Mathematics, Chandigarh University, SAS Nagar (Mohali), Punjab, India

Abstract: In this article, we have discussed the behavior of electrically conducted Blasius flow of non-Newtonian nanofluid under the influence of Forchheimer equation. For non-Newtonian nature of the nanofluid, the Casson model is employed. Heat and mass transfer rates are analyzed under the influence of heat source and sink devices. The Governing boundary layer PDEs are converted to ODEs under proper similarity transformations. RK45 numerical scheme along with the Newton-Raphson shooting technique is utilized to solve the set of ODEs. The effects of dimensionless parameters on velocity, temperature, concentration, heat transfer rate, and mass transfer rate are presented via figures.

Keywords: Forchheimer equation, Casson nanofluid, Magnetic field, Heat source/sink, Shooting method

1. Introduction

Free stream analysis of a 3D Casson nanofluid flowing through forchheimer extended Darcy model for the porous medium is made in this investigation. The magnetic field is considered to be influencing along with the heat source/sink.

The concept of Constantly moving fluid over a motionless surface is observed in many real-life fluids flows [1]. It is important to control the thickness and separation of the boundary layer which is mainly dominated by friction [2]. Ridha [3] computed the solution of a 3Dl Blasius transport numerically. Kachanov and Michalke [4] compared the experimental results with theoretical solutions for the instability of a 3-D Blasius transport. Tsigklifis and Lucey [5] conferred an approach for the inspection of the comprehensive stability of 3D disorders in Blasius transport.

We interact with non-Newtonian fluids in our day-to-day life like honey, blood, toothpaste, paints, juices, and shampoos. These kinds of fluids are flexible and observe the transformation from fluid to solid depending upon relaxation and observation time [12]. Researchers have found new models over time to predict the properties of a non-Newtonian fluid out of which the Casson model is influencing and have unique properties(shear thinning/thickening).

The applications of electrically conducting fluids are found in geophysics, engineering, astrophysics, MHD accelerator, and many more. The magnetic field can restrain the velocity, concentration, and temperature of a fluid. Many researchers have examined this concept in a different types of physical problems. Magnetic field influences on a non-radiative 3Dl flow due to a pressure-supported torus is inspected by Hawley et al. [8]. The magnetic-force-free concept is introduced by Chandrasekhar and Kendall [6]. MHD model for three-dimensional flow in Titans plasma environment is inspected by [7]. Hayat et al. [9] investigated an unsteady MHD three-dimensional flow over a stretching surface. Rakesh et al. [11] analyzed MHD flow in the stagnation region and in presence of velocity/thermal slip.

Fluid Transport through pores and their connectedness is an undetachable part of fluid dynamics [13]. Flow through these geometries has vast applications in plastic-films, the extrusion of polymer, human bones, extraction of petroleum, turbine blades and many more [14]-[15]. Some other important research works in this field are [17]-[19].

2. Mathematical formulation

In this study, we have considered a 3D flow of Casson nanofluid under Blasius conditions, in the presence of Darcy-Forchheimer model of porous surface. Inertia coefficient of porous medium in x and y directions are taken as $F_1 = \frac{c_b}{x\sqrt{K_1}}$ and $F_2 = \frac{c_b}{y\sqrt{K_1}}$ respectively. The system of nanofluid governing equations along with boundaries restrictions formulated as [12]:

$$v_{1_x} + v_{2_y} + v_{3_z} = 0, \tag{1}$$

$$v_1 v_{1_x} + v_2 v_{1_y} + v_3 v_{1_z} = \nu_f \left(1 + \frac{1}{\beta}\right) v_{1_{zz}} + V_1 V_{1_x} + V_2 V_{1_y} - \frac{\nu_f}{K_1}(v_1 - V_1) - F_1(v_1^2 - V_1^2) - \frac{\sigma_f B^2}{\rho_f}(v_1 - V_1), \tag{2}$$

$$v_1 v_{2_x} + v_2 v_{2_y} + v_3 v_{2_z} = \nu_f \left(1 + \frac{1}{\beta}\right) v_{2_{zz}} + V_1 V_{2_x} + V_2 V_{2_y} - \frac{\nu_f}{K_1}(v_2 - V_2) - F_1(v_2^2 - V_2^2) - \frac{\sigma_f B^2}{\rho_f}(v_2 - V_2), \tag{3}$$

$$v_1 \alpha_x + v_2 \alpha_y + v_3 \alpha_z = T_a \alpha_{zz} + \kappa(B_d \alpha_z \beta_z + A_d \alpha_z^2) + q''' \tag{4}$$

$$v_1 \beta_x + v_2 \beta_y + v_3 \beta_z = B_d \beta_{zz} + A_d \alpha_{zz} \tag{5}$$

$$\left.\begin{array}{l} v_1 = v_{1_w}, \quad v_2 = v_{2_w}, \quad v_3 = 0, \quad \alpha = \alpha_w, \quad \beta = \beta_w \quad at \quad z = 0 \\ v_1 = V_1, \quad v_2 = V_2, \quad \alpha \to \alpha_\infty, \quad \beta \to \beta_\infty \quad at \quad z \to \infty \end{array}\right\}. \tag{6}$$

In the above equations, $q''' = \frac{Q}{\rho c_p}(\alpha - \alpha_\infty)$

PDEs are transformed to ODEs utilizing the following similarity transformations.

$$v_1 = ax\varphi_{1'}, \quad v_2 = ay\varphi_{2'}, \quad v_3 = -\sqrt{av}(\varphi_1 + \varphi_2), \quad \varphi_3 = \frac{\alpha - \alpha_\infty}{\alpha_w - \alpha_\infty}, \quad \varphi_4 = \frac{\beta - \beta_\infty}{\beta_w - \beta_\infty} \quad \text{where} \quad \eta = \sqrt{\frac{a}{\nu}}z$$

The obtained coupled ordinary differential equations are

$$\left(1 + \frac{1}{\beta}\right)\varphi_{1_{\eta\eta\eta}} + (\varphi_1 + \varphi_2)\varphi_{1_{\eta\eta}} - \left(\frac{1}{Da} + M\right)(\varphi_{1_\eta} - \lambda_3) - Fr(\varphi_{1_\eta}^2 - \lambda_3^2) + \lambda_3^2 - \varphi_{1_\eta}^2 = 0 \tag{7}$$

$$\left(1 + \frac{1}{\beta}\right)\varphi_{2_{\eta\eta\eta}} + (\varphi_1 + \varphi_2)\varphi_{2_{\eta\eta}} - \left(\frac{1}{Da} + M\right)(\varphi_{2_\eta} - \lambda_4) - Fr(\varphi_{2_\eta}^2 - \lambda_4^2) + \lambda_4^2 - \varphi_{2_\eta}^2 = 0 \tag{8}$$

$$\varphi_{3''} + Pr[Nb\varphi_{4'} + Nt\varphi_{3'}]\varphi_{3'} + Pr(\varphi_1 + \varphi_2)\varphi_{3'} + Q^*\varphi_3 = 0 \tag{9}$$

$$\varphi_{4''} + Sc(\varphi_1 + \varphi_2)\varphi_{4'} + Nr\varphi_{3''} = 0 \quad (10)$$

The deduced restrictions are

$$(\varphi_1 + \varphi_2)(\eta) = 0, \quad \varphi_{1'}(\eta) = \lambda_1, \quad \varphi_{2'}(\eta) = \lambda_2, \quad \varphi_3(\eta) = 1, \quad \varphi_4(\eta) = 1, \quad \text{as} \quad \eta \to 0$$
$$\varphi_{1'}(\eta) = \lambda_3, \quad \varphi_{2'}(\eta) = \lambda_4, \quad \varphi_3(\eta) = 0, \quad \varphi_4(\eta) = 0, \quad \text{as} \quad \eta \to \infty \quad (11)$$

Notations and dimensionless parameters

$$\kappa = \frac{(\rho c_p)_s}{(\rho c_p)_f}, \quad A_d = \frac{T_d}{\alpha_\infty}, \quad Da = \frac{aK_1}{\nu_f}, \quad Q^* = \frac{Q}{a\rho c_p}, \quad Nt = \frac{\kappa A_d(\alpha_w - \alpha_\infty)}{\nu_f}, M = \frac{\sigma_f B^2}{\rho_f a}$$

$$Sc = \frac{\nu_f}{B_d}, \quad Fr = \frac{c_b}{\sqrt{K}}, \quad Nr = \frac{Nt}{Nb}, \quad Pr = \frac{\nu_f}{\alpha_f}, \quad Nb = \frac{\kappa B_d(\beta_w - \beta_\infty)}{\nu_f},$$

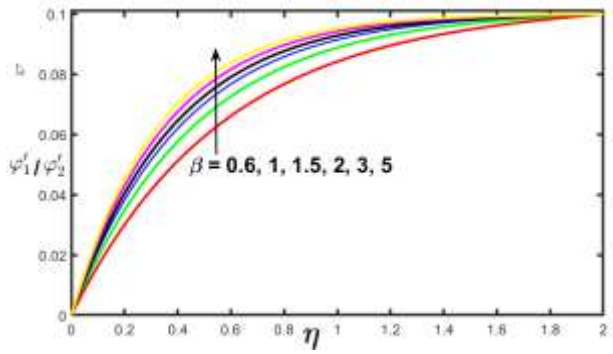

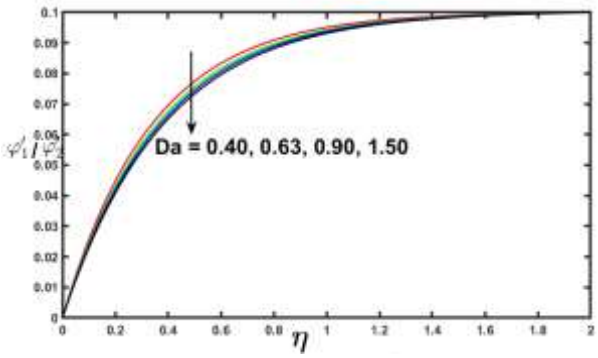

Fig.1: Variability of $\varphi_{1'}$ and $\varphi_{2'}$ with β. Fig.2: Variability of $\varphi_{1'}$ and $\varphi_{2'}$ with Da.

3. Numerical Method

Newton-Raphson shooting scheme with RK45 method is utilized to unravel the equations from (7)-(10), under the restriction (11). We convert our BVP to IVP to make it compatible with RK45. The equations (7-11) are converted to first order ordinary differential equations using the following transformations.

$$\varphi_1 = X_1, \quad \varphi_{1_\eta} = X_2, \quad \varphi_{1_{\eta\eta}} = X_3, \quad \varphi_{1_{\eta\eta\eta}} = X'_3, \quad \varphi_2 = X_4, \quad \varphi_{2_\eta} = X_5, \quad \varphi_{2_{\eta\eta}} = X_6,$$
$$\varphi_{2_{\eta\eta\eta}} = X'_6, \quad \varphi_3 = X_7, \quad \varphi_{3_\eta} = X_8, \quad \varphi_{3_{\eta\eta}} = X'_8, \quad \varphi_4 = X_9, \quad \varphi_{4_\eta} = X_{10}, \quad \varphi_{4_{\eta\eta}} = X'_{10}.$$

The obtained system of first order ordinary differential is

$$X'_1 = X_2 \quad (12)$$
$$X'_2 = X_3 \quad (13)$$
$$X'_3 = \frac{\beta\left[\left(\frac{1}{Da}+M\right)(X_2-\lambda_3)+Fr(X_2^2-\lambda_3^2)+(X_2^2-\lambda_3^2)-(X_1+X_4)X_3\right]}{(1+\beta)} \quad (14)$$
$$X'_4 = X_5 \quad (15)$$
$$X'_5 = X_6 \quad (16)$$
$$X'_6 = \frac{\beta\left[\left(\frac{1}{Da}+M\right)(X_5-\lambda_4)+Fr(X_5^2-\lambda_4^2)+(X_5^2-\lambda_4^2)-(X_1+X_4)X_6\right]}{(1+\beta)} \quad (17)$$
$$X'_7 = X_8 \quad (18)$$
$$X'_8 = -Pr[(NbX_{10} + NtX_8)X_8 + (X_1 + X_4)X_8 + Q^*\varphi_3] \quad (19)$$
$$X'_9 = X_{10} \quad (20)$$

$$X'_{10} = -[Sc(X_1 + X_4)X_{10} + NrX'_8] \quad (21)$$

with boundary conditions

$$X_1(0) = X_4(0) = 0, \quad X_2(0) = \lambda_1, \quad X_5(0) = \lambda_2, \quad X_7(0) = 1, \quad X_9(0) = 1$$

$$X_2(\infty) = \lambda_3, \quad X_5(\infty) = \lambda_4, \quad X_7(\infty) = 0, \quad X_9(\infty) = 0. \quad (22)$$

To solve above system of equations, Firstly we pick the limit for η. Secondly, we chose the initial guesses for $X_3(0)$, $X_6(0)$, $X_8(0)$, and $X_{10}(0) = 0$. Thirdly Runge-Kutta method applied to solve the system. Fourthly it is inspected that if the boundary residual is less than accepted error if not Newton-Raphson method is employed to recalculate the values of $X_3(0)$, $X_6(0)$, $X_8(0)$, and $X_{10}(0) = 0$. The edge of the Runge-Kutta 4th order method over other numerical method is that the implementation of the method is easy. Further, the results are always reliable as the local truncation error for $RK4$ is $O(h^5)$.

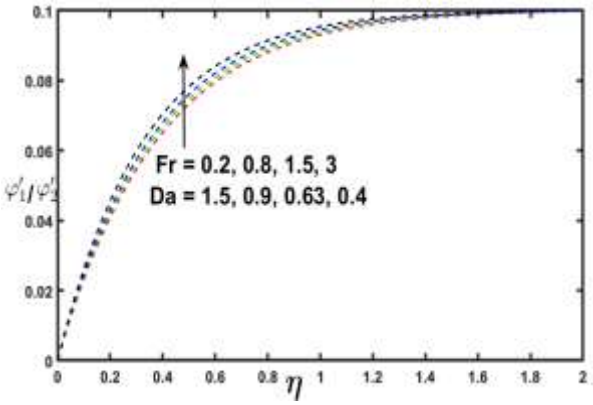

Fig.3: Variability of $\varphi_{1'}$ and $\varphi_{2'}$with Fr and Da.

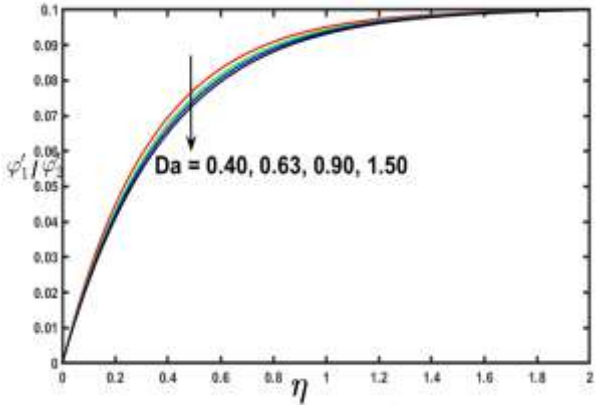

Fig.4:Variability of $\varphi_{1'}$ and $\varphi_{2'}$ with M.

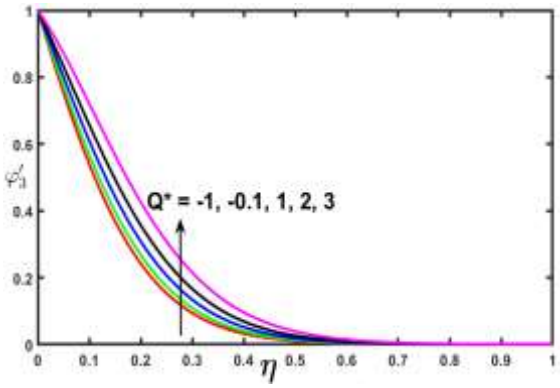

Fig.5:Variability of $\varphi_{3'}$ with heat source ($Q * > 0$) and heat sink ($Q * < 0$)

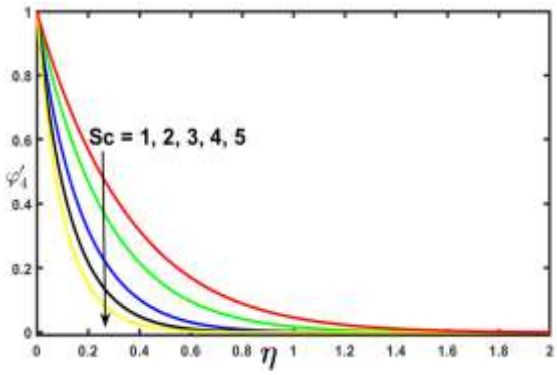

Fig. 6: Variability of $\varphi_{4'}$ with Sc.

4. Results and discussion

This part of the paper consists of plots which demostrate the impacts of concentration, mass transfer, temperature, heat transfer and velocities under Blasius conditions. Values of $\lambda_1 = \lambda_2 = 0$, $\lambda_3 = \lambda_4 = 0.1$(ifnotmentionedseparately) . If not mentioned separately the values of other parameters in both cases are fixed to $Q^* = 3$, $M = 3$, $Sc = 2$, $Pr = 6.07$, $B = 3$, $Fr = 0.2$, $Da = 0.63$, $Nb = 0.05$ and $Nt = 0.02$.

4.1 Variations in velocity

Velocity plots are maintained against the Casson parameter, Darcy number, magnetic

field parameter, and Darcy-Forchheimer number via figures 1-4. It came in to notice that the velocity is increasing with the Casson parameter. Non-Newtonian properties of Casson number enhance the viscosity and curtail the yield stress. This should reduce the velocity of the nanofluid near the surface but contrarily it is increasing because of it has minimal impacts in case of free stream. Boundary layer thickness is noticed shrinking Figure 1. The porous medium permeability is reducing with increasing increments in Da and curtailing with increments in Fr. This forces the velocity of the fluid to grow with decreasing Da and increasing Fr(Please see figure 2-3). Another Figure 4 depicts that the larger electromagnetic force has minimal impacts on free stream velocity. The normally induce magnetic increase in the circular motion of the fluid.

4.2 Variations in temperature and concentration

Figure 5 shows the temperature variation with Q*. with reducing heat sink, the temperature is increasing and with increasing heat source temperature is also increasing. It means the heat sources sink can significantly control the temperature. In another figure 6, the Schmidt number forcing the concentration to curtail. Concentration is reducing since the increasing Schmidt number is related to higher dynamic viscosity and low mass diffusivity.

4.3 Variation in heat and mass transfer

Figure 7-8 are maintained to depict the nature of heat and mass transfer rate. It is concluded that the heat transfer rate in Casson nanofluid can be enhanced by controlling the heat source and Schmidt number. Also if a heat sink is installed then minimum heat loss will be there(See figure 7). The mass transfer rate can be enhanced by controlling the Schmidt number and Brownian motion.

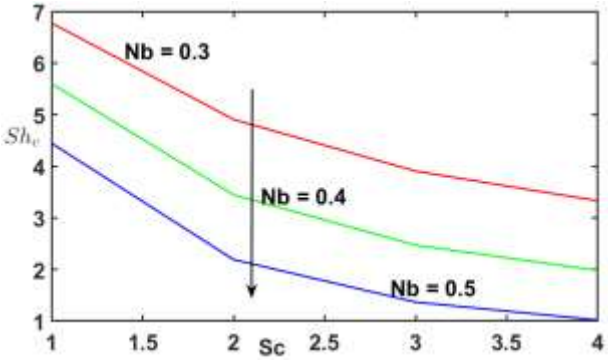

Fig.7: Variability of heat transfer rate with $Q*$ and Sc.

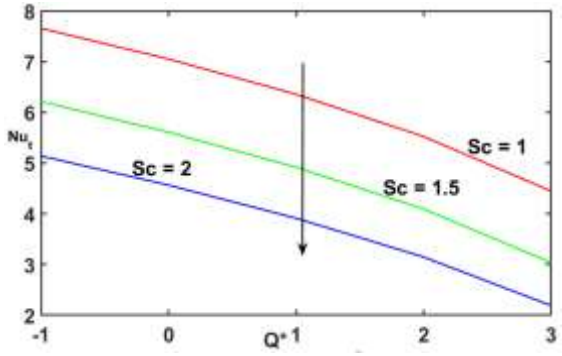

Fig.8:Variability of mass transfer rate with Nb and Sc.

5. Conclusion

Forchheimer effects on an electrically conducted, 3D Casson nanofluid under Blasisus conditions are studied in this paper. The shooting method(Newton-Raphson) along with RK45 is incorporated. The following observations are important to consider.

• Velocity is depicts the identical behaviour with M, Fr, and B that is velocity increasing with increment in these parameters but Da has adverse impact.

• Heat transfer rate of Casson nanofluid for Blasisus type flows can be enhanced by controlling heat source and installing a heat sink device.

• Mass transfer rate of Casson nanofluid for Blasisus type flows can be enhanced by controlling the Schmidt number and Brownian parameter.

• Concentration reduction with Sc and temperature enhancement with $Q*$ is noticed.

References

[1] P.R.H. Blasius, Grenzschichten in Flüssigkeiten mit kleiner Reibung, Druck von BG Teubner, 1907.

[2] Ludwig Prandtl, Motion of fluids with very little viscosity, (1928).

[3] Adhil Ridha, On the three-dimensional alternative to the Blasius boundary-layer solution, Comptes Rendus Mecanique 333(10) (2005) 768-772.

[4] Y.S. Kachanov, A. Michalke, Three-dimensional instability of the Blasius boundary layer, In Laminar-turbulent transition, Springer, Berlin, Heidelberg (1995) 473-480.

[5] K. Tsigklifis, A.D. Lucey, Global stability of three-dimensional disturbances in blasius boundary-layer flow over a compliant panel, In 19th Australian Fluid Mechanics Conference, Melbourne, Australia (2014).

[6] Chandrasekhar, S., & Woltjer L. (1958). On force-free magnetic fields. National Academy of Sciences, 44 (4) 285-289.

[7] Ledvina, S. A., & Cravens, T. E. (1998). A three-dimensional MHD model of plasma flow around Titan. Planetary and Space Science, 46(9-10), 1175-1191.

[8] Hawley, J. F., Balbus, S. A., & Stone, J. M. (2001). A magnetohydrodynamic nonradiative accretion flow in three dimensions. The Astrophysical Journal Letters, 554(1), L49.

[9] Hayat, T., Qasim, M., & Abbas, Z. (2010). Homotopy solution for the unsteady three-dimensional MHD flow and mass transfer in a porous space. Communications in Nonlinear Science and Numerical Simulation, 15(9), 2375-2387.

[10] Chand, K., & Kumar, R. (2012). Hall effect on heat and mass transfer in the flow of oscillating viscoelastic fluid through porous medium with wall slip conditions. Indian Journal of Pure & Applied Physics, 50, 149-155.

[11] Kumar, R., Sood, S., Raju, C. S. K., & Shehzad, S. A. (2019). Hydromagnetic unsteady slip stagnation flow of nanofluid with suspension of mixed bio-convection. Propulsion and Power Research, 8(4), 362-372.

[12] M. Mustafa, J.A. Khan, T. Hayat, A. Alsaedi, Sakiadis flow of Maxwell fluid considering magnetic field and convective boundary conditions, Aip Advances 5(2) (2015) 027106.

[13] T. Hayat, A. Aziz, T. Muhammad, A. Alsaedi, Darcy–Forchheimer three-dimensional flow of Williamson nanofluid over a convectively heated nonlinear stretching surface, Communications in Theoretical Physics 68(3) (2017) 387.

[14] T. Muhammad, A. Alsaedi, T. Hayat, S.A. Shehzad, A revised model for Darcy-Forchheimer three-dimensional flow of nanofluid subject to convective boundary condition, Results in physics 7 (2017) 2791-2797.

[15] T. Hayat, F. Haider, T. Muhammad, A. Alsaedi, Three-dimensional rotating flow of carbon nanotubes with Darcy-Forchheimer porous medium PloS one 12(7) (2017) e0179576.

[16] Vafai, K. (2010). Porous media: Applications in biological systems and biotechnology. CRC Press, Boca Raton.

[17] Vafai, K., & Tien, C. L. (1981). Boundary and inertia effects on flow and heat transfer in porous media. International Journal of Heat and Mass Transfer, 24(2), 195-203.

[18] Vafai, K., & Tien, C. L. (1982). Boundary and inertia effects on convective mass transfer in porous media. International Journal of Heat and Mass Transfer, 25(8), 1183-1190.

[19] Nield, D. A. (1991). The limitations of the Brinkman-Forchheimer equation in modeling flow in a saturated porous medium and at an interface. International Journal of Heat and Fluid Flow, 12(3), 269-272.

An analysis of Julia sets and Noor iterations using a complex Mandelbrot iteration scheme

Deepak Negi
Amrapali Institutes of Technology and sciences, Haldwani, UK (India)
dsingh.negi23@gmail.com

Ashwini Kumar Saini
Govind Ballabh Pant Institute of Engineering & Technology, Pauri Garhwal ,UK (India)
ashu82004@gmail.com

Nitin Pandey
Amrapali Institutes of Technology and sciences, Haldwani, UK (India)
pnnitin@gmail.com

Suresh Chandra Wariyal
Amrapali Institutes of Technology and sciences, Haldwani, UK (India)
swariyal@gmail.com

Ravindra Sharma
Swami Rama Himalayan University, Jolly Grant, Dehradun (India)
Ravindrasharma97@gmail.com

ABSTRACT

In this study, we apply Noor iteration process with complex Mandelbrot set Called composite function, Julia set patterns that are fused to the composite function $f(\square) = \sqrt{\square^3 + \square\square^2 + 1}$ and discuss their dynamical behavior. The classy orbit structure of this function, whose Julia set encloses the entire complex plane, is purported using figurative dynamics. We also present the fixed point scrutiny using proposed iteration function, which using three parameters, and discussed their sequel graphical analysis of complications taking place in the function.

Keywords: Julia Set, Noor iteration, Mandelbrot sets and Feedback process.

1. INTRODUCTION

The fractals are most beautiful and full of real life applications because of their convoluted geometrical structure. Fractals calculation is affectionate of non-Euclidean having algorithms, we sculpt beautiful Julia's pattern which are not generated by any other generation model [6, 8].

Julia set is introduced by grate mathematician Goston Julia in 1918. He studies the iterated polynomials and defines the various set of examples of fractals. And this study is extended by the popular mathematician and researcher Benoit B Mandelbrot in 1975 called Mandelbrot set are most beautiful and classy fractural structure and relate to the different pattern which is not definable at that time such as heartbeat and irregular shape (coastal area).

There are many other procedure to examine fractals, one of them is most popular is the iterated function system which used to find the approximate fixed points of functions under appropriate conditions, the application of fixed point is applied to nonlinear phenomena in different area of science and arts such as computer graphic, biotechnology, physics and engineering etc.

2. PRELIMINARIES

2.1. Mandelbrot set

We select the initial point 0 since it is the single critical point of the quadratic equation $\square_c(z) = z^k + c$, and the Mandelbrot set B is defined as the set of all $c \in \square$ for which the orbit of point 0 is bounded, that is, $\mathrm{B} = \left\{ c \in \square : \left\{ \square_c^{\,k}(0) \right\}; k = 0,1,2,3... \textit{ bounded} \right\}$ an analogous formulation is $\mathrm{B} = \left\{ c \in \square \left\{ \square_c^{\,k}(0) \textit{ does not tends to} \infty \textit{ as } n \to \infty \right\} \right\}$ [13,1].

2.2. Julia set

If $f : \square \to \square$ is a polynomial function with complex values, then the filled Julia set Q is

$$K(Q) = \left\{ z \in \square : \left| Q^k(z) \right|_{k=1}^{\infty} \textit{ does not tend to} \infty, \textit{as } k \to \infty \right\},$$

where complicated space is $\square$ and $Q^k(z)$ is k^{th} iterate of Q the filled Julia set's boundary, ∂KQ ,is referred to as the "Julia set" [13, 1].

2.3. Noor orbit

Let us, take into consideration an iteration sequence $\{x_n\}$ for the starting point $x_0 \in X$, such that the question is.

$$\left\{ \begin{array}{l} x_{k+1} : x_{k+1} = (1-\delta)\, x_k + \delta_k T y_k; \\ y_k = (1-\phi_k)\, x_k + \phi_k T z_k; \\ z_z = (1-\varphi)\, x_k + \varphi_k T x_k; \quad k = 0,1... \end{array} \right\}$$

The sequences away from 0 and converge $\delta_k, \phi_k, \varphi_k \in [0,1]$ and $\{\delta_k\}, \{\phi_k\}, \{\varphi_k\}$. The aforementioned repetitions are known as the Noor orbit, which is characterized by NO , a function of five tuple $(T, x_0, \delta_k, \phi_k, \varphi_k)$. [7]

3. PORPOSED ALGORITHM FOR COMPOSITE MANDELBROT SET

A Mandelbrot set is produced by using the function $f(z) = z^k + c$ where $k \geq 2$, however when creating a composite function, we use the method $f(z) = \sqrt{z^n + cz^2 + 1}$ where $n \geq 3$ see fig1. Here, we are creating a composite function using the iterative Noor technique and the function $f(z) = \sqrt{z^3 + cz^2 + 1}$. The equation displays a basic composite function for $n = 3$ and $\alpha, \beta, \gamma = 1$. Here, we see that when the values of α, β, γ are changed, the wings in the composite Mandelbrot set appear at the beginning, middle, and end points [10, 4, 12]. Likewise, when the values of α and γ are changed, the wings in the composite Mandelbrot set appear at the middle, while the wings in the composite set appear at the starting point when the values of β are changed [5]. And the wings are near the tip of the composite Mandelbrot set when we adjust the α, β, γ values see in fig 2,3,4,5.

Fig1: Composite Mandelbrot set for $\alpha, \beta, \gamma = 1,\ n = 3$

Fig2: Composite Mandelbrot set for $\alpha, \beta, \gamma = .5$, $n = 3$

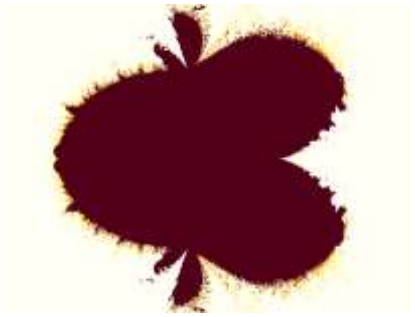

Fig3: Composite Mandelbrot set for $\alpha = .5, \beta, \gamma = 1,\ n = 3$

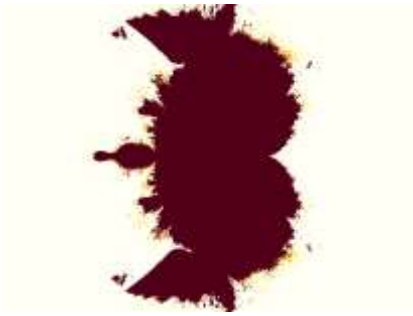

Fig4: Composite Mandelbrot set for $\beta = .5, \alpha, \gamma = 1,\ n = 3$

Fig5: Composite Mandelbrot set for $\alpha, \beta = 1, \gamma = .5,\ n = 3$

3.1 Corresponding Julia sets:

We now have some stunning composite Julia sets with nested and fold symmetry that typically resembles a bush and a dragon curve that alludes to this fractal's most well-known appearance, "The Harter-Heighway Dragon"[9]. These beautiful pictures and realistic-looking natural objects, such bird nests see fig.(8, 9), Peacock wing eye see fig.(6, 7), which we thoroughly examined and discovered to have different points of attachment[11]. When we further examined these, we discovered that they had various points and were giving fixed points, indicating that they were generated by the same formula but were distinct in nature because they followed a dynamical system. Each variable has a unique characteristic that sets it apart from the others, although their origins are the same.

Fig6: Composite Julia set for $\alpha, \beta = 1, \gamma = .5,$ $n = 3\ c = -2.07, 0.62I$

Fig7: Composite Julia set for $\alpha, \beta = 1, \gamma = .5,$ $n = 3\ c = -1.6989, -0.9972I$

Fig8: Composite Julia set for $\alpha, \beta = 1, \gamma = .5,$ $n = 3\ c = -0.84, 1.49I$

Fig9: Composite Julia set for $\alpha, \beta = 1, \gamma = .5,$ $n = 3\ c = -2.69, -2.59I$

3.2 Fixed Points Analysis

A useful framework for examining a variety of nonlinear phenomena appearing in the practical sciences, such as complex graphics, geometry, biology, and physics, is provided by fixed point theory. Fractals and other intricate graphic forms were found to be fixed points in some set maps [2]. Fractals can be thought of as mathematical structures that are similar to themselves and have enough symmetry and resemblance that even very small portions of the overall structure are geometrically similar to it [3]. We selected α, β, γ between zero and one $\alpha = \beta = \gamma \in [0,1]$ for the computational investigation.

Table 1: Orbit of $\lambda(z)$ for $c = -2, 0.4I$ Fixed point for $\alpha = .5, \beta, \gamma = 1$

Total Iteration: n	$\lvert\lambda(z)\rvert$
1	0.4756
2	0.7308
3	0.8177
4	0.7762
.	.
.	.
.	.
54	0.6445
55	0.6445
56	0.6445

Table 2: Orbit of $\lambda(z)$ for $c = -2.1488, 0.0008I$ Fixed point for $\beta = .5, \alpha, \gamma = 1$

Total Iteration: n	$\lvert\lambda(z)\rvert$
1	0.5109
2	0.5470
3	0.5877
4	0.6128
.	.
.	.
.	.
21	0.6262
22	0.6262
23	0.6262

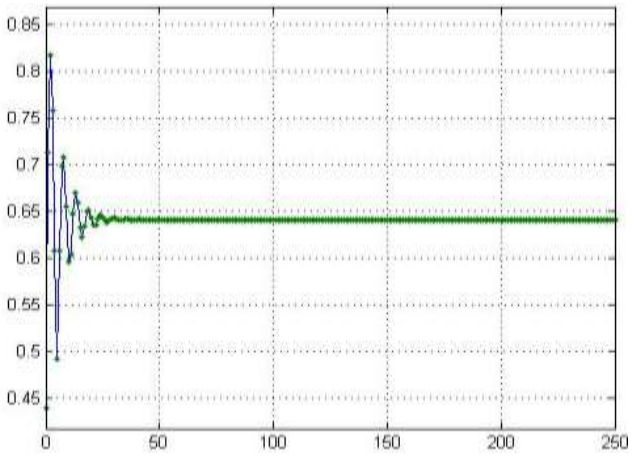

Fig. 10: Observation: In this case, we see that after 54 iterations, the value converges to a fixed point.

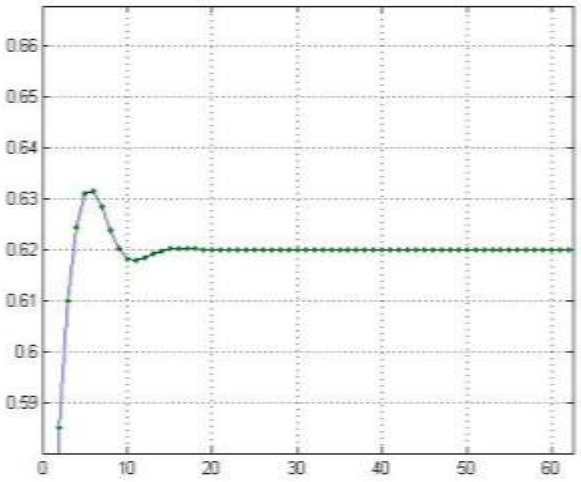

Fig. 11: Observation: Here, we note that after 21 iterations, the value converges to a fixed point.

4. CONCLUSION

The Noor orbit demonstrates that the boundary of the fixed point region is similar to natural features such as bird nests and certain types of peacock wing structures. This is demonstrated by geometrical and numerical analysis of composite Julia sets and composite Mandelbrot sets for the Noor iteration. The escape time computing method hides the intricate structure of these fractals. A variety of orbit traps are developed for the Noor iteration method. The study shows that these sets are completely original and fundamentally different from other known Mandelbrot sets.

5. REFRENCES

[1] D. Negi, A.Negi, and S. Kapoor, "Role of Superior Iterates in Optimizing the Dynamic Noise, "International Journel of Compter Applications, vol. 64, no. 20,2013.

[2] H.F. Walker, and P. Ni, "Anderson acceleration for fixed-pomt iterations," SIAM Journal on Numerical Analysis, vol. 49, no. 4, pp. 1715-1735, 2011.

[3] J. M. Borwein, G. Li, M. K. Tam, " Convergence rate analysis for averaged fixd point iterations in common fixed point problems, "SIAM Journal on Optimization, vol. 27, no. 1, pp. 1-33, 2017.

[4] J. Silverman, " Rational points on, and the arithmetic of, elliptic curves: A tale of two book (and an article)," Bulletin of the American Mathematical Society, vol. 54, no. 4, pp. 591-594, 2017.

[5] K. Kedarisetti, R. Gamini, and V. Thanikaiselvan, "Elliptical Curve Cryptography for Images Using Fractal Based Multiple Key Hill Cipher. " pp. 643-64

[6] M. Akhmet, Domain structured dynamics: unpredicatability, chaos, randomness, fractals, differential equations and neural networks: IOP publishing, 2021.

[7] M. Akhmet, M. O. Fen, and E. M. Alejaily, Dyanamics with chaos and fractals: Springer, 2020

[8] M. Akhmet, M. O. Fen, and E. M. Alejaily, Dyanamics with chaos and fractals: Springer, 2020

[9] M. F. Barnsley, Fractals everywhare: Academic press, 2014.

[10] P. R. Massopust, Fractal functions, fractal surfaces, and wavelets: Academic Press, 2014.

[11] S. D. Balkin, E. L. Golebiewski, and C. A. Reiter, "Chaos and elliptic curves", Computers & graphics, vol. 18, no. 1, pp. 113-117, 1994.

[12] T. Buchanan, Power of Patterns: Fractals: Teacher Created Materials, 2017.

[13] Y.S. Chauhan, R. Rana, and A.negi, "Mandel-Bar Sets of Inverse Complex Function," International Journal of Computer Applications, vol. 975, pp. 8887, 2010.

Designing of Low Power Ring Oscillator with Less Phase Noise for Frequency Synthesizers by using FINFET Techniques

M.Lenin Kumar
Assistant Professor
ECE-Department
Chandigarh University – Punjab

Ajay Vasishth,
Professor,
Physics Department,
Chandigarh University – Punjab

Bikramjit Singh
Assistant Professor,
Chemistry Department,
LRDAVCollege - Punjab

S. Nagaveni
Associate Professor,
Humanities And Sciences Department ,Guru NanakInstitute Of Technology-Hyderabad

Gagan Anand
Basic Science cluster, SOE, University of petroleum and energy studies, Dehradun-248007, India.

Abstract

This research presents a FinFET ring oscillator with adaptive leakage power minimization and reduction in Phase noise margin for Optical energy harvesting. Because these are battery-operated devices, an adaptive body biasing-based leakage power reduction optimizes the optoelectronic biomedical device's leakage power consumption. A five-stage ring oscillator with a frequency of 1 kHz was used to produce the requisite oscillation frequency. The suggested ring oscillator was constructed and Spectre in Cadence Virtuoso Analog Design Environment (ADE) was used to mimic phase noise using 20nm FinFET technology. The suggested ring oscillator's supply voltage is fixed at 50 mV to reduce dynamic and leakage power consumption. The suggested ring oscillator consumes only 41.98 nW of dynamic power, which is 20% less In comparison to the conventional CMOS ring oscillator. The suggested ring oscillator has a leakage power consumption of 4.25 pW. The suggested low-leakage ring oscillator surpasses the competition and is better suited to low-power implantable biomedical devices. The suggested ring oscillator has a phase noise of -156.5 dBc/Hz at 1000 Hz offset frequency and a simulated temperature of 27°C compared to the existing CMOS ring oscillator which is - 114dBc@600KHz.

Keywords- Body Biasing, Optical Energy Harvesting, FINFET, Leakage Power, Ring Oscillator, Phase Noise, Jitter

Introduction

When we convert the optical energy from a laser source using the photo voltaic cell to electrical energy it will be ofthe order of microvolts [1]. To boost up this
energy we gofor an Energy harvesting system. One of the major components of Optical energy harvesting systems is oscillators. This paper is focused on the oscillators which play a major role in Energy harvesting. Oscillators are used in Charge pumps (CP),DC-DC Converters, Phase-Locked-Loop (PLL), etc.

An oscillator can take many forms, such as a ring oscillator or a harmonic oscillator. Harmonic oscillators are very complex and generate stable frequencies with high-quality factors (Q), but they consume a lot of power. Battery-operated implantable biomedical devices cannot be used with them. Ring oscillators, in contrast, are based on very simple circuits and consume very little power, so they are better suited to implantable biomedical systems.

Ring oscillators are used to synchronize the computation processes in any digital system. Ring Oscillators Have a Wide oscillation range, Smaller Size, and Highly integrated multiphase output compared to LC Voltage Controlled Oscillators. Harmonic oscillators provide a stable frequency with a very high-Quality factor but they consume very high power, which isnot suitable for battery-operated devices. Hence Ring oscillators are chosen which consume very less power and are very simple to design. The area occupied by the Ring Oscillator is very less thereby it improves the cost and yield hence well suited for Implantable bio Medical Devices.

In a Ring Oscillators Inverters in an odd number are connected in series with a positive feedback circuit forming a closed loop. This feedback from its last output to the input causes the oscillations There are two different voltage levels 1 or 0 and the output oscillation occurs between these two voltage levels. From this output oscillation, the speed is calculated. The number of inverters defines the stages in the ring oscillator. Say, for instance, if the number of inverters used is three, then it is referred to as a three-stage oscillator. Required output frequency defines stages of inverters in designing the oscillator. If an oscillator is developed with a single inverter, there are no sufficient output oscillations and gain. Random fluctuations in the phase of frequency-domain representation corresponding to time-domain variations from perfect periodicity are known as phase noise in signal processing("jitter"). In general, radio-frequency engineers refer to an oscillator's phase noise.

Varied degrees of periodicity or deviations in periodicity results in Phase noise. Phase noise increases at harmonic frequencies. As the additive noise is so close to the oscillation frequency, it cannot be filtered out. Nonlinear oscillators with well-designed limit cycles will be stable.

In Section II, This article discusses the analysis of phase noise in ring oscillators, and the design of the ring. At the end of the paper, we present the conclusion in section 3.

1. RELATED WORK

[1] Energy harvesting using the hybrid solar/laser light and working of outdoor SC based on storage for self sufficient operation is examined in this work. According to the manufacturer, SC requires the power of 10 W. Millimeter-wave phased-array transceivers are state-of-the-art.

[2] Organic photovoltaic (OPVs) are demonstrated can harvest power for optical wireless data receivers. Furthermore, because their band gap is greater than that of silicon, these OPVs are particularly interesting for indoor applications, as they can better match the spectrum of artificial light. An appropriate combination of a narrow band gap donor polymer and a no fullerene acceptor produces stable OPVs with a power conversion efficiency of 8.8 percent under 1 Sun and 14 percent under indoor illumination conditions.

[3] The photo voltaic effect, which is underutilized in modulators, Optical modulators use semiconductors with light as input and generate electrical energy. This effect is used to show a silicon modulator that uses sub- a/bit electrical energy at sub - GHz rates, which is useful for massively parallel input/output systems such as brain interfaces.

[4] Briefs about the energy harvesting system with a fault-tolerant method and also give the role of oscillators in the energy harvesting system.

[5] For particular power consumption limitations, this paper presents a paradigm for assessing CMOS ring oscillatorphase noise. Both linear and nonlinear operations are taken into account in this model. It implies that for minimal phase noise, quick rail-to-rail switching is required, as well as up-conversion. The current bias/ control circuit's low-frequency noise can have a big impact. This phase noisemodel has been verified using Results of simulation and measurement, In addition, it had a phase noise of 114dBc/Hz coupled-ring oscillator.

2. PURPORTED TIME-DELAY OSCILLATOR

The purported low leakage 5-stage time-delay oscillator has been designed using 20nm FinFET technology. The schematic of the purported time-delay oscillator has been explained. Design of W/L ratio for FinFET inverter. The most important parameter in the Time-delay oscillator is the Threshold voltage (VTH) of the nMOSFET in the inverter. Required VTH can be obtained by properly designing the value of W and L of nMOSFET based on the inverter ratio which is given by equation (7)

$$K\pi = \kappa\pi\,(2)/\kappa\theta * \kappa\sigma \quad \text{----(1)}$$

Where $K\pi$ is the Inverter ratio
$K\theta$ An aspect ratio of nMOSFET
$K\sigma$ is the Aspect ratio of pMOSFET

This 5-stage oscillator uses five inverters to produce therequired oscillation of 1KHz frequency. Adaptive Body Bias can compensate and achieve more uniform transistor performance despite the variations. In the purported low leakage FinFET time-delay oscillator, The maximum leakage Where Kr is the Inverter ratio Kn is the aspect ratio of nMOSFET Kp is the aspect ratio of pMOSFET. Current in the cutoff is given by the nMOSFET hence it is the main leakage power contributor limit leakage power, the inverter's nMOSFET bulk terminal is coupled to a negative bias voltage source via a pMOSFET.

When the nMOSFET is in the cut-off state, a negative bias voltage is provided to raise the threshold voltage. Because the thresholdvoltage and leakage power consumption are inversely proportional, the leakage power consumption

during the NMOSFET cutoff state can be considerably reduced.

Where μn is the electron mobility
Cox is the oxide layer capacitance
W is the FinFET device-width
L is the FinFET device Length

Similarly Eqn 2 $K_p * Tp\, C_{ox}$ ----------(2)

Where μn is the electron mobility and Cox is the oxide layer capacitance.

Substituting Equation (2) and (3) in equation (1) we get the frequency of operation of the time-delay oscillator can be calculated.

The value of L is 20nm from the FinFET library. Hence Wp will be equal to twice that of Wn. The Value of W for nMOSFET is chosen as 50nm hence the value of W for pMOSFET is 100nm. By considering the designed parameter values given in Table 1 the required Threshold voltage and the propagation delay are obtained.

TABLE I DESIGN PARAMETERS OF FinFET INVERTER USED IN PURPORTED TIME-DELAY OSCILLATOR

Wp(nm)	100
We(nm)	50
L(nm)	20

The W/L ratio affects the Time-delay oscillator's Phase Noise Margin. The Phase noise Margin in the Purported Time-delay oscillator is improved by using adaptive body biassing and designed W/L values. The output of the purported low leakage 20nm FinFET time-delay oscillator has been displayed in Figure. 3. The time-delay oscillator produces the square wave with a 50% duty cycle at its output terminal. The input terminal is given with the same output. Hence the time-delay oscillator produces a square wave continuously. The operating frequency is determined by the propagation delay (Td) and the number of stages (N) of the time-delay oscillator.

When the supplied supply voltage is 500mV and the simulated temperature is 27 C, the purported time- delay oscillator has a frequency of 1KHz. To reduce dynamic and leaky power consumption, the minimal supply voltage was chosen to operate the suggested ring oscillator in a low swing.

SIMULATION RESULTS AND DISCUSSION

The design and simulation of the purported work are using 20nm FinFET technology with Cadence Virtuoso Analog Design Environment (ADE) EDA tools. The high-speed spice simulator ‘Spectre’ is used to plot the output waveforms. The simulation parameters which are used to characterize the purported ring oscillator have been listed in Table II. The time-delay oscillator circuit has been simulated with 500mV supply voltage when the simulation temperature is 27oC. Transient simulation has been performed to plot the output waveform.

TABLE III INFLUENCE OF FREQUENCY ON PHASE NOISE

Frequency (Hz)	Phase Noise in dBc/Hz
1	-135
5	-138
10	-144
50	-149
100	-152
500	-153
1000	-156.5

TABLE IV INFLUENCE OF TEMPERATURE ON OSCILLATOR FREQUENCY

Temperature (°C)	Frequency (kHz)
-25	0.948
0	0.964
25	0.983
27	1
50	1.025
75	1.046
100	1.067
125	1.094

Random fluctuations in a waveform's phase, corresponding to time-domain deviations from perfect periodicity, are represented in the frequency domain as phase noise ("jitter"). The Phase Noise of the Time- delay oscillator is -156.5 dBc/Hz at 1000 Hz offset frequency, and the simulation temperature is 27°C. Phase noise is a type of specification in the frequency domain that implies short-term frequency stability. -dBc/Hz is the phase noise unit. Thus, at offset frequency, the offset is -156.5dBc/Hz @ 1000 Hz. When the frequency offset is 1000 Hz, the phase noise is -156.5dBc/Hz. A higher absolute value of phase noise is preferable. Frequency is varied from 1Hz to 1000Hz and the value of Phase noise have been listed in Table III.

The influence of temperature on the frequency of the purported time-delay oscillator has been analyzed by varying the simulation temperature from -25 oC to 125 oC with the step value of 25 oC. The measured values have been listed in Table IV. When the temperature is -25 oC, the oscillator frequency is 0.948 kHz. At room temperature (27oC), the value of oscillator frequency is1 kHz. When the temperature reaches 125 oC, the oscillator frequency is 1.094 kHz. The temperature sweep analysis shows that the oscillator frequency is directly proportional to the temperature.

The Influence of frequency on the Phase noise of the purported time-delay oscillator has been plotted by varying the frequency from 1Hz to 1000Hz. As the simulation frequency increases, the phase noise of the time-delay oscillator decreases.

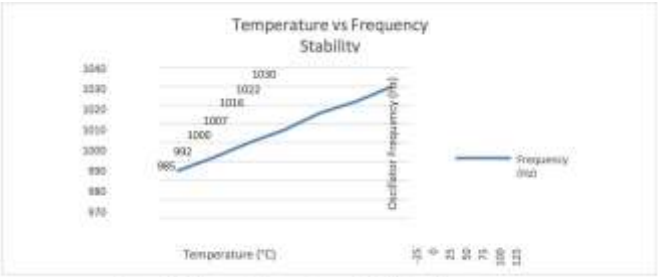

Figure 5. Influence of Temperature on Oscillator Frequency

TABLE V SIMULATION PARAMETERS

Item	Description
EDA Tool	Cadence Virtuoso ADE
Simulator	Specter
Technology	20nm FinFET
Supply Voltage	500mV
Simulation Temperature	27 °C

The influence of temperature on the Oscillation frequency of the purported time-delay oscillator has been plotted by varying the simulation temperature from -25 C to 125 C. As the simulation temperature increases, the oscillation Frequency of the time-delay oscillator increases exponentially as shown in Figure. 5. It gives an astable Frequency of 1KHz at a temperature of 27 C.

The performance metrics of both existing and purported 5-stage time-delay oscillators with 1 kHz operating frequency are analyzed and compared. They are listed in Table V. The purported time-delay oscillator has been designed in 20nm FinFET technology whereas the existing time-delay oscillator circuit was implemented in 0.5µm CMOS technology. The power supply of the purported time-delay oscillator and the existing time-delay oscillator are 500mV and 2.5V respectively. The power consumption ofthe purported time-delay oscillator and the existing time-delay oscillatorare 41.98nW and 150µW respectively.

TABLE VI PERFORMANCE COMPARISON

Parameters	Purported	Existing [1]
Technology	20nm FinFET	0.5µm CMOS
EDA Tool	Virtuoso ADE	Tanner
No. of Stages	5	3
Power Supply (V)	500 mV	2.5 V
Power Consumption (W)	41.98 NW	150 µW
Oscillator Frequency (Hz)	1000	600K
Simulation Temperature	27 ℃	27 ℃
Phase Noise	-156.5dBc@1000Hz	-114dBc@600KHz
Analysis	Transient	Transient

CONCLUSION

This study proposes and implements an adaptive leakage power minimization based FinFET time-delay oscillator with a stable frequency of 1kHz and improved noise performance which is more suitable for Optical Energy harvesting. Since this oscillator produces a stable oscillation, optical energy is harvested without noise. A leakage power minimization method based on adaptive body biasing has been suggested. A time-delay oscillator of five-stage with a frequency of 1 kHz was used to obtain the oscillation frequency. 20nm FinFET technology is used to design the recommended oscillator. 500mV of input reduces dynamic and leakage power consumption. The purported time-delay oscillator consumes only 41.98 nW of dynamic power in comparison to the existing CMOS time-delay oscillator consumes 50 W of power, whereas. The purported time-delay oscillator has a very low leakage power of 4.25 pW. The phase noise of the planned time-delay oscillator is - 156.5dBc/Hz.

REFERENCES

[1] John Fakidis_, Stefan Videv_, Stepan Kuceray, Holger Claussenz, and Harald Haas, “On the design of Optical Energy Harvesting and storage system for outdoor small cells” IEEE Interantional Conference on communication,Apr 2022Iman Tavakkolnia et all,
“Organic photovoltaics for simultaneous energy harvesting and high-speed MIMO optical wirelesscommunications” Official journal of the CIOMP 2047- 7538
[2] M. de Cea 1, A. H. Atabaki1 & R. J. Ram “Energy harvesting optical modulators with subattojoule per bit electrical energy consumption”
Nature Communcation, Apr 2021
[3] Jeneetha Jebanazer, J, Janaki Rani, M.Anand 2021, ‘ Enhanced Energy Harvesting System for Implantable Bio-Medical Devices with Fault Tolerance’, Journal of Green Engineering, vol. 11, no.1, pp 746-767
[4] Liang Dai and Ramesh Harjaani, “Analysis and Design of Low Phase noise Ring Oscillator,” IEEE conf, ISLPED'00, pp. 289-294,
Jul 2002.
[5] A. B. Islam, “Design of wireless power transfer and data telemetrysystem for biomedical applications,” Ph.D. dissertation, Dept. Elect. Eng. Comput. Sci., Univ. Tennessee, Knoxville, TN, USA, 2011.
[6] C. Lu, V. Raghunathan, and K. Roy, “Efficient design of micro-scale energy harvesting systems,” IEEE J. Emerg.

Sel. Topics Circuits Syst., vol. 1, no. 3, pp. 254–266, Sep. 2011.

[7] Sahakoon Panyai, Apinunt Thanachayanont, “ Design and Realization of a Process and Temperature Compensated CMOS Ring Oscillator ”, 2012. *Internal Startup Circuit for Pacemakers", IEEE Transactions On Very Large Scale Integration (VLSI)*

Biography

M. Lenin Kumar received the bachelor's degree in Electronics and Communication Engineering from Anna University in 2011, the master's degree in Electronics and Communication Engineering from Anna University in 2013, and the philosophy of doctorate degree in Electronics & Communication Engineering from Dr MGR University in 2021, respectively. He is currently working as an Assistant Professor at the Department of Electronics and Communication, Faculty of Engineering, Chandigarh University. His research areas in underwater wireless communication and modems. He has been serving as a reviewer for many highly-respected journals.

IMPLEMENTATION OF 64-BIT PARALLEL SUBTRACTOR USING XILINX IP CORES FOR FAST COMPUTING

B.Khaleelu Rehman[1], G.Vallathan[2], Vetriveeran Rajamani[3], Mohammad Salauddin[4], Mudasar Basha[5]

[1]Associate Professor Dept of ECE, Nalla Malla Reddy Engg College, Hyderabad.afridi.1156@gmail.com

[2]Associate Professor, Dept. of ECE, Geethanjali College of Engineering & Technology, Hyd
[3]Associate Professor Grade-1, School of Electronics Engineering (SENSE), Vellore Institute of Technology, Vellore.[1]
[4]Associate Professor Dept of ECE, JBIET,Hyderabad
[5]Assistant Professor, Dept. of ECE, B.V.R.I.T Narsapur, Hyderabad

Abstract. The main objective of the paper is the part of Arithmetic Logical circuits (ALU) i.e Subtractor circuit.64 bit parallel subtractor circuit by using core generator Xilinx IP core and conventional approach is simulated and synthesized with the most advanced Xilinx FPGAs.The proposed system uses less delay as compared to the existing system.RTL, placement and routing, Hardware device utilization parameters, simulation results and power reports are verified by using VHDL programming language. Xilinx I-sim simulator is used for functional verification and timing verification.. X-power analyzer is used to calculate the power.

Keywords. FPGA, VHDL, Xilinx IP.

1.Introduction*:* A N-bit parallel subtractor, subtract the 2 inputs A (Minuend) and B (Subtrahend) as shown in figure 1.FA_1 is the first full adder. Similarly, FA_2 is the second full adder and FA_n is the nth full adder block.Ci_1 is the initialized carry input of the first full adder .S_1, S_2....., Sn_{-1}, S_n, is the sum of the respective full adders. CO_1, CO_2.....CO_{n-1}, CO_n, is the carry of the respective full adders. A_1 is the LSB of Minuend and $B_1$is the complement of Subtrahend. The two's complement of a number can be done by converting the binary format into its equivalent 1's complement. Here 1's complement is to negate the binary number. Here, by appending '1' to the LSB bit of 1's complement, 2's complement notation can be attained [1]. By using basic gates, the 1's complement of 'B' can be attained through the NOT logic gate & '1' is added throughout the carry to get the two's complement notation of 'B_1'. Further, this is added to 'A_1' to perform the subtraction. The value of C_{i1}='1' This procedure will continue till the final full adder like 'FA_n' and it utilizes the carry bit 'C_n' to include with its input 'A_n' as well as 2's complement of 'B_n' to produce the final output bit with final carry bit 'C_{out}'. From the

figure, it can be seen that the first full adder carry FA1 is the input to the second full adder FA2 carry and the FA2 carry is the input to the third full adder FA3 carry [2].To design a 64-bit parallel subtractor the designer requires 64 full adders which are connected in a cascaded manner. For example, the delay of the first full adder is 10ns [3] then to generate the 64th Full adder it requires 10ns×64=640ns to generate the final output

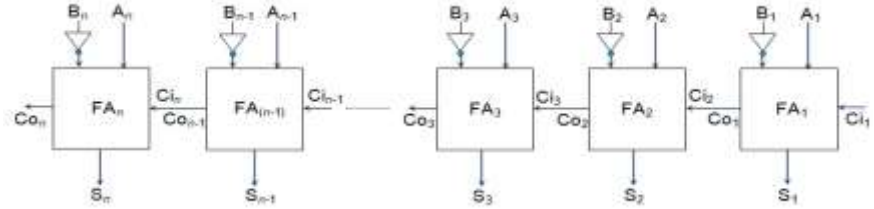

Fig. 1 N-bit parallel subtractor adder block diagram

The I-sim simulated figure as shown in fig 2 depicts One input a [63:0] is the hexadecimal format "0000000000000064" and its base-10 equivalent is 100.similarly the input b[63:0] its hexadecimal is "0000000000000032" and its decimal value is "50".The output diff[63:0] is the hexa equivalent is "0000000000000032" and its base-10 equivalent is 50.The MCPD for the parallel subtractor circuit is 13.146ns through which **1.376ns** for the logic and 11.770ns for the routing the design. Total REAL time to Xst completion requires 44.00secs and total CPU time for finishing time is 44.19secs. Total memory usage of the design 4698524 kilobytes. The table 1.1 shows the hardware device utilized report of the 64-bit parallel subtractor. The number of slices Luts used for the design are 95 out of 17600 available and the bonded Input output blocks are 192 out of 100 available. The synthesis report, RTL view, and simulation waveforms have been targeted with FPGA Zynq XC7Z010 [4] hardware works on 28nm technology and has the ARM processing system [5] and programming logic.

2. Proposed Work: In this digital design era engineers use HDLs for description of any complex logical function. Let us assume that the digital design engineer needs the ALU to design, then one of the components in the ALU design is the subtractor circuit. ALU is used to performs all the arithmetic and logical operations. The operations involved such as subtraction, addition [6] , division and multiplication for signed and unsigned numbers. Logical operations such as logical shifting (left shift, right shift). This paper focuses on the 64 bit parallel subtractor circuit. For designing the parallel subtrator circuit each and every time the engineers have to redesign and code has to be developed at each time they were using .One solution to end up with the above problem is by using Xilinx IP cores[7]. In Xilinx IP cores a piece of code is written for performing a specific task and there by saves the designers time effectively.

2.1 64-BIT PARALLEL SUBTRACTOR: To design a 64-bit parallel subtractor. Below figure 3 shows the Xilinx IP core wizard. The left side shows the FPGA [8] device Zynq XC7Z010 Right side shows the IP(core generator & Architecture wizard). The figure 2.2 shows the Xilinx adder/Subtractor 11.0 IP core.

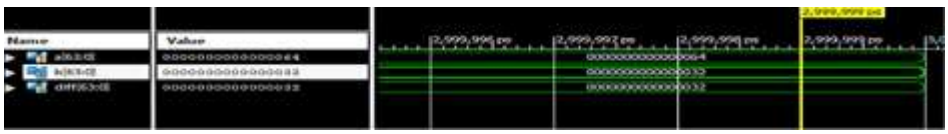

Fig 2 64-bit parallel subtractor simulation

.

Synthesis Report summary		
Logic used	Used	Available
No. of Slice Luts	95	176000
No. of Fully used FF-pairs	0	95
No. of bounded IOBs	100	192

Table 1 64 bit parallel subtractor synthesis report

Adder & Subtractor IP core is used for adding and subtracting the 256-bit unsigned and signed numbers. Apart from adder and subtractor it also performs adder and subtractor in the single design with one control input.

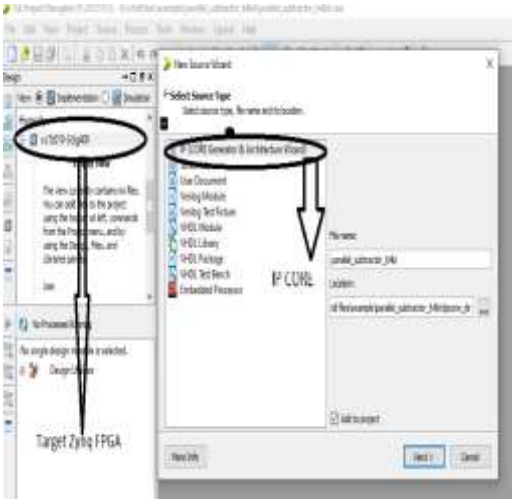

Fig 3 Xilinx ISE IP core

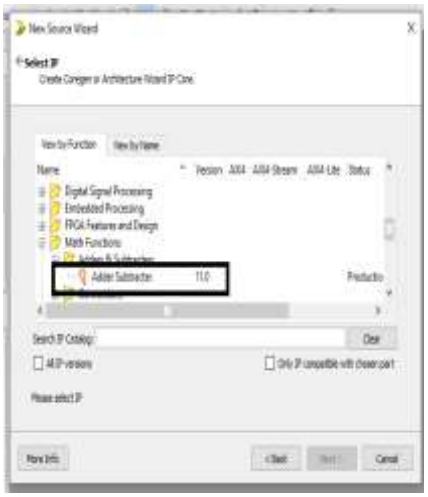

Fig. 4 Xilinx adder/Subtractor IP core.

Figure 2.3 is the 64-bit unsigned parallel subtractor. The figure IP core shown below has two GUI windows. The left GUI part represents the symbolic representation of IP

A[63:0] is one 64-bit input minuend, B[63:0] is another input(Subtrahend), and CLK is

Fig 2.3 64-bit parallel Subtractor

the clock input. The 3 inputs shown are enabled and the remaining ports are disabled the inputs are “ADD” which is used when we select add/subtract module. “C_{in}” is the carry input. And clock enable is representing with “CE”. The outputs are S[63:0], difference output of 64 bits enabled and C_{Out} carry out disabled. The disable pins are optional pins. For any N bit parallel subtractor the carry input should be ‘1’ and the carry output is the output from the previous Full adder

The right side has the component selection. The component selection has 2 options for implementing the design one Fabric and another DSP, through which Fabric uses 64 LUTs and 64 Flip flops.DSP48 is not implemented for 64-bit subtraction. The maximum subtraction is allowed 47 bits with the use of 1 DSP48 processor inside the inbuilt FPGA hardware.

Figure 5 shows the 64-bit parallel subtractor Intellectual property core instantiation the IP core is shown in the highlighted portion in the left side window and below that window, there is the HDL instantiation. The instantiation HDL is with .vho [9] extension an xco file is created and then the instantiation can be done in the VHDL code before “begin” the component declaration and after “begin” the HDL instantiation can be done which is seen in the right side VHDL code. The Register Transfer Level (RTL) diagram of the 64-bit parallel subtractor IP is shown in figure 6. After writing the code and the compilation process completed Xilinx generates a file with extension .ngr for the Register Transfer Level (RTL) schematic. ”clk” is the input signal clock pulse, X(63:0) is one of the input minuends to the subtractor y(63:0) is another input to the adder(subtrahend).z(63:0) is the output difference. Figure 2.3 and 6 are prototype and RTL diagrams respectively.

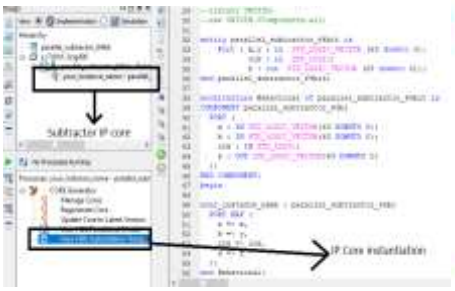

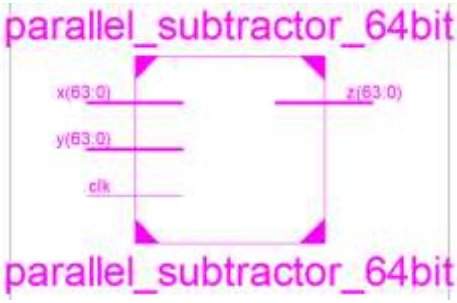

Fig 5 64-bit parallel subtractor IP core. Fig. 6 RTL schematic of 64-bit instantiation parallel subtractor IP core.

Figure 2.6 shows the Xilinx I-SIM simulation [12] timing diagram of the 64-bit parallel subtractor. By default, Xilinx has its own simulator I-Sim but one can install the modelsim[10] also, a product of mentor graphics and X- sim simulator from Xilinx Vivado will also give the same waveforms

One of the input for the above fig 2.6 in the timing window is x[63:0] the Hexadecimal its value “0000000000001086” its decimal value is 4230. Similarly, the input y[63:0] and

its Hexa value is “0000000000000934” its value in the decimal is 2356. The output Z[63:0] is the Hexadecimal “0000000000000752” its decimal value is 1874.CLK is the clock pulse.

The table 2.1 shows the hardware device utilization report of the parallel subtractor Ip-core with respect to the Zynq-7 series FPGA board. The number of slice flip-flops, 4 inputs Slice Luts, I/O blocks, Buffer memories are 166,211,83,193,1 the MCPD for the parallel subtaractor is **1.158** ns through which 0.878ns for the logic to be completed, 0.279ns for the routing. Total REAL time is 37.00secs and total CPU time is 36.43secs. Overall design memory is 4740892 kilobytes. Thus the proposed method gives less delay as compared to the normal subtractor approach.

Logic Utilization	Used	Available	Utilization
Number of Slice Registers	166	35200	1%
Number of Slice LUTs	211	17600	1%
Number of fully used LUT-FF pairs	83	294	28%
Number of bonded IOBs	193	100	193%
Number of BUFG/BUFGCTRLs	1	32	3%

Table 2.1 64 bit parallel subtrator IP core synthesis report

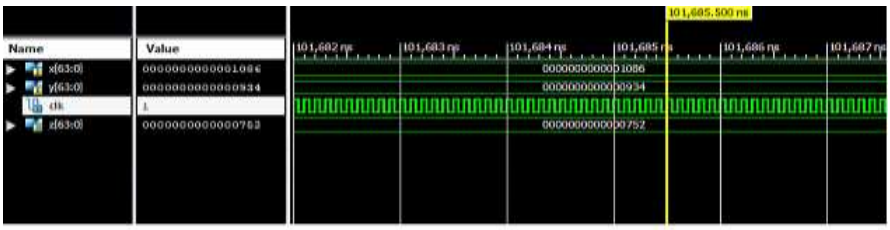

Fig. 2.6 64 bit parallel subtrator simulation using IP Core

3. CONCLUSION:

The HDL implementation of the parallel subtractor circuit using Xilinx Intellectual Property core generation method and conventional approach technique is compared, Its RTL view, synthesis report, power report and timing waveforms has been tested with recent Zynq-7 XC7Z010 series FPGAs which works on 28nm technology.The FPGA parameters like slice Luts,IOBs,LUT-FF pairs, Registers are tabulated and this device has the ARM processing system and programming logic. The proposed design gives less delay as compared to the conventional approach. The IP core approach method gives 1.158 ns of delay. The total power consumption of the design is 0.56 W by using an X power analyzer.

4. REFERENCES

[1] Jaiswal, Manish Kumar, and Ray CC Cheung. "High-performance FPGA implementation of double precision floating point adder/subtractor." International Journal of Hybrid Information Technology 4.4 (2011): 71-80.

[2] Rudnicki, Kamil, and Tomasz P. Stefanski. "IP core of coprocessor for multiple-precision-arithmetic computations." 2018 25th International Conference" Mixed Design of Integrated Circuits and System"(MIXES). IEEE, 2018.

[3] Lee, Boseon, and TaewonSuh. "Towards Characterization of Modern FPGAs: A Case Study with Adders and MIPS CPU." The Journal of Korean Association of Computer Education 16.3 (2013): 99-105

[4] Basha, Mudasar, M. Siva Kumar, Vemulapalli Sai Pranav, and B. KhaleeluRehman. "Approach to Find Shortest Path Using Ant Colony Algorithm." In Intelligent Communication, Control, and Devices, pp. 1243-1252. Springer, Singapore, 2018.

[5] Crockett, Louise H., et al. The Zynq Book: Embedded Processing with the Arm Cortex-A9 on the Xilinx Zynq-7000 All Programmable Soc. Strathclyde Academic Media, 2014.

[6] Kumar, Adesh, Gaurav Verma, Mukul Kumar Gupta, Mohammad Salauddin, B. KhaleeluRehman, and Deepak Kumar. "3D Multilayer Mesh NoC Communication and FPGA Synthesis." Wireless Personal Communications 106, no. 4 (2019): 1855-1873.

[7] Reddy, K. Venkata Siva, P. Vishnu Kumar, K. Maheswari, and B. KhaleeluRehman. "Design and Verification of 16-Bit Vedic Multiplier Using 3: 2 Compressors and 4-Bit Novel Adder." In Proceeding of International Conference on Intelligent Communication, Control, and Devices, pp. 723-732. Springer, Singapore, 2017.

[8] Rehman, B. Khaleelu, Adesh Kumar, and Paawan Sharma. "Modeling and Simulation of ECG Signal for Heartbeat Application." Intelligent Communication, Control, and Devices. Springer, Singapore, 2018. 503-511.

[9] Lysaght, Patrick, et al. "Enhanced architectures, design methodologies, and CAD tools for dynamic reconfiguration of Xilinx FPGAs." 2006 International Conference on Field Programmable Logic and Applications. IEEE, 2006.

[10] Mohammad, Salauddin, R. Seetha, S. Jayamangala, B. KhaleeluRehman, and D. Kumar. "Implementation of FM-Based Communication System with 3-Level Parallel Multiplier Structure for Fast Transmission Using FPGA." In Intelligent Communication, Control, and Devices, pp. 619-626. Springer, Singapore, 2020.

[11] Rehman, B. K., Kumar, A., Mohammad, S., Basha, M., & Reddy, K. V. S. (2020). Detection of DTMF by Using Goertzel Algorithm and Optimized Resource-Sharing Approach. In Intelligent Communication, Control and Devices (pp. 851-856). Springer, Singapore.

Frequency Dependent Surfaces: A Boon in Spatial Filtering

Akshita Gupta, Muskan Bhardwaj, Varun Rana, Ankush Kapoor

Department of Electronics and Communication Engineering, Jawaharlal Nehru Government Engineering College Sundernagar, akshitagupta099@gmail.com, muskanbhardwaj903@gmail.com, ranavarun2002@gmail.com , ankush8818@yahoo.com

Abstract.

In present period, wide variety of technologies are enforced in order to enhance the data rate for better quality of services. In this paper, an elaborated study has been done that substantially focuses on the need and the comparative analysis between different designs of spatial filters. At present, frequency dependent surfaces are used in variety of fields such as satellite communication, radome operation, wireless communication and numerous others.

Keywords. Frequency Dependent Surface (FDS), Resonance frequency, Spatial filter, Polarization, Radome.

1. INTRODUCTION

Frequency dependent surfaces (FDSs) are a type of periodic structures which can act as both band pass as well as band stop filter. These periodic structures are identical and repetitive in their geometry. FDS are planer structures in one or two dimensions. In case of electromagnetics, FDS are called as spatial filters which transmit the desired signals and obstruct the undesired signals. In FDS, transmission and reflection happen when the frequency of incident wave tunes with the frequency of the element which is used for its construction. FDS can be subdivided into two categories on the basis of their geometries that is inductive FDS and capacitive FDS. Inductive FDS often act as a high pass filter and capacitive FDS acts as low pass filter. Coming towards the applications, FDS finds its application in enormous fields in present times such as military, commerce, RCS (Radar Cross Section Control), satellite applications and many more. In order to increase the data speed and to enhance the quality of services, advance antennas are used but they prove to be less sufficient in order to meet the demands. Use of FDS has improved all the antenna parameters by reducing the interference. FDS provides huge dual band separations in order to reduce the risk of being detected by a Radar. It is widely used in military applications. [1-6]

Primarily, FDS is a periodic surface comprises of 2D arrays of components on a dielectric substrate that exhibits transmission and reflection at a certain resonant frequency. When the frequency of an incoming plane wave matches the resonance frequency of FDS, transmission or reflection occurs. FDS has spatial filtering properties and can be implemented as a bandpass or band stop filter with least attenuation of 20dB. When FDS and antenna is integrated gain will increase. The frequency response of FDS is a function of

incident angle, frequency and polarization of incident plane wave. These FDS's are also useful in filtering out unwanted EMI signals and for this purpose fan shaped FDS has been mostly used. [7-11]

For some applications, FDS is required to have an ability of changing the frequency with the change in time. For this purpose, active elements are being inserted inside the structure of FDS surfaces making it as active frequency dependant surfaces (AFDS). AFDS consists of a metallic grid engraved on a dielectric substrate. The geometry of the FDS also plays an important role in its frequency response and radiation characteristics [12-13].

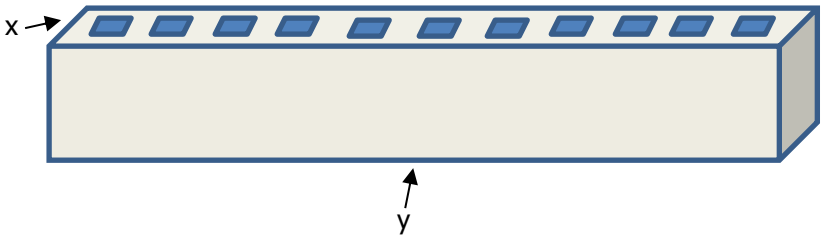

Fig. 1.1 Geometry of FDS

When an EM wave strikes on a unit cell of FDS, then it can be seen as an equivalent lumped circuit comprising of a LC circuit, whose resonance frequency can be calculated on basis of the values of lumped circuit elements [7].

$$f_r = \frac{1}{2\pi\sqrt{LC}} \tag{1.1}$$

$$f_r = \frac{fo}{\frac{\sqrt{\epsilon r+1}}{2}} \tag{1.2}$$

The absorption factor (A) can be given as –

$$A = 1-|\Gamma|^2-|T|^2 \tag{1.3}$$

where, Γ is reflection coefficient and T is transmission coefficient.

2. INSIGHT TO FABRICATION TECHNIQUES

FDS is divided into 3 categories;

Based on array element, there are three types –
i) Basic element- which includes centrally connected looped shapes, patch shapes, combination of all FDS,
ii) Convoluted- used where miniaturized FDS are demanded and flexibility is the main challenge and
iii) Fractal type- where size reduction and multiband behaviour of element is required.

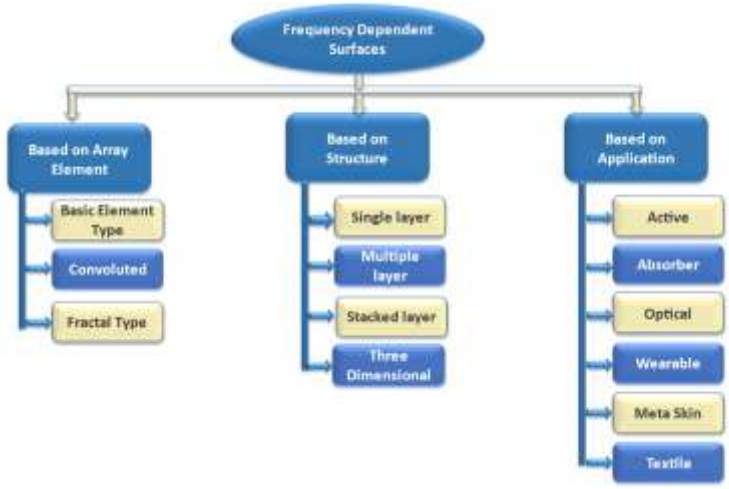

Fig. 2.1 Types of FDS

Based on structure, it can be divided into the following types –

i) Single layer- made up of 2D array of periodic resonant element,
ii) Multilayer- is used when a broadband response is required in a particular frequency range,
iii) AFA - are taken in use to achieve high frequency selectivity and
iv) 3D - grants wide choice of designing methods, sharp cut - off and high flexibility.

On the basis of application, it can be characterized into six different types –

i) Active- are able to control EM performance by tuning the exterior excitation and addition of this element in FDS provides reconfiguration feature,
ii) Absorber- used for absorbing reflected signals in stopband by introducing absorbing array elements,
iii) Optical - used for the applications where a sharp response of frequency is needed with its peak centring the same resonant frequency always,
iv) Wearable- includes temperature sensor which works on modulation of back scatter field and this element can be attained to body,
v) Meta Skin - provides stretchability to the FDS with frequency selectivity and
vi) Textile - used in conferences, screening on clothes and are easy to control.

3. COMPARATIVE ANALYSIS

Ref. No.	Overall Dimensions (mm)	Central frequency (GHz)	ϵr (Relative permittivity)	Substrate material	Bandwidth (GHz)	Remarks
[11]	13 x 13 x 1.6	4.51	4.4	FR4	3.2-5.8	Designed a polarization independent FDS for S and X bands.

[14]	6.5 x 6	9.5	4.4	FR4	5	Designed for frequency range 7.5-11.5 GHz.
[15]	40 x 30	6.6	4.4	FR4	6-8	The proposed model is used for ultra-wideband frequency.
[16]	16 x 16 x 1.57	10.15	2.2	Rogers/RT Duroid 5880	9.5-10.8	High sensitivity, sharp roll-off. Used for designing multi-layer radomes working for X-band frequency.
[17]	7 x 1.41 x 0.5	11	3	Arlon AD300	10-12	Designed FDS for shielding of X-band satellite communication.
[18]	6.2 x 6.2 x 1.6	3.7	4.4	FR4	2.4-5	Proposed design is used for WLAN application.

4. CONCLUSION

This paper dealt with the introduction to different parameters of various frequency dependent surfaces with a classification of them on the basis of various parameters. It showed how the performance of the antennas can be modified and enhanced by using frequency dependent surfaces instead of using traditional antennas. It is interpreted that the parameters and geometry of the frequency dependent surface can be varied according to the requirement, making them particularly application oriented and cost effective. The frequency dependent surface domain holds its use in the coming time and will provide the mankind with a more effective and easily tunable transmission devices.

5. REFERENCES

[1] A. Kapoor, R. Mishra and P. Kumar, 'Novel wideband frequency selective surface-based space borne filters for Sub-6 GHz 5G devices', 4th Biennial International Conference on Nascent Technologies in Engineering (ICNTE), pp. 1-6, 2021.

[2] A. Kapoor, R. Mishra, P. Kumar, 'Frequency selective surfaces as spatial filters: Fundamentals, analysis and applications', Alexandria Engineering Journal, pp. 4263-4293, 2021.

[3] A. Kapoor, K. R. Jha, G. Singh, 'Design and analysis of frequency selective surface at Ka/K/Ku Band for antenna miniaturization', International Conference on Computational Techniques in Information and Communication Technologies (ICCTICT), pp. 25-33, 2016.

[4] Z. Hang, Q.S. Bo, P.W. Dong, L.B. Qin, W.J. Fu, M. Hua, Z.J. Qiu, B. Peng, W.X. Hua, X. Zhuo, 'Dual band frequency selective surface with large band separation and stable performance', Chinese Physical Society, vol.21, no.5, 2012.

[5] A. Kapoor, R. Mishra, P. Kumar, 'Analysis and design of a passive spatial filter for Sub-6 GHz 5G communication systems', Journal of Computational Electronics, vol. 20, pp. 1900–1915, 2021.

[6] P. Janakiram, S. Ajith, S. Bashyam, G.K. Nikhil, R.A. Teja, 'Design and analysis of frequency selective surfaces for Ism and lower ultra-wideband antenna', Journal of Physics: Conference Series, pp.1-11, 2021.

[7] A. Kapoor, R. Mishra and P. Kumar, 'A compact high gain printed antenna with frequency selective surface for 5G wideband applications', Advanced Electromagnetics, vol. 10, no. 2, pp. 27–38, 2021.

[8] A. Kapoor, R. Mishra and P. Kumar, 'Slotted wideband frequency selective reflectors for Sub-6 GHz 5G devices', International Conference on Computing, Communication, and Intelligent Systems (ICCCIS), pp. 786-791, 2021.

[9] X. Hu, C.W. Domier, and N. C. Luhman, Jr., 'Frequency selective surface applications in millimeter wave imaging diagnostics for fusion plasmas', Int. Conf. on Infrared, Millimeter, & Terahertz waves, pp. 1-2, 2015.

[10] A.D. Sabata, L. Matekovits, G. Dassano, A. Buta, A. Silaghi, 'Frequency selective surface for ultra-wide band filtering and shielding', Sensors (Basel), vol.22, no. 5, pp.1-16, 2022.

[11] K. Kaur, A. Kaur, 'Polarization independent frequency selective surface for marine and air traffic radar applications', Sādhanā, vol. 47, no. 81, pp. 1-16, 2022.

[12] S. Azemi, K. Ghorbani, W.S.T. Rowe, '3D frequency selective surfaces', Progress in Electromagnetics Research C, vol. 29, pp. 191-203, 2012.

[13] D. Feng, 'Design of a new active frequency selective surface,' Asia-Pacific Conference on antennas and propagation, pp. 1359-1362, 2014.

[14] P. Das, S. Biswas, S. S. Ridhwaan, R. Ray, D. Ghosh, D. Sarkar, 'Design and analysis of frequency selective surface integrated circular disc antenna', 2nd International Conference on Electronics, Materials Engineering & Nano Technology (IEMENTech) pp. 1-5, 2018.

[15] P. Das, A. Mukherjee, S. Saha, S. K. Ghosh, S. Mitra and S. Das, 'Design and analysis of frequency selective surface integrated microstrip patch antenna', 4th International Conference on Opto-Electronics and Applied Optics (Optronix), pp. 1-4, 2017.

[16] V. K. Kanth, S. Raghavan, 'EM design and analysis of frequency selective surface based on substrate- integrated waveguide technology for air borne radome application', IEEE Transactions on Microwave Theory and techniques, pp.1-13, 2019.

[17] M. Kaharan, E. Aksoy, Y. Yavuz, 'A frequency selective surface design to reduce the interference effect on satellite communication', pp.221-223, 2017.

[18] P. Wei, P.S. Wei, C.N. Chiu, T.L. Wu 'Design and analysis of an ultraminiaturized frequency selective surface with two arbitrary stopbands', IEEE transaction on electromagnetic compatibility, pp. 1-10,2018.

Biographies

Akshita Gupta is a student in electronics and communication engineering from J.N. Government Engineering College Sundernagar Distt. Mandi.

Muskan Bhardwaj is a student in electronics and communication engineering from J.N. Government Engineering College Sundernagar Distt. Mandi.

Varun Rana is a student in electronics and communication engineering from J.N. Government Engineering College Sundernagar Distt. Mandi.

Dr. Ankush Kapoor is working as an Assistant Professor in J.N. Government Engineering College Sundernagar Distt. Mandi H.P. He has more than 20 research articles in national/international journals and conferences being SCI/SCOPUS indexed.

Study of Gravity Tractor efficiency for a NEO

M S Spoorthi, Harshita Saxena, Ramesh Kumar*

[a]*Department of Aerospace Engineering, School of Engineering, University of Petroleum and Energy Studies, Uttarakhand 248007, Dehradun, India*

**Coorosponding Author ramesh_k@hre.iitr.ac.in*

Abstract.

The most talked about topic in the 21st century is climate change and global warming, about how it can cause the extinction of the human race. But there is another unpredictable, yet inevitable event, which could cause mass extinction and catastrophic damage to the Earth, which most researchers believe to be long overdue. It is an event of asteroid collision. This scenario is filled with uncertainty and was previously thought to be unavoidable. But, with the current advancements in space technology, scientists have developed a concept of a spacecraft which is capable of steering the asteroid off its course to prevent a collision. This paper analyses the feasibility of such a spacecraft, i.e., the Gravity Tractors by making use of a strawman asteroid.

Keywords. Gravity Tractor, Asteroid, Near Earth Object, Artificial Gravity

1. INTRODUCTION

Since the dawn of humanity, uncertainty regarding the fragility of civilization has loomed over us. Mostly regarded as a sign of something divinely by the previous generations, meteor showers and comets have always been a subject of interest to humans.

This belief changed after the accidental discovery of the first ever asteroid, Ceres, by Giuseppe Piazzi in 1801 (Asteroids | Exploring the Planets).

And since the discovery of asteroids, we have acquired the knowledge of the threat they pose as well, to humanity as well as our planet Earth. To put it in perspective, it is presumed that an asteroid, approximately 10 kms wide, collided with Earth millions of years ago, resulting in the extinction of the entire species of dinosaurs.

With asteroids having the potential to cause catastrophic damage to the planet, it has become a matter of importance to carefully study and observe these objects. There are more than 27,000 near Earth objects and according to NASA's Center for Near Earth Object Studies, over 26,000 of these objects classify as near-Earth asteroids (Asteroids | Exploring the Planets). Harnessing the clean energy is novel approach for the space mission [1]. For the space mission small thruster like hall and ion will be effectively work , hall thruster draw the attention from the researcher recently.[2]

Hence to tackle this life-threatening problem, many nations have collaborated to start ‘Spaceguard', to study, analyse and survey all the NEOs. In addition to this, Spaceguard has also been researching methods to avoid asteroid collisions.

2. THE KEYHOLE CONCEPT

One of the most significant concepts Spaceguard came up with was the Gravity Tractors. In theory, gravity tractors are deflector machines, using gravity to change the trajectory of the incoming asteroid. To understand how gravity tractors work, you would first require to understand the keyhole concept. When an asteroid in space is predicted to collide with the Earth, it is vital that it follows a certain path to do so. But, before reaching our planet, the NEO has to go through a ‘keyhole’ in space, to ensure its collision. To explain further, just like a ‘lock and key’ system, where a key of particular shape and size only can open the lock, the ‘keyhole’ in space is a similar concept, where the asteroid acts as a key and this particular area as the lock. Upon successfully passing through this area, the asteroid has the maximum possibility to barge into the Earth’s surface. Therefore, a target

plane is usually chosen to define the keyhole, hereby referred to as the b-plane. This plane is perpendicular to the path followed by the asteroid during a close planetary or lunar approach.[3]

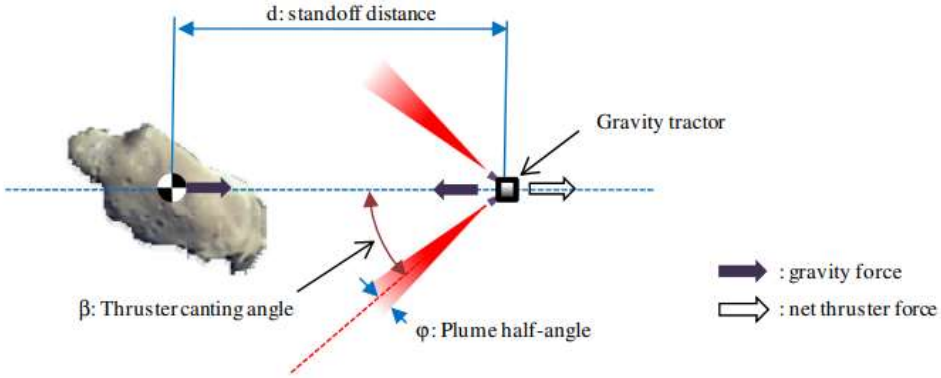

Fig 1: Conceptual figure of a Gravity Tractor [4]

3. WORKING OF GRAVITY TRACTORS

3.1. Theoretical Deflection Formula

When it comes to asteroid collisions, there are two primary planes at play. The A plane is the plane of the asteroid, located in space, whereas, the B plane is the predicted impact area, located on the Earth, i.e., the projected plane. The distance from the Earth's surface to the undeflected impact point is used to calculate the deflection required to be caused by the gravity tractor.

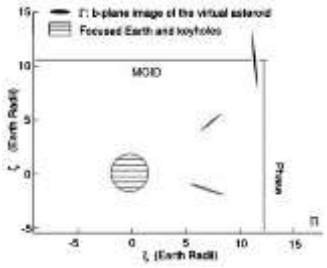

Fig 2: Keyhole and B-plane. MOID - Minimal Orbital Intersection Distance [5]

For example, in Fig.2 no impact on Earth can occur, as the impact location is not on Earth's image. This figure also shows that sometimes the impact plane might not be on Earth, but the close proximity of the asteroid trajectory paves way for future impacts. [5]

A generalised formula of asteroid deflection has been developed by Izzo. [3]

$$\Delta\zeta = -\frac{3a v_{\text{Earth}}(t_s)\sin\theta}{\mu}\int_{t_0}^{t_f}(t_s - t)[\mathbf{v}_{\text{ast}}(t)\cdot\mathbf{A}(t)]\,\mathrm{d}t$$

This formula is used to calculate the deflection on the projected plane of the Earth and here, it denotes the estimated date of collision. From this formula, we get to know that impact intensity is dependent on when the deflection starts, i.e., the earlier the deflection starts, the more is the final deflection.

3.2. Working

In Izzo's concept of a gravity tractor, a spacecraft is sent into orbit, near the potentially harmful asteroid. It is then positioned either in front of or behind the NEO. To keep its relative position, the vehicle, with mass m1, is

required to continuously apply a thrust of T, to maintain its relative position. Absence of thrust would lead to the crashing of the spacecraft into the asteroid.

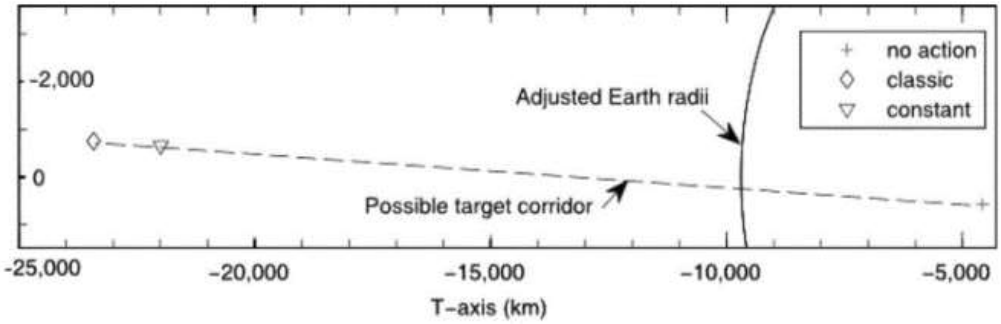

Fig 3: Classic and Constant profiles comparison [6]

The tilt in Fig.3, marked as possible target corner, is necessary, to avoid the crash of spacecraft onto the asteroid. Otherwise, in any other case, it would result in the generation of counteract force due to mutual gravity. This in turn adds thrust to the asteroid, lesser than the magnitude of gravitational potential binding force at that point.

4.3 Dynamics

The gravity tractor advances under the influence of both the asteroid as well as the Sun. The relative motion of the IDM with respect to the selected asteroid in heliocentric reference frame, given by the Newtonian dynamics is, [5]

$$\mathbf{f}_{sc}(\mathbf{x}_{sc}, \mathbf{x}_{ast}, \mathbf{u}; t) = \begin{bmatrix} \Delta\mathbf{v}(t) \\ -\mu_{sun}\left(\frac{\Delta\mathbf{r}(t)+\mathbf{r}_{ast}(t)}{\|\Delta\mathbf{r}(t)+\mathbf{r}_{ast}(t)\|^3} - \frac{\mathbf{r}_{ast}(t)}{\|\mathbf{r}_{ast}(t)\|^3}\right) - \mu_{ast}\frac{\Delta\mathbf{r}(t)}{\|\Delta\mathbf{r}(t)\|^3}\left(1+\frac{m_{sc}(t)}{m_{ast}}\right) + \frac{T}{m_{sc}(t)}\mathbf{u}(t) \\ -\frac{2F_{th}}{g_0 I_{sp}}\|\mathbf{u}(t)\| \end{bmatrix}$$

Where,

$$\Delta\mathbf{r} = \mathbf{r}_{sc}(t) - \mathbf{r}_{ast}(t),$$

$$\Delta\mathbf{v} = \mathbf{v}_{sc}(t) - \mathbf{v}_{ast}(t)$$

$$\mathbf{x}_{sc} = [\Delta\mathbf{r}, \Delta\mathbf{v}, m_{sc}]$$

5. Objective

This paper mainly focuses on analysing the viability of the concept of gravity tractors, mainly dealing with near earth objects' (NEO) impact mitigation.

6. Methodology

Since we are not equipped with the software and data to study and simulate the required objective, we have taken information from research conducted by NASA's JPL.[3]To understand how the asteroid behaves, we have to assume the required data of an asteroid: A strawman NEO with the following characteristics was selected as the target asteroid:

Table 1: Asteroid data [3]

Category	**Description**
Asteroid name	2016 NM4
V∞	5-10 km/s (with respect to Earth in the range)
Effective diameter	140 m
Bulk density	2.0 g/cm3
Axial ratios	1:1:2
Rotation period	12 hr
Rotation pole obliquity	45°
Size and spin	Varied
Discovery time	2016
Impact location	5400 km south of Los Angeles and 1500 km NW of Easter Island in the southern part of the Pacific Ocean
Impact time	2049

Fig 4: Impact location [3]

6.1 Understanding the asteroid's orbit

The hypothetical asteroid we considered comes under the Aten-class asteroids. Its mean motion ratio is close to 13:10, 13 indicates the revolution of the asteroid and 10 indicates the time period (in years) after which its orbit will repeat. The asteroid's closest approach occurs in 2046, where its minimum distance is about one lunar distance.

For the required calculations in this project, the motions of other objects were assumed based on the available data. The bodies include the Sun, the Moon, all the planets and 4 other asteroids, in addition to the effects of solar relativity.

Date	Body	Dist.(AU)
2016 Aug 27.94383	Earth	0.042706
2017 Oct 30.31594	Venus	0.080965
2020 Dec 5.38243	Venus	0.062307
2024 Jan 7.88372	Venus	0.046527
2026 Aug 15.82433	Earth	0.055507
2027 Feb 5.14327	Venus	0.042289
2030 Mar 5.01357	Venus	0.040493
2033 Mar 29.28549	Venus	0.052710
2036 Apr 17.59255	Venus	0.073968
2036 Aug 31.82278	Earth	0.033996
2039 May 11.61451	Venus	0.081424
2042 Jun 4.36096	Venus	0.087426
2045 Jun 26.60054	Venus	0.094500
2046 Sep 13.67208	Earth	0.002772
2049 Sep 11.98767	Moon	0.001902
2049 Sep 12.35720	Earth	0.000019

Table 2. Mapping the timeline of close approaches within 0.1 AU of 2016 NM4 from discovery to impact. [3]

7. Results

The probability of post-deflection orbit of the asteroid missing the keyhole is very high, despite the probability being only 10-4.

The close approach in 2046 enables us to increase the effectiveness of the gravity tractor, which increases the 2049 b-plane deflection factor relative to the 2046's b-plane of 100.

The t-Gt in the simulation can achieve an acceleration of 2.5 x 10-12 m/s2, which is 6.5 μm/s per month. The force corresponding to the asteroid's mass is 7.2 mN. It is assumed that the asteroid was successfully deflected before the secondary impact in 20149.

8. Conclusion

The concept of a gravity tractor spacecraft would not only prevent Earth-collisions, but also would help in mitigating the uncertainty of safety during any deep-space explorations. This paper studied the efficiency of the spacecraft, along with the asteroid trajectory, yielding positive results. The manufacturing and implementation of this vehicle would signify a great milestone in space-technology.

The problem of space debris is one drawback to this idea. We have deep dived the space-debris clean up system as a way to lessen this. We will launch our space debris clean up system, which will during the first stage reach the debris particles' speed, once we have determined the positions and speeds of the debris particles. The space debris clean up device and the debris are both relatively stationary. Following that, the space debris removal system will approach the debris and smash with it at a sufficient impact velocity for the debris to be cold welded to the system. We can remove a group of space debris particles since most small debris particles cluster around the earth's orbit. The space debris removal system experiences a lot of atmospheric drag after removing space debris from a group. As a solution for this, it uses its propulsion system to adjust its orbit to the International Space Station's height, where the collected debris is being removed. The system is then again put into use [7].

As Mars is the next big destination, due to its closeness to our planet, there are many reasons to explore this Red Planet and search for human existence and getting prepared for future human [8]. Therefore, with the growing need for space explorations, not just for Earth, but, this concept can be used to avoid asteroid collisions on any planet.

9. Bibliography

[1] A. Bohrey, R. Kumar, A. Thakran, and H. Soni, "Vertical Axis Airborne Wind Turbine: Future of Renewable Energy," in *AIAA Propulsion and Energy Forum, 2021*, 2021. doi: 10.2514/6.2021-3369.

[2] S. Badoniya, R. Kumar, A. Dubey, S. Thakur, and R. Thakur, "MUTATION OF PERMANENT MAGNET HALL THRUSTER: CENTRAL CATHODE CONFIGURATION," 2020.

[3] K. Yeomans *et al.*, "NEAR-EARTH OBJECT (NEO) ANALYSIS OF TRANSPONDER TRACKING AND GRAVITY TRACTOR PERFORMANCE Submitted to B612 Foundation Final Report Study carried out and report written by D," 2008.

[4] C. Foster, J. Bellerose, D. Mauro, and B. Jaroux, "Mission concepts and operations for asteroid mitigation involving multiple gravity tractors," *Acta Astronaut*, vol. 90, no. 1, pp. 112–118, 2013, doi: 10.1016/j.actaastro.2012.10.010.

[5] J. T. Olympio, "Optimal control of gravity-tractor spacecraft for asteroid deflection," *Journal of Guidance, Control, and Dynamics*, vol. 33, no. 3, pp. 823–833, 2010, doi: 10.2514/1.46378.

[6] N. Ummen and V. Lappas, "Polyhedron tracking and gravity tractor asteroid deflection," *Acta Astronaut*, vol. 104, no. 1, pp. 106–124, Aug. 2014, doi: 10.1016/j.actaastro.2014.07.024.

[7] H. Dhawan and R. Kumar, "Cold welding based space debris removal system," *INCAS Bulletin*, vol. 13, no. 2, pp. 31–36, 2021, doi: 10.13111/2066-8201.2021.13.2.4.

[8] R. Kumar, H. Dhawan, A. Bohrey, and P. Adhlakha, "Space Habitat solar thermal energy system a novel approch," in *AIAA Propulsion and Energy Forum, 2021*, 2021. doi: 10.2514/6.2021-3714.

Behavioral Modeling of Direct-Conversion Transmitter by Incorporating Augmented concept with MoE

Manoj Bhatt and Sanjay Mathur*
*Department of Electronics and Communication Engineering, College of Technology, Govind Ballabh Pant University of Agriculture and Technology, Pantnagar, India
mb914491@gmail.com, sanjaymathur.ece@gbpuat-tech.ac.in
* Corresponding author.

Abstract

In this research, an Augmented Mixture of Experts (A-MoE), a modified form of a committee machine i.e., (MoE), is used to provide a one-step solution for predicting dynamic non-linear behavior of wideband RF power amplifier (PA) along with other impairments of the direct-conversion transmitter (DCT) such as I/Q imbalance and DC offset. For data acquisition for modeling, we have utilized a class AB-PA-driven transmitter with a wideband three-carriers Long-Term Evolution (LTE) signal. The modeling performance for behavioral modeling of DCT obtained for the A-MoE model show better performance than multilayer perceptron (MLP) neural networks (NNs) and other machine learning methods for actual device data in term of normalized mean squared error (NMSE). Hence, the purposed method provides a noval solution for efficient behavioral modeling of PA or DCT's, reporting the performance level much better than comparative methods.

Keywords. PA nonlinearity, Mixture of Expert, Direct-Conversion Transmitter, transmitter impairments, Long-Term Evolution (LTE) signal.

1. INTRODUCTION

In modern communication systems, for enhancing spectrum efficiency with restricted spectrum resources, researchers have utilized higher-order modulation techniques like quadrature amplitude modulation (QAM), wideband code division multiplexing (WCDM), and orthogonal frequency division (OFDM). Due to wideband envelope varying signals with high peak-to-average power ratio (PAPR), these higher-order modulation techniques are more sensitive to the non-linear behavior of PA and produce more non-linear distortion than other similar average power leveled low PAPR modulation-based communication systems. Hence to compensate for nonlinearity in PA, different linearization techniques have been used in the digital domain of the transmitter section, in which digital predistortion is the most popular and widely used linearization technique [1].

In a wideband communication system, the high PA starts to show the memory effect because of the input signal's larger bandwidth. In such cases, memoryless models [2-4] attain limited linearization performance, and hence memory capable models comprising structures capable of modeling them are used. The Volterra series is taken as a reference model for the accurate modeling of dynamic (memory-based) non-linear systems [5]. A large number of coefficients (Volterra kernels) is one major drawback of the Volterra model and the number of coefficients increases exponentially in the Volterra model with an increase in the nonlinearity degree and memory depth of the series, which in turn surges the computational complexity of the model with slow convergence. A comparative study between various Volterra-based methods, such as Memory polynomial (MP), generalized memory polynomial (GMP), and Dynamic Deviation Reduction (DDR), etc. was done based on the complexity and performance of the models by Ghannouchi et al. [6] and concluded that these polynomial models present higher modeling accuracy of the narrow band signal or less complex PA or moderately non-linear PA. But these methods still have large hardware complexity and numerical instability due to dispersion coefficient and data matrix ill-conditioning.

A DCT chain/system of communication system has several imperfections, i.e., DC offset and I/Q imbalance, etc., and these imperfections are generated by the gain and phase mismatch behavior of the non-ideal local oscillator (LO) carrier leakage and the modulator [7], respectively. In various instances, PA nonlinearity-based distortions also additionally distort the performance of the communication system degrading the output signal. Most of the aforementioned techniques only emphasize PA nonlinearity-based distortions, which essentially generate the need for developing a convenient solution for compensating all the mentioned impairments associated with the DCT chain in parallel.

Recently, due to the capability of universal approximation and excellent adaptive nature, NNs are proficiently used for the behavioral modeling of static and dynamic PAs having time-delay tap [8]. Unlike existing linearization methods, such as Volterra and its variants, NN-based linearization methods [9,10] provide a one-step process solution for estimating and linearizing the DCT without any extra branch. NN models have also been integrated with the augmentation concept [10] etc. to provide enhanced performance.

This article uses the MoE method with an augmented concept for digital-domain behavioral modeling of PA or DCT's imperfections. In this line, the remaining paper is organized as follows. Section 2 gives the details of transmitter distortion parameters values and PA device/signal details utilized for implementing the behavioral modeling of the amplifier. Section 3 demonstrates the modeling methodology of MoE with the aforementioned concept. Section 4 presents the results and discussion related to the A-MoE method and compares its results with different neural networks and machine learning methods like Multilayer perceptron (MLP), Adaboost, K-Neighbors, Linear Regression, Linear Support Vector Regression (SVR), and Decision tree and lastly, a brief conclusion is presented in Section 5.

2. TRANSMITTER DISTORTION PARAMETERS AND PA DEVICE/SIGNAL INFORMATION

The complete equation of the impaired signal at the output of the modulator ($\mathrm{V_{t-impair}(t)}$) of the DCT can be given as (1) [9].

$$\mathrm{V_{t-impair}(t)} = I_n(\mathrm{t})\cos(\omega_c \mathrm{t}) - Q_d(\mathrm{t})\sin(\omega_c \mathrm{t}) + \zeta(\mathrm{t}) \quad (1)$$

where $I_n(\mathrm{t})$ and $Q_d(\mathrm{t})$ are the I/Q components of the baseband input signal respectively, ω_c is the carrier's angular frequency, and $\zeta(\mathrm{t})$ is the overall impairment error demonstrated by the DC offset and I/Q imbalance [9].

Table 1 Different DCT distortion considerations

	Distortion Parameters	**Level of Distortion**
Condition 1	PA nonlinearity	PA nonlinearity: 4 dB compression
Condition 2	PA nonlinearity and I/Q imbalance	PA nonlinearity: Same as condition 1 I/Q imbalance: 1 dB gain compression and 3-degree phase compression
Condition 3	PA nonlinearity and DC offsets	PA nonlinearity: Same as condition 1 DC offsets: 3 and 5 % for I and Q respectively
Condition 4	PA nonlinearity, I/Q imbalance, and DC offsets	PA nonlinearity: Same as condition 1 I/Q imbalance: same as condition 2 DC offsets: same as condition 3

Table1 shows the several conditions of distortion utilized for behavioral modeling of DCT in the present work. The effect of these distortion parameters can be observed as AM/AM and AM/PM characteristics of the DCT in the form of distortion [11]. Since DPD linearization techniques are based on the capability of performing behavioral modeling using the considered model, and if the considered model is inept in precisely recording the effect of these modifications, the system performance might severely degrade [7].

The present work utilizes class AB-PA for developing behavioral modeling of a DCT system. The whole chain of the transmitter considered a device under test (DUT), is operated through a three-carriers wideband LTE input signal. This input signal carries two carriers in the ON state with the middle carrier in the OFF state (LTE101) at two bandwidths, 11 MHz (10.68 dB PAPR) and 16 MHz (11.39 dB PAPR). The other system conditions are 2 GHz center frequency with 92.16 MHz sampling frequency.

3. MODELING METHODOLOGIES OF A-MOE

Many methods have been introduced to enhance the performance of the solo DPD method. Out of them, the augmentation concept is one that has been successfully implemented [12] to show better behavioral modeling and mitigating abilities with respect to individual behavioral/DPD methods. The improved performance results inspire us to inculcate an augmentation scheme in the MoE method for enhancing the performance of MoE behavioral modeling. The architecture associated with A-MoE is presented in Figure1 (a). MoE [13] is an example of supervised learning and has a modular structure [14]. MoE has two core parts in its structure i.e., a set of experts network and a single gate network having a single-layer NN, comprising of K neurons where every neuron is allocated a specific expert. Both the experts and gate networks act synchronously to solve a non-linear supervised problem statement through Divide-and-Conquer operating principle [14]. Figure1(b) and (c) are representing the expert's signal flow graph and the gating network's signal flow graph respectively. If, the input vector to the kth expert is given by (**x**), and (w_k) is the synaptic weight vector of this expert network along with the bias term (b), then the output (y_k) generated by expert k is given by equation (2)

$$y_k = w_k^T \boldsymbol{x} + b \tag{2}$$

where the input vector ($\boldsymbol{x}(n)$) form utilized in the proposed work is given as,

$$\boldsymbol{x}(n) = \begin{bmatrix} I_{in}(n), I_{in}(n-1), I_{in}(n-2), I_{in}(n-3), \ldots, I_{in}(n-M) \\ Q_{in}(n), Q_{in}(n-1), Q_{in}(n-2), Q_{in}(n-3), .., Q_{in}(n-M) \\ I_{in}(n)^3, I_{in}(n)^5, \ldots., I_{in}(n)^N \\ Q_{in}(n)^3, Q_{in}(n)^5, \ldots, Q_{in}(n)^N \\ |\boldsymbol{x}_{in}(n)|, |\boldsymbol{x}_{in}(n)|^3, \ldots, |\boldsymbol{x}_{in}(n)|^L \end{bmatrix} \tag{4}$$

where $I_{in}(n)$ and $Q_{in}(n)$ are in and quadrature-phase elements of the current samples, $I_{in}(n-M)$ and $Q_{in}(n-M)$ are in and quadrature-phase elements of the past samples, *M*, *N*, and *L* represent the input signal's memory depth, phase component's odd orders, and input signal's absolute value respectively.

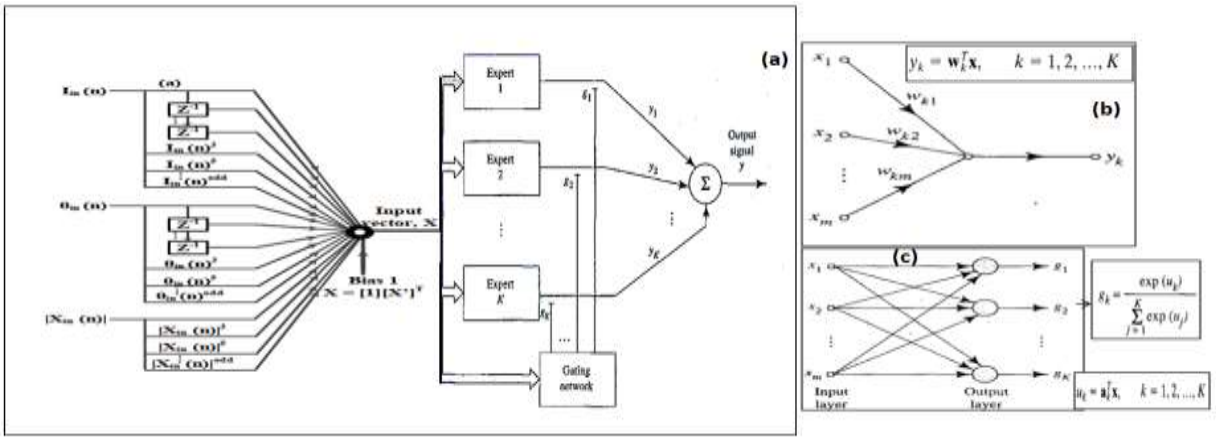

Figure 1. (a) Architecture of A-MoE, (b) Expert network's signal flow graph,
(c) Gating network's signal flow graph

The probability of determining the target vector corresponding to a specific input through the MoE model is calculated through the following equation (5) [13],

$$P\left(y|\boldsymbol{x}, \emptyset_g, \emptyset_e\right) = \sum_{l=1}^{L} g_l\left(\boldsymbol{x}, \emptyset_{\boldsymbol{g}}\right) P\left(y|\boldsymbol{x}, l, \emptyset_e\right) \tag{5}$$

where $g_l\left(\boldsymbol{x}, \emptyset_{\boldsymbol{g}}\right)$ represents gating function providing selection probability for l^{th} expert, $P\left(y|\boldsymbol{x}, l, \emptyset_e\right)$ is the occurrence probability of output *y* for a given input $\boldsymbol{x}$ using l^{th} expert, $\emptyset_g$ and $\emptyset_e$ are gate and expert's set of

parameters. The modified gating form for the modeling has been adapted from Xu *et al*. [15]. Further, detailed information on the MoE method has been given in [11, 13].

Here, we are using two A-MoE networks for behavioral modeling of the DCT, where one network has been utilized for the input signal's in-phase components while the other is for the input signal's quadrature-phase component. The final output signal is obtained by combining these two outputs from individual A-MoE networks, i.e., in-phase and quadrature-phase components of the output signal, and the final form of the output signal is given by the following equation (8)

$$y_{out} = I_{out} + j * Q_{out} \tag{8}$$

4. SIMULATION RESULTS AND DISCUSSION RELATED TO DYNAMIC BEHAVIORAL (CLASS AB-PA) MODELING CAPABILITY OF A-MOE FOR VARIOUS SIGNALS

For modeling purpose, 13 number of experts have been optimized in the A-MoE model by analyzing NMSE performance, the most vital system performance element. The values of *M*, *N*, and *L* are 2, 5, and 3 respectively. The number of samples which are used for the training and validation purpose is 38 K and 35 K, respectively. NMSE is determined as,

$$\boldsymbol{NMSE = 10\,log_{10}\left(\frac{\sum_{i=1}^{Z}(I-I_{desired})^2+(Q-Q_{desired})^2}{\sum_{i=1}^{N}(I_{desired})^2+(Q_{desired})^2}\right)} \tag{9}$$

where *Z* is the sample length.

The performance related to behavioral modeling of the A-MoE model in terms of NMSE has been mentioned in Table2 for three carriers' LTE signals. The values of NMSE in Table2 reflect that the A-MoE model is efficiently capable of performing behavioral modeling corresponding to every signal with different impairment conditions of DCT which have already been mentioned in section 2.1.

Table 2. A-MoE behavioral modeling performance for DCT/ PA characteristics in terms of NMSE

A-MoE (LTE (4G) Signal)		**NMSE (dB)**	
		Training	**Validation**
LTE101 (3-5-3)	**Condition 1**	-37.15	-37.01
	Condition 2	-37.57	-38.10
	Condition 3	-36.92	-36.78
	Condition 4	-38.53	-38.04
LTE101 (3-3-10)	**Condition 1**	-38.63	-37.16
	Condition 2	-36.50	-36.01
	Condition 3	-35.92	-35.56
	Condition 4	-36.88	-35.62

Now, we are comparing the behavioral modeling performance of the proposed method with NNs and machine learning-based methods in terms of NMSE for both the LTE101 signals with different bandwidths for various impairment conditions. Table3 shows the NMSE of different methods with the A-MoE method, which shows that the A-MoE method, overshadows all the considered methods.

A-MoE methods performance capability was further analyzed in the time domain through AM/AM and AM/PM characteristics (Figure2); and frequency domain using a power spectral density (PSD) plot (Figure3). From Figure2, it can be observed that the proposed model precisely captures PA/DCT's non-linear characteristics in presence of I/Q imbalance and DC offset for the validation dataset and expresses its efficient capability for modeling.

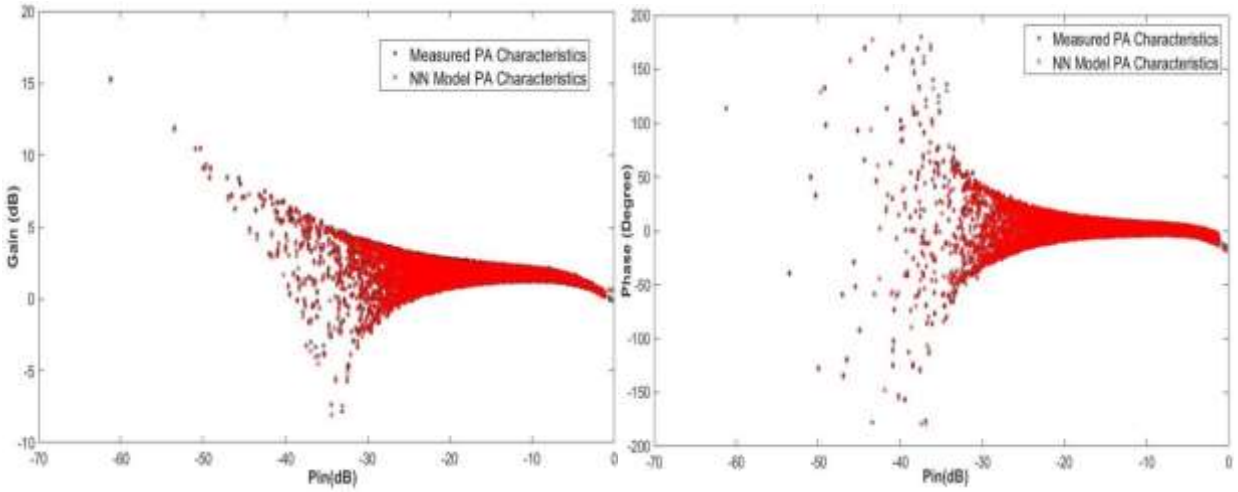

Figure 2. (a) AM/AM, (b) AM/PM characteristics of DCT's non-linear characteristics using proposed A-MoE model corresponding to LTE (101) 3-5-3 signal

Table 3. NMSE Performance comparison of A-MoE with different NNs and Machine learning methods for modeling of PA/DCT characteristics

Methods	**Signal Bandwidth (LTE (4G) Signal) & Distortion Components**							
	LTE101 (3-5-3) (TWO Memory elements in Input Data Vector)				**LTE101 (3-3-10) (TWO Memory elements in Input Data Vector)**			
	Condition 1	**Condition 2**	**Condition 3**	**Condition 4**	**Condition 1**	**Condition 2**	**Condition 3**	**Condition 4**
	NMSE	**NMSE**	**NMSE**	**NMSE**	**NMSE**	**NMSE**	**NMSE**	**NMSE**
A-MoE	**-37.01**	**-38.10**	**-36.78**	**-38.04**	**-37.16**	**-36.01**	**-35.56**	**-35.62**
MLP	-34.78	-35.85	-35.83	-35.80	-35.97	-35.91	-35.68	-34.61
Adaboost	-18.96	-18.38	-18.45	-18.33	-17.30	-17.74	-17.49	-17.58
K Neighbors	-34.22	-35.21	-35.21	-35.22	-35.44	-35.46	-35.48	-34.26
Linear Regression	-23.82	-23.93	-23.8	-23.85	-23.98	-23.99	-23.85	-23..80
Linear SVR	-22.77	-22.88	-22.77	-22.76	-22.97	-23.02	-22.82	-22.72
Decision Tree	-33.8	34.1	-34.20	-34.27	-34.37	-34.39	-34.39	-33.26

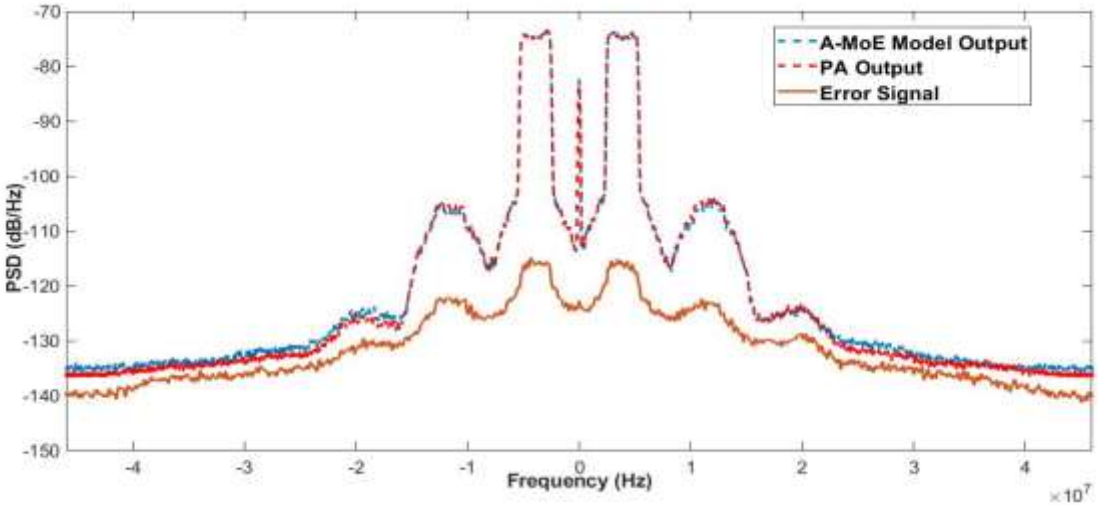

Figure 3. PSD plot with DCT's output corresponding to proposed A-MoE for LTE (101) 3-5-3 (Distortion consideration: Condition 4)

Figure3 depicts the frequency domain performance characteristics of the proposed A-MoE model. Both, the PSD plot of model output and measured output at DCT output accurately follow each other for in-band frequency as well as out-band frequency. This determines that the proposed A-MoE method is very much capable of performing behavioral modeling for entire-band data and the results significantly outperform as compared to the conventional NN methods.

5. CONCLUSION

In this paper, behavioral modeling analysis of DCT is achieved through the A-MoE framework. The modeling results of A-MoE has an excellent limit of resemblances with AM/AM and AM/PM characteristic of PA/DCT's imperfections. The method provides a single-step modeling solution to model any kind of distortion/imperfection as tabulated in the DCT chain without modifying the basic architecture of the system, which is an additional advantage as compared to other methods, where additional RF circuitry is always required to model I/Q imbalance and DC offsets. Based on performance metioned in Table 3, it is clear that the A-MoE method gives higher NMSE performance than other used methods, it is between 1 to 3 dB higher than MLP and K Neighbors, around 4 to 5 dB higher than tree- based ML method i.e., Decision tree and more than 5 dB as compared to other used machine learning methods for all the condition metioned in Table 1. So on the basis of this, we can clearly see the better performance results as compared to various NNs and machine learning methods like MLP, Adaboost, K Neighbors, Linear Regression, Linear SVR, and Decision Tree.

6. REFERENCES

[1] F. M. Ghannouchi, and O Hammi, 'Behavioral modeling and predistortion' 2009;52–64.

[2] Rapp C., Effects of HPA-nonlinearity on 4-DPSK / OFDM-signal for a digital sound broadcasting system', 2018.

[3] M. Ibnkahla, J. Sombrin, F. Castanie, et al., 'Neural networks for modeling nonlinear memoryless communication channels', IEEE Trans Commun. 1997;45:768–771.

[4] JHK. Vuolevi, T. Rahkonen, JPA. Manninen, 'Measurement technique for characterizing memory effects in RF power amplifiers', IEEE Trans Microw Theory Tech. 2001.

[5] S. Boyd, LO. Chua., 'Fading Memory and the Problem of Approximating Nonlinear Operators With Volterra Series', IEEE Trans circuits Syst. 1985;CAS-32:1150–1161.

[6] FM. Ghannouchi, O. Hammi, M. Helaoui, 'Behavioral Modeling and Predistortion of Wideband Wireless Transmitters. Behav. Model. Predistortion Wideband Wirel', Transm. 2015.

[7] JK. Cavers, 'The Effect of Quadrature Modulator and Demodulator Errors on Adaptive Digital Predistorters for Amplifier Linearization', IEEE Trans Veh Technol. 1997;46:456–466.

[8] M. Rawat and F. M. Ghannouchi, 'Distributed spatiotemporal neural network for nonlinear dynamic transmitter modeling and adaptive digital predistortion', *IEEE Trans. Instrum. Meas.*, vol. 61, no. 3, 2012.

[9] M. Rawat and F. M. Ghannouchi, 'A mutual distortion and impairment compensator for wideband direct-conversion transmitters using neural networks', *IEEE Trans. Broadcast.*, vol. 58, no. 2, 2012.

[10] D. Wang, M. Aziz, M. Helaoui, and F. M. Ghannouchi, 'Augmented Real-Valued Time-Delay Neural Network for Compensation of Distortions and Impairments in Wireless Transmitters', *IEEE Trans. Neural Networks Learn. Syst.*, vol. 30, no. 1, pp. 242–254, 2019.

[11] M. Bhatt, M. Rawat, and S. Mathur, 'A Committee Machine Neural Network for Dynamic and its Inverse Modeling of Distortions and Impairments in Wireless Transmitters', IETE JOURNAL OF RESEARCH., 2021.

[12] M. Hui, T. Liu, M. Zhang, Y. Ye, D. Shen, and X. Ying, 'Augmented radial basis function neural network predistorter for linearisation of wideband power amplifiers', Electron. Lett., vol. 50, no. 12, pp. 877–879, 2014.

[13] R. A. Jacobs, M. I. Jordan, S. J. Nowlan, and G. E. Hinton, 'Adaptive Mixtures of Local Experts', *Neural Comput.*, vol. 3, pp. 79–87, 1991.

[14] Haykin S. Neural networks: A comprehensive foundation. Pearson Educ. 1997.

[15] L. Xu, M. I. Jordan, and G. E. Hinton, 'An alternative model for mixtures of experts', Nips, no. 7, 1994.

A Research survey on implementation of Artificial Intelligence in underwater autonomous vehicles by using MIMO-OFDM for Underwater wireless communication

M.Lenin Kumar
Assistant Professor
ECE-Department
Chandigarh University –Punjab

Ajay Vasishth,
Professor,
Physics Department,
Chandigarh University – Punjab

Bikramjit Singh
Assistant Professor,
Chemistry Department,
LRDAVCollege - Punjab

S.Nagaveni
Associate Professor,
Humanities And Sciences Department, Guru NanakInstitute Of Technology-Hyderabad

Gagan Anand
Basic Science cluster, SOE,
University of petroleum and energy studies,
Dehradun-248007, India.

Abstract

The interest in customary checking for marine environment and examination is growing rapidly. Limited bandwidth and slow speed of signals brief the result of uninformed throughput. The objective of this work is to make the modem more responsive and act automatically for disturbances in case of both optical and acoustic signal transmission during plate disturbances, signals from underwater living organisms, detecting submarines, other underwater vehicles, etc., can be tackled. The basic principle of Deterministic Artificial Intelligence (DAI) is asserting the deterministic self- awareness programs based on the self-identification or physics of underlying problems. An optoacoustic communication system that provides high throughput with reduced latency to an underwater vehicle. The optical links make modem operations much easy in cluttered environments without the need for a tether. Controlling the modem is done through automatic devices. Python is used for development with OFDM. The real-time applications are set as the future study.

Keywords-- underwater communication, Artificial Intelligence, low power, bandwidth- light sound, Opto-acoustic modem, optical sensor.

I. INTRODUCTION

We aim at fixing artificial intelligence in the most adopted way as the first principle for the need of autonomous way of desired trajectory. This paper briefs the exploratory effects of framework for controlling the submerged robot which utilizes our proposed opto-acoustic modem interface using the computerized reasoning. The proposed modem accomplishes high speed with low dormancy. The range of applications varies from pipeline perxception, improvement acknowledgement in ocean side to submarines where there is need of tracking the moving articles is needed. First all the systems in correspondence are arranged and natural communication channels is made through and then they are modified for lowered correspondence communication channels suiting the need of artificial intelligence. Hence submerged opto-acoustic is viewed as the most ideal arrangement. A wider area of survey is done for the implementation of AI applications in underwater communication.

Our proposed modem allows a onland user to operate the robot using the human input device for real time study. The system is found to achieve a real time control with OFDM. A link and the acoustic sensor are used for a quick update of the link between the land and underwater connectivity which is being operated from land with the mission parameters and goals. The optical link also enables the receiving high fidelity images and videos that are transmitted from the robot. The comparison of parameters between optical, acoustic, optoacoustic, and AI-based optoacoustic modems. Table 1 shows the above-said comparison of parameters.

II. LITERATURE SURVEY

With the great advancement in mechanization in science, the upgradation in artificial intelligence is a key part in various areas such as public areas communicating space, submerged, and earth-situated language. The ease of computerized reasoning is based on the understanding of the automation of human ideas. The objective of this paper is to provide a better way of approach to making an underwater communication modem for AI-based applications. The uniqueness of man-made thought is the capacity in justifying and deciding the right moves in accomplishing a particular task. The possibility of the human

made consciousness is based on the human idea. This work throws more light on making a new path for the underwater communication modems with AI applications and to develop insights on what really a "responsible AI" means. This work proposes a hybrid solution to overcome the bandwidth limitation in optical and acoustic communication with the help of acoustic-assisted aligned channel between the optical transceivers.

Underwater robots need to tackle numerous challenges. Some of the naturally occurring disturbing are underwater currents, marine life, unexpected vegetation, unmanned vehicles, etc., and restricted possibilities and reduced vision are some of the technical barriers. Hence the robots are need to design to manage all such barriers on its own without any external support. Hence, machine learning based modern technology and AI is now being adopted for designing a robot such that they operate autonomously in tackling the challenges they undergo. Before we decide to choose a robot for an environmentally safe activities for underwater communication, they should be made such that we can rely on them for the sole purpose. The robots should be capable of working on their own on worst situation for accomplishing the missions safely and in a better way by making the right decisions. They should get back to its base stations for charging before it is out of power.

III. OPTO-ACOUSTIC AI MODE

The idea for implementing the opto-acoustic modem with AI is made with the face growing pace of AI in real time applications and its diversity. The proposed modem is based on both the optical and acoustic signal calculator. The new of modem is saving the data about the unknown entry in ocean body, study of underwater creatures, natural disaster, any unusual disturbances at the backend. The proposed hybrid modem for both opticl and acoustic signals adds as advantage for implementing the AI technology into the system. Overcoming the long multipath spreading in underwater communication is well tackled by OFDM, hence it is more preferred for UWA channels. Figure 1 shows some of the real time applications of AI.

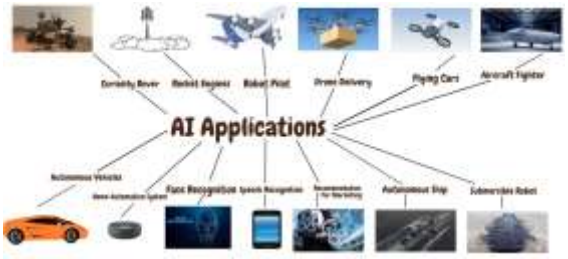

Figure 1 AI Applications

The need for interfacing with high level programming making the analysts free from details an generating models of high level leading to the increase in the productivity and improved reliability and quality analysis. AI with knowledge based systems provide an opportunity to meet the need.

The mathematical model processing for an AI system is shown in figure 2.

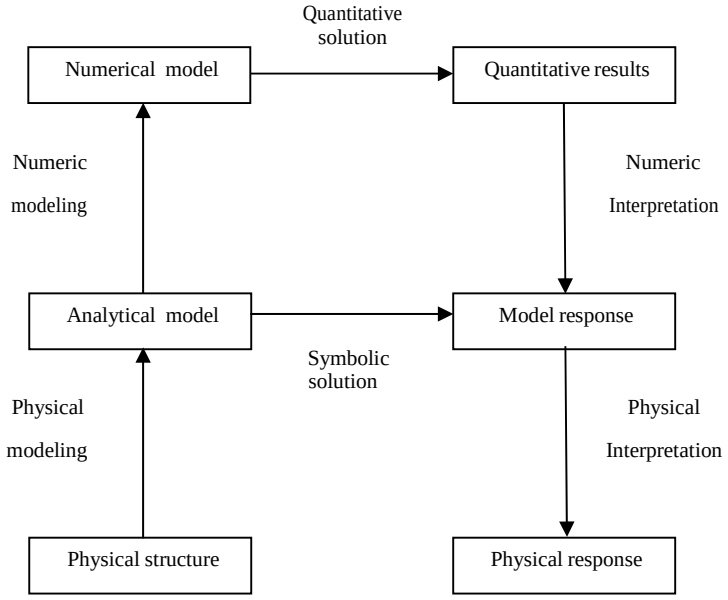

Figure 2 Mathematical model processing of an AI system

The factors influencing the oceanic environment and the need of AI system to monitor an assess the health an alert if there is need.

Factors for a AI system to have a healthy ocean

- Marine litter prediction.
- Real time monitoring of pollution levels.
- Over fishing & protection.
- Automated fish catch threshold.
- Aquaculture monitoring & illegal fishing.
- Real time monitoring of oceanic temp. & PH, phytoplankton, oceanic currents, coral reef ecosystem.
- Monitoring marine habits, coral reef mapping, AUV deep sea assessment, quantities of oceanic species & location.

IV. MIMO OFDM based underwater opto-acoustic AI modem

One of the best approach to overcome the bandwidth limitation in opto-acoustic communication channel is using Multiple Input Multiple Output (MIMO) technology. Multiple transmitting elements simultaneously transmit the independent information streams in the same bandwidth using AI. Thus bandwidth requirement is significantly reduced. The great advantage of MIMO is brought out by studying the shallow water channel using AI. Channels for submerged acoustic communication are very limited and also reverberant. Numerous high recurrence tests are conducted in shallow water. An investigation under different circumstances on drift information collected in shallow water has been carried out in this work to study the delineation of sea conditions (arbitrary sea medium, surface waves) influencing the sign properties. Differences at various stages, fleeting clarity of individual waves, spatial intelligence of multipath waves at different time scales are incorporated in channel properties. limited bandwidth, rapid time variation, fading, refractive properties of communication medium, limited bandwidth and Doppler shifts. Numerous multipath exists in shallow water due to water surface proximity and interfaces at the bottom level resulting in longer delay spread. This is considered to be the most challenge in configuring the underwater acoustic communication.In the opto-acoustic modem architecture of the system controls an underwater robot through an optical link. The system comprises of three high level components. The input for the system is fed from two optical and sound sources. After receiving the input, an encoder control gadget in the movement controlled framework to and electrical sign which can be pursued by the movement controlled framework. The channel for the opto-acoustic system reaches MUX with the use of a multiplexer. The design of the proposed opto-acoustic AI modem for underwater communication is shown below

The concatenated signal is then divided into two separate signals at the MUX as OP and AC signals. All the signals are collected by the MUX and then forwarded into OFDM transmitter. The figure 3 shows the OFDM part permitting the high effectiveness as its regulation plan and transporter power can be controlled independently by every transporter. QPSK is first applied on the information in the QPSK side and then it is exposed to create and the received OFDM signal is examined. The fundamental concept of OFDM is breaking down the high rate information signal into numerous low rate streams. All these broken low rate data streams are simultaneously sent over subcarriers. The received signals are processed in the MIMO OFDM block. The output is then processed as OP and AC.

For instance, consider that two modems are used for Underwater communication say modem1 and modem2. Modem 1 is fitted on land and modem 2 is installed at aquatic area with both light and sound sensors being installed in it. These sensors will generate a data connection web system which transfers the signal back and forth between a mode. With the implementation of AI technology, these data is stored and the installed modem is made to learn to generate the feedback for vibration and signals received. These stored data have various uses as discussed in the earlier part.

- **Proposed OFDM Transmitter**

As signals are transmits the signals, sampling is one which breaks own the continuous signals into discrete time signal. The MIMO block of the transmitter multiplies the capacity and then the signal is forwarded to AI block. Raspberry pi is used for integrating the system which greatly reduces the cost of the entire system. AI block transforms the signal into computerize code and it is resent to FFT for further transmission. Finally the signal is sent to MUX. Figure 3 shows the block diagram of the proposed OFDM transmitter.

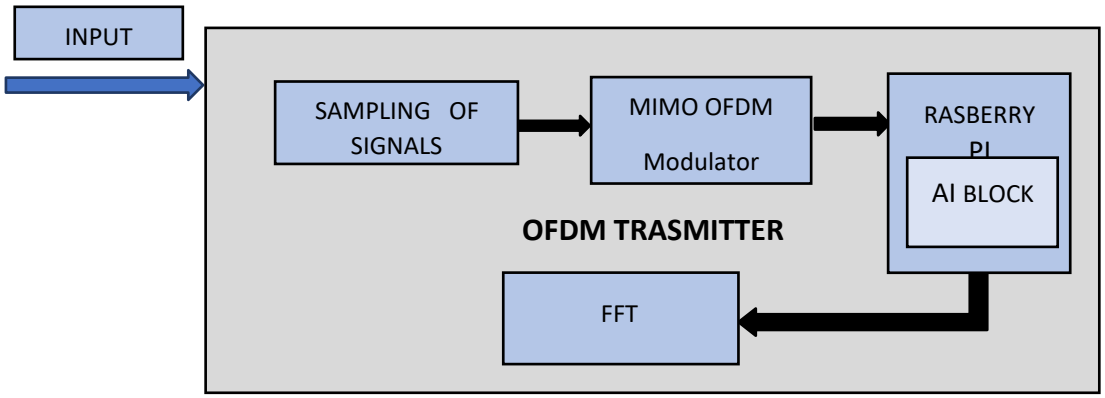

Figure 3 OFDM transmitter

- **Proposed OFDM receiver**

The OFDM receiver receives the signals where the frequency domain signal samples are converted into time domain signals. The samples received by MIMO OFDM demodulator recovers the information from the modulator carrier wave. From here the sampling signals undergo discrete time signalling. Raspberry pi is used to integrate the signals for generating continuous high bandwidth with high data rate signals of OP and AC outputs form the opto-acoustic AI modem. Figure 4 shows the block diagram of proposed OFDM receiver.

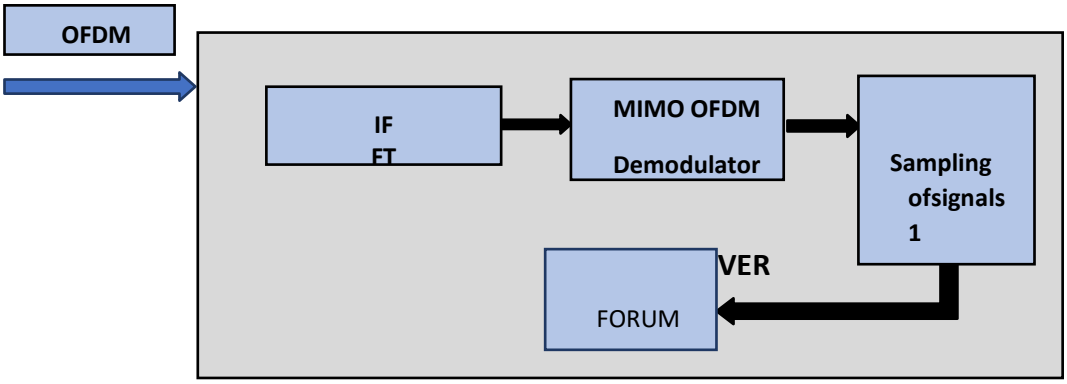

Figure 4 Proposed OFDM transmitter

- **SENSE -PROCESS -ACT- LEARN**

The loop system of Sense-process-act-learn of learning is followed and is shown in figure 5. The signals are first sensed by the underwater robots. Both the optical and sound signals are processed by the robots which act on the target venue to evaluate the data set by recording various acquittal activities and itself self-using Artificial intelligence as how to respond back to the system. Again the entire paradigm is followed. It turns into a channel associated with a criticism regulator. While considered beneath the degree of man-made reasoning, channels and regulators for detecting and acting are a fundamental fixing. Inertial route frameworks are channels giving solid and evaluated assessments to specialist states, both surface and subsea. Moreover, powerful control frameworks regularly balance out directionally unsteady ships and submarines. The inertial route framework (INS)- to direction regulator sense-act circle depicts numerous independent marine robots: ready to execute a mission script however unfit to comprehend to respond shrewdly to the climate. Figure 5 Sense-process-act-learn. Figure 5 shows the process of Sense-process-act-learn.

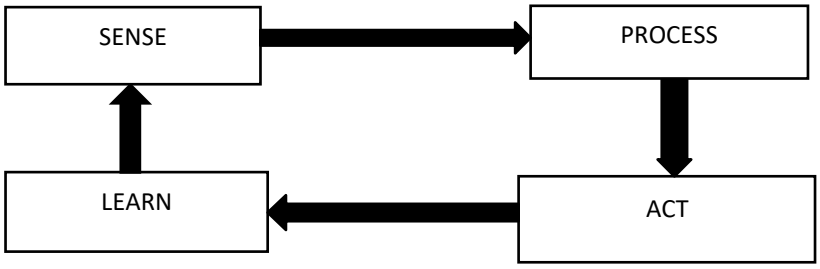

Figure 5 Sense-process-act-learn

V. RESULTS AND DISCUSSION

Comparison of various parameters of optical, acoustic, opto-acoustic modem and AI-based opto-acoustic modem are compared and shown in table 2.

Implementation of raspberry pi using python is used for developing a new generation of Opto-acoustic AI modem having higher bandwidth, greater transmission speed, higher power with great technology is required in developing such a modem with the use of artificial technology. It is carried over with the help of the Underwater system and implementation of the higher categorized simulation part of the opto-acoustic modem in the AI system. Figure 6 shows the sample Database collection of optical signal attenuation under various oceanic conditions through AI implementation. Base on the signal level received under water condition, the system will automatically calculate the level of attenuation that can occur through the database of the signals and its corresponding level of attenuation already attained. So the system automatically generates the messages about the signals based on the previous experience.

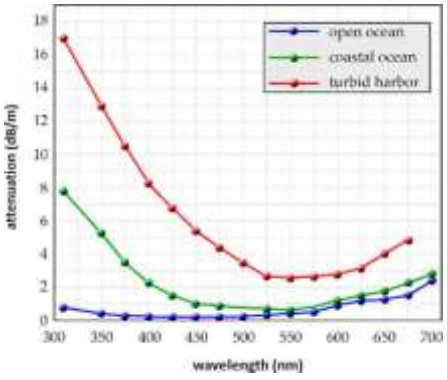

Figure 6 Database of attenuation of optical signals under different oceanic condition

Figure 7 shows a study sample of percentage of level of disturbances observed in the modem implanted oceanic area. All these types of observations are carried out by the AI part of the communication system. Hence under the intruding of any new signals will also be stored in the database and if it is observed in future, the messages will be automatically sent to the nearby or base station for the necessary action. If the received signals are already in the stored database then it will not be stored once again but the response will be automatically performed from the system as the previous response. If the signals are new, it will be stored and will be indicated to the nearby station for action. Thus, AI proves its need in alerting system.

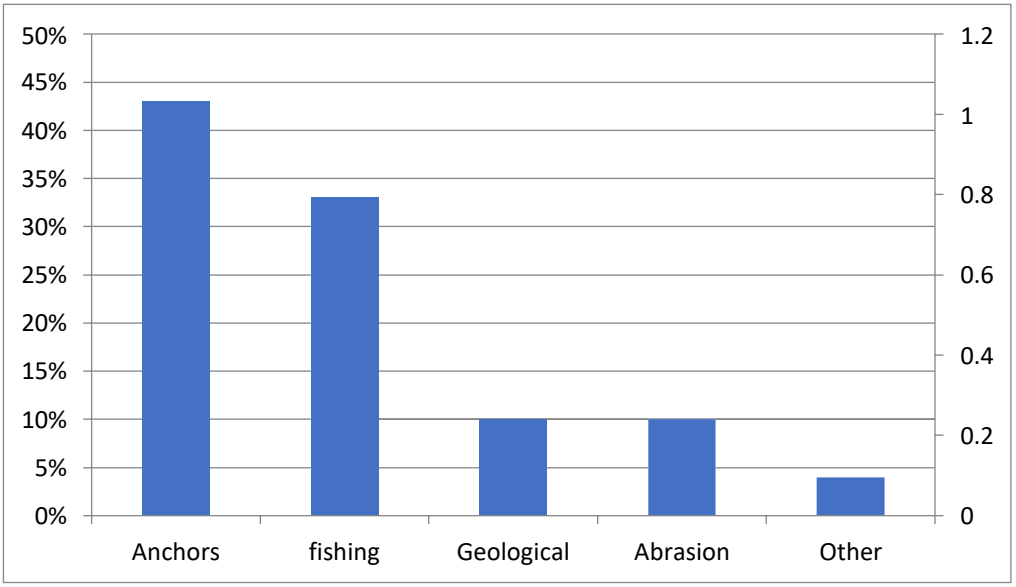

Figure 7 survey based on AI system of observation in underwater prevailing conditions

The observed acoustic signal speed achieved at different oceanic depths by the AI system with reference to the prevailing conditions of temperature and pressure in the implanted oceanic area. Based on the database of acoustic wave speed, the alert will be made by the AI system for the prevailing oceanic conditions like temperature, pressure, turbidity and living organisms which will greatly affect the communication of acoustic signals, alerts will be made for the transmitter in advance.

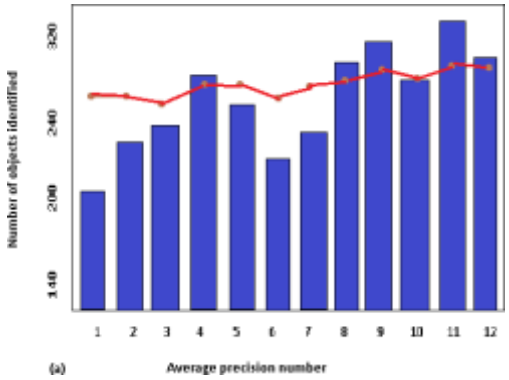

Figure 8 Response of AI system in object identified under different turbidity conditions of water condition

Monitoring the underwater environment impact is an important application of AI which helps it more scalable an automated. The AI system is ingested with an underwater data centre which is nothing but the sample or reference data for the AI system. Based on the level of distraction in the received signal, it is analyzed and response is made by the AI system. Figure 8 shows the detection of received signals with respect to direction and object distraction in the path of signal transmission and reception. The trajectory is framed by the AI system based on the signal communication level through dynamic model simulation. Observations on three sequential scenarios are made with trail planned to make the waypoint in real time scenario. Figure 9 shows the simulation of analysis of AI system over the trajectory of the signal.

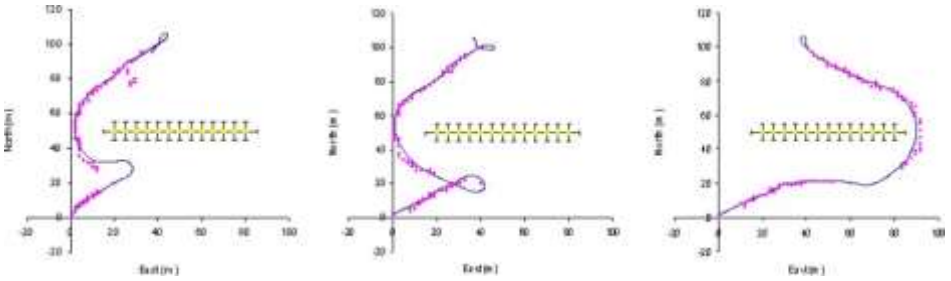

Figure 9 SimulationofavoidingtrajectoryanalyzedbyAIsystem

Autonomous Target Recognition is made to find the unmanned underwater vehicles in the path of communication. This survey is analyzed by the AI system to make a response for a successful communication.

VI. Conclusion and Future Scope

In this paper, an Opto-acoustic AI modem basic architecture for submerged correspondence has been proposed and illustrated. From the reproduction results acquired, with the utilization of the proposed hybrid modem a strong association is attained between the earthbound and submerged world. This will trade signals and store all information involving light and sound sensors as hotspots for energy utilized for recording different submerged exercises. The modem advances by carrying out AI and creating feedback mechanism. The collection of both optical and sound signs through a solitary modem demonstrates the outcome of the proposed Opto-acoustic AI modem. Basically, the proposed modem additionally remains a straightforward answer for more prominent information rate and bandwidth for the impending age of fast submerged optical/acoustic correspondence. The future start of a submerged flagged world with incredible communication can be achieved by some modifications in a couple of more OFDM methods. We can carry out the modem utilizing Machine learning with a high-level Algorithm which will start the future framework headway. In this paper, a comprehensive survey of the issues in implementing artificial intelligence in underwater communication by underwater opto-acoustic modem and the significant challenges posed by them for a successful communication is surveyed. A review on the research and the development of artificial intelligence in underwater communications has been addressed and Response of a AI system in signal distraction due to object identified under different turbidity condition of water condition is shown .Also Simulation of avoiding trajectory analyzed by AI system was briefed .Based on the summary of the research developments, the challenges of AI in underwater communication are types of algorithms and different types of data manipulation for synchronizing ,designing of a predictor model and the basic challenges like noise and attenuation, absorption and scattering, multi path, path loss etc. Here we are enabling MIMO - OFDM (multiple input multiple output) in receiver and transmitter side with best sampling system theorems or mathematical calculations. We also code an AI for making the modem to sense the water quality and salinity etc. This modem also enables to study regarding the light and sound system. And also the placement of transmitter and receiver for a proper flow process in AI is also to be found.

REFERENCES

1. I. F. Akyildiz, D. Pompili and T. Melodia, 2005, “Underwater acoustic sensor networks: research challenges,” Ad Hoc Networks. Vol. 3, no. 3, pp. 257–279
2. G. Baiden, Y. Bissiri and A. Masoti, 2009, “Paving the way for a future underwater omni-directional wireless optical communication systems,” Ocean Engineering. Vol. 36, pp. 633–640
3. C. Gabriel, M. A. Khalighi, S. Bourennane, P. Léon, and V. Rigaud, 2013, “Monte-Carlo-based channel characterization for underwater optical communication systems,” IEEE Journal of Optical Communication Networks, Vol.5, no. 1, pp. 1-12
4. A. Munafò, E. Simetti, A. Turetta, A. Caiti, and G. Casalino, 2011, “Autonomous underwater vehicle teams for adaptive ocean sampling: a data-driven approach,” Ocean Dynamics, Vol. 61, no. 11, pp. 1981-1994
5. W. Cox and J. Muth, 22014, “Simulating channel losses in an underwater optical communication system,” Journal of Optical Society in America, Vol. 31, no.5, pp.920-934
6. P. Lacovara, 2008,“High-bandwidth underwater communications,” Marine Technology Society Journal. Vol. 42, no.1, pp. 93-102
7. S. Arnon, 2010, “Underwater optical wireless communication network”, Optical Engineering, Vol. 49, no. 1
8. J. Heidemann, M. Stojanovic, and M. Zorzi, 2012, “Underwater sensor networks: applications, advances and challenges,” Philoshopical Transactions of the Royal Society, Vol. 358, pp. 158–175
9. S. Tang, Y. Dong, and X. Zhang, 2014, “Impulse response modeling for underwater wireless optical communication links,” IEEE Transactions in Communications, Vol. 62, no. 1, pp. 224-236
10. B. M. Cochenour and L. J. Mullen, 2012, “Free-space optical communications underwater,” in Advanced Optical Wireless Communication System, Cambridge University Press, pp. 201–239
11. F. Hanson and S. Radic, 2008, “High bandwidth underwater optical communication,” Application in Opticals, Vol. 47, no.2, pp.277–283
12. K. Nakamura, I. Mizukoshi and M. Hanawa, 2-15, “Optical wireless transmission of 405 nm, 1.45 Gbit/s optical IM/DD-OFDM signals through a 4.8 m underwater channel,” Optical Expressions, Vol. 23, no.2, pp. 1558-1556

Performance analysis and enhancement of the performance of solar air heater using multiple ribs

Geetanjali Raghav

**University of Petroleum and Energy Studies, India*

Abstract.

The Industrial Revolution led to the establishment of additional industries, which in turn led to a rise in the usage of energy in the form of fossil fuels. Due to problems with the usage of fossil fuels, alternative forms of energy have gained importance and relevance in the modern era. These resources are said to as renewable since they, like the sun and wind, can never run out. They have a less carbon footprint and are additionally known as unconventional sources of energy. Thermal pollution can be considerably decreased. They have the potential to be inexhaustible, limitless sources of energy. The majority of renewable, polluted air energy sources are typically clean. Investigations have focused on the following things: The majority of renewable, pollution-free energy sources are typically clean. Researchers have studied the effects of the factors relative width distance (Gd/Lv), relative gap width (g/e), relative roughness height (e/D) and roughness width ratio (W/w),. The optimal rib hardness parameter values have indeed been reviewed and analyzed. Using experimentally obtained data, correlations for Nu &friction factor as functions of Re have been constructed. A multi-V-shaped rib with gap parameters has been investigated.

Keywords: solar air heater, ribs, heat transfer

1 INTRODUCTION

The thermal efficiency of the solar air heaters is enhanced by the rise in heat transfer area. Use of this type of heater was advised by Lof et al, having an advantage of negligible pressure loss and is quite effective for a slight temperature increase. However, the price of the device increases because to the demand for a huge glass surface. As a result, it is preferable for turbulence to be generated only in the viscous sub-layer region, which is where thermal resistance occurs, which is located close to the absorber. Artificial roughness is surface texture that has been produced artificially. This can be accomplished by identifying ribs in various configurations, such as hill transverse, inclined, V-shaped, multi-V, or W ribs. These researchers looked at how heat transmission and friction factor in applications for cooling gas turbines and heat exchangers were affected by geometric characteristics of roughness element Momin and others (2002 For a fixed relative roughness of 10 and a Reynolds number range of 2500- 18000, the effects of relative roughness height and angle of attack were experimentally explored. The impact of V-shaped rib array on the friction and heat transfer of fully developed flows in a square channel was studied by Lau et al. in 1991. In order to predict the impact of the rib heads chamfer angle inside a rectangular channel with integral chamfered ribs, Karwa et al. (1999) conducted an experimental analysis. Ahu etal (2005) carried out an experimental analysis of a comparable geometry with broken transverse ribs for solar air heaters. Aspect ratio of 8, roughness height of 10–30 mm, height of the ribs of 1.5 mm, and Reynolds number variation of 3000–12,000 were the factors that the experiment examined. Regular imperfection geometries that can be created as voids and ribs were studied by Donne and Meyer [7, 8]. Transverse rib roughness was the focus of earlier studies on rib smoothness by Webb et al.In a different study, Prasad and Saini [10] used circular wires to artificially roughen the heated plate's inner surface. They claimed that there had been a considerable improvement in the heat transfer coefficient. The ideal values for the rib roughness parameter have been determined and discussed. Using experimentally obtained data, correlations for Nu and f as functions of Re have been developed. A multi-V-shaped rib with gap parameters has been investigated.

2. METHODOLOGY

The appropriate values or range of values for all pertinent parameters for the collector system, categorized into fixed and variable parameters. With an objective of the investigating the exergetic performance of the solar air heater for a given set of system and operating parameters.

Table 2.1: System and operating parameters

		Parameter	Value/Range
System parameter	Fixed	Collector length (L), m	2
		Collector width (W), m	1
		Duct depth (H), m	0.025
		Thickness of collector plate (t_p), m	0.002
		Number of glass covers (N)	1
		Thermal conductivity of insulation (k_i), W/m-K	0.037
		Thickness of insulation (δ_i), m	0.05
		Transmittance–Absorptance product ($\eta\alpha$)	0.80
		Emissivity of the absorber plate (ε_p)	0.90
		Emissivity of the glass cover (ε_g)	0.88
		Thickness of glass cover (t_g), m	0.004
		Air gap between absorber plate and glass cover (L_{gw}), m	0.025
		Thickness of collector edge (t_c), m	0.1
		Slope of collector (β), degree	43
	Variable	Relative roughness height (e/Dh)	0.019-0.043
		Relative roughness pitch (p/e)	3-8
		Flow angle of attack (α), degree	30-75
		Relative roughness width(W/w)	1-10
Operating parameter	Fixed	Ambient temperature (T_a), K	300
		Wind velocity (V_w), m/s	1
	Variable	Temperature rise parameter ($\Delta T/I$), K-m²/W	0.002-0.025
		Solar radiation intensity (I), W/m2	600-1000

2.1 Procedure for evaluation of exergetic Components and Exergetic Performance:

The solar air heating is assumed to suck in surrounding atmosphere for the purposes of this study, producing input air that is the same temperature as the surrounding. The projected global temperature of the air passing through the duct (T) and the entrance air temperature are used to compute the output air temperature.

$$T_O = T_i + \Delta T$$

Mean film temperature (T_{fm})

$$T_{fm} = \frac{T_i + T_o}{2}$$

Now from the value of mean film temperature, average and estimated initial mean plate temperature is presumed

$$T_{pm} = T_{fm} + 10$$

The Mullick et al [85] equation;

$$U_t = \left[\left\{\frac{12.75\left((T_{pm}-T_c)\cos\beta\right)^{0.264}}{(T_{pm}+T_c)^{0.46}L_s^{0.21}} + \frac{\sigma(T_{pm}^{2}+T_c^{2})(T_{pm}+T_c)}{\frac{1}{\varepsilon_p}+\frac{1}{\varepsilon_c}-1}\right\}^{-1} + \left\{h_w + \frac{\sigma\varepsilon_c(T_c^{4}-T_s^{4})}{(T_c-T_a)}\right\}^{-1} + \frac{t_g}{k_g}\right]^{-1}$$

Back loss coefficient U_b, is expressed as,

$$U_b = \frac{K_i}{\delta_i}$$

Table 2.2: Estimation of the thermal performance

Parameter	Formula
Thermal efficiency	$\eta_{th} = Q_u/A_pI$
Effective efficiency	$\eta_{eff} = \frac{Q^{\bullet}_u - \frac{P^{\bullet}_m}{C}}{A_pI}$
Absolute or net Exergy flow	$E^{\bullet}_n = IA_p\eta_{th}\eta_c - P^{\bullet}_m(1-\eta_c)$
Carnot Efficiency	$\eta_c = 1 - \frac{T_a}{T_{im}}$
Exergy inflow	$E^{\bullet}_s = A_pI\eta_{ex} = IA_p\left(1-\frac{T_a}{T_{sun}}\right)$
Exergetic efficiency	$\eta_{II} = \frac{E^{\bullet}_n}{E^{\bullet}_s}$
Optical exergy	$E^{\bullet}_{LO} = IA_p\eta_{ex}(1-\tau\alpha)$

3. RESULTS AND DISCUSSION

3.1 Impact of relative roughness height, pitch, and width ratio on exergy loss components:

For different system (flow angle of attack) and operational parameter values, the exergetic components of a solar air heater with multiple purposefully roughened V-ribs have been found. The appropriate roughness parameter values (angle of attack) that will result in the best exergetic performance from a solar air heater have been identified. The following exergy losses components are explored individually:

3.1.1 Optical Exergy Losses ($\dot{E}_{LO}$)

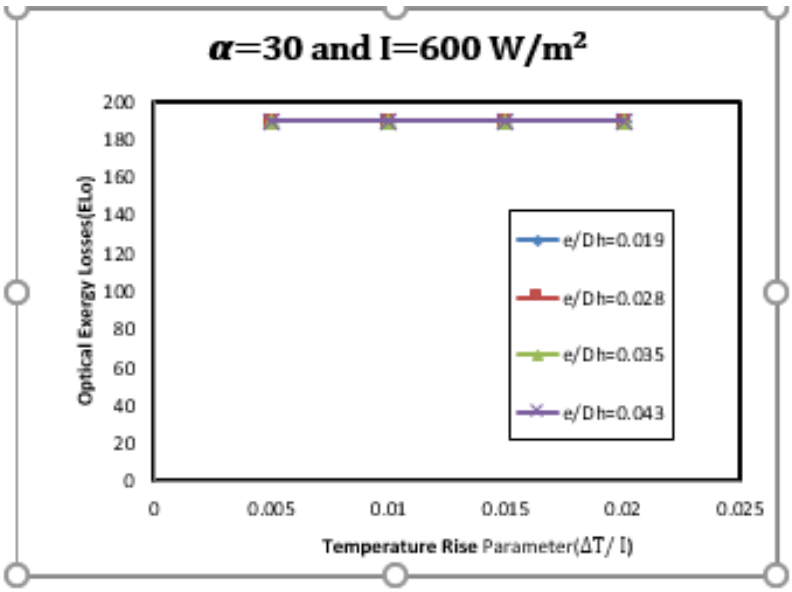

Fig 3.1 Variation of energy losses (optical)

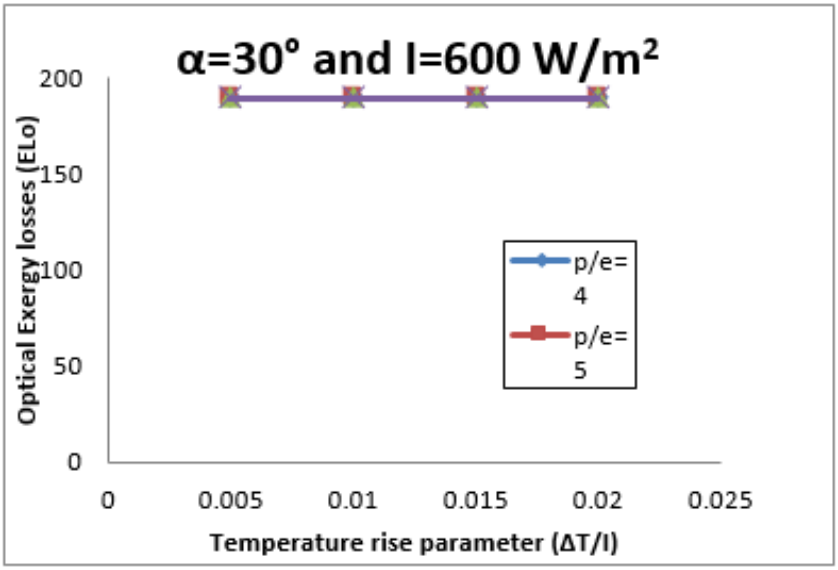

Fig. 3.2 Effect of temperature rise on energy losses

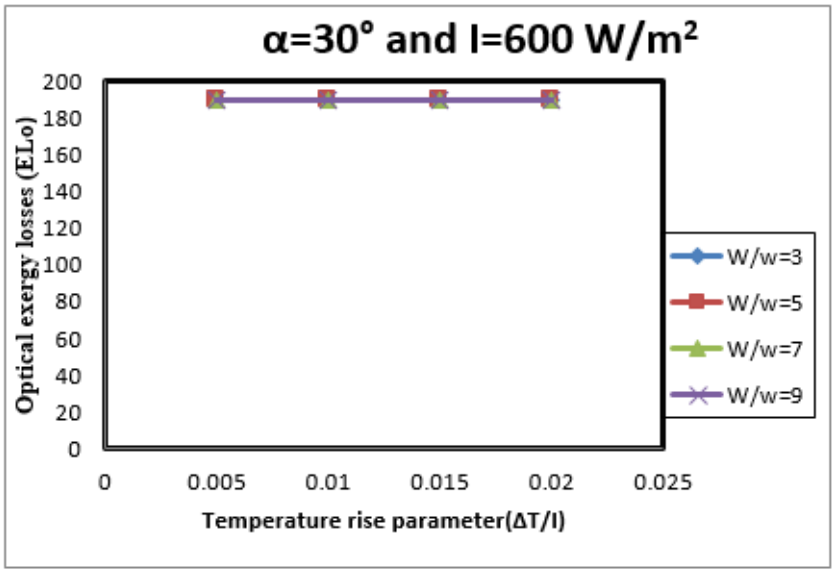

Fig.3.3 Variation of ELo with temperature rise parameter (ΔT/I) for different (W/w).

For given values of various roughness as well as operating parameters, Figs. 3.1, 3.2, and 3.3 demonstrate that the optical exergy inefficiencies are independent of the temperature rise factor (T/I), comparative roughness height (e/Dh), relative roughness pitch (p/e), & relative roughness width ratio.That's because the energy destroyed as a result of the cover's transmission and the importer plate's assimilation is independent of both the temperature of the cover and the absorber plate and only rely on the transmittance – absorptance(αr) product, which has been anticipated to be constant.

3.2.2 Exergy loss occur due to the absorber's irradiation during assimilation (ĖLA):

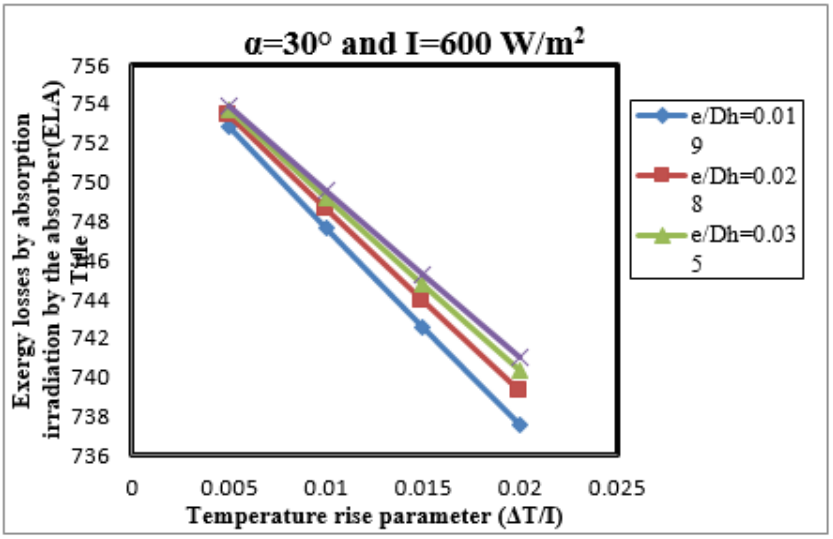

Fig .3.4 Variation of ELa with temperature rise parameter(ΔT/I) for different(e/Dh).

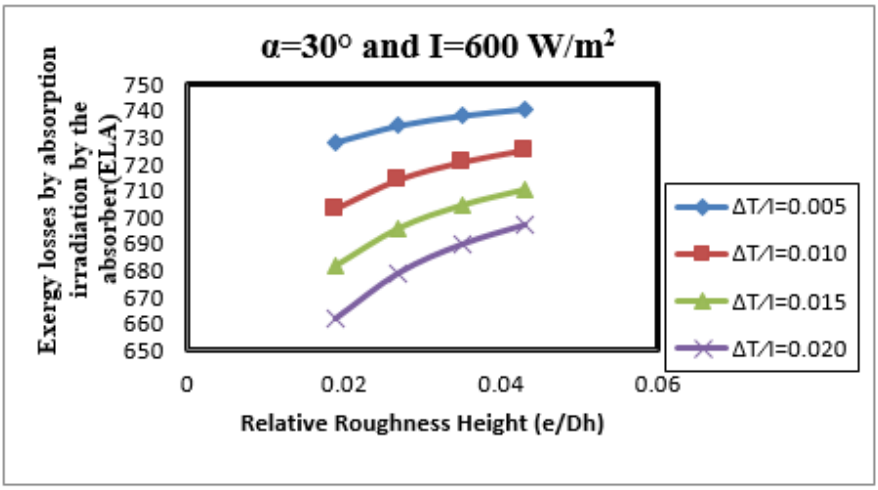

Fig .3.5 Variation of ELa with Relative roughness Hight (e/Dh) for different(**ΔT/I**)

As shown in Figs. 3.4 and 3.5, At mean sheet temperature Tpm, the absorber's Radiation exposure absorption accounts for the majority of energy losses; the value decreases as the temperature rise parameter (T/I) is raised. It exhibits the greatest losses at the lowest temperature rise parameter value (T/I=0.005) and the smallest losses at the highest temperature rise parameter value (T/I=0.025). Additionally, the relative roughness height has an impact, with an increase in relative roughness height leading to an increase in exergy losses. Since energy at higher temperatures implies bigger amounts of exergy, a high absorber temperature reduces exergy losses through absorption. A higher absorber plate temperature and, hence, more energy are created for a similar amount of absorbed energy when the "roughness height" parameter is set to l..

4. Conclusion

The effectiveness of a solar-powered air heater with multiple V rib shape that has been artificially roughened has been investigated using a mathematical modelling technique. Studies have been done on how system and operating characteristics affect different energy component types. The amount of energy lost during the transfer of heat from the absorber dish to the working medium increases with the temperature rise parameter, decreases with the ratio of relative looking to upgrade, pitch, and breadth, and is at its lowest value at an angle of attack of 60 degrees. As the temperature rise factor grows, the energetic efficiency of the collector rises as well. However, excessively low values

of this factor may provide a negative result because of the heat transfer process that takes place between the absorber surface and medium

REFERENCES

[1] Prasad, B.N., Saini, J.S., 1988. Effect of artificial roughness on heat transfer and friction factor in a solar air heater. Solar Energy 41 (6), 555–560.

[2] Gupta, D., Solanki, S.C., Saini, J.S., 1993. Heat and fluid flow in rectangular solar air heater ducts having transverse rib roughness on absorber plates. Solar Energy 51, 31–37.

[3] Bhagoria, J.L., Saini, J.S., Solanki, S.C., 2002. Heat transfer coefficient and friction factor correlations for rectangular solar air heater duct having transverse wedge shaped rib roughness on the absorber plate. Renewable Energy 25, 341–369.

[4] Karwa, R., Solanki, S.C., Saini, J.S., 1999. Heat transfer coefficient and friction factor correlations for the transitional flow regime in rib roughened rectangular ducts. International Journal of Heat and Mass Transfer 42, 1597–1615.

[5] Momin, A.-M.E., Saini, J.S., Solanki, S.C., 2002. Heat transfer and friction in solar air heater duct with V-shaped rib roughness on absorber plate. International Journal of Heat and Mass Transfer 45, 3383–3396.

[6] Muluwork, K.B., Saini, J.S., Solanki, S.C., 1998. Studies on discrete RIB roughened solar air heaters. In: Proceedings of National Solar Energy Convention, Roorkee; pp. 75– 84.

[7] Jaurker, A.R., Saini, J.S., Gandhi, B.K., 2006. Heat transfer and friction characteristics of rectangular solar air heater duct using rib-grooved artificial roughness. Solar Energy 80 (8), 895–907.

[8] Sahu, M.M., Bhagoria, J.L., 2005. Augmentation of heat transfer coefficient by using 90_ broken transverse ribs on absorber plate of solar air heater. Renewable Energy 30, 2057– 2063.

[9] Saini, R.P., Saini, J.S., 1997. Heat transfer and friction factor correlations for artificially roughened ducts with expanded metal mesh as roughened element. International Journal of Heat and Mass Transfer 40 (4), 973–986.

Design and Analysis of 2x2 MIMO Antenna using Reshape Hexagonal Geometry for Wideband Wireless Application

Sanjay Chouhan[1], Aditi Soni[1], Ganesh Mukati[1], Kishor Kumbhare[1], *Jitendra Yadav[2,] Santosh Kurre[2]

[1]*Dept. of ECE, Jawaharlal Institute of Technology, Borawan*

[2]*Department of Mechanical Engineering, School of Engineering, University of Petroleum and Energy Studies, Bidholi, Dehradun-248007, India.*

Author Emails

**Corresponding author: jyadav@ddn.upes.ac.in*

Abstract:

In this study, an antenna with four port is designed and analyzed by utilizing latest multiple input multiple output techniques for 3.3 to 6.0 GHz frequency band and Wi-Fi applications. The designed antenna covers wi-fi applications at 3.6 GHz, and 5 GHz band. The low-profile microstrip patch antenna was used in the design of the antenna (MPA).The MPA is the antenna which can place in any metallic surface. In the initial work of the thesis single antenna is discussed and optimized using CST-Microwave Suit software, then it converted in four element antenna and optimized. The antenna is developed with Wi-Fi applications in mind. The various results are calculated like gain, efficiency, envelop correlation coefficient, far field parameters etc. The resonating frequency is 5.1 GHz and return loss coefficient (S11) is -31 dB and isolation coefficient (S12, S13, S14, S21, S31, S41, S23, S24, S42, S32 etc.) is below -11 dB. A 5.14 db gain is at resonant frequency while the directivity is 5.94 dB at resonant. The antenna has a radiation efficiency of higher than 80%.The approximate bandwidth of the reshaped hexagonal four ports multiple inputs multiple output antenna is 2.6 GHz. All other antenna parameters are evaluated and discussed.

Keywords: Antenna, Efficiency, MPA, Surface current Distribution, gain

1. INTRODUCTION

Antenna plays very vital role in the field of communication. An electrical device known as an antenna or aerial transforms electrical energy into radio waves and vice versa. An Antenna can be used as transmitter and as a receiver. An antenna converts information in the form of voltage and current into the electromagnetic signal, which is then transmitted into air. As the name implies, electromagnetic waves are made up of magnetic and electric fields of varying strengths. E and H are parallel to one another, and they are also parallel to the direction in which waves propagate. The definition of an antenna provided by Stutzman and Thiele for the official IEEE [1], follows the concept: "Antenna is the part of a transmitting or receiving system that is designed to either receive or radiate the electromagnetic waves in a specific direction with define polarization".

It is very important to have knowledge about the existing research work in the field of microstrip antenna have been done by researcher and existing project of the same. A lot of sources are there by which we can get full fledge knowledge such as internet, antenna related books, old IEEE papers and many other sources. There has been a tonne of research done in the topic of mutual coupling reduction, size reduction of antenna, improvement of isolation between various antenna elements; improve the bandwidth utilization, directivity and gain of antenna. Laurent Desclos et al. describe a quarter-wavelength diversity patch setup for the 2.4 GHz ISM band PC card application in [2-4]. The framework is composed of two patches having the length is equal to quarter of wavelength which is separated by a distance to achieve the single side space diversity on a substrate. It has a high cross polarization factor and offers superior impedance matching.

Small Printed Antennas are designed and performed by M. Agarwal et al. [5]. This study looks closely at electrically tiny microstrip patches with shorting posts. These antennas are appropriate for mobile communication systems that call for a small antenna size. Performance patterns are identified, and methods to increase these antennas' bandwidth are offered. These trends provide important information about the ideal design, which consists of a wide bandwidth, a small size, and ease of production. Mark et al. conduct an experimental study of a single layer wideband electromagnetic linked microstrip patch antenna in [6]. A dual wideband antenna printed in a substrate is proposed which is designed especially for WLAN (wide local area network) and WI-MAX services. It uses a microstrip feeder line which excites the antenna and a trapezoidal conductor utilized [7-9] for band widening that is positioned in the back plane. The measured 10 dB bandwidth for return loss spans the 2.4/5.2/5.8 GHz WLAN bands and the 2.5/3.5/5.5 GHz WI-MAX bands, and it is between 2.01 and 4.27 GHz and 5.06 and 6.79 GHz, respectively. A technique for

creating a microstrip patch antenna array with linear polarization utilizing a microstrip line feed has been developed by Baskar. With the help of quarter wave transformer the array of microstrip patch antenna designed. This array [10-15] works on 8000 MHz to 12GHz frequency range. This band is used to receive unsupervised signal in radio communication and transmit this to the host. The resonant frequency for each element is quite different than other and each antenna element operates on their own resonant frequency.
Using a patch [16-18] with slots in it, Atser A. described a method for boosting microstrip patch antenna bandwidth. A rectangular patch that is 32 mm wide and 24 mm long generates the three alternate geometry forms U, E, and H. Simulation of such antenna was done [19-22] by Sonnet software tool and result of software compared with conservative rectangular microstrip patch antenna. One can find several applications wherein proposed research work may be implemented [23-29.] The comparison of these two antenna It is evident that placing an E, U, or H-patch over the substrate will increase the bandwidth of a standard patch antenna by 28.89% (630 MHz), 4.81% (100 MHz) to 28.71% (610 MHz), and 9.13% (110 MHz), respectively. Present work intend to design and analyze a four port antenna by utilizing latest multiple input multiple output techniques for 3.3 to 6.0 GHz frequency band and Wi-Fi applications. The designed antenna covers wi-fi applications at 3.6 GHz, and 5 GHz band [30-37].

2. ANTENNA DESIGNING PARAMETER

In the microstrip patch antenna design, the rectangular patch contains a built-in feed line power source. The antenna in present work has a modified hexagonal configuration and resonates at 5.1 GHz. Antennas are mounted atop a copper common ground plane and an electrically insulating dielectric layer. The table 1 will make the criteria clear.

Table 1 Design parameters for Microstrip Patch Antenna

Description	Size	Material
Substrate width (SW)	50 mm	FR-4
Substrate Length (SL)	50 mm	FR-4
Substrate height (SH)	1.524 mm	FR-4
Ground Width (GW)	50 mm	Copper
Ground Length (GL)	13 mm	Copper
Ground Height (GH)	0.07 mm	Copper
Feed width (FW)	2.9 mm	Copper
Feed length	2.74 mm	Copper
Feed width-2	0.99 mm	Copper
Feed length-2	20 mm	Copper
Radius of patch	14.7 mm	Copper
Patch height (PH)	0.07 mm	Copper

3. ANTENNA DESIGN

The design of reshaped hexagonal geometry based microstrip patch antenna is shown in figure 1. In which four patches are mounted on a single substrate. Figure 2 shows the proposed antenna's back view. In the initial level of design, single element of complete hexagonal shaped patch is designed thereafter one cut is produced in the hexagonal geometry results in reshaped hexagonal geometry.
The proposed antenna's ground is depicted in the diagram. Four identical ground with equal length and width are there. The single ground length and width is 50 x 13 mm^2.

4. RESULTS AND DISCUSSION

4.1 S- Parameter Calculation

The simulation results of above microstrip patch antenna structure GHz is shown in graphs below. It has a return loss coefficient below -30 dB and an isolation coefficient below -11 dB, and it resonates at 5.1 GHz. The front view shows the four element antenna which has hexagon modified geometry. Single feed line is there with two different feed widths. The isolation coefficient like S12, S13, S14 are discussed in figure 3, the S12 is below -11 dB in the complete frequency band. In the proposed band the isolation coefficient S13 is below -18 dB and the isolation coefficient S14 is below -16 dB. All other parameters like S23, S24 etc. are not discussed just because of symmetry in the geometry.

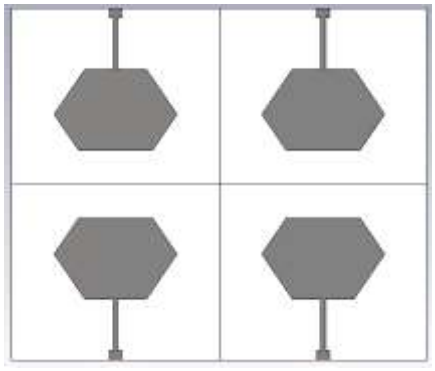

Figure 1 Front aspect of a microstrip patch antenna

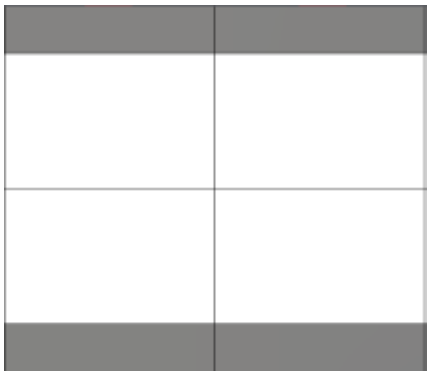

Figure 2 Design of Patch Antenna back view

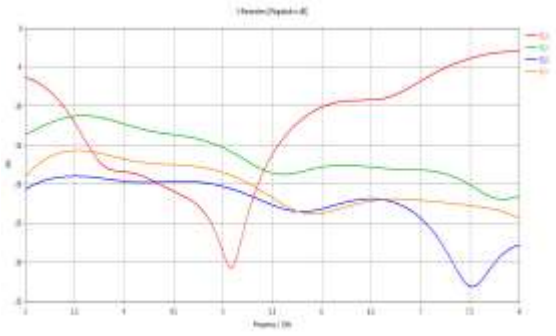

Figure 3: S- Parameter of proposed antenna.

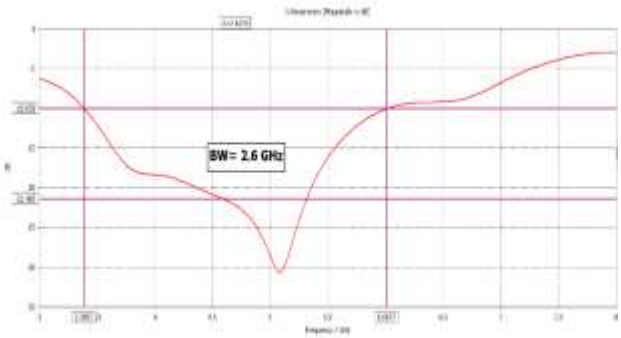

Figure 4 Bandwidth of proposed antenna.

4.2 Bandwidth of Proposed Antenna

The proposed antenna has a 2.6 GHz total bandwidth and operates between 3.3 and 6 GHz. Applications in the 3.6 GHz and 5.0 GHz Wi-Fi frequency bands are covered by the wideband of frequency. Figure 4 shows the antenna's bandwidth plot.

4.3 FAR-Field

Figure 5 and figure 6 show the E-field and H-field characteristics of proposed antenna respectively. The major lobe magnitude of E-field is 15.7 dBV/m at 217^0. An angular width of pattern is 39 degree while the side lobe level is -0.9 dB. All the E-filed results are evaluated for resonance frequency 5.1 GHz. The major lobe magnitude of H-field is -34.3 dBA/m at 136^0. An angular width of pattern is 42.5 degree while the side lobe level is -7.1 dB. All the H-filed results are evaluated for resonance frequency 5.1 GHz. Antenna gain is an antenna's ability to emit more or less in any direction in comparison to theoretical antenna. Figure 7 talks about the MIMO antenna's gain. Since each antenna element is the same, every port experiences the same gain. The antenna's gain at resonance frequency is 5.1 dB. The directivity results of antenna are shown in figure 8. The uniform directivity is found at resonance frequency. The directivity is 5.94 dBi at resonance frequency.

4.4 Efficiency

The effectiveness of the antenna is determined by the power supplied to it in comparison to the power it emits. A high efficiency antenna radiates the majority of the power that is present at the antenna's input. An antenna with low efficiency loses the bulk of the power it consumes either internally or externally due to impedance mismatch. Figure 9 shows the efficiency plot of the suggested antenna. Radiation is present in more than 80% of the graph outcomes. The surface current distribution shown in figure 10.

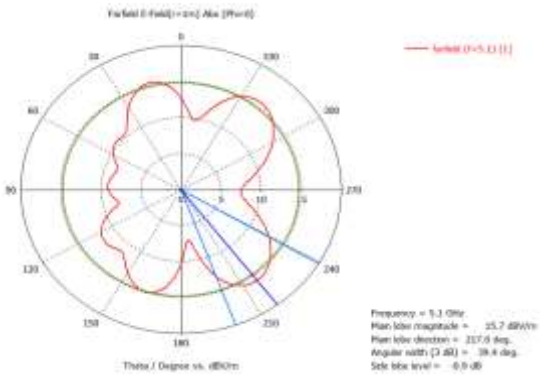

Figure 5: E field characteristics (port 1)

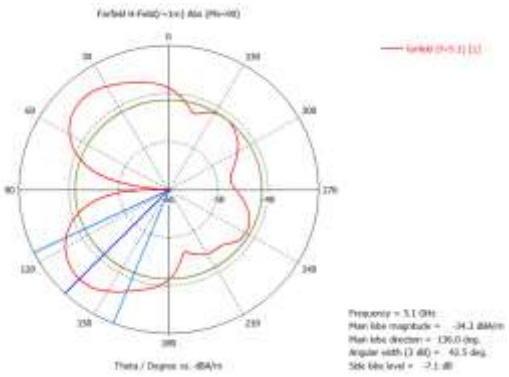

Figure 6: H field characteristics (port 1)

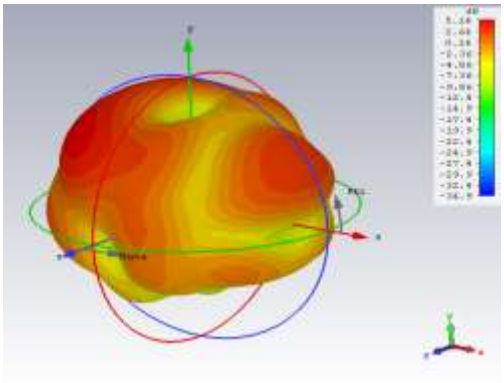

Figure 7: Gain of proposed antenna element

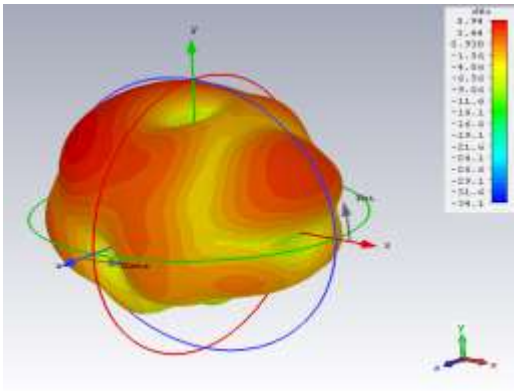

Figure 8: Directivity of proposed antenna at 5.1 GHz

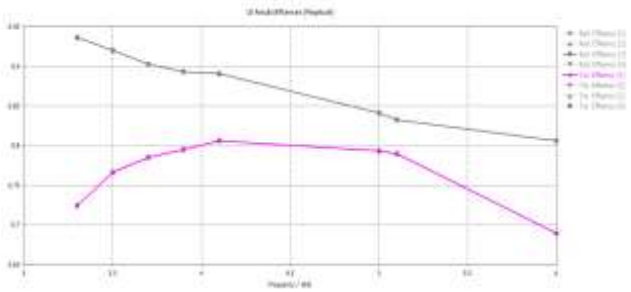

Figure 9: Efficiency of proposed antenna element

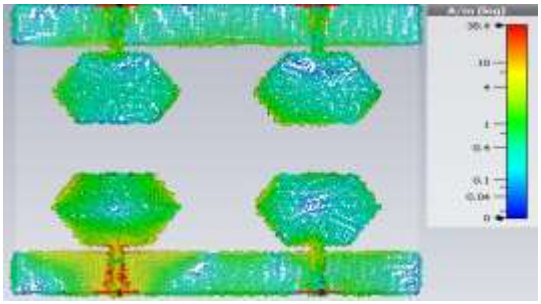

Figure 10: Surface current distributions at port 1

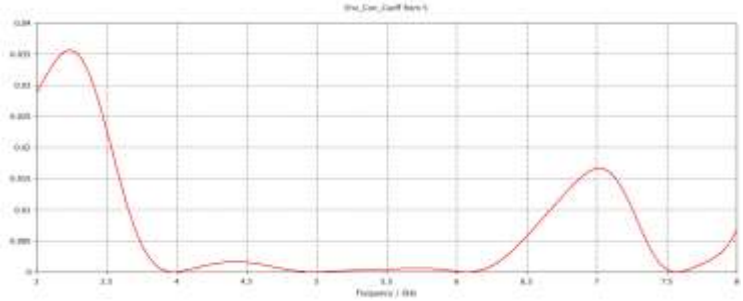

Figure 11: Envelop correlation coefficient

4.5 ECC (Envelope Correlation Coefficient)

The envelope correlation coefficient calculates the relationship between MIMO radiation patterns (ECC). ECC has a value between 0 and 1. It denotes that a correlation between the radiation patterns at 0 and a full correlation at 1 is indicated. From figure 11, it is concluded that ECC results are acceptable. The ECC is less than 0.03 in whole band.

5. CONCLUSIONS

The antenna is made of FR-4 substrate with dimensions of h = 0.078 mm, t = 0.07 mm, and frequency of 5.1 GHz. The findings show that this structure prevents a significant amount of surface current from accessing a neighboring patch antenna. The antenna has return loss coefficient (S11) is -30 dB and isolation coefficient (S12, S13, S14, S21, S31, S41, S23, S24, S42, S32 etc.) is below -11 dB. The antenna has a gain of 5.4 dB and a directivity of 5.94 dBi. The proposed antenna has a radiation efficiency of higher than 80%.The other MIMO antenna parameter are also discussed and analyzed for the proposed frequency band and it is satisfactory.

REFERENCES

1. Arun, Henridass, et al. "Deployment of modified serpentine structure for mutual coupling reduction in MIMO antennas." *IEEE antennas and wireless propagation letters* 13 (2014): 277-280.
2. Matin, M. A., M. P. Saha, and H. M. Hasan. "Design of broadband patch antenna for WiMAX and WLAN." *2010 International Conference on Microwave and Millimeter Wave Technology*. IEEE, 2010.
3. Suganthi, T., et al. "Design and analysis of rectangular microstrip patch antenna for GSM application." *IJISET-International Journal of Innovative Science, Engineering & Technology* 1.2 (2014): 245-249.
4. Immadi, Govardhani, et al. "Design of coaxial fed microstrip patch antenna for 2.4 GHz BLUETOOTH applications." *Journal of emerging trends in computing and information sciences* 2.12 (2011): 686-690.
5. Agarwal, Mayank, Ashis Kumar Behera, and Manoj Kumar Meshram. "MIMO-configured WLAN access point antenna with high port isolation." *Journal of ElEctromagnEtic WavEs and applications* 31.10 (2017): 1007-1019.
6. Gupta V., Kumar R., Mishra R.G., Semwal A., Siwach S., "Design and optimization of luggage tracking system on airport", Proceeding of International Conference on Intelligent Communication, Control and Devices Advances in Intelligent Systems and Computing (2016), pp. 833-838, doi:10.1007/978-981-10-1708-7_97.
7. Chouhan, Sanjay, et al. "Multiport MIMO antennas with mutual coupling reduction techniques for modern wireless transreceive operations: A review." *International Journal of RF and Microwave Computer-Aided Engineering* 28.2 (2018): e21189.
8. Abdulraheem, Yasir I., et al. "Design of frequency reconfigurable multiband compact antenna using two PIN diodes for WLAN/WiMAX applications." *IET Microwaves, Antennas & Propagation* 11.8 (2017): 1098-1105.
9. Ahmet Kayabasi, AbdurrahimToktas, EnesYigit, KadirSabanci, "Triangular quad-port multi-polarized UWB MIMO antenna with enhanced isolation using neutralization ring", AEU - International Journal of Electronics and Communications vol. 85, pp. 47-53, February 2018.
10. Bing Yanga, MinzheChenb, Lingyun Li, "Design of a four-element WLAN/LTE/UWB MIMO antenna using half-slot structure", AEU - International Journal of Electronics and Communications vol. 93, pp. 354-359, September 2018.
11. WaelA.E.Ali, Ahmed A.Ibrahim, "A compact double-sided MIMO antenna with an improved isolation for UWB applications", AEU - International Journal of Electronics and Communications, vol. 82, pp. 7-13, December 2017.
12. Chouhan, Sanjay, Debendra Kumar Panda, and Vivek Singh Kushwah. "Modified circular common element four-port multiple-input-multiple-output antenna using diagonal parasitic element." *International Journal of RF and Microwave Computer-Aided Engineering* 29.2 (2019): e21527.
13. AlishirMoradikordalivand, Chee Yen Leow, TharekAbd Rahman, SepidehEbrahimi, Tien Han Chua, "Wideband MIMO antenna system with dual polarization for WiFi and LTE applications", International Journal of Microwave and Wireless Technologies, vol. 8, pp. 643-650, 2016.
14. AlishirMoradiKordalivand, Tharek A. Rahman, and Mohsen Khalily, "Common elements wideband MIMO antenna system for WiFi/LTE access-point applications", IEEE antennas and wireless propagation letters, vol. 13, pp. 1601-1604, 2014.
15. R. Kumar, N. J. Ahuja, M. Saxena, and A. Kumar, "Modelling and Simulation of Object Detection in Automotive Power Window," Indian J. Sci. Technol., 2016;9 (43) doi: 10.17485/ijst/2016/v9i43/104393.
16. S.RaniPatre, S. P. Singh, "Shared radiator MIMO antenna for broadband applications", IET Microwaves, Antennas &Propagation,vol 12, pp. 1153-1159, June 2018.
17. S. Chouhan, L.D. Malviya, "Four-port shared rectangular radiator with defected ground for wireless application" International Journal of Communication System, Vol. 33, Issue 9, pp. 1-8, 12 March 2020.

18. Sanjay Chouhan, D.K. Panda, V.S Kushwah and P.K Mishra, "Octagonal-shaped wideband MIMO antenna for human interface device and S-band application", International Journal of Microwave and Wireless Technologies, pp. 1-10, 2018.
19. Chouhan, Sanjay, et al. "Spider-shaped fractal MIMO antenna for WLAN/WiMAX/Wi-Fi/Bluetooth/C-band applications." *AEU-International Journal of Electronics and Communications* 110 (2019): 152871.
20. Taha Ahmed, Bazil, et al. "(3.1-20) GHz MIMO antennas." *AEU-INTERNATIONAL JOURNAL OF ELECTRONICS AND COMMUNICATIONS* 94 (2018): 348-358.
21. Rekha, Vutukuri Sarvani Duti, et al. "Dual band notched orthogonal 4-element MIMO antenna with isolation for UWB applications." *IEEE Access* 8 (2020): 145871-145880.
22. Chouhan, Sanjay, Vivek Singh Kushwah, and Jitendra Yadav. "Two element multi-slotted MIMO antenna for dual band applications using FR-4 material." Materials Today: Proceedings (2021).
23. Maan A., Pitta P., Yadav J. (2018) Performance Evaluation of Rectangular Fins by Modeling and Simulations. In: Siddiqui N., Tauseef S., Abbasi S., Rangwala A. (eds) Advances in Fire and Process Safety. Springer Transactions in Civil and Environmental Engineering. Springer, Singapore
24. Yadav J., Agnihotri G. (2018) Circumvention of Friction-Induced Stick-Slip Vibration by Modeling and Simulation. In: Singh R., Choudhury S., Gehlot A. (eds) Intelligent Communication, Control and Devices. Advances in Intelligent Systems and Computing, vol 624. Springer, Singapore
25. Jitendra Yadav and Geeta Agnihotri (2017), "Modeling and Simulation of the Dynamic Response of a Generic Mechanical Linkage for Control Application Under the Consideration of Nonlinearities Imposed by Friction", In Springer Proceedings of the International Conference on Nano-electronics, Circuits & Communication Systems, Lecture Notes in Electrical Engineering 403
26. Jitendra Yadav & G. Agnihotri, "Proposed Critical Damping for a Spring Mass System to Avoid Stick Slip" ,Springer Journal of the institution of engineers (India): Series C Volume 96, Number 3, PP 331-335, July-September 2015.
27. Yadav, Jitendra, et al. "Nonlinear dynamics of controlled release mechanism under boundary friction." Results in Engineering 11 (2021)
28. Yadav J., Pitta P., Maan A. (2018) Swing Tower of Loader Backhoe Arm for Dynamics and Stress Analysis by Modeling and Simulation. In: Siddiqui N., Tauseef S., Abbasi S., Rangwala A. (eds) Advances in Fire and Process Safety. Springer Transactions in Civil and Environmental Engineering. Springer, Singapore
29. Dravid Shriram, Jitendra Yadav, and Santosh Kumar Kurre. "Comparison of loosening behavior of bolted joints using plain and spring washers with full-threaded and plain shank bolts." Mechanics Based Design of Structures and Machines (2021)
30. R. Kumar, R. K. Pachauri, P. Badoni, D. Bharadwaj, U. Mittal, and A. Bisht, "Investigation on parallel hybrid electric bicycle along with issuer management system for mountainous region," J. Clean. Prod., 2022; 362:132430, doi: 10.1016/j.jclepro.2022.132430.
31. Kumar, R., Kumar, A., Gupta, M. K., Yadav, J., & Jain, A. (2022). Solar tree-based water pumping for assured irrigation in sustainable Indian agriculture environment. Sustainable Production and Consumption, 33, 15-27, doi.org/10.1016/j.spc.2022.06.013.
32. Yadav, Jitendra, et al. "Identification of damping prohibiting stick-slip form friction influenced dynamic system." Proceedings of the Institution of Mechanical Engineers, Part C: Journal of Mechanical Engineering Science (2022): 09544062221135517.R.
33. Kumar, K. Bansal, A. Kumar, J. Yadav, M. K. Gupta, and V. K. Singh, "Renewable energy adoption: Design, development, and assessment of solar tree for the mountainous region," Int. J. Energy Res. 2021; 1–17 doi: 10.1002/er.7197.
34. R. Kumar and A. Kumar, "Design and hardware development of power window control mechanism using microcontroller," 2013 Int. Conf. Signal Process. Commun. ICSC 2013;61–365 doi: 10.1109/ICSPCom.2013.6719813.
35. A. Kumar, K. Bansal, D. Kumar, A. Devrari, R. Kumar, and P. Mani, "FPGA application for wireless monitoring in power plant," Nucl. Eng. Technol.2020; 53(4); 1167–1175 doi: 10.1016/j.net.2020.09.003.
36. A. Kumar, P. Sharma, M. K. Gupta, and R. Kumar, "Machine Learning Based Resource Utilization and Pre-estimation for Network on Chip (NoC) Communication," Wirel. Pers. Commun., 2018; 102 (3): 2211–2231 doi: 10.1007/s11277-018-5376-3.
37. R. Kumar, Divyanshu, and A. Kumar, "Nature Based Self-Learning Mechanism and Simulation of Automatic Control Smart Hybrid Antilock Braking System," Wirel. Pers. Commun., 2021; 116(4); 3291–3308 doi: 10.1007/s11277-020-07853-7.

APPLICATION OF 7-LEVEL NPC CONVERTER FOR LOW VOLTAGE WIND ENERGY CONVERSION SYSTEM

[1]M.D. Sharique, [2]Kavita Kushwah, [3]Ashish Kumar Singhal

Dept of EE, Sagar Institute of Science Technology and Engineering Bhopal, India, Shariquecoolsmart@gmail.com, kushwahkavita101@gmail.com, ashishee@gmail.com

Abstract.

There are many types of converters that can be utilized in low voltage applications. Unfortunately, most of them are not suitable for this type of operation. Choosing the correct converter topology is very important in order to ensure that the system performs efficiently and effectively. In this paper, we present a 7-level multilevel power converter that was utilized to manage the performance of a wind energy conversion system. The power converter was designed using maximum clamping diodes. In addition, the performance of a neutral point-clamp converter is also examined. The goal of this paper is to provide an overview of the various facets of wind energy conversion. It also explores the different techniques that are utilized in the development of such systems.

Keywords. Wind Energy System, WECS, DC-DC Converter, NPC, Switching devices, Grid system etc.

1. INTRODUCTION

This paper aims to discuss the various aspects of wind energy conversion in the world. In the next section, we will talk about the various works that are being carried out in the field of WECS. Also, we will talk about the need of application in this field. A large-scale VSC and a transformer are required to convert AC to DC voltage. An offshore platform is also required to be installed in place of these components. The working of these components will increase the installation and maintenance costs. There are two types of switches used in this process: the isolated switch and the bypass switch. If a fault occurs in the generator, the first step is to block the converter. Then, the insulation switch should be opened and the bypass switch should be closed. This will prevent the faulty converter from working. The rest of the system will operate normally. The proposed configuration of the WECS and the gear box will increase the wind generator's speed. This will result in the output voltage and frequency of the generator being equal to 50 hertz. A PMSG is used as the Wind Generator [1]. A 7-level inverter is also used as the wind power converter. The constant current and the

magnitude of the PMSG's output voltage are the main factors that make this component a reliable and high-quality component. As the technology used in the oil and gas industry continues to develop, more sophisticated components and systems are being developed. These are ideal for various applications, such as renewable energy. The desire to have offshore wind energy installations is not just motivated by global warming. It also takes a certain amount of commitment to make this possible.

2. MULTILEVEL CONVERTER (7L-NPC)

A multilevel converter can provide output voltages at higher levels than two. This type of device can be used in combination with a rectifier or inverter to produce a higher voltage output. The lowest type is the three-stage converter, which has a output frequency that's similar to that of a bridge converter. The three-level converter is referred to as a 5-level converter, and its basic topology consists of a frequency converter, a neutral point compensated, and a modular multilevel converter. To achieve high output voltage, switching devices have to be regulated properly. A simple step-through-a-scunder is used to create multiple Direct Current supplies using various DC sources, such as solar photovoltaic arrays and wind turbines. These components need a single supply to operate properly[3][7].The other type of converter is a modular multilevel converter, which requires multiple separated and balanced supplies. A magnetic link can be used to create multiple DC supplies for this device.

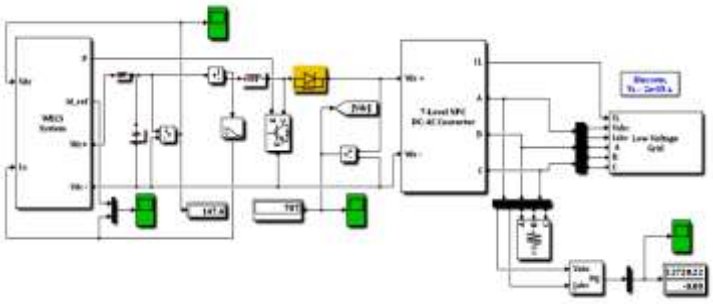

Fig.1.SIMULINK Model of 7-Level NPC Fed Low Voltage Grid Interface WECS

Due to the increasing number of renewable energy sources such as wind turbines and solar photovoltaics, the need for additional diodes is increasing. Six diodes are required for a three-phase converter. Wind turbine mechanical strength can be derived by determining the wind speed, air density, and swept region. The kinetic energy is converted into mechanical energy by the wind turbine [4][5].
The mechanical power output of the wind turbine is,

$$P_m = \frac{1}{2}\rho v_b^2 - \frac{1}{2}\rho v_b v_d^2 = \frac{1}{2}\rho A\left(\frac{v+v_d}{2}\right)\left(v^2 - v_d^2\right) \qquad 2.1$$

Where, P_m is mechanical power by wind turbine, v_d is the downwind speed in ms^{-1} and v is the upwind speed. From the aforementioned equation, it can be shown that the mechanical

strength of the wind turbine is directly proportional to the cube of wind speed. Any wind turbine has its limit (approximately 59%) which ensures how much energy can be extracted from the wind. Turbine will never extract any of the kinetic energy present in the atmosphere, because if it will then there will be little downwind behind the turbine. Fig 2 shows that the upwind and downwind regions are distinct [8][9]. As a result, upwind speed would be greater than downwind speed.

3. SYSTEM OF WECS

The key component of the simulation is wind energy conversion. This technology is based on electromechanical conversion. Wind energy conversion systems are made up of a mechanical turbine and an electrical generator. So, for the simulation, two components are used: one for the drive train portion and the other for the electrical generator portion. The wind turbines drive train (mechanical components) is made up of a blade-pitching mechanism, a blade hub, and a rotor shaft (for wind turbine converters, relative long). The turbine and generator are used in the design of the drive train in this study. The moment of inertia of the wind wheel (blade-fed hub) is approximately 90% of the overall train moment, whereas the inertia rotor generator time is around 10%. In addition, the generator has the maximum torsion rigidity. To represent the WTGS driver train system, a three-mass model, a two-mass model, a one-luminous mass model, or even a six-mass model can be employed. For correct transient analyses of WTGSs, a six-mass drive train model is necessary. Despite this, a six-mass driver-train system increases simulation time in modest stages because to the complicated and extensive numerical measurement.

a) MPPT

The basic aim of MPPT is to operate at that point where maximum power is generated at the wind speed. MPPT generate the pulses for the operation of boost converter which is connected to the output of the WECS.

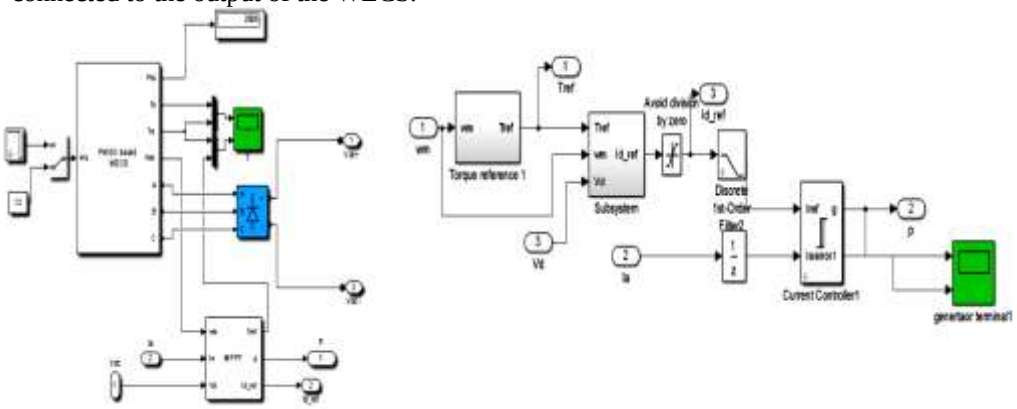

Fig. 2. SIMULINK Model of WECS with MPPT & MPPT used in WECS

4. GRID INTEGRATION OF PMSG WITH WIND TURBINE SYSTEM

Power electronic devices are used to incorporate the grid into WECS that are capable of transforming the power into a useful form. To synchronise WECS with a grid with a constant frequency, a constant voltage and a high-power factor. The voltage level of the MLI can be

generated by a staircase. It depends on the number of DC sources used. The harmonic material in the generated voltage decreases with increasing DC sources. The upcoming MLI topologies must have the following things:

- Less switching devices as much as possible.
- Lower switching frequency.
- Capable to stand with very high power and voltage application

a) Model of IGBT Switches in 7-Level NPC

Here in this each leg of three phases supply is connected with diode clamped converter for the converting DC voltage to the AC voltage. Each leg has two different type of connections. Upper part is used for producing positive part of AC cycle and lower part is used for negative part of AC cycle. Figure 6 shows the switching connection of upper and lower part of each leg. Here IGBT switch is used for switching action of the power converter.

i) Switching Schemes for 7-Level NPC Converter

A switching pattern between the carrier signals of a certain cell can be created by adding a phase level shift between the two adjacent cells. This process can be used to create a multilevel multi-channel converter. The converter can be equipped with either a line-shifted or phase-shifted conveyor. If the reference signal is the frequency of fm, the converter's frequency modulation index can be determined:

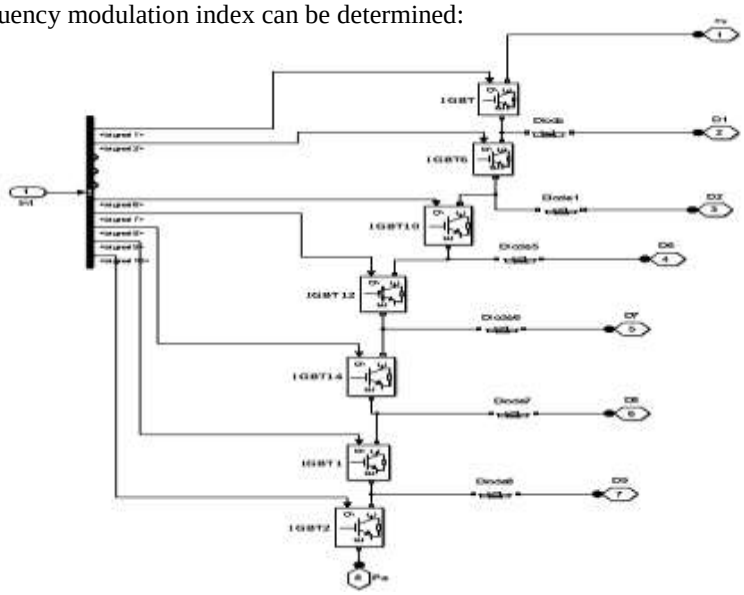

Fig. 3 SIMULINK Model of IGBT Switches in 7-Level NPC

The phase-shifted conveyor is ideal for converting FC and MMC signals. The index of the amplitude modulation can be calculated by comparing the Am and Ac peak-to-peak signals. The block diagram for the 7-level converter of the phase-shifted switching scheme. Three signals are required on this modulation scheme. 120 ^{0} moved by each other. The number of carrier signal depends on the number of conversion levels; in total are $\frac{m-1}{2}$ in multilevel converter. The carrier phase shifted towards the particular pair of cell can be determined as:

$$\theta_{ps} = \frac{360^0}{m-1}$$

the phase shifted signal generated in PWM scheme for 7-level NPC converter system. Each signal is used for upper-level switch for producing pulses for on/off strategy of the NPC.

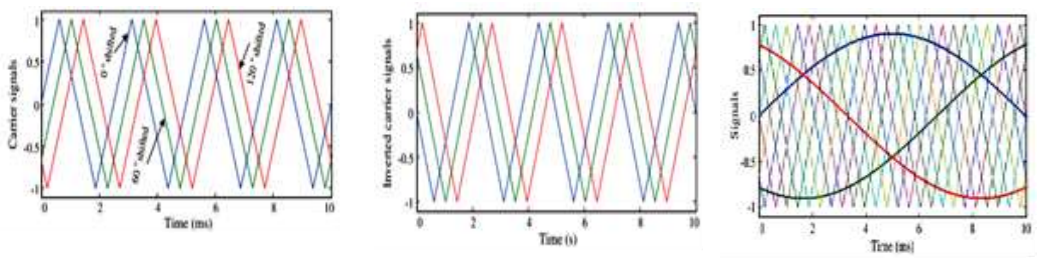

Fig. 4. Three phase carrier signal for phase shifted PWM for 7-Level NPC

5. RESULT ANALYSIS

The whole model of the proposed system is designed in MATLAB. MATLAB is the powerful SIMULINK tool which is used for design a prototype of the working model for testing and validation. The data which is used in the simulation in MATLAB is always standardizing with the IEEE society. Table-1 Shows the parameter used in the simulation work.

TABLE I. SIMULINK PARAMETER

Parameter	**Value**
Wind Turbine Data	
Mechanical Power	8.5 kW
Base Wind Speed	12 m/s
Pitch Angle	0
Max Power at base speed	0.8
Generator Data	
Type of Generator	PMSG
Generator Specification	10 Nm, 300 Vdc, 2300 RPM
Load Data	
3 Phase Star Connected load	400 V, 50 Hz, 15 kW
Grid Side Converter Data	
Switch Used	IGBT
DC Link Capacitor	2200*5 µF
Carrier Signal Frequency	5 kHz

Filter inductor	2 mH
Filter Capacitor	5µF

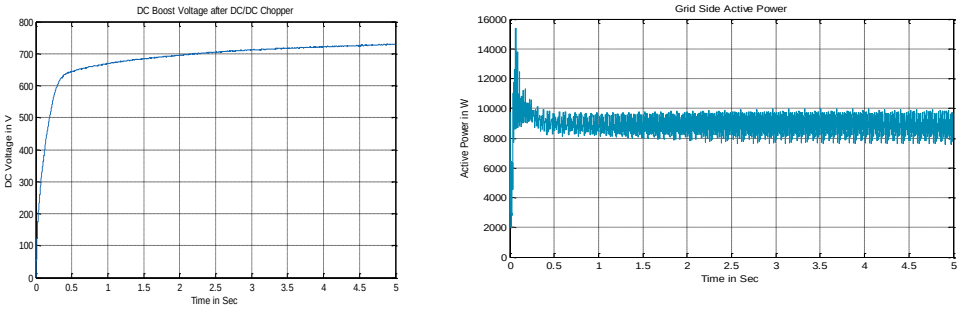

Fig. 5. DC Boost Voltage Generation by Wind Generator & Grid Side Active Power

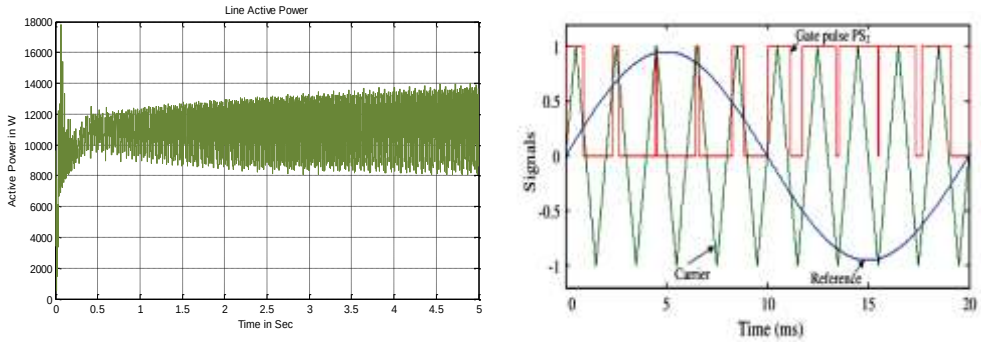

Fig. 6. Line side Power & Inverter Output Line Voltage

6. CONCLUSION

The multilevel inverter holds attractive features, usage of more switches in the conventional configuration poses a limitation to its wide range application. In this paper, the 7-level NPC is proposed on generator and grid-side converters. The 7-level NPC multilevel inverter using 5 switches is successfully introduced in simulation the circuit using MATLAB/Simulink and observed that it decreases the R_{DC} by which switching losses reduced. Therefore, a renewed 7-level NPC multilevel inverter topology is introduced incorporating the least number of unidirectional switches and MPPT used, thereby ensuring the minimum switching losses and reducing size and installation cost.

7. REFERENCES

[1] K.Bedoud, A.Rhif, T.Bahi, H.Merabet,"Study of a double fed induction generator using matrix converter: Case of wind energy conversion system" International Journal of Hydrogen Energy, Volume 43, Issue 25, Pages 11432-11441, 2018.

[2] Naziha Harrabi, Mansour Souissi, Abdel Aitouche, Mohamed Chaabane, “Intelligent control of grid-connected AC–DC–AC converters for a WECS based on T–S fuzzy

interconnected systems modelling", IET Power Electronics, Volume 11, Issue 9,p. 1507 – 1518, 2018.

[3] Kotb B.Tawfiq, Arafa S.Mansour, Haitham S.Ramadan, Mohamed Becherif, E.E.El-kholy, "Wind Energy Conversion System Topologies and Converters: Comparative Review", Energy Procedia Volume 162, April 2019, Pages 38-47, 2019.

[4] Aghiles Ardjal, Adel Merabet, Maamar Bettayeb, Rachid Mansouri, Labib Labib, "Design and implementation of a fractional nonlinear synergetic controller for generator and grid converters of wind energy conversion system", Energy, Volume 186, 115861, 2019.

[5] Shijia Zhou, Fei Rong, Wenlong Sun, Sheng Huang, Qiuwei Wu, "AC/AC grid connection of six-phase wind power generator based on enneagon MMC converter", International Journal of Electrical Power & Energy Systems, Volume 118, Page no.105810, 2020.

[6] N. Ramesh Babu, Ramji Tiwari, “Recent developments of control strategies for wind energy conversion system", Renewable and Sustainable Energy Reviews, Volume 66, Pages 268-285, 2016.

[7] René Aubrée, François Auger, Michel Macé, Luc Loron, "Design of an efficient small wind-energy conversion system with an adaptive sensor less MPPT strategy", Renewable Energy Volume 86, Pages 280-291, 2016.

[8] Asma Tounsi; Hafedh Abid; Maher Kharrat; Khaled Elleuch, "MPPT algorithm for wind energy conversion system based on PMSG", 18th International Conference on Sciences and Techniques of Automatic Control and Computer Engineering (STA), 2017.

[9] Essam. H. Abdou; Abdel-Raheem Youssef; Salah Kamel, "Adaptive P&O MPPT for Wind Energy Conversion System Based 1.5 MW DFIG", 019 IEEE Conference on Power Electronics and Renewable Energy (CPERE)”, IEEE Conference on Power Electronics and Renewable Energy (CPERE), 2019.

[10] Dwivedi, Priya, Ashish Kumar Singhal, Aayush Shrivastava, and Subinoy Roy. "Hybrid RE energy system based modified maximum peak power tracking technique" Solid State Technology 63, no. 6, page no. 20429-20434, 2020.

[11] Singhal, Ashish. "A Sustainable Growth of Clean Energy In India: A Target 2022." INFORMATION TECHNOLOGY IN INDUSTRY 9.2, page no. 1069-1076, 2021.

[12] Anshu Sharmaa, Ashish Singhal, “Designing of Three Level 3 Phase Inverter Using Improved SPWM Modulation for different Loads” Turkish Journal of Computer and Mathematics Education, Vol.12 No.3, page no. 4513-4520, 2021.

Overview of Hydrogels and Hydrogels based Actuators for Biomedical Applications

Rohit Sharma[1], Iqbal Singh[2], Ajay Vasishth[3], Sourbh Thakur[4]

[1]Satyam Engineering & Technology, Amritsar, Punjab, India-143107

[2]Satyam Polytechnic & Pharmacy College, Amritsar, Punjab, India-143107

[3]University Institute of Sciences, Chandigarh University, Mohali,

Punjab, India- 140413

[4]Department of Organic Chemistry, Bioorganic Chemistry and Biotechnology,

Silesian University of Technology, B. Krzywoustego 4, 44-100 Gliwice, Poland

Email: rohitsharma3940@gmail.com

Abstract

Hydrogels are three-dimensional polymeric chains that are widely employed in many applications due to their extraordinary and unique abilities. Nowadays, hydrogels are being incorporated more and more into various bio-medical applications because of their characteristics like biocompatibility, biodegradability, imitation of extracellular matrices, and bioactive molecules. This paper aims to provide a brief overview of hydrogels, their classifications, and types of hydrogel actuators based on their response to different types of stimuli like electric fields, light, magnetic fields, pressure, temperature, solvent composition, ions, pH, and specific molecular recognition. Applications of hydrogel actuators in the biomedical field and current challenges have also been discussed.

Keywords: Hydrogel, polymer, stimuli-responsive, actuator, biomedical applications

1. INTRODUCTION

Hydrogels are three-dimensional polymeric networks that contain water in their structure and show the property of swelling without dissolving in water [1]. The tendency to hold water in hydrogels depends upon the presence of hydrophilic

groups, cross-linking degree, polymer-polymer and polymer-water physical interactions, temperature, pH, and ionic strength. Its characteristics, like softness, elasticity, biodegradability, and the ability to expand and contract, make it a potential candidate for various biomedical applications [2]. The polymeric network of hydrogels is formed through the chemical or physical interactions between homopolymers and copolymers. Hydrogels can be moulded into any shape and size, such as nanoparticles, microparticles, coatings, slabs, and films. The use of hydrogels in biomedical applications has increased significantly in recent years due to their phenomenal stretching and flexibility, biocompatibility, and stimuli sensitivity. Furthermore, new hydrogel nanocomposites are being explored because the already present hydrogels have many limitations and inabilities, such as poor mechanical strength, low strain, and low thermal stability. So, to address most of these problems, scientists are synthesizing new hydrogel nanocomposites from various nanomaterials [3]. This paper sheds light on hydrogels, their classification, hydrogel actuators, their biomedical applications and current challenges.

2. CLASSIFICATION OF HYDROGELS

Hydrogels are classified into several types. Based on sources, hydrogels are classified into natural and artificial/synthetic origins [4]. Hydrogels can be obtained naturally from proteins of natural products such as collagen and gelatine and polysaccharides and using chemical compositions in synthetic ways. Though synthetic polymers are much stronger than natural polymers, but in recent years, the usage of natural hydrogels in various applications has significantly increased. Further, according to polymeric compositions, hydrogels are also defined into three categories: homopolymeric hydrogels, copolymers, and multi-polymers (interpenetrating polymeric hydrogels). First, homopolymeric hydrogels are polymer networks produced from only one type of monomer. On the basis of the type of monomer and the polymerization process, they may result in a cross-linked skeletal structure [5]. Second, copolymers are formed from at least two or more distinct species of monomers having one hydrophilic constituent which are then organised with polymeric network chains in a pseudorandom, block, or alternating pattern [6]. Third, hydrogels are defined as multipolymer interpenetrating polymeric hydrogels (IPH). In this type, hydrogels are constructed using two freely cross-linked synthetic and/or natural polymer components, whereas semi-interpenetrating polymeric hydrogels contain one cross-linked and another the non-cross-linked polymeric component [7, 8]. Further, depending on the type of cross-linking, hydrogels are defined as chemically cross-linked and physically cross-linked. Apart from this, based on chemical composition and physical interactions, hydrogels through cross-linking are classified as amorphous, semi-crystalline, and crystalline. Moreover, according to the presence or absence of electrical charge located on the cross-linked chains, hydrogels are classified as non-ionic, ionic, amphoteric electrolyte and zwitterionic. Furthermore, it is possible to tailor the mechanical strength, biodegradability, and response of

hydrogels to different stimuli by choosing the right combination of monomers and cross-linking agents for a specific biomedical application.

3. HYDROGEL ACTUATORS AND THEIR TYPES

A simple actuator is defined as a device that converts any sort of energy, such as electrical, optical, air, or hydraulic energy, into mechanical energy to achieve physical movements, whereas hydrogel actuators convert the received energy into mechanical energy with a soft motion like a living being. Hydrogel actuators are sensitive to external stimuli. There are different types of stimuli. One is physical stimuli, which contain electric fields, light, magnetic fields, pressure, solvent composition, sound, and temperature, whereas the other is chemical or biochemical stimuli having ions, pH, and specific molecular recognition. Hydrogel actuators can be optimized by changing the variety of input stimuli. Based on input stimuli, hydrogel-based soft actuators are divided into six types.

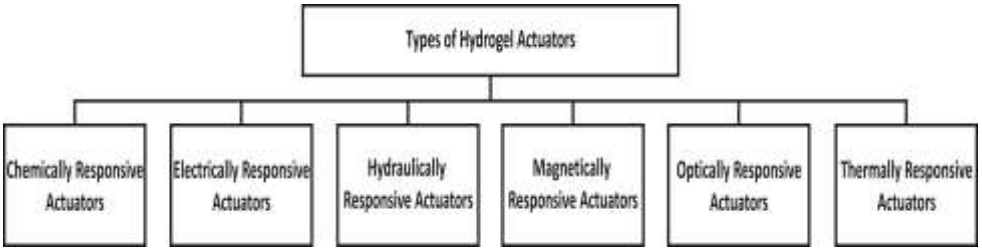

Figure 1. Schematic classification of hydrogel actuators on the basis of input stimuli

3.1. Chemically Responsive Actuators

This type of hydrogel actuator can convert the chemical energy of the surroundings directly into mechanical motion [9]. These actuators are fabricated with chemically responsive hydrogels and depend on the volumetric adjustments that occur in hydrogels in reaction to chemical stimuli. They are further divided into three types of actuators; solvent-responsive, pH-responsive and biomolecule-responsive. In solvent-responsive actuators, the differential in hydrophobicity between the polymer network and the solvent determines how much volume can be changed by this actuator [10]. Further, in pH-responsive hydrogel actuators under the required pH environment, the volumetric changes rely on the ionization of the polymer network [11]. Further, the biomolecular-responsive actuators are based on the reversible association and dissociation of biomolecular complexes to change the volumetric quantity [12].

3.2. Electrically Responsive Actuators

These types of hydrogel actuators change their shape according to electrical stimuli. Without the need for any complex conversion of stimuli, only computational circuits are required to control the volumetric changes very efficiently and accurately [13]. Electrically responsive actuators are further divided into electrically induced osmotic pressure actuators and dielectric elastomer actuators. In these actuators, osmotic pressure is created via the formation of an ion gradient, which leads to the swelling of hydrogel asymmetrically. Second, the dielectric elastomer actuator consists of a dielectric elastomer layer between the two ionic conductive hydrogels. The hydrogel/elastomer interfaces along each hydrogel accumulate opposite-charged ions when a high voltage is placed between the two materials. This creates Maxwell tension between the hydrogels, and resultantly, the elastomer layer shrinks in thickness and enlarges in area. [14].

3.3. Hydraulically Responsive Actuators

Hydraulic pressure plays a pivotal role in changing the shape of the hydrogel in hydraulically responsive actuators. In comparison with other types of actuators, hydraulically responsive actuators can achieve higher speeds and actuation forces. Furthermore, they are transparent by nature, so they are widely used in underwater activities owing to the same refractive index of these actuators as hydrogel and water. Moreover, they can easily eschew the sonic radars because of their same impedance as water, so they are also used in applications where stealth purposes are required [15].

3.4. Magnetically Responsive Actuators

In magnetically responsive actuators, external magnetic fields are responsible for the shape change of the hydrogels. They typically contain nano- or micro-sized magnetic particles and can be controlled remotely without a physical connection. When a magnetic field is applied externally, the hydrogel matrix changes shape as a result of the magnetic force being transmitted to it through the scattering of magnetic particles in the hydrogel. Nowadays, magnetically responsive hydrogels are used in artificial muscles and the manufacturing of implantable medical devices [16].

3.5. Optically Responsive Actuators

Light irradiation is used for volumetric changes of the hydrogels in optically responsive actuators. Energy can be transferred wirelessly with this type of actuator, and no physical connection is required. These actuators are also responsive to multiple wavelengths. Further, in response to specific wavelengths, reversible isomerization occurs in photoswitchable molecules like spiropyran and azobenzene. Under ultraviolet (UV) light, spiropyran dissociates, and under visible light, it changes back into a ring-closed structure. Hydrophobicity changes are

directly responsible for the reverse isomerization that leads to changing the shape of the hydrogels. Furthermore, an optically responsive actuator which involves spiropyran can function as a reversible photo-valve for microfluids [17].

3.6. Thermally Responsive Actuators

These kinds of hydrogel actuators change their shape according to variations in temperature. These actuators create large deformations by selectively reacting to a specific temperature range. Due to their tunable temperature range, they can be widely used in applications such as soft robotics. Thermally responsive hydrogel actuators are divided into lower critical solution temperatures (LCST) and upper critical solution temperatures (UCST). LCSTs generally shrink when temperatures rise above critical and swell when temperatures fall, whereas UCSTs expand when temperatures rise above critical and contract to their normal position at lower temperatures [18].

4. BIOMEDICAL APPLICATIONS OF HYDROGEL ACTUATORS AND CURRENT CHALLENGES

The hydrogel-based actuators have proven productive in biomedical field and are becoming popular for various applications such as navigating medicine in the arteries and holding and releasing drugs in drug delivery systems [19]. They are widely employed in biomedical industries, such as implanting chips on human body organs (heart, liver, skin, kidneys) via microfluidic devices [20]. Moreover, microfluidic devices are also employed in cell culture, medical examination, wound healing and dressing, and the manufacturing of pharmaceutical devices in a quick, precise, and high-throughput manner [21]. In addition to this, smart robotics arms, or usually microrobotics arms, are becoming very popular in the biomedical field. Microactuators are also employed in smart robotic arms using polypyrrole. Furthermore, hydrogel actuators are playing tremendous role in bioprinting applications such as tissue engineering and steriolithography via 3D bioprinting and 4D bioprinting of neural stem cell attachments and natural collagen fibre imitation [22, 23]. Hydrogel scaffolds are extremely useful to repair or regrow damaged biological tissue and are essential for providing a supportive matrix for embedded cells. Scaffold matrices serve a significant role in development of new tissue morphogenesis by directing the growth of cells placed inside them. Scaffolding is used to deliver cardiac cells into cardiac muscles and it plays a pivotal role in the tissue regeneration process [24].

5. CURRENT CHALLENGES

Hydrogel actuators have evolved with the passage of time and undergone significant advancements, but they are still facing some challenges in contemporary times. Firstly, the biggest limitation of hydrogel actuators is related to their power efficiency. It is observed that hydrogel actuators that work on the expansion/shrinking phenomenon yield low power conversion efficiency. Till

date, much research has been carried out to improve the energy efficiency of hydrogels, but the obtained efficiency is not as high as required for feasible biomedical applications. Another limitation of hydrogel actuators is related to their fabrication techniques. For practical biomedical applications, it is required to muster different hydrogels with multiple properties and fuse them into one material, but in fact, it is a hectic task to amass distinct hydrogel properties into one material and create an advanced hydrogel actuator. So far, much research has focused on tailoring the properties related to stimulus response of hydrogel actuators; however, there are still some challenges, such as lower mechanical power, UV carcinogenesis, stability factors, and the virulence of some materials that need to be addressed. Further, all the present hydrogels have a longer response time to stimuli. This response time creates a bottleneck in many practical biomedical applications that require a very fast response time in nanoseconds.

6. CONCLUSION

In summary, hydrogel-based biomaterials are widely used in many interdisciplinary fields but over the past decade, the usage of hydrogels in the biomedical area has grown significantly owing to their biocompatibility with human organs/tissues. Hydrogel actuators are used in drug delivery, bioprinting, microrobotics, microfludic devices and tissue scaffold fabrication. So far tremendous progress has been made in development of hydrogel based actuators but few issues should be addressed to use hydrogel actuators in efficient manner. In the stimulus-responsive hydrogels, there is need of fabricating actuators that can work with minimal input of stimuli. Furthermore, reducing the response time to stimuli from several minutes to the millisecond level especially in applications that require a quick response is still a challenge that provides scope for future research.

7. REFERENCES

[1] E.M. Ahmed, et. al., ‘An innovative method for preparation of nanometal hydroxide superabsorbent hydrogel’, Carbohydrate Polymers, vol. 91, pp. 693-698, 2013.

[2] E. Caló, V.V. Khutoryanskiy, ‘Biomedical applications of hydrogels: a review of patents and commercial products’, European Polymer Journal, vol. 65, pp. 252-267, 2015.

[3] A.K. Gaharwar, N. A. Peppas, A. Khademhosseini, ‘Nanocomposite hydrogels for biomedical applications’, Biotechnology and Bioengineering, vol. 111, pp. 441-453, 2014.

[4] W. Zhao, et. al., ‘Degradable natural polymer hydrogels for articular cartilage tissue engineering’, Journal of Chemical Technology & Biotechnology, vol. 88, pp. 327-339, 2013.

[5] T. Iizawa, et. al., ‘Synthesis of porous poly (n-isopropylacrylamide) gel beads by sedimentation polymerization and their morphology’, Journal of Applied Polymer Science, vol. 104, pp. 842-850, 2007.
[6] L.Yang, J.S. Chu, J.A. Fix, ‘Colon-specific drug delivery: New approaches and in vitro/in vivo evaluation’, International Journal of Pharmaceutics, vol. 235, pp. 1-15, 2002.
[7] Z. Maolin, et. al., ‘The swelling behavior of radiation prepared semi-interpenetrating polymer networks composed of polynipaam and hydrophilic polymers’, Radiation Physics and Chemistry, vol. 58, pp. 397-400, 2000.
[8] F. Machado, E. L. Lima, J. C. Pinto, ‘A review on suspension polymerization processes’, Polimeros, vol. 17, pp. 166-179, 2007.
[9] P. Techawanitchai, et. al., ‘Photo-switchable control of pH-responsive actuators via pH jump reaction’, Soft Matter, vol. 8, pp. 2844-2851, 2012.
[10] P. Etienne, et. al., ‘Reversible patterning and actuation of hydrogels by electrically assisted ionoprinting’, Nature Communications, vol. 4, pp. 2257, 2013.
[11] J. Duan, et. al., ‘Bilayer hydrogel actuators with tight interfacial adhesion fully constructed from natural polysaccharides’, Soft Matter, vol. 13, pp. 345-354, 2017.
[12] J. Kim, et. al., ‘Review of soft actuator materials’, International Journal of Precision Engineering and Manufacturing, vol. 20, pp. 2221-2241, 2019.
[13] E. Acome, et. al., ‘Hydraulically amplified self-healing electrostatic actuators with muscle-like performance’, Science, vol. 359, pp. 61-65, 2018.
[14] P. J. Glazer, et. al., ‘Role of pH gradients in the actuation of electro-responsive polyelectrolyte gels’, Soft Matter, vol. 8, pp. 4421-4426, 2012.
[15] H. Yuk, et. al., ‘Hydraulic hydrogel actuators and robots optically and sonically camouflaged in water’, Nature Communications, vol. 8, pp. 14230, 2017.
[16] S.Y. Chin, et. al., ‘Additive manufacturing of hydrogel-based materials for next-generation implantable medical devices’, Science Robotics, vol. 2, pp. eaah6451, 2017.
[17] J. T. Schiphorstet. et. al., ‘Molecular design of light-responsive hydrogels, for in situ generation of fast and reversible valves for microfluidic applications’, Chemistry of Materials, vol. 27, pp. 5925-5931, 2015.
[18] W. J. Zheng, et. al., ‘Tough Al-Alginate/Poly (N-Isopropylacrylamide) hydrogel with tunable LCST for soft robotics’, ACS Applied Materials & Interfaces, vol. 7, pp. 1758-1764, 2015.
[19] S. Fusco, et. al., ‘Self-folding mobile microrobots for biomedical applications’, Proc. of IEEE Int. Conf. on Robotics and Automation, pp. 3777-3782, 2014.
[20] Q. Wu, et. al., ‘Organ-on-a-Chip: Recent breakthroughs and future prospects’, Biomedical Engineering Online, vol. 9, pp. 19, 2020.

[21] M. Ibrahim, M. K. Richardson, ‘Microfluidic devices for cell, tissue and embryo culture’, Recent Patents on Regenerative Medicine, vol. 3, pp. 249-263, 2013.

[22] S. Shin, H. Kwak, J. Hyun, ‘Melanin nanoparticle-incorporated silk fibroin hydrogels for the enhancement of printing resolution in 3d-projection stereolithography of Poly(Ethylene Glycol)-Tetraacrylate bio-ink’, ACS Applied Materials & Interfaces, vol. 10, pp. 23573-23582, 2018.

[23] J.M. McCracken, et. al., ‘3D-printed hydrogel composites for predictive temporal (4D) cellular organizations and patterned biogenic mineralization’, Advanced Healthcare Materials, vol. 8, pp. 1800788, 2019.

[24] C. Lin, C.S. Ki, H. Shih, ‘Thiol-Norbornene photo-click hydrogels for tissue engineering applications’, Journal of Applied Polymer Science, vol. 132, pp. 41563, 2015.

Simulink Computed Torque Control of a Novel 15-DOF Anthropomorphic Robotic Fingers

Deepak Bharadwaj[#], Roushan Kumar

Department of Mechanical Engineering, School of Engineering, University of Petroleum and Energy Studies, Dehradun, India

[#]Corresponding Author: *Deepak Bharadwaj, Email: dbharadwaj@ddn.upes.ac.in*

Abstract

Joint control is the prominent issue observed during finger interaction with the environment. Internal collision of finger movement during grasping of the object occurs while picking the object. This research work focuses on the placement of joint motor, so that finger collision can be avoided. Due to compact size and advancement of sensing and actuation, the flat plate motor was directly mounted between the finger joint. Touch sensors were placed on the surfaces of the finger. A simple master-slave control was adopted for the finger joint motion control. A smooth operation of grasping was observed during finger interaction.

Keywords: Collision, Control architecture, Finger interaction, Computed torque control

1. INTRODUCTION

Finger gripper controlling is a tedious task. The main problem arises due to actuator size. Placing of larger size actuator between the fingers is not possible and also for mobile applications, there is a chance of collision [1]. Earlier design work on the pulley system, four-bar chain mechanism, and gear mechanism. The conventional mechanism is limited to the workspace for the finger during grasping the object [2],[3]. The conventional mechanism has no flexibility to deal with the unknown shape and size of the object. Due to the larger size of the mechanism and more weight of the actuator, grasping is not done properly. With the advancement of flat plate EC motors, such type of problems can be minimized. Flat plate motor sizes vary from 10 mm thickness to 50mm thickness and the diameter of rotor size varies from 2mm-20mm. The flat plate EC motor has an inbuilt quadrature encoder. The current trends in robotics research shifted to the placement of the plate motor [4]. These motors can easily be fitted between the joints. This research work focuses on the placing of the plate motor between the joints.

Controlling of 15_DOF finger joint is also a very tough task. A simple master and slave control architecture was used for the finger gripper control. The advantage of master and slave type control architecture did not put the controller to do computation. The Master is controlling the finger position and the slave is controlling each joint position. The feedback was sent to the master controller and the master controller the correction if any deviation happens while the interaction of the finger gripper during the grasping of the object.

2. MECHANICAL DESIGN

A 3-D model was prepared on the Solid work plate form. The dimension was kept approximately to the human finger dimension. The model consists of 15 joints. Each finger has three joints [5]. Each joint was connected with one flat plate motor. To simplify the control, one common shaft is connected to a flat plate motor. One motor is controlling the three joints simultaneously. The schematic details of the finger gripper are shown in figure 1.

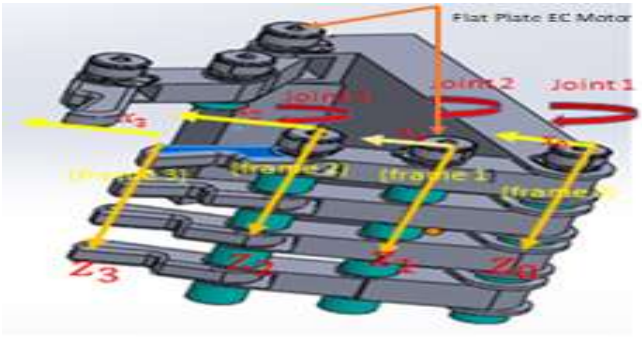

Figure 1. 3-D Modelling of Finger Gripper

3. CONTROL ARCHITECTURE

In its environment, a finger gripper completes the designated activities, which fall into two categories: contact-type tasks and non-contact-type jobs [6]. Actuators that impart a force or a torque to the links in order to move them are what power and drive each individual joint of a finger manipulator [7]. The manipulator control system gives the actuator commands necessary to move the manipulator and produce the desired end effector motion [8]. These instructions are based on the control set points produced from the collection of joint torque time histories that the trajectory planner collected. To obtain precise motion, the control system might be given back with the actual joint and/or end effector positions and their derivatives. The control system may use input on the actual joint locations and velocities, as indicated by the dotted lines for the feedback. The parameter q , $\dot{q}$ and $\ddot{q}$ and τ and so on. Joints cannot move independently, and a complex control algorithm will be required. A master control system that synchronises and controls n-joints makes up the usual robot control architecture for an n-DOF manipulator [9]. Sending "set point" instructions to each of the joint controllers is the responsibility of this master control. The set point data is used by the n-joint controllers to instruct the joint actuator to move the joint. The joint controller may employ feedback to the master controller. The Multi-Input –Multi-output (MIMO), nonlinear dynamics model of the n-DOF manipulator becomes

$$\tau = M(q)\ddot{q} + H(q,\dot{q}) + \dot{G}(q) \qquad (1)$$

Fig. 2. Manipulator control system

Because this controller is based on a more accurate dynamic model of a manipulator, it provides better trajectory performances than linear controllers do. The controller discussed here employs the computed torque control law to modify the system effectively decouple and linearize it [10]. The computed torque control scheme also comprises two portions- a model-based and a servo portion [11],[12]. The schematic diagram of a manipulator control system is shown in figure 2. The model-based portion defines the nx1 vector of control torques τ using a structure. Where $\dot{\tau}$ is the nx1 torque vector specified by the servoposition.

$\tau = M(q)\dot{\tau} + H(q,\dot{q}) + \dot{G}(q)$ (2)

$\dot{\tau} = \ddot{q}$ (3)

By using nonlinear feedback of the real locations and velocities of joints, the model-based portion efficiently linearizes and decouples the dynamics of the system. Figure 3 illustrates the schematic depiction of this nonlinear control strategy.

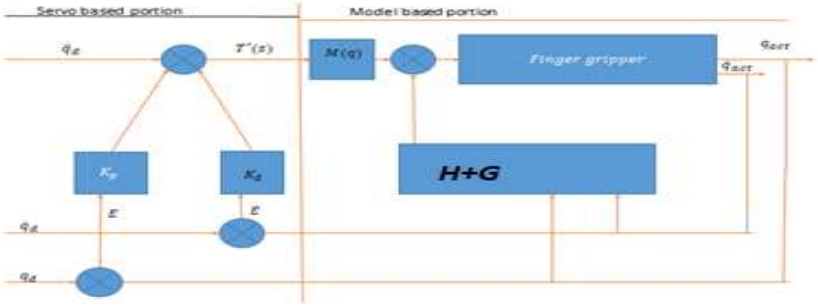

Fig .3. Control architecture of computed control

The control law of the servo portion based on the nx1 vectors E and $\dot{E}$ of the servo errors in joint positions and velocities, respectively. The servo portion of the computed torque control scheme is, therefore, defined as

$E(t) = q_d(t) - q(t)$ *(4)*

And $E(t) = \dot{q}_d(t) - \dot{q}(t)$ *(5)*

Where $q$and q_d denote the nx1 vectors of actual and desired joint positions respectively. The servo portion of the computed torque control scheme is, therefore, defined as

$\dot{\tau} = \ddot{q}_d + K_d\dot{E} + \dot{K}_pE$ *(6)*

Where $K_p$and K_d are the nxn matrices of position and velocity gains, respectively. Usually $K_p$and K_d are chosen as diagonal matrices with constant gains. This serves to decouple the error dynamics of the individual joints [13],[14]. The model of error behavior or error dynamics is obtained from

$\ddot{q} = \ddot{q}_d + K_d\dot{E} + \dot{K}_pE$ *(7)*

or with $\ddot{E} = \ddot{q}_d - \ddot{q}$ *(8)*

$\ddot{E} + K_d\dot{E} + \dot{K}_pE = 0$ *(9)*

This shows that the error dynamics of a closed–loop system are specified by a second-order linear error equation. This vector equation is decoupled if K_p and K_d are diagonal matrices with constant gain. Hence the error equation could be written on a joint-by-joint basis. For joint i the error equation is

$\ddot{e}_i + K_{di}\dot{e}_i + K_{pi}e_i = 0$ *(10)*

Where $K_{pi}$and K_{di} are the position and velocity gains, respectively, for joint i. For the critically damped performance of joints, the relationship between $K_{pi}$and K_{di} is obtained in equation i.e

$K_{di} = 2\sqrt{K_{pi}}$ *(11)*

3.1 Gain Parameter

The equation specifies the methodology for setting the control gains K_p and K_d.A direct consequence of the control law, equation, is that the servo error at any instant of time is zero provided there is no initial error and the computation time for the computer is zero, i.e the actuator torque is computed as a continuous function of time [15],[16]. In reality, the time taken to compute the servo error, the PD law control gains, and to command a new value of torque, is nonzero and is known as the cycle time. This

is the resulting command torque $\dot{\tau}_a$ is a staircase function and the servo error is non-zero at the beginning of each cycle [17]-[19]. The controller will reduce this nonzero servo error to zero during each cycle [20-23]. Based on these parameters the control gain K_p and K_d are computed as listed in Table1.

Table 1. Control gain values of K_p and K_d

Gain/Joint	K_p	K_d
Joint 1	12	8
Joint 2	10	6
Joint 3	8	4

Hence the actual trajectory tracked will be close to, but not the same as desired trajectory. Apart from a damping ratio of unity, another factor that constrains the selection of control gains is the flexibility of links, which are assumed to be rigid bodies in the development of the joint model. The unmodeled structural flexibility of the link and other mechanical elements produces resonance at frequencies other than natural frequency. Because these structural flexibilities have been ignored, the controller must be designed so as not to excite these unmoulded resonances. The lowest unmoulded resonance, which corresponds to the maximum value of the effective inertia seen by the actuator,I_{max} has a resonance frequency

$$\omega_{res} = \omega_o \sqrt{\frac{I_o}{I_{max}}} \qquad (12)$$

where ω_o is the structural frequency when the effective inertia is I_o. To prevent exciting these structural oscillations and also ensure structural stability, the controller's natural frequency ω_n must be limited to $0.5\omega_{res}$.i,e

$$\omega_n \leq 0.5\omega_{res} \text{ and } K_p \leq (0.5\omega_o)^2 \frac{I_o}{I_{max}} \qquad (13)$$

4. RESULTS AND DISCUSSION

The simulation was carried out for the planned trajectory of the different joints. The cubic spline polynomial equation has been used for trajectory planning. The boundary condition is applied at the start and end of the trajectory.

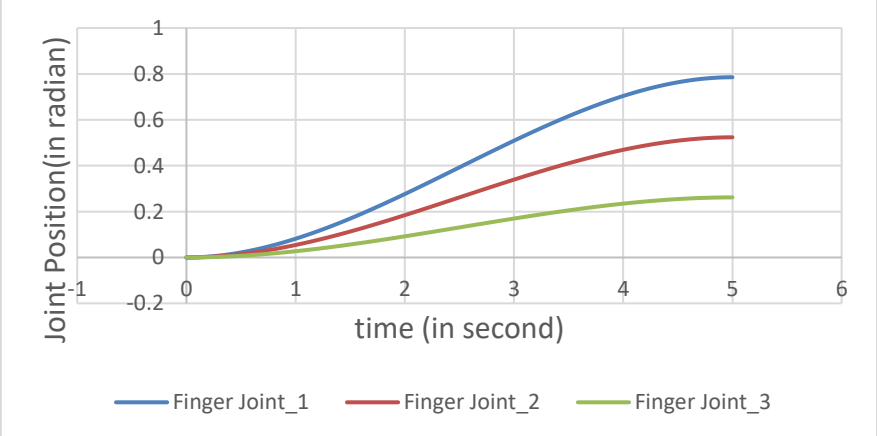

Fig .4. Planned trajectory

Initially, the joint position and velocity are zero. Hence there is no jerk coming at the start and the end of the motion. The cubic spline polynomial equation creates the smooth trajectory of the joint movement. The finger joint speed up for 2.5 seconds of travel and the next half comes to speed down. The simulation was carried out for 5 seconds for the minimum and maximum values of the individual joints. Figure 4 shows the finger joint position with respect to time. Coriolis and centrifugal force resist the motion of the finger joint to reach the desired position. The proportional gain and derivative gain were taken [12; 10; 8] and [8; 6:4] based on the values obtained from the equation. Tuning of the gain can increase the joint position reached near the grasped object. A deviation can be observed in figure 5 between the planned and actual trajectory of the finger

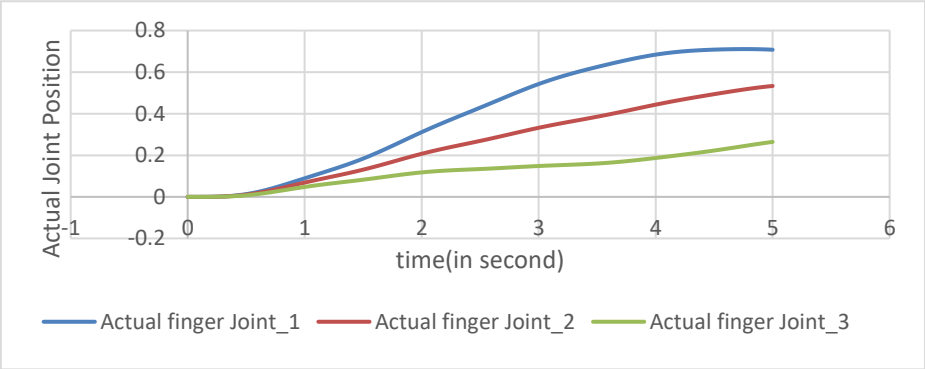

Fig .5. Actual trajectory of finger joint

5. CONCLUSION

A new finger gripper design was considered for the grasping of the unknown shape and size of the object in the unknown environment. The 3-point touch of the finger during an interaction makes the robotic finger gripper flexible. A large workspace was observed compared to the conventional design. The master-slave approach of the control system makes the system very easy to manipulate the object.

References

[1] M. Liu, L. Hao, W. Zhang, and Z. Zhao, "A novel design of shape-memory alloy-based soft robotic gripper with variable stiffness," *Int. J. Adv. Robot. Syst.*, vol. 17, no. 1, pp. 1–12, 2020, doi: 10.1177/1729881420907813.

[2] R. Kumar, N. J. Ahuja, M. Saxena, and A. Kumar, "Modelling and Simulation of Object Detection in Automotive Power Window," Indian J. Sci. Technol., 2016;9 (43) doi: 10.17485/ijst/2016/v9i43/104393.

[3] M. Honarpardaz, M. Tarkian, J. Ölvander, and X. Feng, "Finger design automation for industrial robot grippers: A review," *Rob. Auton. Syst.*, vol. 87, pp. 104–119, 2017, doi: 10.1016/j.robot.2016.10.003.

[4] R. Kumar, Divyanshu, and A. Kumar, "Nature Based Self-Learning Mechanism and Simulation of Automatic Control Smart Hybrid Antilock Braking System," Wirel. Pers. Commun., 2021; 116(4); 3291–3308 doi: 10.1007/s11277-020-07853-7.

[5] M. Kaur and W. S. Kim, "Toward a Smart Compliant Robotic Gripper Equipped with 3D-Designed Cellular Fingers," *Advanced Intelligent Systems*, vol. 1, no. 3. p. 1970032, 2019, doi: 10.1002/aisy.201970032.

[6] D. Bharadwaj and M. Prateek, "Kinematics and dynamics of lower body of autonomous humanoid Biped Robot," *Int. J. Innov. Technol. Explor. Eng.*, vol. 8, no. 4, 2019.

[7] D. Gan *et al.*, "Actuation-Coordinated Mobile Parallel Robots With Hybrid Mobile and Manipulation Functions," *J. Mech. Robot.*, vol. 14, no. 4, Mar. 2022, doi: 10.1115/1.4053821.

[8] M. Takizawa, S. Kudoh, and T. Suehiro, “Design and implementation of a multi-DOF hand and basic motions for rope-knotting tasks,” *Adv. Robot.*, vol. 36, no. 10, pp. 463–473, 2022, doi: 10.1080/01691864.2022.2070866.
[9] Kumar, R., Gupta, N., Bharadwaj, D., Dutt, D., & Joshi, A. (2022). Design and development of electronic clutch control unit for manual transmission. Materials Today: Proceedings. https://doi.org/10.1016/j.matpr.2022.08.470
[10] D. Bharadwaj, M. Prateek, and R. Sharma, “Development of reinforcement control algorithm of lower body of autonomous humanoid robot,” *Int. J. Recent Technol. Eng.*, vol. 8, no. 1, 2019.
[11] Kumar, R., Gupta, M. K., Kumar, A., Sharma, P., & Deorari, R. (2022). Analysis of electronic clutch control unit for manual transmission vehicle oriented toward safety. Materials Today: Proceedings. https://doi.org/10.1016/j.matpr.2022.08.473
[12] S. Nicosia and A. TORNAMBÈ, “Use of asymptotic observers in the parameter estimation of robotic manipulators having elastic joints,” *Adv. Robot.*, vol. 5, no. 4, pp. 349–376, 1990, doi: 10.1163/156855391X00250.
[13] R. Kumar, K. Bansal, A. Kumar, J. Yadav, M. K. Gupta, and V. K. Singh, “Renewable energy adoption: Design, development, and assessment of solar tree for the mountainous region,” Int. J. Energy Res. 2021; 1–17 doi: 10.1002/er.7197.
[14] H. Tourajizadeh and S. Manteghi, “Design and optimal control of dual-stage Stewart platform using Feedback-Linearized Quadratic Regulator,” *Adv. Robot.*, vol. 30, no. 20, pp. 1305–1321, 2016, doi: 10.1080/01691864.2016.1212735.
[15] R. Kumar, R. K. Pachauri, P. Badoni, D. Bharadwaj, U. Mittal, and A. Bisht, “Investigation on parallel hybrid electric bicycle along with issuer management system for mountainous region,” J. Clean. Prod., 2022; 362:132430, doi: 10.1016/j.jclepro.2022.132430.
[16] Kumar, R., Kumar, A., Gupta, M. K., Yadav, J., & Jain, A. (2022). Solar tree-based water pumping for assured irrigation in sustainable Indian agriculture environment. Sustainable Production and Consumption, 33, 15-27, doi.org/10.1016/j.spc.2022.06.013.
[17] R. Kumar, N. J. Ahuja, M. Saxena, and A. Kumar, “Automotive Power Window Communication with DTC Algorithm and Hardware-in-the Loop Testing,” Wirel. Pers. Commun., 2020;114 (4): 3351–3366 doi: 10.1007/s11277-020-07535-4.
[18] C. S. Meera, S. Sunny, R. Singh, P. S. Sairam, R. Kumar, and J. Emannuel, “Automated precise liquid transferring system,” 2014:1-6 doi: 10.1109/IICPE.2014.7115831.
[19] Kurre, S.K., Yadav, J., Thakur, S. (2022). Comparative Study of the Rear and Rear Side Impact on a Roll Cage Using FEM. In: Singh, M.K., Gautam, R.K. (eds) Recent Trends in Design, Materials and Manufacturing. Lecture Notes in Mechanical Engineering. Springer, Singapore. https://doi.org/10.1007/978-981-16-4083-4_37.
[20] Yadav, J., Kurre, S.K., Thakur, S. (2022). FEM-Based Impact Analysis of Roll Cage of an All-Terrain Vehicle. In: Singh, M.K., Gautam, R.K. (eds) Recent Trends in Design, Materials and Manufacturing. Lecture Notes in Mechanical Engineering. Springer, Singapore. https://doi.org/10.1007/978-981-16-4083-4_17.
[21] Yadav, Jitendra, Santosh Kumar Kurre, and Shubham Thakur. "Estimation of the dynamic response of roll cage under impact loading by modeling and simulation." Materials Today: Proceedings 50 (2022): 2181-2188. https://doi.org/10.1016/j.matpr.2021.09.445
[22] Yadav, Jitendra, et al. "Nonlinear dynamics of controlled release mechanism under boundary friction." Results in Engineering 11 (2021): https://doi.org/10.1016/j.rineng.2021.100265
[23] Dravid Shriram, Jitendra Yadav, and Santosh Kumar Kurre. "Comparison of loosening behavior of bolted joints using plain and spring washers with full-threaded and plain shank bolts." Mechanics Based Design of Structures and Machines (2021): 1-19. https://doi.org/10.1080/15397734.2021.2008258.

Optimum point trajectory tracking of a robotic manipulator system using Extremum Seeking control

Devendra Rawat, Mukul Kumar Gupta, Abhinav Sharma

Department of Electrical & Electronics, University of Petroleum & Energy Studies, Dehradun, India[1,2,3], Devendra.rawat85@gmail.com

Abstract.

Robotic manipulators have extensive applications including grasping, recognition, and viewpoint optimization. Trajectory tracking is extremely important in such applications. Some of the applications require the optimum tracking of trajectory. The complexity, uncertainty, and nonlinearities of the robotic manipulators make it difficult. Extremum-seeking control (ESC) gives the ability to track a varying maximum of a performance variable. It is an adaptive and model-free approach that provides the ability to track the optimum path of a robotic manipulator. In this paper, a perturbation-based ESC controller has been designed that tracks the optimum point of the trajectory of a robotic manipulator. Robotic manipulators being multi-input multi-output (MIMO) systems two objective functions are required. A sinusoidal perturbation has been added to the control input. Objective functions have been designed utilizing the control input. Furthermore, the applications of ESCs have been discussed and presented here, which imparts an understanding of this technique in various application areas.

Keywords. Extremum- seeking control, Robotic-manipulator, trajectory tracking.

1. INTRODUCTION

Robotic manipulators are highly uncertain, nonlinear, and complex systems. With the advent of technology robotic systems have gained much popularity and have been employed in many industrial applications. Robotic systems provide ease and comfort to human lives by embedding a certain amount of autonomy. Because of the large applications in industry effective control methods are extremely important. Researchers are continuously exploring ways to control these robotic systems and provide autonomous solutions for performing industrial tasks. ESC is a control strategy that tracks a varying maximum or minimum of a performance function [1]. This technique is an adaptive approach that adapts to parameter changes A sinusoidal perturbation is added to the control input u, making it perturbation type ESC. Based on the control law, this method provides the optimum value of the objective function [2]. In some applications, a robotic manipulator has to track the optimum position in the specified trajectory to perform the task, ESC can track that optimum value. In [6] the authors proposed a novel fractional order extremum seeking control (FOESC) that improved the convergence, robustness, and performance by incorporating the fractional calculus in ESC. Simulation and experimental analysis validate the proposed scheme and

show better performance as compared to the classic extremum-seeking algorithm. ESC provides a robust and stable response. *Meroslav Kristic et-al*. [7] performed stability analysis of ESC and proved the stability of ESC by averaging method and singular perturbation analysis further author suggested improvement in stability and performance of ESC by including a dynamic compensator in the ESC algorithm [8]. Researchers are continuously finding ways to improve the ESC. In [9], The authors designed a novel fast ESC to improve the static and dynamic performance of ESC without any steady state oscillations. In this paper, the authors designed the perturbation-based extremum-seeking controller for tracking of optimum trajectory value for a two-link robotic manipulator.

2. MATERIAL AND METHODS

The dynamics of a two-link robotic manipulator has been given as follows:

$$M(q)\ddot{q} + C(q,\dot{q})\dot{q} + G(q) = \tau \quad (1)$$

The $q, \dot{q}$ are the angular positions and velocities of both the links. *M(q)* is the mass matrix, *C(q)* is centripetal coriolis matrix and $G(q)$ is the gravitational force and τ is the applied torque to the robot manipulator. This section illustrates the ESC technique, types of ESC and its applications in various sectors.

2.1. Extremum Seeking Control (ESC)

Tracking a varying maximum or minimum of a performance function called extremum seeking control [1]. It is an equation-free adaptive control approach that adapts to parameter changes. It is an optimization technique in which a sinusoidal perturbation is added to the control input u. Based on the control law, this method provides the optimum value of the objective function [2]. Extremum-seeking controller tracks that optimum value. Extremum-seeking control is a local optimizer and changes in the system dynamics are faster than the perturbations. Figure 1. describes the extremum-seeking control method.

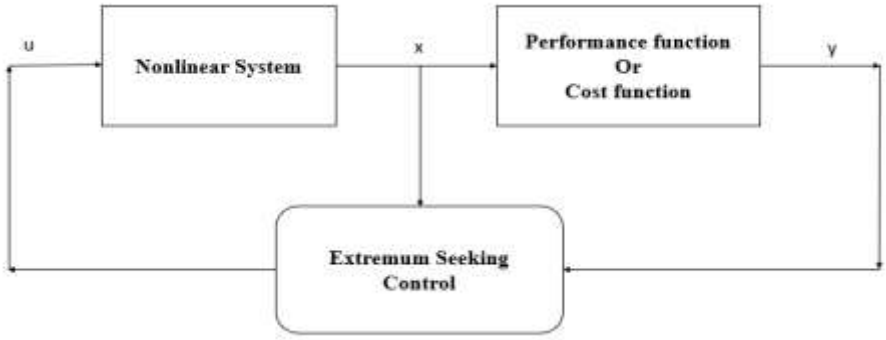

Figure 1. Block diagram of Extremum Seeking Control

Berk Calli et.al. [4] presented a detailed analysis of the ESC techniques by performing a comparison and robustness analysis of each of the ESC techniques. Authors characterized these techniques as sliding mode ESC, neural network-based ESC, approximation-based ESC, and adaptive ESC. Robotic systems have high nonlinearities, uncertain dynamics, and high disturbance, perturbation-based ESC gives robust trajectory performance. In

conclusion, the authors suggested the use of approximation-based ESC when noise is not much effective, neural network ESC is preferred in the presence of significant noise while perturbation-based ESC is much more effective when a high level of noise and uncertain dynamic effects are present. Thus, perturbation-based ESC is found to be the most robust. ESC techniques are classified as shown in Figure 2. [4].

Figure 2. Classification of Extremum Seeking Control Techniques [4][5]

2.2. Applications of ESC

Extremum-seeking control is suitable for the system's disturbances and variations in the parameters. It has applications in areas like renewable energy (solar array optimization), the automotive industry, and robotic systems [3]. ESCs have applications in the systems that have disturbances and variations in the parameters over time. ESCs find applications in most of the fields mainly the have applications in Automotive Industry, Renewable energy, process control, and robotic systems. ESC is a model-free approach this property makes it popular thus ESC finds applications in many different areas where the optimum value is required. *Denis dochain et.al.* [10] presented a survey of ESC techniques and their applications to process and reaction systems. The authors implemented two approaches the perturbation-based ESC and model-based ESC on an isothermal reaction system. For model-based approaches, two conditions namely model structure is known and unknown have been used. Simulation results show the stability and convergence of both control approaches. In [11] [12], the authors presented an adaptive ESC for continuous stirred tank bioreactors and a non-isothermal CSTR without knowing much about the growth dynamics. An adaptive seeking algorithm has been implemented to maximize the cost function. ESC has been used in renewable energy for applications like solar array optimization and wind turbine power enhancement. Due to varying external conditions, sometimes it is required to change the operating conditions to get the desired power output out of the system. This is referred to as solar array optimization and maximum power point tracking. In [13] authors presented the maximum power point tracking using ESC. Researchers [14] [15] have been implanting this technique in solar energy to get the maximum power through optimization of the parameters. In [16], the authors have designed the ESC to maximize the power output of a wind turbine with load reduction. Control and optimization of power in wind energy [17] [18] systems find wide applications of ESC. Automotive electronics is a rapidly improving industrial application that imparts safety and comfort to human beings. ESC finds applications in

antilock braking system (ABS) design [19] to optimize the forces applied on the breaks. Thus, ESC has wide applications in various fields.

3. RESULTS AND DISCUSSIONS

Robotic manipulators being highly nonlinear, uncertain, and multi-input multi-output (MIMO) systems, two separate ESCs using two different objective functions have been designed for two different links. A cubic polynomial trajectory has been considered as the reference, having optimum values of π/4 and π/6 respectively. J_1 and J_2 are the objective functions used to track the optimum value of trajectories of the links.

$$J_1 = (pi/4) - (0.89 - u)\text{^}2 + C \tag{2}$$

$$J_2 = (pi/6) - (0.72 - u)\text{^}2 + C \tag{3}$$

u is a control input, and a sinusoidal perturbation is added to this control input. C is a constant term. Figure 3. shows the reference cubic polynomial trajectory of both links.

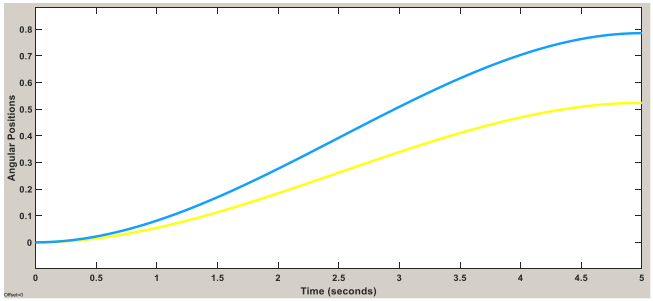

Figure 3. References Trajectories

Figure 4. shows the output of ESC for both links. Figure 5. shows the optimum value trajectory tracking for both links, where both objective functions have been able to track the optimum value of trajectories. It is clear from both figures that the designed controller is able to seek the optimum value in the reference trajectories.

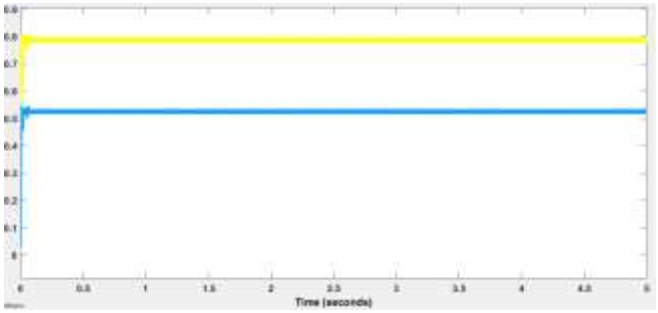

Figure 4. Output of ESC

The Simulink model of the ESC has been shown in Figure 6. The polynomial trajectory as shown in Figure 3. has been given as a reference. A sinusoidal perturbation has been included in the control law, this changes the control law and estimates the best input.

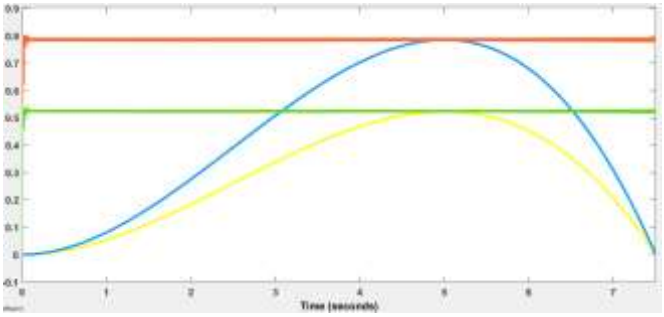

Figure 5. optimum value tracking of the reference trajectory

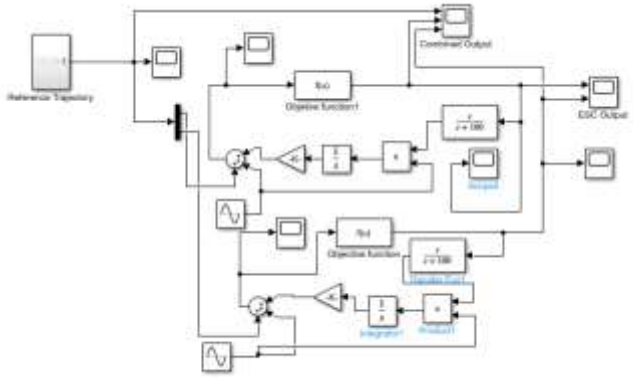

Figure 6. Simulink diagram of ESC design of robotic manipulator.

Two different objective functions have been incorporated each on the different links of a robotic manipulator. The output of the proposed controller has been shown in ESC output.

4. CONCLUSION

Robotic manipulators have various applications in industry, some of the applications require tracking of optimum value of the desired trajectory. Because of the complex, nonlinear, and uncertain nature of the robotic system, it becomes much more difficult to track the optimum value in such applications. Extremum-seeking control is a real-time adaptive optimization approach that adapts the system parameters to unknown dynamics with the help of an objective function. In this paper, a perturbation-based ESC is designed to track the optimum value of the cubic reference trajectory with the help of the objective functions. Because of the MIMO nature of robotic manipulators, two objective functions have been designed utilizing the control input. Furthermore, the applications of ESCs have been discussed and presented here, which imparts an understanding of this technique in various application areas.

5. REFERENCES

[1] Z. Chunlei, R. Ordóñez, 'Extremum-seeking control and applications: a numerical optimization-based approach', Springer Science & Business Media, 2011.

[2] A. Kartik, M. Krstic, Real-time optimization by extremum-seeking control. John Wiley & Sons, 2003.

[3] M. Kristic, H-H. Wang, 'Stability of extremum seeking feedback for general nonlinear dynamic systems', Automatica-Kidlington 36.4, pp.595-602, 2002.

[4] B. Calli. et. al., Comparison of extremum seeking control algorithms for robotic applications, Int. Conf. on Intelligent Robots and Systems. pp. 3195-3202, 2012.

[5] C. Olalla, et.al., 'Analysis and comparison of extremum seeking control techniques', IEEE Inter Symposium on Industrial Electronics, pp. 72-76, 2007.

[6] H. Malek, Y. Chen, 'Fractional order extremum seeking control: performance and stability analysis', IEEE/ASME Transactions on Mechatronics, 21(3), pp.1620-1628, 2016.

[7] M. Krstic, H.H. Wang, 'Stability of extremum seeking feedback for general nonlinear dynamic systems' Automatica-Kidlington, 36(4), pp. 595-602, 2000.

[8] M. Krstić, 'Performance improvement and limitations in extremum seeking contol', Systems & Control Letters, 39(5), pp.313-326, 2000.

[9] L. Wang, S.Chen, K. Ma, 'On stability and application of extremum seeking control without steady-state oscillation', Automatica, 68, pp.18-26, 2016

[10] D. Dochain, M. Perrier, M. Guay, 'Extremum seeking control and its application to process and reaction systems: A survey', Mathematics and Computers in Simulation 82.3, pp.369-380, 2011.

[11] M. Guay, D. Dochain and M. Perrier, 'Adaptive Extremum Seeking Control of Continuous Stirred Tank Bioreactors with Unknown Growth Kinetics', Automatica, 40, pp.881-888, 2004.

[12] M. Guay, D. Dochain, M. Perrier, 'Adaptive extremum seeking control of nonisothermal CSTR', Chem. Eng. Science, 60(13), pp. 3671-3681, 2005.

[13] S.L. Brunton, et. al., 'Maximum power point tracking for photovoltaic optimization using ripple-based extremum seeking control' 'IEEE transactions on power electronics 25(10) pp.2531-2540, 2010.

[14] N. Bizon, 'Global Maximum Power Point Tracking (GMPPT) of Photovoltaic array using the Extremum Seeking Control (ESC): A review and a new GMPPT ESC scheme', Renewable and Sustainable Energy Reviews 57, pp. 524-539,2016.

[15] R. Leyva, et. al., 'MPPT based on sinusoidal extremum-seeking control in PV generation', International Journal of Photoenergy 2012.

[16] Y. Xiao, Y. Li, M.A. Rotea, 'Multi-objective extremum seeking control for enhancement of wind turbine power capture with load reduction', Journal of Physics: Conference Series. Vol. 753. No. 5. IOP Publishing, 2016.

[17] A. Ghaffari, M. Kristic, S. Seshagiri, 'Power optimization and control in wind energy conversion systems using extremum seeking', IEEE transactions on control systems technology 22.5, pp.1684-1695, 2014.

[18] Z. Chunlei, R. Ordonez, 'Numerical optimization-based extremum seeking control with application to ABS design', IEEE Transactions on Automatic Control 52.3 pp. 454-467, 2007.

[19] D. Erkin, B. A. Güvenç, T. Acarman, 'Extremum-seeking control of ABS braking in road vehicles with lateral force improvement', IEEE Transactions on Control Systems Technology 22.1, pp. 230-237, 2012.

Design and Development of Alcohol Detection Sensor Mechanism for Safe Driving in Automobile

Jitendra Yadav *, Santosh Kumar Kurre, Shubham Thakur
Department of Mechanical Engineering, School of Engineering, University of Petroleum and Energy Studies, Bidholi, Dehradun-248007, India.
Author Emails
** Corresponding author: jyadav@ddn.upes.ac.in*

Abstract

The present work describes the design and develop an alcohol detection sensor system that ensures safe driving of vehicle. The mechanism is capable of instrumenting a locking system that will ensure the start of vehicle only after checking the level of alcohol taken by the driver. The proposed system make use of pre-existing alcohol sensor (MQ-3), which is integrated with Arduino board. The system is also capable of sending the messages to the nearest competent authorities and dear one's of the driver, as soon as alcohol consumption is detected through the app integrated with the system. This paper includes designing of the sensor, Algorithm for app development, material description for the sensor. The proposed work if adopted as a regulation by the government agencies, will lead to prevent many casualties due to road accidents.
Keywords: Locking system, MQ-3, Arduino, App development.

1. INTRODUCTION

Product development and simulation has emerged as a powerful research tool [1-3]. A lot of work have been reported on research on vehicle performances in terms ensuring vehicle safe design [4-6] and modification in functionalities [7-10], but a very few work have been reported about the proficiency of driver. The increased hazardous rate due to road accidents by the consumption of alcohol should be the area of concern for the automobile industries and government agencies. There is a need of design, development and implementation of an alcohol detection sensor mechanism which will be primarily targeting on saving lives of people by not allowing the driver to start the car with alcohol consumption. The consumption of liquor is a typical propensity in numerous societies, related with customs' merriments, however even a little amount of liquor will influence human behavior [11]. In the past there had been many researches done on detecting toxic gases, vehicle location and accident, instrumenting locking system of vehicle for security purposes, implementation SMS based alcohol detection with vehicle controlling etc. Safety of vehicle is of prime concern amongst these aspects. Public safety in general and roads safety in particular. The idea is characterized by being deliberately dependent on personal contribution [12]. Research are continuously being done to get optimum solutions for tracking and locking automatically. The automobile industries are now also considering these issues seriously [13].
Many researches have been found in literature on using GPS and GSM module for tracking but the information that was provided through it, was sometimes a bit confusing in exact identification, because the SMS receives location in terms of latitudes and Longitude, which is tough to interpreter. K Sandeep et al. [14] proposed the use of the Internet of things (IOT) device as Raspberry Pi three model B as a core. It mainly includes Touch sensor, alcohol concentration detection sensor, Facial recognition, Heart beat rate, to safeguard the drowsy driver. Izanoordi Ahmad et al. [15] Proposed a model based on MQ-3 alcohol sensor with HC-05 Bluetooth module. Whenever system crosses the threshold value of alcohol the system is used to send the message to one of its relative via Bluetooth transmission. S.V. Altaf et al. [16] used MQ-3 alcohol sensor with microcontroller ATS8951 in which the sensor was fitted in front of the driver seat. The proposed system work on the concept when MQ-3 sensor detects the alcohol the car ignition will immediately will be turned off and it detects while driving then it will reduce the fuel supply [17-22].

However a lot of work is done to provide the safe driving mechanism but a lot has remained in term of integration of these technologies for the optimal solution. Present work provides a way to deal with the most sophisticated and advanced system which prohibits the driving by a alcohol consumed person. The present work addresses the development of an alcohol sensor by using pre-existing technologies followed by app development on android studio [22-29]. The safeguards are provided with the help of GPS module, Triggering an alarm and Automatic ignition off etc. Alcohol sensor mechanism is developed with the help of MQ-3 sensor, Microcontroller (ATS 8051), LCD Display, Buzzer, Relay, Analog to Digital Converter, DC Motor (For System Demonstration), GPS and GSM Module followed by CATIA model, proteus model and value proposition canvas. The app was

developed on android studio [29-32]. The main purpose of the app is to send the location of a car with drunk driver to one of its family member and competent authority.

2. PROPOSED SYSTEM

The Prosed system is shown in figure 1. Alcohol sensor mechanism is developed with the help of MQ-3 sensor, Microcontroller (ATS 8051), LCD Display, Buzzer, Relay, Analog to Digital Converter, DC Motor (For System Demonstration), GPS and GSM Module followed by CATIA model, proteus model and value proposition canvas.

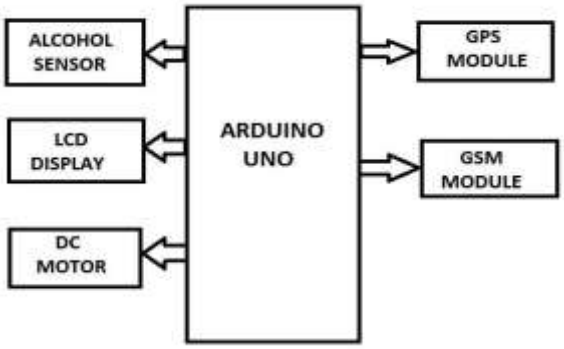

Figure 1 Proposed system

2.1 MQ-3 Sensors

MQ-3 Model is based on Taguchi design with a coating of oxide sensing[8]. In MQ-3 MQ stands for metal oxide semi-conductor (MOS) type gas sensor. MQ-3 sensor provide fine range for detection of alcohol particles in the air varies from 25 to 50 ppm with a accuracy of +/- 6.7 ppm and it is suitable for making breathalyzer. The MQ-3 sensor works on 5V draws 800MV. Table 1 shows the specification of MQ-3.

Table1: Specification of MQ-3 sensor

Operating voltage	5V
Load resistance	200 KΩ
Heater resistance	33Ω ± 5%
Heating consumption	<800mw
Sensing Resistance	1 MΩ – 8 MΩ
Concentration Scope	25 – 500 ppm
Preheat Time	Over 24 hour

2.2 Analog to Digital Converter

Analog to digital converter allows microcontroller ATS8051 to complete it circuit. Analogue signal regularly change their value, which come from mQ-3 sensor. In analog signal there is continuous change in value in terms of voltage, sensors while in case of binary the representation of value is only in one and zero so, here analog to digital converter comes into play which shows real life value which is easily monitored.

2.3 Microcontroller ATS8051

Microcontroller consist of CPU, Ram, and it is the main part of the system. The microcontroller has bit address for data, which makes transmission of data, which make transmission of data very smooth. The single chip contain four port, two timers and one serial port and during assembly, it can be easily programmed.

2.4 LCD Display

LCD stands for liquid crystal display it is a flat board display or other electronically adjusted optical equipment, which do not transmit light straight forward. LCD is made of substance, which is permanent liquid substance LCD provide a good quality contrast, brightness and clear images.

2.5 GPS and GSM Module

GPS module is used for tracking it is a satellite based navigation system. GPS is used to navigate or locate the location of cars. GPS convert received signal into longitude and latitude. GSM Module is a technology of second generation (2G). GSM is a cost-effective device, which applies sim card of any operator to transmit message from one person to another person. The model will also send the message of whereabouts of the vehicle through SIM900A. Another reason to choose GSM Module is that it support all mobile system.

2.6 Relay

Relay is very important part of the circuit as relay helps in closing and opening of the circuit if the relay is open it energized the circuit while if relay is closed it does not energized the circuit and if the circuit of the relay analyze the fault current in the circuit it give energy to the magnetic which produce magnetic field. It works on the principle of electromagnetic attraction.

3. METHODOLOGY

The experimental set for the sensor is shown in figure 2. For assembling of sensors, we are using pre-existing technologies. Microcontroller act as a heart of the system [6]. The main eight components for development of sensor are MQ-3 sensor, Microcontroller ATS8051, Analog to Digital Converter, GPS and GSM Module, LCD Display, Buzzer, Relay, DC Motor (For System Demonstration) and there are other off components which are in use. The flow chart works when a person sitting inside a car on driver seat has consumed alcohol or not. If person has not consumed alcohol then car will run smoothly else, if MQ-3 sensor detects alcohol particles in the air then it will show the value of alcohol concentration on LCD display if value is more than recommended level the microcontroller give signal to buzzer circuit and buzzer is turned on and at the same time relay is turned off due to this ignition of the car is deactivated. Alcohol detection system with buzzer indicate project is extend by adding an ignition key at the input and a DC motor at a output. The input ignition key is given to the microcontroller. It is used to find out the car whenever a car is started whenever a key is inserted into the ignition lock at the that time the alcohol detection process is started [17] as soon as alcohol detects sensors GPS and GSM Module comes into play it will helping us in sending the location to one of its family member to pick up from the location and the location will be shared through the app developed during this project. The proteus model is also developed for this project.

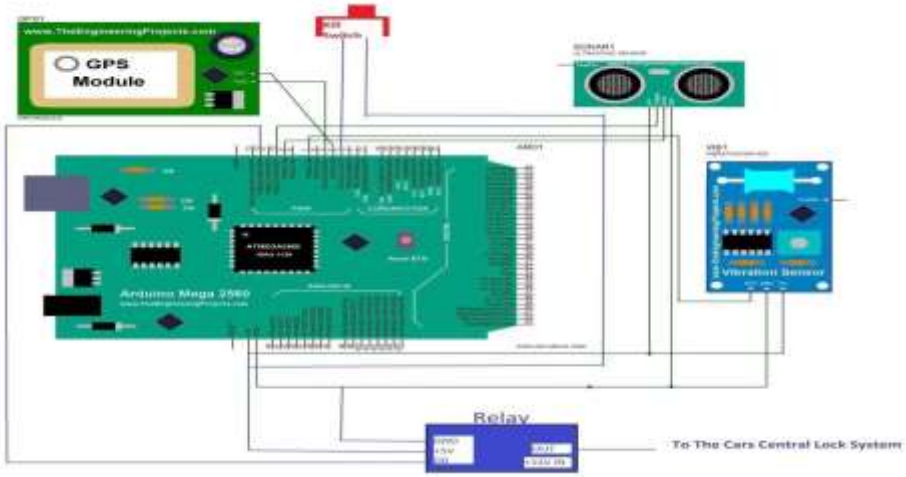

Figure 2 Experimental set up of sensors

4. RESULTS AND DISCUSSION

4.1 Modelling of the Sensors

In development of any prototype designing plays an important role In order to understand the dimension, size, function. The sensor is designed in such a way that it will easily install on the steering of the car keeping in mind that MQ-3 sensor has a fine sensitivity range of 2 meter. Figure 3 shows the drafting model of the sensors.

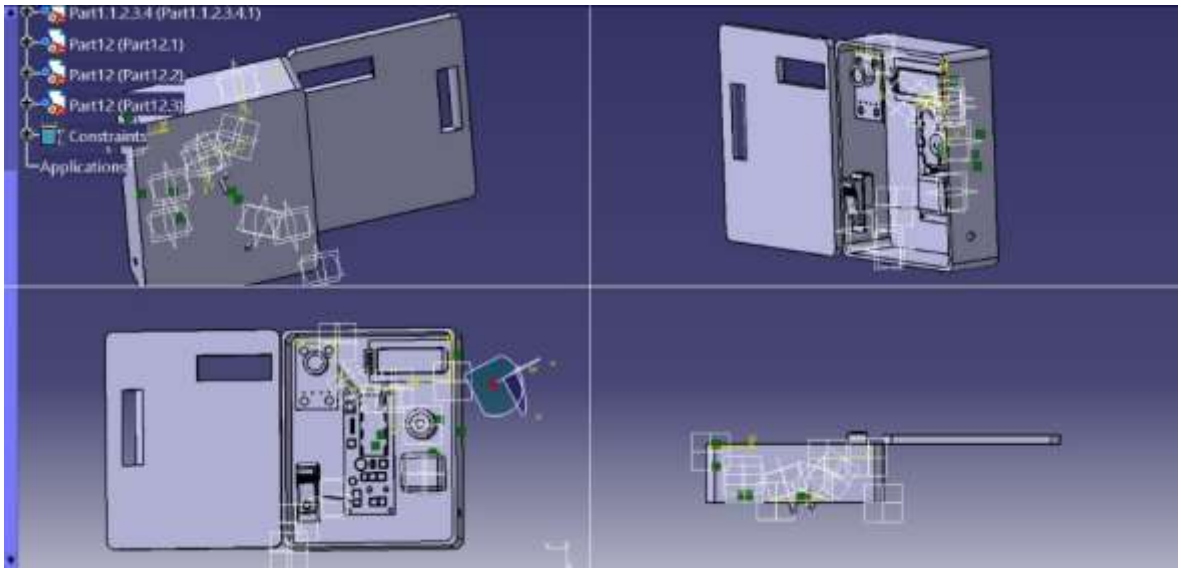

Figure 3 Drafting model of the sensors

4.2 Algorithm for an App Development

Figure 4 shows interface of an app development. The steps for algorithm for the app development is as follows:
Step 1- Getting the Google Map API key
Step 2- Create a New Android Project
Step 3- Select Google Map Activity, click next, and finish.
Step 4- Open google_map_api.xml, where you will enter the Google Map API KEY and now build the Gradle.

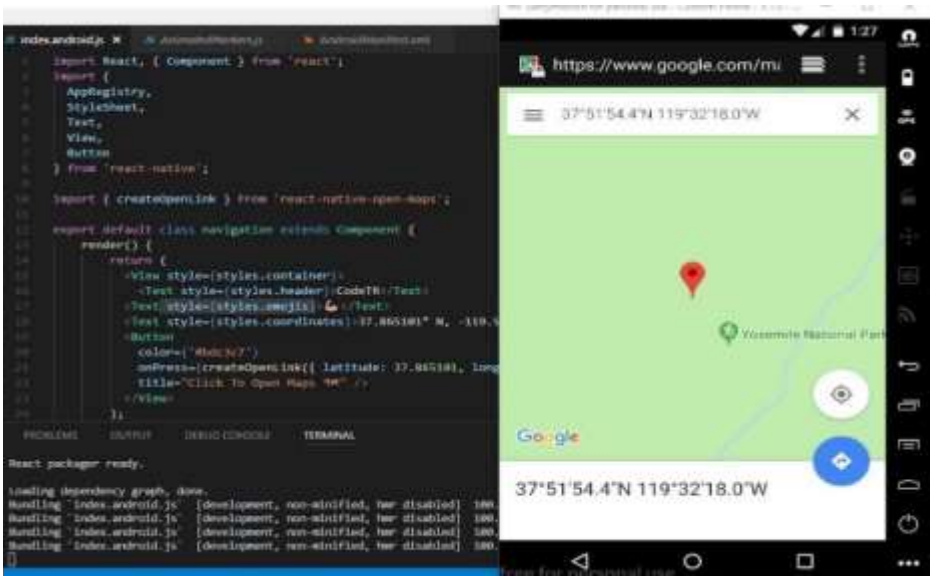

Figure 4: Interface of an app development

Step 5- Define internet and location permission in Android Manifest
Access_fine_location
Internet
Step 6- Code MapsActivity.java file for inserting functions in Google Maps.
Step 7-Functions needed
OnMapReady () - it is used when the map is ready to use.

OnConnected ()-when device connection is successful.
OnConnectionSuspended ()-device is in disconnected state.
OnConnectionFailed ()-failed to connect.
OnLocationChanged ()-when there is change in location of device.
GoogleApiClient () - build this to use google play services to ensure that the permissions are granted and to build its object and add API () to specify which API are requested by your app.
AddConnectionCallbacks () - to receive connection events from GoogleApiClient ().
AddOnConnectionFailedListener () - to receive connection failed events from GoogleApiClient ()
Step 8- Change map types, zoom controls.
Step 9 - Run the app with internet connections.

5. CONCLUSION

The proposal system check whether the person has consumed alcohol or not while driving the car, which will help us in reducing in car accident due to drunk driving. The project is categorized into three parts. The first part discuss about the electronic control unit that is used in this prototype that comprises of Arduino board, Sensor, Microcontroller. The second part is designing of the sensor to check the compatibility, availability of the passage in the car to fix it. The third category comprises of development of a navigation system to locate the car.

REFERENCE

1. Yadav J., Pitta P., Maan A. (2018) Swisng Tower of Loader Backhoe Arm for Dynamics and Stress Analysis by Modeling and Simulation. In: Siddiqui N., Tauseef S., Abbasi S., Rangwala A. (eds) Advances in Fire and Process Safety. Springer Transactions in Civil and Environmental Engineering. Springer, Singapore https://doi.org/10.1007/978-981-10-7281-9_18
2. Maan A., Pitta P., Yadav J. (2018) Performance Evaluation of Rectangular Fins by Modeling and Simulations. In: Siddiqui N., Tauseef S., Abbasi S., Rangwala A. (eds) Advances in Fire and Process Safety. Springer Transactions in Civil and Environmental Engineering. Springer, Singapore 10.1007/978-981-10-7281-9_26
3. Yadav, Jitendra, et al. "Nonlinear dynamics of controlled release mechanism under boundary friction." Results in Engineering 11 (2021): https://doi.org/10.1016/j.rineng.2021.100265
4. Yadav, J., Kurre, S.K., Thakur, S. (2022). FEM-Based Impact Analysis of Roll Cage of an All-Terrain Vehicle. In: Singh, M.K., Gautam, R.K. (eds) Recent Trends in Design, Materials and Manufacturing. Lecture Notes in Mechanical Engineering. Springer, Singapore. https://doi.org/10.1007/978-981-16-4083-4_17
5. Yadav, Jitendra, Santosh Kumar Kurre, and Shubham Thakur. "Estimation of the dynamic response of roll cage under impact loading by modeling and simulation." Materials Today: Proceedings 50 (2022): 2181-2188. https://doi.org/10.1016/j.matpr.2021.09.445
6. Kurre, S.K., Yadav, J., Thakur, S. (2022). Comparative Study of the Rear and Rear Side Impact on a Roll Cage Using FEM. In: Singh, M.K., Gautam, R.K. (eds) Recent Trends in Design, Materials and Manufacturing. Lecture Notes in Mechanical Engineering. Springer, Singapore. https://doi.org/10.1007/978-981-16-4083-4_37
7. R. Kumar and A. Kumar, “Design and hardware development of power window control mechanism using microcontroller,” 2013 Int. Conf. Signal Process. Commun. ICSC 2013;61–365 doi: 10.1109/ICSPCom.2013.6719813.
8. R. Kumar, N. J. Ahuja, and M. Saxena, “Improvement and approval of impediment recognition and activity for power window,” 2018, doi: 10.1007/978-981-10-5903-2_89.
9. R. Kumar, N. J. Ahuja, M. Saxena, and A. Kumar, “Modelling and Simulation of Object Detection in Automotive Power Window,” Indian J. Sci. Technol., 2016;9 (43) doi: 10.17485/ijst/2016/v9i43/104393.
10. R. Kumar, Divyanshu, and A. Kumar, “Nature Based Self-Learning Mechanism and Simulation of Automatic Control Smart Hybrid Antilock Braking System,” Wirel. Pers. Commun., 2021; 116(4); 3291–3308 doi: 10.1007/s11277-020-07853-7.
11. Gasparesc, G. (2018). Driver Alcohol Detection System Based on Virtual Instrumentation. IFAC-PapersOnLine, 51(6), 502–507. https://doi.org/10.1016/j.ifacol.2018.07.110
12. Al-Youif, S., Ali, M. A. M., & Mohammed, M. N. (2018). Alcohol detection for car locking system. ISCAIE 2018 IEEE Symposium on Computer Applications and Industrial Electronics, 230–233. https://doi.org/10.1109/ISCAIE.2018.8405475
13. Prof. Bhavana Patil, Harsh Amrite, Kailas Gaikwad, J. D. & S. H. (2018). smart car monitoring system using Arduino. International Research Journal of Engineering and Technology (IRJET), 05(03), 1554–1557. www.irjet.net

14. Sandeep, K., Ravikumar, P., & Ranjith, S. (2017). Novel Drunken Driving Detection and Prevention Models Using Internet of Things. Proceedings - 2017 International Conference on Recent Trends in Electrical, Electronics and Computing Technologies, ICRTEECT 2017, 2017-Decem, 145–149. https://doi.org/10.1109/ICRTEECT.2017.38
15. Ahmad, I., Suhaimi, M. F., & Yusri, N. A. N. (2019). Development of alcohol sensor detector with engine locking system for accident prevention. AIP Conference Proceedings, 2129(July), 1–7. https://doi.org/10.1063/1.5118204
16. Altaf, S. V, Abhinay, S., Ansari, E., & Anwer, R. (2017). Alcohol Detection and Motor Locking System. International Journal of Advanced Research in Electrical, Electronics and Instrumentation Engineering, 6(2), 989–993.https://doi.org/10.15662/IJAREEIE.2017.0602062
17. Krivec, M., Mc Gunnigle, G., Abram, A., Maier, D., Waldner, R., Gostner, J. M., Überall, F., & Leitner, R. (2015). Quantitative ethylene measurements with MOx chemiresistive sensors at different relative air humidities. Sensors (Switzerland), 15(11), 28088–28098. https://doi.org/10.3390/s151128088
18. R. Kumar, R. K. Pachauri, P. Badoni, D. Bharadwaj, U. Mittal, and A. Bisht, "Investigation on parallel hybrid electric bicycle along with issuer management system for mountainous region," J. Clean. Prod., 2022; 362:132430, doi: 10.1016/j.jclepro.2022.132430.
19. Kumar, R., Kumar, A., Gupta, M. K., Yadav, J., & Jain, A. (2022). Solar tree-based water pumping for assured irrigation in sustainable Indian agriculture environment. Sustainable Production and Consumption, 33, 15-27, doi.org/10.1016/j.spc.2022.06.013.
20. R. Kumar, N. J. Ahuja, M. Saxena, and A. Kumar, "Automotive Power Window Communication with DTC Algorithm and Hardware-in-the Loop Testing," Wirel. Pers. Commun., 2020;114 (4): 3351–3366 doi: 10.1007/s11277-020-07535-4.
21. C. S. Meera, S. Sunny, R. Singh, P. S. Sairam, R. Kumar, and J. Emannuel, "Automated precise liquid transferring system," 2014:1-6 doi: 10.1109/IICPE.2014.7115831.
22. A. Pal, R. Kumar, and V. R. Sanal Kumar, "Conceptual design of an automatic fluid level controller for aerospace applications," Proc. IEEE Int. Conf. Soft-Computing Netw. Secur. ICSNS 2015, 2015, doi: 10.1109/ICSNS.2015.7292433.
23. R. Kumar, K. Bansal, A. Kumar, J. Yadav, M. K. Gupta, and V. K. Singh, "Renewable energy adoption: Design, development, and assessment of solar tree for the mountainous region," Int. J. Energy Res. 2021; 1–17 doi: 10.1002/er.7197.
24. Yadav, Jitendra, et al. "Identification of damping prohibiting stick-slip form friction influenced dynamic system." Proceedings of the Institution of Mechanical Engineers, Part C: Journal of Mechanical Engineering Science (2022): 09544062221135517.
25. R. Kumar, P. K. Dwivedi, D. Praveen Reddy, and A. S. Das, "Design and implementation of hydraulic motor based elevator system," 2015, doi: 10.1109/IICPE.2014.7115821.
26. A. S. Das, P. K. Dwivedi, A. K. Mondal, R. Kumar, R. M. Reddy, and A. Kumar, "Storage optimization of automated storage and retrieval systems using breadth-first search algorithm," 2017, doi: 10.1007/978-981-10-2999-8_18.
27. A. Kumar, K. Bansal, D. Kumar, A. Devrari, R. Kumar, and P. Mani, "FPGA application for wireless monitoring in power plant," Nucl. Eng. Technol.2020; 53(4); 1167–1175 doi: 10.1016/j.net.2020.09.003.
28. Dravid Shriram, Jitendra Yadav, and Santosh Kumar Kurre. "Comparison of loosening behavior of bolted joints using plain and spring washers with full-threaded and plain shank bolts." Mechanics Based Design of Structures and Machines (2021): 1-19.
29. Yadav J., Agnihotri G. (2018) Circumvention of Friction-Induced Stick-Slip Vibration by Modeling and Simulation. In: Singh R., Choudhury S., Gehlot A. (eds) Intelligent Communication, Control and Devices. Advances in Intelligent Systems and Computing, vol 624. Springer, Singapore
30. Jitendra Yadav and Geeta Agnihotri (2017), "Modeling and Simulation of the Dynamic Response of a Generic Mechanical Linkage for Control Application Under the Consideration of Nonlinearities Imposed by Friction", In Springer Proceedings of the International Conference on Nano-electronics, Circuits & Communication Systems, Lecture Notes in Electrical Engineering 403, DOI 10.1007/978-981-10-2999-8_26
31. Jitendra Yadav & G. Agnihotri, "Proposed Critical Damping for a Spring Mass System to Avoid Stick Slip" ,Springer Journal of the institution of engineers (India): Series C Volume 96, Number 3, PP 331-335, July-September 2015.
32. Jitendra Yadav & G. Agnihotri, "Modeling and simulation of hydraulic actuator with viscous friction", International Journal of Advanced Technology in Engineering and Science, Volume No 03, Special Issue No. 01, March 2015

The impact & usage of digital payment system in India during the Covid-19 pandemic

Ajay Prasad Nautiyal[1], Sapna Bisht[2], Kapil Rajput[3]

[1]*Department of Computer Science Engineering Uttaranchal University, ajaynautiyal16@gmail.com*

[2]*Department of Civil Engineering Uttaranchal University, sapnabisht18@gmail.com*

[3]*Department of Computer Science Engineering Uttaranchal University, kapilrajput1984@gmail.com*

Abstract.

The COVID-19 pandemic spread the use of digital & online modes of payment, according to the Annual report 2020-21 by RBI. The prospects for FinTech in India's financial system in 2021-2022, according to the RBI, would be determined by the degree to which digital usage has become entrenched. During the lockdown period of the Covid19 pandemic, the usage of online transactions and electronic currency transfers was motivated. Furthermore, the use of digital payment and e-wallets should be motivated to avoid unnecessary bank visits, apply social distancing, avoid physical contact while exchanging cash in the presence of the COVID-19 pandemic in India, and to give a positive attitude among Indian people toward cashless economy adoption. The goal of this research was to look into the use of digital payments and e-wallets.

Keywords. Covid-19, digital payment, lockdown, e-wallets.

1. INTRODUCTION

During the Covid19 lockdown, the use of electronic transactions skyrocketed in order to reduce the number of physical visits to bank branches around the country (by Oliver-Balch 2020). The number of people visiting the bank branch was also reduced as a result of the lockdown. Due to the growth of electronic commerce and the increased use of digital and virtual payment methods, the Global Payment Gateways Processing Solutions Market (GPGPSM) forecasted the trend of the payment gateways industry up to 2024, amid and after Covid-19, and the global payment market is expected to grow $23.40 USD billion in the years 2020-24. (by Jesse Maida (2020)) [1].

Instead of physical transactions, digital payment and e-wallets allow consumers to conduct cashless transactions via mobile applications or online banking. Open digital wallets, semi-closed e-wallets, and closed e-wallets are the three categories of e-wallets. Some e-wallet

applications do not require a bank account, and users can conduct digital transactions using digital money deposited into the application (Octal IT Solution, 2020). In the near future, the growing smartphone users will be a critical element in boosting the number of digital wallet users. In a variety of situations, including pandemics and lockdowns, e-wallets and other electronic cash transfer systems come in handy (by RBI Governor, in 2020) [1].

Many players offer e-wallet services to customers in India, including Google Pay, Paytm, FreeCharge, PayPal, Phone Pay, PayUMoney, and MobiKwik, to name a few. Furthermore, e-wallets will help to minimise the need for physical contact during pandemic situations, as well as the need to visit a bank branch to transfer money from a bank account during the Covid-19 lockdown period.

We never expected COVID-19 would turn out to be such a pandemic calamity for the entire human species when the news first broke. Furthermore, we Indians are not immune to the pandemic's effects [2].Academic lectures moved from offline to online, corporate employment moved from offline to online, travel ticket booking moved from offline to online, and online food orders grew as a result of COVID-19. Similarly, payment systems, which are at the heart of all transactions, have seen an increase in people switching from offline to online [2].

2. STATEMENT OF PROBLEM

The Union Government's declaration of a statewide lockdown beginning on March 24, 2020, had a significant impact on how business was done during lockdown days. To avoid Covid19, social distancing and avoiding physical contact are used as preventative methods. As a result, clients are encouraged to use the convenience of digital cash transactions and payment methods to eliminate unwanted physical visits and touch while transferring or remitting money [3]. As a result, people began to use digital, mobile, and online wallets to cope with the covid-19, paving the way for more cashless payments in the country. To overcome the challenges to effective adoption in the consequence of Covid19, it is necessary

to study the use of digital payment systems as well as users' preferences and motivations for using digital currency transactions [4].

3. LITERATURE REVIEW

Anup Kumar et al. (2017) the effect of perceived grievance and safety on the decision to keep using mobile wallets in India. The researcher conducted an empirical investigation on the desire to keep using e-wallets using a confirmatory theoretical approach. The results support the Technology Adoption Model hypothesis that perceived usefulness and ease of use have a significant and favorable impact on perceived security and that perceived security and grievance redressal have a favorable and mediating effect on a developing country's desire to use e-wallets [5].

Biplab Datta & Amit Shankar (2018) delivered an offline and online survey to investigate the systematic equation model for factors impact the adoption of mobile payments in India. To assess the adoption of TAM in the context of Indian clients, the researcher used a descriptive and hypothetical research design. The results demonstrate that whereas personal inventiveness and subjective norms do not significantly and favourably influence Indian consumers' propensity to use mobile payment, perceived utility, trust, and self-efficacy do [6].

Pranav Mishra & Bhawna Mukaria (2019) attempted to Examine the variables affecting Indian e-wallet customers' opinions of public and private mobile wallet providers. The researchers used a hypothetical study design and survey approach to obtain primary data from 433 respondents in the form of a structured questionnaire. Using IBM SPSS software, the Independent Sample t test was performed. According to the findings, public sector e-wallet providers have a lower perception than private sector operators. Between PSU and private sector digital-wallet service providers in India, there is a considerable mean difference in perceptions of difficulties, customer service, and personal risk [7].

According to G.Sudha and M.Thangajesu Sathish's (2020) article, shops will use digital payment systems following demonetization. The researcher looked at payment methods before and after demonetization to see how they changed. The majority of retailers accepted payments through a variety of apps.

According to RBI (January 2021), digital payments in India have seen an exponential surge since the Covid-19 pandemic hit in March 2020. The Reserve Bank of India (RBI) reported a 40 percent year-on-year (YoY) increase in the index to 304.06 in September 2021, up from 217.74 in September 2020, indicating that India's digital payments are deepening [8].

According to the Statista Research Department (Jan, 2022), the results of a poll among Indians on the impact of COVID-19 and its thereafter lockdown, a huge number of respondents utilised Paytm to conduct e- payments. Over 30% of those who took part in the poll said they had increased their use of online payments. On March 24, 2020, India went under lockdown, the world's largest, confining 1.2 billion people, which was extended until 3rd May, 2020 [9].

4. OBJECTIVE OF THE STUDY

- To examine how digital payments were used during COVID-19.
- To investigate the demography characteristics of Indian digital-wallet users.
- To learn more about respondents' e-wallet preferences and motivations.

5. ANALYSIS AND INTERPRETATION

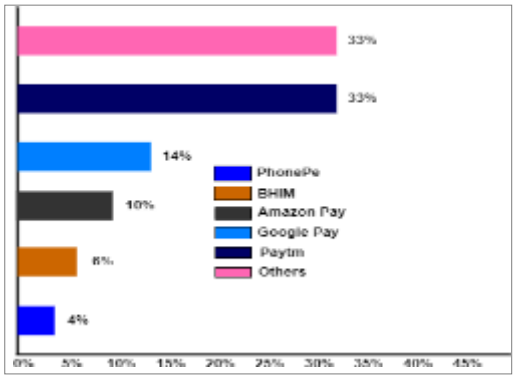

Figure 1. COVID-19 Impact- on e-payment applications usage in India (April -2020) (Source - www.statista.com)

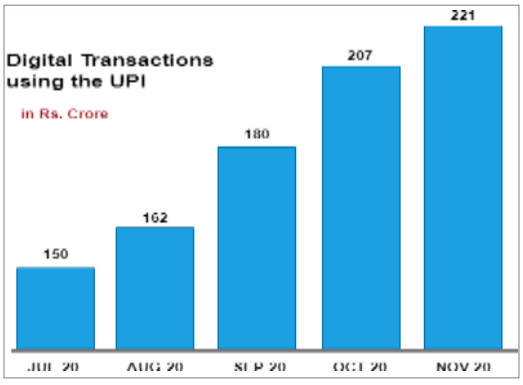

Figure 2. Digital Transactions using the UPI (in Rs. Crore) in 2020 (Source - www.paytm.com)

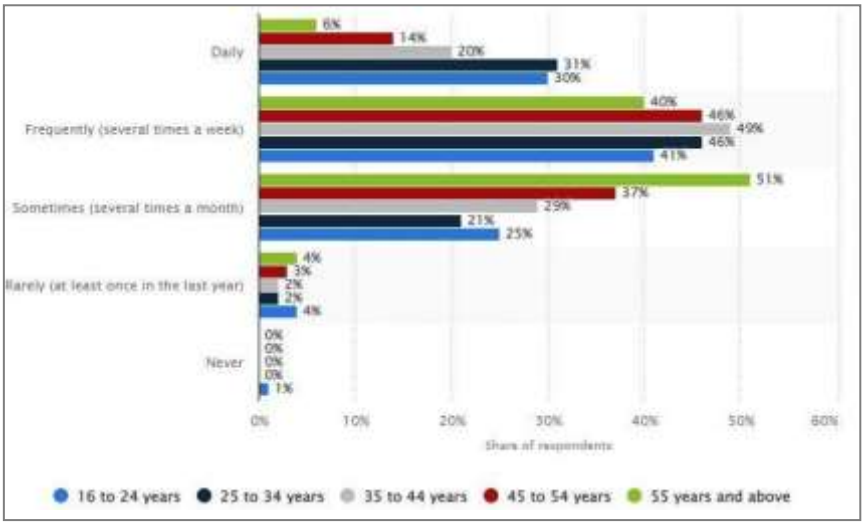

Figure 3. Frequency of using digital payment services by Indians during 2020, age group (Source - www.statista.com)

Table 1. Cumulative Payment Transactions in 2020

Month	Transaction No. (Crore)	(%)Growth (month - month)
January 2020	436.43	
February, 2020	847.44	94.17(%)
Mar, 2020	1262.84	49.02(%)
April, 2020	1566.22	24.02(%)
May, 2020	1890.23	20.69(%)
June, 2020	2298.85	21.62(%)
July, 2020	2699.06	17.41(%)
Aug, 2020	3132.43	16.06(%)
Sept, 2020	3620.51	15.58(%)
Oct, 2020	4108.29	13.47(%)
Nov, 2020	4623.25	12.53(%)
Dec, 2020	4764.28	03.05(%)

As shown in Table 1, Since January 2020, there has been an increase in the number of digital payment transactions. From January to February 2020, it increased by over 94.17 percent, from 436.43 crore to 847.44 crore in transactions. In addition, the proportion of increase was decreasing. The percentage change from February to March 2020 was 49.05 percent. From November 2020 to December 2020, it boosts the percentage decline to 03.05 percent. The total number of transactions in December was 4764.28 crore [10].

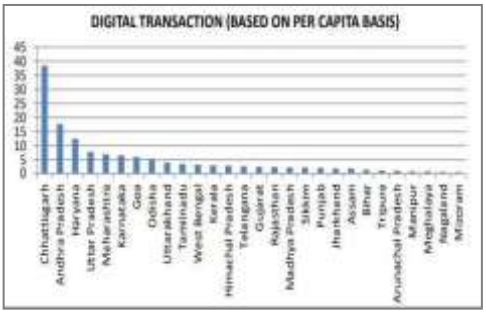

Figure 4. State-wise distribution of online Payment Transaction (BHIM , Rupay Card on POS only) (Source-RBI)

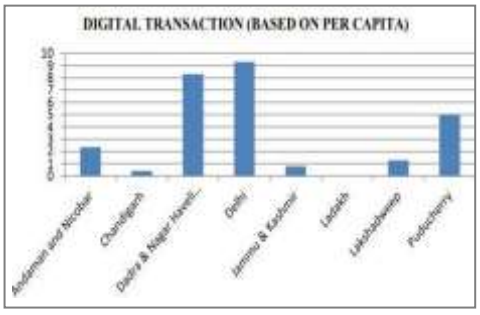

Figure 5. UT State-wise distribution of Digital online Transaction (BHIM Rupay Card on POS only) (Source- RBI)

As shown in FIGURE 4 and FIGURE 5, Chhattisgarh was the highest number of digital transactions per capita (38.481), followed by Andhrapradesh (17.68%) and Haryana (12.42%). The next was UP at 7.73. It is 6.94 in Maharashtra, Manipur, Meghalaya, Nagaland, and Mizoram had the fewest digital transactions per capita, with 0.8, 0.765, 0.584, and 0.548 respectively. There are 8.311 digital transactions in Union Territory, followed by 4.991 in Dadra & Nagar Haveli & Daman and Diu [11].

Figure 6 shows the monthly growth of BHIM-UPI transactions from April 2020 to March 2021 as per the DigiDhan Govt. of India dashboard [12].

Figure 6. Monthly Growth Of BHIM-UPI Transactions (Apr 2020-March 2021) (Source -https://digipay.gov.in/)

Figure 7 shows the monthly growth of BBPS (Bharat BillPay) transactions from April 2020 to March 2021 as per the DigiDhan Govt. of India dashboard [12].

Figure 7. Monthly Growth Of BBPS (Bharat BillPay) Transactions (Apr 2020-March 2021) (Source -https://digipay.gov.in/)

Figure 8 shows the monthly growth of BHIM-UPI transactions from April 2021 to March 2022 as per DigiDhan Govt. of India dashboard [12].

Figure 8- Monthly Growth of BHIM-UPI Transactions (Apr 2021-March 2022) (Source -https://digipay.gov.in/)

Figure 9 shows the monthly growth of BBPS (Bharat BillPay) transactions from April 2021 to March 2022 as per DigiDhan Govt. of India dashboard [12].

Figure 9- Monthly Growth Of BBPS (Bharat BillPay) Transactions (Apr 2021-March 2022) (Source -https://digipay.gov.in/)

The National Payments Corporation of India (NPCI) is an umbrella body established by banks under the direction of the RBI that is de facto responsible for all retail payments made in India. It serves as a middleman for a variety of digital payment methods, including IMPS, UPI, and Bharat BillPay, among others. Examining the value and volume of these transactions from January 2020 to June 2020, as depicted in Figure 10, demonstrates a decline in payments in India as a result of COVID-19 and related containment efforts, but a quick recovery in consecutive months across several modalities [13].

The lockdown period was characterized by significant restrictions on consumer spending as well as the deferral of multiple ordinary monthly payments. Consumers were left in a state of limbo when it came to making decisions about the amount and timeliness of pending and unpaid bills. This is reflected in a 49% drop in the value of overall NPCI payment goods across all digital payment modes in April 2020, compared to payments in March 2020. [13].

FIGURE 11 shows the Cumulative Payments Transactions (Last 12 Months – Oct 2021 to up to 12 Sep 2022) [12].

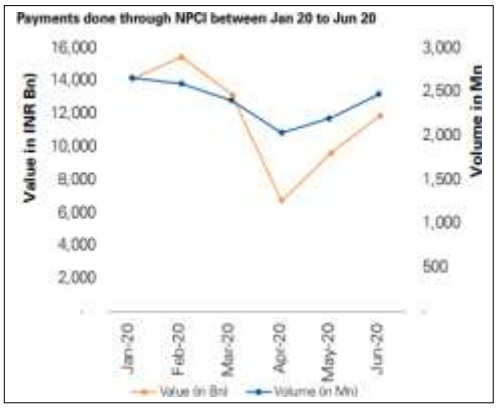

Figure 10. Payments dare donethrough NPCI between Jan 20 to Jun 20 (Source - NPCI payments database as accessed in July 2020.)

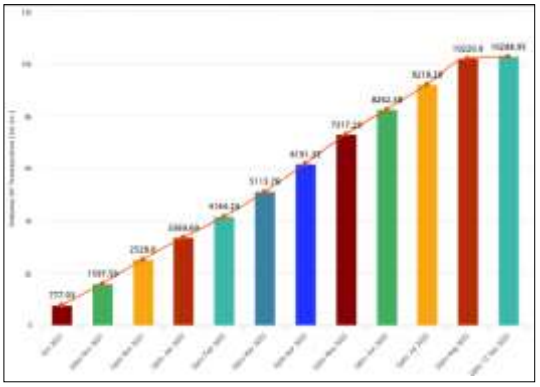

Figure 11. Cumulative Payments Transactions (Last 12 Months – Oct 2021 to up to 12 Sep 2022)

6. CONCLUSION

According to the survey, users of e-wallets have expressed a strong desire to adopt them. In every corner of the country, peers, friends, and family members have been taught the need of using an e-wallet during a pandemic to reduce physical monetary transactions. Existing users of digital payment and electronic wallets are encouraged to educate others about the importance, performance, use, and benefits of digital payment over traditional payment methods. Service providers believe that better design and content will persuade more customers to use and use e-wallets in their daily lives in pandemics and other similar emergency scenarios. Furthermore, in order to avoid the Covid19 virus or other similar epidemics, digital payment and e-wallets can be utilized to conduct monetary transactions.

7. REFERENCES

[1] Dr.Rajbir Saha,Digital payments usage during covid19 pandemic with special reference to e-wallet users, IJMER,January -2021.

[2] Dr.Rashmi M Mate,Impact of covid-19 on digital payment usage in India, UGC Care Group 1 Journal,December 2021.

[3] Rashi Singhal,Impact of covid-19 on digital payment services at towns and villages,International Journal of Creative Research Thoughts (IJCRT),May 2021.

[4] V. Sornaganesh,Impact of Covid-19 Outbreak in Digital Payments,International Journal for Innovative Research in Multidisciplinary Field,October 2020.

[5] https://government.economictimes.indiatimes.com/news/digital-payments/digital-payments-swell-as-42-indians-make-multiple-online-payments-during-covid-19-lockdown/75172943
[6] https://paytm.com/blog/payments/upi/upi-transaction-features-benefits-maximum-limit/

[7] https://www.statista.com/statistics/1111087/india-coronavirus-impact-on-digital-payment-app-usage/
[8] https://inc42.com/buzz/digital-payments-index-up-by-40-in-september-2021-rbi/
[9] M. P. Brown and K. Austin, The New Physique(Publisher Name, Publisher City, 2005), pp. 25–30.
[10] M. P. Brown and K. Austin, Appl. Phys. Letters 85, 2503–2504 (2004).
[11] R. T. Wang, "Title of Chapter," in Classic Physiques, edited by R. B. Hamil (Publisher Name, Publisher City, 1999), pp. 212–213.
[12] https://digipay.gov.in/dashboard/Default.aspx
[13] https://assets.kpmg/content/dam/kpmg/in/pdf/2020/08/impacting-digital-payments-in-india.pdf [7] Intel, 'Turning challenges into opportunities in the data center', White Paper,

Biographies

Mr. Ajay Prasad Nautiyal received the bachelor's degree in computer science & engineering from Uttarakhand Technical University in 2013, and the perusing in masters in computer science & engineering from Kurukshetra University, Haryana. He is currently working as Lecturer at the Department of Computer Engineering, Uttaranchal University. His research areas include IoT, deep learning, data science, data analytics and social network analysis. He has published many patents and conference papers in reputed journals.

Ms. Sapna Bisht received the bachelor's degree in Civil Engineering from Graphic Era University in 2013, and master's in Environmental engineering from Uttaranchal University, Dehradun. She is currently working as an Assistant Professor at the Department of Civil Engineering, Uttaranchal University. Her research areas include Civil Engineering, Environmental Sciences, IoT, data science, data analytics and social network analysis. She has published many patents and conference papers in reputed journals.

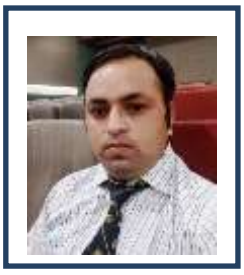

Mr. Kapil Rajput received the bachelor's degree in computer science & engineering from UPTU University in 2009, and master's in computer science & engineering from Uttaranchal University Dehradun. He is currently working as an Assistant Professor at the Department of Computer Science Engineering, Uttaranchal University. His research areas include ML, IoT, data science, data analytics and social network analysis. He has published many patents and conference papers in reputed journals.

Palm Print Recognition Based on Correlation Features

Ritika Raturi[1], Deval Verma[2]

[1]Department of Mathematics, Chandigarh University, Punjab- 140413
raturiritika2000@gmail.com
[2]School of Computer Science Engineering and Technology
Bennett University, Times Group
Greater Noida-201310
deval09msc@gmail.com

Abstract

The performance of a palmprint recognition system is determined by one of its essential components, the comparator. However, in the realm of palmprint recognition system, the purpose of analysis and comparator development is weakened. The main contribution of this study is the analysis of comparators using theory and experiments. The investigation investigates the possibility that a ground truth of palmprint images could contain identical data. Experimental analysis makes use of the receiver operating characteristic (ROC) curve. It has been found that comparators based on the similarity measure functions of the normalised correlation coefficient (NCC) perform well.

Keywords. Palmprint Recognition, NCC, Comparators, Metrics, ROC curve, Correlation

1. INTRODUCTION

Biometrics is an approach of automatically recognising a person based on his physical or behavioural features. Wherever there is a need for user verification, biometric solutions are necessary [1]. Over the last decade, palm-print-based biometric identification systems have gotten a lot of attention. Principle lines, wrinkles ridges, tiny points, unique points, and texture patterns are some of the traits that might be referred to as biometric characteristics [2]. The tri-radiated region, also known as the inter-distal region, is the area beneath the finger that is bordered by the cardiac line. This part of the palm comprises traits that are both distinctive and generally distinguishable [14]. Palm prints are a more accurate way to identify people than fingerprints because they cover a larger surface area. Palm print sensors are therefore larger and more expensive than fingerprint sensors [3]. The use of these systems for large-scale personal authentication will necessitate additional work to increase performance significantly [11].

In the field of biometrics, the objective is to generate a data representation that separates the real and imposter score distributions well. Numerous effective faces and palmprint recognition systems utilise conventional image processing methods to extract features utilising image filters that improve discriminative information while decreasing noise [13].

The most cutting-edge biometric technology, with over 20 decades of research and development, is automatic fingerprint verification. There are still certain challenges to be resolved despite the abundance of scanning methods, feature extraction, pre-processing, and matching algorithms that have been propounded for fingerprint verification [15, 16]. Hand geometry can only provide limited precision in accordance with the simple aspects of the hands, and its capacity to differentiate individuality is still an open subject [17].

Palm region extraction is the process of selecting and orienting the core section of palmprints, also termed as the region of interest (ROI). It's used to match different palmprint photos by aligning them. Many algorithms have been developed to extract the ROI of palmprints for effective feature extraction [12,18]. There are five components of a standard palm print recognition system. The first is a palm-print scanner, which gathers photos of palm prints. Pre-processing establishes a coordinate system for aligning palmprint images. The third stage, known as feature extraction, extracts useful features from pre-processed palmprints. The fourth feature is a palmprint matcher, which compares two palmprint attributes. This study looks at how different comparators affect the palm matching process while assuming that a correlation coefficient must be treated similarly to the positive.

Additionally, a formula for calculating a comparator parameter for the pattern matching system's maximum decision accuracy is obtained by theoretical research.

To analyse the comparator and confirm the formula, experiments are conducted on a variety of palmprint matching systems. Here is a description of the remaining paper. There are definitions of preliminaries in section 2. Proposed methodology is discussed in section3. Experiments and results are discussed in section 4 and 5.

2. PRELIMINARIES

2.1. Dataset Description

For research purposes, the Casia palmprint database [18] has been used. 312 persons are represented by 5,502 images in this database. The format of the palmprint pictures is "xxxx m/f l/r xx.jpg". These jpeg photos of palm prints are in 8-bit grayscale. Where the letters "xxxx" stand for a person's unique identification number, which spans from 0000 to 0312, "m/f" for male or female, and "l/r" for left or right palm, respectively.

2.2. Normalised Cross Correlation coefficient (NCC)

The degree of similarity between two photographs is calculated using the normalised cross correlation coefficient (NCC) [8]. Because NCC is less sensitive to direct changes in the amplitude of brightening in two compared images [14,10], it is more significant than cross correlation. With the aid of palm lines, one common use of pattern matching is palmprint matching, which is used for fortune telling. Mathematical formula is given in Figure 2.21.

FIG:1 0001_m_l_01

FIG:2 0001_m_l_02

$$\eta(x_1, y_1) = \frac{\sum_{l=1}^{M}\sum_{m=1}^{N}\{x_1(l,m).y_1(l,m)\}}{\sqrt{\sum_{l=1}^{M}\sum_{m=1}^{N}\{x_1(l,m)\}^2}.\sqrt{\sum_{l=1}^{M}\sum_{m=1}^{N}\{y_1(l,m)\}^2}} \in [0,1]$$

Figure2.21. Evaluation of NCC, η (x1, y1)

3. PROPOSED METHODOLOGY

A comparator consists of two components: a function and a threshold that determine how similar two palm images are to one another. If there is a greater degree of resemblance between two palm images than the threshold, the two are considered to match. palm images are not matched if this is not the case. A general comparator is defined mathematically as follows in Figure 3.1:

$$C_{(\tau,\ \mathrm{sim})}(x_1, x_2) = \begin{cases} \text{match} & \text{if } \mathrm{sim}(x_1, x_2) \geq \tau \\ \text{no match} & \text{otherwise} \end{cases},$$

Figure 3.2. Evaluation of Similarity (x1, x2)

False positive rate (FPR) and false negative rate (FNR) for both measures are calculated by using following equations in Figure 3.2.

$$FPR = \frac{\sum(FP)}{\sum(TP) + \sum(FP)} \qquad FNR = \frac{\sum(FN)}{\sum(FN) + \sum(TN)}$$

Figure 3.2. Evaluation of Similarity (x1, x2)

4. EXPERIMENTS, RESULTS AND ANALYSIS

In this section, we've discussed our experimental work. The major goal of this research is to compare two images using the performance factors NCC to determine how comparable they are. then use a ROC curve to compare how similar they are. Both parameters have [0, 1] ranges. Casia database contain 5,502 images in this database, out of them the results of 30

palm images are shown in given Table 4.1. NCC values are computed for both left and right hand in Table 4.1 and it is observed that on taking some threshold value it is decided for match and not match.

Table 4.3. NCC value of Right /Left Hand, NM (no match), M(match) range [0,1]

Palm No.jpg	**Type**	**NCC values for left palm**	**Decision based on NCC (Th=0.9)**	**NCC values for right palm**	**Decision based on NCC (Th=0.9)**
palm0001	L	1	M	0.8776	NM
palm0002	L	0.924316286	M	0.83537232	NM
palm0003	L	0.908045649	M	0.893865815	NM
palm0004	L	0.911274144	M	0.8916082	NM
palm0005	L	0.922325198	M	0.872080946	NM
palm0006	L	0.905877726	M	0.89605427	NM
palm0007	L	0.901073111	M	0.894218908	NM
palm0008	L	0.876557038	NM	0.870822589	NM
palm0009	R	0.860061145	NM	1	M
palm0010	R	0.858743713	NM	0.998018839	M
palm0011	R	0.83510893	NM	0.935007229	M
palm0012	R	0.840590762	NM	0.971519321	M
palm0013	R	0.888537342	NM	0.929232254	M
palm0014	R	0.89001467	NM	0.931723599	M
palm0015	R	0.887452513	NM	0.934980282	M
palm0016	R	0.834901091	NM	0.930568405	M
palm0017	L	0.916501824	M	0.897225417	NM
palm0018	L	0.898084337	NM	0.882776414	NM
palm0019	L	0.904247812	M	0.862085519	NM
palm0020	L	0.875981741	NM	0.867090231	NM
palm0021	L	0.861540544	NM	0.864350786	NM
palm0022	L	0.882046809	NM	0.858687178	NM
palm0023	L	0.876204649	NM	0.848362653	NM

palm0024	R	0.807131267	NM	0.914954649	M
palm0025	R	0.791954271	NM	0.906271612	M
palm0026	R	0.882320735	NM	0.841548278	NM
palm0027	R	0.801373396	NM	0.905876433	M
palm0028	R	0.818123168	NM	0.890212266	NM
palm0029	R	0.798173497	NM	0.892508208	NM

A two-dimensional plot of the false positive rate FPR (defined as the ratio of the total number of incorrect matches to the total number of matches) versus the false negative rate FNR (defined as the ratio of the total number of incorrect non-matches to the total number of non-matches) is known as a ROC curve. Every part of a palmprint matching system is necessary for FPR and FNR. FPR and FNR have a [0,1] range. The optimal point on a ROC curve is (FPR, FNR) = (0,0). In Figure 4.1 shows the ROC curve of FPR and FNR of NCC values corresponding to the given dataset.

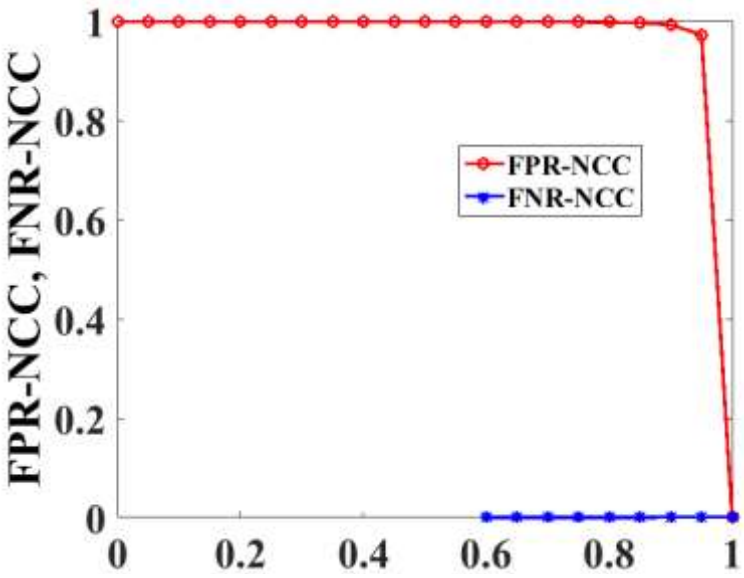

Figure 4.4. ROC Curve for NCC range [0,1]

5. CONCLUSIONS

This study presents an investigation of palmprint matching based on NCC similarity measurement. The primary goal of this work was to determine the palmprint matching accuracy. On several palmprint images, experiments have been conducted. NCC and similarity measurements are used to evaluate the effectiveness of their matching. To

determining accuracy, we have calculated FPR and FNR using various threshold values. The findings show that NCC delivers the least value at the 0.760 threshold, whereas NCC gives the least value at the threshold value of 1.

6. REFERENCES

[1] N. Duta, A. K. Jain, K. V. Mardia, 'Matching of palmprints', Pattern Recognition Letters 23 (2002) 477-485.

[2] G. S. Badrinath, P. Gupta, 'Stockwell transform based palm-print recognition', Applied Soft Computing 11 (2011) 4267-4281.

[3] D. Brown, K. Bradshaw, 'Deep Palmprint Recognition with Alignment and Augmentation of Limited Training Samples', SN Computer Science (2022) 3:11.

[4] A. Kong, D. Zhang, M. Kamel, 'A survey of palmprint recognition', Pattern Recognition, vol.42(7), pp.1408–1418, 2009.

[5] P. H. H. Yeomans, B. V. K. V. Kumar, M. Savvides, 'Palmprint classification using multiple advanced correlation filters and palm-specific segmentation', IEEE TRANSACTIONS ON INFORMATION FORENSICS AND SECURITY, VOL. 2, NO. 3, SEPTEMBER 2007.

[6] D. Zhang, W. Zuo, F. Yue, 'A comparative study of palmprint recognition algorithms', ACM Comput. Surv. 44, 1, Article 2 (January 2012), 37 pages. http://doi.acm.org/10.1145/2071389.2071391

[7] J. You, W. Li, D. Zhang, 'Hierarchical palmprint identification via multiple feature extraction', Pattern Recognition 35 (2002) 847–859.

[8] D. M. Sai, T. L. Chien, 'Fast normalized cross correlation for defect detection', Pattern Recognition Letters, Vol. 24, pp. 2625-2631, 2003

[9] J. Chen, Y. S. Moon, M. F. Wong, G. Su, 'Palmprint authentication using a symbolic representation of images', Image and Vision Computing 28 (2010) 343–351.

[10] D. Zhang, A. W. K. Kong, J. You, M. Wong, 'Online palmprint identification', IEEE Trans. Pattern Anal. Mach. Intell., vol. 25, no. 9, pp. 1041–1050, Sep. 2003.

[11] A. Kumar, 'Incorporating Cohort Information for Reliable Palmprint Authentication', Sixth Indian Conference on Computer Vision, Graphics & Image Processing.

[12] X. Bao, Z. Guo, 'Extracting Region of Interest for Palmprint by Convolutional Neural Networks', 978-1-4673-8910-5/16/$31.00 ©2016 IEEE.

[13] J. Svoboda, J. Masci, M. M. Bronstein, 'Palmprint recognition via discriminative index learning', 2016 23rd International Conference on Pattern Recognition (ICPR) Cancún Center, Cancún, México, December 4-8, 2016.

[14] L. Di. Stefano, S. Mattoccia, M. Mola, 'An Efficient Algorithm for Exhaustive Template Matching based on Normalized Cross Correlation', IAPR Int. Conf. on Image Analysis and Processing (ICIP 2003), September 17-19, Mantova, Italy, pp. 322-327, 2003.

[15] Kong, A. W. K., Zhang, D.: Feature-Level Fusion for Effective Palmprint Authentication, ICBA 2004, LNCS 3072, pp. 761-767, 2004. © Springer-Verlag Berlin Heidelberg 2004.

[16] G. Lawton, Biometrics: a new era in security, Computer, vol. 31, no. 8, pp. 16-18, 1998.

[17] "CASIA Palmprint Database, http://biometrics.idealtest.org/"

Breast Cancer Prediction Using Statistical Features

Shruti Sharma[1] and Deval Verma[2]

[1]Chandigarh University
1Department of Mathematics, Chandigarh University, Punjab- 140413
srts1906@gmail.com
[2]Bennett University, Times Group
School of Computer Science Engineering and Technology
Greater Noida-201310
deval09msc@gmail.com

Abstract

As we all know breast cancer is a very devastating disease. By each passing day number of deaths in women are increasing because of breast cancer. The accuracy rate of each technique varies depending on the situation, tools, and datasets. Since their effectiveness has been established, machine learning techniques have gained popularity as a field of study. They can greatly help with the early diagnosis and prediction of breast cancer processes. In this work a logistic regression and random forest machine learning techniques were used to detect and predict breast cancer. In this work, breast cancer prediction is carried out using statistical properties and classified using Random Forest Classifier and Logistic Regression on Wisconsin Breast Cancer Diagnosis Dataset.

Keywords. Breast Cancer Prediction, Machine Learning, Ensemble Techniques, Data Mining, Deep Learning, Algorithms.

1. INTRODUCTION

The proportion of women who die from breast cancer worldwide has increased dramatically in the last few decades, making it the most lethal and heterogeneous disease of our time. Women die from this disease more often than any other disease [1]. Breast cancer is caused by abnormal growth of fatty and fibrous tissues in the breast. A combination of data mining and machine learning algorithms is being used to predict breast cancer [2]. One of the most important tasks is finding the most appropriate and suitable algorithm to predict breast cancer. Breast Cancer begin to spread when cellular growth becomes unchecked, leading to malignant tumours [3]. There are different stages of cancer caused by the cancer cells spreading throughout the tumours. A cancerous condition caused by the spread of cells and tissues throughout the body is breast cancer.

When we collect data of various types of breast cancer prevailing worldwide, we get to know that it's a huge raw dataset which we need to clean and analyse, using data mining

techniques, and algorithms. Any kind of disease can be discovered with the help of these functions. Statistics and machine learning are employed in the diagnosis of cancer disorders such as, lung cancer, prostate cancer and leukaemia [6], as well as databases, fuzzy sets, storage warehouses, and neural networks can be used. In traditional cancer detection, three tests are conducted: clinical examination, radiological imaging, pathology tests. This method is called "the gold standard [7]". The model is aimed at predicting unseen data and delivering good results in both the training and testing phases [8]. As far as machine learning is concerned, it is based on three main strategies-feature selection, pre-processing, classification.

There are three sections in this paper: the first discusses related work for prediction of benign and malignant classes, and the second discusses proposed methodology, the third section discusses experiments and results for breast cancer diagnosis.

2. SURVEY FOR BREAST CANCER PREDICTION

As we know, machine learning models are those algorithms which learn from the data of the past. Based on a machine learning model, we analyse many data and predict the future based on those data [9]. Based on regression and classification models, the decision tree is constructed. Subsets of the dataset are divided into smaller ones. It is possible to make predictions with the highest level of precision using smaller sets of data [12]. In this K-Nearest Neighbour (KNN) algorithm, more dependent variables are included in the learning process. Using this algorithm, a binary response is generated. Based on a particular set of data, logistic regression [11] can provide a continuous outcome. A statistical model with binary variables is used in this algorithm [10]. In Naive Bayes Algorithm (NB) an assumption is made that the training dataset will be large in this model. By using the Bayesian method, the probability is calculated [13]. In support vector machine (SVM) classification and regression problems are solved using this supervised learning algorithm [14]. It consists of large datasets that can be predicted with the highest accuracy rate using this method. In addition to using 3D and 2D modelling, it is an effective machine learning method [11], [15]. In K-Mean Algorithm, using a clustering algorithm, the K-mean algorithm divides data into small clusters. Data is compared using an algorithm to determine their similarity. Data containing at least one cluster can be used to evaluate a large dataset [17]. In this work we have used two machine learning algorithms which are used to predict breast cancer are as below:

- Random Forest (RF): A Random Forest algorithm is an efficient way to solve problems of supervised learning both for classification and regression. In machine learning, this is a basic building block that is used to predict new data based on previous datasets [11].

- Logistics Regression (LR): In this algorithm, more dependent variables are included as part of the supervised learning process. Responses from this algorithm are binary in nature. It is possible to obtain a continuous outcome of specific data using logistics regression [11]. The algorithm is based on the use of a binary variable statistical model [10].

3. PROPOSED METHODOLOGY

The seven phases of the suggested framework are as follows:

In this paper, the goal is to create a method for predicting the benign and malignant classes using regression and classification of breast cancer.

3.1. Dataset Description

On the UCI machine learning repository, a dataset is accessible. 569 samples in all are included in this collection. Our samples have a malignant (M) or benign (B) classification (B). These are medical terminology that describe the two types of tumour cells that we discussed earlier: benign and malignant. The properties have all their values. The distribution of our samples shows that 357 are benign and 212 are malignant. Figure 3.1 and Figure 3.2 shows the images of benign and malignant cancer.

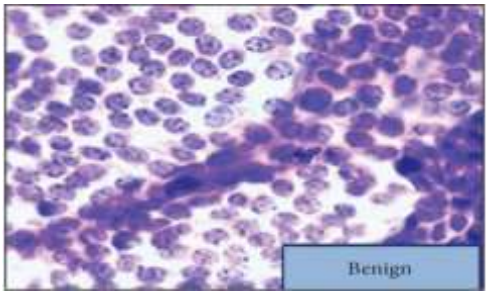

Figure 3.1: Benign Class

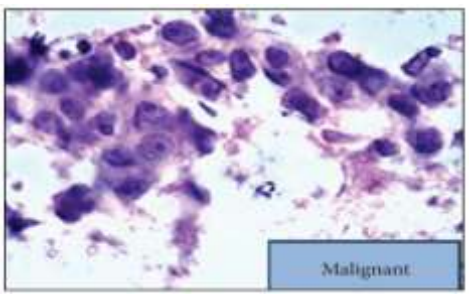

Figure 3.2 Malignant Class

Figure 3.1 shows benign cancer cells which are abnormal in nature but non-cancerous collection of cells. It grows very slowly and doesn't spread to additional bodily parts whereas malignant cancer cells are shown in Figure 3.2. These cells grow rapidly and invade other body organs very soon, it is cancerous and metastatic in nature. Figure 3.3 represents the number of malignant and benign cells present in our dataset.

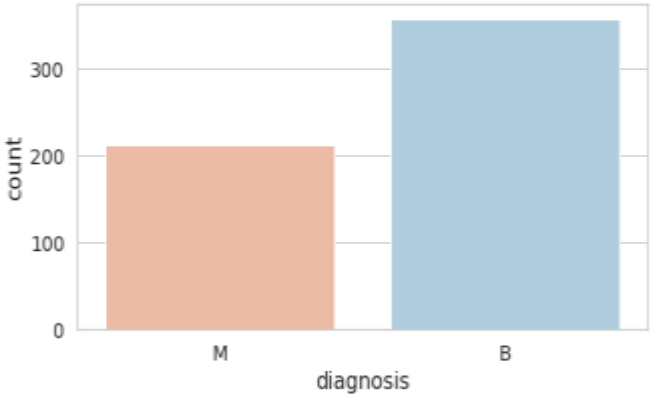

Figure 3.3. Wisconsin Breast Cancer Diagnostic Dataset

3.2. Feature Extraction

There are a total of 31 features namely, mean of radius, texture mean, mean value of perimeter, mean value of area, smoothness mean, mean of compactness, mean of concavity, mean of concave points, mean of symmetry, mean of fractal dimension, worst texture, worst perimeter, worst area, worst smoothness, worst compactness,worst part of concavity, worst part of concave points, worst part of symmetry, and worst part of fractal dimension.

4. EXPERIMENTS AND RESULTS

All experiments are performed using Sci-Kit Learn library available in Python programming language. The dataset is splitted into various ratios for training and testing samples. Using data inputs, our predictive algorithm will determine whether a cancer is benign or malignant in nature. In this study, we have applied two machine learning techniques to know which algorithm is more accurate in prediction. Firstly, we imported the required libraries such as NumPy and Pandas in our python then download the dataset from Kaggle. Then we got the information about our dataset and checked for the missing values. In this dataset, there is no missing value. So, we have spitted data into training and testing for both classifiers.

4.1. Performance Analysis

After splitting the data, we have evaluated accuracy score of training data which was 99% in Logistic regression and 99.5% in Random Forest classifier. After this, we tested our model accuracy on test data on confusion matrix. The important parameters are recall, F1 score, precision, accuracy on which we tested our model and compared with each other. In logistic regression model, the confusion matrix was [TP=86, TN=50, FP=4, FN=3] and in Random Forest Classifier the confusion matrix was [TP=87, TN=51, FP=3, FN=2] after applying the accuracy formula in both we got 95.10% and 96.5% testing accuracy respectively. The results are as below-

	Algorithm	Training Accuracy	Testing Accuracy
1.	Logistic Regression	99%	95.10%
2.	Random Forest Classifier	99.5%	96.50%

4.2. Comparative Analysis

The comparative analysis of both performances is shown in Figure 4.1:

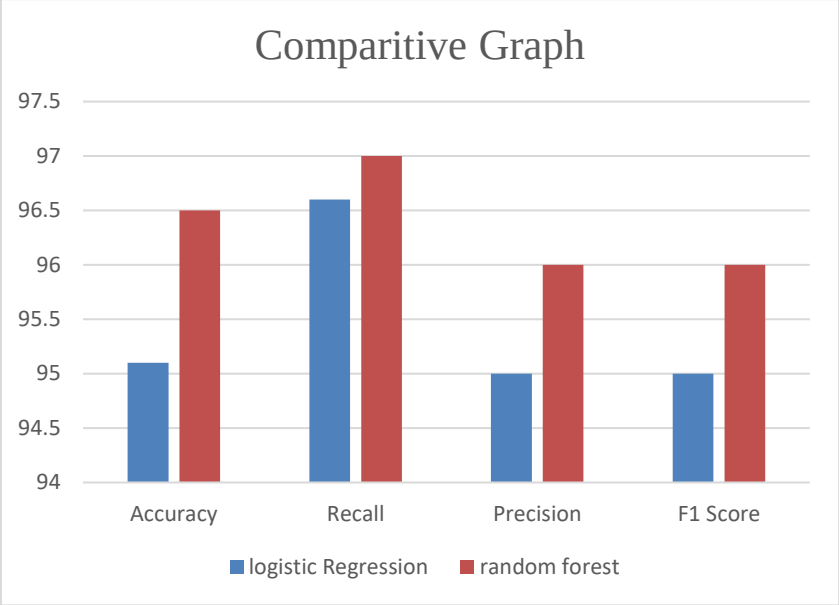

Figure 4.1. Comparative Graph

5. CONCLUSIONS

In this work, breast cancer prediction is carried out using statistical properties and classified using Random Forest Classifier and Logistic Regression. The results are evaluated and compared, based on accuracy's a result, the Random Classifier model can be used to predict breast cancer because it performed well in terms of accuracy of prediction (96.5%), which will greatly aid doctors in making an accurate prediction. The limitation we have seen that is after being accurate Random Forest classifier model can predict wrong as it is not 100% accurate Several issues still need to be addressed in future research. As we all know data is everything in every domain. Hence, it can be said that data availability is the most significant challenge for deep learning and machine learning in predicting breast cancer. Most researchers are now searching for medical images of patients with cancer, which contain sensitive information, and are publicly available as raw images. To overcome the problem of limited patient data, many researchers are now using data augmentation schemes, such as cropping, filtering, rotating, and cleaning. Data from more patients can be obtained using this technique.

6. REFERENCES

[1] Y. S. Sun et al., 'Risk factors and preventions of breast cancer', International journal of biological sciences, vol.13, no.11, pp.1387, 2017.

[2] Y. Khourdifi and M. Bahaj, "Applying best machine learning algorithms for breast cancer prediction and classification," in 2018 International Conference on

Electronics, Control, Optimization and Computer Science (ICECOCS), pp. 1–5, IEEE.

[3] Y. Lu, J. Y. Li, Y. T. Su, and A. A. Liu, 'A review of breast cancer detection in medical images', IEEE Visual Communications, and Image Processing (VCIP), pp. 1–4, IEEE in 2018.

[4] F. K. Ahmad and N. Yusoff, 'Classifying breast cancer types based on fine needle aspiration biopsy data using random forest classifier', 13th International Conference on Intelligent Systems Design and Applications, pp. 121–125, IEEE, 2013

[5] R. Hou et al., 'Prediction of upstaged ductal carcinoma in situ using forced labelling and domain adaptation', IEEE Transactions on Biomedical Engineering, Vol. 67, no. 6, pp. 1565-1572, 2019.

[6] D. Delen, 'Analysis of cancer data: a data mining approach', Expert Systems, vol. 26, no. 1, pp.100–112, 2009.

[7] A. Reddy, B. Soni, and S. Reddy, 'Breast cancer detection by leveraging machine learning', ICT Express, vol. 6, no. 4, pp. 320-324, 2020.

[8] Z. Salod and Y. Singh, 'Comparison of the performance of machine learning algorithms in breast cancer screening and detection: A protocol', Journal of Public Health Research, vol.8, no. 3, pp. 1677-1686, 2019

[9] C.M. Bishop, 'Pattern recognition and machine learning' Springer, vol. 4, no. 4, pp. 738). New York: springer. 2006.

[10] H. Tran, 'A survey of machine learning and data mining techniques used in multimedia system', no. 113, pp.13-21, 2019.

[11] C.Y.J .Peng ,K.L.Lee, and G.M.Ingersoll, 'An introduction to logistic regression analysis and reporting', The journal of educational research, vol. 96, no. 1, pp. 3–14, 2002.

[12] H. Sharma and S. Kumar, 'A survey on decision tree algorithms of classification in data mining', International Journal of Science and Research (IJSR), vol. 5,no. 4, pp.2094–2097, 2016.

[13] A. A. Ibrahim, A. I. Harshad and N.E.M. Shawky, 'A Comparison of Open-Source Data Mining Tools for Breast Cancer Classification', pp. 636–651.IGI Global, 2017

[14] T. Evgeniou and M. Pontil, 'Support vector machines: Theory and applications', in Advanced Course on Artificial Intelligence, pp. 249–257, Springer, 2005.

[15] Y. Yang, J. Li, and Y. Yang, 'The research of the fast SVM classifier method', in 12th International Computer Conference on Wavelet Active Media Technology and Information Processing (ICCWAMTIP), pp. 121–124, IEEE,2015.

[16] L. Breiman, 'Random forests', Machine Learning, vol. 45, no. 1, pp. 5–32, 2001.

[17] Y. Li and H. Wu, 'A clustering method based on k-means algorithm', Physics Procedia, vol. 25, pp. 1104–1109, 2012.

An Insight on the Swastika Shaped Antenna Design

Kumar Abhinandan Patial[1], Simran Dogra[2], Ankush Kapoor[3]

Department of Electronics and Communication Engineering, Jawaharlal Nehru Government Engineering College, Sundernagar, patial2273@gmail.com, simrandogra253@gmail.com, ankush8818@yahoo.com

Abstract.

This work proposes a study of an innovative compact monopole antenna comprising with a microstrip patch engraved in the shape of a Swastika design. The study of various feeding methods for wireless microstrip patch antennas, is addressed in this paper. The various design aspects of the swastika shaped patch antenna are discussed. The performance parameters are reported in form of comparative analysis of the existing literatures.

Keywords. Feeding methods, MSA, SSA, substrate and 5G frequency.

1. INTRODUCTION

Microwave and wireless engineers take a great interest in research on relatively small microstrip antenna (MSA) designs. A drastic improvement on the structural designs has been reported in the recent years which is the need for latest 5G wireless communication. The important properties of the antennas which are focussed in the transmission devices are their weight and size which are desired to assist with the high mobility needs of a wireless communication system [1]. MSAs have numerous blessings, including mild weight, low cost and can be utilized in applications like aircraft, satellite, and wi-fi communication [2]. The cheap fabrication cost of MSAs is a result of their simplicity of mass manufacture by utilizing printed circuit technology [3]. The properties which validate the design of the MSA include better return loss, high gain and high input impedance. The various modifications in the design geometry play an important role in improving the properties of the MSA [4-5]. The limited bandwidth of an MSA is among its most critical disadvantages. A number of studies and approaches have been applied for improving the bandwidth of the MSA [6]. A swastika shaped antenna (SSA) has been recently developed by the researchers which has exhibited improved radiation properties with better polarization [7-8]. The design of the SSA has been taken from a holy sign in Hindu mythology, and has exhibited enhancement in the bandwidth of an MSA. The compact monopole patch antenna, which consists of a patch in the Swastika form, is briefly described in this article. The rectangular slots of the SSA helps in modifying the surface current distribution of the patch. The shape basically helps the charge particles in accelerating and deaccelerating, which improves the bandwidth and radiation characteristics. This article presents research investigations for various applications employing this sort of swastika-shaped antenna.

2. SWASTIKA SHAPED PLANAR PATCH DESIGN

To build an MSA, first the substrate is chosen, then the length of the patch is calculated using the design equations. The designer's ability lies in choosing an appropriate feeding mechanism. Basically, the two feeding methods that are most often utilised are probe feed and microstrip line feed for the SSA design. Designing a MSA and SSA requires careful consideration of the thickness and choice of dielectric material [8]. The basic design equations for the SSA are formulated as [5]:

Width of Antenna (w):

$$w = \frac{c}{2f_o\sqrt{\frac{(\epsilon r+1)}{2}}} \tag{2.1}$$

Effective Dielectric Constant (ϵ_{eff}):

$$\epsilon_{\text{eff}} = \frac{\epsilon r+1}{2} + \frac{\epsilon r-1}{2}\left[1 + 12\frac{h}{W}\right]^{\frac{-1}{2}} \tag{2.2}$$

Effective Length (L_{eff})

$$L_{\text{eff}} = \frac{c}{2f_0\sqrt{\epsilon \text{eff}}} \tag{2.3}$$

Length Extension (ΔL)

$$\Delta L = 0.412h\ \frac{(\epsilon eff+0.3)(\frac{W}{h}+0.264)}{(\epsilon eff-0.258)(\frac{W}{h}+0.8)} \tag{2.4}$$

Effective Length (L)

$$L = L_{\text{eff}} - 2\Delta L \tag{2.5}$$

As shown in Figure 2.1, the geometric configuration of the SSA is presented engraved in FR4 substrate.

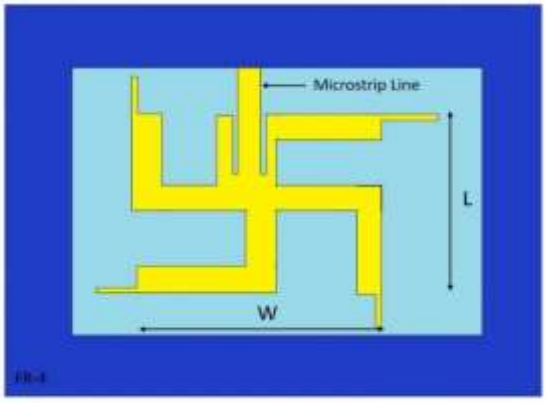

Figure 2.1: Swastika MSA's top view

It consists of four arms in opposite directions with four slots between the arms. FR-4 substrate is mostly used because of its less cost, dominant availability and use at various

frequencies [9-10]. Further, feeding plays a very important role for matching the input impedance and getting SSA to work efficiently. [11-12].

3. FEEDING MECHANISMS

There are various feeding methods used for Swastika MPA. These methods basically are of two types: contacting and non-contacting.

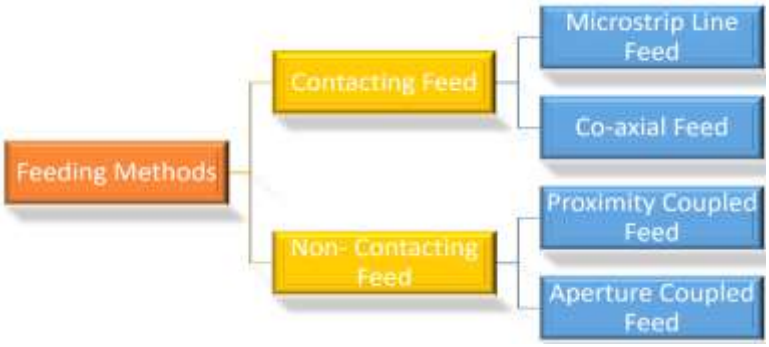

Figure 3.1: Flow chart of feeding techniques

3.1 Contacting feed - This approach uses contacting components like a microstrip or coaxial line to supply power at radio frequency directly to a patch of MSA. The most popular method of contacting feed are coaxial cable (CB) and microstrip line (ML).

3.2 Non-contacting feed - The MSA is not supplied with radio frequency power directly in this approach. Through electromagnetic coupling, the feed line's power is transmitted to the route. Aperture Coupled (AC) and Proximity Coupled (PC) are the two most used non-contacting feeding approaches. [10-11]

A. ML Feed

It makes use of a conducting strip, which is physically joined to the border of the MSA. The benefit of this type of feeding mechanism is in the form of planar structure as the feed is engraved in the same substrate. Furthermore, s-waves and artificial feed radiation also rise with the height of the dielectric material being employed, which lowers the antenna's bandwidth, unwanted cross-polarized radiation is also caused. The straightforward planar design of this approach makes it beneficial.

B. CB Feed

The CB feed mechanism is a very well-liked approach of feeding MSA. The patch antenna is joined to the coaxial connection's inner conductor, which is enclosed in the dielectric and is welded to it, while the connection's outer part of the conductor is fastened to the ground plane. The main advantage of this is the freedom with

which the feed may be placed within the patch to optimally adjust the input impedance. Its main flaws are a constrained bandwidth and modelling challenges brought on by the need to drill a hole in the substrate and the connection sticking out beyond the ground plane, which prevents it from being precisely flat for thick substrates.

C. PC Feed

This type of feeding mechanism for the patch antennas is based on the electromagnetic coupling. The radiating patch is positioned on top of the upper substrate, with the feed line sandwiched between the two dielectric substrates. The major benefit of this feed approach is the removal of stray feed radiation and the very high bandwidth (up to 13%) it offers owing to the overall increase in microstrip patch antenna thickness.

D. AC Feed

The ground plane acts as a barrier between the feed line and the radiating patch surface in this sort of feed technology. A slot or aperture in the ground plane helps to couple the patch and the feed line. The fluctuations in the coupling depend on the aperture's size (length and breadth), which is adjusted for greater bandwidths and lower return losses.

Because of benefits including no direct touch between the feed and radiator, broader bandwidths, and improved isolation makes AC feeding as appealing.

4. COMPARATIVE ANALYSIS

REF.	OVERALL DIMENSIONS (in mm)	CENTRE FREQUENCY (GHz)	SUBSTRATE DIELECTRIC CONSTANT (εr)	BANDWIDTH
[1]	28.8 × 37.2 × 1.6	2.5	4.2	43.758%
[3]	32 × 32 × 1.6	2.9/5.2/6.9/8.2 and 12.9	4.4	200/300/280/400/500 MHz
[5]	52.29 × 67.74 × 1.6	1.7 to 2.6	4.2	21.7%
[9]	40 × 40 × 1.6	2.4	4.4	109.9 MHz

5. CONCLUSION AND FUTURE SCOPE

The current study conducts a survey to get insight into the design of swastika patch antennas and finds that little research has been done on this sort of patch antenna. The various feeding methods as well as the employed design equations are discussed. Swastika-shaped antennas have found utility in a variety of products, including wireless communication equipment's

and medicinal devices. The study on the polarisation dependency and phase shifting where this form of antenna may put its candidacy for use has not yet been revealed which can be a great scope of research.

6. REFERENCES

[1] R. Mishra, R. Dandotiya, A. Kapoor, P. Kumar, 'Compact high gain multiband antenna based on split ring resonator and inverted F Slots for 5G industry applications', Applied Computational Electromagnetics Society Journal (ACES), vol. 36, no.8, pp. 999-1007, 2021.

[2] A. Sharma, R. K. Vishwakarma, 'Microstrip antenna with swastik slot for UWB applications', 2014 IEEE Students' Conference on Electrical, Electronics and Computer Science, pp. 1-5, 2014.

[3] P. Nagaraju, I. Khan, H. V. Kumaraswamy, D. H. Sachina, K. R. Sudhindra, 'Analysis of SWASTIK-shaped slotted MSPA antenna for 5G sub band applications', Global Transitions Proceedings, vol. 3, issue 1, pp. 80-85, 2022.

[4] I. Singh, Dr. V.S. Tripathi, 'Micro strip patch antenna and its applications: A survey', International Journal of Computer Applications in Technology, vol. 2, issue 5, pp. 1595-1599, 2011.

[5] A. K. Maurya, A. Singh, B. Pandey, S. Srivastava, R. Singh, 'Design and analysis of swastik slot loaded microstrip antenna at FR4 lossy substrate on L-band', International Journal of Engineering Sciences & Research Technology, vol. 4, issue 5, pp. 74-79, 2015.

[6] R. Verma, N. Vyas, R. Rana, V. Kaushik, A.K. Arya, 'Design study of microstrip antenna with various feeding techniques: A Review', International Journal of Engineering Research & Technology, vol. 3, issue 5, pp. 619-622, 2014.

[7] U. Raithatha, S. S. Kashyap, D. Shivakrishna, 'Swastika shaped microstrip patch antenna for ISM band applications', International Research Journal of Engineering and Technology, vol. 02, issue 02, pp.516-519, 2015.

[8] K. Sivakami, Vaisakhi V S, Kavitha B. Kumar, 'A design of swastika shaped microstrip patch antenna for wireless communication', International Journal of Scientific & Engineering Research, vol. 8, issue 7, pp. 156-160, 2017.

[9] S. Burlakoti, P. Rai, 'Performance comparison of swastika and rectangular shaped microstrip patch antenna', Kathford Journal of Engineering and Management, vol. 1, issue 1, pp. 11-14, Nov., 2018.

[10] A. Arora, A. Khemchandani, Y. Rawat, S. Singhai, G. Chaitanya, 'Comparative study of different feeding techniques for rectangular microstrip patch antenna', International Journal of Innovative Research in Electrical, Electronics, Instrumentation and Control Engineering, vol. 3, issue 5, pp. 32-35, 2015.

[11] A. Kumar, J. Kaur, R. Singh, 'Performance analysis of different feeding techniques', International Journal of Emerging Technology and Advanced Engineering, vol. 3, issue 3, 2013.

[12] A. Kapoor, R. Mishra and P. Kumar, 'A compact high gain printed antenna with frequency selective surface for 5G wideband applications', Advanced Electromagnetics, vol. 10, no. 2, pp. 27–38, 2021.

Biographies

Kumar Abhinandan Patial is pursuing the bachelor's degree in electronics and communication engineering from J.N. Government Engineering College, Sundernagar.

Simran Dogra is pursuing the bachelor's degree in electronics and communication engineering from J.N. Government Engineering College, Sundernagar.

Dr. Ankush Kapoor is working as an Assistant Professor in J.N. Government Engineering College Sundernagar Distt. Mandi H.P. He has more than 20 research articles in national/international journals and conferences being SCI/SCOPUS indexed. He has around 10 years of experience in academics. His research interests include Frequency selective surfaces, Design and Analysis of Microstrip Antennas and metamaterials.

Designing of smart grid system in Indian Scenario

Prashant Kumar, Woxsen University Hyderabad,

Paramjeet Singh Paliyal, Electrical cluster, UPES Dehradun

Surajit Mondal, Electrical Cluster, UPES Dehradun

Abstract

In terms of energy utilisation, the aim of this research is to build a smart small-scale electrical power system termed as a smart microgrid. One of the biggest trends in the electricity system right now is energy utilization. Energy is lost in enormous amounts due to the imbalance between energy production and consumption. Microgrids are crucial for generating energy from renewable sources like photovoltaic systems in response to demand. In a MATLAB and Simulink framework with standard distribution elements, the microgrid system has been modelled. Solar energy systems serve as the microgrid energy sources, while during normal operation, the main grid supplies electricity to residential areas. Another component of this microgrid is AC power generation. To accelerate simulation speed, the model employs the Phasor solution of Specialized Power Systems.

Keywords- Smart Grid, Micro grid, Renewable energy, solar energy, Wind energy.

1. Introduction

A microgrid is a local electrical grid with control features, allowing it to operate independently and cross over to the old grid. A grid connected to mid-generation sources enables the use of electrical appliances, heat, cooling systems, and electronics devices in homes, buildings, stores, and other facilities. Distributed generators, batteries, and renewable energy sources like solar panels, wind farms can be used as a dedicated power source for the Smart Microgrid . The world's population is requisite to increase by almost a billion every year, that bringing the total population to more than 30 billion by 2030. Two things will result from this population growth: an increase in energy demand and issues with power grids.

A microgrid can enhance the quality of the power network from the perspective of the consumer. Both the likelihood of depletion and overall energy expenses will be decreased. The microgrid can reduce the flow of energy through the transmission and distribution lines, as well as their losses and burden on the network. It can also make it easier to maintain the network in the event of a malfunctions. Microgrids can operate in island mode and while connected to the main grid. A strong loading / production network can be built using this program's assistance in resolving RES problems and uncertainties. The Microgrid program's adoption will benefit the environment by lowering our reliance on fossil fuels and, the threat of climate changes. The future of energy systems is definitely the implementation of this programme with RES as an additional energy resource.

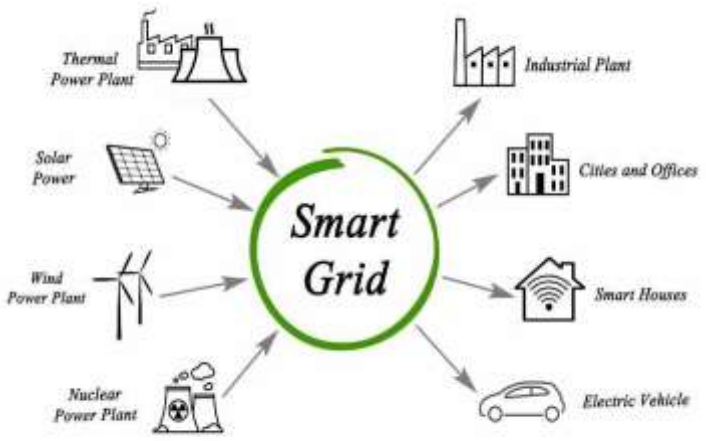

Fig 1: Smart grid scope and applications

2. Routes and challenges to using Smart grid in India.

As previously mentioned, the smart power grid is being transformed from a state-of-the-art technology to a functional level via smart grid technology. In order to provide relevant data to relevant Indian State stakeholders, the Department of Energy (Ministry of Power) engaged "The Climate Group" and "The Global e-Sustainability Initiative" at the System Modelling and Advancement in Research Trends. However, IT capabilities have totally improved and strengthened the simplification of the distribution side networks, which has improved the grid network by delivering personalised user service.

Table 1: Smart Grid Technologies, Challenges and Obligations.

Technology	Challenges	Obligations
Self – Healing Action	Security	Exploited from Internet Attacks (Spam, Worms, Virus etc.), National Question
	Reliability	Failure Loyalty during natural disasters, systemic exit and total darkness
Integration of Renewable Energy	Forecasting of Solar and Wind generation	Long term and unpredictable, random energy sources, unscheduled power flow and dispatch
	Power Flow Optimization	
Energy Storage Systems	Cost	Expensive energy saving systems such as Ultra capacitors, S.M.E.S, C.A.E.S etc
	Complexity	Complication of Complexities Complex design module and networks
	Non – Flexibility	Unique non-flexible designs for all individual networks do not make it easy to get used to
Consumers	Security	Malware, data capture, data corruption, illegal power management and Smuggling.
	Privacy	Sharing causes privacy attacks, copyright infringement, downside etc.
	Consumer awareness	Corruption and system threats like security and privacy issues.
	Disturbance	Grid Redesign Seeking balance and strength of the power system by grid weight.
	Harmonics Suppression	System instability during sag, dips or power fluctuations such as low voltage, volume power, electric lights etc.
Reliability	Grid Automation	The need for a strong data security system, with a secure and confidential network for reliable security, communication and control
	Grid Reconfiguration	System stability with grid complexity. And Generation demand equilibrium.

3. DESIGN AND SIMULATION OF MICROGRID

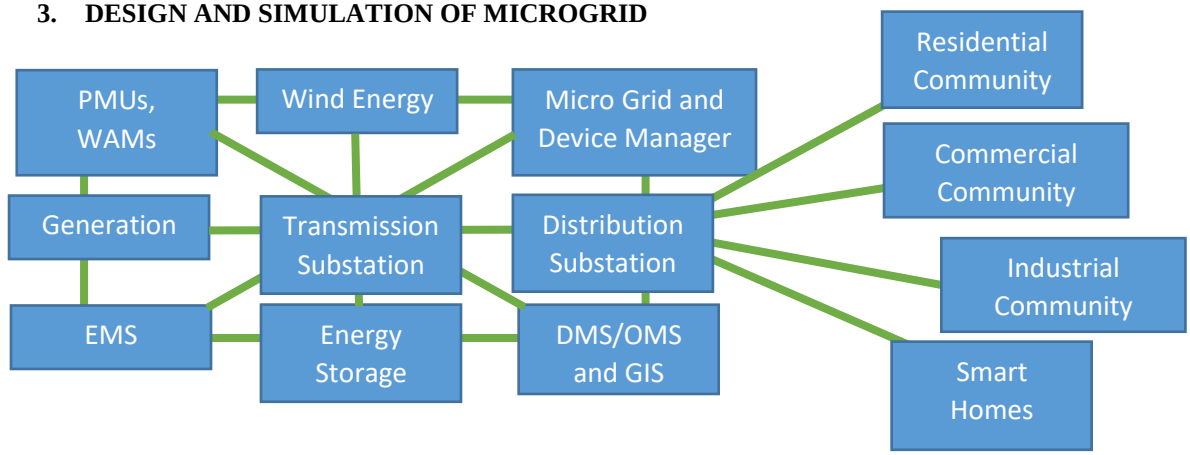

Fig 2: Block Diagram for smart grid hierarchy

Simulink Toolbox for MATLAB will be used to simulate the microgrid system. The simulation of AC power, a PV panel, a battery, and loads is represented in this image below.

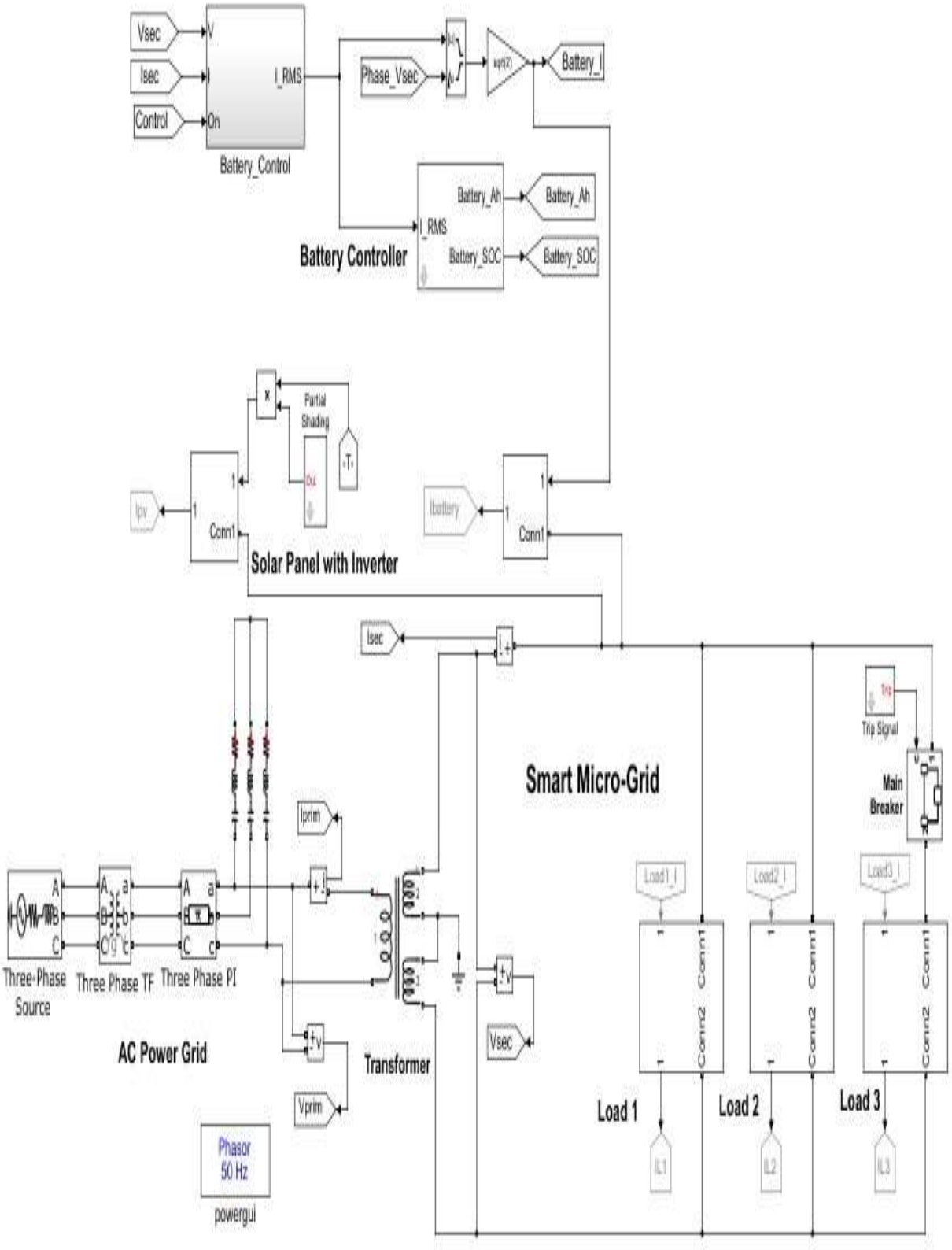

Fig 3: Smart microgrid design in Simulink

4. Simulation Results:

The simulation results below in figure shows the output waveform of the power generated with help of PV plant and the secondary AC grid, the first display scope is showing the waveform of the power generated by the PV and the maximum value is taken at 5000MW approx. The second display scope is showing the waveform of AC connected grid and the maximum value is taken at 4000MW approx. The third display scope is showing the power through the load side. All the values can be monitored by using the field data devices and by using the simulation we can find the real time performance in our smart grid system.

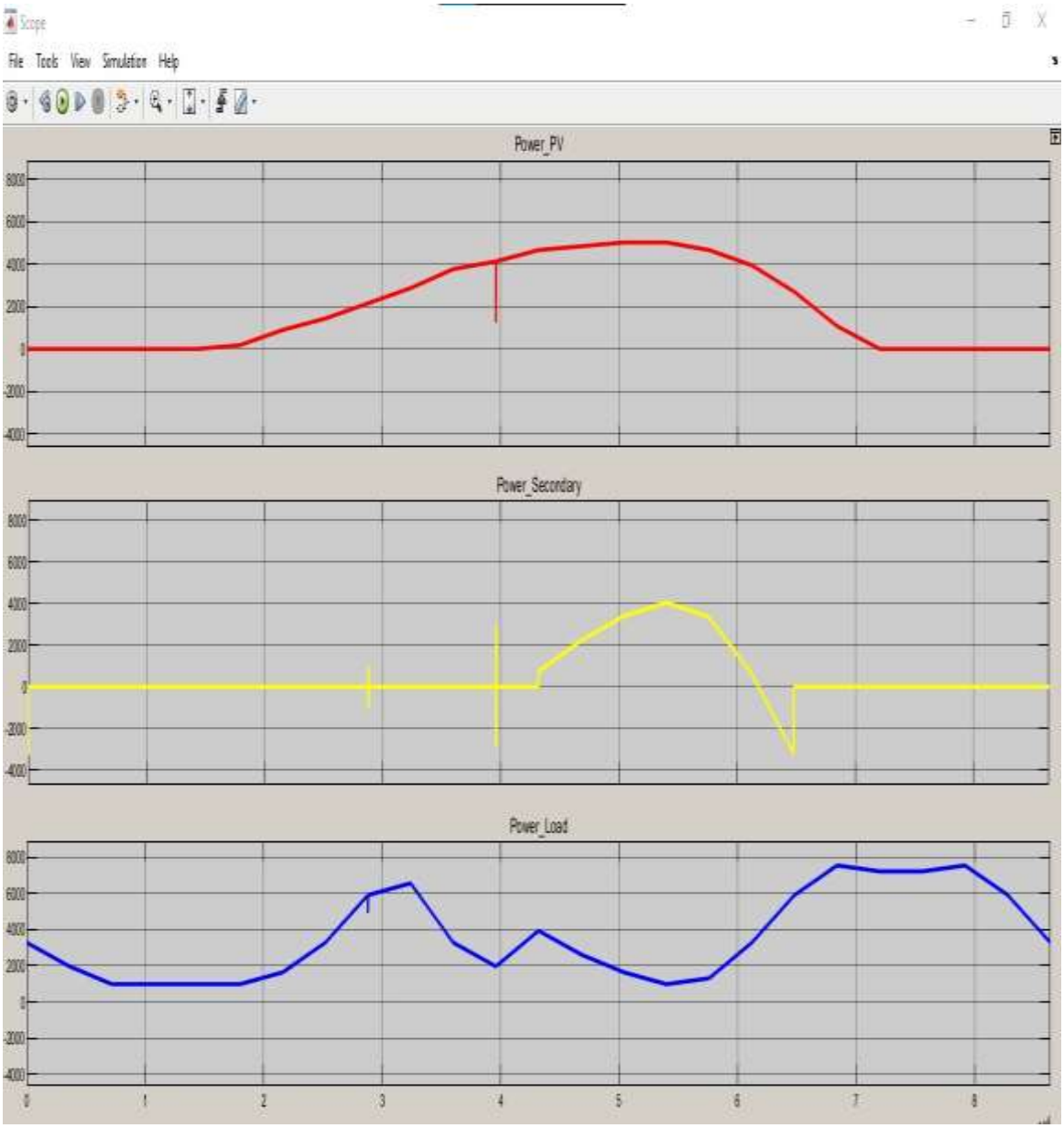

Fig 4: Power generation output waveform

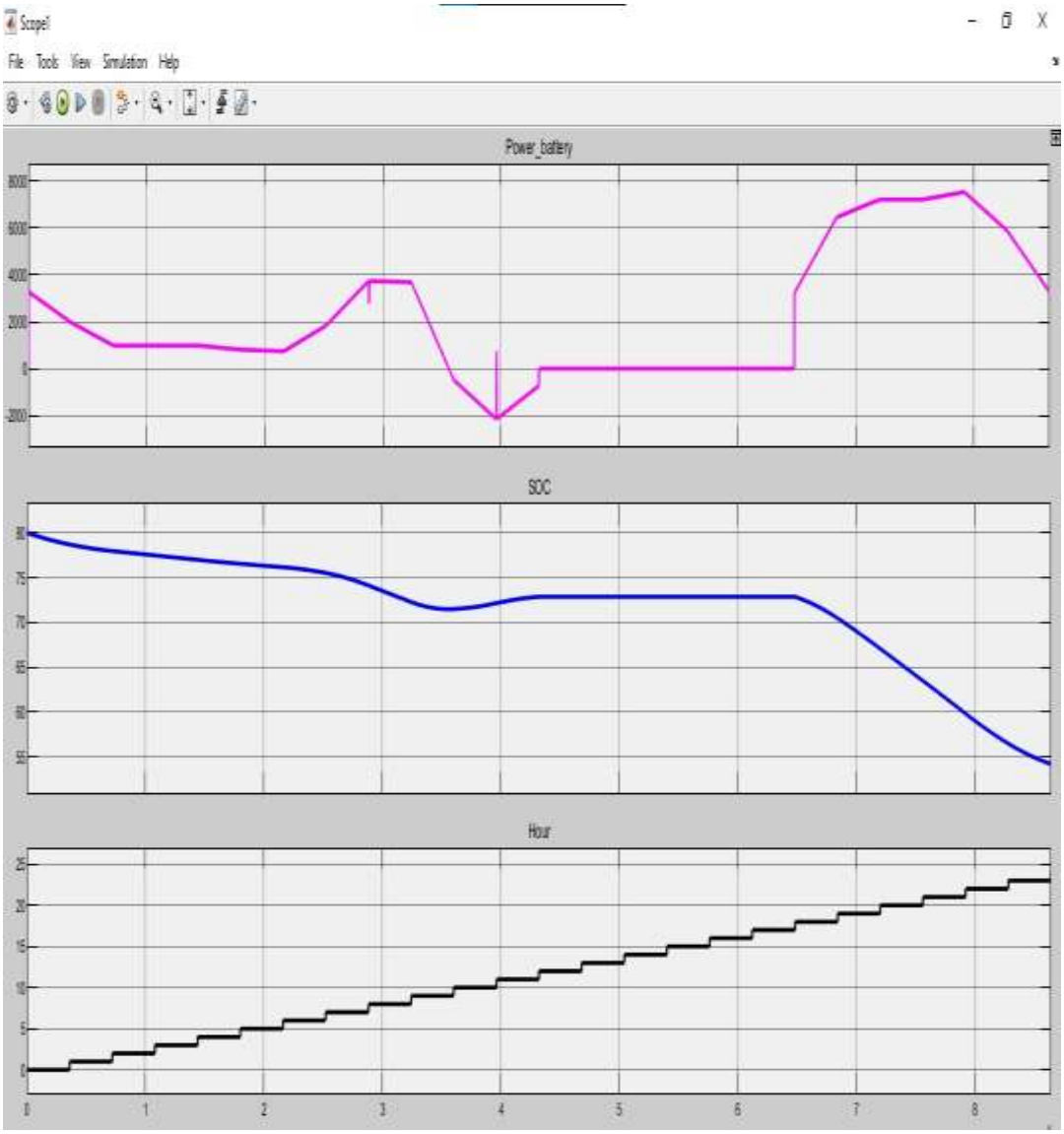

Fig 5: power battery, SOC, Time duration

The above figure shows the wave forms for the power through the battery, the waveform for the state of charge and the time duration. The above graph clearly shows how the power is varying with respect to time.

Conclusion and future scope:

A new generation of grid technology is being developed by smart microgrid in the fields of power management, automation of power generation and control to the other energy sources via energy storage devices. The dynamic and distributed control mechanisms are discussed using the Managing General Agents (MGAS) framework in a report above In line of this, the reports may serve as a reference point for future regulations that will direct the Indian power system to deploy the Smart grid in collaboration with RES.

A grid connection for power generation is an important factor of the study that was intended to build on photovoltaics and the design of photovoltaic grid connections in the Indian state. Furthermore, only few other micro grid and hybrid power-related projects have a power storage system that is expected to be completed soon. The ongoing research vision will be purposefully act as an advocate for the position and national development strategies in power and capacity in relation to the present and future need for power once the entire study has been completed.

Introducing the smart grid in the currently existing power system will enhance the efficiency, reduce the losses and give the better monitoring for the field data devices, research in this area will never stops, more the research

will make smarter the power system. The best way to make the power system smarter is to work more with renewable energy as it is more abundant in nature and is sufficient to fulfil the load demands.

References:

[1] Sinha, A.; Neogi, S.; Lahiri, R.N.; Chowdhury, S.; Chowdhury, S.P.; Chakraborty, N.; , "Smart grid initiative for power distribution utility in India," IEEE Power and Energy Society General Meeting, 2011 , vol., no., pp.1-8, 24-29 July 2011

[2] "The Green Grid: Energy Savings and Carbon Emission Reductions Enabled by a Smart Grid," EPRI Palo Alto, CA: 2008

[3] V.S.K. Murthy Balijepalli, S.A. Kharparde, R.P. Gupta, Yemula Pradeep, "SmartGrid Initiatives and Power Market in India" Proc. Of IEEE Power and Energy Society General Meeting, pp.1-7, Jul. 2010.

[4] Bossart, S.J.; Bean, J.E.; , "Metrics and benefits analysis and challenges for Smart Grid field projects," Energytech, 2011 IEEE , vol., no., pp.1-5, 25-26 May 2011.

[5] "Electricity Act '2003", Govt. of India, New Delhi, 2003 [6] Central Electricity Authority, 2010. [Online] Available: http://www.cea.nic.in/reports/electricity_act2003.pdf

[7] Ministry of Power, Government of India Website. [Online] Available: http://powermin.nic.in, Nov. 2009

[8] Pradeep, Y.; Thomas, J.; Sabari, C.L.; Balijepalli, V.S.K.M.; Narasimhan, S.R.; Khaparde, S.A.; , "Towards usage of CIM in Indian Power Sector," IEEE Power and Energy Society General Meeting, 2011 , vol., no., pp.1-7, 24-29 July 2011.

[9] Central Electricity Authority, 2010. [Online] Available: http://www.cea.nic.in/reports/yearly/energy_generation_10_11.pdf.

[10] Raoot, M.G.; Pentayya, P.; Khaparde, S.A.; Usha, S.; , "Complexities in integrating IPPs in Indian power system," IEEE Power and Energy Society General Meeting, 2010, vol., no., pp.1-9, 25-29 July 2010.

[11] Central Electricity Authority, 2010. [Online] Available:http://www.cea.nic.in/powersecreports/executive summary/201008/index.htm.

[12] Power Grid Corporation of Indian Limited, "Unified Load Despatch & Communications Scheme", Nomination for CSI-TCS Best IT Usage Award, National IT Awards, 2003.

[13] Y. Pradeep, S. A. Khaparde, and Reji Kumar, "Intelligent Grid Initiatives in India", Proc. Of 14th IEEE International Conference on Intelligent System Applications to Power Systems (ISAP), Kaoshiung, Taiwan, Nov 4th–9th, 2007.

14] J. P. Conti, "Let the grid do the thinking," IET Power Engineer, pp. 34– 37, April/May 2006.

[15] Balijepalli, V.S.K.M.; Khaparde, S.A.; Gupta, R.P.; , "Towards Indian Smart Grids" , Proc. Of TENCON 2009 - 2009 IEEE Region 10 Conference, vol., no., pp.1-7, 23-26 Jan. 2009.

[16] Technology Roadmap, Smart Grid, International EnergyAgency (IEA),http://www.iea.org/papers/2011/smartgrids_roadmap.pdf, pp. 6, 2011

[17] The Climate Group http://www.theclimategroup.org).

Biographies:

Dr. Prashant Kumar: Dr. Prashant Kumar is an Assistant Professor, Department of Electrical & Electronics Engineering at Woxsen University. He did his Master of Technology and Doctorate from NITTTR, Chandigarh and Doctorate from Maharana Pratap University of Agriculture and Technology, Udaipur, Rajasthan. In his 13 years of teaching and research duration, he has published eight research papers, including high repute International journals, International conferences. He has two design grants, four patents published, and two copyright grant on his account. He also has experience of organizing short term training programs, symposium and workshops. His research area includes Energy Storage, Demand Side Management, Electric Vehicle Integration, Integration of Distributed Energy Resources, and Smart Grid.

Dr. Surajit Mondal: Dr. Mondal did his Ph.D. on the Application of Solar Thermal Energy in 2020. Currently, he is associated with the Electrical and Electronics Engineering Department of the University of Petroleum and Energy Studies as an Assistant Professor-Senior Scale. He has published more than 35 International research and review articles as an author or co-author. He has issued 48 patents and granted 12 patents against his name.

Mr. Paramjeet Singh Paliyal: Mr. Paramjeet is the PHD Scholar in Electrical cluster in University of Petroleum Studies Dehradun. He has done his M.Tech in Power System Engineering from Uttarakhand Technical University, Main Campus, Dehradun. He has two publications and has two years of teaching experience.

IoT enabled Solar PV Maximum Power Tracking System

Mohd Nazim[1], Faizan Arif Khan[2], Ahmad Faiz Minai[3], Mohammed Asim[4], Mohammad Arifuddin Mallick[5], Mahfooz Ahmad[6]

[1,2,3,4,5]Department of Electrical Engineering Integral University Lucknow, India

[6]Deptt of Electronics & Comm. Engg. Integral University, Lucknow, India

Abstract: There have been significant technological growth in photovoltaic systems worldwide in recent years. It has increased environment-friendly electricity production. The Internet of Things (IoT) is one of the developing technologies with huge probabilities. IoT's association with renewable energy systems increases reliability and improves the controlling applications. Similarly, a solar PV system with IoT tracking is presented and analyzed in this work. Maximum energy production from solar cells is a preferable required criterion. This condition required a better leading power point tracking scheme which maximizes the power production of the photovoltaic cell in various odd conditions. Accordingly, the full proficiency of the solar power system can also increase by improving MPPT schemes. Over the past decade, many methods have been anticipated to implement maximum power tracking in a solar PV system. A novel idea of interfacing an IoT system and a photovoltaic system under partial shading conditions is proposed in this article.

Keywords: Solar PV, Internet of Things, P&O, MPPT,

1. INTRODUCTION

With the rising rate of power consumption and greenhouse emissions worldwide, many clean and environmentally friendly alternative renewable sources of energy generation have been. It has expanded the demand for renewable resources like solar photovoltaic devices [1]. Solar PV systems are executed either in off-grid or on-grid applications. Solar panels can be implemented on the rooftop or a plainer surface, according to system size and space availability [2]. Maximum power point tracking (MPPT) is a significant technical advancement used for the ultimate energy tapping from the solar PV system. Solar PV MPPT maintains the alignment of solar panels in the direction of maximum solar radiation fall. The MPPT method is efficiently performed under partial shading situations. Recently, several MPPT techniques have been projected for solar PV systems [3]. The performance of the solar photovoltaic system can be improved by adding different MPPT techniques. Currently, the Internet of Things (IoT) is a rising technology. It provides a connection between computing strategy and physical devices (such as mechanical devices, devices for animals, or human beings) through the internet for telemetric controlling. In the present scenario, the association of the Internet of Things with Solar PV MPPT schemes increases the performance of the whole arrangement. IoT technology collects the panel's statistics and is despatched to the cloud through the internet. The MPPT controlling devices utilize the IoT and additionally monitor many parameters of the Solar PV Monitoring System. It sends the command to start or stop the system scheme according to calculated records by the person from a remote place through the internet [4]. This paper presents a solar PV monitoring system using IoT-based MPPT techniques. The work given here shows better solar energy tracking performance than the other method.

2. METHODOLOGY

The solar energy application is growing at a rapid rate globally. In general, solar cells show nonlinear characteristics with changes in the weather. The power-voltage and current-voltage curves of the solar PV scheme keep a nonlinear property that primarily relies upon surroundings temperature, solar irradiance, and connected load [5]. The MPPT techniques have been developed for obtaining the Maximum Power from the photovoltaic cell. Several methodologies are used for tracking the maximum power and operating the solar PV panel at MPP more efficiently. Recent works include incremental conductance, perturb and observe, inherent neural networks, AI-based schemes and fuzzy logic control [6-8]. A combined operation of Solar PV systems with IoT-based MPPT tracking is proposed in this work. The complete procedure of the whole system follows the flow chart shown in figure1.

3. SOLAR PV SYSTEM

It is widely known that the Solar PV panels are made of solar cells. The solar cells are carrying the properties of semiconductors as they are basically member of semiconductor diode family sensitivity to the solar radiations. Therefore output of photovoltaic cells, responds for the solar irradiance, temperatures, shades, and dirt. At present, several models for solar cells are used for analysis by the different scholars [6-9].

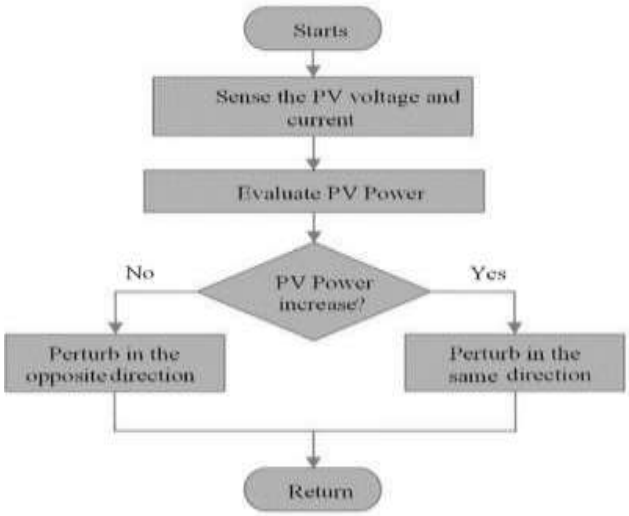

Figure 1: Flow chart of proposed system.

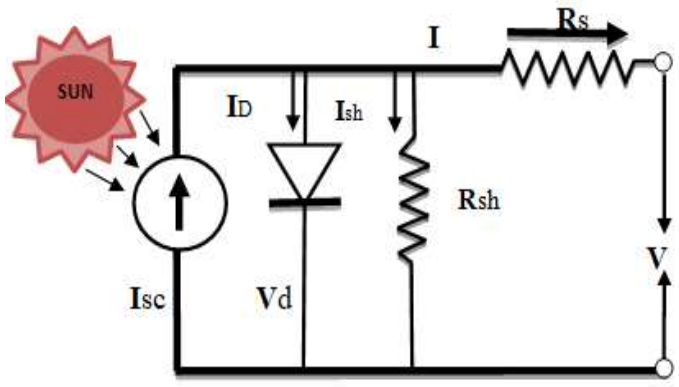

Figure 2: Schematic representation of a solar PV cell in Single diode model [11].

The single diode version is observed more efficient as compared to the double diode model. Therefore, a schematic arrangement of single-diode based photovoltaic scheme is considered for the solar cells study as illustrated in Figure 1. The short-circuit current also known as photo-current is presented by equation (1).It is generated by the fall of solar radiations on the solar modules.

$$I_{sc} = G/1000\ [I_{scr} + K_i\ (T_c - T_r)] \quad (1)$$

Where,

I_{sc} = Photo-current, G = solar irradiance, K_i= Temperature coefficient, I_{scr} = Reverse saturation current, T_r = Reference temperature, T_c = Cell temperature,

The output (V_{oc}) in the single diode model of the solar PV cell can be given by equation (2).

$$V_{oc} = \ln\ (I_{sc}/I_o + 1)\ (nkT_c) \quad (2)$$

Where,

V_{oc}= Open circuit voltage, n = Ideality factor, I_o = Saturation current, k = Boltzmann constant, T_c= Cell temperature,

The voltage and current relation of the solar cell is given by Equation (3)

$$I = I_o\ [\exp\ (qV/kT) - 1] - I_{ph} \quad (3)$$

Where,

V= voltage across the diode, T = absolute temperature, I_{ph} = light generated current.

$$I = Isc - I_0 \left[\exp\left(\frac{V+R_sI}{\frac{N_sKT}{q}a}\right) - 1\right] - \left(\frac{V+R_sI}{Rsh}\right) \quad (4)$$

Where,

Ns = series-connected cell, T = temperature of the PN junction, , Rs = Series resistance, Rsh = Shunt resistance

If the thermal voltage of the solar array is V_t = Ns KT/q, then Equation (4) may be rewritten as:

$$I = I_{sc} - I_0 \left[\exp\left(\frac{V+R_sI}{V_ta}\right) - 1\right] - \left(\frac{V+R_sI}{Rsb}\right) \quad (5)$$

4. MPPT(Maximum Power Point Tracker)

In general, the solar panel tried to be inclined toward the solar rays to get the highest absorbance. The accurate tracking of solar rays may be possible by using the MPPT mechanism. The axis of the solar panel is connected with the MPPT controlling technique. The tracking action occurs in the direction of the maximum tapping solar radiation [8]. The solar PV module uses tracking schemes for collecting solar radiation and moving structures among different periods of flexibility used to manipulate the oblique angle. The tracking motion can be controlled via either an inherent or a remote controller. The most common popular MPPT techniques are P&O and incremental conductance. Most of the researcher proposes the Perturb and observe algorithm as the best and most cost-effective method for implementing MPPT in solar panels. In this scheme set of rules can be easily adapted together with the software program and the hardware platform [10]. As a result, the Perturbed and observe algorithm is used in many cases to implement solar tracking. When P&O is turned on, the voltage in the panel array is completely disrupted. Figure 3 represent the P–V curve whilst the Perturbed, and observed algorithm and flowchart given in 4 is active. The output energy of a maximum power point constantly oscillates around the MPP. By decreasing the perturbation step rate, the oscillations of the P–V curve can be minimised.

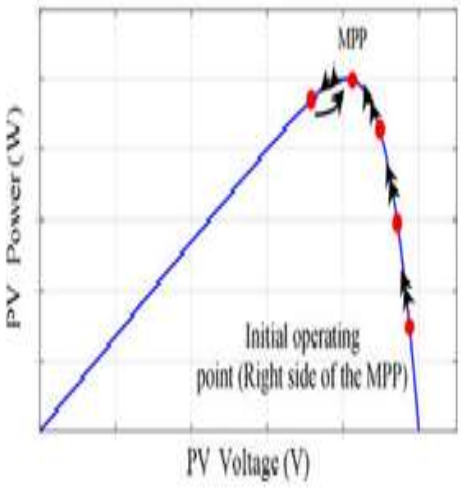

Figure 3 P-V curve of the Solar PV arra

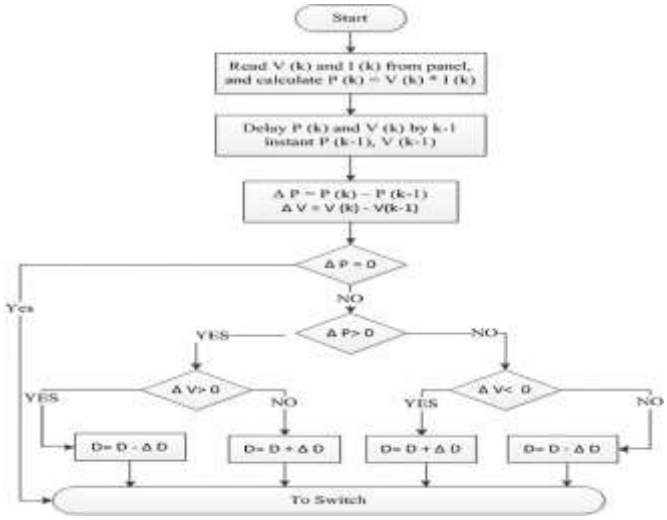

Figure 4. Proposed flowchart of P&O [10]

5. IoT (Internet of Things)

IoT has the capability to connect or control information without any human-to-human or device-to-computer physical interface. It works with the generation of unique ID, transmitted through wireless connection and operated by smartphone or any other device. The IoT is a rising technology have a tremendous ability to be applied for renewable energy, mainly solar photovoltaic cells. Maximum energy manufacturing is the general standard for any solar PV cell. The IoT is a spectre that combines numerous technologies in the conflux of power systems, data generation, elixirs, nanotechnology, and biotechnology. The Internet of Things system is primarily based on information apprehension systems, which include RFID, infrared sensors, GPS, laser scanners, and other different sensors, that can companion with the Internet to deal with teaching according to the protocol, which fetters sensible identification, locality and path, supervision, and management. In the intended system, we start the stain enumerate technique for monitoring sensors [10]. Cloud-based computing can also be accessed for different applications of IoT over the Internet. Cloud estimation is a large-scale processing opportunity that advances the system, as well as a complete generation that is entirely based on IP [12].

6. DESIGNING OF SOLAR ENERGY MONITORING SYSTEM USING IOT TECHNIQUES

The IoT-based monitoring and controlling solar devices using this device's online display makes use of power, voltage, current, temperature, climate changes, monitoring daylight, and dirt cleaning with the assistance of wipers. In the present work, IoT is used to track the MPP for the solar PV array. The application of this device tracking is to analyse daily data and controls solar wipers and daylight towards the motion of the solar panel [13]. The tracking and controlling are executed with the Arduino controller, the RPi, and sensors.

The implementation of an IoT-based monitoring and controlling system for PV panels is presented in figure 5. The components' features are then accumulated through a set of commands applied to a utility server to interrupt the solar energy tracking, determine the maximum power, and pick out uncommon occasions. This segment presents the framework of the Solar Energy tracking System using IoT techniques. Figure 5 depicts the observation of data transfer to the cloud via RPi. The schematic details of each block are discussed below.

6.1. Solar Panels

The Solar panels are made of solar cells arrangements. These cells are carrying the properties of semiconductors as they are basically member of semiconductor diode family sensitivity to the solar radiations. Therefore output of photovoltaic cells, responds for the solar irradiance, temperatures, shades, and dirt [14].

6.2. Sensor Unit

To recognize the alignment of the solar modules, an LDR was used as a light sensor, converting an alteration in resistance into a change in voltage [15].

6.3. Arduino Unit

An Arduino Uno is used to implement the sun tracking algorithm and controlling the motor. The voltage outputs of the LDR circuits are fed to the Arduino analog pins which are used for two servo motors. The Arduino board controlling scheme determines the voltage and once implemented, the solar panel block diagram determines the direction the panel should move.

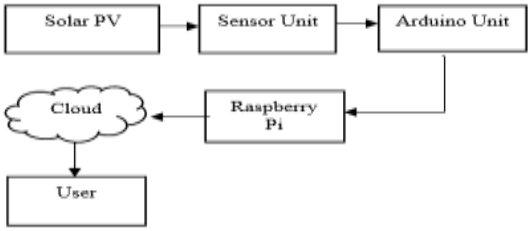

Figure.5: System Design of IoT based MPPT.

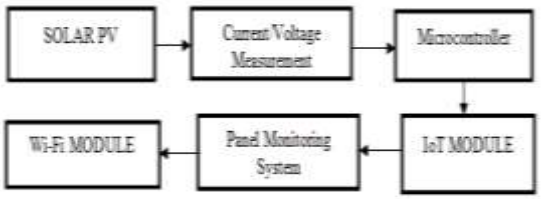

Figure 6. Solar PV Panel tracking Using IoT

7. WORKING SCHEME OF SPV TRACKING USING IOT

The schematic arrangement of SPV Tracking Using IoT is shown in Figure 6. The proposed hardware system is shown in Figure 7. Arduino detected the electrical parameters through a current and voltage sensor. The Raspberry PI provides information on Arduino output through the interface. Raspberry sends a review for the cloud. The cloud presents confirmation data in the form of signals that the entire patron can understand. The system design primarily ensures the observation of maximum power output in terms of the current and voltage estimation of the PV cell. The tracking information is transmitted between the controller and the PV server through the IoT channel. The controller unit processed the information about current and voltage to facilitate the server using the remote transmission.

The evaluation of current and voltage is checked and sent to the IoT module. In this work, the rural location of village Dasauli is considered for the hardware application situated at26º57.5'N, 80º60.0'E in the Tehsil BK Talab Distt Lucknow (UP) [13]. The annual solar radiation, clearness index and observed temperature are given in Figures 9 and 10. The peak season of solar radiation and temperature in May is considered for the study. The comparative values of load and power produced are displayed at the controlling location [19]. From this server, the current and voltage values of the PV panels can be controlled anytime, anywhere in the established PV system. The proposed solar system is tested by implementing an improved solar tracking P&O algorithm in hardware. Two servo motors are used for moving the solar panels. One is north-south, and the other is east-west. The controlling signal causes the servo-motor to move toward maximum radiation. Although the solar tracker monitors and adjusts the leading position of the solar modules, the solar output is constantly changing due to cloudy weather and solar radiation. The proposed improved P & O algorithm is applied for low-voltage solar systems using Arduino-UNO [14-15]. The outcome is transferred to software over the serial port and data from the Arduino output. It is observed that MPPT successfully tracked the maximum power from Solar panels. The PV characteristics of the solar panel traced the continuous operation of the PV module at that MPPT point.

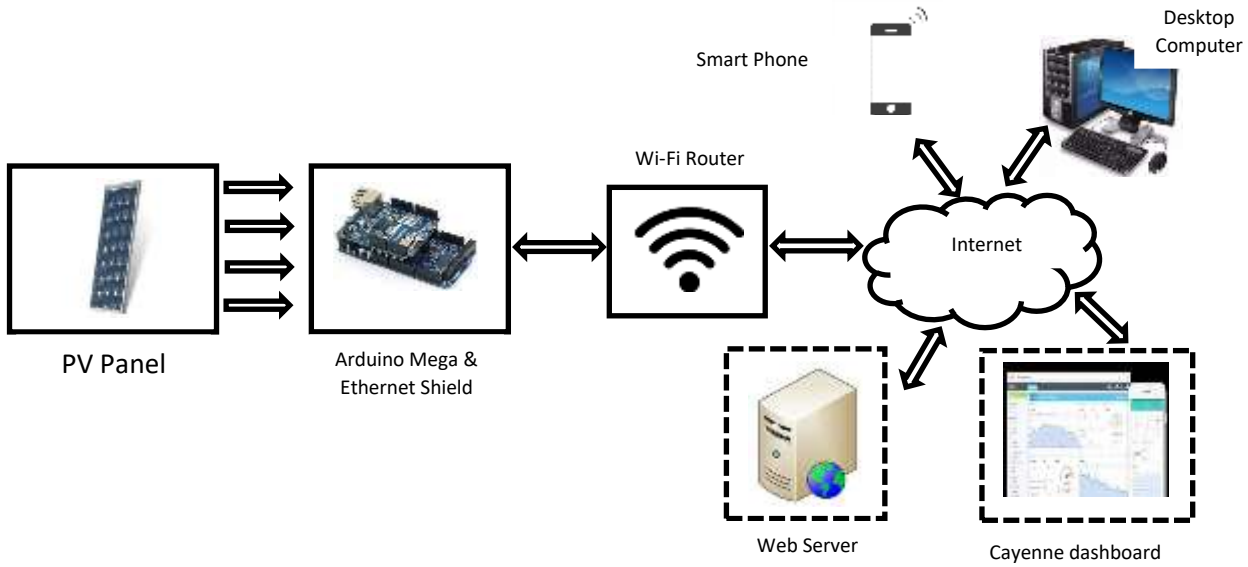

Figure 7: The experimental installation

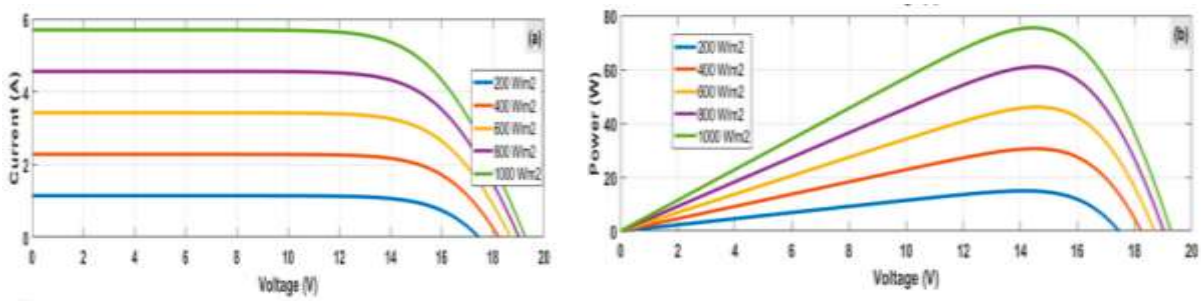

Figure 8: PV, VI characteristics of Working setup

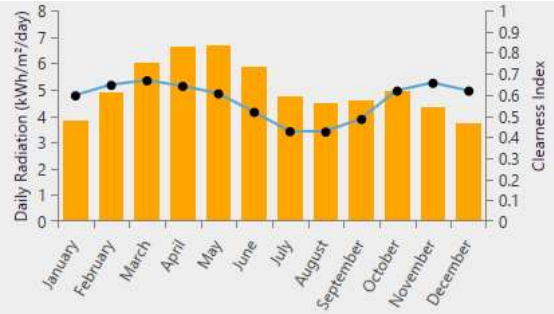

Figure 9: Solar radiation and clearness Index at considered location [20].

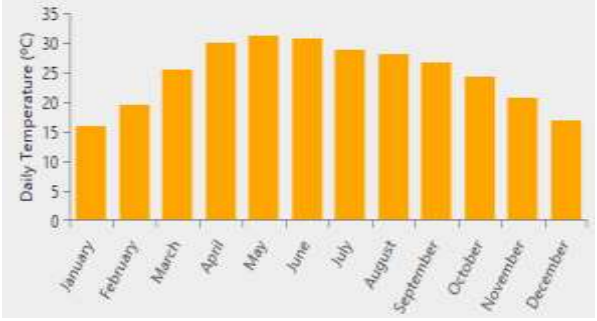

Figure 10: Annual Temperature at considered location [20]

8. RESULT AND DISCUSSION

The hardware scheme has arranged as shown in the schematic diagram. The system is performed for two conditions: the first condition is obtaining the result without IoT association in MPPT tracking. In the second, the monitoring is performed for the IoT-based arrangements. The obtained results are assimilated in Table 1 for both the conditions without IoT on the same day and with IoT performed in terms of voltage, current, and Power produced. There are many differences between the obtained result while using IoT and without IoT. Hardware system without IoT at 07:00 AM, gives the voltage and current as 10.80 V and 0.70 A, while it gives the voltage and current as 14.80V and 13.32A with IoT. A similar gap continues in both situations from 07:00 AM to 05:00 PM in voltage and current, as presented in Table 1. In addition, the power production also shows the gap between conditions with and without IoT: at 07:00 AM, the Power in both cases is 07.56 W and 13.32 W. The Power produced is approximately double the value without IoT. The comparative power curve for 24

hours is presented in Figure 11. It is very much clear from the figure that the system with IoT is more valuable because of getting the high value of the Power than the without IoT system.

Table 1: Comparative analysis of Power output with and without IoT association

Time in Hrs.	Case 1 (Without IoT)			Case 2 (With IoT)		
	V(V)	I(A)	P(W)	V(V)	I(A)	P(W)
07:00 AM	10.80	0.70	07.56	14.80	0.90	13.32
08:00 AM	10.70	1.00	10.50	14.60	1.20	17.52
09:00 AM	11.10	1.18	13.09	14.70	1.30	19.11
10:00 AM	11.30	1.20	13.56	15.20	1.40	21.28
11:00 AM	11.40	1.22	13.90	15.70	1.50	23.55
12:00 PM	11.50	1.30	14.90	16.00	1.60	25.60
01:00 PM	12.00	1.35	16.40	16.30	1.70	27.71
02:00 PM	12.80	1.42	18.15	16.80	1.75	29.40
03:00 PM	12.20	1.36	16.60	16.20	1.71	27.70
04:00 PM	11.40	1.25	14.25	15.80	1.62	25.59
05:00 PM	11.10	1.16	12.88	15.30	1.52	23.60

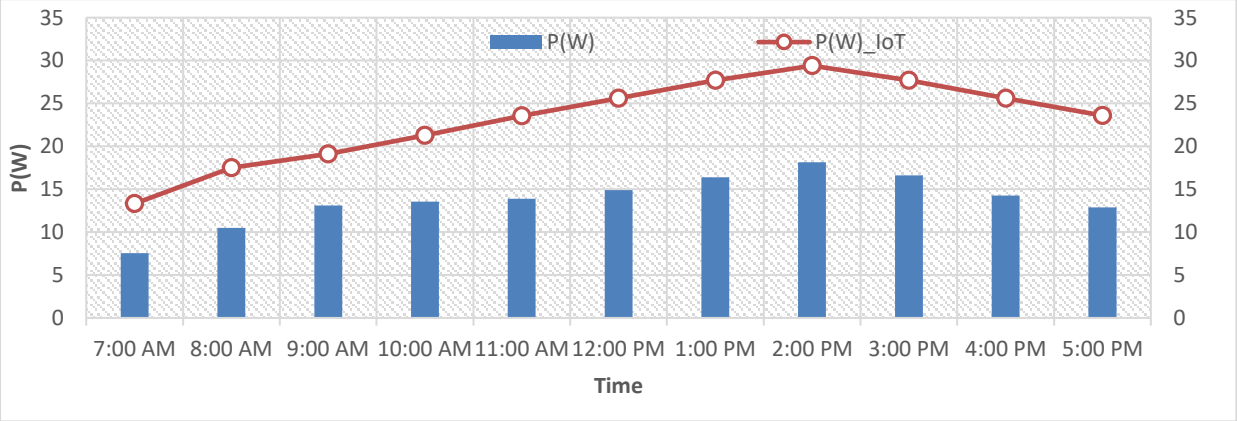

Figure 11: Comparative Power curve at considered location.

9. CONCLUSION

Renewable energy resources are gaining popularity as compared to traditional energy. It became helpful in degrading fossil fuel consumption and greenhouse gas emissions. The efficiency and reliability of renewable energy are continuously improving through the research and development processes. The current work presents a suitable solution for green energy production from solar PV. In this paper, an advanced MPPT technology for photovoltaic applications has discussed. Different methods of solar PV tracking have been explored, focusing on various parameters. A real-time data-based comparative analysis is presented using the necessary features to choose the suitable MPPT for the specific application. The proposed system is an efficient way to obtain the desired results. This IoT-based system can be advantageous for rural Solar PV applications. The P-V and V-I characteristics of the proposed MPPT methodology for PV panels are comparatively analysed. The IoT-based MPPT scheme has been successfully implemented to extract maximum power from solar PV. The present work also allows precise monitoring of the maximum output of solar PV arrangement.

REFERENCE

[1] M. Kumar, A. F. Minai, A. A. Khan and S. Kumar, "IoT based Energy Management System for Smart Grid," 2020 International Conference on Advances in Computing, Communication & Materials (ICACCM), 2020, pp. 121-125, doi: 10.1109/ICACCM50413.2020.9213061.

[2] Kwon, Jung Min, Bong Hwan Kwon, and Kwang Hee Nam. 2008. “Three-Phase Photovoltaic System with Three-Level Boosting MPPT Control.” *IEEE Transactions on Power Electronics* 23(5): 2319–27.

[3] R. K. Pachauri, A. F. Minai, V. Pandey, Shashikant, V. Goyal and R. Swain, "Optimal Placement of Modules in PV Array Systems to Achieve Higher GMPP under Obscured Irradiations," 2021 International Conference on Control, Automation, Power and Signal Processing (CAPS), 2021, pp. 1-7, doi: 10.1109/CAPS52117.2021.9730692.

[4] Subudhi, Bidyadhar, and Raseswari Pradhan. 2013. “A Comparative Study on Maximum Power Point Tracking Techniques for Photovoltaic Power Systems.” IEEE Transactions on Sustainable Energy.
[5] A. A. Khan, A. F. Minai, L. Devi, Q. Alam and R. K. Pachauri, "Energy Demand Modelling and ANN Based Forecasting using MATLAB/Simulink," 2021 International Conference on Control, Automation, Power and Signal Processing (CAPS), 2021, pp. 1-6, doi: 10.1109/CAPS52117.2021.9730746.
[6] Ram, J. Prasanth, T. Sudhakar Babu, and N. Rajasekar. 2017. “A Comprehensive Review on Solar PV Maximum Power Point Tracking Techniques.” Renewable and Sustainable Energy Reviews.
[7] Goetzberger, Adolf, Christopher Hebling, and Hans Werner Schock. 2003. “Photovoltaic Materials, History, Status and Outlook.” Materials Science and Engineering R: Reports 40(1): 1–46.
[8] Ali, Ali Nasr Allah, Mohamed H. Saied, M. Z. Mostafa, and T. M. Abdel- Moneim. 2012. “A Survey of Maximum PPT Techniques of PV Systems.” In 2012 IEEE Energytech, Energytech 2012,.
[9] Faizan Arif Khan, Nitai Pal, Syed Hasan Saeed,Chapter 31 - Stand-alone hybrid system of solar photovoltaics/wind energy resources: an eco-friendly sustainable approach, In Advances in Nonlinear Dynamics and Chaos (ANDC), Renewable Energy Systems, Academic Press,pp 687-705,2021,https://doi.org/10.1016/B978-0-12-820004-9.00030-9.
[10] Minai, A.F., Usmani, T., Uz Zaman, S., Minai, A.K. (2022). Intelligent Tools and Techniques for Data Analytics of SPV Systems: An Experimental Case Study. In: Malik, H., Ahmad, M.W., Kothari, D. (eds) Intelligent Data Analytics for Power and Energy Systems. Lecture Notes in Electrical Engineering, vol 802. Springer, Singapore. https://doi.org/10.1007/978-981-16-6081-8_16
[11] Fatima, K., Minai, A.F., Malik, H. (2022). Intelligent Approach-Based Maximum Power Point Tracking for Renewable Energy System: A Review. In: Malik, H., Ahmad, M.W., Kothari, D. (eds) Intelligent Data Analytics for Power and Energy Systems. Lecture Notes in Electrical Engineering, vol 802. Springer, Singapore. https://doi.org/10.1007/978-981-16-6081-8_19
[12] Sarkar, P. R., Khan, F. A., & Ahamad, I. (2015). Performance enhancement of Multilevel Inverter in PV system with new topology. *International Journal of Advance Engineering and Research Development*, *2*(1), 301-307.
[13] Locations of the selected site in the north India, viewed on 12 Sep 2020. <https://www.google.com/maps/d/viewer?mid¼1PRNsTVTx_mxFS944bTNCFZldOoI&ie¼UTF8&t¼h&oe¼UTF8&msa¼0&ll¼26.974934600000008%2C81.00161589999999&z¼18.>
[14] F. A. Khan, S. H. Saeed, M. Asim, S. Rahman and P. R. Sarkar, "Cost Optimization by adding SPV Plant at Load end in a Grid Connected System," *2018 International Conference on Computational and Characterization Techniques in Engineering & Sciences (CCTES)*, 2018, pp. 65-70, doi: 10.1109/CCTES.2018.8674149.
[15] Ahmad, Eahraz and Khan, Faizan A and Sarkar, Prabhat R, Modelling & Simulation of PV Module Connected with Three-Port DC Converter (July 8, 2021). http://dx.doi.org/10.2139/ssrn.3882303
[16] Saifur Rahman, Alwadie A., Faizan A Khan. Generation Of Electricity Using Renewable Energy Resources published in International Conference on Renewable Energies and Power Quality (ICREPQ’17) Malaga (Spain), 4th to 6th April, 2017,in Renewable Energy and Power Quality Journal,Vol.1, No.15, April 2017, ISSN 2172-038 X, https://doi.org/10.24084/repqj15.238,
[17] Uzma Aslam, Faizan A. Khan, Prabhat Ranjan Sarkar, Abu Shoban “Comparative Study on various Custom Devices” published in the International Journal Of Innovative Research In Electrical, Electronics, Instrumentation And Control Engineering, Vol. 4, Issue 2, February 2016, ISSN (Online) 2321-2004, ISSN (Print) 2321-5526, DOI 10.17148/IJIREEICE.2016.4230.
[18] Mahfooz Ahmad, Faizan A. Khan, Saifur Rahman, Saima Rahman “Development of a Digital Multimeter: A Low-Cost Design Approach” published with the “International Journal of Engineering and Management Research”, Volume-6, Issue-2 of March-April 2016. ISSN (Online): 2250-0758, ISSN (Print): 2394-6962
[19] SM Asmer Saeed Kazmi, F. A. Khan, P. R. Sarkar, A. F. Minai , Performance Analysis of Solar PV based Flying Capacitor Multilevel Inverter using MATLAB/Simulink International Journal of Engineering Research and Applications ISSN: 2248-9622, Vol. 10, Issue 8, (Series-III) August 2020, pp. 62-66. DOI: 10.9790/9622-1008036266.
[20] https://www.firstgreen.co/climate-zone-map-of-india/

Survey on Optical technologies used for Communication

[1,5]Shivmanmeet Singh, [2]Harmandeep Kaur, [3,5]Lakhveer Singh, [4,5]Rehan Dhir [6]Ajay Vasishth

[1]*Department of Electronics and Communication Engineering, Guru Nanak Dev Engineering College, Ludhiana, India*

[2]*Department of Computer Application, Guru Nanak Dev Engineering College, Ludhiana, India*

[3]*Department of Mechanical and Production Engineering, Guru Nanak Dev Engineering College, Ludhiana, India*

[4]*Department of Mechanical Engineering, Guru Nanak Dev Engineering College, Ludhiana, India*

[5]*Center for Multifaceted Learning, Guru Nanak Dev Engineering College, Ludhiana, India*

[6]*Department of Physics, Chandigarh University, Mohali, India*

Email:, shivmanmeet@gmail.com, harmandeepkaur156@gmail.com, lakhveerbathinda@gmail.com, rehan2000.rd@gmail.com, ajay.e8023@cumail.in

Abstract.

Future high data rate fifth Generation mobile networks services will need more frequency transmission, which is now inadequate to do so. A potential answer to the radio frequency spectrum dilemma is optical wireless communication as it can be used on an extremely broad range of unregulated spectrum. In the last ten years, it has drawn increasing scientific attention from all around the globe for both outdoor and indoor applications. OWC offloads applications from radio frequency networks that generate a lot of data. Through OWC, a 100 Gigabit per second data rate has already been demonstrated. Both indoor and outdoor services are available, and communication ranges from a few nm to more than 10,000 km. In this work, optical wireless technologies are reviewed and given a technical overview. We review the most important technologies for comprehending OWC and provide cutting-edge standards. Clarifying the distinctions between many prospective related current radio frequency technologies is the main contribution of this research.

Keywords. Internet of Things (IoT), Electric (E), magnetic (M), and electromagnetic (EM).

1. INTRODUCTION

The latest work in mobility communication is 5G communication. With the superior system capacity, huge interconnections, lowest energy consumption, ultra-high security and exceptionally high experience quality [1]–[6], it will provide novel services. It can be anticipated that 5G communication would use densely branched heterogeneous networks, with a 1000-fold increase in mobile data volume per area and a 100-fold increase the number of wireless devices connected, compared to the number of current wireless networks [1]. Radio frequency (RF) is now an extensively utilised technology in many wireless

applications but the spectrum is not enough to support the IoT paradigm and the rising need for 5G wireless bandwidth. It is anticipated that existing wireless technologies will not be able to capture the enormous connectivity requirement of future mobile data traffic because the electromagnetic spectrum, which has advantageous communication properties below 10 GHz, has almost been exhausted by current wireless technologies [12]. In addition, the band (below 10 Gigahertz) includes restrictions such as a band with narrow spectrum, laws governing the usage of the spectrum, and intense RF interference from neighbouring access points. As a result, for wireless communication connection, researchers are exploring new complementing spectrum, such as mm and nm waves [11]. The electromagnetic spectrum's RF band spans a range of frequencies from 3 Kilohertz to 300 Gigahertz. Local and international authorities have severe regulations on the usage of this band. Most of the time, only a few operators, such as point to point television broadcasters, microwave connections and cellular phone companies, are granted full licences for RF sub-bands. Future high density, high-capacity networks are predicted to be developed using the optical spectrum, which is seen as a potential option. Using the optical spectrum, wireless connection is called OWC (OWC). It can provide quality services both indoors and outside. However, OWC systems struggle because of their susceptibility to obstruction blocking and their low transmitted power. Thus, the cohabitation of OWC and RF systems may provide a practical answer to the enormous needs of the impending 5th Generation mobile networks and beyond communication systems.

2. OVERVIEW

2.1. What do OWC Technologies consist of?

Using directed visible light (VL), ultraviolet (UV) or infrared (IR) spectrum as the propagation medium, optical transmission is referred to as OWC. OWC systems that use this band are often referred to as visible light communication systems. VLC can provide lighting and location all at once. IR, UV, and VL frequencies are used for satellite to earth systems. Line of sighting process and non-sighting process is used for optical communication lines thereafter possible working using UV communication.

2.2 Platforms for OWC Applications

Applications for OWC span a broad spectrum [12]. Number of settings where OWC may be used, including business, healthcare, railroad stations, transportation, residences, workplaces, malls, underwater environments, and space.

2.3. OWC for IoT and 5G

Optical Wireless Communication (OWC) has emerged as a viable solution for enabling high data date trans receiver stations [6] to overcome the problem of distance, speed and time. Furthermore, high-capacity backhaul support for 5th Generation mobile networks and beyond communication systems may be efficiently provided via FSO, LiFi, and VLC. OWC technologies use relatively little power, which is essential for 5G [2].

2.4. Classification by OWC

OWC systems can be broadly divided into five groups based on communication range. Ultra-short range OWC: Communications at the nm/mm level take place in this subcategory of

OWC. Nm distance chip to chip communication is an example of this kind of communication. Medium range OWC: This particular communication range includes outdoor V2X communications and WLANs based on VLC. Long-range OWC: This particular range of communication allows for km-range connections, for instance, between buildings. Ultra-long range OWC. This particular communication range includes linkages between satellites, between satellites and the Earth, between satellites and aircraft, between aircraft and other aircraft, and between aircraft and the ground.

3. TECHNOLOGIES USED

The architecture and operating principles of each optical technology (VLC, OCC, LiFi, FSO and LiDAR) are distinct. Additionally, they could vary in terms of communication medium, sending and receiving systems, and modulation techniques. The fundamental structures of the different OWC technologies. As physical transmitters, several OWC devices employ either LDs or LEDs. Physical receivers are PDs, cameras, or ISs, while communication mediums are IR, VL, or UV spectra. This diagram illustrates how the transmitter, receiver, and communication medium of the different OWC systems vary from one another.

3.1. Communication with Visible Light (VLC)

Over the decade, VLC which is a fragment of OWC, has become an encouraging technology. VLC might be crucial in achieving this goal since IoT makes it possible for several devices to be linked for resource sharing, monitoring, and sensing. Compared to RF-based solutions, VLC technology provides 10,000 times larger bandwidth capacity. Significant prospects for applications in homes, workplaces, vehicles, aircraft, trains, and roadways are offered by VLC based on the VL spectrum. Additionally, it does not hurt anyone.

3.2. Light Fidelity (LiFi)

Light Fidelity falls within the category of nm-wave communication. Light Fidelity and Visible Light Communication differ primarily in that Light Fidelity is a bidirectional communication system, whereas VLCS can be either unidirectional [3] or bidirectional [4], (ii) VLCS can be either unidirectional [3] or bidirectional [4], and (iii) Light Fidelity must provide seamless user mobility, whereas mobility support is not required for Visible Light Communication; and (iv) Visible Light Communication systems can be either unidirectional [3] or bidirectional. Thus, Light Fidelity creates a new tiny at to cell layer inside existing heterogeneous wireless networks since it is a full-featured wireless networking system that facilitates smooth user mobility. In light of this, a Visible Light Communication system will only be considered a Light Fidelity system if it contains Light Fidelity capabilities (such as multiuser communication, point-to-multipoint and multipoint-to-point communications, and seamless user mobility). However, a Light Fidelity system may only be considered a Visible Light Communication system when VL is utilised as a transmission medium.

3.3. Communication using optical cameras (OCC)

We are now quite used to having smart gadgets in our daily lives. Majority of these gadgets have front and/or back facing camera/cameras with Light Emitting Diodes flashes. This enables it to build OWC utilising devices in an easier way where the transceiver pair is a flash and a camera. No more hardware modifications are needed for this approach. OWC implementation employing Light Emitting Diodes, screens or other light sources, it might

be considered an Optical Camera Communication system. Additionally, when an Optical Camera Communication system employs VL as the communication medium, it may be regarded as a Visible Light Communication.

3.4. Optical Free Space Communication (FSOC)

A subclass of OWC called FSOC [7]-[9] is often operated utilising the Near Infrared channel. Additionally, it can be controlled utilising the UV and VL spectra. The levels of attenuation are lower while employing IR, however. In FSO, illumination is not necessary. Instead of using LEDs for the transmission, FSO often employs LDs. The inputted source information data must be sent to a distant location. The raw data is first encoded. Prior to modulation, channel coding is an optional step. OOK/PM/OFDM modulation is carried out by the modulator. If necessary, an optical amplifier may be utilised to boost the modulated beams of laser power intensity. Light beam is then gathered and can be refocused using beam forming optics prior to transmission [7]. An LD is often used as an optical source in FSO systems [2]. Some manufacturers further use beam collimators and high-power LEDs. In FSO systems, the optical source should be able to supply relatively power for temperature. The optical filters and lens on the receiver front-end gather and concentrate into receiver. The voltage is then created from the PD output current.

3.5. Light Detection and Ranging (LiDAR)

Light Detection and Ranging (LiDAR) is an appealing optical remote sensing technique which helps to determine a target's range and/or other details about it [2], [3]. NIR and VL are often used by LiDAR to image things. The laser installed on an aeroplane, for instance, can be utilised to map topography with a resolution of 300 mm or greater. In order to construct points for 3D mapping, beams of laser are employed to find the characteristics of dispersed light. Similar technologies and concepts are used by LiDAR and RADAR to track the positions and motions of objects, respectively. Each technology functions differently, and each has a different set of applications that it is best suited for. Both technologies employ the energy reflected off the things they are aiming at to infer different information about those items. In contrast to RADAR, LiDAR employs optical light as its source of energy rather than microwaves. The energy in the form of optical light is sent from a transmitter as a signal in both LiDAR and RADAR. An item reflects a little of the energy of the original signal when it gets affected by the transmitted signal. The receiver at the site of the source of energy subsequently receives this reflected energy, which is then used to obtain the object's distance, size and other properties. Additionally, most of these things that can be accurately measured and found using RADAR and LiDAR range are size and makeup.

4. UNRESOLVED PROBLEMS AND PROSPECTIVE RESEARCH LINES

4.1. Hybrid Network Architecture

In particular, optical wireless is a strong contender for delicate applications where RF interference must be minimised. A hybrid network may be useful for load balancing, improving link stability, providing wireless access in far-off locations (such as deep space, ocean and earth conditions), and therefore reducing interference. The researchers were

drawn to this problem because of this. Switching from one communication method to another in an adaptable and seamless manner is a key difficulty for hybrid systems.

4.2. High data rate optical backhaul

High capacity backhaul networks are a critical problem for 5G and beyond communications [3]. An interesting area for investigation is optical wireless networks, such as VLC or FSO, which can act as a nice addition to the current wired and wireless backhaul communication.

4.3. UV communication via NLOS and Inter Cell Interference (ICI)

UV communication, a key characteristic of the UV band, allows for high-data-rate NLOS communication. Future study should focus on a thorough evaluation and utilisation of trans receiver geometrical configuration needs. ICI is a concern for dense validation of LED's for LiFi/VLC small cell/attocell design. The optical spectrum may be extended beyond the UV band, which has several advantages thanks to powerful and reasonably priced sources.

4.4. Wireless optical communication underwater

As several applications for oil pipe inquiry, and off-shore investigation have been presented, underwater wireless optical communication has recently gained a lot of interest. Many underwater communication applications need long-distance, fast connectivity.

4.5. Mobility with ease and in vehicle communication

OWC systems are necessary for providing the user mobility. At best, LiFi currently offers seamless connectivity [11]. Thus, researchers are trying to validate vertical handovers [4] in hybrid networks [1]. To maintain smooth connections, it is crucial to have a handover mechanism. This is a difficult problem that has to be thoroughly researched. There is thus a tonne of room to improve air loss mitigation in OWC systems. IEEE 802.11p employs an unlicensed RF spectrum and is also called Wireless Access in Vehicular Environments (WAVE). The OWC system may potentially be used for traffic control.

4.6. OWC for positioning and in drone application

High precision, licence-free operation, lack of electromagnetic interference, affordable frontends, etc., are the main reasons of attention of LED positioning [10]. Also, might be the next big thing in transportation. Numerous problems, including accurate location and dependable drone communication, will emerge from its large-scale deployment. Due to the shortcomings of RF-based technologies, OWC might be a useful supplementary strategy to resolve these problems.

4.7. Red, Green and Blue (RGB) LED-based OCC

[5], [8] OCC employing Red, Green and Blue LEDs and colour cameras (or IS) is a potential method for successful parallel (‖) visible light communications. Numerous scientists are focusing on RGB LEDs to create effective communication technologies.

5. CONCLUSION

The rapid surge in demand for wireless bandwidth for 5th Generation mobile networks and future communications cannot be met by the present RF technology. Visible, infrared and ultraviolet sub-bands of the exceptionally broad optical spectrum may be exploited for

wireless networking to enable 5G and IoT. The issues brought on by a lack of spectrum for RF-based wireless communication will be solved by using optical bands in addition to RF. Many applications that presently rely on RF communication are being converted to OWC by researchers. Healthcare, industry, places of public meeting, stadiums, homes, workplaces, transits, retail markets and malls, underwater communication, and space will all significantly benefit from optical wireless technology. We have showcased a broad overview of upcoming OWC technologies in this survey report. To ensure a brighter future, optical wireless technologies are undoubtedly promising. In the coming time, 5G and beyond heterogeneous wireless networks, we anticipate that OWC systems will play a significant complementary role to RF-based technologies, and we believe that this comparative assessment will be a critical asset for further research in these areas.

References

[1] P. Pirinen, "A brief overview of 5G research activities," in Proc. of *International Conference on 5G for Ubiquitous Connectivity (5GU)*, Nov. 2014, pp. 17-22.

[2] M. Shafi, A. F. Molisch, P. J. Smith, T. Haustein, P. Zhu, P. D. Silva, F. Tufvesson, A. Benjebbour, and G. Wunder, "5G: a tutorial overview of standards, trials, challenges, deployment, and practice," *IEEE Journal on Selected Areas in Communications*, vol. 35, no. 6, pp. 1201-121, Jun. 2017.

[3] M. Jaber, M. A. Imran, R. Tafazolli, and A. Tukmanov, "5G backhaul challenges and emerging research directions: a survey," *IEEE Access*, vol. 4, pp. 1143-1166, May 2016.

[4] D. Zhang, Z. Zhou, S. Mumtaz, J. Rodriguez, and T. Sato, "One integrated energy efficiency proposal for 5G IoT communications," *IEEE Internet of Things Journal*, vol. 3, no. 6, pp. 1346-1354, Dec. 2016.

[5] H. A. U. Mustafa, M. A. Imran, M. Z. Shakir, A. Imran, and R. Tafazolli, "Separation framework: an enabler for cooperative and d2d communication for future 5G networks," *IEEE Communication Surveys & Tutorials*, vol. 18, no. 1, pp. 419-445, 2016.

[6] J. G. Andrews, S. Buzzi, W. Choi, S. V. Hanly, A.Lozano, A. C. K. Soong, and J. C. Zhang, "What will 5G be?," *IEEE Journal on Selected Areas in Communications*, vol. 32, no. 6, pp. 1065-1082, Jun. 2014.

[7] A. A. Fuqaha, M. Guizani, M. Mohammadi, M. Aledhari, and Moussa Ayyash, "Internet of things: a survey on enabling technologies, protocols, and applications," *IEEE Communication Surveys & Tutorials*, vol. 17, no. 4, pp. 2347-2376, 2015.

[8] P. Schulz, M. Matthé, H. Klessig, M. Simsek, G. Fettweis, J. Ansari, S. A. Ashraf, B. Almeroth, J. Voigt, I. Riedel, A. Puschmann, A. M. Thiel, M. Müller, T. Elste, and M. Windisch, "Latency critical IoT applications in 5G: perspective on the design of radio interface and network architecture," *IEEE Communications Magazine*, pp. 70-78, Feb. 2017.

[9] M. R. Palattella, M. Dohler, A. Grieco, G. Rizzo, J. Torsner, T. Engel, and Latif Ladid, "Internet of things in the 5G era: enablers, architecture, and business models," *IEEE Journal on Selected Areas in Communications*, vol. 34, no. 3, pp. 510-527, March 2016.

[10] W. A. Hassan, H.-S. Jo, and T. A. Rahman, "The feasibility of coexistence between 5G and existing services in the IMT-2020 candidate bands in Malaysia," *IEEE Access*, vol. PP, no. 99, 2017.

[11] A. Ijaz, L. Zhang, M. Grau, A. Mohamed, S. Vural, A. U. Quddus, M. A. Imran, C. H. Foh, and R. Tafazolli, "Enabling massive IoT in 5G and beyond systems: phy radio frame design considerations," *IEEE Access*, vol. 4, pp. 3322-3339, Jul. 2016.

[12] D. Tsonev, S. Videv, and H. Haas, "Towards a 100 Gb/s visible light wireless access network," *Optics Express*, vol. 23, no. 2, pp. 1627-1637, Jan. 2015.

Four Element Modified Rectangular Slotted Antenna for Wireless Application

Sanjay Chouhan[1], Khelta Ram Jadhaw[1], Ganesh Mukati[1], Kishor Kumbhare[1], *Jitendra Yadav[2], Santosh Kumar Kurre[2]

[1]Dept. of ECE, Jawaharlal Institute of Technology, Borawan

[2]Department of Mechanical Engineering, School of Engineering, University of Petroleum and Energy Studies, Bidholi, Dehradun-248007, India.

Author Emails

**Corresponding author: jyadav@ddn.upes.ac.in*

Abstract

The creation of low-cost, low-profile, light-weight antennas that can sustain good performance across a broad spectrum of frequencies is now necessary due to the advancement of communication systems. A four-element, slotted, modified, compact MIMO antenna is suggested. The suggested patch antenna is created using the optimal Envelop correlation coefficient and tested using the CST microwave studio software. Quarter wave feed line and slot lessen the impact of mutual coupling between radiating elements. The size of single antenna is 24 x 27 mm^2. The obtained isolation is more than 20 dB in proposed band. The bandwidth of proposed antenna is 3.7 GHz which is ranges from 10.0 to 13.8 GHz. The proposed antenna has a directivity of 6.12 dBi, a gain of 4.23 dBi, and an ECC.

Keywords: MIMO, Antenna Design, Bandwidth, directivity, surface current distribution

1.INTRODUCTION

In recent years, there has been an increase in demand for additional services and features for mobile equipment. [1-3]. A larger data rate is required for these new functions and services to operate effectively. GPS, Wi-Fi, Bluetooth, infrared, and other features are now commonplace in mobile devices. To transmit and receive signals, all of these applications require an antenna. The antenna's isotropic radiation, improved radiation efficiency, compact design, efficient impedance matching to receive and transmit paths, and ease of construction are required for optimum antenna system performance. A correct antenna design should be taken into account because a change in any physical parameter [4-7] may have an effect on the antenna's effectiveness and bandwidth.

The utilization of multiple antenna systems using MIMO [8-12] technology to transmit the same power utilizing. The interest in antennas at the transmitter and receiver has increased recently because it increases channel capacity without consuming more bandwidth or power. The MIMO technology has some challenges like isolation amongst ports [13-16]. The good isolation is achieved by some techniques like parasitic elements between the radiators, metamaterials, isolating networks, SSR resonators, orthogonal polarization techniques etc. [17-22].One can find several applications wherein proposed research work [23-29] may be implemented. In the present work, we propose a multi-input multi-output (MIMO) antenna operating at 12.1 GHz..The antenna system's component antennas are placed close to one another [30-37].

2.ANTENNA DESIGN

Design Parameters- A single patch's design parameter is calculated. On a FR-4 substrate, a patch antenna operating at 12.1 GHz is currently being developed. The FR-4 substrate is 1.524 mm tall with a dielectric constant of 4.3.
Width and length of patch antenna can be calculated by the equations 1 to equation 4.

For Width B

From equation (1),

$$\mathbf{B} = \frac{c}{2f_r\sqrt{\frac{\epsilon_r+1}{2}}} \quad \text{.....(1)}$$

For Length,

Effective dielectric constant from equation (2),

$$\boldsymbol{\epsilon_{reff}} = \frac{\epsilon_r+1}{2} + \frac{\epsilon_r-1}{2}\left[1 + 12\frac{h}{B}\right]^{-\frac{1}{2}} \quad \text{.....(2)}$$

The additional length derived from equation (3)

$$\Delta\mathbf{L} = \mathbf{0.412}\frac{(\epsilon_{reff}+.3)(\frac{B}{h}+0.264)}{(\epsilon_{reff}-.258)(\frac{B}{h}+0.8)} \text{ ... ...(3)}$$

Now, the equation (4) can be used to determine the patch antenna's effective length.

$$\mathbf{L_{eff}} = \frac{\mathbf{c}}{\mathbf{2f_r\sqrt{\epsilon_r}}} - \mathbf{2} \times \Delta L \text{.....(4)}$$

The geometry of the suggested MIMO antenna system is shown in Figure 1(a) and (b).The antenna system is made up of four radiating elements that are printed on a shared FR4 substrate that is 1.524 mm thick and 24 x 27 mm^2 in size. The substrate has a dielectric constant of 4.3. The radiator is a rectangular patch, and A 50 micro strip line separately feeds each radiator. The antenna is 96 x 27 mm^2 in total. Table 1 listed the optimized data of antenna.

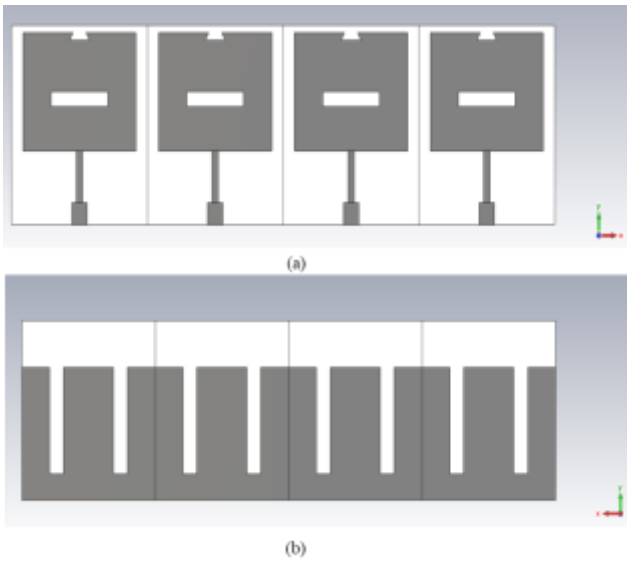

Figure 1. (a) Front view of antenna (b) Back view of antenna

Table 1: Optimized dimensions of suggested MIMO antenna

Parameter	**Description**	**Size in mm**	**Material**
Sw	Substrate width	24	FR-4 (Dielectric cont. 4.3)
Sl	Substrate Length	27	FR-4 (Dielectric cont. 4.3)
Sh	Substrate height	1.524	FR-4 (Dielectric cont. 4.3)
Gw	Ground Width	24	PEC (Copper)
Gl	Ground Length	20	PEC (Copper)
Gh	Ground Height	0.07	PEC (Copper)
Pw	Patch Width	20	PEC (Copper)
Pl	Patch Length	16	PEC (Copper)
Ph	Patch height	0.07	PEC (Copper)
Slot width	-pw/4 to pw/4	10	Nickle
Slot height	----	2	Nickle
Fw1	Upper Feed width	1.1	PEC (Copper)
Fl1	Upper Feed length	7	PEC (Copper)
Fw	Bottom Feed width	2.3	PEC (Copper)
Fl	Bottom Feed length	3	PEC (Copper)

3.RESULT AND DISCUSSION

Software called CST MICROWAVE STUDIO is used to simulate a four-element MIMO antenna. At resonance frequency 12.1 GHz, the simulated values of S-parameters and bandwidth are got and isolated. The results of simple rectangular patch antenna shows in figure 2 which resonate at 12.1 GHz and return loss of -49 dB and In the whole frequency range, isolation The result of same antenna with only S11 parameter and isolation coefficient is discussed separately.

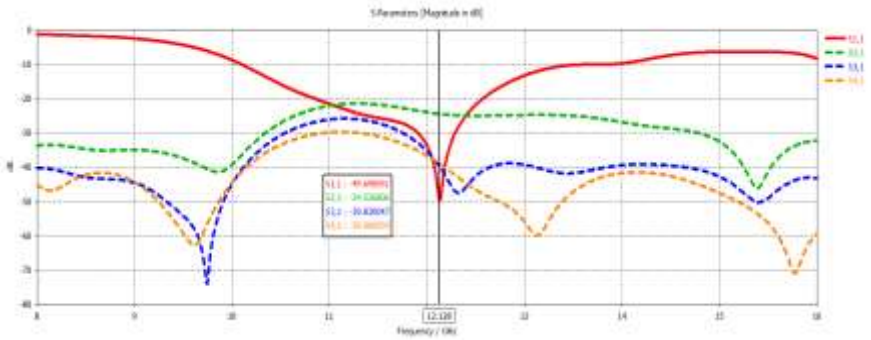

Figure 2: S-parameter MIMO antenna

The suggested basic rectangular microstrip patch antenna's bandwidth graph is shown in figure 3, along with antennas with parasitic and slotted ground. The proposed simple antenna is obtained bandwidth of 3.7 GHz.

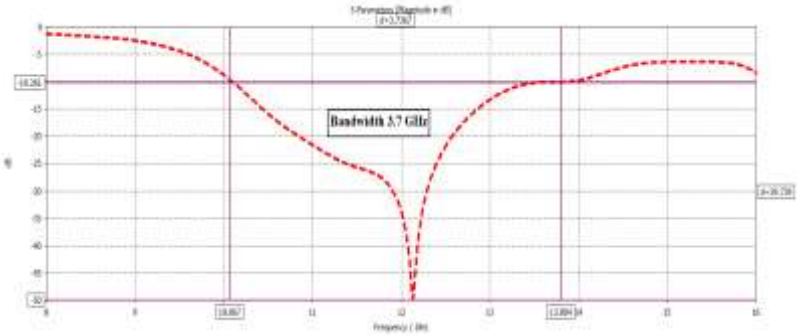

Figure 3: Bandwidth of proposed MIMO antenna

At 12.1 GHz resonant frequency, the far-field radiation patterns of a 4-port MIMO antenna are measured. E- and H-modules can be used to define the effects of a simulated distant field on four-element MIMO E- and H-planes. According to figures 4 to 7, the proposed antenna's directivity is 6.12 dBi and its gain is 4.23 dBi. The envelope correlation coefficient "" in a MIMO antenna system illustrates the impact of various radio frequency signal propagation channels that disperse the antenna components. The envelope correlation coefficient calculates the correlation between the radiation patterns of MIMO receiving antenna pairs (ECC). Its values vary from 0 to 1, with 0 signifying no connection and 1 signifying complete correlation of the radiation patterns. The graphic clearly shows that the suggested structure's ECC is below 0.008. Here, the dispersal of surface current at the antenna system patch is predetermined. An analytical picture of the amount and direction of current flow in the antenna is provided by surface current. Additionally, it is the current direction of current flow. One port is activated, while the remaining ports are turned off by 50, to detect the impact of surface current distribution on the antenna.

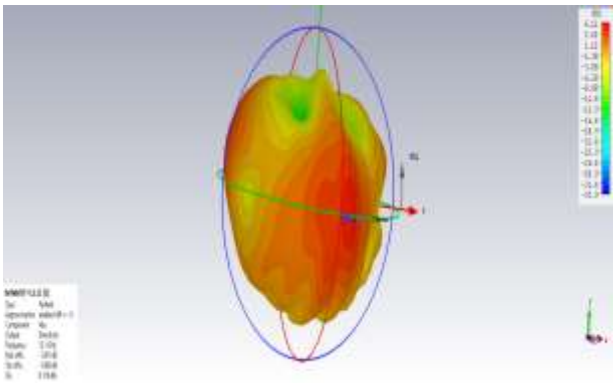

Figure 4: Directivity of antenna

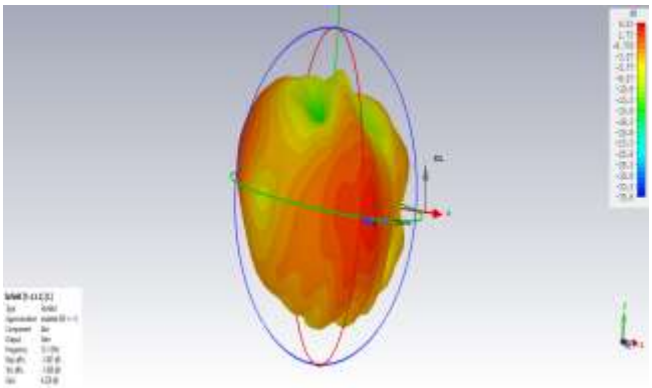

Figure 5: Gain of antenna

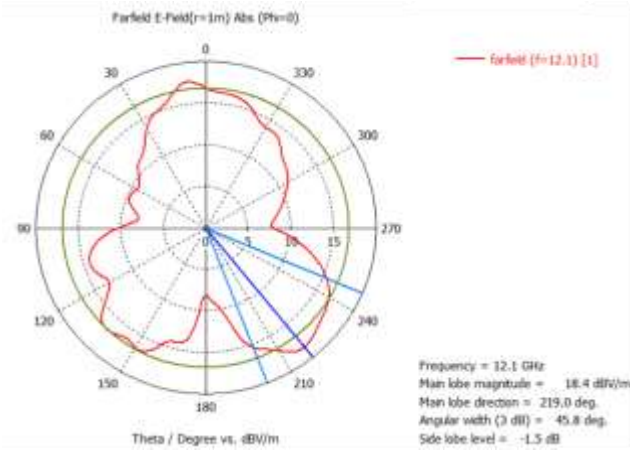

Figure 6: E-field

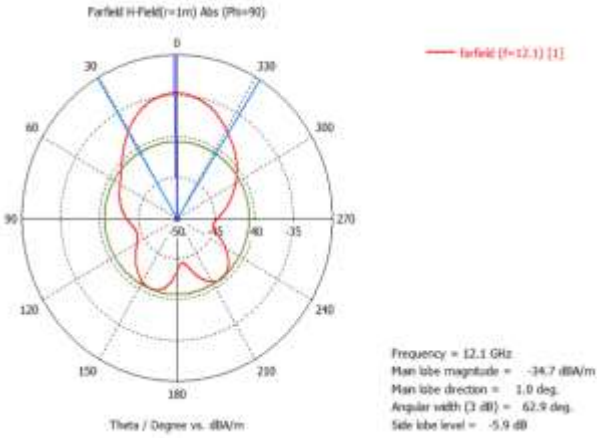

Figure 7: H-field

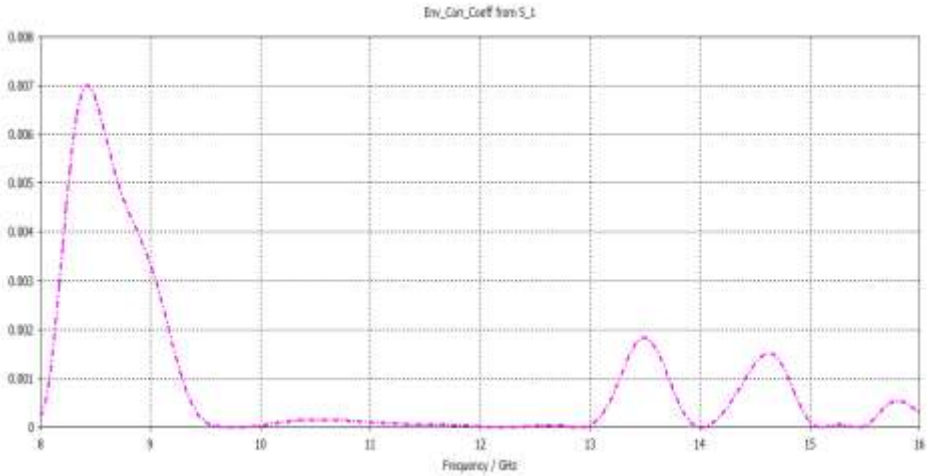

Figure 8: ECC structure

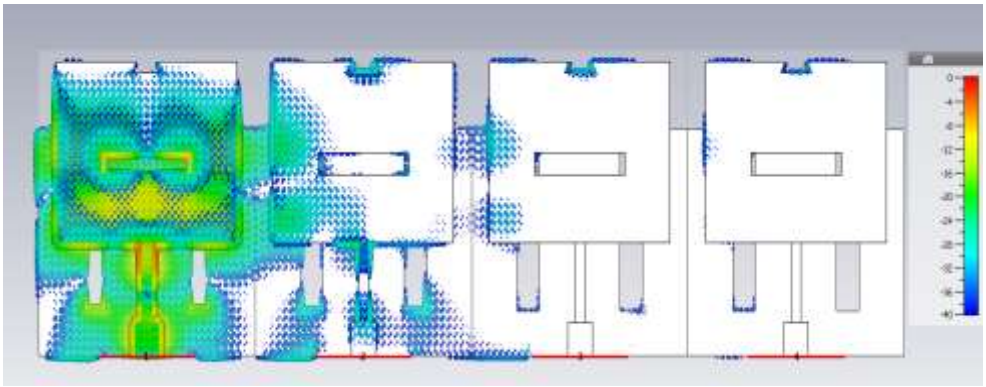

Figure 9: Surface current distribution of antenna when port 1 excited.

4.CONCLUSIONS

For wireless communication at 12.1 GHz, a small four-element single-band MIMO antenna with modified rectangular geometry is presented. Through the use of slotted arrangements and modified ground, the influence of conjoint coupling between radiating elements is lessened. The frequency bands have minimal ECC and encompass the range of 10–13.7 GHz. The suggested antenna is 96 x 27 mm2 in total. The results also showed that this antenna operates efficiently over its whole operational bandwidth. The obtained isolation between radiating elements is greater than 20 dB At 12.1 GHz, the obtained gains were more than 4 dBi for each antenna. ECC is measured at very low resonance frequencies. This design strategy offers a wideband antenna solution with good antenna properties. The isolation between ports is increased by the slots in patches.

REFERENCES:

1. Saqer Al Ja'afreh, Yi Huang, Lei Xing "Low profile and wideband planar inverted-F antenna with polarisation and pattern diversities" IET Microw. Antennas Propag., 2016, Vol. 10, Iss. 2, pp. 152–161
2. Saber Soltani, Parisa Lotfi, and Ross D. Murch, " A Port and Frequency Reconfigurable MIMO Slot Antenna for WLAN Applications" IEEE TRANSACTIONS ON ANTENNAS AND PROPAGATION, VOL. 64, NO. 4, APRIL 2016
3. Anitha Ramachandran, and Vasudevan Kesavath, "A Four-Port MIMO Antenna Using Concentric Square-Ring Patches Loaded With CSRR for High Isolation" IEEE ANTENNAS AND WIRELESS PROPAGATION LETTERS, VOL. 15, 2016
4. Syeda Irum Jafri, Rashid Saleem, Muhammad Farhan Shafique, Anthony Keith Brown, "Compact reconfigurable multiple-inputmultiple-output antenna for ultra wideband applications" IET Microw. Antennas Propag., 2016, Vol. 10, Iss. 4, pp. 413–419
5. Beegum S. Femina and Sanjeev K. Mishra "Compact WLAN Band-notched Printed Ultrawideband MIMO Antenna with Polarization Diversity" Progress In Electromagnetics Research C, Vol. 61, 149–159, 2016
6. Gunjan Srivastava and Akhilesh Mohan, "Compact MIMO Slot Antenna for UWB Applications" IEEE ANTENNAS AND WIRELESS PROPAGATION LETTERS, VOL. 15, 2016
7. J. Malik, D. Nagpal and M.V. Kartikeyan, "MIMO antenna with omnidirectional pattern Diversity" ELECTRONICS LETTERS 21st January 2016 Vol. 52 No. 2 pp. 102–104
8. Aswathy K. Sarma, Henridass Arun, Malathi Kanagasabai, Sangeetha Velan, Chinnambeti Raviteja, M. Gulam Nabi Alsath "Polarisation diverse multiple input–multiple output antenna with enhanced isolation" IET Microwaves, Antennas & Propagation
9. Jing-Yi Zhang, Fan Zhang, Wen-Peng Tian and Yong-Lun Luo, "ACS-fed UWB-MIMO antenna with shared Radiator" ELECTRONICS LETTERS 20th August 2015 Vol. 51 No. 17 pp. 1301–1302
10. Shrivishal TripaAkhilesh Mohan and Sandeep Yadav, "A Compact Koch Fractal UWB MIMO Antenna With WLAN Band-Rejection" IEEE Antennas And Wireless Propagation Letters, Vol. 14, 2015
11. Sultan Shoaib, Imran Shoaib, Nosherwan Shoaib, Xiaodong Chen and C.G. Parini, "A 4x4 MIMO Antenna System for Mobile Tablets" The 8th European Conference on Antennas and Propagation (EuCAP 2014)
12. Jamal Nasir, Mohd Haizal Jamaluddin, Mohsen Khalily, Muhamad Ramlee Kamarudin, Irfan Ullah, "Design of an MIMO Dielectric Resonator Antenna for 4G Applications" Wireless Pers Communication (2016) 88:525–536
13. Han Wang, Longsheng Liu, Zhijun Zhang, YueLi, Member and Zhenghe Feng, "Ultra Compact Three-Port MIMO Antenna With High Isolation and Directional Radiation Patterns"IEEE ANTENNAS AND WIRELESS PROPAGATION LETTERS, VOL. 13, 2014
14. Jie Lu, Zhenqi Kuai, Xiaowei Zhu, and Nianzu Zhang, "A High-Isolation Dual-Polarization Microstrip Patch Antenna With Quasi-Cross-Shaped Coupling Slot" IEEE Transactions On Antennas And Propagation, Vol. 59, No. 7, July 2011
15. H. Li, J. Xiong, Z. Ying and S.L. He "Compact and low profile co-located MIMO antenna structure with polarisation diversity and high port isolation" Electronics Letters 21st January 2010 Vol. 46 No. 2
16. N. S. Awang Da, M. R. Dzulki°i, and M. R. Kamarudin "Polarization Diversity Monopole Antenna" PIERS Proceedings, Cambridge, USA, July 8, 2010
17. AtifJamill, Mohd Zuki YUSOffl, Noorhana Yahya, "Current Issues and Challenges ofMIMO Antenna Designs".
18. Arogyaswami J. Paulraj Dhananjay A. Gore, Rohit U. Nabar, And Helmut Bölcskei, "An Overview of MIMO Communications—AKey to Gigabit Wireless" Proceedings Of The IEEE, VOL. 92, No. 2, February 2004
19. K. Chung and J.H. Yoon. "Integrated MIMO antenna with high isolation characteristic" ELECTRONICS LETTERS 15th February 2007 Vol. 43 No. 4

20. Sema Dumanli, Chris J. Railton, and Dominique L. Paul, “A Slot Antenna Array With Low Mutual Coupling for Use on Small Mobile Terminals” IEEE Transactions On Antennas And Propagation, Vol. 59, No. 5, May 2011
21. Belgacem Aouadi and Jamel Belhadj Tahar, “Improved antenna diversity system by low correlation between elements exploiting Single-Negative Metamaterials” 2012 24th International Conference on Microelectronics (ICM)
22. Chouhan, Sanjay, Vivek Singh Kushwah, and Jitendra Yadav. "Two element multi-slotted MIMO antenna for dual band applications using FR-4 material." Materials Today: Proceedings (2021).
23. Maan A., Pitta P., Yadav J. (2018) Performance Evaluation of Rectangular Fins by Modeling and Simulations. In: Siddiqui N., Tauseef S., Abbasi S., Rangwala A. (eds) Advances in Fire and Process Safety. Springer Transactions in Civil and Environmental Engineering. Springer, Singapore
24. Yadav J., Agnihotri G. (2018) Circumvention of Friction-Induced Stick-Slip Vibration by Modeling and Simulation. In: Singh R., Choudhury S., Gehlot A. (eds) Intelligent Communication, Control and Devices. Advances in Intelligent Systems and Computing, vol 624. Springer, Singapore
25. Jitendra Yadav and Geeta Agnihotri (2017), “Modeling and Simulation of the Dynamic Response of a Generic Mechanical Linkage for Control Application Under the Consideration of Nonlinearities Imposed by Friction”, In Springer Proceedings of the International Conference on Nano-electronics, Circuits & Communication Systems, Lecture Notes in Electrical Engineering 403
26. Jitendra Yadav & G. Agnihotri, “Proposed Critical Damping for a Spring Mass System to Avoid Stick Slip” ,Springer Journal of the institution of engineers (India): Series C Volume 96, Number 3, PP 331-335, July-September 2015.
27. Yadav, Jitendra, et al. "Nonlinear dynamics of controlled release mechanism under boundary friction." Results in Engineering 11 (2021)
28. Yadav J., Pitta P., Maan A. (2018) Swing Tower of Loader Backhoe Arm for Dynamics and Stress Analysis by Modeling and Simulation. In: Siddiqui N., Tauseef S., Abbasi S., Rangwala A. (eds) Advances in Fire and Process Safety. Springer Transactions in Civil and Environmental Engineering. Springer, Singapore
29. Dravid Shriram, Jitendra Yadav, and Santosh Kumar Kurre. "Comparison of loosening behavior of bolted joints using plain and spring washers with full-threaded and plain shank bolts." Mechanics Based Design of Structures and Machines (2021)
30. R. Kumar, R. K. Pachauri, P. Badoni, D. Bharadwaj, U. Mittal, and A. Bisht, “Investigation on parallel hybrid electric bicycle along with issuer management system for mountainous region,” J. Clean. Prod., 2022; 362:132430
31. R. Kumar, N. J. Ahuja, M. Saxena, and A. Kumar, “Automotive Power Window Communication with DTC Algorithm and Hardware-in-the Loop Testing,” Wirel. Pers. Commun., 2020;114 (4): 3351–3366
32. C. S. Meera, S. Sunny, R. Singh, P. S. Sairam, R. Kumar, and J. Emannuel, “Automated precise liquid transferring system,” 2014:1-6
33. A. Kumar, R. Kumar, A. Jain, A. Pandey, S. Thapliyal, and A. Sharma, Automatic street lighting system, vol. 624. Springer Singapore, 2018.
34. A. Pal, R. Kumar, and V. R. Sanal Kumar, “Conceptual design of an automatic fluid level controller for aerospace applications,” Proc. IEEE Int. Conf. Soft-Computing Netw. Secur. ICSNS 2015, 2015,
35. R. Kumar, K. Bansal, A. Kumar, J. Yadav, M. K. Gupta, and V. K. Singh, “Renewable energy adoption: Design, development, and assessment of solar tree for the mountainous region,” Int. J. Energy Res. 2021; 1–17
36. R. Kumar, P. K. Dwivedi, D. Praveen Reddy, and A. S. Das, “Design and implementation of hydraulic motor based elevator system,” 2015
37. Yadav, Jitendra, et al. "Identification of damping prohibiting stick-slip form friction influenced dynamic system." Proceedings of the Institution of Mechanical Engineers, Part C: Journal of Mechanical Engineering Science (2022): 09544062221135517.

Face Recognition using Shape Invariant Features

Avtar Singh[1], Deval Verma[2]

[1]Department of Mathematics, Chandigarh University, Punjab- 140413
avtarsingh78611@gmail.com
[2]School of Computer Science Engineering and Technology
Bennett University, Times Group
Greater Noida-201310
deval09msc@gmail.com

Abstract

Face recognition is a traditional trend that is necessary for security measures. It may be utilized for detection and authenticating to affirm a person's identification and to recognize persons, respectively. But the cost and maintenance of the ideas vary to the idea of logic. This paper reviews the face recognition process with different approaches and related studies as well as some practical implementations, types, methods, and other details. Fundamentally Histogram of Oriented Gradients (HOG) is the basis of the face detection and the classifier used is the linear support vector machine (SVM) which instantly determines these methods' respective weights, and the Deep Convolutional Neural Network is trained on a picture used in the background to create 128 measures for each face to decrease the time of detection.

Keywords. Face Detection, Face Recognition, HOG, SVM, Neural Networks

1. INTRODUCTION

Facial recognition algorithms attempt to identify a human face based on its two-dimensional representation, which is three-dimensional and modifies appearance depending on lighting and facial emotion. Kelly completed the first piece of work pertaining to automatic facial recognition to identify the same individual among a group of photos recorded by a television camera [1]. Due to their unpredictable look and the variety of stances they might take, humans can be difficult to identify in photographs. The first need is a strong feature set that enables clean human form discrimination even in cluttered backgrounds with poor lighting. Biometrics recognition system which is one of the applications of face detection [2,3,4,5,6,7,8]. There are several different approaches with which we can detect a face and recognize it. Some of them are Eigen space: Among the most effective approaches for computational recognition of faces as in digital pictures is Eigen space-based high accuracy face recognition [13] [22]. Holistic face recognition identifies people by using global information from their faces [21]. The global characteristics of the pattern are considered by holistic methods [9,10,11,12,13,14,15,16,17,18,19,20,21,22,23]. According to [19] the influence of facial feature dislocation under position changes is eliminated to achieve posture tolerance.

In this work, we introduce a novel algorithm for face alignment that runs in milliseconds and delivers face detection. Since the key elements of earlier face alignment algorithms were identified, they were then streamlined and added to a series of high-capacity regression functions that were learned via gradient boosting, which resulted in speed improvements

over existing techniques. The organization of the paper is as follows: section II discusses the related work; section III discusses preliminaries and covers basics of HOG and Cascade of Regressors. The section IV explains the proposed technique. Results and discussion are discussed in section V. A conclusion is given in section VI.

2. PRELIMINARIES

2.1. Histogram of Oriented Gradients (HOG)

An image is just a discrete function of (x, y), the gradient of an image may also be determined. Images have a horizontal (x-direction) and a vertical (y-direction) gradient that is computed at each pixel. Values for gradients are assigned to 0-255. The [7][8]and [9] have depicted how a face and human gestures can be detected with the help of HOG. The orientation (magnitude) is provided in [10].

2.2. Cascade of Regressors (COR)

In this work, which should simulate facial changes under different head postures and facial expressions, is too difficult to resolve in a single step of regression. Therefore, rather of regressing in a single step, an adaptive cascade regression model [6] is used that learns the frontal-profile connections in a cascade fashion and gradually approaches the optimum. x represents shape of frontal face and non-frontal is x_0. Where regression can be expressed as $R(x_0)$. Here $x - x_0 = \Delta x$, $x_0 + \Delta x = R(x_0)$, Given in Figure 2.21.

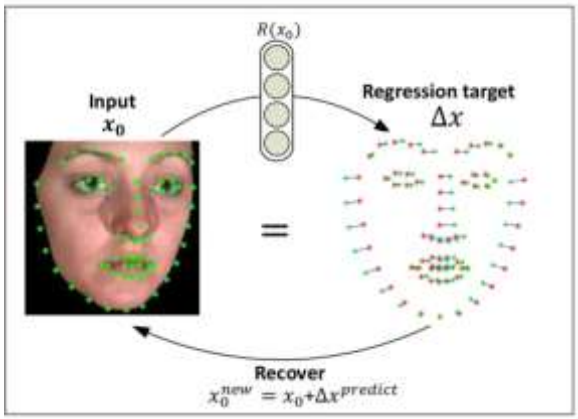

Figure 2.21. Cascade regression process

This technique is used for finding 68 markers on each face.

3. PROPOSED METHODOLOGY

Step1: To create a condensed version of an image, encode the image using the HOG algorithm [7]. Find the region of the image that most closely resembles a general HOG encoding of a face using this simplified version. (Given in Figure 2.21)

Step2: A series of regression functions can be used to tackle the problem of facial alignment [15]. By identifying the key facial landmarks, determine the facial position. Use those

markers to warp the image once we've located them so that the eyes and mouth are in the middle.

Step3: Use a deep neural network architecture that is trained to measure facial traits to run the centred face image. The 128 measurements should be saved.

Step3: Find the individual whose measurements are the most like our face's measurements among all the faces we have previously measured. That's our opponent shown in Figure 3.1.

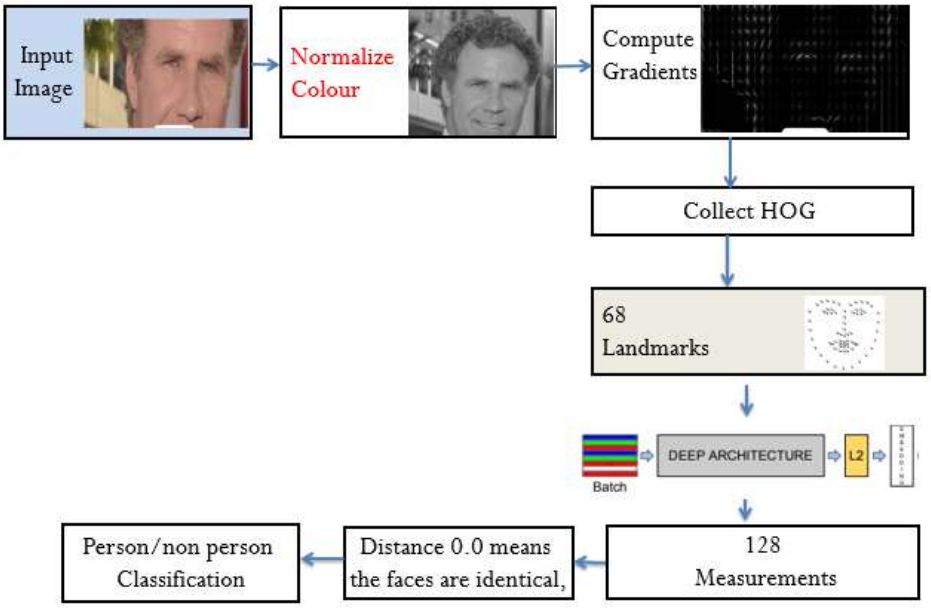

Figure 3.1 Proposed Methodology

4. EXPERIMENTAL AND RESULTS

We have taken 60 sample images from Kaggle dataset for experimental work. These images are a collection of different facial expression of Elon Musk. Experiments have been performed on the data set of images “Elon Musk” Each image is RGB image and convert it into binary image. All the experiments have been performed on PYTHON 3.10- and 64-bit version for windows. Table 4.1 shows the experimental results.

Table 4.1. Results

Figure 4.1 Image A

Figure 4.2 Image B

Figure 4.3. Blur image 1

Figure 4.4. Blur image 2

Figure 4.5. Output image1

Figure 4.6. Output image2

In accordance with [7] and [15] we learned to use HOG and face alignment to decrease the detection time. In this experiment Figure 4.1. i.e., Image A is the train image for encoding and Figure 4.2. i.e., Image B is the Test image for comparison which shows the result that it is the matching image of Elon Musk and the distance between the face locations is 0.43. The less the distance between the face distance, more precise the face matching is done. In the images above we have seen the input images are blurry or may be taken from a low-quality camera, despite the fact still the results shown in the output images are matched with the input images in most of the cases which are output image 1 with 0.50 face distance, image 2 with 0.47 face distance and image 3. with 0.51 face distance as shown in Figures 4.1, 4.2, 4.3, 4.4, 4.5 and 4.6.

5. CONCLUSIONS

We have calculated the 128 measurements and based on that we can tell that our face matched or not. To check how similar is the face matched, for that we have calculated the face distance (the Euclidian distance) for each comparison face and the distance tells how similar the face is. Out of all other complex models this technique is very effective for a simple cost-effective purpose and suggests for the face extraction from a mass group to detect the terrorist/culprits from that group. There are other approaches to face recognition that we have seen, but CNN and HOG serve as the foundation for face recognition as well as various alternative methods.

6. REFERENCES

[1] M. D. Kelly, 'Visual identification of people by computer', PhD thesis, Stanford University, CA, USA, 1971

[2] V. Blanz and T. Vetter, 'Face recognition based on a 3d morphable model', IEEE Trans. Pattern Anal. Mach. Intell., 25(9), 2003.

[3] P. Viola and M. J.Jones, International Journal of Computer Vision, Springer , pp. 137-154, 2004.

[4] N. Dalal and B. Triggs, 'Histograms of Oriented Gradients for Human Detection, INRIA Rhone-Alps, 655 avenue de l'Europe, Montbonnot 38334, France

[5] G. Bradski and A. Kaehler, 'Learning OpenCV', 1st edn. O'Rielly books, USA, 2008.

[6] Y Wang, X Dong, G Li, J Dong, H Yu, 'Cascade regression-based face frontalization for dynamic facial expression analysis', Cognitive Computation., Sep; vol. 14, no. 5,pp.1571-84, 2022.

[7] N. Dalal and B. Triggs, 'Histograms of oriented gradients for human detection', 2005 IEEE Computer Society Conference on Computer Vision and Pattern Recognition (CVPR'05), pp. 886-893 vol. 1, 2005.

[8] W. T. Freeman and M. Roth. 'Orientation histograms for hand gesture recognition'. Intl. Workshop on Automatic Faceand Gesture- Recognition, IEEE Computer Society, Zurich, Switzerland, pp. 296–301, June 1995.

[9] W. T. Freeman, K. Tanaka, J. Ohta, and K. Kyuma, 'Computer vision for computer games', 2nd International Conference on Automatic Face and Gesture Recognition, Killington, VT, USA, pp. 100–105, October 1996.

[10] M. Chandrakala and P. Durga Devi, 'Two-stage classifier for face recognition using HOG features, vol 47, Part 17, Pages 5771-5775,2021.

[11] J. Harguess and J. K. Aggarwal, 'A case for the average-half-face in 2D and 3D for face recognition', IEEE Computer Society Conference on Computer Vision and Pattern Recognition Workshops, pp.7-12,2009.

[12] King, Davis E, Dlib-ml: A machine learning toolkit, The Journal of Machine Learning Research, vol 10, 1755-1758, 2009.

[13] J. Ruiz-del-Solar and P. Navarrete, 'Eigenspace-based face recognition: a comparative study of different approaches', in IEEE Transactions on Systems, Man, and Cybernetics, Part C (Applications and Reviews), vol. 35, no. 3, pp. 315-325, Aug. 2005.

[14] R. Gopalan, D. Jacobs, ‘Comparing and combining lighting insensitive approaches for face recognition’, Computer Vision and Image Understanding, Volume 114, Issue 1, pp. 135-145, 2010.

[15] Q. Liu, J. Deng, J. Yang, G. Liu and D. Tao, ‘Adaptive Cascade Regression Model For Robust Face Alignment’, in IEEE Transactions on Image Processing, vol. 26, no. 2, pp. 797-807, Feb. 2017.

[16] J. M. Pandya, D. Rathod, J.J. Jaadav, ‘A survey of face recognition approach’, International Journal of Engineering Research and Applications (IJERA), pp. 632-635, 2013.

[17] H. Moon, ‘Biometrics Person Authentication Using Projection-Based Face Recognition System in Verification Scenario’, in International Conference on Bioinformatics and its Applications. Hong Kong, China, pp.207-213, 2004.

[18] D. McCullagh, ‘Call It Super Bowl Face Scan 1’, Wired Magazine, 2001.

[19] X. Zhang and Y. Gao, ‘Face recognition across pose: A review, Pattern Recognition’, pp. 2876-2896, 2009.

[20] D. R Sun, L. N Wu, ‘A local-to-holistic face recognition approach using elastic graph matching’, International Conference on Machine Learning and Cybernetics, vol. 1, no. 1 pp. 240-242, 2002.

[21] S Karamizadeh, S.M. Abdullah, M Zamani, ‘An Overview of Holistic Face Recognition’, International Journal of Research in Computer and Communication Technology, vol. 2, no. 9, pp.738-741, 2013.

[22] M. A. Turk and A. P. Pentland, ‘Face recognition using eigenfaces’, IEEE Computer Society Conference on Computer Vision and Pattern Recognition, pp. 586-591, 1991.

[23] Y. Wu and Q. Ji, ‘Facial Landmark Detection: A Literature Survey’, International Journal of Computer Vision, Springer, vol.127, no. 2, pp.115-142, 2019.

Efficiency Evaluation and Ranking of Indian PSBs: An Application of Data Envelopment Analysis

Reshampal Kaur

Associate Professor, Division of Mathematics, UIS, Chandigarh University, Mohali-140413, India, reshampal0304@gmail.com

Abstract.

Efficiency analysis in a relative environment is a requisite for any entity for optimization of sustainable development. Among many other tools available for performance analysis, the most appropriate and preferred tool worldwide is Data envelopment analysis (DEA), with diverse applications in public as well as private sector, in a multiple-input-output environment of Decision-making units (DMUs), in a competitive environment. This paper aims to present a comparative performance analysis of Indian public sector banks (PSBs) using conventional Charnes, Cooper and Rhodes (CCR) DEA model for efficiency evaluation as well as the advanced super-efficiency DEA model for the ranking of DMUs, for the year 2020. Findings from the application of DEA models, reveal that half of the Indian PSBs under study are relatively inefficient. As PSBs contribute majorly in Indian economy, efforts should be made for their efficiency enhancement. Also, it has been found that the results calculated using super-efficiency models are more appropriate and comprehensive for a rigorous efficiency comparison of all DMUs including efficient ones.

Keywords. Data envelopment analysis (DEA), Optimization, Efficiency, Decision making units (DMUs), Performance, Public sector banks (PSBs).

1. INTRODUCTION

For optimization of sustainable development, organizations must use their resources efficiently. Moreover, they need to consistently analyse their performance amongst their peers, to explore their scope of efficiency enhancement, using limited resources available to them. Data envelopment analysis (DEA) is a tool based in the scope of linear programming and has been used abundantly on the global level for an efficiency evaluation in comparative environment, among peer entities, across verticals [1]–[3]. The application areas of DEA include not only governmental entities like schools, military or hospitals, but also in banking, airlines, warehouses, transports, financial markets and stocks [4]–[13]. In the frameworks of DEA, such entities are termed as Decision making units (DMUs), which are peer entities using similar resources, called inputs to produce multiple desired goods or services, called outputs. If required, these input and output variables can be assigned weights, as per their importance. In an analysis dealing with the comparative study in a single time period , non-parametric technique DEA synchronises the inter-relationships of various input-output variables, without any assumption of functional structures [14], for the DMUs under study

and identifies the units performing efficiently and further forming the frontier [15]. Also, it identifies comparatively inefficient units along with sources of inefficiency.

Public sector banks (PSBs) play an important role in Indian economy. In present times when there is a tough competition in public, private and foreign banks operating in India, PSBs with limited resources and strict regulations, are facing tough competition for survival as well as for growth. Such circumstances make it desirable to analyse the performance of Indian PSBs, to identify the domains to be improved for enhancement in efficiency.

The present study adopts the non-parametric technique DEA to assess the performance of Indian public sector banks (PSBs) and analyses the comparative inferences regarding efficiency and ranking of these banks, taken as DMUs, using Charnes, Cooper and Rhodes (CCR) DEA model and Super-efficiency DEA model. This paper has been set out as the following. The second section describes the materials and the methods used in this paper along with the details of the data used for the purpose, followed by discussion on results in section three. Further, section four discusses the overall observations of the results followed by a conclusion.

2. MATERIALS AND METHODS

This section describes the approach, techniques and the models used for the analysis, in this study. The description of data and variables used in the study has been provided in the subsection 2.1.

In a framework following Charnes et al. [1], for n DMUs, say DMU1, DMU2, …, DMUn such that the DMUk uses 'm' inputs x_{ik} $(i = 1,2, \dots, m)$ to produce 's' outputs y_{rk} $(r = 1,2, \dots, s)$, in a given time period. All the input and output values considered here are non-negative numbers, using constant returns to scale and following an input-oriented approach.

Taking input weights as $Iv = (a_{1,}a_{2,\dots,}a_m)$ and output weights as vector $Ov = (b_{1,}b_{2,\dots,}b_s)$, Each DMUk has a LPP to optimize the objective function

$$\text{Maximize } \theta = b_1y_{1k} + b_2y_{2k} + \cdots + b_sy_{sk}$$

$$s.t.\ a_1x_{1k} + a_2x_{2k} + \cdots + a_mx_{mk} = 1$$

$$\text{and } b_1y_{1j} + b_2y_{2j} + \cdots + b_sy_{sj} \leq a_1x_{1j} + a_2x_{2j} + \cdots + a_mx_{mj}$$

$$for\ every\ j = 1, 2, \dots, n.$$

$$\text{Also, } a_1, a_2, \dots, a_m \geq 0\ and\ b_1, b_2, \dots, b_s \geq 0 \qquad (1)$$

Thus, taking k = 1, 2, …, n, equation (1) above represents 'n' LPPs such that each such LPP can be solved to find most suitable weights for input as well as output variables, corresponding to each DMU.

CCR model of DEA evaluates efficiency scores of the DMUs, this score is a positive value less than or equal to one. The units with efficiency score 'one', are identified as efficient DMUs, which form the frontier. Rest of the units are considered as comparatively inefficient units, with potential scope of improvement, which are assigned with one or more efficient units as benchmarks. These assigned benchmarks and the corresponding inefficient units

have same set of variable weights in DEA analysis, thus providing insights for a feasible and achievable target to the inefficient unit, to become efficient.

The conventional CCR DEA model, in which either an input orientation or output orientation can be considered, with constant returns to scale, has numerous extensions. Although there are abundant applications of the basic conventional DEA models, even then these basic models have a shortcoming that they assign efficiency score 'one' to all the efficient DMUs, thus identifying more than one DMU as efficient, which provides similar ranks for many DMUs, hence don't provide the 'most efficient' unit. As a result, not able to provide any information for comparing efficient DMUs.

To resolve this problem, Andersen and Petersen [18] introduced a new DEA model, called Super-efficiency DEA model. In this model, efficiency scores are evaluated by a comparative analysis of efficient units, with respect to a reference technology, which is comprised of rest of the units. As a result, providing non-identical efficiency scores to each of the DMUs and enhanced information on the functioning of units, along with identifying better performing DMU among any pair of DMUs, selected at random.

Present study evaluates the performance of eighteen Indian PSBs, for the year 2020, using the results of the findings of DEA CCR model and DEA Super-efficiency model, considering input-orientation of optimization with constant returns to scale (CRS) of variables.

2.1. Data and Variables

The performance analysis in the present study is based on the eighteen public sector banks of India for the year 2020. The banks under study and the respective symbols are Allahabad bank(B1), Andhra bank(B2), Bank of Baroda(B3), Bank of India(B4), Bank of Maharashtra(B5), Canara bank(B6), Central bank of India(B7), Corporation bank(B8), Indian bank(B9), Indian overseas bank(B10), Oriental bank of commerce(B11), Punjab and Sind bank(B12), Punjab national bank(B13), State bank of India(B14), Syndicate bank(B15), UCO bank(B16), Union bank of India(B17), United bank of India(B18), considered as DMUs for the DEA models.

For the efficiency evaluation using DEA, selection of the variables is the most critical phase, which largely impacts the interpretations. Researchers have varied opinion on the selection and the number of variables selected for the analysis [8], [19], [20]. The present study uses four inputs such as borrowings, owned funds, wage bills and total deposits. Also, there are two output variables, namely total other income and the spread, as shown in a self-sketch figure 1.

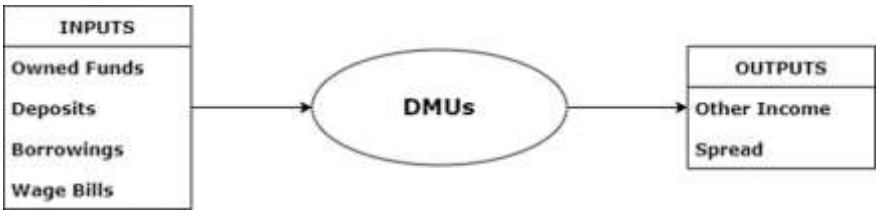

Figure 1. Input and Output Variables Used in DEA Models

The data values related to the DMUs, corresponding to the selected input-output variables, in Million INR, have been sourced from RBI published annual statistical tables. The data values are then normalized and the descriptive statistics like mean and standard deviation, have been calculated, using R programming software. The results thus found have been listed in Table 1.

TABLE 1: DESCRIPTIVE STATISTICS OF INPUT AND OUTPUT VARIABLES

Variables	N	Mean	S.D.	Median	Skewness	Kurtosis
Owned funds	18	36273.67	52300.45	17874.36	2.88	7.94
Total Deposits	18	502689.99	720579.37	245167.06	3.02	8.63
Borrowings	18	39432.20	72776.31	14912.32	2.98	8.40
Wage Bills	18	6391.32	10020.24	3521.32	3.33	10.19
Other Income	18	6562.04	9991.97	3336.07	3.18	9.47
Spread	18	13788.77	21938.63	7079.66	3.12	9.14

Source: Authors own calculations; All data values in Crores of INR.

3. RESULTS

This section includes the results of the tools, used in this study. The performance of each DMU, as per the findings received from CCR and Super-efficiency models of DEA, has been given in Table 2.

TABLE 2: EFFICIENCY SCORES OF DMUS FROM CCR AND SUPER-EFFICIENCY DEA MODELS

DMUs	CCR DEA	Super-eff CRS	Rank
B1	0.89888	0.898878202	16
B2	1	1.201578921	4
B3	1	1.04029503	8
B4	0.92399	0.923989726	12
B5	1	1.264321665	3
B6	0.90562	0.905617061	15
B7	0.91107	0.91107119	14
B8	1	1.756742858	1
B9	1	1.071503337	7
B10	0.91672	0.916722592	13
B11	0.86109	0.861085027	17
B12	0.81198	0.811975669	18
B13	0.95522	0.955217477	11

B14	0.99015	0.990147412	10
B15	1	1.026979216	9
B16	1	1.105953206	6
B17	1	1.142041177	5
B18	1	1.374446839	2

The findings of the DEA CCR model, as efficiency scores, with an input orientation and using a constant return to scale, have been given in Table 2, column 2. As analyses from these results, nine DMUs namely, Andhra bank(B2), Bank of Baroda(B3), Bank of Maharashtra(B5), Corporation bank (B8), Indian bank(B9), Syndicate bank(B15), UCO bank(B16), Union bank of India(B17), United bank of India(B18) are efficient with efficiency score equal to one whereas remaining nine DMUs are relatively inefficient in performance, with efficiency score less than one.

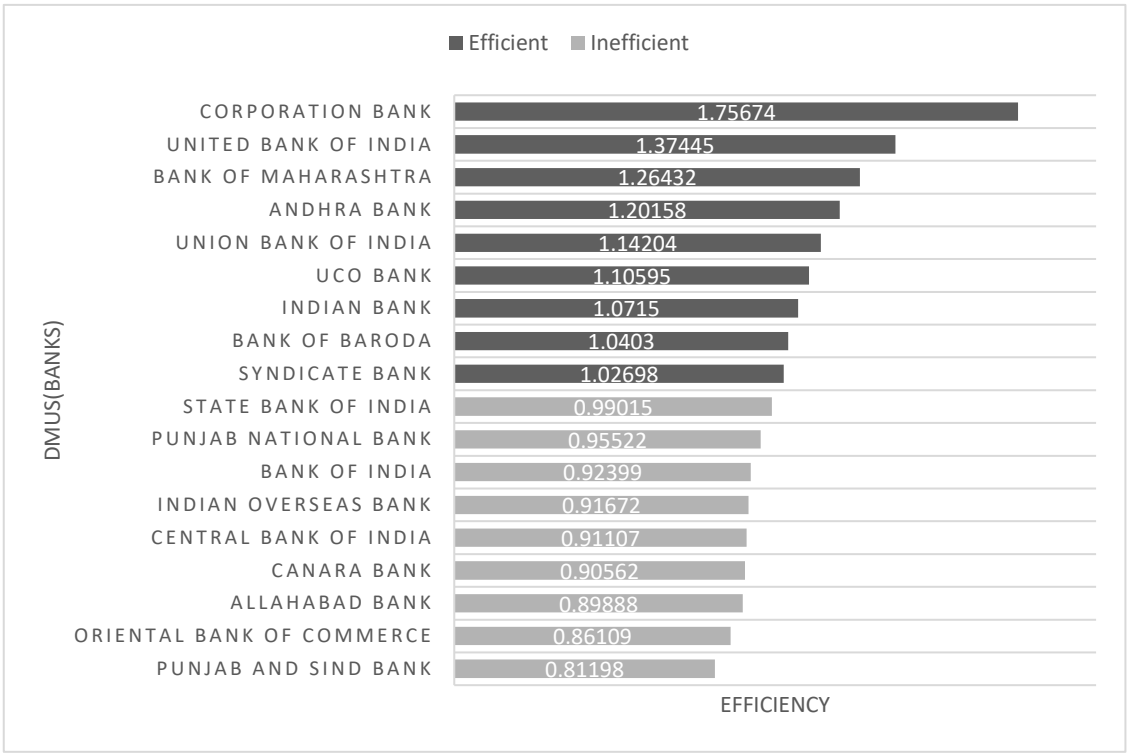

Figure 2. Performance Analysis Using DEA Models

It has been observed from the findings that all efficient DMUs have score equal to one, which makes it difficult to assign benchmarks to these units, for identification of further efficiency improvement. To overcome this problem, DEA super-efficiency model has been

used. The findings of this model have been provided in Table 2, column 3. In addition to the identification of efficient and inefficient DMUs, as given by CCR model, this model also evaluates distinct efficiency score to each efficient DMU, providing a clear efficiency ranking of all DMUs, as given in Table 3, column 4, for an easy comparison of performance and benchmarking. Figure 2 represents the identification of efficient and inefficient DMUs as well as the rank wise efficiency scores of DMUs, using Super-efficiency DEA model.

It has been observed from the results that among efficient DMUs, Corporation bank(B8) is leading with rank 1, followed by United bank of India(B18) on rank 2, Bank of Maharashtra(B5) on rank 3, Andhra bank(B2) on rank 4, Union bank of India(B17) on rank 5, UCO bank(B16) on rank 6, Indian bank(B9) on rank 7, Bank of Baroda(B3) on rank 8 and Syndicate bank(B15) on rank 9. Further lower ranks have been obtained by inefficient DMUs.

4. CONCLUSION

Data envelopment analysis (DEA) is an efficient tool, which can be applied for a comparative efficiency evaluation, in a multiple input-output framework. In spite of a vast application areas, conventional DEA models have some shortcomings, like these conventional models provide efficiency score ‘one’ to all efficient DMUs, thus do not provide any parameter to further compare these DMUs for their comparative performance analysis. This shortcoming can be improved by using Super-efficiency model of DEA, which provides non-repeated efficiency scores to the DMUs, thus helping in identification of better performing DMU among any pair of DMUs selected at random. These results further can be helpful for benchmarking also, for a targeted improvement in efficiency.

Present study uses conventional CCR and the advanced Super-efficiency models of DEA, to analyse the efficiency of eighteen Indian public sector banks (PSBs), for the year 2020. Findings reveal a poor performance of Indian PSBs under study, where only half of the banks under study are efficient. Top five rankers are Corporation bank, United bank of India, Bank of Maharashtra, Andhra bank and Union bank of India.

It is required to further analyze the inefficient banks and explore the causes of their low efficiency. Also, for efficiency enhancement of these relatively inefficient PSBs, they should be assigned with efficient benchmarks, to provide an easy-to-follow targets, which can help the low performing unit to have guiding factor for an efficiency enhancement.

5. REFERENCES

[1] A. Charnes, W. Cooper, and E. Rhodes, “Measuring the efficiency of decision making units,” Company European Journal of Operational Research, vol. 2, pp. 429–444, 1978.

[2] L. M. Seiford, “A bibliography for Data Envelopment Analysis (1978-1996),” Ann Oper Res, vol. 73, pp. 393–438, 1997.

[3] W. D. Cook and L. M. Seiford, “Data envelopment analysis (DEA) - Thirty years on,” Eur J Oper Res, vol. 192, no. 1, pp. 1–17, Jan. 2009, doi: 10.1016/j.ejor.2008.01.032.

[4] R. Markovits-Somogyi, “Measuring efficiency in transport: The state of the art of applying Data Envelopment Analysis,” Transport, vol. 26, no. 1, pp. 11–19, 2011, doi: 10.3846/16484142.2011.555500.

[5] G. Raphael, “A DEA-Based Malmquist Productivity Index approach in assessing performance of commercial banks: Evidence from Tanzania,” European Journal of Business and Management, vol. 5, no. 6, pp. 25–34, 2013, [Online]. Available: www.iiste.org

[6] A. Mohammadi and H. Ranaei, “The Application of DEA based Malmquist Productivity Index in Organizational Performance Analysis,” International Research Journal of Finance and Economics, vol. 62, pp. 68–76, 2011, [Online]. Available: http://www.eurojournals.com/finance.htm

[7] X. Xue, Q. Shen, Y. Wang, and J. Lu, “Measuring the Productivity of the Construction Industry in China by Using DEA-Based Malmquist Productivity Indices,” J Constr Eng Manag, pp. 64–71, 2008, doi: 10.1061/ASCE0733-93642008134:164.

[8] W. P. Wong, “A global search method for inputs and outputs in data envelopment analysis: Procedures and managerial perspectives,” Symmetry (Basel), vol. 13, no. 7, Jul. 2021, doi: 10.3390/sym13071155.

[9] M.-C. Chang, C.-P. Chen, C.-C. Lin, and Y.-M. Xu, “The Overall and Disaggregate China’s Bank Efficiency from Sustainable Business Perspectives,” Sustainability, vol. 14, no. 7, p. 4366, Apr. 2022, doi: 10.3390/su14074366.

[10] M. Feng and X. Li, “Evaluating the efficiency of industrial environmental regulation in China:A three-stage data envelopment analysis approach,” J Clean Prod, vol. 242, Jan. 2020, doi: 10.1016/j.jclepro.2019.118535.

[11] A. Karande et al., “Performance Analysis of Storage Warehouses in a Food Grain Supply Chain using Data Envelopment Analysis,” 2019.

[12] G. Fancello, M. Carta, and P. Serra, “Data Envelopment Analysis for the assessment of road safety in urban road networks: A comparative study using CCR and BCC models,” Case Stud Transp Policy, vol. 8, no. 3, pp. 736–744, Sep. 2020, doi: 10.1016/j.cstp.2020.07.007.

[13] J. S. Liu, L. Y. Y. Lu, W. M. Lu, and B. J. Y. Lin, “A survey of DEA applications,” Omega (United Kingdom), vol. 41, no. 5, pp. 893–902, Oct. 2013, doi: 10.1016/j.omega.2012.11.004.

[14] W. W. Cooper, S. Li, L. M. Seiford, R. M. Thrall, and J. Zhu, “Sensitivity and Stability Analysis in DEA: Some Recent Developments,” Joumal of Productivity Analysis, vol. 15, pp. 217–246, 2001.

[15] W. W. Cooper, L. M. Seiford, K. Tone, and J. Zhu, “Some models and measures for evaluating performances with DEA: Past accomplishments and future prospects,” Journal of Productivity Analysis, vol. 28, no. 3, pp. 151–163, Dec. 2007, doi: 10.1007/s11123-007-0056-4.

[16] R. D. Banker, A. Charnes, and W. W. Cooper, “SOME MODELS FOR ESTIMATING TECHNICAL AND SCALE INEFFICIENCIES IN DATA ENVELOPMENT ANALYSIS*,” Manage Sci, vol. 30, no. 9, pp. 1078–1092, 1984, doi: https://dx.doi.org/10.1287/mnsc.30.9.1078.

[17] W. W. Cooper, L. M. Seiford, and K. Tone, Data envelopment analysis: A comprehensive text with models, applications, references and DEA-solver software: Second edition. 2007. doi: 10.1007/978-0-387-45283-8.

[18] N. C. Petersen and P. Andersen, “A Procedure for Ranking Efficient Units in Data Envelopment Analysis A Procedure for Ranking Efficient Units i n Data

Envelopment Analysis," Source: Management Science, vol. 39, no. 10, pp. 1261–1264, 1993.

[19] T. Subramanyam, R. Donthi, V. Satish Kumar, S. Amalanathan, and M. Zalki, "A new stepwise method for selection of input and output variables in data envelopment analysis," Journal of Mathematical and Computational Science, vol. 11, no. 1, pp. 703–715, 2021, doi: 10.28919/jmcs/5205.

[20] C. P. Barros, O. Goncalves, and N. Peypoch, "French regional public airports technical efficiency," International Journal of Transport Economics, vol. 39, no. 2, 2012.

Biographies

Reshampal Kaur received the post-graduation degree in Mathematics from Punjab University, Chandigarh. She is CSIR-NET qualified and did her PHD from Punjab Technical University, in Operations Research. She is currently working as an Associate Professor at Department of Mathematics, Chandigarh University. Her research areas include mathematical modelling, multivariate data analysis and optimization.

Solar Power Integration Impact on Power Grid Perfomance

[1]Sulekha Singh Marko[**], [2]Suneel Kanojiya, [3]Aayush Shrivastava, [4]Ashish Singhal

Sagar Institute of Science technology and engineering[1,2,3,4],
marko.sulekhasingh2107@gmail.com[1], suneelkanojiya18@gmail.com[2],
mr.aayushshrivastava@gmail.com[3], ashishee@gmail.com[4]

Abstract.

A study has been conducted on the integration of solar power into power grids. The main aim of this study to analyse the impact of solar PV penetration on the power grid performance and its futuristic solution to overcome those issues. In the overall study found that the current variation at some place reach beyond the highest level of fault current, volage levels improved at busses and power losses decreases in the network about the 50% at 80% solar PV penetration level.

Keywords. Solar power, Penetration, Power factor, fault current, voltage and current variation, power losses.

1. INTRODUCTION

Renewable energy sources produce electricity using natural resources, which are less harmful to the environment than those that rely on conventional fuels. These sources can also help lower the overall power losses and pollution levels in the system. Although renewable energy sources can help lower the pollution levels and power losses in the system, they have various issues that need to be considered before they can be added to the system. Some of these include over-voltage, under-voltage, harmonics, and transient stability [1][2][3].

The increasing capacity of renewable energy sources such as solar power has increased the risk of short circuits in the grid. This is especially true when a microgrid is running in its own mode. One of the most common calculations that electrical designers have to make is the short circuit calculation. An electrical apparatus should be able to withstand the current and voltage of a fault for a certain period of time[4]. Protective equipment should also be designed to remove any potential faults that may be present in the system. Faults in these components should be fixed within the equipment's tolerance. Through extensive research, electrical engineers have been able to thoroughly examine the various facets of transient analysis. The goal of this process is to determine the minimum and maximum currents that a system's fault should have. All electrical equipment should have the necessary ability to withstand a fault at a given level.[5]. The maximum and minimum currents of the system are usually determined for the building of an earthing system and for the protection of an advanced protection system. Having the necessary knowledge about the type of defect that can be found in the system is very important to ensure that the equipment is protected. In order to protect the equipment, the pickup setting should be chosen using the lowest available fault current. The use of the electrical transient analysis programming, known as the ETAP, can greatly reduce the time it takes to perform a short circuit calculation[6][2][1]. In this study, the Electrical Transient and Analysis Program is used to investigate the best placement

for PV plants and their maximum penetration level (ETAP 19.5). To confirm the choice, the IEEE 14 bus system is emulated. To select the best outcomes for a given objective function, ETAP has the capacity to simultaneously execute several scenarios[2].

2. LOAD FLOW CALCULATION

A load flow analysis is a process that involves analyzing the flow of electricity through a power system. It can determine the voltage magnitude and the amount of current that' is flowing down the lines. It can also calculate the real and reactive power losses. The results of this procedure are used to start studies on the electric power system's components. This process is very important in the planning of a system's new extension or installation. The study performed on this project took into account the 1.3kV lines that are running through the IEEE 14 bus feeder network. The total operational load of the system is 259 megawatts, while the reactive load is around 73.5 MVAR. The results of the analysis were analyzed using the Gauss-Sidel method. The four solar PV plants are connected to the distribution feeders of IEEE 14. The total load of the network is determined by taking into account the overall energy usage by the renewable energy sources. The analysis also took into account the different power injection levels[1] [6].

In this case, solar PV has no impact on the system's load. Case 2, 3, and 4 show that it has fulfilled the system's 20%, 40%, and 60% load requirements, Case 5: Solar PV has fulfilled the 80% of the system's active load. Case 6: It has also fulfilled the 100% of the system's active load, case 7: fulfil the 120% of the system active load.[2].

A single line diagram is used to describe systems since it is assumed that their distribution is uniform. The load flow solution calls for generating an admittance matrix of dimension where n is the system number (n x n). A bus's own admission is represented by the diagonal elements of the admittance matrix, whereas mutual bus admission is represented by the off-diagonal elements[6][7].

$$Y = \begin{bmatrix} Y_{11} \dots \dots \dots Y_{44} \\ \dots \dots \dots \dots \dots \\ \dots \dots \dots \dots \dots \\ Y_{55} \dots \dots \dots Y_{88} \end{bmatrix} \quad (1)$$

The initial Gauss Sidle method, calculated voltage magnitude and angle of the particular bus provide as the parameters that define actual and reactive power and non-linear equation is solving by iterative methods (Gauss Sidle and Newton Raphson)

Real Power

$$P_i = \sum_{j=1}^{n} |V_i||V_j||Y_{ij}| \cos(\theta_{ij} - \gamma_i + \gamma_j) \quad (2)$$

Reactive power

$$Q_i = \sum_{j=1}^{n} |V_i||V_j||Y_{ij}| \sin(\theta_{ij} - \gamma_i + \gamma_j) \quad (3)$$

The calculated values known as power residuals for the terms ΔP_i and ΔQ_i is represented as:

$$\Delta P_i = P_i^{sch} - P_i \quad (4)$$

$$\Delta Q_i = Q_i^{sch} - Q_i \quad (5)$$

One or more transmission lines, loads, and generators can be connected to one another at a point or node called a bus. Each bus in a power system study has four values associated with it: the voltage magnitude (|V|), the voltage phase angle (γ), the active power (P), and the reactive power (Q). Two of these bus quantities are known, and the other two need to be calculated by solving an equation. The two known quantities that have been mentioned are

used to categories the buses. Three categories are used to group buses. The three bus types: Swing (P & γ), and Generator (P & V) Load Bus, (P&Q constants)[8][6].

This issue can be resolved in two different ways. First off, the measured real-and reactive-value requires internal iteration if the variables are picked up and determined at the beginning of the resolution approach (eq. 2 & 3). Second, to detect power inaccuracies and intolerance, improved accuracy iterations are necessary (eq. 4 and 5). The first iteration in this study is referred to as a calculation iteration, while the second iteration is referred to as a precision iteration.

TABLE NO. 1 - PENETRATION LEVEL OF SOLAR PV CONNECTED IN CASE WISE.

Total connected active load (kW) in network = 310 Kw							
% Penetration	**PV1 at Bus 2**	**PV2 at Bus 3**	**PV3 at Bus 4**	**PV4 at Bus 6**	**PV5 at Bus 13**	**PV6 at Bus 14**	**Total Solar PV (kW)**
Case1(0%)	0	0	0	0	0	0	0
Case2(20%)	51.8	0	0	0	0	0	51.8
Case3(40%)	51.8	51.8	0	0	0	0	103.6
Case4(60%)	51.8	51.8	51.8	0	0	0	155.4
Case5(80%)	51.8	51.8	51.8	51.8	0	0	207.2
Case6(10%)	51.8	51.8	51.8	51.8	51.8	0	259
Case7(120%)	51.8	51.8	51.8	51.8	51.8	51.8	310.8

TABLE NO. 2 – SOLAR PV PANEL RATING

Parameter Rating of solar PV	
Short-Circuit Current (Isc) Module	8.33 A
Open -Circuit Current (Voc) Module	33.97 V
Voltage & Current at Maxpower (Vmp, Imp) Module	27.19 V,7.89 A
Sun irradiance MAX. level	1000W/m2

3. RAISING THE VOLTAGE AT THE 14 BUS FEEDER

As seen from the simulation results, the level of PV penetration rises as well as the voltage of the buses also rising. The voltage of each of the 14 buses is shown in Fig. 2 with solar PV penetration rising from 0% to 120%. The level of solar PV penetration rises together with the percentage of voltage. The rise in voltage at various nodes continues to be within the prescribed limit (0-1.5%).

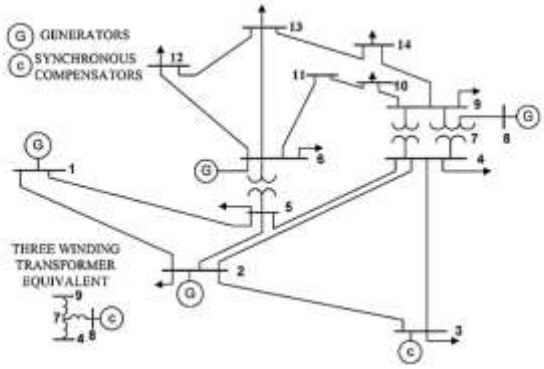

Fig.1 – Integration of Solar PV at Bus 2,3,4,6,13,14 In IEEE 14 Bus System

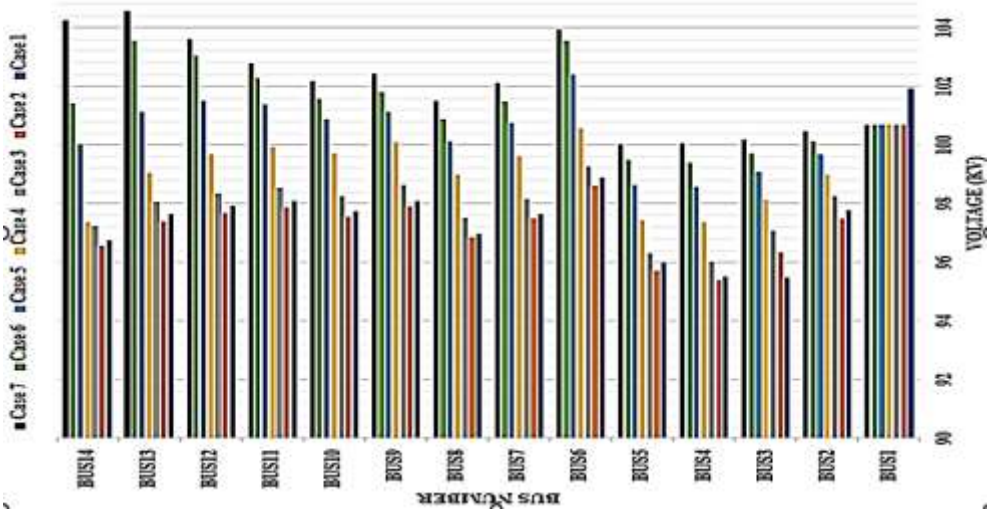

Fig2. – Voltage variation analysis with respect to Solar PV penetration

4. THE EFFECT OF SOLAR PV PLANTS ON POWER LOSSES IN THE DISTRIBUTION SYSTEM

The magnitude of power flow is inversely personal to the rate of power loss. PV technology has altered how the distribution network is used, resulting in atypical and bidirectional power flows. Therefore, the presence of PV systems and the consequent altered power flows may significantly affect power losses. Figure 3 illustrates this finding from an study of PV penetration that power loss lowers as PV penetration rises till 80% after 80% power loss increases gradually for case 6 & case 7.

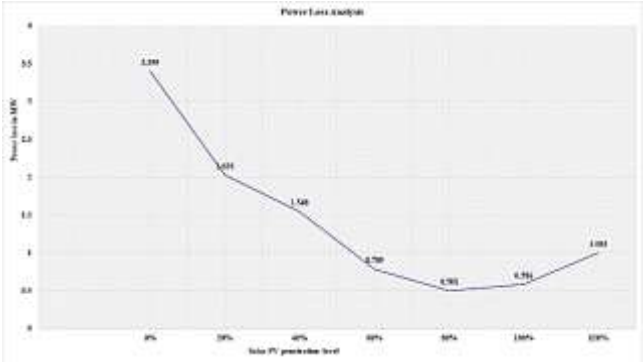

Fig3. – **Power Losses analysis for all penetration levels.**

5. THE EFFECT OF SOLAR PHOTOVOLTAICS ON POWER FACTOR.

The power factor is a significant aspect since it is essential for the efficient operation and reliable transmission of electric power. A decrease in power factor results from increased power output from the PV system. The increased active power from the PV system without any generation of reactive power may be used to interpret this. Because the grid supplies less active power while retaining the same level of reactive power, the power factor decreases as a result [9][6][10].

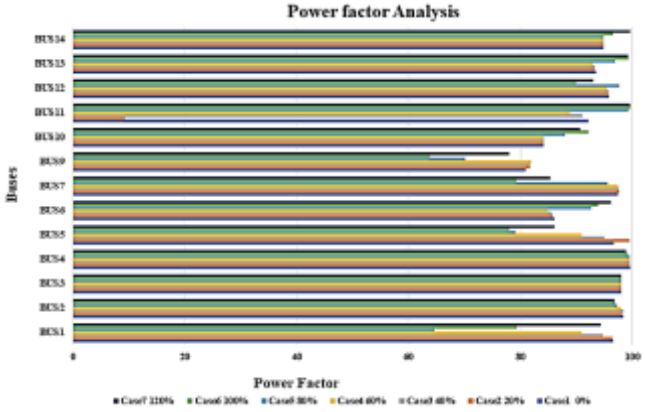

Fig4. – power factor of each case of solar PV penetration

6. SHORT CIRCUIT CURRENT WITH SOLAR PV

The goal of short circuit analysis is to determine the asymmetrical and symmetrical fault currents and their contribution to the overall electrical system. This process influences the short circuit ratings of equipment used in the distribution grid. The three types of fault that can be divided are the line to line, line to ground, and double line to ground. In this paper, the corresponding graphs are shown for the simulations of the L-G and L-L faults [1]. The results of this exercise show the magnitude of the buses that were involved in the line-to-line fault that was performed by an ETAP. Figs 4 and 5 illustrate the varying current values as the grid's penetration level changes. The results of the exercise show the significant faults in the micro-grid. The current values exhibited in these scenarios are shown in varying phases, with the former remaining above marginal in some areas and decreasing in others.[1][11].

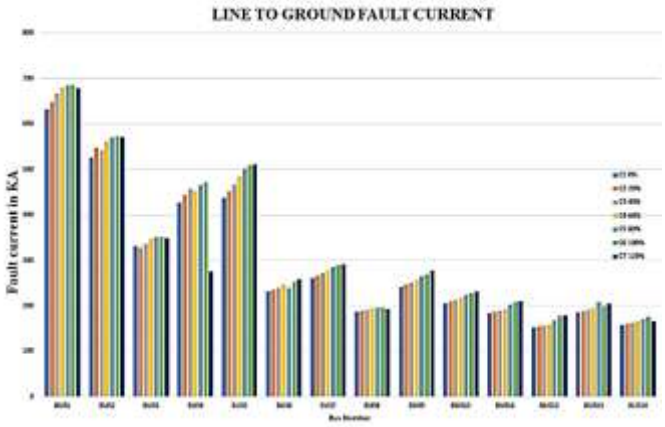

Fig 5. – Analysis Of L-G Fault Current for IEEE 14 Bus Distribution Feeder

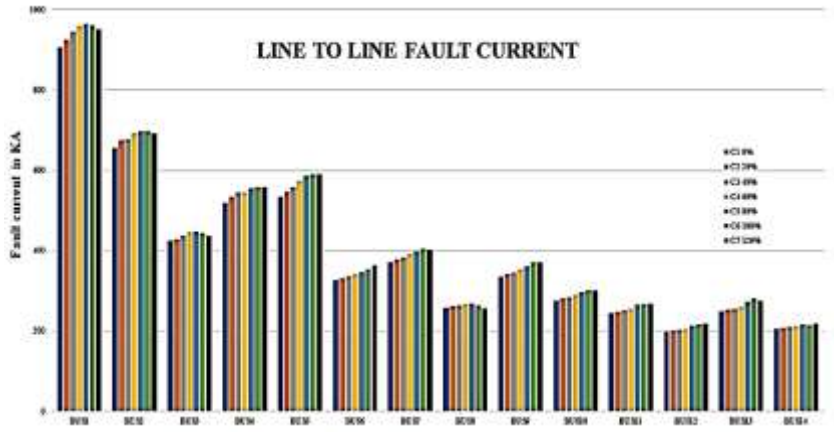

Fig 6. – Analysis Of L-L Fault Current for IEEE 14 Bus Distribution Feeder

The main bus that connects the various sub-buses and loads is shown in Figure 6. The distribution of the current during the line-to-ground fault is shown in Figure 5. The result shows that the defective phase of each bus leads to a large gain in the rated current, while the other phases experience an unequal displacement.

7. CONCLUSION

In the study found that the current variation in the penetration level of the connected devices can affect their system efficiency and life span. It is also found that the power factor of the system can vary at different penetration levels, which can cause it to be unbalanced. The study revealed that as the penetration level of the connected devices increases, the power losses decrease. However, after reaching a certain level of penetration, the power losses increase slightly. This research can should be used to develop an energy policy for renewable energy and its will be useful for the independent system operator for defining the integration capacity of RE.

References

[1] R. R. Waqfi and M. Nour, "Impact of PV and wind penetration into a distribution network using Etap," 2017 7th International Conference on Modeling, Simulation, and Applied Optimization, ICMSAO 2017, May 2017, doi: 10.1109/ICMSAO.2017.7934892.

[2] M. Al Talaq and C. A. Belhaj, "Optimal PV Penetration for Power Losses Subject to Transient Stability and Harmonics," Procedia Computer Science, vol. 175, pp. 508–516, Jan. 2020, doi: 10.1016/J.PROCS.2020.07.072.

[3] S. Bimenyimana, G. N. O. Asemota, J. D. D. Niyonteze, C. Nsengimana, P. J. Ihirwe, and L. Li, "Photovoltaic solar technologies: Solution to affordable, sustainable, and reliable energy access for all in Rwanda," International Journal of Photoenergy, vol. 2019, 2019, doi: 10.1155/2019/5984206.

[4] S. P. Ramezanzadeh, M. Mirzaie, and M. Shahabi, "Reliability assessment of different HVDC transmission system configurations considering transmission lines capacity restrictions and the effect of load level," International Journal of Electrical Power & Energy Systems, vol. 128, p. 106754, Jun. 2021, doi: 10.1016/J.IJEPES.2020.106754.

[5] M. Almaktar, A. M. Elbreki, and M. Shaaban, "Revitalizing operational reliability of the electrical energy system in Libya: Feasibility analysis of solar generation in local communities," Journal of Cleaner Production, vol. 279, p. 123647, Jan. 2021, doi: 10.1016/J.JCLEPRO.2020.123647.

[6] P. R. Kadukar, P. S. Shete, and S. P. Gawande, "Transient Analysis of Distributed Generation AC Microgrid using ETAP," Proceedings of the 2018 International Conference on Current Trends towards Converging Technologies, ICCTCT 2018, Nov. 2018, doi: 10.1109/ICCTCT.2018.8550987.

[7] D. K. Saini, A. Shrivastava, K. Saini, and M. Pandit, "Distribution Grid Parameter Variation due to Solar PV Power Integration," INTERNATIONAL JOURNAL of RENEWABLE ENERGY RESEARCH A. Shrivastava et al, vol. 10, no. 3, 2020.

[8] R. A. Shalwala and J. A. M. Bleijs, "Impact of grid-connected PV systems on voltage regulation of a residential area network in Saudi Arabia," 2010 1st International Nuclear and Renewable Energy Conference, INREC'10, 2010, doi: 10.1109/INREC.2010.5462580.

[9] A. S. Siva, S. Sathieshkumar, and T. Santhosh Kumar, "Analysis of Stability in IEEE 14 Bus System using ETAP Software," in Proceedings of the 4th International Conference on Inventive Systems and Control, ICISC 2020, Jan. 2020, pp. 935–938, doi: 10.1109/ICISC47916.2020.9171115.

[10] A. K. S. A. S. S. R. Priya Dwivedi, "Hybrid RE energy system based modified maximum peak power tracking technique," Solid State Technology, vol. 63, no. 6, pp. 20429–20434, Dec. 2020, Accessed: Jul. 17, 2021. [Online]. Available: http://www.solidstatetechnology.us/index.php/JSST/article/view/8479.

[11] A. Shrivastava, A. Sharma, M. Pandit, V. Jately, and B. Azzopardi, "Hybrid Protection Scheme Based Optimal Overcurrent Relay Coordination Strategy for RE Integrated Power Distribution Grid," Energies 2021, Vol. 14, Page 7192, vol. 14, no. 21, p. 7192, Nov. 2021, doi: 10.3390/EN14217192.

Overview and Design of Mecanum Wheel

[1,5]Shivmanmeet Singh, [2]Harmandeep Kaur, [3,5]Lakhveer Singh, [4,5]Rehan Dhir [6]Ajay Vasishth

[1]*Department of Electronics and Communication Engineering, Guru Nanak Dev Engineering College, Ludhiana, India*.

[2]*Department of Computer Application, Guru Nanak Dev Engineering College, Ludhiana, India*.

[3]*Department of Mechanical and Production Engineering, Guru Nanak Dev Engineering College, Ludhiana, India*.

[4]*Department of Mechanical Engineering, Guru Nanak Dev Engineering College, Ludhiana, India*.

[5]*Center for Multifaceted Learning, Guru Nanak Dev Engineering College, Ludhiana, India*.

[6]*Department of Physics, Chandigarh University, Mohali, India*.

Email:, shivmanmeet@gmail.com, harmandeepkaur156@gmail.com, lakhveerbathinda@gmail.com, rehan2000.rd@gmail.com, ajay.e8023@cumail.in

Abstract.

Mobile robots are quite sophisticated and have many difficulties to overcome. The capacity to manoeuvres in small spaces is one of the key obstacles. This ability mostly relies on the wheel's design. The primary goals of this project are to increase wheelchair mobility and, as a result, the quality of life for users. Mecanum wheels were used for this project for that reason. This essay discusses the recently developed mechanical design as well as the best way to create a circular-shaped roller.

Keywords. Mecanum wheel, automobile, rollers, vehicle, omnidirectional.

1. INTRODUCTION

Recently, researchers have been concentrating on studies concerning the utilisation of wheeled omnidirectional running mechanisms. Storage and transportation, military, social services and many other field areas have all made extensive use of magnum omnidirectional vehicles in particular [1]. Omnidirectional robotic vehicles have several benefits over traditional vehicles when it comes to manoeuvrability in congested areas. They are capable of carrying out activities with ease in crowded areas that are predicted to have static impediments, dynamic obstacles, or restricted spaces. These kinds of settings are often present in industries, workshops, warehouses, hospitals, etc. Traditionally, omnidirectional vehicles have been specially designed to move on hard, flat and smooth surfaces. On ground, omnidirectional vehicles have three DOF. They are suited for highly manoeuvrable, constrained, or precise placement situations since omnidirectional vehicles can do motions such as longitudinal, lateral, center point steering and any composite motion of the previously mentioned three. The wheel velocity of an omnidirectional wheel may be broken

down into the sections that are in the active and passive direction. The active component of the force is oriented parallel (∥) to the axis of the roller which is in contact with the ground, whilst the passive component of force is perpendicular (⊥) to the axis of the roller. Figure 1 illustrates basic mecanum wheel's design. Minimum of one and a maximum of two rollers are in touch with the ground while a mecanum wheel is turning. The roller only makes touch with the ground at one point, however, theoretically. Depending on how the wheel is rotating, this surface area moves across the roller from side to side. This forces the force of traction to be determined by the traversing feel of the contact of the roller with the surface.

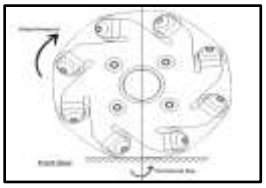

Figure 1. Degrees of Freedom in Mecanum Wheel

According to tests carried out for numerous researchers around the world, the Mecanum wheels' biggest problem is that they are unable to move laterally in the sand because the dirt and sand particles piles up between the rollers and on the side of the wheels and stops it from motion after the dirt and sand pile reaches a certain height with respect to the wheel size [2],[3]. They also have difficulty triumphing over obstacles during the motion in lateral direction. The main key goals of our study, which was motivated by these issues, was to develop a new kind of mecanum wheel capable of resolving those issues.

2. REGULAR MECANUM WHEELS

In a mecanum wheel, a group of k congruent rolls are assembled and arranged symmetrically around the wheel body. Each roll's face is a component of a revolution surface (R), whose b axis is skewed to the wheel's a axis [4]. There have been several comparable ideas put out, however these designs vary in terms of the number (k) of rollers, the manner of linkage of the rollers to the hub, the fixed angle at which rollers are in relation to wheel, the various materials utilised, etc. [2]. Some of the major issues faced are large vibrations and limited loading capacity. Slippage is another issue with them; as a consequence, even with the equivalent rotation of the wheel, the lateral and longitudinal movement of vehicle distances vary. In figure 2, a classic mecanum wheel is shown.

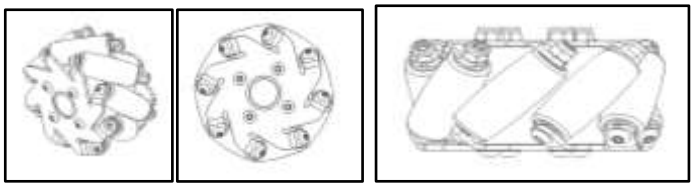

Figure 2. Conventional Mecanum Wheel

3. DESIGN OF ROLLERS

To ensure motion continuity is one of your primary concerns when building a new drive system. The true significance of this is that there are sufficient rollers and contact lines to

cover the wheel's curvature, in this example, a circumference. Additionally, there is a certain count of rollers used in the wheel that creates an optimal balance between possessing a few big size rollers per wheel and a number of small size rollers per wheel. Equation 1 is used to compute the moving continuity, which is denoted by.

$$\varepsilon = \frac{N(y-2\theta_o)R}{2\pi R} = \frac{N}{2\pi}(y - 2\theta_o)$$

There are five parameters listed in equation (1). These variables (R, N, ε, y, θ) are utilised to construct the rollers for the circular wheel components. As shown in Figure 3, R is the wheel's overall radius, N is number of rollers requires, y is angle at which the helical line is rotated around the z-axis of wheel, and θ is angle between the starting motion of point C travelling adjacent to the helical line (Figure 3).

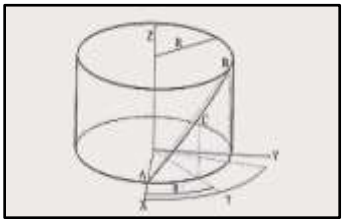

Figure 3. Configuration of the Rollers Scheme

A value of ε<1 in Equation (1) indicates that the length of the roller will be inadequate and will not function because the rollers will be small in comparison to the number of rollers in the wheel. The motion continuity may be ensured even when ε>1, but ε=1 is the best number since in this instance the length of the rollers satisfies all necessary wheel features. The number must therefore be as near to 1 as feasible because as it rises, the wheel becomes thicker, the roller's length increases, and the generatrix begins to oscillate, which renders the curve insufficient. The rollers in this paper's new design have a circular form, and changes have been made to the materials and the technique the rollers are attached to the hub. Figure 4 shows an example of the new design that is suggested.

Figure 4. Proposed and exploded view of macanum Wheel

The form of the rollers is defined in this design by the circular shape. In this instance, the coordinates A, B, and C in Figure 3 must be defined. These are how those points are defined:

$$A\ (R, 0, 0) \mid B\ (R\cos\gamma, R\sin\gamma, R\gamma) \mid C\ (R\cos\theta, R\sin\theta, R\theta)$$

The vectors "A" and "B" are then established using the definitions listed below.

$$\overrightarrow{AC} = \begin{Bmatrix} R(\cos\theta - 1) \\ R\sin\theta \\ R\theta \end{Bmatrix} = \begin{Bmatrix} P_1 \\ P_2 \\ P_3 \end{Bmatrix}$$
$$\overrightarrow{AB} = \begin{Bmatrix} R(\cos\gamma - 1) \\ R\sin\gamma \\ R\gamma \end{Bmatrix}$$

The unit vector parallel to A and B is written as follows:

$$\vec{u} = \frac{\overrightarrow{AB}}{|\overrightarrow{AB}|} = \frac{\overrightarrow{AB}}{R\sqrt{2 - 2\cos\gamma + \gamma^2}} = \begin{Bmatrix} u_1 \\ u_2 \\ u_3 \end{Bmatrix}$$

$$u_1 = \frac{\cos\gamma - 1}{D} u_2 = \frac{\sin\gamma}{D} u_3 = \frac{\gamma}{D}$$

$$D = \sqrt{2 - 2\cos\gamma + \gamma^2}$$

The curvature of the roller may be efficiently determined using this information. However, to do this, vectors A and C must be rotated around vector at an angle to produce numerous contact lines. Using this approach, the equations shown below are produced.

$$\begin{aligned} P_1' = {} & [\cos\tau + u_1^2(1 - \cos\tau)]P_1 \\ & + [u_2u_1(1 - \cos\tau) - u_3\sin\tau]P_2 \\ & + [u_3u_1(1 - \cos\tau) + u_2\sin\tau]P_3 \\ P_2' = {} & [u_2u_1(1 - \cos\tau) + u_3\sin\tau]P_1 \\ & + [\cos\tau + u_1^2(1 - \cos\tau)]P_2 \\ & + [u_3u_2(1 - \cos\tau) - u_1\sin\tau]P_3 \\ P_3' = {} & [u_3u_1(1 - \cos\tau) - u_2\sin\tau]P_1 \\ & + [u_3u_2(1 - \cos\tau) + u_1\sin\tau]P_2 \\ & + [\cos\tau + u_3^2(1 - \cos\tau)]P_3 \end{aligned}$$

The roller's surface equation is thus stated as follows

$$x = x(\theta, \tau) = R + P_1'$$
$$y = y(\theta, \tau) = R + P_2'$$
$$z = z(\theta, \tau) = P_3'$$

After that, the roller's maximum and minimum radii were calculated using the roller's surface equation in order to create a circular profile for the roller with the highest potential efficiency. Here, the other parameters of the equation, (L, l, l), may be determined by defining the number of rollers. L is the roller's length, is the angle formed by the hub and roller axis, and l is the width of the wheel are used to determine the roller's maximum and lowest radii. If N, the number of rollers, is known, may be used to determine roller length:

$$L_r = 2R\frac{\sin{}^{\varphi}/_{2}}{\sin\alpha} = 2R\frac{\sin{}^{\pi}/_{N}}{\sin\alpha}$$
$$\varphi = \frac{2\pi}{N}$$

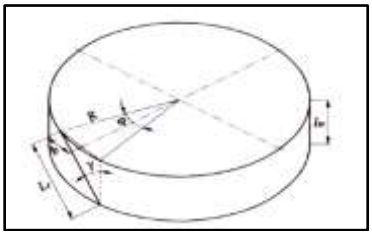

Figure 5: Wheel specifications

The wheel width will therefore be:

$$l_w = L_r \cos\alpha = 2R\frac{\sin {}^{\pi}/_{N}}{\tan\alpha}$$

The maximum radius of the roller may be calculated from these, and it is represented as:

$$r_{max} = R - \left(\frac{L_r \sin\alpha}{2\tan {}^{\pi}/_{2}}\right)$$

And the following equation is used to get the minimum radius:

$$r_{min}^2 + (2R - 2r_{max})r_{min} + R^2\left(\sin {}^{\varphi}/_{2}\right)^2 + r_{max}^2 - 2Rr_{max} = 0 \qquad (3)$$

The terms, r(max) and r(min) stand for the roller's maximum and lowest radii, respectively.

4. MECHANUM WHEEL SIMULATION

MATLAB programme was written with the goal of identifying the ideal silhouette for the roller. 750 interactions were performed in order to get the optimal outcome, with the number of rollers set between 8 and 14. The moving continuity coefficient was chosen between 1.008 and 1.031, and the width range is between 30 and 40 mm. The parameters α, θo, τ and R were previously specified in order to determine the roller's surface curve. The final set of required parameters were 45, 11, and 70. Regarding the parameter R, it was established in accordance with the project's goal, which will be covered in the next issue. As a result, the vehicle's top speed was set at 5 km/h, and its weight limit was set at 100 kg. Accordingly, the mecanum wheel's radius R should be 50mm. The driving torque was given to each of the four revolute joints that joined the body and the four mechanical wheels. Table 1 is a list of the wheel's primary properties. Figure 6 shows that the curve is simply rotated 360 degrees to create the roller.

Table 1. Parameters to define the curve of the roller

Parameters to define the curve of the roller					
Width (mm)	Maximum radius of roller (mm)	Minimum radius of roller (mm)	Helical Line Angle (°)	Roller Length (mm)	Continuity Coefficient
35	12	9	67.5	50	1.01

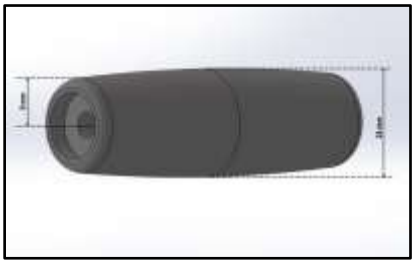

Figure 6. Roller's 3D model (Dimensions in millimetres)

5. OUTCOMES

On the basis of continuity coefficient, simulations were run with varying values for the number of rollers, with a range chosen between 8 and 14. In the end, the number of rollers set at 12 produced the best performance. This occurred as a result of the rollers touching one other while being displaced with 10 and 11 rollers, which caused unfavourable vibrations. The wheel becomes thicker and the curve that creates the roller is insufficient when using 13 and 14 rollers because the length of the rollers is too long.

Table 2. Fixed parameters to define the curve of the roller

Fixed parameters to define the curve of the roller				
Number of Rollers	Rotational axis of wheel (α)	Starting angle of Helical Line (θo)	Rotation of wheel contact line around roller axis of rotation (τ)	Radius of the wheel (mm)
12	45º	11º	70º	75

Table 2 lists the primary variables that were fixed to produce the roller's curve when the number of rollers was set at 12. Figure 7 illustrates the outcomes after setting the roller's maximum radius to a range of 10 to 12 mm.

As shown in Figure 7, the roller length will rise as the maximum radius decreases, necessitating a thicker wheel. Additionally, the generatrix has a tendency to fluctuate, making the curve insufficient for the roller's creation. As a consequence, the Maximum radius setting of 10 to 12 mm produced the greatest results, as indicated in Table 3.

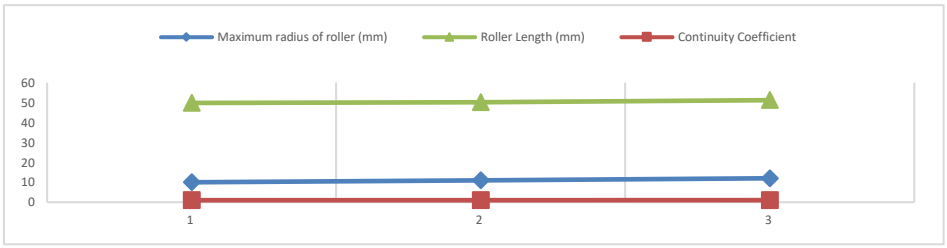

Figure 7. Relation among the main parameters (Maximum radius range: 10 to 12 mm's)

Table 3. Results of the parameters when the Maximum radius range is between 10 and 12

Results of the parameters when Maximum radius range is between 10 and 12

Maximum radius of roller (mm)	Minimum radius of roller (mm)	Helical Line Angle (°)	Roller Length (mm)	Continuity Coefficient
10	7	67.1	49.8	1.008
11	8	67.5	50.1	1.012
12	9	67.9	51.2	1.031

6. CONCLUSION AND DISCUSSION

In this research, an investigation of how the roller's geometry was created in accordance with the project concept was carried out. To create the most ideal roller curvature and improve the agility of the vehicle utilising this mechanical wheel, simulations using MATLAB and SOLIDWORKS were done. The mecanum wheel-based platform whose concept design is analysed, can be utilised in the future for multiple purposes as its final application.

REFERENCES

[1] Yunan Zhang, Tao Huang. 'Research on a Tracked Omnidirectional and Cross-Country Vehicle". Mechanism and Machine Theory 87 (2015) 18-44.

[2] A. Ramirez-Serrano, R. Kuzik, G.Solana. "Elliptical double Mecanum wheels for autonomously traversing rough terrain".

[3] S. Ransom, O. Krömer, and M. Lückemeier, "Planetary rovers with mecanum wheels," 16thISTVS Intl Conf, 25-28 Nov, 2008, Torino, Italy.

[4] A. Gfrerrer. "Geometry and kinematics of the Mecanum wheel". Computer Aided Geometric Design 25 (2008) 784-791

[5] Ioan DOROFTEI, Bogdan STIRB. "Design, modeling and Control of an Omni-directional Mobile". Solid State Phenomena Vols. 166-167 (2010) pp 173-178.

[6] SOLIDWORKS Inc., 2016. SolidWorks help Guide. s.l.: s.n.

[7] MATLAB Inc., 2018. MATLAB Help Guide.s.l.: s.n.

ELEKX - Adding Mental Health Perspective to a Chatbot

Ruchi[1], Suniti Dutt[2], Mitali Sinha[3], Aditay Kalia[4], Saksham Kanwar[5], Sanchit Khatkar[6], Ayush Srivastav[7], Ajay Vasishth[8]

[1-8] Chandigarh University, Mohali.

Email: ruchi061179@gmail.com

Abstract.

Typically, mental health professionals such as therapists treat mental disorders. Nevertheless, there is a universal human resource shortfall to provide such mental health services. Because of the scarcity and cost concerns, the Artificial Intelligence (AI) industry has taken matters into their own hands. The development of AI systems capable of producing human- like responses is currently a very popular research domain. Creating a virtual psychotherapist AI is one step closer to realizing the dream of human-like bot. In this work, a metal health bot for responding to users via text, i.e., a chatbot named "ELEKX" is proposed. The name Elekx is derived from the Greek word Elex which means man's defender or warrior. This chatbot allows patients to converse in the language they are most comfortable with from anywhere. This chatbot has been built using dialog flow to understand the mental health of a patient and engage them in a conversation by understanding their problems, suggesting remedies and seeking to lower their anxiety, stress and depression. The developed chatbot ELEKX is capable of aiding users in their day-to-day affairs and detecting any signs of negative change in mental health, and, if required, for alerting the concerned healthcare workers and immediate family members. Elekx is having an omnichannel messaging support and it provides sentimental analysis to our conversation.

Keywords. Artificial Intelligence, Assistance, Design-Based Research, Emotional Health, Values.

1. INTRODUCTION

A chatbot is a computer programme that communicates with people in real time utilising verbal medium, textual, facial, and bodily language [1]. Chatbot is also known as chatterbot, dialogue system, virtual agent, machine conversation system, and Conversational User Interface (CUI). A chatbot's basic goal is mimicking of a human conversation. Chatbots are generally driven by text, along with pictures and integrated widgets, thereby making it easier to initiate a conversation with a bot. Intelligent chatbots employ Artificial Intelligence (AI) for comprehending the purpose and circumstance of a user text and replying back. Un-intelligent or rule based chatbots produce a conversation based on certain established rules such as decision trees [2]. Over the past few years, chatbot usage in health care has increased. Chatbots for healthcare are popular for supporting the patients, their families, and the health care workers [3] by offering specialised cognition, therapeutic aid, and behavioural changes (such as Wysa, that offers cognitive behaviour therapy) [4], or assistance with disease management (such as Babylon Health, which offers digital health consults) [5].

Pharmacotherapy or psychotherapy are typically used to address mental health issues [6]. The demand for mental health experts, however, is greater than the supply in many countries.

According to global estimates, there are nine psychiatrists available for every 100,000 individuals in rich nations [7] and one psychiatrist for every 10,000,000 individuals in underdeveloped nations [8]. The WHO estimates that roughly 45% of individuals in industrialised nations and 15% of individuals in developing nations bear accession to mental health care [9]. When individuals with mental health illnesses are not treated, suicide thoughts and fatality rates might rise [10].

The chatbots are generally comprised of four primary modules: a text interpreting module, a conversation manager, a response generation module, and, a database which stores many kinds of data required for the training and operation of chatbot. A chatbot architecture and the connections among its constituents is shown in Figure 1. There are still technological restrictions even if AI can realise and aid in the creation of chatbots. The inability of current systems to recall earlier talks might result in improper answers [12]. To solve this problem, information about the patient's mental state must be gathered and preserved for further encounters with chatbot. Due to a lackof understanding or emotional intelligence, a chatbot reply may frustrate or be insufficient for a user [12]. Existing mental health chatbots have general abilities, a tendency to repeat themselves, and interactions that frequently resemble those found in self-help books [13].

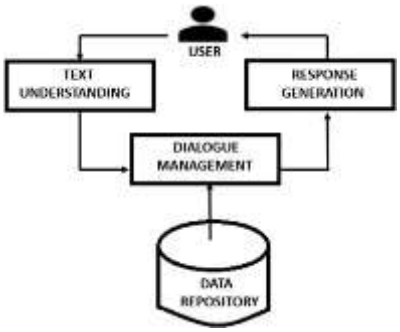

Figure 1. Chatbot architecture [11]

The problem here is that the technological constraints of the created mental health chatbots are not thoroughly studied in the present research. Evaluations primarily rate user experience and usefulness [14, 15]. The app stores are filled with mental health chatbots, but many of them lack evidence-based practises or, at the very least, do not have practises that are supported by pertinent research [16]. Mental health chatbots should rely on clinical data in order to be trustworthy and useful, which means integrating therapeutic procedures that are already in use in clinical practise and have proven helpful. Additionally, there is less research regarding the therapeutic value of mental health chatbots [16, 17]. Chatbots must maintain the privacy and confidentiality of user data regarding their mental health due to the sensitivity of such information [18]. Contrary to doctor-patient interactions, where patient privacy and confidentiality are guaranteed, chatbots frequently overlook these factors. Users

cannot interact anonymously with the majority of chatbots, notably those found on social networking networks [18].

2. BACKGROUND

A technique for putting word segmentation into practise was described by Mohammed Javed et al. in [19]. This algorithm's authors suggested calculating the character spaces within the sentences. All different kinds of gaps between characters should be included in the character spacing. They consist of word gaps, punctuation, and letter gaps. The method is based on the quantity of blank space or characters between each sentence unit. To get the mean average between the characters in the sentence, the character spacing are first computed [20].

People have used a variety of design and development methods for chatbots ever since they were first developed. Modern approaches for dialogue creation and management are more and more utilising machine and deep learning techniques [20–22]. This is due to the growing acceptance of machine learning and artificial intelligence techniques in a variety of applications. For people who have a little psychological disability, there is a smartphone application called SERMO [23]. It helps emotional control and uses techniques from Cognitive Behaviour Therapy (CBT). The programme is a conversational agent that prompts users to submit their feelings and ideas about commonplace occurrences that are established on Albert Ellis' theory of situation, emotions and thoughts. The theory takes the stance that inputs are assessed, whether intentionally or unintentionally, and that these assessments result in certain emotions and actions [24]. For people who feel embarrassed in revealing their mental health difficulties to a health care practitioner owing to stigmatisation, chatbots are also appropriate for offering mental health therapy. Lucas and colleagues found that veterans who used a chatbot revealed greater Post-Traumatic Stress Disorder (PTSD) symptoms than those who used anonymised or non-anonymised variants of a self-administered questionnaire [25]. Because they lack the high-quality human engagement that face-to-face interactions with health care professionals give, most computerised therapies are characterised by higher dropout rates as well as low adherence, even if they can be successful in ameliorating mental health [25, 26]. Through their intuitive, human-like, and enjoyable user interactions, chatbots can develop into a potential replacement for those treatments and increase users' adherence [27]. The fact that AI algorithms are often trained with massive data sets presents another significant challenge for the creation of chatbots for mental health. Another issue is that training with data of other fields can inject information into the system which could increase the risks of patient damage. Other methods that use lesser data for training or employ transfer learning are being developed. Furthermore, when the training data are poorly sampled or data are unavailable for particular sub-groups, trained models might become biased towards specific demographic groupings. The problem here is that the technological constraints of the created mental health chatbots are not well studied in the existing research [28, 29]. Evaluations primarily rate user experience and usability [28, 29].

Chatbots can't communicate human emotions or attend to all of a patient's demands. They could be useful for less difficult activities like data gathering or administrative and organisational chores, but whenever in-depth patient knowledge is required, they may falter [29]. It is necessary to improve their capacity to comprehend user input and respond properly. The accuracy of identifying emergency situations and developing a suitable

response after an emergency situation has been identified is a significant difficulty. Another unresolved issue is the customization or personalization of chatbots for specific users [30]. A number of patients, doctors, insurance companies, researchers, tech firms, and programme officials from the US National Institute of Mental Health established a unanimous statement on requirements for mental health mobile apps [31].

3. ELEKX - THE PROPOSED CHATBOT

The following are some advantages of the proposed ELEKX:

● With the help of ELEKX, users will be easily able to deal with day-to-day stress, depression, and anxiety.

● The user's data and progress about the user's mental health conditions will be stored and analysed.

● The user's mood can be enhanced and cheered up using a positive approach, humour, and CBT (Cognitive Behavioural Therapy).

● CBT will be used in the form of suggestions to help users lessen the effects of daily stress, depression, and various other mental health problems.

4. EXPERIMENTAL SETUP

For the implementation of ELEKX, Google Colaboratory online platform has been used here. Google Colaboratory, which is particularly well suited to machine learning, data analysis, and teaching, enables anybody to develop and run arbitrary Python code through the web. The dataset is then downloaded from Kaggle's Mental

Health FAQ [32]. This data set comprises of 98 questions and answers regarding mental health. There are three columns in it: Question ID, Questions, and Answers. Since NLP (Natural Language Processing) enables chatbots to learn and imitate the patterns and styles of human speech, ELEKX uses NLP. It links user input to an intent in order to categorise the message for the best potential predetermined response For this model, regularization is employed to control the model complexity which will make our model prone to overfitting, and the best model is retained for final comparisons based on training and validation accuracy and loss. We have used dropout regularization in our chatbot.

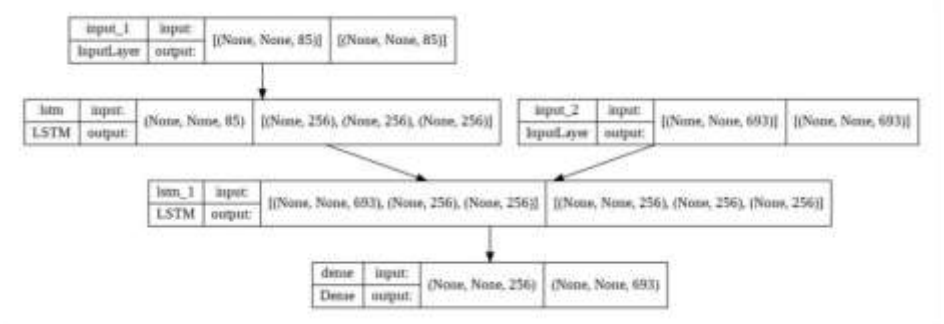

Figure 2. Complex model plot of ELEKX based on LSTM

Here, The Convolutional Neural Network (CNN) design appears to produce the greatest outcomes. Three layers make up the model: a CNN layer, an embedding layer, and a fully linked layer.

Figure 2 portrays the training as well as validation accuracies of the proposed chatbot. An encoder-decoder model is trained on the used data set. A seq2seq model, known as the encoder-decoder model, employs LSTM (Long Short-Term Memory) to generate text from the training corpus. Figure 3 depicts the training losses of the model.

Here, the model's training accuracy demonstrates how well it can categorise the two photos while being trained on the training dataset, whereas the model's validation accuracy demonstrates how well it can categorise the images on the validation dataset. It predicts a word from the user's input, and then it uses that word's probability or likelihood of occurring to forecast each of the subsequent words.Figure 4 shows the demonstration of ELEKX. It can be seen that ELEKX has run successfully after implementing the code in the software. It can provide quick solution of questions regarding mental health for its users.

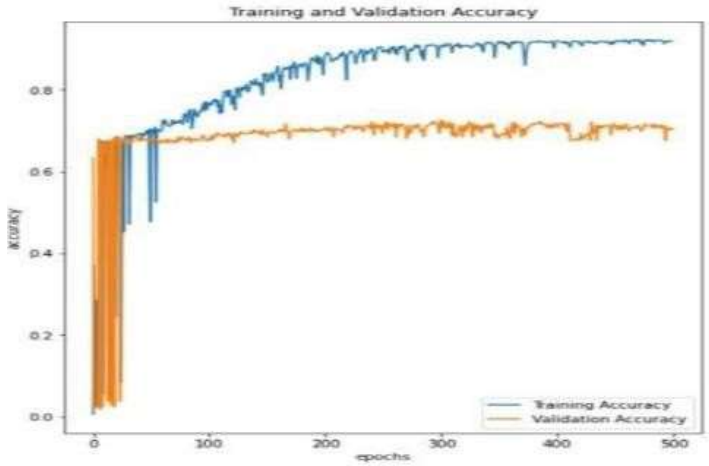

Figure 3. Training as well as validation losses

5. CONCLUSION

It is observed that the field of internal health assistants and chatbots in psychology and psychotherapy operations is expanding. The application of cutting-edge natural language technologies in conjunction with psychotherapy can result in tools that can, to a large extent, fill gaps in the delivery of internal care. ELEKX has been developed as a friendly chatbot so that users can feel at ease when they are counting on it for solutions regarding their mental health.

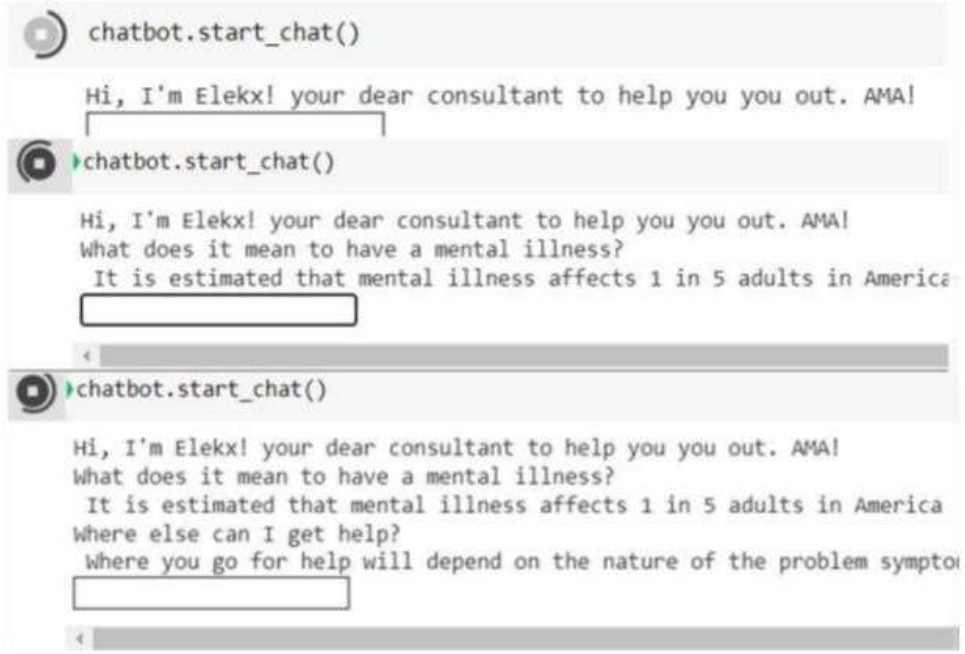

Figure 4 Working demonstration of ELEKX

6. REFERENCES

[1] Sansonnet J-P, Leray D, Martin J-C Architecture of a Framework for Generic Assisting Conversational Agents. In, Berlin, Heidelberg, 2006. Intelligent Virtual Agents. Springer Berlin Heidelberg, pp 145-156

[2] Hussain S, Ameri Sianaki O, Ababneh N A Survey on Conversational Agents/Chatbots Classification and Design Techniques. In, Cham, 2019. Web, Artificial Intelligence and Network Applications. Springer International Publishing, pp 946-956

[3] Fadhil A, Gabrielli S (2017) Addressing challenges in promoting healthy lifestyles: the al-chatbot approach. Paper presented at the Proceedings of the 11th EAI International Conference on Pervasive Computing Technologies for Healthcare, Barcelona, Spain

[4] Inkster B, Sarda S, Subramanian V (2018) An Empathy-Driven, Conversational Artificial Intelligence Agent (Wysa) for Digital Mental Well-Being: Real-World Data Evaluation Mixed-Methods Study. JMIR Mhealth Uhealth 6 (11):e12106. doi:10.2196/12106

[5] Tschanz M, Dorner TL, Holm J, Denecke K (2018) Using eMMA to Manage Medication. Computer 51 (8):18-25. doi:10.1109/MC.2018.3191254.

[6] Cuijpers P, Sijbrandij M, Koole SL, Andersson G, Beekman AT, Reynolds CF, 3rd(2013) The efficacy of psychotherapy and pharmacotherapy in treating depressive and anxiety disorders: a meta-analysis of direct comparisons. World psychiatry : official journal of the World Psychiatric Association (WPA) 12 (2):137-148. doi:10.1002/wps.20038

[7] Murray CJ, Vos T, Lozano R, Naghavi M, Flaxman AD, Michaud C, Ezzati M, Shibuya K, Salomon JA, Abdalla S, et al (2012) Disability-adjusted life years (DALYs) for 291 diseases and injuries in 21 regions, 1990-2010: a systematic analysis for the Global Burden of Disease Study 2010. Lancet (London, England) 380 (9859):2197- 2223. doi:10.1016/s0140-6736(12)61689-4

[8] Oladeji BD, Gureje O (2016) Brain drain: a challenge to global mental health. BJPsych international 13 (3):61-63. doi:10.1192/s2056474000001240 13. Anthes E (2016.) Mental Health: There's an App for That. Nature 532 (7597): 20–23

[9] Hester RD (2017) Lack of access to mental health services contributing to the high suicide rates among veterans. International Journal of Mental Health Systems 11 (1):47. doi:10.1186/s13033-017-0154-2.

[10] Bickmore TW, Caruso L, Clough-Gorr K, Heeren T (2005) 'It's just like you talk to a friend' relational agents for older adults. Interacting with Computers 17 (6):711-735. doi:https://doi.org/10.1016/j.intcom.2005.09.002

[11] Zeineb Safi, Alaa Abd-Alrazaq, Mohamed Khalifa,; Mowafa Househ, Division of Information and Computing Technology, College of Science and Engineering Hamad Bin Khalifa University Qatar Foundation P.O. Box 34110: Journey of medical internet search.

[12] Abd-alrazaq AA, Alajlani M, Ali N, Denecke N, Bewickd BM, Househ M (2020)Patients' attitudes toward using chatbots for mental health: Scoping review. Journal of Medical Internet Research.

[13] Laranjo L, Dunn AG, Tong HL, Kocaballi AB, Chen J, Bashir R, Surian D, Gallego B, Magrabi F, Lau AYS, Coiera E (2018) Conversational agents in healthcare: a systematic review. Journal of the American Medical Informatics Association 25(9):1248-1258. doi:10.1093/jamia/ocy072

[14] Kretzschmar K, Tyroll H, Pavarini G, Manzini A, Singh I (2019) Can Your Phone Be Your Therapist? Young People's Ethical Perspectives on the Use of Fully Automated Conversational Agents (Chatbots) in Mental Health Support. Biomedical informatics insights 11:1178222619829083. doi:10.1177/1178222619829083

[15] Miller E, Polson D (2019) Apps, Avatars, and Robots: The Future of Mental Healthcare. Issues in Mental Health Nursing 40 (3):208-214. doi:10.1080/01612840.2018.1524535

[16] Vaidyam AN, Wisniewski H, Halamka JD, Kashavan MS, Torous JB (2019)Chatbots and Conversational Agents in Mental Health: A Review of the Psychiatric Landscape. The Canadian Journal of Psychiatry:0706743719828977

[17] Stiefel S (2018) 'The Chatbot Will See You Now': Mental Health Confidentiality Concerns in Software Therapy. doi:http://dx.doi.org/10.2139/ssrn.3166640

[18] Luxton DD, Anderson SL, Anderson M (2016) Chapter 11 - Ethical Issues and Artificial Intelligence Technologies in Behavioral and Mental Health Care. In: Luxton DD (ed) Artificial Intelligence in Behavioral and Mental Health Care. Academic Press, San Diego, pp 255-276.

[19] Mohammed Javed, P. Nagabhushan, B.B. Chaudhari, "A Direct Approach for Word and Character Segmentation in Run-Length Compressed Documents with an Application to

Word Spotting", 13th International Conference on Document Analysis and Recognition (ICDAR), 2015.

[20] Serban IV, Klinger T, Tesauro G, Talamadupula K, Zhou B, Bengio Y, et al. Multiresolution Recurrent Neural Networks: An Application to Dialogue Response Generation. 2016. URL: http://arxiv.org/abs/1606.00776 [accessed 2020-02-12]

[21] Henderson M, Budzianowski P, Casanueva I, Coope S, Gerz D, Kumar G, et al. A Repository of Conversational Datasets. 2019. URL: http://arxiv.org/abs/1904.06472 [accessed 2020-02-12]

[22] Guo J, Lu S, Cai H, Zhang W, Yu Y, Wang J. Long Text Generation via Adversarial Training with Leaked Information. 2018 Presented at: The Thirty-Second AAAI Conference on Artificial Intelligence (AAAI-18); February 2–7, 2018; New Orleans, LA.

[23] Denecke K, Vaaheesan S, Arulnathan A (2020) Regulating Emotions with the Chatbot SERMO. IEEE Transactions on Emerging Topics in Computing:1-13. doi:10.1109/TETC.2020.2974478

[24] Wilken B (2015) Methoden der Kognitiven Umstrukturierung: Ein Leitfaden für die psychotherapeutische Praxis" (Methods for cognitive restructuring – A guideline for psychotherapeutic practice). 8th edn. Kohlhammer Verlag,

[25] Lucas GM, Rizzo A, Gratch J, Scherer S, Stratou G, Boberg J, Morency LP (2017) Reporting mental health symptoms: Breaking down barriers to care with virtual human interviewers. Front Robot AI 4 (OCT). doi:10.3389/frobt.2017.00051

[26] Nooijer JM, Oenema A, Kloek G, Brug J, De Vries H, De Vries NK (2005) Bevordering van gezond gedrag via Internet, nu en in de toekomst.

[27] Grolleman J, van Dijk B, Nijholt A, van Emst A Break the habit! designing an e-therapy intervention using a virtual coach in aid of smoking cessation. In: International Conference on Persuasive Technology, 2006. Springer,

[28] Abd-alrazaq AA, Safi Z, Alajlani M, Warren J, Househ M, Denecke K (2020) Technical metrics used to evaluate healthcare chatbots: Scoping review Journal of Medical Internet Research

[29] Laranjo L, Dunn AG, Tong HL, Kocaballi AB, Chen J, Bashir R, Surian D, Gallego B, Magrabi F, Lau AYS, Coiera E (2018) Conversational agents in healthcare: a systematic review. Journal of the American Medical Informatics Association 25

[30] Palanica A, Flaschner P, Thommandram A, Li M, Fossat Y (2019) Physicians' Perceptions of Chatbots in Health Care: Cross-Sectional Web-Based Survey. J Med Internet Res 21 (4):e12887. doi:10.2196/12887

[31] Kocaballi AB, Berkovsky S, Quiroz JC, Laranjo L, Tong HL, Rezazadegan D, Briatore A, Coiera E (2019) The Personalization of Conversational Agents in Health Care: Systematic Review. J Med Internet Res 21 (11):e15360. doi:10.2196/15360

[32] https://www.kaggle.com/datasets/narendrageek/mental-health-faq-for-chatbot

ROLE OF LINEAR ALGEBRA IN IMAGE COMPRESSION

Dhruv Sharma[1], R K Chaurasia[2], and Gagan Anand[3]

[1]Dhruv Sharma, FST , ICFAI University. Jaipur

[2]Assistant Professor, FST, ICFAI University, Jaipur 302031.

[3]Basic Science Cluster, Department of Physics, SOE, University of Petroleum and Energy Studies, Dehradun- 248007, India.

Abstract.

A comparison will be made between Singular Value Decomposition (SVD) and Block Truncation Coding (BTC) in this paper, as well as analyse how Algebra contributes to image compression and Block Truncation Coding (BTC). We will also examine how Algebra influences image compression. The input picture will be compressed first using the SVD method to reduce the image matrix rank, BTC will then be used to compress the matrix produced. The suggested approach improves the JPEG compression process by adding lossless compression, resulting in a compression rate of over 99 percent.

Keywords. Linear Algebra, BTC, SVD & PSNR.

1. INTRODUCTION

1.1. Image Processing

Basically, it's a way of processing images by extracting their characteristics or altering their inputs. Image processing is one of the most quickly evolving technology in today's world. It is also an important research field in computer science and engineering.

The following phases that makeup the image processing is:

- Input of the image data via software.
- Analysing and changing the input.
- And generating an output that could be a changed image or a report based on analysis.

When using digital techniques, all sorts of data must go through three general processing steps: pre-processing, enhancement, and display. Information extraction is the last of these steps.

1.2 Digital image processing (DIP)

The process of converting digital photos into digital images is called DIP. Analogue image processing can be compared to DIP as a subset of digital signal processing. It offers many procedures to choose from and apply to the input image, as well as discarding some issues such as noise and or unwanted distortion during the process. Image processing can be viewed as a multidimensional system because images can be displayed in 2D or more.

1.2. Image Compression

Digital image processing is a tool to process digital photos using the digital computer A procedure is used to process digital photos electronically with the help of a digital computer. processing. It offers many algorithms to choose from Image compression can be accomplished in a variety of ways. Internet users primarily use GIF and JPEG compression for graphic images. GIF is most often used for line art and graphics with simple geometric patterns, while JPEG is more often used for photos.

1.3. Linear Algebra

We all underestimated Linear Algebra's potential. It is composed of algorithms and approaches that are extremely useful in the real world, particularly in image analysis and manipulation. Images are one of the most widely used forms of communication in today's digital and social environments.
The two fundamental elements of linear algebra are the vector and matrix. A matrix is a linear mapping that converts vectors from one space to another, whereas a vector is a Euclidean space point (both the spaces could be of the same or different dimensions).

1.3.1. Eigenvalue and Eigenvector□λ

An equation as simple as Av = λv could be so significant. A matrix's eigenvalues and eigenvectors can be used to solve many problems, from machine learning to quantum computing. In other words, λ is the eigenvalue of A, and *v* is the eigenvector,

if

□□ = □□

From a visual point of view, A*v* and the eigenvector *v* appear to be on the same plane.

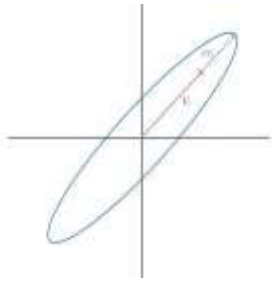

It doesn't always follow that x equals Ax. Only a few exceptional vectors meet the criteria. Here is an instance of eigenvectors.

$$\begin{matrix} 1 & -3 & 3 \\ 3 & -5 & 3 \\ 6 & -6 & 4 \end{matrix} \begin{matrix} 1/2 \\ 1/2 \\ 1 \end{matrix} = 4 \begin{matrix} 1/2 \\ 1/2 \\ 1 \end{matrix}$$

The related Av_i will grow if the eigenvalue is bigger than one. It will shrink if it is less than one.

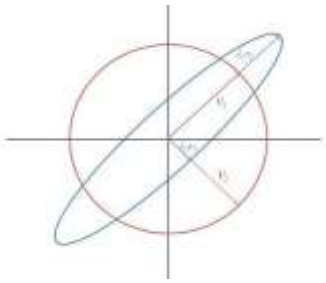

2. SINGLE VALUE DECOMPOSITION

Single Value Decomposition (SVD). SVD can decompose any matrix into three matrices, unlike other decompositions that need a square matrix to be decomposed, SVD allows you to decompose a rectangle matrix (a matrix that has different numbers of rows and olumns).

Q^T, , and T are Z's decomposed matrices. As a result, any linear map may be deconstructed into these three fundamental transformations, this process known as Singular Value decomposition (SVD).

$$B = TQZ^t \qquad \ldots (1)$$

Figure 1: Example of Factorisation of *B* to *TQZ*^{t}

Where *T* is an $a \times a$ orthogonal matrix

$$T = [t_1, t_2, \ldots t_r, t_{r+1}, \ldots, t_m] \qquad \ldots\ldots\ldots (2)$$

column vectors $\mathbf{t_i}$, for $i = 1, 2, \ldots, m$, form an orthonormal set:

And Z is an $b \times b$ rectangular matrix

$$Z = [\, z_1, z_2, \ldots z_r, z_{r+1}, \ldots, z_n] \qquad \ldots (3)$$

column vectors $\mathbf{v}i$ for i = 1, 2, …, n, form an orthonormal set:

Here, Q is an $a \times b$ diagonal matrix with

singular values (SV) on the diagonal. The matrix Q can be as shown :

Q = σ1 0 --- 0 0 ---- 0

0 σ2 --- 0 0 --- 0

- - - - - - - -

- - - - - - - -

0 0 --- σr 0 ----- 0

0 0 --- 0 σ(r+1) ----- 0

- - --- - ------ ----- -

0 0 --- 0 0 ----- σr

0 0 --- 0 0 ----- 0

For $i = 1, 2, \ldots, n$, σ_i are called Singular Values (SV) of matrix B. It can be proved that

$\sigma_1 \geq \sigma_2 \geq \ldots \geq \sigma_r \geq 0$, and

$\sigma_{r+1} = \sigma_{r+2} = \ldots = \sigma_n = 0 \qquad \ldots (5)$

For $i = 1, 2, \ldots, n$, is called Singular Values (SVs) of B. The $\mathbf{v}i$'s and $\mathbf{t}i$'s are called right and left singular vectors of B [1].

Digital images can be compressed to reduce the quantity of information they require. Compression is attained by reducing three essential data severances: 1) coding redundancy, caused by poor coding quality; 2) interpixel redundancy, caused by pixel correlations; and 3) psychovisual redundancy, caused by data disregard by the System of visual perception in humans.

Its singular values decrease rapidly. Based on the rank of an asymmetric matrix increases. This property can be useful for reducing noise and compressing matrix data by removing single values or higher ranks.

We present detailed steps to demonstrate the SVD image compression process:

$$B = TQZ^t$$

i.e. *B* can be epitomized by the external as BB^T

product expansion:

$$BB^T = TQZ^TZDT^T$$

By truncating the sums after the first k terms, the closest matrix of rank k is obtained:

$$Bk = \sigma_1 t_1 z_1 + \sigma\ 2t\ 2z\ 2t + \text{----------} + \sigma_{K1} t_{K1} z_{K1}$$

The total storage for Bk will be

k(a + b+1)

A digital picture that corresponds to Bk will remain substantially similar to the original image even if the integer k is less than n. On the other hand, the remaining k will have a diverse storage and picture. With typical k selections, A_k will require less than 20% of storage.

Compressed Images at different values of K.

Original Image

- **Result of Experimentations for Image Compression**

3. BLOCK TRUNCATION CODING

As a result, moments for each picture block are preserved. It is known as moment-preserving block truncation. In order to implement the BTC algorithm, following steps must be taken:

The first step is to divide the image into rectangular parts that don't overlap with each other. In order to simplify the process, we decided to make the blocks squares measuring m x m.

In the second step, each pixel in the block is quantized into two brightness values using a two-level quantizer (1 bit). The mean x and the standard deviation σ are these values.

$$\underline{\square} = 1/\square \sum_{\square=1}^{\square} \square\square$$

$$\sigma = \sqrt{1/\square} \sum_{\square=1}^{\square} (\square\square - \underline{\square}i)^2$$

Step 3: The two values x and σ are referred to as BTC quantizers. Two-level bit planes are generated by comparing each pixel value xi to the threshold value x.

$$\square = 1 \; \square\square \geq \underline{\square}$$

$$0 \; \square\square < \underline{\square}$$

Each block is converted to a bit plane using this method. A block of 4 × 4 pixels, for example, will yield 32-bit compressed data, or 2 bits per pixel (bpp).

The fourth step involves rebuilding an image block in the decoder by replacing "1"s in the bit plane with "H", and "0"s with "L", as shown in the following equations:

$$H = \underline{\square} + \sigma\sqrt{\square/\square}$$

$$L = \underline{\square} + \square\sqrt{\square/\square}$$

The number of 0's and 1's in the compressed bit plane is denoted by p and q, accordingly.

Original Compressed Image

- **Result of Experimentations for Image Compression**

4. PSNR

Two images are compared to calculate their peak signal-to-noise ratios (in decibels). In this ratio, original and compressed images are compared for quality. With increasing PSNR, the quality of the compressed or rebuilt image improves.
In this ratio, the original and compressed image quality are compared. In PSNR, the peak error is represented by the PSNR, whereas in MSE, By MSE, we can measure the squared error between the original and compressed images. TUsing MSE as a measure of error is in inverse relationship with the error. PSNR is calculated in two stages: calculating mean square error and calculating PSNR.

$$MSE = \frac{1}{M * N}\{[f(a,b) - f'(a,b)^2]\}$$

M and N in the above equation stand for the input pictures' respective rows and columns. The block then uses the following calculation to get the PSNR:

$$PSNR = 10log10\frac{R^2}{MSE}$$

A picture's input data type has the greatest variation when viewed in the previous equation. The R value is 1, for instance, if the key picture uses floating (double-precision) points. A data type that is 8 bits unsigned has R = 255, for example.

5. CONCLUSION

When the singular value of an SVD increases, the quality of compressed image is enhanced significantly but the size also increases. The image's visual quality degrades as the block size increases, and the compression size does not shrink as much.
The block truncation coding (BTC) scheme is effective in terms of higher compression ratios

as inferred from our findings. When data loss is unacceptable, Singular Value Decomposition (SVD) may be used for passwords, financial information, and confidential papers; however, BTC can be used when the focus is more on transmission than what information is included in the picture.

REFERENCES

1. Adiwijaya, M. Maharani, B.K. Dewi, F.A. Yulianto and B. Purnama et al., 2013. digital image compression using graph colouring quantization based on wavelet-SVD. J. Phys. Conf. Series, 423: 1-1. DOI: 10.1088/1742-6596/423/1/012019
2. Mrak M., Grgic S. and Grgic M., Picture Quality Measures in image compression systems, IEEE EUROCON, Ljubljana, Eslovenia, September 2003.
3. Mande M., Singular Value Decomposition, Department of computer science of the Technological Institute of Bombay India, august 2003.
4. Rafale C. Gonzalez, Richard Eugene. Digital Image Processing. Pearson, Edition 3, 2012.
5. Somasundaram K. and MS.S.Vimala, Efficient Block Truncation Coding: (IJCSE) International Journal on Computer Science and Engineering. Vol. 02, No. 06, 2010, 2163-2166.
6. Somasundaram, K. and I. Kaspar Raj. “Low Computational Image Compression Scheme based on Absolute Moment Block Truncation Coding “. May 2006. Vol. 13.
7. R. H. Myers, D. C. Montgomery, G. G. Vining, T. J. Robinson, Generalized linear models: with applications in engineering and the sciences, vol. 791, John Wiley & Sons 2012.
8. Naseem, R. Togneri, M. Bennamoun, Linear Regression for Face Recognition IEEE Trans. Pattern Anal Mach Intell, vol. 32 no. 11, pp. 2106-2112, 2010.
9. Mr. Chandresh K Parmar, Prof. Kruti Pancholi, "A Review on Image Compression Techniques" Journal of Information, Knowledge and Research in Electrical Engineering ISSN: 0975 – 6736 volume – 02, Issue – 02 Nov 12 to Oct 13.
10. L. J. Revell, Phylogenetic Signal and Linear Regression on Species Data Methods in Ecology and Evolution, vol. 1, no. 4, pp. 319-329, 2010.

Biographies

Dhruv Sharma currently pursuing B,Tech (CSE) from ICFAI University, Jaipur.

Dr. R.K Chaurasia is Head of Department of Electronics & Communication Engineering. He has 19 years of teaching and research experience. He has published 40 research paper in national and international journal like Elsevier, Springer and IEEE proceeding. He has also chair session and Reviewer of prestigious Journal like IET, IEEE and Springer conferences. His key areas are Wireless Communication, Signal Processing. He has also published two books in Lambert publication.

Dr. Gagan Anand has been associated with the University of Petroleum and energy studies as a **Professor** in the Department of Physics, School of engineering studies since July 2011. He worked on the concentration of Calcium in Strontium Bismuth titanate ceramics for high-temperature sensor applications an alternative to Lead-based materials like PZT/PLZT etc. His vast teaching experience has been spanned over **22** years across various leading colleges in India.

Vectorization of Text in Natural Language Processing

[1]Parth Sethi, [2]Deval Verma
[1]Department of Mathematics, Chandigarh University, Punjab- 140413
parthsethi85@gmail.com
[2]School of Computer Science Engineering and Technology
Bennett University, Times Group
Greater Noida-201310
deval09msc@gmail.com

Abstract

(NLP) Natural language processing is the field where computers can comprehend and use natural language text or voice for beneficial purposes. Some pre-processing and feature encoding techniques are applied over unstructured text data. The text will then be transformed into numerical feature vectors so that it may be fed to computers for machine learning applications. In this work, a statistical or frequency-based word embedding techniques are used. That are Continuous Bag of Words (CBOW), (TF-IDF) Term Frequency-Inverse Document Frequency and Skip-Gram Models. This work shows a comparison of all these techniques.

Keywords: NLP, Textual data, lemmatization, stemming, TF-IDF, CBOW and Skip gram models

1. INTRODUCTION

Natural language processing helps us to deal with this important aspect of humanity. NLP is a branch of machine learning that provides computers the ability to comprehend human text and speech. For example, humans feel more connected through stories; moreover, stories are an efficient way to transmit important information from one person to another. Stories are fundamental to humans for example: “Humans like to think in tales versus facts, statistics, or calculations, and the more straightforward the story, the better.”– Yuval Noah Harari

The above quote from the book [1] clearly highlights the importance of stories for humanity. Human race is a social animal and research has shown that stories are more engaging and influencing for the brain, that is the reason why some literature is banned by the governments of various countries. Humans feel more connected through stories; moreover, stories are an efficient way to transmit important information from one person to another. Stories are fundamental to humans [1, 2, 3,4].

Some of the use cases of NLP include speech recognitions, sentiment analysis, and language translators. NLP is playing a huge role in improving the healthcare sector and it is helping in providing better results for the patients [5,6,7,8,14]. Word embedding are numerical representations of words in the shape of a low dimensional vector, we need

word embedding because machine algorithms can understand only numbers and not text or words [9,10,11,12,14]. It can take a word out of its textual context. Words that are similar will have close vectors, for instance words happy and jovial will have vectors that are akin to each other. Word embedding is also capable of capturing semantic and syntactic similarities of texts. Semantic refers to similarity of the meaning of the given texts or words and syntactic similarities refer to the similarity of words of the given texts [13,14]. There are many techniques to attain word embedding; some of the most popular techniques are listed below:

- Binary Encoding
- TF-IDF Encoding
- Word2Vec Embedding

1.1. Binary Encoding

In one binary encoding, every word which is a part of the text is represented in vector form. A word will be labelled as 0 or 1, that is how this technique gained its name. It is also known as one hot encoding. For instance, consider the following sentences “I love to read” and “I like to read”. Both sentences have semantic and syntactic similarities. Before we can encode these sentences, we must tokenize them. These two sentences will have the following vectors if we use binary encoding as our encoding technique [4].

On the left-hand side of the figures are the indices of the words. For example, look at the vector for “I like to read”, at index 0 there is the alphabet “I” so it’s one hot encoding representation is [1,0,0,0] followed by the word “like” at index 1 which will have vector [0,1,0,0]. One hot encoding technique has dimensionality problems. In the above used sentences the vocab size is extremely small, Vocab size = Number of distinctive words. So, the vocab size for the sentence “I like to read” is 4 and the same is for the sentence “I love to read.” From the above figures, we can see that most of the vectors are taken up by zeroes and single ones. Now, assume that we have a text with a vocabulary size of 10,000. Each word in that vocab will be represented by 9999 0’s and a single 1. This is not computation friendly.

It is difficult to attain syntactic and semantic information of the text if we use binary encoding. Syntactic refers to the grammatical structure of the sentence and semantic refers to the meaning of the sentence [5,6].

	I	love	read	to
0	1	0	0	0
1	0	1	0	0
2	0	0	0	1
3	0	0	1	0

	I	like	read	to
0	1	0	0	0
1	0	1	0	0
2	0	0	0	1
3	0	0	1	0

Figure 1.1. Binary encoding vectors

The above statement examples (Figure:1.1) are like each other but looking at the derived vectors we cannot obtain any information about the similarity. Binary encoding techniques cannot extract the essence of the text. We also lose the order of the words in which they appear in the text. We used sentences “I like to read” and “I love to read” but when we binary encoded those sentences words “read” and “to” lose their order, this might lead to the loss of the meaning of the entire text.

1.2. Term Frequency-Inverse Document Frequency Encoding

Term Frequency-Inverse Document Frequency is abbreviated as TF-IDF. Its score is obtained by using the following formula in (1.21):

$$tf - idf(w, d, C) = tf(w, d) * idf(w, C) \quad (1.21)$$

It is obtained by multiplying the number of times word w appears in document d with the inverse document frequency of word w in the corpus C. Most popular uses of this technique include text mining, Keyword extraction etc. Before we can understand how tf-idf works, we first must understand tf and idf, as these are multiplied to attain tf idf score [7,8] as shown in Table 1.1.

Term Frequency (TF): TF measures the frequency with which a word appears in the text. Length of the documents can greatly impact the term frequency, TF is the quantity of is directly proportional to occurrences of a word i.e., as the number of occurrences of a word increase, term frequency also increases [6]. Each document has its own term frequency. For instance, there is a high probability that a word such as "this" can appear more times in a document with 500 words as compared to the document with 50 words. To deal with these problems we perform normalization of the frequency of the words appearing in a document. This can be done by using the following formula in (1.22):

$$tf(w, d) = \frac{Number\ of\ times\ word\ w\ appears\ in\ document\ d}{Total\ number\ of\ words\ in\ the\ document} \quad (1.22)$$

For instance, our document contains 2 sentences. First sentence is "What a beautiful day", and the second sentence is "Sun is shining bright". Now, our vocabulary will look like

{"What", "a", "beautiful", "day", "Sun", "is", "shining", "bright"}

Table1.1 Values of tf (A) and tf (B)

Term	**tf(A)**	**tf(B)**
What	1/4	0
a	1/4	0
beautiful	1/4	0
day	1/4	0
Sun	0	1/4
is	0	1/4
shining	0	1/4
below	0	1/4

Inverse Document Frequency (IDF): Document frequency refers to the number of documents in a corpus that contains the term. IDF can be calculated using the following formula in (1.23).

$$IDF(w) = \int \frac{Total\ number\ of\ documents\ in\ a\ Corpus}{Number\ of\ documents\ with\ word\ w\ in\ it} \quad (1.23)$$

IDF is the measure of the significance of a word in a corpus. We need IDF because while calculating term frequency each word is given equal importance. For instance, we need to calculate the term frequency of an article about renewable sources of energy, however words such as „this", „that, „of „ may have more number of occurrences as compared to words such as „renewable", „natural" and in our case these less occurring terms holds more importance and to deal with this we will compute IDF [6]. IDF score will be less for more frequent terms and high for the rare terms. To understand IDF better, assume that we have a corpus of 5 documents and each document contains a single sentence.

Document 1 = "There might be rain today"

Document 2 = "I like to read"

Document 3 = "It may not rain today"

Document 4 = "I love to read George Orwell's work"

Document 5 = "It is such a beautiful day"

IDF score for word "I" will be calculated using these values 52 and it will be 0.39. Total number of documents in the corpus is 5 and the documents which contain the word "I" are 2. Similarly, calculate the IDF for the word "George Orwell", 51 and it will be 0.69.

Now, let's get back to tf idf. It is obtained after multiplying the term frequency with the inverse document frequency. For simplicity purposes assume we have weather corpora that contain 1000 documents and in a document of 500 words "sun" occurs 100 times. So, the term frequency of the word wills 100500 or 0.2, and "sun" is occurring in 50 documents, so the inverse document frequency will be 100050 or 1.30. The tf-idf score will be the product of tf and idf: 0.2 * 1.30 = 0.26.

1.3. Word2Vec

Word2vec converts a word into a vector, and various arithmetic operations can be performed on these vectors; it's a multilayer neural network model [13]. Similar words will have similar vectors, for instance word lion and forest will have similar vectors [8,9]. We can identify both semantic and syntactic similarity using this word embedding. This method utilizes "**Cosine similarity**" to find out the closeness of words. Quoting the famous example here, we can do king - man = queen. Word embedding can be obtained using two methods [10,11,12,13]:

- CBOW model
- Skip-gram model

1.4. CBOW model and Skip-gram model

A continuous bag of words (CBOW), which determines the word based on context. Whereas Skip-gram predicts context based on word [5,6,7]. These models capture syntactic and semantic similarities between words; cosine similarity is utilized to find similar words and both models use neural networks to produce word embedding.

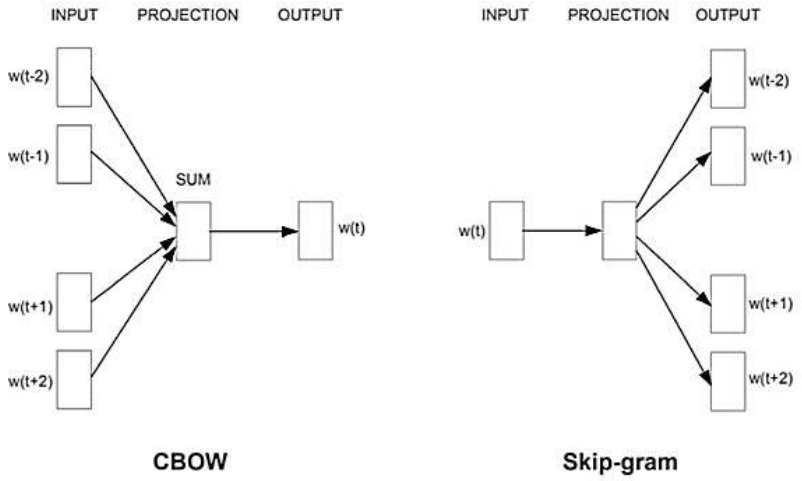

Figure 1.41. Architecture of the CBOW and skip-gram

In the given, Figure 1.41 we can see the word embedding for the word “trees”, now using this word embedding the models can predict similar words as shown in Figure 1.42.

```
array([-3.1647831e-03,  6.6352432e-04, -4.3224380e-03, -3.2030789e-03,
       -3.2577547e-03,  2.3196186e-03, -2.1934137e-04, -3.5526946e-03,
       -4.3959594e-03,  3.6182536e-03,  5.0039287e-03, -1.6665216e-03,
        1.0310774e-03,  4.8572265e-03, -3.9254529e-03,  2.6369265e-03,
        1.4008979e-03, -3.3607757e-05,  2.3548059e-04,  5.0829898e-04,
        5.0335978e-03, -2.8610714e-03,  2.9744555e-03, -1.5639713e-04,
        2.0028965e-05, -3.4813008e-03, -4.4373344e-03,  4.3749912e-03,
        2.1769165e-03, -3.4617835e-03, -3.2318819e-03,  2.5144881e-03,
       -3.7870089e-03,  1.0379617e-03,  1.4049141e-03,  4.5789471e-03,
       -2.0588420e-03,  9.4364729e-04,  2.1561191e-03, -3.5151306e-03,
        2.8693476e-03,  4.9358369e-03,  1.8326265e-03,  6.0908357e-04,
       -3.5187874e-03,  4.5093838e-03, -2.1001834e-03,  2.5853562e-05,
        4.6728244e-03,  1.0346936e-03, -2.5840461e-03, -1.3534208e-03,
        3.7168451e-03,  5.2585325e-04,  3.7305017e-03, -4.0082322e-03,
        2.4603755e-03,  5.3490091e-04,  3.9507668e-03, -4.1897088e-04,
        2.4129493e-04, -2.0739404e-03, -1.7915292e-03, -2.8138754e-03,
       -4.9105008e-03,  4.9478668e-03,  2.8109606e-03, -2.0268252e-04,
        3.1278927e-03,  4.5318729e-03,  3.2669005e-03,  4.6174284e-03,
       -2.1689201e-03, -4.2771120e-03,  7.3322898e-04,  2.8674718e-04,
        3.5741110e-03,  5.7364105e-05,  2.8834697e-03, -3.0618829e-03,
       -3.8231914e-03,  2.9396319e-03, -2.2789377e-03,  1.2001503e-03,
       -1.1800561e-03,  3.4961426e-03,  1.1842416e-03,  5.6611816e-04,
        4.2340956e-03,  6.8602688e-04,  2.1409253e-03, -9.1481837e-04,
       -3.2595231e-03, -1.6708935e-04,  3.9600485e-04,  4.8093372e-03,
        1.4168725e-03, -1.3021023e-03, -2.4729986e-03, -3.5623604e-04],
```

Figure 1.42 Word embedding array of word “trees”

2 ARCHITECTURES OF THE MODELS:

- Pre-Processing the unstructured text data is the first stage in NLP.
- A further step may be added to the process to exclude or convert emotions to ASCII digits. A model is created in NLP, that can solve our problem,
- Input layer of the CBOW model takes the one hot encoded vector of the context word(s) of size V.
- The second layer of the model or hidden layer to the model uses N Neurons and finally the output layer returns a SoftMax vector of length V [7].
- In CBOW the order of the word does not matter. We must declare a window size, it's a tuneable parameter. Let's assume we have an environment article (processed) and we declared the window size as 2, then the context words and target word will look like in Figure 2.1:

```
[(['trees', 'play', 'role', 'for'], 'critical'),
 (['play', 'critical', 'for', 'people'], 'role'),
 (['critical', 'role', 'people', 'and'], 'for'),
 (['role', 'for', 'and', 'the'], 'people'),
 (['for', 'people', 'the', 'planet'], 'and')]
```

Figure 2.1 Context and target words.

3 EXPERIMENTS AND RESULTS:

In the above figure 2.4, the words in a list represent the context words and the words outside of it represent the target word. Our first sentence is "trees play critical role for", according to our parameter the target word should be between the first 2 words and the last 2 words in a sentence and that results in "critical" being our target word in this case [8].

After the algorithm finds out the target and context words, the one hot vector of size V is passed in the first layer of the model then the second layer of the model which contains N neurons. The second layer tries to predict the target words using the one hot encoded vector of the context words, in our case we'll pass the vectors of words trees, play, role and for in the first layer of our model then the second layer will try to predict the word "critical" then the third layer will produce a SoftMax vector of size V. Finally, the algorithm will compare the predicted target word with the actual target word and then the weights of the second layer are updated using the error.

3 CONCLUSIONS:

Skip-gram works in a similar way as that of CBOW except it uses the target word to predict the context words. To make things simple, we'll use the same example as we used in the CBOW model. For "trees play critical role for" the skip-gram model will use the label word i.e., "critical" for prediction of context words. Whether to use skip-gram or CBOW depends on the problem and the dataset that you're looking at. Skip-gram is slower, but it works well with large datasets whereas CBOW is faster and is preferred for small corpus.

2. REFERENCES

[1] Y. N. Harari, '21 Lessons for the 21st Century', Signal, 2018.

[2] P. M Nadkarni, L Ohno-Machado, and W. W. Chapman, 'Natural language processing: an introduction', Journal of the American Medical Informatics Association vol.18, no. pp. 544-551,2011

[3] J. Hirschberg and M. D. Christopher, 'Advances in natural language processing', Science, vol. 349, no. 6245, 261-266 2015.

[4] S., Krishnan, J., Wang, E., Wu, M.J. Franklin, K., Goldberg, 'Active clean: interactive data cleaning for statistical modelling', Proceedings of the VLDB Endowment, vol. 9, no. 12, pp. 948– 959, 2016.

[4] P., Bojanowski, E., Grave, A., Joulin, T., Mikolov, 'Enriching word vectors with subword information', Transactions of the association for computational linguistics vol. 5, pp.135-146, 2017.

[5] D., Coppersmith, S.J., Hong, J.R. Hosking, 'Partitioning nominal attributes in decision trees', Data Mining and Knowledge Discovery, vol. 3, no.2, pp. 197–217 1999.

[6] X., Rong, Word2vec Parameter Learning Explained, 2022.

[7] T., Mikolov, K., Chen, G. Corrado, and J., Dean, "Efficient Estimation of Word Representations in Vector Space", 2022.

[8] B., Yoshua, D., Raejean, P., Vincent, and J., Christian, "A neural probabilistic language model", The Journal of Machine Learning Research, 3: pp. 1137–1155, 2003.

[9] T., Mikolov, S., Kombrink, L., Burget, J., Cernocky, and S., Khudanpur, "Extensions of recurrent neural network language model", In Acoustics, Speech and Signal Processing (ICASSP), 2011 IEEE International Conference on, pp. 5528– 5531. IEEE, 2011

[10] D., Peter, Turney, "Distributional semantics beyond words: Supervised learning of analogy and paraphrase", In Transactions of the Association for Computational Linguistics (TACL), pp. 353–366, 2013.

[11] K., Grabczewski, N., Jankowski, "Transformations of symbolic data for continuous data-oriented models", In: Artificial Neural Networks and Neural Information Processing, pp. 359–366. Springer 2003.

[12] W., Kim, B.J., Choi, E.K., Hong, S.K., Kim, D. Lee, "A taxonomy of dirty data", Data mining and knowledge discovery vol.7, no. 1, pp.81–99, 2003.

[13] K., J., Berry, P., W., Mielke, P.W., Jr, H., K., Iyer, 'Factorial designs and dummy coding', Perceptual and motor skills, vol. 87, no. 3, pp. 919–927, 1998.

[14] K. Chowdhary, 'Natural language processing', Fundamentals of artificial intelligence. pp. 603-49, 2020.

Miscellaneous Artificial Intelligence and Machine Learning Models For Multimedia and Medical Applications

[1]Akash Goel, [2]Amit Kumar Goel, [3]Adesh Kumar

[1, 2] Department of Computer Science & Engineering, Galgotia's University, Greater Noida, NCR, India

[3] Department of Electrical & Electronics Engineering, School of Engineering, University of Petroleum and Energy Studies, Dehradun, India

adeshmanav@gmail.com

Abstract.

The research article presents the study on artificial neural networks and machine learning in different research domains and bids in interactive human, medical and real-world multimedia applications. The AIML has been proven in healthcare to link genetic codes, increase hospital productivity, and power surgical robots. In medical applications, It has been used extensively for electronic health records, sensor data, imaging, -omics, and medical text are some of the data types that are most frequently utilized for machine learning in biomedical research. The different models of ANN have provided good accuracy for the prediction and evaluation of the performance of different medical and multimedia systems.

Keywords. Machine Learning, Artificial Neural Networks, Deep Learning, Multimedia Applications, Medical Information

1. INTRODUCTION

Machine learning (ML) has advanced particularly quickly in the last ten years in the field of healthcare. Many healthcare requirements [1] that are expected to enhance patient care, lessen the burden on healthcare workers, reorganize healthcare operations, and give people more control over their health [2] have already begun to take shape. The development of image-based triage and second readers is one instance where machine learning for healthcare has been successful in translating computer vision. The utilization of electronic health records (EHRs) to foretell the risk and course of certain diseases has also made rapid progress. There are innumerable uses for ANN. To get the most out of the operational front, technology and AI applications can be implemented across a wide range of sectors and businesses [3]. The healthcare sector is now testing and using AI for surgical procedures [4] in operating rooms as well as medication administration and various patient treatments.

2. APPLICATIONS OF AIML

Machine learning modes have been used extensively for different multimedia applications [5] such as stock market prediction, social media, medical diagnosis, healthcare, defence, aerospace, electronics software, hardware accelerators [20], forensics and signature verifications, weather forecasting, facial recognition, and robotics applications [21]. Fig.1 presents the overview of the different applications of the AIML. The healthcare service system serves a crucial role in the medical area, which has great demands on human life. In order to advance, healthcare experts in developing countries are using cutting-edge technologies like machine learning and AI. Improvements in the healthcare sector have sparked research on intelligent, human-cantered healthcare systems. AI technologies have an impact on the development of monitoring and critical care units in clinics and hospitals. Modern discoveries in prediction, inhibition, medicine, and healthcare are quickly, cheaply, and more effectively addressed by these developments. The process of medical diagnosis welcomes a variety of AI applications to enhance service delivery, improved disease detection, prediction accuracy, and

many other areas. AI-assisted medical procedures are revolutionizing the field's reliance on the extensive study. These activities include the creation of new drugs, clinical diagnostics research, individualized medicine, robotic surgery, skilled human prenatal care, radiography, reviewed prescriptions, and evaluated patient information analytics.

Fig. 2 Major domains of AI and ML

3. MODEL STUDY & RESULTS

Table 1 summarizes the miscellaneous ANN and machine learning models for medical diagnoses and multimedia applications

Table 1 Miscellaneous model and applications

Description	**Accuracy**	**AI-ML**	**Application**
Csernansky et al. [1]	76.9%	Logistic Regression Model	MRI
Paikaray et al. [2]	95.10%	Random forest	Heart stroke predictions
Nadakinamani et al. [3]	100 %	Random Tree	cardiovascular disease
Kumar et al. [4]	93.00 %	Decision tree classifier and algorithm	Hardware in loop testing and automation in power window control

Kumar et al. [6]	88.12%,	Multiple linear regression	Brain Tumor detection and MRI image segmentation
Hooda et al. [7]	91.70%	K-means clustering	Estimation for the surface roughness of superhydrophobic coated surfaces in self-clearing solar panels
Yang et al. [8]	88.2%	Dirac Delta Net	Hardware accelerator and Co-design for ConvNet with embedded FPGAs
Mohsin et al. [9]	100%	K-Nearest Neighbor Classification	Hardware accelerator with embedded FPGAs for mobile devices
Rani et al. [10]	75.16%, 74.03%, 83.50%, 85.81%	K-Nearest Neighbor (75.16%), Bayesian Network (74.03%), Regression Tree (83.50%), and Support Vector Machine (SVM)	Recognition in human-robot interaction
Zhao et al. [11]	95.00 %	Boosted regression tree	Robot-assisted surgery in healthcare organizations
Wang et al. [12]	92.5%, 91.3% 95.4%,	K-nearest neighbors (k-NN) (92.5%), Support vector machine (SVM) 91.3%, and Logistic regression (LR) (95.4%)	Data augmentation and robot-assisted surgery
Raju et al. [13]	99.40%	Component Analysis (PCA) with the integration of Discrete Wavelet Transform	Global and local facial recognition
Gui et al.[14]	90.20%	short-term memory (LSTM) and random forest model	Perdition of flight delay for surveillance-broadcast
Rhee et al. [15]	64.00 %	Random tree	Forecasting the meteorological drought for remote sensing and ling range
Prashanth et al. [16]	96.40%	Naive Bayes + SVM	Early detection of Parkinson's disease using multimodal features

Firdausi et al. [17]	96.8%	Decision tree	Malware detection on the internet
Kumar et al. [18]	97.99 %	Decision tree regressor (92.74) Random forest regressor (92.49) Multiple linear regressors (97.99)	Hardware chip design analysis for pre-synthesis and resources projections for network-on-chip communication
Banna et al. [19]	90.00 %	CNN	Robotics and automation industries for cognitive behavior and dynamic actions.
Goel et al. [21] [24]	81.00 %	Level set methods	Providing the review of AI and machine learning for the different real-time applications in medical applications and brain tumor is one of the applications which is reviewed and analyzed using different methods such as level set, Otsu etc.
Kumar et al. [22]	71.42% 78.26% 86.95% 84.34% 80.45% 91.39%	Otsu's method Watershed algorithm DWT K-means Level set CNN	For brain tumor study, analysis, and prediction for the different diseases and cases. Deep learning applications for a brain tumor and further use for analyzing the type of tumor.
Dhyani et al. [23]	91.00 % 83.00%	ResRNN Classifier (91.00), and DesNet which is working g with multiscale deep fusion neural networks.	For the study and analysis of the performance evaluation of the ECG database for the prediction of the Arrhythmia diseases
Khatter et al. [24]	>90.00%	Controlled Competitive Learning	Used for clustering and medical data analysis
Agarwal et al. [25]	73.84%	Deep Convolution Adversarial Networks	Detecting melanoma, a form of advanced skin cancer

4. CONCLUSIONS

Supervised learning, unsupervised learning, and reinforcement learning are the three categories into which ML algorithms are divided. Supervised learning is the paradigm used the most frequently for machine learning operations. It is typically used for data where it fits to analyse the input and output variables to analyse the closeness. Examples of supervised learning include linear regression, support vector machines, random forests, gradient boosting, logistic regression, and artificial neural networks. Since the data are not implicitly divided into different categories, an unsupervised learning system does not have labelled data. The outcome of this study reveals that ANN has been used extensively for several medical applications, diagnosis, and healthcare industries. The different versions of ANN algorithms such as CNN, RNN, and feedforward ANN, have proven better accuracy of > 90 % in comparison to other algorithms and models for the same diagnosis and multimedia applications.

5. REFERENCES

[1] Csernansky, J. G., Wang, L., Jones, D., Rastogi-Cruz, D., Posener, J. A., Heydebrand, G., ... & Miller, M. I. (2002). Hippocampal deformities in schizophrenia characterized by high dimensional brain mapping. American Journal of Psychiatry, 159(12), 2000-2006.

[2] Paikaray, D., & Mehta, A. K. (2022). An extensive approach towards heart stroke prediction using machine learning with ensemble classifier. In Proceedings of the International Conference on Paradigms of Communication, Computing and Data Sciences (pp. 767-777). Springer, Singapore.

[3] Nadakinamani, R. G., Reyana, A., Kautish, S., Vibith, A. S., Gupta, Y., Abdelwahab, S. F., & Mohamed, A. W. (2022). Clinical Data Analysis for Prediction of Cardiovascular Disease Using Machine Learning Techniques. Computational Intelligence and Neuroscience, 2022..

[4] Kumar, R., Ahuja, N. J., Saxena, M., & Kumar, A. (2020). Automotive Power Window Communication with DTC Algorithm and Hardware-in-the-Loop Testing. Wireless Personal Communications, 114, 3351-3366.

[5] Kumar, A., Sharma, P., Gupta, M. K., & Kumar, R. (2018). Machine learning based resource utilization and pre-estimation for network on chip (NoC) communication. Wireless Personal Communications, 102(3), 2211-2231.

[6] Kumar, A., Chauda, P., & Devrari, A. (2021). Machine Learning Approach for Brain Tumor Detection and Segmentation. International Journal of Organizational and Collective Intelligence (IJOCI), 11(3), 68-84.

[7] Hooda, A., Kumar, A., Goyat, M. S., & Gupta, R. (2021). Estimation of surface roughness for transparent superhydrophobic coating through image processing and machine learning. Molecular Crystals and Liquid Crystals, 1-15.

[8] Yang, Y., Huang, Q., Wu, B., Zhang, T., Ma, L., Gambardella, G., ... & Keutzer, K. (2019, February). Synetgy: Algorithm-hardware co-design for convnet accelerators on embedded fpgas. In Proceedings of the 2019 ACM/SIGDA International Symposium on Field-Programmable Gate Arrays (pp. 23-32).

[9] Mohsin, M. A., & Perera, D. G. (2018, June). An FPGA-based hardware accelerator for K-Nearest neighbor classification for machine learning on mobile devices. In Proceedings of the 9th International Symposium on Highly-Efficient Accelerators and Reconfigurable Technologies (pp. 1-7).

[10] Rani, P., Liu, C., Sarkar, N., & Vanman, E. (2006). An empirical study of machine learning techniques for affect recognition in human–robot interaction. Pattern Analysis and Applications, 9(1), 58-69.
[11] Zhao, B., Waterman, R. S., Urman, R. D., & Gabriel, R. A. (2019). A machine learning approach to predicting case duration for robot-assisted surgery. Journal of medical systems, 43(2), 32.
[12] Wang, Z., & Fey, A. M. (2018). Deep learning with convolutional neural network for objective skill evaluation in robot-assisted surgery. International journal of computer assisted radiology and surgery, 13(12), 1959-1970.
[13] Raju, K., Chinna Rao, B., Saikumar, K., & Lakshman Pratap, N. (2022). An Optimal Hybrid Solution to Local and Global Facial Recognition Through Machine Learning. In A Fusion of Artificial Intelligence and Internet of Things for Emerging Cyber Systems (pp. 203-226). Springer, Cham.
[14] Gui, G., Liu, F., Sun, J., Yang, J., Zhou, Z., & Zhao, D. (2019). Flight delay prediction based on aviation big data and machine learning. IEEE Transactions on Vehicular Technology, 69(1), 140-150.
[15] Rhee, J., & Im, J. (2017). Meteorological drought forecasting for ungauged areas based on machine learning: Using long-range climate forecast and remote sensing data. Agricultural and Forest Meteorology, 237, 105-122.
[16] Prashanth, R., Roy, S. D., Mandal, P. K., & Ghosh, S. (2016). High-accuracy detection of early Parkinson's disease through multimodal features and machine learning. International journal of medical informatics, 90, 13-21.
[17] Firdausi, I., Erwin, A., & Nugroho, A. S. (2010, December). Analysis of machine learning techniques used in behavior-based malware detection. In 2010 second international conference on advances in computing, control, and telecommunication technologies (pp. 201-203).
[18] Kumar, A., Sharma, P., Gupta, M. K., & Kumar, R. (2018). Machine learning-based resource utilization and pre-estimation for network on chip (NoC) communication. Wireless Personal Communications, 102(3), 2211-2231.
[19] Al Banna, M. H., Haider, M. A., Al Nahian, M. J., Islam, M. M., Taher, K. A., & Kaiser, M. S. (2019, January). Camera model identification using deep CNN and transfer learning approach. In 2019 International Conference on Robotics, Electrical and Signal Processing Techniques (ICREST) (pp. 626-630). IEEE.
[20] Rawat, A. S., Rana, A., Kumar, A., & Bagwari, A. (2018). Application of multi-layer artificial neural network in the diagnosis system: a systematic review. IAES International Journal of Artificial Intelligence, 7(3), 138.
[21] Goel, A., Chikara, D., Srivastava, A. K., & Kumar, A. (2016). Medical Imaging with Brain Tumor Detection and Analysis. International Journal of Computer Science and Information Security, 14(9), 228.
[22] Kumar, A. (2022). Study and analysis of different segmentation methods for brain tumor MRI application. Multimedia Tools and Applications, 1-23.
[23] Dhyani, S., Kumar, A., & Choudhury, S. (2023). Arrhythmia disease classification utilizing ResRNN. Biomedical Signal Processing and Control, 79, 104160.
[24] Khatter, H., Aggarwal, V., & Ahlawat, A. K. (2016, February). Performance analysis of the competitive learning algorithms on Gaussian data in automatic cluster selection. In *2016* Second International Conference on Computational Intelligence & Communication Technology (CICT) (pp. 48-53). IEEE.
[25] Agarwal, Nidhi, Vikas Singh, and Pratham Singh. "Semi-Supervised Learning with GANs for Melanoma Detection." 2022 6th International Conference on Intelligent Computing and Control Systems (ICICCS). IEEE, 2022.

Analysis of various factors affecting the life of concentrated solar power systems in real Environmental condition.

Geetanjali Raghav

**University of Petroleum and Energy Studies, India*

E-mail: graghav@ddn.upes.ac.in

Abstract.

Thermal solar concentration collectors use mirrors to reflect sunlight and focus it on a receiver. These collectors can be parabolic or linear, depending on whether they focus sunlight on a focal point or a segment of a straight line. The fluid that exits the panel from this one spot is heated to a temperature of more than 100°C.This study, which examined how optical defects affected the interceptor factor and, ultimately, the optical efficiency or performance of a solar parabolic trough system, focuses on the parabolic trough collector (PTC). The optical efficiency was evaluated using solar trace for slope errors, 0–6 m rad secularity errors, tracking errors, and misalignment errors. In the ensuing simulations, a parabolic trough collector with a focal of 1.84 m, a length of 5 m, and a receiver radius of 0.035 m is used. In the simulations, three different concentration ratios—20, 30 The findings demonstrate that mistakes in slope and specularity have an effect on the heat flux concentration on the receiver's absorber tube. Additionally, they demonstrate that optical efficiency rapidly decreases as slope errors rise.

Keywords. Parabolic trough collector: PTC, Monte Carlo Ray Tracing: MCRT, Heat Collection Element HCE, Concentration Ratio CR.

1. INTRODUCTION

Numerous studies have helped to significantly lower the cost of concentrated solar thermal electricity. Solar energy has many uses and has been regarded as a clean and sustainable energy source since the 1970s, according to a study by Zhiyong Wu, Shidong Li, Guogeng Yuan, Quang Qiang Lei, and Zhifeng Wang published in 2014. Three-dimensional numerical analysis of the heat transfer performance of parabolic dish receivers demonstrates this. A key element of parabolic trough systems is a collector, which is a parabolically coiled mirror with a high reflectivity for capturing incident solar energy. The heat collection element (HCE), also known as the receiver tube, is where the solar rays that strike the mirror are focussed and reflected, creating thermal energy. The receiver is made of a metallic absorber tube that is enclosed in glass. The glass envelope and tube are separated by a vacuum to lessen receiver Additionally, this absorber tube is selectively coated to provide it maximum incoming radiation absorption and low infrared emission.The design of the collector, the materials used in construction, and the numerous mistakes that were made both

during the development and operation of the system all have an impact on the optical performance of the PTC, which affects the performance of the overall system (3. Güven and Bannerot, 1986).The optical performance will be impacted by 4 mistakes on the interceptor factor. The interceptor factor is the ratio of energy reflected by the concentrating collector to Guven and Bannerot's formula for the optical performance of a parabolic trough system is where the interception factor is and the product is, respectively, the reflexion, the transmittance, and the absorptance. It displays the compositional characteristics. Guven and Bannerot claim that the impact of the angle of incidence, including cosine losses and end losses, affects optical performance. However, this quantity is equivalent to 1 in situations with a fully tracking collector or when the angle of incidence is zero. As a result, we won't consider this effect of angle of incidence in this study and instead focus on the optical performance that was mentioned earlier.These academics provide an in-depth explanation of the many PTC fault categories. One of these is a material error, which includes flaws in the glass cover's transmissivity, the reflectivity of the reflecting material, and the coating's absorptivity on the absorber tube. 2: manufacturing and assembly problems, such as incorrect local slopes, reflector misalignment during assembly, and incorrect receiver tube placement. 3: operational errors, such as tracking errors, wind loading errors, and temperature impact problems. To determine how these inaccuracies affect the interceptor factor, numerous research have been conducted. This study employs an optical modelling programme called Sol Trace that is based on Monte Carlo Ray Tracing to analyse optical data and determine the real heat flux distribution on the receiver's absorber tube (4. SolTrace, 2012)

Parabolic reflector: It is the mirror in the form of parabolic shape which reflects all the radiation at the focus of a parabola. This reflector is mounted over a structure which can move from east to west with the help of sun tracker.

Absorber tube or receiver: It is a metal pipe or tube coated with black nickel or chromium and sealed with glass tube. Black coating increase the absorption of tube while glass glazing decreases the convection losses from tube. The sun tracker is the mechanism that rotates the entire building from east to west. It uses a sensor-based algorithm and a timer algorithm to function. The system's geometry needs to be specified in order to achieve the PTC's maximal optical performance. A parabolic trough collector system under consideration is seen in 3D in figure 1. The real parabolic trough systems are constructed from a variety of panels that have been combined. It is expected that the performance of the system would not be significantly impacted by the space between the various panels. This illustration depicts a condensed collector with a continuous parabolic surface.

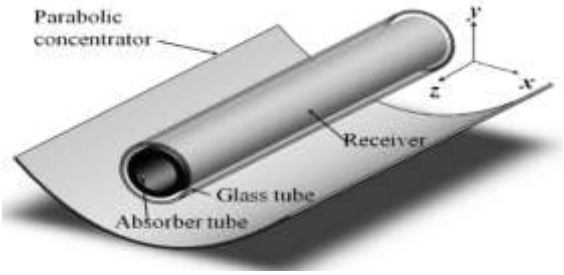

Figure 1: schematic of the parabolic trough collector

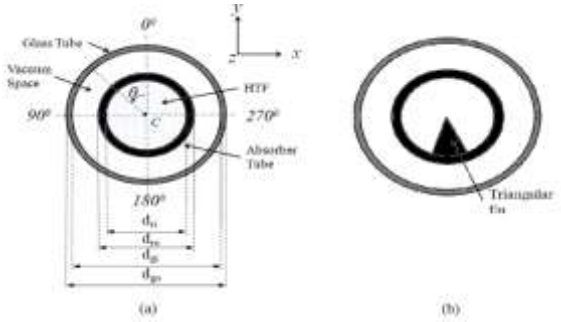

Figure 2: Cross sectional view of receiver (a) plain absorber tube (b) finned absorber tube

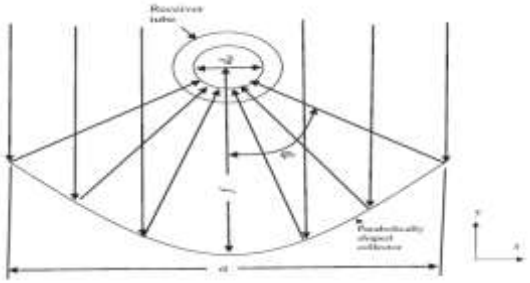

Figure 3: Cross sectional view of the PTC system with a trace of some incident rays

The figure 3 above shows a cross sectional view of the collector The equation of a parabola gives the following description of the collector's geometry:

$$x^2 = 4fy$$

The aperture's width and rim angle are connected

$$f = a/4\tan(\varphi_r/2\ )$$

Any two parameters can be used to define the shape of the collector using these two equations. For each of the next three simulations on the programme SolTrace, the concentration ratio C r, which links the predicted area of the collector to the projected area of both the absorber tube, will be altered.

$$C_r = \frac{A_a}{A_r} = \frac{a \times L}{d_{ri} \times L}$$

For the next simulations, we want to have C_r equals to 20,30 and 40. For this we calculate the aperture and we put 4,398 m for the concentration ratio 20 , 6,597 m for 30, 8,796 m for 40.

Parameter	Symbol	Value
Aperture width	W	5m
Glass tube inner diameter	d_{gi}	0.109m
Glass tube outer diameter	d_{go}	0.115m
Absorber tube inner diameter	d_{ri}	0.066m
Absorber tube outer diameter	d_{ro}	0.070m
Focal length	f	1.84m

Parameter	Symbol	Value
Absorber tube absorptivity	α_r	0.92
Absorber tube reflectivity	ρ_r	0.08
Glass tube transmissivity	τ_g	0.935
Glass tube reflectivity	ρ_g	0.045
Mirror reflectivity	ρ_m	0.93
Mirror transmissivity	τ_m	0

Table 1: *optical and geometrical properties of PTC system used in the current study*

A simulation using ray tracing was run for the PTC system described in Table 1presents the optical characteristics of the PTC components taken into consideration in the investigation. For all ray tracing simulations, the tracking mechanism of the PTC was considered to be flawless, and the direct normal irradiation was set at 1000W/m². For the ray tracing simulation, the mirror's slope and specularity error were taken into account as 3 mrad. The thermal analysis covered in the following part introduces the sun flux distribution discovered using ray tracing as a boundary. Figure 4 is a sample SolTrace

Figure 4: Ray tracing in SolTrac

RESULTS & DISCUSSION

Concerning the simulations, several errors were considered like the slope error,the specular error, the tracking error and the misalignement following x and ywhere the effect of the

errors on the optical performance which is $\eta_{opt} = (\varphi T\ \alpha)\ \gamma$ with $\gamma = \frac{E_{abs}}{E_{ref}}$ is the interceptor factor.

i) Slope error and specular error

Also, we don't see clearly the effect of the slope error on the tracking error in comparison with what we saw in the other graphs ploted before. The effect of the tracking error on the interceptor factor is less appearant thant that of the slope error**.**

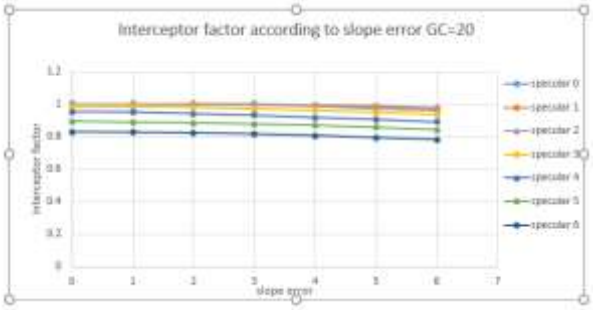

ii) Slope error and tracking error

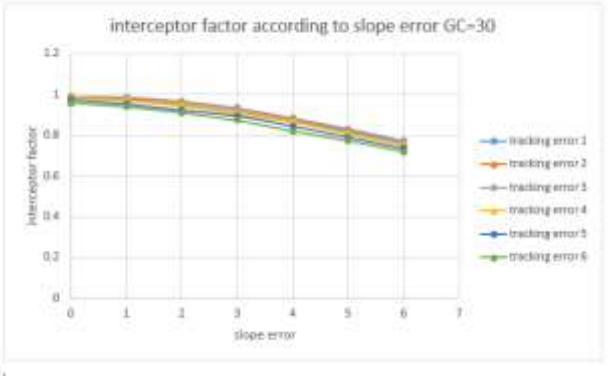

Exploring the platform of the Sheffler dish

Because of the rain and the inconvenient weather in Dehradun, I can't do the optical or the thermal experiments on the parabolic trough collector. For this, I learn more about the Sheffler dish.The point of focus is the axis of rotation. As long as it is in place, it collects concentrated heat, which is then transferred to water thru the receiver to produce hot water or high-pressure steam.Water from the header pipe travels to the recipient (thermosiphon principle). The header pipe collects the hot water or steam gathered at the receiver and transports it to the intended use.

Figure 6: Températures' sondes (inner, outer)

Conclusion

This study examines the effects of tracking, slope, specularity, and misalignment errors on a parabolic trough system's optical and electronic properties. The study's results demonstrate that slope inaccuracies have a substantial impact on the heat flux distribution on the absorber tube of the receiver. As a result, the optical efficiency declines as the slope. Additionally, it was shown that tracking or specularity faults on the heat flux distribution on the recipient's absorber tube do not significantly affect the interceptor factor. It is demonstrated that when the slope error is fixed at 3 mrad, the misalignment after z is significantly altered compared to the misalignment following due to the optical characterisations completed throughout the course of my internship's first two months, I have come to the conclusion that the error slope has the greatest impact on optical performance. Studying the thermal characterization and assessing the thermal efficiency in relation to this slope inaccuracy would be interesting.

REFERENCES

[1] Tsoutsos T, Gekas V, Marketaki K. Technical and economical evaluation of solar thermal power generation. Renew Energy 2003; 28 (6):873–86.

[2] Mills D. Advances in solar thermal electricity technology. Sol Energy 2004; 76(1–3):19–31.

[3] Larson DL. Final report of the Coolidge solar irrigation project. New Mexico: Sandia National Laboratories; 1983.

[4] Lippke F. Simulation of the part-load behavior of a 30 MWe SEGS plant. New Mexico: Sandia National Laboratories; 1995.

[5] Thomas A. Solar steam generating systems using parabolic trough concentrators. Energy Convers Manage 1996; 37(2):215–45.

[6] Kalogirou S, Lloyd S, Ward J. Modelling, optimisation and performance evaluation of a parabolic trough solar collector steam generation system. Sol Energy 1997; 60(1):49–59.

[7] Zarza E, Valenzuela L, Leo´n J, Hennecke K, Eck M, Weyers H, et al. Direct steam generation in parabolic troughs: final results and conclusions of the DISS project. Energy 2004;29 (5-6):635–44.

[8] Almanza R, Lentz A. Electricity production at low powers by direct steam generation with parabolic troughs. Sol Energy 1998; 64 (1–3):115–20.
[9] Singh N, Kaushik SC, Misra RD. Exergetic analysis of a solar thermal power system. Renew Energy 2000; 19:135–43.

[10] Price H, Hassani V. Modular trough power plant cycle and systems analysis. Colorado: National Renewable Energy Laboratory; 2002.
[11] Prabhu E. Solar trough organic rankine electricity system (STORES) stage 1: power plant Optimization and economics. California: National Renewable Energy Laboratory; 2006.
[12] Solid media thermal storage for parabolic trough power plants Doerte Laing et al., Solar Energy 80(2006-08):1283-1289 · October 2006.

Coastal Surveillance and Detection of Intruder – A Mechanism using Antenna Arrays

Madhukant Patel, Suhani Patel

ReveSoils Pvt Ltd, madhukant.patel@reveautomation.com

ReveSoils Pvt Ltd, suhani.patel@reveautomation.com

Abstract.

In this paper the Intrusion Detection over a wide coastal line is tested using the developed Antenna Arrays on a Laboratory Setup as well as the live coastal region. The foundation of implementation methodology is laid on the Microwave Detection mechanism where Microwave beams are used in the sensor technology, where a transmit antenna generates the beams to form a spot on the receiver. If the receiver detects a difference in the received power, the system immediately begins to analyse the intrusion possibilities and, if the predetermined conditions for an incursion are met, an alarm is sounded to alert the control room. The system is capable of working even in non-favourable weather conditions. The entire system was implemented and tested at Laboratory in a simulated environment as well as live on the river site in Ahmedabad. As a result the data obtained from the simulated laboratory environment and river site were deeply analysed through 'Digital Signal Processing Techniques". The outcomes obtained are encouraging, where human and non-human intrusions were detected, after 'Digital Signal Processing' with an existing 'Edge Gateway Electronic System' located near the receiver antenna at the coastal site .

Keywords. Microwave Technology, Device free localization, Transmission and Receiver, Gain and Power

1. INTRODUCTION

India has a long coastline with a thriving fishing sector that relies on the resources of the sea. As previous occurrences have demonstrated, effective surveillance with tracking of the coast is very important to maintain the nation's security and economic strength. The paper referred [1] presents two radio frequency sensors with different directivities designed and tested for device-free localization in an indoor environment. Mostly, in smart homes and smart offices, people may be irritated by wearing the device on them all the time. As compared with device-based localization, the proposed sensors can localise dynamic targets without affecting the privacy of the people around. Both sensors are tested to detect the change in received signal strength (ΔRSS) due to the presence of an obstacle. RF sensors operate in the ISM band of 2.4–2.5 GHz frequencies.. Experimentation shows that the higher directivity provides better ΔRSS [1]. The designed Microwave imaging system is based on Microwave Object Detection Algorithms that will be able to detect human and other 'intrusive' objects without human intervention. [2] The sensor node will efficiently send the sensor data to the hub through wireless link. The prototype model is set up in the simulated lab to address the detection of intrusion sensing, alarm communication and assessment. The algorithm based on correlation method is employed for intrusion detection

in long, flat, narrow geometrical zones/border areas [3]. Advancements in 'Microwave image processing' have been recently proved as promising imaging tools, which could play a fundamental role to efficiently manage emergencies related to stroke and haemorrhages. This paper focuses on the radar imaging (through microwave sensors) approach and in particular on the processing algorithms of the backscattered signals. [4] Assuming the use of Microwave Imaging Space-Time beamforming algorithm, Artefacts removal is an essential step of any microwave radar imaging system and currently considered artefact removal algorithms have been shown not to be effective in the specific scenario of brain imaging [5]. The reliable prediction of coverage footprint resulting from an airborne wireless radio base station, is of utmost importance, when it comes to the new emerging applications of air-to-ground wireless services. [6] These applications include the rapid recovery of damaged terrestrial wireless infrastructure due to a natural disaster, as well as the fulfilment of sudden wireless traffic overload in certain spots due to massive movement of crowds. In this paper, we propose a statistical propagation model for predicting the air-to-ground path loss between a low altitude platform and a terrestrial terminal.[7] A fast microwave imaging method for brain stroke detection is presented. The method estimates the power distribution of the scattering waves inside the head based on the measured multistatic scattered signals around the head. [8] In that regard, Average Trace Subtraction (ATS) and Bessel function are used to remove the background reflections and calculate the scattering electromagnetic waves in the frequency domain. [9] The imaging algorithm is verified using a round-shaped 8-element antenna array which surrounds a realistic head model in the simulation environment. The obtained images using the presented technique demonstrate its ability in brain stroke detection and localization. [10]

2. Test setup and Data collection

Figure 1 illustrates the Lab setup for capturing the experimental data. The input signal (0 dB) of 10 GHz is fed to the RF amplifier. The transmitting gain is set to 20 dB. The RF amplifier power is fed to the transmit antenna.

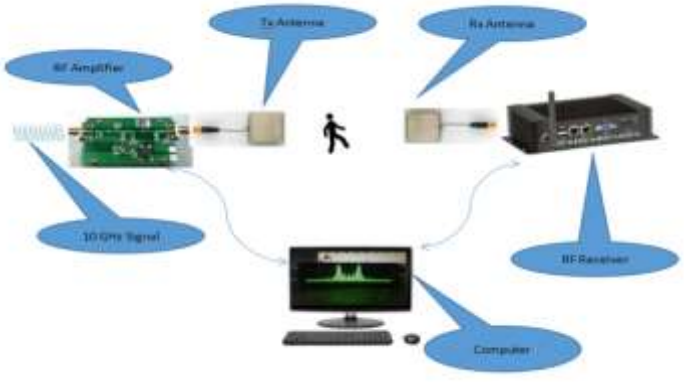

Figure 1. Schematic block of Test setup to capture intruder data.

A receiving antenna is connected to an RF receiver on the receiver side. The computer is connected to an RF receiver to collect the signal of the receiving antenna. The data was captured at every step of the intrusion and were recorded on the computer.

The detailed functioning of receiver and transmitter are illustrated in terms of block diagram as shown in Figure 2 and Figure 3 respectively.

As an intruder moves from top to bottom at different distances from Tx-antenna, the power drop pattern changes as tabulated in Table 1. The scale of the model is scalable by controlling the transmit power for desired distance from 1 to 10 kilometers. The developed patch antenna framework is designed to work under the scale factor of 1:100 under the Lab framework.

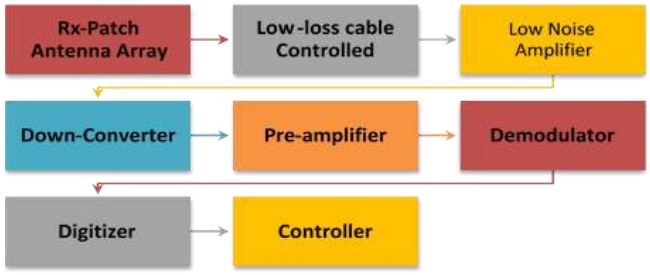

Figure 1.2. Block diagram illustrating the functioning of Transmitter

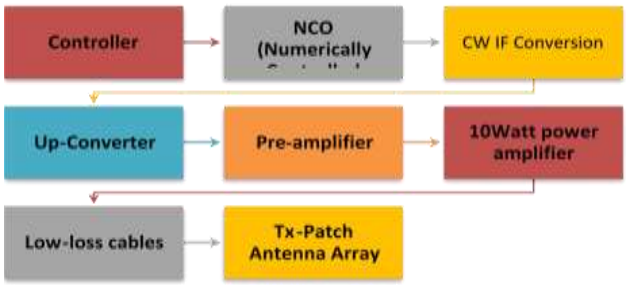

Figure 1.3. Block diagram illustrating the functioning of Receiver

3. Results and Discussion

Under the research the target parameters of power drop 20 to 22 dB, distance of 8 to 10 km. Through the adopted methodology, the target achieved as 19 to 22 dB attenuation with human intrusion, and 10 km and with enhanced parameters of Rx-receiver, it can be achieved as high as 25 km.

The reasons for the difference are environmental conditions, inaccuracies in sensor fabrications and instrument errors. The excellent data were received in the Lab condition which are tabulated in Table 1. Considering safety against the high power RF radiations, the transmitter power is kept at a safe level of less than 10dBm.

For calculating the scalability of the model used in the Lab, the following equation, which will calculate the Free Space Path Loss at given frequency.

$$FSPL = 20\log d + 20\ lof\ f + 20\ lof\ (4\pi c) - G\ (T_x) - G(R_x) \quad (1)$$

Here, G(Tx) and G(Rx) are the gain of the transmitting and receiving antenna respectively, whereas d is the distance between the antennas.

In actual site conditions, d = 10 km. f = 10 GHz, G(Tx) = 14, G(Rx) = 14. Transmitter amplifier gain = 2, Receiver amplifier gain = 60. Free space path loss = 71 dB.

The distance between transmitting and receiving antennae of 10 km are comfortably detectable with the sensitivity of the receiver of -60 dBm. The distance can be increased 25 km by increasing the sensitivity of the Rx-receiver by 10 more dB.

Table-1 shows the statistics of the received power based on the intruder entering tangential to the 'beam' and the distance from the Tx sensor.

Table-1 data received against the movement of intruder

	Distance from Transmitting sensor in Meters (m)								
Step No	**1m**	**3m**	**5m**	**7m**	**9m**	**11m**	**13m**	**15m**	**17m**
Step 1	1.3	1.2	1.1	1	0.9	0.75	0.5	0.3	0.15
Step 2	1.4	1.3	1.2	1.1	1	0.9	0.6	0.45	0.3
Step 3	1.5	1.4	1.3	1.2	1.1	1	0.75	0.55	0.4
Step 4	1.6	1.5	1.4	1.3	1.2	1.1	0.85	0.62	0.46
Step 5	1.7	1.6	1.5	1.4	1.3	1.2	0.95	0.75	0.55
Step 6	1.9	1.8	1.7	1.69	1.63	1.23	1.09	1.04	0.8
Step 7	2.8	2.5	2.43	2.05	2.01	1.98	1.87	1.54	1.38
Step 8	3.6	3.45	3.37	3.2	3.08	2.5	2.03	1.6	1.4
Step 9	5.58	5.15	4.72	4.05	3.7	2.8	2.23	2.03	1.9
Step 10	11.66	11.2	10.74	9.8	8.9	8.44	7.96	7.5	7.04
Step 11	16.32	15.9	15.45	14.93	13.8	13.38	12.96	12.5	12.08
Step 12	22.1	21.1	20.11	19.11	18.11	17.11	17.62	17.14	16.66

Step 13	22.5	21.5	20.5	19.4	18.4	17.4	20.42	19.92	19.44
Step 14	22	21.2	20.21	19.21	18.21	17.96	17.54	17.11	16.69
Step 15	15.94	15.5	15.05	14.3	13.3	12.86	12.42	11.98	11.54
Step 16	10.3	9.9	9.5	8.89	7.9	7.5	7.1	6.7	6.3
Step 17	4.88	4.5	4.12	3.46	2.87	2.66	2.28	1.87	1.49
Step 18	3.7	3.56	3.43	3.21	2.63	2.39	2.16	1.76	1.34
Step 19	2.9	2.76	2.64	2.57	2.38	2.27	2.05	1.63	1.21
Step 20	1.8	1.68	1.53	1.42	1.35	1.26	1.17	1.04	0.85

To eliminate the noise and interferences, the received signal was sampled at 100 times in the second and was averaged on 100 datasets. So, one sample is connected at every second. The noise and interference is further reduced by applying 6^{th} order polynomials, and the detection ability increases and falls alarms get reduced significantly. To remove static background, multiple backgrounds have been generated. One will be a master background, which will be derived from several backgrounds under different light and tide conditions. Besides, floating vegetation, leaves, etc has been removed to detect the target efficiently.

Through the experiments, it is found that the received power fluctuates within 1 to 2 dB. If human or human sized objects intrude between the transmit and receive sensors, the power received on the receive sensor falls down by 7 to 10dB than nominal power received at the receiving sensor under “no intrusion” conditions. . Based on the geographical and environmental conditions of the site, the “Alert threshold” is set between 3 to 5dB. Drop in received power is the function of the object size and the distance from the transmitting sensor.

The Microwave Imaging can be optimized for many more use cases. Microwave imaging approach enhances to detect and identify unknown objects and security threat level detection as well.

4. CONCLUSION

This paper provides a method of the end application of the customised patch antenna arrays fabricated using highly customised dielectric material. The effect of the intruder is tabulated, which numeracies as the drop of the received power as function of the size and speed of the intruder.

5. REFERENCES

[1] Rehman A., Ellahi Z., Iqbal A., Ullah F., Ali A., Kwak K.S. (2019) Design and Implementation of Directional Sensors for Privacy-Ensured Device-Free Target Localization in Indoor Environment, Wireless Communications and Mobile Computing, Vol. 2019, Article ID 8391307, 8 pages, 2019.

[2] Ricci E., Di Domenico S., Cianca E., and Rossi T. (2015) Artifact removal algorithms for stroke detection using a multistatic MIST beamforming algorithm, 2015 37th Annual International Conference of the IEEE Engineering in Medicine and Biology Society (EMBC), pp. 1930-1933,

[3] Perez M. D., et al., (2018) New Approach for Clinical Data Analysis of Microwave Sensor Based Bone Healing Monitoring System in Craniosynostosis Treated Pediatric Patients, IEEE Conference on Antenna Measurements & Applications (CAMA), pp. 1-4.

[4] Al-Hourani A., Kandeepan S., and Jamalipour A. (2014) Modeling air-to-ground path loss for low altitude platforms in urban environments, IEEE Global Communications Conference, pp. 2898-2904.

[5] Belkebir K., Kleinman R. E., and Pichot C. (1997) Microwave imaging-Location and shape reconstruction from multifrequency scattering data, IEEE Transactions on Microwave Theory and Techniques, Vol. 45, no. 4, pp. 469-476.

[6] Zamani A., and Abbosh A. M. (2015) "Fast multi-static technique for microwave brain imaging," IEEE International Symposium on Antennas and Propagation & USNC/URSI National Radio Science Meeting, pp. 536-537.

[7] Li, H., Gu H., Han Y., and Yang J. (2010) “Object-oriented Classification of High-resolution Remote Sensing Imagery Based on an Improved Color Structure Code and a Support Vector Machine.” International Journal of Remote Sensing 31 (6), pp 1453–1470.

[8] Shi Z. (2010) Image Semantic Analysis and Understanding. In: Shi Z., Vadera S., Aamodt A., Leake D. (eds) Intelligent Information Processing V. IIP 2010. IFIP Advances in Information and Communication Technology, Vol 340.

[9] Van den Berg P. M., and Abubakar A. (2001). Contrast Source Inversion Method: State of Art. Progress In Electromagnetics Research, 34, pp 189–218.

[10] Ravindra K., and Sarma A.D., Prasad M.V.S.N. (2002) An adaptive polynomial path loss model at UHF frequencies for mobile railway communication, Indian Journal Radio and Space physics, Vol. 31, pp, 278-284.

Biographies

	**Dr. Madhukant Patel** Received PhD degree from University of Petroleum Studies (UPES), Dehradun, Masters degree from DDIT, Nadiad, Bachelors from LD College of Engineering Ahmedabad. He is a seasoned professional with over 4.5 decades rich experience in IoT based system designs, Sensor Technologies for BioTech designs, Communications & firmware based Product Development, Project Management, Strategy Planning, and Corporate training, Team Management with well known organisations in Electronics, Communication, Instrumentation, Automation, Robotics, etc.
	**Ms. Suhani Patel** received the bachelor degree in Electronics and Communication from Government Engineering College, Gujarat, India in 2020. She is currently a Data Scientist and Director at ReveSoils Pvt Ltd. Ahmedabad. Her research areas include Data analytics, Hyperspectral Imaging(HSI), deep learning, predictive models, IoT, Massive data analytics for the "Biotech", Spectroscopy, Image processing.

Computation of Singular Posture of New 15-DOF Anthropomorphic Robotic Fingers

Deepak Bharadwaj[#], Roushan Kumar

Department of Mechanical Engineering, School of Engineering, University of Petroleum and Energy Studies, Dehradun, India
***[#]Corresponding Author:** Deepak Bharadwaj, Email: dbharadwaj@ddn.upes.ac.in*

Abstract

A new finger gripper design had been proposed in the present work. The existing design of finger gripper has limitations in manipulability. Earlier the tension wire and pulley system has been used for the finger gripper movement. Due to that, the load-carrying capacity of the finger gripper is very low. The proposed design has a combination of serial linkage and parallel linkages. Each finger has 3-DOF. The four fingers of the gripper are attached to the common shaft, and the joint was actuated by one flat plate EC motor. The last finger is attached separately to the shaft and each joint was actuated separately. The dimension of the finger gripper is kept approximately to the anthropomorphic finger. Jacobian and singularity postures were computed for different orientations.

Keywords: Finger Gripper, linkages, Singularity, Posture, Anthropomorphic.

1. INTRODUCTION

The robotic finger gripper design can increase the dexterity and manipulability of the robotic hand. A proper design of a robotic finger can easily grasp the object and avoid collision between the fingers. The automation of a multi-finger robotic end effector plays a crucial role in agile manufacturing for grasping objects [1]. The recent trends have changed in finger gripper design. In place of rigid finger gripper, the research community focus on flexible soft robotic grippers [2]. The soft robotic gripper can easily manipulate the object in an unknown environment [3].

The EMG control interfaces closely interact with the object and perform the task. Multi-finger joint control is an issue. A single actuator control differential mechanism is used to operate the closing and opening of the fingers. Soft robotics emerges in clinical operations as an alternative for therapeutic abilities [4]. A single actuator Differential mechanisms reduced the actuator requirement and possess convenient grasps [5],[6]. The help of a flexible roller chain and simple mechanism allow the finger gripper to grasp a big object. The tendon movement and elastic force of the spring help the finger to open and close very easily. 3- D printed robotic finger was fused with the thermoplastic polyurethane. The fused soft robotic finger has pneumatic sensing chambers. The control of finger force, as well as position, was achieved with the help of a pneumatic sensing chamber. The biomimetic and biomechanics properties were implemented in a new robotic finger gripper. The robotic finger gripper was actuated using five pneumatic cylinders. The motion is obtained similarly to the human upper limb finger. The efficacy were obtained 0.93 i.e closer to the human finger movement [7].

Soft and actuate robotic finger gripper has an advantage over rigid finger gripper. The compliance feature of the soft gripper has a broad range of object manipulability [8],[9]. Controlling the multi-finger robotic gripper is a tedious task. The grasping force of the finger with an object depends on the hemispherical fingertip radius of contact. In the biomimetic finger gripper. Muscle force and moments were tendon driven and match with human finger capability [10]. Generally, lightweight materials like

elastomer material were used for developing the finger gripper. Elasto materials are lightweight and durable and very easy to maintain [11].

The proposed research work was carried out for the combination of serial and parallel multi-finger joint actuation. The development of a flat plate EC brushless DC motor enables to actuation of the finger joint individually. The flat plate DC motor size was varying from 6mm -19mm in diameter and the length is varying from 10-20mm. The finger length is kept the same approximately to the anthropomorphic finger. There is no motion between the crossed fingers. The combination of the serial and parallel finger increases the manipulability of grasping the object and load carrying capacity also increased.

2. CONCEPTUAL DESIGN AND MODELLING

The design was developed in the Solid Work software. Each finger has three parts. The first part of the finger is named as finger base. The center distance between the two ends of the finger base is 37.5 mm and 15mm in width. The detail of the finger base is shown in figure 1. An assembly has been developed by adding the EC flat motor and shaft. The first part of the finger is connected to the palm. The base of all the finger base parts is concentric. The shaft is inserted in the hole, i.e. also concentric to the base part. Each finger is bolted on the shaft so that each finger move simultaneously. The flat plate motor is supported on the palm and drives the shaft, so that the finger base part has the same motion. The finger's second part is also connected in the same way. The EC flat motor is supported on the finger base part and drives the shaft. During motion, all the second parts of the finger move simultaneously and there is no collision between the first part and the second part. The last part of the finger is also connected in the same fashion. The fifth finger i,e thumb is connected in the same way, but actuation is done with the help of three individual flat plates EC motors [12]. A 3-D model of robotic fingers were shown in figure 1.

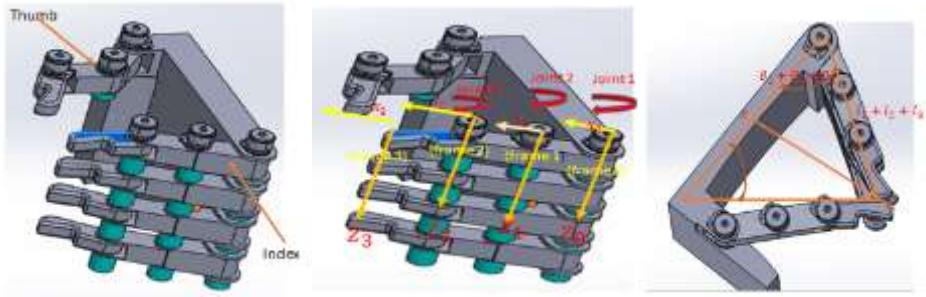

Fig. 1 a) 3-D view of robotic Fingers b) Joint-link description c) Collision detection

2.1. **Forward & Inverse Kinematics**

The kinematic model describes the finger movement in space. Each finger has 3-DOF. All the joints are revolute and active joints. The four fingers of the gripper has the same orientation and moved in the same plane. Each of the four fingers is separated by a distance of 10mm. So there is no collision occurs in the crossed finger position, because the mechanical configuration of the finger does not allow it to move in another direction. The fifth finger has the same orientation but rotates in the opposite direction so that it can grasp the object. Each finger can be modelled as a kinematic chain with three links connected by the three joints [13]. The Denaavit-Hartenberg method was adopted for finding the workspace of the finger. The workspace of all the fingers is the same. The joint notation scheme and complete frame assignment are shown in figure 1 a, 1b, and 1c and joint link parameter for the finger gripper are determined and tabulated in table 1.

Table 1. Joint link parameter for the finger gripper

Link	Parameters 1 (θ_i)	Joint parameters (d_i)	Parameters 2 (l_i)	Parameters 3 (a_i)
	θ_1	0	l_1	0
	θ_2	0	l_2	0
	θ_3	0	0	0

Where θ_i is a rotation about Z_{i-1} axis,d_i is the translation along Z_{i-1} axis, a_i is the translation by a distance along x_i axis,α_i is the rotation about x_i axis. The workspace of index finger 1 is evaluated as follows

$$ {}^0_3T = {}^0_1T * {}^1_2T * {}^2_3T \quad (1) $$

=

$$ \begin{bmatrix} \cos(\theta_1+\theta_2+\theta_3) & -\sin(\theta_1+\theta_2+\theta_3) & 0 & l_2\cos(\theta_1+\theta_2)+l_1\cos(\theta_1)+l_3\cos(\theta_1+\theta_2+\theta_3) \\ \sin(\theta_1+\theta_2+\theta_3) & \cos(\theta_1+\theta_2+\theta_3) & 0 & l_2\sin(\theta_1+\theta_2)+l_1\sin(\theta_1)+l_3\sin(\theta_1+\theta_2+\theta_3) \\ 0 & 0 & 1 & 0 \\ 0 & 0 & 0 & 1 \end{bmatrix} $$

Similarly, the workspace of the other finger was evaluated. The joint displacements$(\theta_1, \theta_2, \theta_3)$ that lead the finger gripper to a certain position and orientation T can be found by solving the kinematic model equations for unknown joint displacements. The close-form solution was obtained for different values of finger joint with equations (1) to (5).

$$ \theta_2 = \cos^{-1}\frac{(d_x-l_3n_x)^2+(d_y-l_3n_y)^2-{l_2}^2-{l_1}^2}{2l_1l_2} \quad (2) $$

$$ \theta_1 = \varphi - \psi + \cos^{-1} C \quad (3) $$

Where $\varphi = \theta_1+\theta_2+\theta_3 = \tan^{-1}\frac{n_y}{n_x} + 180° \quad (4)$

$\psi = \tan^{-1}\frac{B}{A}$,

$x = {d_x}^2 + {d_y}^2 - {l_2}^2 - {l_1}^2 - {l_3}^2 - 2l_1l_2\cos(\theta_2)$.

$A = 2l_1l_3 + 2l_3l_2 * u$, $B = 2l_3l_2 * v$

$u = \cos(\theta_2)$, $v = \sin(\theta_2)$,

$C = \frac{x}{\sqrt{A^2+B^2}}$

$$ \theta_3 = \tan^{-1}\frac{n_y}{n_x} + 180° - \theta_2 - \theta_1 \quad (5) $$

2.2 Jacobian & Singular Posture

The finger movement depends on the finger joint velocities. The Jacobian describes the finger joint position with respect to time. The Jacobian relates the joint velocity of the finger to the end finger velocity. The closing and opening of the gripper depend on the Jacobian matrix[14]. The Jacobian matrix for the first finger is computed as follows with equations (6) and (7).

$$ J(q) = [J_1 \quad J_2 \quad J_3] \quad (6) $$

Where

$$J_1 = \begin{bmatrix} -l_2 \sin(\theta_1 + \theta_2) - l_1 \sin(\theta_1) - l_3 \sin(\theta_1 + \theta_2 + \theta_3) \\ l_2 \cos(\theta_1 + \theta_2) + l_1 \cos(\theta_1) \\ 0 \\ 0 \\ 0 \\ 1 \end{bmatrix}$$

$$,J_2 = \begin{bmatrix} -l_2 \sin(\theta_1 + \theta_2) - l_3 \sin(\theta_1 + \theta_2 + \theta_3) \\ l_2 \cos(\theta_1 + \theta_2) + l_3 \cos(\theta_1 + \theta_2 + \theta_3) \\ 0 \\ 0 \\ 0 \\ 1 \end{bmatrix}, J_3 = \begin{bmatrix} -l_3 \sin(\theta_1 + \theta_2 + \theta_3) \\ l_3 \cos(\theta_1 + \theta_2 + \theta_3) \\ 0 \\ 0 \\ 0 \\ 1 \end{bmatrix}$$

The loss of motion of the finger will start at the point from where the finger is coming into contact with the other finger. Since there is no lateral degree of freedom, due to other finger is not affecting the motion of the other finger. But possibility occurs at the point from where the thumb finger is coming into contact with the index finger. Two types of singularity were computed. The interior singularities were occurs when the tip of the finger is located inside the reachable workspace of the finger gripper. These are caused when two or more joint axes become collinear and at a specific end-effector configuration [15]. The computational of internal singularities can be carried out by analyzing the rank of the Jacobian matrix[16]- [22]. The Jacobian matrix loses its rank and becomes vanishes [23]-[27], that is $\det|J| = 0$. This is computed by portioning the Jacobian matrix into three $2X2$ submatrices.

$$J_1 = \begin{bmatrix} -l_2 \sin(\theta_1 + \theta_2) - l_1 \sin(\theta_1) - l_3 \sin(\theta_1 + \theta_2 + \theta_3) & -l_2 \sin(\theta_1 + \theta_2) - l_3 \sin(\theta_1 + \theta_2 + \theta_3) \\ l_2 \cos(\theta_1 + \theta_2) + l_1 \cos(\theta_1) + l_3 \cos(\theta_1 + \theta_2 + \theta_3) & l_2 \cos(\theta_1 + \theta_2) + l_3 \cos(\theta_1 + \theta_2 + \theta_3) \end{bmatrix}$$

$$J_2 = \begin{bmatrix} -l_2 \sin(\theta_1 + \theta_2) - l_3 \sin(\theta_1 + \theta_2 + \theta_3) & -l_3 \sin(\theta_1 + \theta_2 + \theta_3) \\ l_2 \cos(\theta_1 + \theta_2) + l_3 \cos(\theta_1 + \theta_2 + \theta_3) & -l_3 \cos(\theta_1 + \theta_2 + \theta_3) \end{bmatrix} \quad (7)$$

$$J_3 = \begin{bmatrix} -l_2 \sin(\theta_1 + \theta_2) - l_1 \sin(\theta_1) - l_3 \sin(\theta_1 + \theta_2 + \theta_3) & -l_3 \sin(\theta_1 + \theta_2 + \theta_3) \\ l_2 \cos(\theta_1 + \theta_2) + l_1 \cos(\theta_1) + l_3 \cos(\theta_1 + \theta_2 + \theta_3) & -l_3 \cos(\theta_1 + \theta_2 + \theta_3) \end{bmatrix}$$

From expression (7), the interior singular position was obtained by solving the expression

$$\det|J_1| = l_1 l_2 \sin(\theta_2) + l_1 l_3 \sin(\theta_2 + \theta_3) = 0 \quad (8)$$

$$\det|J_2| = l_2 l_3 \sin(\theta_3) = 0 \quad (9)$$

$$\det|J_3| = l_2 l_3 \sin(\theta_3) + l_1 l_3 \sin(\theta_2 + \theta_3) = 0 \quad (10)$$

Since the thumb finger and index finger i.e. finger1 and finger2 are parallel in orientation. During grasping, both fingers made contact at three points. Condition 1 occurs at the point where both finger 1 and finger 2 comes in contact. Condition 1 is shown in figure 2. These points were computed by the expression (7) to (11).

$$\theta_1 + \theta_2 + \theta_3 = \sin^{-1} \frac{x}{2(l_1 + l_2 + l_3)} \quad (11)$$

3. RESULTS

The first singularity posture was obtained at $\theta_3 = 0° \; and \; 180°$, the second singularity posture was obtained at $\theta_2 = 0° \; and - 180°$. The actuation constraint does not allow the $\theta_1$to rotate more than

90°. Singular postures were obtained at a different computed angle. Figures 2 and 3 show the simulated result of singular posture.

Fig. 2. Singular posture of the fingers including thumb finger and index finger

Fig. 3. Collision detection in all the fingers

4. CONCLUSION

The robotic finger gripper design has been considered for the grasping of the object. : A new finger gripper design had been proposed in the present work. The propped design can actuate the four joints of the finger simultaneously. The other two joints of the finger have also actuated with the help of a flat plate EC motor. The index finger was actuated separately. Singularities were computed for the different angles. A collision-free movement of the gripper was observed during the operation.

REFERENCES

[1] M. Honarpardaz, M. Tarkian, J. Ölvander, and X. Feng, "Finger design automation for industrial robot grippers: A review," *Rob. Auton. Syst.*, vol. 87, pp. 104–119, 2017, doi: 10.1016/j.robot.2016.10.003.

[2] Z. Chen, H. Rahimi Nohooji, and C.-M. Chew, "Development of Topology Optimized Bending-Twisting Soft Finger," *J. Mech. Robot.*, vol. 14, no. 5, Feb. 2022, doi: 10.1115/1.4053159.

[3] M. Liu, L. Hao, W. Zhang, and Z. Zhao, "A novel design of shape-memory alloy-based soft robotic gripper with variable stiffness," *Int. J. Adv. Robot. Syst.*, vol. 17, no. 1, pp. 1–12, 2020, doi: 10.1177/1729881420907813.

[4] M. Zhu, M. Xie, X. Lu, S. Okada, and S. Kawamura, "A soft robotic finger with self-powered triboelectric curvature sensor based on multi-material 3D printing," *Nano Energy*, vol. 73, no. March, p. 104772, 2020, doi: 10.1016/j.nanoen.2020.104772.

[5] J. Zhou, J. Yi, X. Chen, Z. Liu, and Z. Wang, "BCL-13: A 13-DOF soft robotic hand for dexterous grasping and in-hand manipulation," *IEEE Robot. Autom. Lett.*, vol. 3, no. 4, pp. 3379–3386, 2018, doi: 10.1109/LRA.2018.2851360.

[6] R. Kumar, N. J. Ahuja, M. Saxena, and A. Kumar, "Automotive Power Window Communication with DTC Algorithm and Hardware-in-the Loop Testing," Wirel. Pers. Commun., 2020;114 (4): 3351–3366 doi: 10.1007/s11277-020-07535-4.

[7] C. Gosselin, F. Pelletier, and T. Laliberté, "An anthropomorphic underactuated robotic hand with 15 dofs and a single actuator," *Proc. - IEEE Int. Conf. Robot. Autom.*, pp. 749–754, 2008, doi: 10.1109/ROBOT.2008.4543295.

[8] R. Kumar, K. Bansal, A. Kumar, J. Yadav, M. K. Gupta, and V. K. Singh, "Renewable energy adoption: Design, development, and assessment of solar tree for the mountainous region," Int. J. Energy Res. 2021; 1–17 doi: 10.1002/er.7197.

[9] Gupta V., Kumar R., Mishra R.G., Semwal A., Siwach S., "Design and optimization of luggage tracking system on airport", Proceeding of International Conference on Intelligent Communication, Control and Devices Advances in Intelligent Systems and Computing (2016), pp. 833-838.
[10] C. Y. Chu and R. M. Patterson, "Soft robotic devices for hand rehabilitation and assistance: A narrative review," *J. Neuroeng. Rehabil.*, vol. 15, no. 1, pp. 1–14, 2018, doi: 10.1186/s12984-018-0350-6.
[11] K. Xu and H. Liu, "Continuum Differential Mechanisms and Their Applications in Gripper Designs," *IEEE Trans. Robot.*, vol. 32, no. 3, pp. 754–762, 2016, doi: 10.1109/TRO.2016.2561295.
[12] R. Kumar, Divyanshu, and A. Kumar, "Nature Based Self-Learning Mechanism and Simulation of Automatic Control Smart Hybrid Antilock Braking System," Wirel. Pers. Commun., 2021; 116(4); 3291–3308.
[13] S. E. Baek, S. H. Lee, and J. H. Chang, "Design and control of a robotic finger for prosthetic hands," *IEEE Int. Conf. Intell. Robot. Syst.*, vol. 1, pp. 113–117, 1999, doi: 10.1109/iros.1999.812990.
[14] C. Tawk, H. Zhou, E. Sariyildiz, M. In Het Panhuis, G. M. Spinks, and G. Alici, "Design, Modeling, and Control of a 3D Printed Monolithic Soft Robotic Finger with Embedded Pneumatic Sensing Chambers," *IEEE/ASME Trans. Mechatronics*, vol. 26, no. 2, pp. 876–887, 2021, doi: 10.1109/TMECH.2020.3009365.
[15] Y. Mishima and R. Ozawa, "Design of a robotic finger using series gear chain mechanisms," *IEEE Int. Conf. Intell. Robot. Syst.*, vol. 1, no. IROS, pp. 2898–2903, 2014, doi: 10.1109/IROS.2014.6942961.
[16] Kumar, R., Kumar, A., Gupta, M. K., Yadav, J., & Jain, A. (2022). Solar tree-based water pumping for assured irrigation in sustainable Indian agriculture environment. Sustainable Production and Consumption, 33, 15-27, doi.org/10.1016/j.spc.2022.06.013.
[17] Kumar, R., Kumar, A., Gupta, M. K., Yadav, J., & Jain, A. (2022). Solar tree-based water pumping for assured irrigation in sustainable Indian agriculture environment. Sustainable Production and Consumption, 33, 15-27, doi.org/10.1016/j.spc.2022.06.013.
[18] B. S. Homberg, R. K. Katzschmann, M. R. Dogar, and D. Rus, "Haptic identification of objects using a modular soft robotic gripper," *IEEE Int. Conf. Intell. Robot. Syst.*, vol. 2015-Decem, pp. 1698–1705, 2015, doi: 10.1109/IROS.2015.7353596.
[19] D. Chadefaux, J. L. Le Carrou, M. A. Vitrani, S. Billout, and L. Quartier, "Harp plucking robotic finger," *IEEE Int. Conf. Intell. Robot. Syst.*, pp. 4886–4891, 2012, doi: 10.1109/IROS.2012.6385720.
[20] R. Kumar, R. K. Pachauri, P. Badoni, D. Bharadwaj, U. Mittal, and A. Bisht, "Investigation on parallel hybrid electric bicycle along with issuer management system for mountainous region," J. Clean. Prod., 2022; 362:132430, doi: 10.1016/j.jclepro.2022.132430.
[21] Kumar, R., Gupta, N., Bharadwaj, D., Dutt, D., & Joshi, A. (2022). Design and development of electronic clutch control unit for manual transmission. Materials Today: Proceedings.
[22] Kumar, R., Gupta, M. K., Kumar, A., Sharma, P., & Deorari, R. (2022). Analysis of electronic clutch control unit for manual transmission vehicle oriented toward safety. Materials Today: Proceedings.
[23] Maan A., Pitta P., Yadav J. (2018) Performance Evaluation of Rectangular Fins by Modeling and Simulations. In: Siddiqui N., Tauseef S., Abbasi S., Rangwala A. (eds) Advances in Fire and Process Safety. Springer Transactions in Civil and Environmental Engineering. Springer, Singapore.
[24] Yadav J., Agnihotri G. (2018) Circumvention of Friction-Induced Stick-Slip Vibration by Modeling and Simulation. In: Singh R., Choudhury S., Gehlot A. (eds) Intelligent Communication, Control and Devices. Advances in Intelligent Systems and Computing, vol 624. Springer, Singapore.
[25] Jitendra Yadav and Geeta Agnihotri (2017), "Modeling and Simulation of the Dynamic Response of a Generic Mechanical Linkage for Control Application Under the Consideration of Nonlinearities Imposed by Friction", In Springer Proceedings of the International Conference on Nano-electronics, Circuits & Communication Systems, Lecture Notes in Electrical Engineering 403, DOI 10.1007/978-981-10-2999-8_26
[26] Jitendra Yadav & G. Agnihotri, "Proposed Critical Damping for a Spring Mass System to Avoid Stick Slip" ,Springer Journal of the institution of engineers (India): Series C Volume 96, Number 3, PP 331-335, July-September 2015. https://doi.org/10.1007/s40032-015-0173-1
[27] Yadav, Jitendra, et al. "Nonlinear dynamics of controlled release mechanism under boundary friction." Results in Engineering 11 (2021): https://doi.org/10.1016/j.rineng.2021.100265

Predicting Coma patient emotions based on a Real-World Study, using Machine Learning and Deep Learning Techniques

Parth vyas, R. K. Chaurisia, A. K. Saini

Authors affiliation, ICFAI University, Jaipur/FST

parthv.btech2020@iujaipur.edu.in, rkchaurasia@iujaipur.edu.in, aksaini@iujaipur.edu.in

Abstract.

Psychology, cognitive science, and, more lately, engineering have all paid close attention to emotion modelling and recognition. Despite the fact that behavioural modes have been the subject of extensive investigation, physiological signals have received less attention. Dialectical behaviour therapy (DBT), which was created to lessen dysregulated emotions in personality disorders, is employed with patients with eating disorders (ED) because it is a transdiagnostic phenomenon. Emotional interactions are advantageous in a variety of contexts because they have a significant positive impact on cognitive functions like learning, memory, perception, and problem-solving in the human brain. Additionally, it may be pertinent in today's healthcare, particularly when dealing with people who are stressed or depressed. Additionally, it would be extremely beneficial for a rehabilitation application to direct patients through rehabilitation training while adjusting to the patient's emotional condition.

Keywords. Ecg AI; CNN; ANN; Deep convolution; Linear generation; Extraction and selection; Polynomial network

• Introduction

The Effective Computing Research Group at MIT has generated a lot of attention in the academic and scientific communities over the past 20 years as they work to enhance how people feel when using technology. [7] Several issues revolve around deepening machine learning and deep algorithms in order to ensure that the emotion detection system has a high accuracy as well as processing robustness of physiological data. Heart rate variability (HRV), blood volume pulse, and other physiological measurements (BVP), skin temperature (SKT), electrocardiogram (ECG), [22, 23] and electrodermal activity (EDA), which both the peripheral and central neural systems as their source, have been used to identify affective states. Subjective emotions are categorized as having a valence or stimulating orientation. The extent to which each focus is reflected in the other adds feelings to one's own conscious affective experience. Unlike the focus of arousal, which promotes the activation or deactivation of emotions, stimulus valence focus is related to positive or negative features. Affective states and physiological signals, which are the results of people's self-reported feelings, are correlated in some datasets. [6] To characterize the dimensions of arousal and valence, emotional categories are constructed in a circular structural model that includes basic emotions (for example, enthusiastic, happy, delighted, relaxed, quiet, peaceful, drowsy, bored, sad, nervous, angry, and angry) [12]. Research on identifying emotional patterns for enhancing user experience in many contexts was made possible by the development of sensors and wearable technology as mechanisms for gathering physiological data from individuals in their daily lives. [1,10,15] Research in tourism management research This highlights the significance of this kind of tool for emotional recognition in various ways, such as enhancing the tourist experience through the personalization of services where the expectations of the visitor are assessed throughout the course of three stages (before, during, and after a

visitor's visit) for various aspects of tourist activities. Recommendation systems are a useful tool before traveling to a tourist location, especially when taking into account the size of the attraction. In a similar vein, [17] the World Tourism Organization acknowledges that in an increasingly competitive tourist destination market, emotional benefits are more likely to be emphasized than physical attributes and trip cost. This research investigates deep convolutional neural network (CNN) models as a framework for emotion identification and compares them to conventional machine learning techniques for effective recognition. The AMIGOS data collection was used to generate experimental assessments for the categorization of emotional dimensions of arousal and valence. [25] In the initial planning stage, QRS detection techniques were employed to get RR intervals of the ECG and transform physiological signals. Likewise, the time series Peaks of GSR signals were found in the skin conductance response (SCR). [1] Physiological ECG signals and GSR properties are extracted and correlated to determine the efficiency factor for emotion prediction. As a result, we developed an algorithm and dataset for a deep face reading system in the medical industry using convolution and CNN. With this approach, we created a dataset indicating that coma patients are terrible because they cannot move or speak, but the AMIGOS data collection was used to generate experimental assessments for the categorization of emotional dimensions of arousal and valence. [25] They They frequently alter their facial expressions to convey physiological messages. [26,22] We developed an algorithm using a data set of all the emotions.

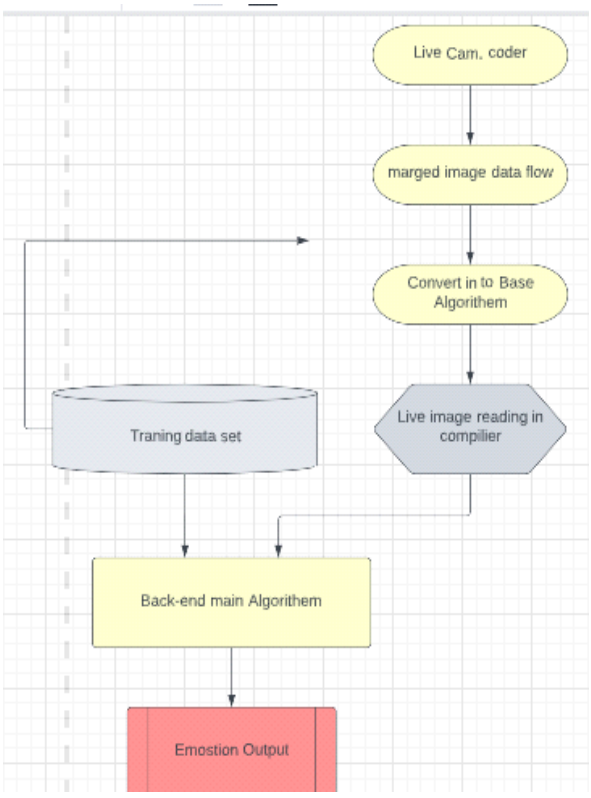

Figure 2.1. Typical Datacentres Infrastructure

- **Multimodal Dataset**

In reaction to the elicitation, a person's emotional response to change in the environment is reflected in their affective states. Humans employ their senses to express their emotions through gestures, speech, or physiological responses [5, 8, 20]. Multimodal affect recognition is determined by correlations between physiological data and emotions. Images, movie clips, and music videos have been utilized as emotional triggers to assess users using explicit measurements that allow for the verification of arousal and valence levels. The consolidation of a multimodal emotional data set that contrasts people's affective responses is made possible by the implicit recognition of emotions elicited by multimedia information utilizing physiological and brain signals, on the other hand. In reaction to the elicitation, a person's emotional response to change in the environment is reflected in their affective states. Humans employ their senses to express their emotions through gestures, speech, or physiological responses [5, 8, 20]. ECG and GSR physiological registration signals, EEG, and activity faces of 58 individuals were used to quantify multimodal effects induced by 36 video clips with durations ranging from 58 to 128 seconds. By recording the EEG, ECG, and GSR signals of the stimulus produced during short and lengthy viewing, the AMIGOS dataset examines 40 participants' moods, affects, and personalities. Abadi and his colleagues To To investigate the physiological The ASCERTAIN dataset compares brain signals (EEG and magnetoencephalogram) from 30 people (GSR, BVP, SKT, EOG, and EMG) and has a strong influence on ECG, electrooculogram (EOG), and trapezius-electromyogram personality and emotion recognition responses (EMG). Likewise, the multimodal MAHNOB-HCI database contains physiological signals (ECG, GSR, SKT, and respiration), eye gaze, and EEG from 20 emotional videos, 14 short videos, and 28 images. The EEG efficacy of DEAP and MAHNOB-HCI in predicting arousal is higher, and physiological signals produce superior results with valence. Although AMIGOS exhibits the same behaviour as EEG signals, it performs better when excited. The DECAF physiological characteristics recognized arousal in movie clips, and the AMIGOS affective dataset was used to test the machine learning methods suggested in this study for emotion recognition.

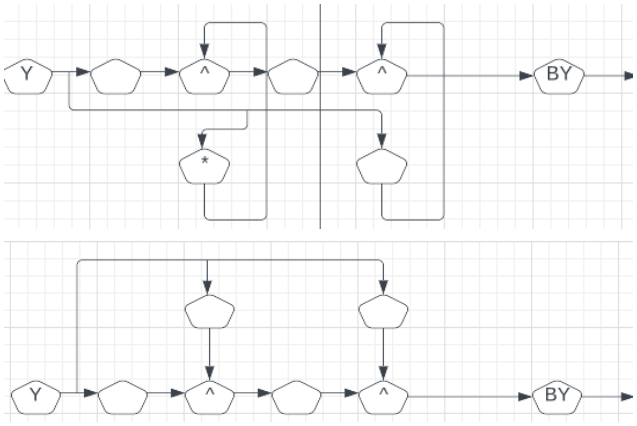

fig(2)Showing the machine learning model

The expressiveness of (deep) neural networks: [24] (Deep) neural networks have been successfully applied to a in recent years, it has seen a wide range of applications. Several factors, including a) the availability of massive datasets, b) massively running machine learning libraries and parallel hardware, and c) training improvements, can be attributed to the increase in performance. Training enhancements include a) optimizer enhancements, b) network capacity expansion, and c) regularization techniques. However, for several decades, the paradigm for each layer has largely remained unchanged: each layer consists of a linear transformation and an element-wise activation function. Despite the wide range of linear transformations and activation functions, the effort to broaden to date, this paradigm has received little attention. Recently, hierarchical models have demonstrated exceptional performance in the learning of expressive generative models. For example, the recent BigGAN performs a hierarchical composition by skipping noise from a multi-resolution generator via z-join. Similarly, the concept appeared in Style GAN, a step forward from the GAN that grows gradually (ProGAN). StyleGAN, like ProGAN, is a complex network that generates convincing results on simulated 2D images. [21] The authors use arguments from the style transfer literature to explain the improvements in style GaN vs. Pagan. We believe that these enhancements can be better explained in light of our proposed polynomial function approximation. Despite the hierarchy to achieve the more accurate approximation proposed in these works, we present a method based on polynomial expansion. We also

show how a polynomial expansion of this type can be used in image generation, image classification, and graph representation learning, which are all examples of machine learning.

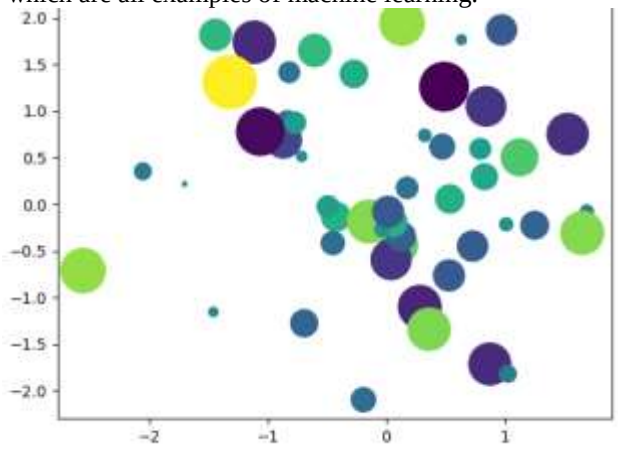

Graph plotting of datasets.

- **Polynomial Network.**

Polynomial relationships were investigated using two different types of networks: a) self-organizing networks like datasets with hard-coded feature selection and b) pi-sigma networks for indemnification. The group data processing method is responsible for the concept of learnable polynomial features (GMDH). Sub-descriptors that represent quadratic correlations between two input features. Higher-order polynomials are used, and multiple input elements are allowed. [22] The method cannot scale to high-dimensional data correlation because the input to each sub-descriptor is predefined (a subset of the input elements). Shin et al. present the pi-sigma network, a one-hidden-layer neural network. The multiply affine data transformation is learned; the output is obtained by multiplying all of the functions. Regularization is one way to improve the pi-sigma network. To obtain the output by training in or using multiple units of the product In sigma-pi-sigma neural networks, the pi-sigma network is extended (SPSNN). To obtain each output, the SPANN concept relies on summing different pi-sigma networks. On each pi-sigma subnet, SPS filters the input functions on a predefined basis (overlapping rectangular pulses). Despite using polynomial properties or products, such networks do not scale well for high-dimensional signals. Furthermore, unlike modern generative models, which use a finite number of samples from high-dimensional ground-truth distributions, experimental evaluation is done only on signals with known ground truth distributions (and up to 3-dimensional input/output).

- **Compression Between Models.**

Although all three models are based on polynomial expansion, their recursive forms and decompositions differ. In recent years, it has seen a wide range of applications. In this paper, we use NCP for image generation comparison and NCP-Skip for image classification. Based on the settings in Sec. 4, our preliminary CCP and NCP experiments show comparable performance.

- There are three models are based on polynomial expression.
- All activation function must be removed.
- The order of expression with (I P r2) must be performed.
- The encephalopathies are infectious 6-9 or not 9-12.

2. At least two mechanisms are thought to be involved in intracranial hypertension causing brain damage.

- Low ischemia is caused by cerebral perfusion pressure (CPP = MAP*ICP)

- If pressure difference exists between the anterior and posterior brain compartment one or both temporal lobes can herniate through the tentorium.

- **Linear Generation.**

Nets of Adversaries (GAN). We create a GAN in which the generator is implemented as a polynomial product (via the NCP decomposition) and the discriminator is used. The generator employs no activation functions, only a single hyperbolic tangent (tanh) in image space.

- We create a GAN in which the generator is implemented as a polynomial product (via the NCP decomposition).
- The generator employs no activation functions only a single hyperbolic tangent in image space.
- In first model we used the 100 patients' data to train the model.
- The majority of the 76 patients were men between the age of 18-40 and the other patient due to trauma.
- We use their temperature facial expression electrography and the over model.

- **Linear classification.**

To demonstrate this empirically, we use ResNet without activations for classification. the polynomial's power. Residual Networks (ResNet) and their variants have been used to perform a variety of Object detection and image generation. The answer is almost certainly "yes" regardless of whether the encephalopathies are infectious 6-9 or not 9-12; regardless of the debate over Monitoring has many advantages, including the prevention of death and disability in the acute setting.

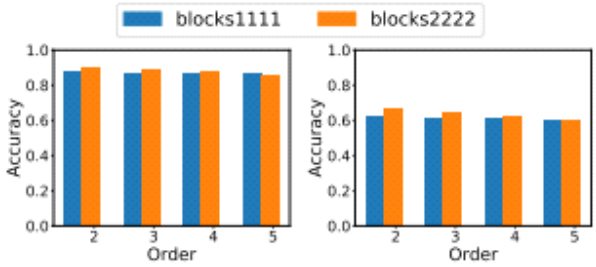

At least two mechanisms are thought to be involved in intracranial hypertension causing brain damage. First, low Ischemia is caused by cerebral perfusion pressure (CPP = MAP ICP) [2]., particularly in border zones between major arterial regions; it may be associated with seizures, as However, it is frequently clinically silent in hypertensive encephalopathy.

the pressure difference between the posterior fossa and the spinal canal is large enough (inferior pontine and medullary herniation syndromes). Brain herniation causes direct mechanical damage as well as ischemia and haemorrhage as a result of vascular dysfunction.

The following are the crucial steps: I have developed the habit of serially examining the patient's level of consciousness (Table 1) and brainstem reflexes in relation to these concepts so that progression is immediately recognized; (ii) remembering the stages of progressive herniation compatible with intact survival (in bold in Tables 2 and 3); (iii) learning the control algorithm so that action is taken as soon as possible.

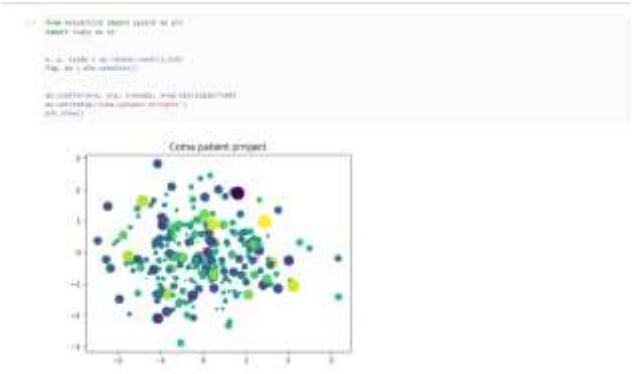

for graphical plotting using deep learning and MATLAB process

- ## Machine Learning.
  - **Data pre-processing**

The detection of ECG and GSR signal peaks is performed as a preliminary step to extract physiological signal features because emotions cause significant changes in these segments. The pulse-to-beat interval (RR interval) can be determined using heart rate variability (HRV) analysis. [16] Values between RR of the interval corresponding the standard wave of the QRS complex was used to calculate the time between the two peaks of R. To transform the ECG signal, the proposed Pan Tompkins QRS detection algorithm is used. With cut-off frequencies of 0.5 and 15 Hz, the signal is filtered to reduce noise, and the QRS detection complex employs an adaptive threshold. Similarly, a bandpass noise reduction filter with cut-off frequencies of 0.05 and 0.19 Hz is used to pre-process the GSR signal. It is then resampled using a digital phase filter with a frequency of 10 Hz. To detect the SCR peak, a standard method is used, which identifies the maximum, minimum, and offset index of the signal GSR. As a result, the amplitude threshold is calculated, as are the properties between the SCR peaks.

- **Extraction and selection of features**

Adequate feature extraction signals that correlate with self-reported emotional states are required for influence detection. In other words, it establishes the relationship between traits, emotions, and physiological reactions and serves as an input to the predictor. Adequate feature extension singles that correlate with self-reported emotional states are required for influence detection. In contrast to CNN the physiological ECG and GSR signals were manually extracted. The variance of feature signals derived from ECG and GSR described the feature extension process deep learning and machine learning algorithm are used to filter out redundant.

Prediction results from machine algorithms are typically similar to or slightly higher than those obtained in the previous study. As a result, CNN achieves better performance in excitation recognition using EEG signals as opposed to the GSR signal, which is better at predicting valence. Given the AMIGOS dataset's physiological data limitations, it was proposed that the depth learning model be validated using EEG and ECG signal data. For every signal, 10,000 points were used to segment and normalize the data. 90% of the information was used. For training and the remaining 10% for testing, resulting in the validation model was assigned 965 instances.

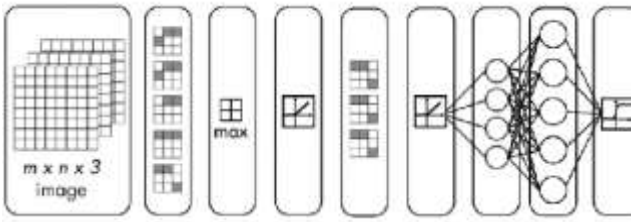

flow of Emotion Reading Process.

• Conclusion.

We introduce a new class of DCNN. Which uses a polynomial neural network to approximate function. We demonstrate the expressivity of polynomials in sequence experiment and demonstrate the effectiveness of -nets in both discriminative and generative tasks. The performance of the most modern architecture in image generation, image and sound classification and networking learning representation improves continuously with minor modifications. The focus of this study is on using computational models on data collection by camera and wearable devices to recognize emotions from physiological signals.

The direction of the low index below 0.8 for more than two hours on 111 transcranial Doppler ultrasound is highly suggestive of irreversible brainstem death. 112 HE Convolutional networks versus classical networks Machine learning algorithms have outperformed humans despite being designed for object recognition, image recognition, and detecting emotions in physiological signals.

The focus of this study is on using computational models on data collected by wearable devices to recognise emotions from physiological signals.

• Acknowledgement.

We value the hardware contributions from Nvidia and the cloud credits from Amazon Web Services. A DTA from Imperial College helped to support the work of GC, SM, and GB. JD received a portion of the Imperial President's Ph.D. Scholarship to help with his study. The EPSRC Fellowship DEFORM: Large Scale Shape Analysis of Human Deformable Models (EP/S010203/1) and a Google Faculty Award both contributed to the funding of SZ's study. An early version of it using single polynomials for the generative settings can be seen there. The Telematic Applications and Services Group (GAST) of the Universidad Carlos III de Madrid is responsible for the AMIGOS project. The authors thank the anonymous reviewers for their constructive criticism. The Colombian government is funding this study endeavour.

• References.

[1] R.W. Picard, Affective Computing. MIT Press, July 2000.
[2] P. Ekman, R.W. Levenson, and W.V. Friesen, “Autonomic Nervous System Activity Distinguishes Among Emotions, "Science," vol. 221, pp. 1208-1210, Sept. 1983.
[3] F. Honig, A. Batliner, and E. Noth, “Real-Time Recognition of the Affective User State with Physiological Signals,” Proc. Doctoral Consortium Conf. Affective Computing and Intelligent Interaction, pp. 1-8, 2007.
[4] J. Anttonen and V. Surakka, “Emotions and Heart Rate While Sitting on a Chair,” Proc. SIGCHI Conf. Human Factors in Computing Systems, pp. 491-499. 2005,
[5] C.M. Jones and T. Troen, “Biometric Valence and Arousal Recognition,” Proc. 19th Australasian Conf. Computer-Human Inter- action, pp. 191-194, 2007.
[6] R.L. Mandryk, T.W. Inkpen, and K.M. Calvert, “Using Psycho-physiological Techniques to Measure User Experience with Entertainment Technologies,” Behaviour and Information Technol- ogy, vol. 25, no. 2, pp. 141-158, Mar.-Apr. 2006.
[7] R. Sinha, W.R. Lovallo, and O.A. Parsons, “Cardiovascular Differentiation of Emotions,” Psychosomatic Medicine, vol. 54, pp. 422-435, 1992.

[8] R.W. Picard, E. Vyzas, and J. Healey, "Toward Machine Emotional Intelligence: Analysis of Affective Physiological States," IEEE Trans. Pattern Analysis and Machine Intelligence, vol. 23, no. 10, pp. 1175-1191, Oct. 2001.
[9] J. Kim and E. Andre, "Emotion Recognition Based on Physiological Changes in Music Listening,"IEEE Trans. Pattern Analysis and Machine Intelligence, vol. 30, no. 12, pp. 2067-2083, Dec. 2008.
[10] F. Nasoz, K. Alvarez, C.L. Lisetti, and N. Finkelstein, "Emotion Recognition from Physiological Signals Using Wireless Sensors for Presence Technologies," Int'l J. Cognition, Technology, and Work, special issue on presence, vol. 6, no. 1, pp. 4-14, Feb. 2004
[11] K. Kim, S. Bang, and S. Kim, "Emotion Recognition System Using Short-Term Monitoring of Physiological Signals," Medical and Biological Eng. and Computing,
vol. 42, no. 3, pp. 419-427, May 2004.
[12] R.L. Mandryk and M.S. Atkins, "A Fuzzy Physiological Approach for Continuously Modeling Emotion during Interaction with Play Technologies,"Int'l J. Human Computer Studies, vol. 65, no. 4, pp. 329-347, 2007.
[13] P.J. Lang, M.M. Bradley, and B.N. Cuthbert, "Int. Affective Picture System (IAPS): Instruction Manual and Affective Ratings," Technical Report A-5, 2001.
[14] A. Haag, S. Goronzy, P. Schaich, and J. Williams, "Emotion Recognition Using Bio-Sensors: First Steps towards an Automatic System,"Affective Dialogue Systems,vol. 3068, pp. 36-48, 2004.
[15] L. Sornmo and P. Laguna, " Bioelectrical Signal Processing in Cardiac and Neurological Applications." Elsevier, 2005.
[16] J.T. Catalano, " Guide to ECG Analysis." J.B. Lippincott, 1993.
[17] R. Shouldice, C. Heneghan, P. Nolan, and P.G. Nolan, "PR and PP ECG Intervals as Indicators of Autonomic Nervous Innervation of the Cardiac Sinoatrial and Atrioventricular Nodes," Proc. First IEEE Int'l Conf. Neural Eng., pp. 261-264, Mar. 2003.
[18] R. Virtanen, A. Jula, J.K. Salminen, L.M. Voipio-Pulkki, H. Helenius, T. Kuusela, and J. Airaksinen, "Anxiety and Hostility Are Associated with Reduced Baroreflex Sensitivity and Increased Beat-to-Beat Blood Pressure Variability," Psychosomatic Medicine, vol. 65, pp. 751-756, 2003.
[19] S. Booth-Kewley and H.S. Friedman, "Psychological Predictors of Heart Disease: A Quantitative Review," Psychological Bull., vol. 101, no. 3, pp. 343-362, 1987.
[20] G.H.E. Gendolla, M. Richter, and A. Friedrich, "Task Difficulty Effects on Cardiac Activity,"Psychophysiology,
no. 45, pp. 869-875, 2008.
[21] J. Blascovich, M.D. Seery, C.A. Mugridge, R.K. Norris, and M. Weisbuch, "Predicting Athletic Performance from Cardiovascular Indexes of Challenge and Threat,"
J. Experimental Social Psychology, vol. 40, no. 5, pp. 683-688, 2004.
[22] H. Ue, I. Masuda, Y. Yoshitake, Y. Inazumi, and T. Moritan"Assessment of Cardiac Autonomic Nervous Activities by Means of ECG R-R Interval Power Spectral Analysis and Cardiac Depolarization-Repolarization Process,"Annals of Noninvasive Electrocardiology,
vol. 5, no. 4, pp. 336-345, 2000
[23] W.L. Wasmund, E.C. Westerholm, D.E. Watenpaugh, S.L. Wasmund, and M.L. Smith, "Interactive Effects of Mental and Physical Stress on Cardiovascular Control," J. Applied Physiology, vol. 92, pp. 1828-1834, 2002.
[24] R. Pramila, J. Sims, R. Brackin, and N. Sarkar, "Online Stress Detection Using Psychophysiological Signals for Implicit Human- Robot Cooperation,"Robotica,vol. 20, no. 6, pp. 673-685, 2002.
[25] M. Dambacher, W. Eichinger, K. Theisen, and A.W. Frey, "RT and Systolic Blood Pressure Variability after Sympathetic Stimulation during Positive Tilt in Healthy Volunteers," Proc. Computers in Cardiology, pp. 573-576, Sept. 1994.
[26] G. Andrassy, A. Szabo, G. Ferencz, Z. Trummer, E. Simon, and A. Tahy, "Mental Stress May Induce QT-Interval Prolongation and T-Wave Notching," Annals of Noninvasive Electrocardiology, vol. 12, no. 3, pp. 251-259, 2007.
[27] A.F. Folino, G. Buja, P. Turrini, L. Oselladore, and A. Nava, "The Effects of Sympathetic Stimulation Induced by Mental Stress on Signal Averages Electrocardiogram,"
Int'l J. Cardiology,vol. 48, pp. 279-285, 1995.
[28] A. Szabo, "The Combined Effects of Orthostatic and Mental Stress on Heart Rate, T-Wave Amplitude, and Pulse Transit Time," European Journal of Applied Physiology, vol. 67, no. 6, pp. 540-544, 1993.
[29] H. Scher, J.J. Furedy, and R.J. Heslegrave, "Phasic T-Wave Amplitude and Heart Rate Changes as Indices of Mental Effort and Task Incentive," Psychophysiology, vol. 21, no. 3, pp. 326-333, 1984.

Biographies

Parth vyas Student at IcfaiTech, IcfaiTech, The ICFAI University Bachelor of Technology - CSE \ I am a Computer science Student and Currently I'm working on Image processing development with Python language And with this course gaining knowledge of Digitel image processing.

Dr. AK Saini Professor & Dean at IcfaiTech,The ICFAI University,Jaipur working in the field of higher education for last 20 years. Area of specializations are Machine Learning, Artificial Intelligence, Computer Vision, Computer Architecture etc. For last 10 years in educational administration along with teaching.

Dr. RK Chaurisia Assistant Professor ,Icfai university jaipur ,Total Experience 20 years Published 50 research paper in national/International journal Research Area are wireless communication, Image processing, Machine lerning ITS, The ICFAI University, Jaipur-302031

Extraction of Features in Number Plate using Contour Spotting

Harshita Prashar[1], Deval Verma[2]

[1]Department of Mathematics, Chandigarh University, Punjab- 140413
harshitaprashar97@gmail.com
[2]School of Computer Science Engineering and Technology
Bennett University, Times Group
Greater Noida-201310
deval09msc@gmail.com

Abstract

This Number plate recognition (NPR) of a vehicle's become very important nowadays. Also, it isn't easy to verify the car's owner. They drive very fast and violate traffic rules. Identification of owners and traffic control is a crucial problem in every country. In every city, 90% of people own their vehicle, so it becomes challenging to trace every car; many examples include tracking stolen vehicles, managing the toll barriers, parking tolls, infringed traffic lights, and monitoring. Because our police officers may not be able to catch the cars due to over speeding and occasionally the number plates appear dirty, it is difficult to apprehend everyone and punish them. That is why it is essential to develop NPR to solve all these problems. ANRP is in a large amount and several in numbers. Yet, it is a challenging task because of the diversity in number plates, different colours, different languages, and different characters; also, people may place non-standard types of plates in their vehicles and illumination during image acquisition. In this paper, we introduced NPR using some algorithms, different morphological operations, image size, character segmentation and contour spotting methodologies for plate pinpointing. An Artificial Neural Networks is used for recognition and character classification. An extension and future trends of NPR are suggested at the end of the paper

Keywords. Number Plate Recognition (NPR), Character Segmentation, License Plate (LP), Artificial Neural Networks (ANN), Image Processing, Machine Learning, Technologies.

1. INTRODUCTION

Energy In the last few years, license plate recognition (LPR) has been one of the practical advancements for vehicle superintendence Automatic number plate recognition (ANPR) is widespread surveillance that photographs moving targets and deciphers their license plates. An ANPR system can be used for various purposes, Automated traffic monitoring and tracing, toll collecting for park and highways, fuelling store automated, and trip time monitoring. A growing amount of traffic flow analysis using ANPR is done to support

smart mobility [1]. The fundamental justification is that, in contrast to Ultra High Frequency Radio Frequency Identification systems [2], ANPR system identifies registered number plate with no additional [3]. Modern ANPR cameras can scan license plates and provide other relevant data like counting, direction, groups of cars, and speed. The ability of ANPR technology to detect and browse many moving vehicles has led to its integration into many areas of the current digital landscape. To offer an exact way of contemplating a vehicle without earthling intercession. It is used for a variety of services, including access control, parking management, tolling, user billing, delivery tracking, traffic management, policing and security services, customer assistance and instructions, red light and lane imposition, cavalcade stretch guesstimate, and numerous others [4]. The prime focus of this paper is to locate regular licence plates, segment characters, and identify them from a car image. Different scales, distances, angles, resolutions, and lighting requirements must be accommodated by the system. The problem statement will be presented in Section 2. The suggested solution will present in Section 3. The paper is finally concluded in Section 4.

1.1. Related Work

Researchers may have discovered various techniques for locating license plate inputs and neural networks. Rodolfo and Stefano developed an approach based on vector quantization in 2000. (VQ). In this system, they provide suggestions about picture regions, and by this, they improve location performance. By coding Mechanism, VQ image representation was explained. Neural networks were employed by Park et al. (1999) to locate license plates [5]. HSI values are used as filters to determine whether each small window of an image contains a license plate. A post-processor then combines these filtered images and finds the bounding boxes of license plates in the picture. Zimic et al. in 1997 located license plates by fuzzy logic. In This logic, some functions were made for the vague as “Dark and bright sequences” [6] But due to its sensitive role, it needs a lot of time for processing. In 2002, Zhu et al. and Wei et al. in 2001 used the colour feature to locate the plate, but this was not enough for different environments. Again, Ming et al. (1996) improves the edge detection method by eliminating the lowest and highest parts of edge density to simplify the complete image. But some parts of the plate will be lost in this method.

1.2. How actual ANPR works

One of the most precise uses for computer vision systems is ANPR. Autonomous number plate recognition systems use visual character recognition (OCR) to detect car licence plates. Webcams quickly capture number plate scans, and software is then used to segment, confirm their order, and convert the image to text.

1. Initially, the ANPR camera records photos with a licence plate (video stream or image).
2. The plate is then located using machine vision techniques (object detection).

1.3. Applications of ANPR works in real life

We offer a robust actual ANPR framework that is meticulously working on CCTV video footage received from cams that are not explicitly set up for ALPR. The current ALPR algorithms are predicated on the idea that the input video will be captured using a specialized, high-resolution, high-speed camcorder and is/or assisted by controlled capture surroundings, with the best camera height, focus, activity speed, and lighting settings [8].

Furthermore, typical video forensic applications could call for looking for a car with a particular licence plate on noisy surveillance video released by unspecialized, medium- to higher cameras operating in low-light scenarios [9]. Border patrol: The identification number is registered at the country's entryways and used to trace border crossings. Signalization: Relying on the cars' entry permit, the traffic can be routed to multiple lanes. The technique lessens both the number of stewards and road congestion. Analysing the travel time: Officials use journey time analysis (JTA) as a powerful instrument to track passage through vehicles and the length of time they take to go from one node to the other. Also, these statistics help congestion managers plan their routes more precisely [10].

2. PROPOSED METHODOLOGY

We find a different solution for character recognition and image segmentation for the LPR framework. We have used three stages to identify these kinds of frameworks. The license plate region must first be located and extracted from a larger scene image. Then, starting from the area of the license plate, the alphanumeric characters on the license plate must be separated from the background. In the third step, send them to an OCR system for recognition. To successfully identify an automobile by reading its license plate, finding the plate in the scene image provided by any acquisition device is crucial (e.g., video or still camera) [7]. ANPR Required four major stages to complete their process that is shown below in Figure 2.1.
Pre-processing, NPR (Number Plate Recognition), Segmentation of Characters, Recognition of Characters

2.1. Pre-processing

The automatic number plate identification system has numerous difficulties. To improve the input image and make it more suited for the following processing processes, this step is crucial. Pre-processing starts with applying a minimal filter to the image to improve the dark values by expanding their region as shown in Figure 2.1.

Figure 2.1. A car picture with Number plate which we are going to detect below.

This step increases the image's saturation to improve colour separation [16]. The idea is then changed from colour to grayscale. Then, to separate the background from highlights, we increase the image contrast.

2.2. License Plate Recognition

The output of this stage will be a sub-image that includes the license plate because the location of the license plate is in this stage [4]. This process involves essential steps like the Exact location of the Number Plate and finding large rectangles around the Number plate.

2.3. Segmentation of Characters

Exact location of the Number Plate and finding large rectangles around the Number plate. To segment, a picture is divided into smaller portions for further processing. Such as - Line level segmentation, word level segmentation [13], and character level segmentation are the order in which images are segmented

2.4. Recognition of Characters

Computers can recognize written or printed characters, such as numbers or letters, and convert them into a format that the computer can use through a process called character recognition [14].

3. GENERAL PROCESS OF ANPR SYSTEM

Using a camera to recognise licence plates requires taking images of the target scene's licence plates. After taking a high-quality photo of the surroundings or the car, any ANPR system's essential dependence is on its algorithms' trustworthiness [11][12]. Tens of thousands of lines of software coding are required for these algorithms to provide the desired results and manage the system complexity.

3.1. Python ANPR with Open CV and OCR

Firstly, Let's Understand the term OpenCV [18] and OCR sing a camera to recognise licence plates requires taking images of the target scene's licence.

"Optical Character Recognition" (OCR): "Optical Character Recognition" It is a piece of technology that can discern text in digital images. A real paper document or an image can be turned into a text-rich, readable electronic version using OCR software. Other OCR technologies may transform the characters into editable text back right in the image, while some merely export the text [17, 18]. Mainly we must follow 6 steps for Detect a number plate:

- Import after installing dependencies.
- Image blur, read in grayscale.
- Track down the localization edges.
- Then, place the mask over the contours.
- To read text, use simple OCR.
- Outcome of Rendering

3.2. Read the image, Grayscale and Blur

To read in our image and perform some Gray scaling, we have used the open cv imread function shown in Figure 3.1.

Figure 3.1. Output after using Gray scale on original image

3.3. Apply Filter and find the edges for localization

The next thing that we're going to do is apply a little bit of filtering and some edge detection, so our filtering will basically allow us to remove noise from our image. As shown in Figure 3.2

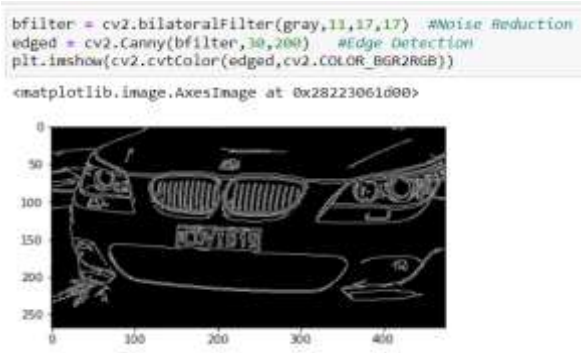

Figure 3.2. Output after using Gray scale on original picture

To do so, we've used the Canny algorithm [14], which allows us to detect edges; here again, we've got several parameters that we can pass through, which can be tuned depending on what you find works.

3.4. Find Contours and Apply Mask

The next step that we must complete is contour detection, which entails locating these lines and locating polygons within those lines [15]. Ideally, shapes should be visible in our images because a rectangle is most likely going to be the shape of our license plate. We are looking for a contour with four points. The ideal result for our number plate portion is a contour with four points. In the next line we have grabbed our contours using imutils. Grabcontours (), this basically simplifies how our contours are returned.

3.5. Masking the image

The next thing that we're going to do is apply a contour search, we've accurately detected where our number plate is located. The next step is to just isolate this numberplate portion because doing so will make it much simpler to feed the data to easy OCR as shown in Figure 3.3. The next thing that we're going. To achieve so, we first started by identifying every single portion of our image that isn't black.

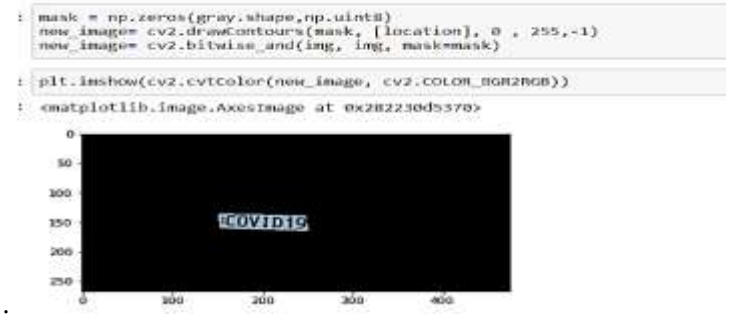

Figure 3.3. Output After Masking the original image

After clipping the image, we are putting those in variables x and y and obtaining a set of coordinates that reflects every section's now visible in numberplate shown in Figure 3.4.

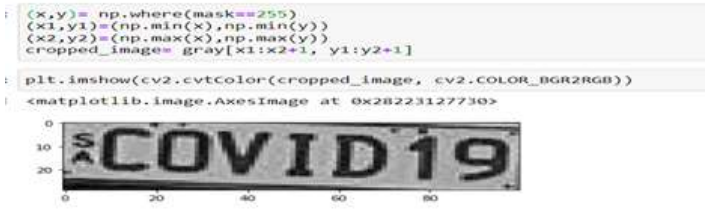

Figure 3.4. Output of the number plate

As a result, when everything is put together, we have our cropped image, which represents our number plate. MNIST dataset is used for character recognition, and ANN (Artificial neural network) Classifier is used to check the accuracy of our number plate.

4. CONCLUSIONS

Using It is well known that now days there are infinite IOT things through which one can capture an image, but how to utilize these things for the security should be of concern. ANPR should also be utilized in such appliances which can give a shorthand to security and help the people. Through this paper we have seen how to locate regular licence plates, segment characters, and identify them from a car image which will help a lot for security purposes but there are some difficulties that still needs to be resolved:

- Dark shaded portions at night
- Hiding numberplate with Infrared Light so that camera cannot capture the image
- Bright light emitting by plates

The algorithm is good to go but all these factors may affect the image capturing process which is the basic need of the algorithm. Also, we have seen how old methods were helpful for the numberplate recognition but keeping the above shortcomings in mind a new technique and appliances should be developed so that there is no act of hindering the detection system.

5. REFERENCES

[1] N. Mufti, S.A.A. Shah, ‘Automatic number plate Recognition: A detailed survey of relevant algorithms’, Sensors, vol. 21, no. 9, pp. 3028, 2021.

[2] S. Du, M. Ibrahim, M. Shehata, ‘Automatic license plate recognition (ALPR): A state-of-the-art review’, IEEE Transactions on circuits and systems for video technology, vol.23, no. 2, pp.311-325, 2012.

[3] X. Luo, D. Ma, S. Jin, Y. Gong, ‘Queue length estimation for signalized intersections using license plate recognition data’, IEEE Intelligent Transportation Systems Magazine, vol.11, no. 3, pp. 209-220, 2019.

[4] H. Y Lin, J.M Dai, L.T Wu, L.Q Chen, ‘A vision-based driver assistance system with forward collision and overtaking detection’, Sensors, 20(18), pp.5139, 2020.

[5] S. K. Thangallapally, R Maripeddi, ‘E-Security System for Vehicle Number Tracking at Parking Lot (Application for VNIT Gate Security’, IEEE International

Students' Conference on Electrical, Electronics and Computer Science (SCEECS) pp. 1-4, IEEE, 2018.

[6] I. T. Negassi, G. G., Araya, M., Awawdeh, and T. Faisal, 'Smart car plate recognition system', 1st international conference on advanced research in engineering sciences (ARES), pp. 1-5, IEEE, 2018.

[7] D. Kanteti, D. V. S., Srikar, & T. K. Ramesh, 'Intelligent smart parking algorithm', International Conference on Smart Technologies For Smart Nation pp. 1018-1022, IEEE, 2017.

[8] R. Shreyas, B.V.P Kumar, H.B. Adithya, 'Dynamic traffic rule violation monitoring system using automatic number plate recognition with SMS feedback', 2nd International Conference on Telecommunication and Networks (TEL-NET) pp. 1-5, IEEE 2017.

[9] B. Chaithra, K.V Karthik, D. Ram Kishore, 'Monitoring traffic signal violations using ANPR and GSM', International conference on current trends in computer, electrical, electronics and communication (CTCEEC), pp. 341-346, IEEE, 2017.

[10] A. Y Felix, A. Jesudoss, J.A. Mayan, 'Entry and exit monitoring using license plate recognition', IEEE international conference on smart technologies and management for computing, communication, controls, energy, and materials (ICSTM), pp. 227-231, 2017.

[11] Y. HE, P. SHE, L. ZUO, C. ZHANG, 'Study on Frequency Shift in Mutual Coupling Effect of Ultra-high-frequency Radio Frequency Identification Near-field System', vol.41, no.3, pp. 602-610, 2019.

[12] https://towardsdatascience.com/segmentation-in-ocr-10de176cf373

[13] R., Song, Z., Zhang, H. Liu, 'Edge connection-based Canny edge detection algorithm', Pattern Recognition and Image Analysis, vol.27, no.4, pp.740-747, 2017.

[14] V. K., Govindan, A. P. Shivaprasad, 'Character recognition—a review', Pattern recognition, vol. 23, no.7, pp.671-683, 1990.

[15] S., Mori, C. Y., Suen, K. Yamamoto, 'Historical review of OCR research and development', Proceedings of the IEEE, vol.80, no.7, pp.1029-1058, 1992.

[16] M. M. Fahmy, 'Toward low-cost traffic data collection: automatic number-plate recognition', In IEE Colloquium on Toll Systems (pp. 65-67). IET,1992.

[17] D. J., Higham, N. J. Higham, 'MATLAB guide', Society for Industrial and Applied Mathematics, 2016

[18] I., Culjak, D., Abram, T., Pribanic, H., Dzapo, M. Cifrek , 'A brief introduction to OpenCV', In proceedings of the 35th international convention MIPRO pp. 1725-1730, IEEE, 2012.

Real Time Cloud enabled Water Quality Supervising and Aerator Actuation in Shrimp Farming

Mocherla Chakradhar Abhinay *[1], Seetharam Reddy Ramireddy [2], Vamsiram Gandham [3], Vaegae Naveen Kumar [4]

School of Electronics Engineering, Vellore institute of Technology, Vellore, Tamilnadu, India
[1]chakradhar.abhinay@gmail.com, [2]seetharamreddy30@gmail.com, [3]vamsiramg@gmail.com, [4]vegenaveen@vit.ac.in

Abstract. In general, the water sample from shrimp ponds is sent for testing once in 10 days, and there are cases where the water sample gets changed within these 10 days and it can sometimes adversely affect the growth of shrimps. This paper proposes and develops a real-time cloud based water quality monitoring and automated aerator actuation in shrimp farming system. The prototype mainly consists of sensor modules, relay modules, Long Range Radio (LoRa) transmitter, LoRa receiver, node microcontroller unit (NodeMCU) and other interfacing circuitry. This system uses the low power LoRa module as transceiver connected with an Arduino which interfaces various sensors and NodeMCU which sends the sensor data to the Google database. The parameters like dissolved oxygen, pH, turbidity, total dissolved solids (TDS), temperature and conductivity are measured to assess the water quality in shrimp pond. The dataset is formed based on the acquired values of the parameters and machine learning algorithms are used to predict water quality index. Water quality index is predicted by training the system using various machine learning models. The performance of various machine learning algorithms is compared. Problem of high electricity charges faced by aqua farmers is also addressed by turning on the aerators only when oxygen level in water is insufficient for the rearing of shrimps. The use of machine learning models to forecast water quality and the LoRa module for communication, effectively and remotely monitors the shrimp farming system, which saves time, money, and hazards.

Keywords: Shrimp farming, Arduino Uno, NodeMCU, LoRa module, Machine learning algorithms, Sensors.

1 INTRODUCTION

Shrimp farming is a significant economic activity in many nations since it increases employment prospects in the fields of production, processing, marketing, transportation, and other related services. Good quality of water is needed for shrimp growth which in return results in farm profit. The water parameters such as dissolved Oxygen, pH, turbidity, total dissolved solids (TDS), temperature and conductivity are few of the main conditions that are to be tested often in the pond [1]. Water quality monitoring is done manually in shrimp farms. The conventional way of water quality monitoring is to collect the water sample from the pond and send it to the test center. But, by the time the report is received from the test center, the characteristics of the aquaculture pond changes. This proves to be ineffective if the farmer wants to take any immediate action in order to control the damage to the shrimps.

Periodic sampling of shrimp pond is highly necessary to monitor, their growth performance. The Internet of Things (IOT) assists smart farming by connecting people and farm remotely through various gadgets. Based on shrimp parameters, IOT is used to estimate and forecast trends in the quality of water conditions utilizing water quality index (WQI) models. Different approaches came into existence for the determination of WQI in the aquatic environment. Rahman et al. [2] proposed a classification problem. A Multivariate time series data set obtained from time series data of aforementioned parameters, is applied as input to the machine learning model. There exist different approaches for the estimation of WQI in the aquatic environment such as particle swarm optimization [3], statistical and deterministic models [4-6].

Long et al. [7] developed a system with a sensor node that measures the water's pH, dissolved oxygen, and temperature. The results can be viewed on Android devices once the sensed data was relayed through Zigbee to a distant server. Aerators and pumps can both be controlled remotely by the server. The device was equipped with a camera module to transmit a real-time view of the producing pond. Rajesh et al. [8] proposed a system that enables users to check water temperature, turbidity, and pH on any internet-connected device without having to join the system's WiFi network. Cesar et al. [9] stored data with MYSQL server for further processing, communication between sensor block and the Arduino via UART, then transmission of data through Zigbee to the server and cloud service. Kuang et al. [10] proposed an extreme learning algorithm for the prediction of dissolved oxygen. The performance of the ANN-based estimation models was explained and compared with the multi linear regression (MLR) based model [11]. Carbajal et al. [12] used fuzzy inference system for assessment of WQI of shrimp pond.

Even though there are so many methods of automatic monitoring of shrimp framing are proposed, the following problems needs to addressed and solved. At present, the water sample from shrimp ponds is sent for testing once in 10 days, and there are cases where the water sample gets changed within these 10 days and it can sometimes adversely affect the growth of shrimps. The shrimp farmers also face problem of high electricity charges as most of them keep their aerators turned on even when oxygen level in water is sufficient for the rearing of shrimps. The other major problem that we tried to solve in this system is the lack of internet connection at the location of the shrimp farm. These issues motivated us to propose a system for real time cloud enabled water quality supervising and aerator actuation in shrimp farming. Various sensors such as analog turbidity sensor, analog pH sensor, TDS sensor, temperature sensor, dissolved Oxygen sensor are interfaced with Adrunio Uno, NodeMCU, LoRa transreceiver. The NodeMCU, ESP8266 is integrated with LoRa module to automate and remotely monitor the shrimp pond. The uniqueness of the system is the usage of two LoRa modules to transmit bi-directional information over a long range. In absence of internet connectivity, monitoring and controlling of the sensor values and the relay states can be done with the help of GSM module. In this paper we used both IBM cloud and Google database for storage of data and communication. Also, we used seven machine learning algorithms mainly, support vector machine, K-nearest neighbours, Gaussian Naïve-Bayes, decision Tree, multi-layer perceptron, logistic regression and random forest for accurate prediction of WQI

to assess the survival of shrimp with a confidence score ‘1’ or ‘0’ along with percentage of survival.

2 IMPLEMENTATION OF PROPOSED SHRIMP FARMING SYSTEM

The block diagram of proposed real-time cloud based water quality monitoring and automated aerator actuation in shrimp farming system is depicted in figure 2.1. In a typical shrimp pond, the parameters which are to be kept in optimal levels are dissolved oxygen, temperature, salinity, turbidity, pH level, alkalinity and hardness, ammonia and nutrient levels. Of these parameters the major ones which are required to supervise the water quality are found to be dissolved oxygen, pH, turbidity, temperature, and TDS. For real time monitoring and control of a shrimp farming system, the vital parameters required to supervise the water quality are dissolved oxygen (> 3 mg/l), pH (7.0 – 8.5), turbidity (< 1500 NTU), temperature (15 – 45 °C), and TDS (< 1100 ppm). Sensors required to obtain the values of the above-mentioned parameters are incorporated within a prototype so that all these values can be dynamically monitored. The prototype mainly consists of sensor modules, relay modules, LoRa transmitter, LoRa receiver, NodeMCU and other interfacing circuitry. A dataset is formed based on the acquired values of the parameters and machine learning algorithms are used to predict water quality index. These values are continuously monitored by the user in real time and necessary action can be taken whenever it is required to do so. The following sections describe various modules and procedures of the proposed system.

2.1 Hardware Design

As shown in the Figure 2.1, sensors are calibrated and placed in the water and the sensor values are periodically monitored by Arduino UNO which reads sensor values from all sensors and serially transmits the sensor values to LoRa module. The LoRa module wirelessly transmits these sensor values up to a range of 15 KM. At the receiver LoRa which is placed within 15 KM range of the shrimp pond, the NodeMCU circuit serves the webpage and sends sensor data, relay state and water quality information to the Google sheets database and also IBM cloud. It even notifies users about abnormal sensor readings, changes in relay states and internet connectivity issues through text and email notifications. The machine algorithms will use the dataset available in the Google database to predict the water quality index.

The sensor values are periodically monitored by the NodeMCU and are serially transmitted to the LoRa Transmitter module. At the receiver, the LoRa module will wirelessly transmit these values to Blynk App and are updated in the IBM cloud. The NodeMCU will also send the data to Google database. In this paper we used both IBM cloud and Google database for storage of data and communication. If the measured values are not in optimal range, the user can supervise the sensor values anywhere in the world where there is internet connectivity. The predicted WQI of the machine learning model will assist the LoRA receiver to transmit back the control information to NodeMCU at the shrimp pond. This NodeMCU thereby control the aerator connected to Arduino Uno through Relay module. The Figure 2.2 depicts the flow chart of the two way communication between the NodeMCU and LoRa modules.

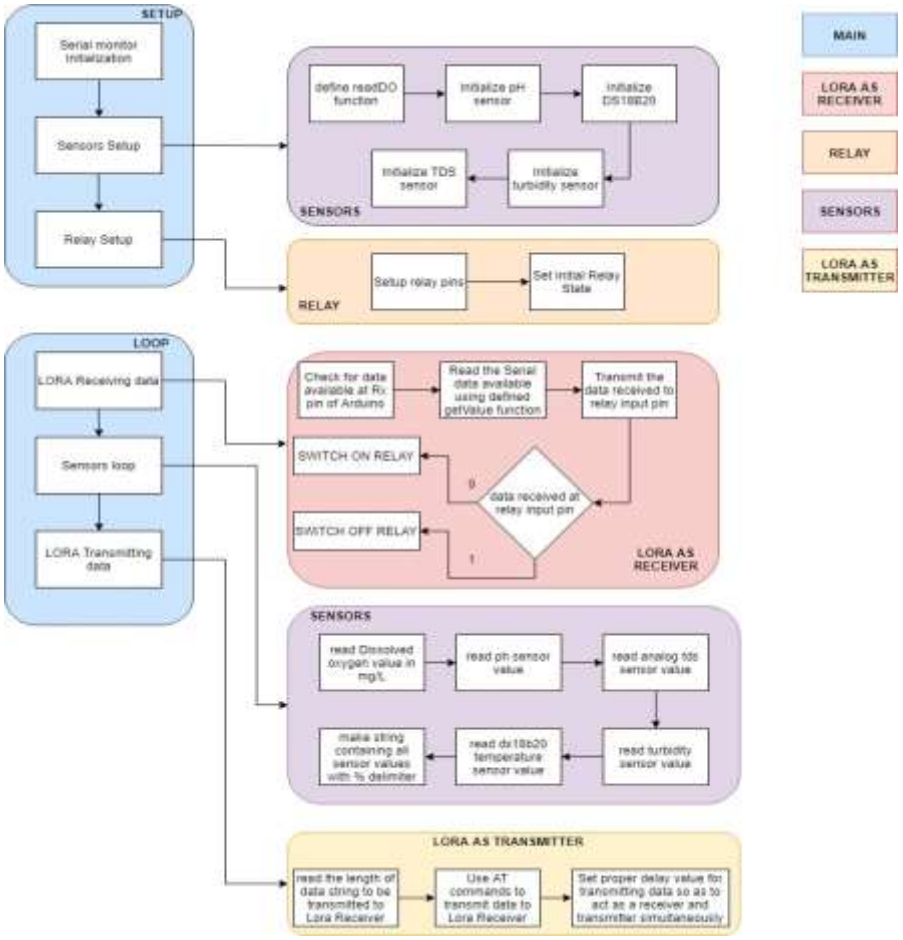

Figure 2.1. Block diagram of proposed real-time cloud based water quality monitoring and automated aerator actuation in shrimp farming system.

*2.2 **Acquisition of Dataset and Machine Learning Algorithms***

Water Quality Index (WQI) can help the user to understand the condition of the shrimp pond and notify necessary steps to be taken to improve the water quality. To predict water quality, a binary value is assigned to WQI. A dataset is formed by collecting 6507 samples at different life cycles of the shrimp with each containing an array of sensor values as in the order of dissolved Oxygen, pH, turbidity, TDS, temperature and conductivity are collected. This dataset is used to train different machine learning models to predict the water quality. Given a random sample of water, the sensor modules sense the six parameters. These are applied as inputs to different machine learning algorithms. Support vector machine [13], K-Nearest

neighbour [13], Naïve-Bayes [14], multilayer perceptron [15], logistic regression [16], decision tree [17] and random forest [18] are the different machine learning models used for prediction of WQI. These models predict the water quality whether it is good (with label 1) or bad (with label 0) and returns a Water Quality Index.

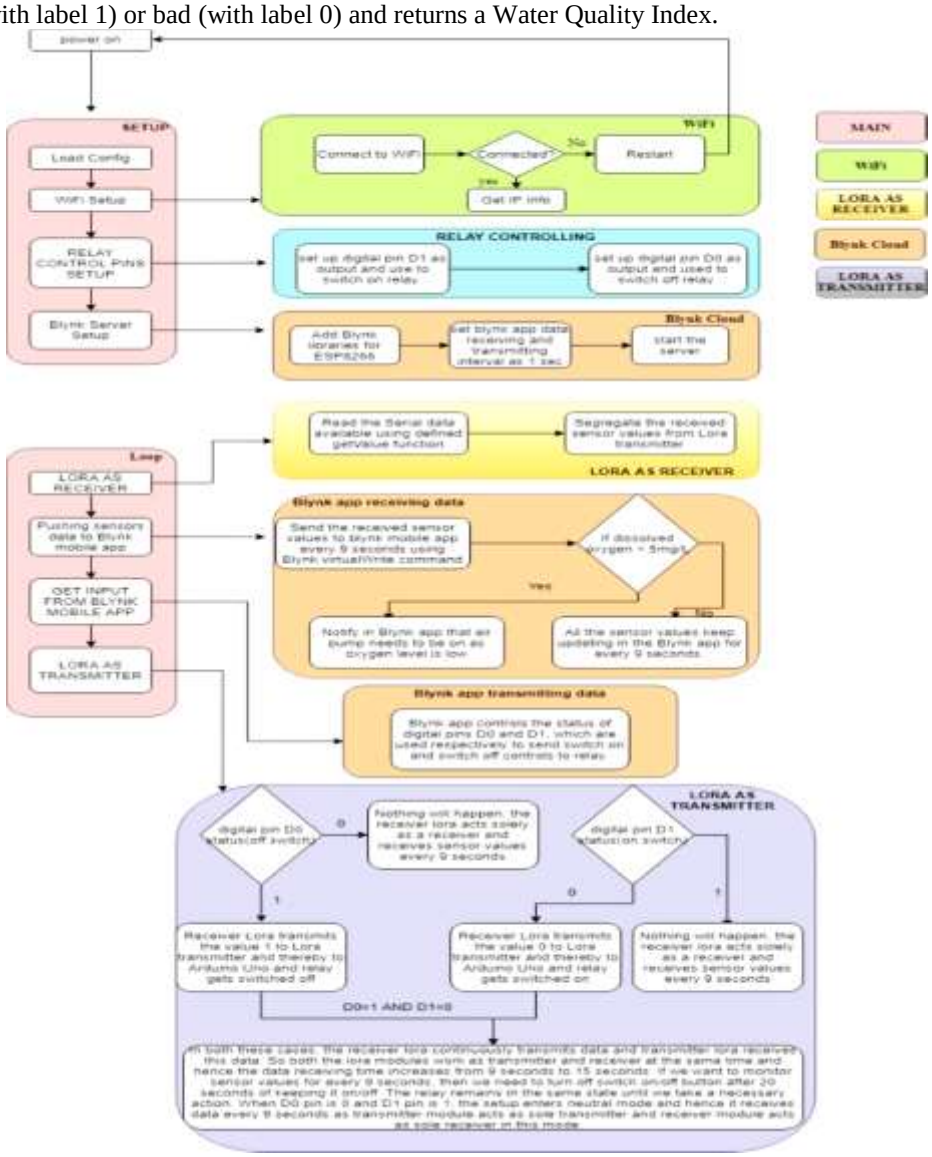

Figure 2.2. Two way communication between the two LoRA modules and NodeMCU

3 RESULTS AND DISCUSSIONS

The experimental set-up of sensor modules and related interfacing circuitry of the proposed system is shown in figure 3.1. The Arduino Uno reads sensor values from all sensors and serially transmits the sensor values to LoRa module. The LoRa module transmits these sensor values to LoRa receiver station which is up to a range of 15 KM. The sensor values are periodically monitored by the NodeMCU and are serially transmitted to the LoRa Transmitter module. At the receiver, the LoRa module will wirelessly transmit these values to Blynk App and are updated in the IBM cloud. The NodeMCU will also send the data to Google database. The LoRa module can even receive back the information about relay states from our receiver NodeMCU circuits and thereby control the aerator connected to Arduino UNO through Relay module. In this paper we used both IBM cloud and Google database for storage of data and communication. If the measured values are not in optimal range, the user can supervise the sensor values anywhere in the world where there is internet connectivity. The predicted WQI of the machine learning model will assist the LoRA receiver to transmit back the control information to NodeMCU at the shrimp pond.

In the training of the models, an acquired dataset of 6507 samples are used. The performance of machine learning algorithms mainly support vector machine, K-Nearest neighbour, Naïve Bayes, multilayer perceptron, logistic regression, decision tree and random forest are compared. The performance of these models is summarized in Table 1. The random forest model prediction has highest accuracy.

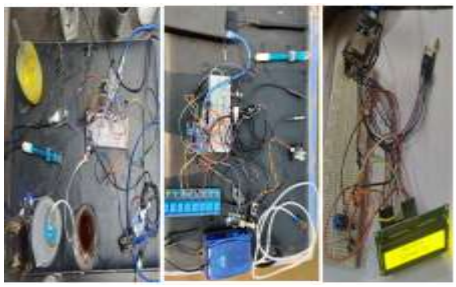

Figure 3.1. Hardware of proposed system

TABLE 1. ACCURACY COMPARISON

Algorithm used for model	**Accuracy Score (in percent)**
SVM	74.96
KNN	96.15
Naive Bayes	86.94
Decision Tree	99.94
MLP Neural Network	97.23
Random Forest	99.89
Logistic Regression	97.49

In this paper, real time cloud enabled water quality supervising and aerator actuation in shrimp farming project solves the problems that aquaculture farmers are facing right now. In this system, we are continuously monitoring the water quality every 10 seconds and the values are continuously stored in a database and are displayed in a website. Whenever the water quality degrades, we immediately notify the farmer through text messages, website notifications and even email notifications are sent regarding the same information. In order to cut down their electricity charges, we are using relay module to control aerators and we can now turn on the aerators only when the oxygen level goes below the fixed threshold value. The aerators can be controlled from our website when there is an internet connection and can be controlled through GSM module when there is no internet connection. The other major problem that we tried to solve in this system is the lack of internet connection

at the location of the shrimp farm. We are using LoRa module, which wirelessly transmits sensor data up-to a range of 15 kilometers. Even in case if we still lose our internet connection after finding a perfect place within 15-kilometer range for our LoRa receiver modules, we interfaced SIM800A GSM module, so that we can still read sensor values and control our aerator in farm. We have also deployed a machine learning model using seven algorithms mainly, support vector machine, K-nearest neighbours, Gaussian Naïve-Bayes, decision Tree, multi-layer perceptron, logistic regression and random forest. These Algorithms are used to for accurate prediction of survival of shrimp with a confidence score '1' or '0' along with percentage of survival.

4 CONCLUSION

In this paper, a novel prototype is developed for effective monitoring and control of the shrimp farming system. The real time cloud enabled water quality supervising and aerator actuation in shrimp farming addresses the problems of aquaculture farmers. The proposed system continuously monitors the water quality every 10 seconds and the values are continuously stored in a database. Whenever the water quality degrades, the system immediately notifies the farmers through text messages, website notifications and even email notifications. The user may remotely monitor their farm from anywhere with the usage of NodeMCU and LoRa modules. It has achieved all of the necessary goals, thus the system now automatically monitors the shrimp farm, resulting in high accuracy and a decrease in the amount of manpower required. This system saves sensor data in the cloud over an internet connection. The integration of the LoRA transmitter and receiver for this prototype results in superior quality data for the owner of the shrimp farm. Finally this system offers efficiency and accuracy while being economical.

5 REFERENCES

[1] A, Davor, Viktor Pocajt, Aleksandra Perić-Grujić, and Mirjana Ristić. "Modelling of dissolved oxygen in the Danube River using artificial neural networks and Monte Carlo Simulation uncertainty analysis." Journal of Hydrology 519 (2014): 1895-1907.

[2] Rahman, Ashfaqur, Stuart Arnold, and Joel Janek Dabrowski. "Identification of variables affecting production outcome in prawn ponds: A machine learning approach." Computers and Electronics in Agriculture 156 (2019): 618-626.

[3] Deng, Changhui, XinJiang Wei, and LianXi Guo. "Application of neural network based on PSO algorithm in prediction model for dissolved oxygen in fishpond." In 2006 6th World Congress on Intelligent Control and Automation, vol. 2, pp. 9401-9405. IEEE, 2006.

[4] Miao, Xinying, Changhui Deng, Xiangjun Li, Yanping Gao, and Donggang He. "A hybrid neural network and genetic algorithm model for predicting dissolved oxygen in an aquaculture pond." In 2010 International Conference on Web Information Systems and Mining, vol. 1, pp. 415-419. IEEE, 2010.

[5] Ghosh, Lopa, and G. N. Tiwari. "Computer modeling of dissolved oxygen performance in greenhouse fishpond: an experimental validation." international journal of agricultural research 3, no. 2 (2008): 83-97.
[6] Hu, Xuemei, Yingzhan Hu, and Xingzhi Yu. "The soft measure model of dissolved oxygen based on RBF network in ponds." In 2011 Fourth International Conference on Information and Computing, pp. 38-41. IEEE, 2011.
[7] Guangli, L. O. N. G. "Design of an aquaculture detection system based on internet of things." Int J Simul Syst Sci Technol 17, no. 31 (2016): 28-1.
[8] Huy, Thong Nguyen, Khanh Nguyen Tuan, and Thanh Tran Trung. "An Application of WSN in Smart Aquaculture Farming." In Intelligent Computing in Engineering, pp. 975-984. Springer, Singapore, 2020.
[9] Encinas, Cesar, Erica Ruiz, Joaquin Cortez, and Adolfo Espinoza. "Design and implementation of a distributed IoT system for the monitoring of water quality in aquaculture." In 2017 Wireless Telecommunications Symposium (WTS), pp. 1-7. IEEE, 2017.
[10] Kuang, Liang, Pei Shi, Chi Hua, Beijing Chen, and Hui Zhu. "An Enhanced Extreme Learning Machine for Dissolved Oxygen Prediction in Wireless Sensor Networks." IEEE Access 8 (2020): 198730-198739.
[11] Folorunso, Taliha A., A. M. Aibinu, Jonathan Gana Kolo, Suleiman Omeiza Eku Sadiku, and Abdullahi Muhammad Orire. "Water Quality Index Estimation Model for Aquaculture System Using Artificial Neural Network." (2019).
[12] Carbajal-Hernández, José Juan, Luis P. Sánchez-Fernández, Jesús A. Carrasco-Ochoa, and José Fco Martínez-Trinidad. "Immediate water quality assessment in shrimp culture using fuzzy inference systems." Expert Systems with Applications 39, no. 12 (2012): 10571-10582.
[13] Pulluri, Kranthi Kumar, and Vaegae Naveen Kumar. "Qualitative and Quantitative Detection of Food Adulteration Using a Smart E-Nose." Sensors 22, no. 20 (2022): 7789.
[14] Grodniyomchai, Boonyawee, Khattiya Chalapat, Kulsawasd Jitkajornwanich, and Saichon Jaiyen. "A deep learning model for odor classification using deep neural network." In 2019 5th International Conference on Engineering, Applied Sciences and Technology (ICEAST), pp. 1-4. IEEE, 2019.
[15] Kumar, Vaegae Naveen, and Komanapalli Venkata Lakshmi Narayana. "Development of an intelligent pressure sensor with temperature compensation." Journal of Engineering Science and Technology 12.7 (2017): 1723-1739.
[16] Pulluri, Kranthi Kumar, and Vaegae Naveen Kumar. "Development of an Integrated Soft E-Nose for Food Quality Assessment." IEEE Sensors Journal 22, no. 15 (2022): 15111-15122.
[17] Tobing, Fenina Adline Twince, Muhammad Iqbal Dzulhaq, Marlinda Vasty Overbeek, and Eko Anto Setiawan. "Design of decision support system with C4. 5 algorithm methods in determining results vaname shrimp cultivation." In 2019 5th International Conference on New Media Studies (CONMEDIA), pp. 195-200. IEEE, 2019.
[18] Kaewchote, Jirabhorn, Sittichoke Janyong, and Wasit Limprasert. "Image recognition method using Local Binary Pattern and the Random forest classifier

to count post larvae shrimp." Agriculture and Natural Resources 52, no. 4 (2018): 371-376.

Research Trends of Network Security in IoT: A Comparative Review

Kapil Joshi[1]

Department of CSE, Uttaranchal of Technology, Uttaranchal University, Dehradun, India

Kapilengg0509@gmail.com

Adarsh Kumar[2]

School of Computer Science, University of Petroleum and Energy Studies, Dehradun, Uttrakhand, India

adarsh.kumar@ddn.upes.ac.in

Minakshi Memoria[3]

UIT, Uttaranchal University, Dehradun, India

minakshimemoria@gmail.com

Rajiv Kumar[4]

Uttaranchal School of Computing Sciences, Uttaranchal University, Dehradun, India

rajiv.gill1@gmail.com

Abstract.

In the last decade, Technology is constantly evolving and producing new products numerous revolution. The Internet of Things (IoT) is a concept regarded as one of the most significant technological transformation. (IoT) connects two worlds: virtual and physical. We discuss in this paper conduct a comprehensive review of the literature on the various factors, challenges and threats that have had an impact on network security in the IoT domain. To identify the articles for the systematic review, on selected databases, we conducted a keyword search. There are 712 full-text articles in total were discussed, and the findings disclosed that several architectures and protocols are used to secure the IoT. The findings also emphasized the importance of improved IoT network security. In this paper, We also conversed about future studies opportunities, which are expected to inspire more research in the area of IoT network security.

Keywords. Internet of Things (IoT), Network Security, Internet of Things Devices.

1. INTRODUCTION

The Internet of Things (IoT) refers to a collection of physical objects connect via as well as cyberspace communication procedure that takes place inside it. The system facilitates the exchange of massive transferring large amounts of data between devices [1] without the need for Human intervention is required. According to Gartner, The number of people who use interconnected devices will reach 6.4 billion by 2016, which is 30 times the quantity of connected devices in 2009. According to projections, this figure will surpass 20.8 billion by 2020. These devices are now being used in a variety of industries. Indeed, there is a rise in demand for these gadgets in a variety of direction as such as smart homes, wearable's, e-health, manufacturing automobile, automation, agricultural farming, supply chain, as well as other operational technologies. Regardless of how unexpected surge there are still a little available Concerns about the security of these devices that must be addressed. According to a study conducted by HP, approximately 70% of the majority of commonly used Wearable computing (IoT) devices is vulnerable in user access permissions, encryption, password [2] security, and other areas. These dangers primarily include PUAs, Distributed Rejection of Service (DDoS), or other forms of cybercrime of cybercrime. Some human values are shown in figure 1.1.

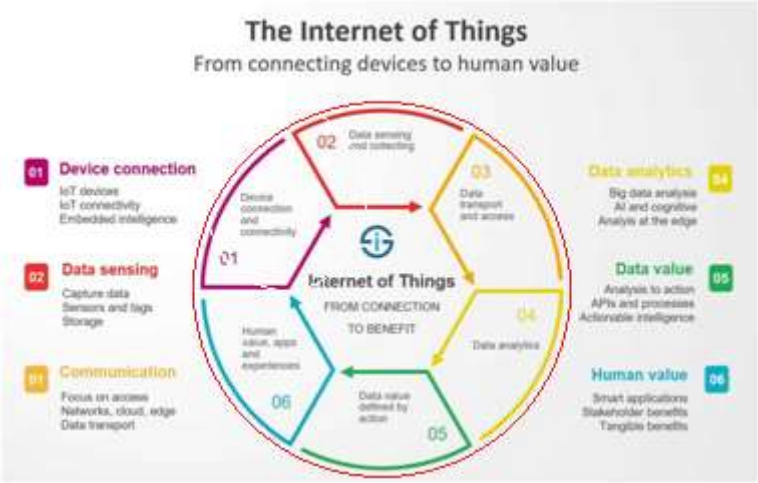

Figure 1.1. IoT for human values [3]

Because IoT devices can communicate with networks require multiple layers of protection. A variety of protocols, security policies, procedures and algorithms, are used to ensure the layers' security. These measures are critical [3] in the fundamental security implications of IoT, which is also the central concept investigated within this paper.

The following is how article is organized: Section 2 goes into great detail about the research process. Section 3 discusses the review's findings, which form the basis for the

main discussion in Section 4. Section 5 contains an overview of our significant contribution and a discussion of the study's restriction.

2. RESEARCH APPROACH

We have conducted a systematic research approach on multiple methods. Further we are classifying the three categories. These are as below:

2.1. Research Overview

We conducted a systematic review addressing the research questions posed above using a non-experimental approach based on content analysis. The content analysis contributes to the development of a methodical and structured reach to identifying and trying to describe text materials in the current body of knowledge [4]. We refined the text materials in this paper using a table of contents with to categories the key components of the text content that [3] will serve as appropriate examples, use categories and sub-categories. We documented our findings, and Sections 3 and 4 of this article discuss our findings based on those observations.

2.2. Classification Framework

We discuss in this paper used the procedures [4] proposed by Higgins and Green as well as Kitchenham et al. for conducting a thorough analysis of classification guidelines was conducted. The rulebook includes six descriptors: journal year, or title, conference, volume number, associated SDLC Phase, author keywords, security phase relevance, as well as key security terms.

2.3. Data Collection

We used keyword searches to search the databases of Science Direct, Springer, ACM Digital Library, IEEE Xplore, and Wiley InterScience [5]. To choose the texts or publications for analysis, use the phrase 'IoT but also NETWORK SECURITY' in the 'AND' format. The search term was used in Full Text and Metadata. The procedure was carried out throughout the months of November and December of 2016. During the search, we excluded standards, prefaces, editorials, courses, workshops, tutorials, poster sessions, and other English language articles. Text substances or articles are retrieved during in the lookup of the databases [6].

There are 2906 matches listed there are duplicates in Table 1. We filtered the pulled articles further to determine their suitability for use. We used to detect exclusion articles applicable to the Internet of Things and network security domains [6]. Database analyses are performed in figure 2.1.

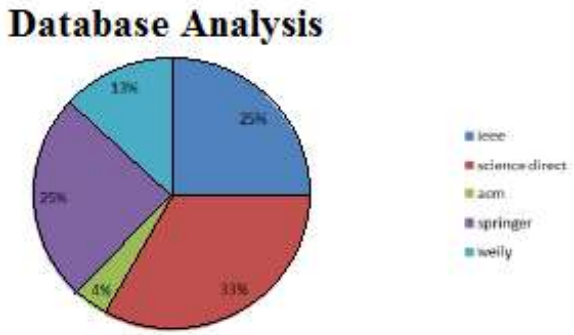

Figure 2.1. Database Analysis in Various Journal

Table 2.1 Results on Database

Sr. No.	Database (Conference & Journal)	No. Of Hits
1	IEEE Xplore	740
2	ACM Digital Library	121
3	Science Direct	974
4	Springer Link	725
5	Wiley Inter Science	390
6	**Total**	**2,950**

3. FINDINGS

We conducted a systematic review of 712 articles resulting from the database selection process. There are 627 journal articles, 5 booklets, but also 80 conference proceedings among the number 712. 535 papers have been published among these years 2010, 2013, 2017 and 2021. Papers submitted among 2014 and 2016 (including both years), and eight articles published between the years 1983 and 2009. Given the range of annual publications, it is clear that fascination with an emphasis on IoT safety has increased exponentially in the last 3 years when compared to previous years [7].

We identified critical security issues associated with IoT networks that are highly dynamic and have highlighted network characteristics in this paper. We discovered that every IoT device should be secure and dependable in order to satisfy the privacy requirements, particularly when these devices are used together including applications such as defence, sciences of medicine, automobiles, and so on, where the primary concern is security. However, because of their Despite their small shape, such IoT devices have a lot of power limited computational ability, making [8] It is difficult to provide security as a result of risks associated with securing these devices against eavesdroppers, Computer viruses,

Denial of Provider Phishing, Spoofing, and other threats others have emerged as critical topics to research in the sense of Internet of Things security. Because of Because of the limited authority of such IoT devices, it is difficult to create an effective architecture for sensor data storage and networking.

The division these things can be grouped together as "communities" used to ensure the security of the Internet of Things. Furthermore, when appropriate authorization is obtained, these communities can communicate with one another. As a result, data transmission is dangerous. As a result, Data traffic security among devices and cloud must also be a priority [9]. There are numerous available methods for enforcing data reliability. Encryption methods Additional Security Surface (SSL) and Transport Layer Security (TLS) are two examples (TLS). There are also Secure Mesh protocols, for example, have been used in Environmental noise Assisted Living (AAL), especially in e-Healthcare is a lightweight DDoS defense algorithm attacks, and Wireless protocols are layered (Internet, PHY/MAC, and Capacity for innovation). IPv6/IPv4, TCP/UDP, and 6LoWPAN are all part of the network/communication layer. The Wireless HART, UWB, IrDA, but also PLC 802.X series are all part of the PHY/MAC layer. CoAP, SNMP, DNS, and DLMS are examples of application layer protocols.

There are some numerous There are protection alternatives available for wireless networks, but 802.15.4 link-layer safety is the most common widely used. Unless data integrity is important, a concern, the 6LoWPAN system is operational the way to go because It is capable of supporting per-hop security arrangements via Cryptographic devices with symmetric keys [10] This system guarantees confidential operation, Authentication at the source, replay safety, data transformation, and semantic protection In addition, the network provides straight web entry via standards that are open In relation to network IP Security (IPSec) procedures are embedded for security the TCP/IP protocol stack is implemented using software in the operating system, Linux and NetBSD are two examples. Even so, the protocol is computationally demanding, which has a significant impact on network performance. Previously, web access or web transfer relied based upon that application layer CoAP method allowed with web transfer limited Networks and nodes. This procedure incorporates NoSec, PreShared-Key, Raw Public Key, as well as Identification card are examples of security modes have been shown to be useful in terms of transport layer security However, CoAP remains less secure putting data dependability at risk, particularly DDoS attacks are prevented. As a result, Security of the Datagram Network Layer (DTLS) protocol is used to ensure the required genuineness, confidentiality, and integrity Cookies in the web protocol domain provide protection. Typically, a collection of application layer protocols is put in place. ZigBee is a popular collection that is built around the IEEE 802.15.4 Mac. The protocol set is capable of be used to build effective and efficient network meshes with 216 devices are possible. These mesh networks have been shown to be have low energy consumption. They have a low data rate and are self-configuring [11].

Each and every of the protocols mentioned above send metadata, such as the source and destination identifies between nodes that are highly vulnerable to a variety of attacks, the most common of which are eavesdropping and packet injection. The Wireless HART protocol is useful for gaining maximum control so over process environment for

measurement. Because of The procedure is robust and reliable due to the TDMA-based MAC sub layer incorporated within using TSMP technology and ratio of availability of more than 99.73 percent. There are some restrictions in the architecture of security that must be addressed. The Procedure for trying to carry Authentication for Internet Connectivity (PANA) is a different network protocol that allows authenticated network access can be used to address questions about webbing access authenticity on the architecture. It is an EAP that uses UDP protocol that operates between an EAP authenticator and an EAP peer [12].

A deep-packet anomaly detection reach with high performance and low weight can run on small Internet of Things devices is as well a viable option. The method employs n-gram bit-patterns for modeling payloads efficiently and flexibly, with the n-gram dimension varying by dimension. Elliptic Curve Cryptography (ECC) is beneficial for developing portable Public Key Cryptosystems to achieve lightweight integration (PKC). It is primarily due to the system's key size is small, short and operand length relatively minimal arithmetic requirements Authority over the protection of the data and communication transfer pathway is also exercised available for the Black Network via Black SDN is an IoT network architecture employs As the trusted third-party link, an SDN controller is used. Using encryption to protect the top corner and payload protect against a variety One surefire method is the use of attacks. The ICN, a fresh (inter-) connectivity paradigm, is often used to connect all networks of such network functions and protocols, as well as to the system's core, information identifiers ICN is most advantageous in terms of information [13] retrieval flexibility. Through flexible semantic-rich identifiers, ICN enables information "advertisement" and "retrieval." It differs because of location -based IP addresses have been examples of identifiers.

In this case study, we examined IoT security and analyzed security features and requirements at various layers. It is possible, based on findings that as the Internet of Things evolve increased security issues will emerge.

4. DISCUSSIONS

This paragraph discusses the findings as part of our comprehensive study of 712 IoT network security articles As analyzed, the goal of the majority of the object was to find a method of conveying data security in Iot systems. This research paper adheres to positivism as a paradigm, which studies observable and classifiable facts. The writings that were the qualitative research methodology were used in the review to find outcome that focused on achieving IoT network security. There are a few examples Instances where both qualitative methods are used noteworthy. Both approaches were used in these articles to develop algorithms, architecture, and procedures [14] that are efficient.

We also observe that the primary approach used in articles about network security in IoT is experimental research. The approach's main goal has been to identify various network security potential attacks. The use it is also possible to use real case analysis as a method strategy noteworthy, with specific configurations chosen to deal with problems such as IoT network security [15].

In terms of distribution of articles, and over half of those centered on IoT [16] network security have been published because 2010 The rise in the number of published object

demonstrates how the domain is attracting researchers from all around the world Growing system complexities, diverse business scenarios [17], and an extremely competitive and vibrant global market to function [18], survive, and sustain could explain the increased interest. We discovered that the majority of the articles focused on providing IoT security. Traditional methods are giving way to more advanced techniques that improve the security of IoT devices [19]. This study also had the following limitations:

- Using different keywords for the search may result in different results. As a result, the keywords were used selected to give a concise overview of the current trends in IoT network [20-23] safety.
- It used as the same keyword in multiple places different libraries in various locations times may yield mismatch results (For example, because of a search engine or library updates).

As per the current record, we found the latest graph on available data mentioned in figure 4.1

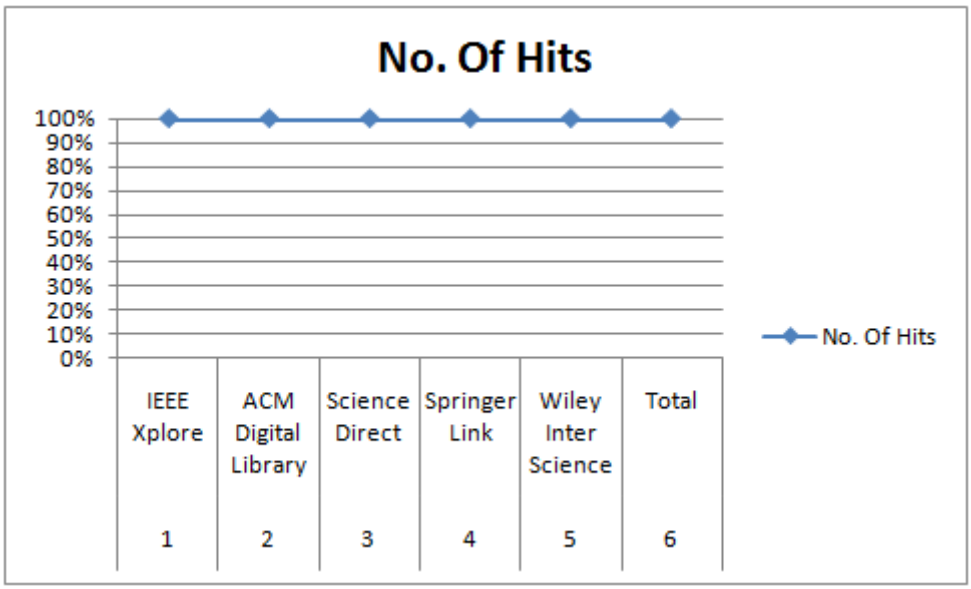

Figure 4.1. Number of Hits (As per Year)

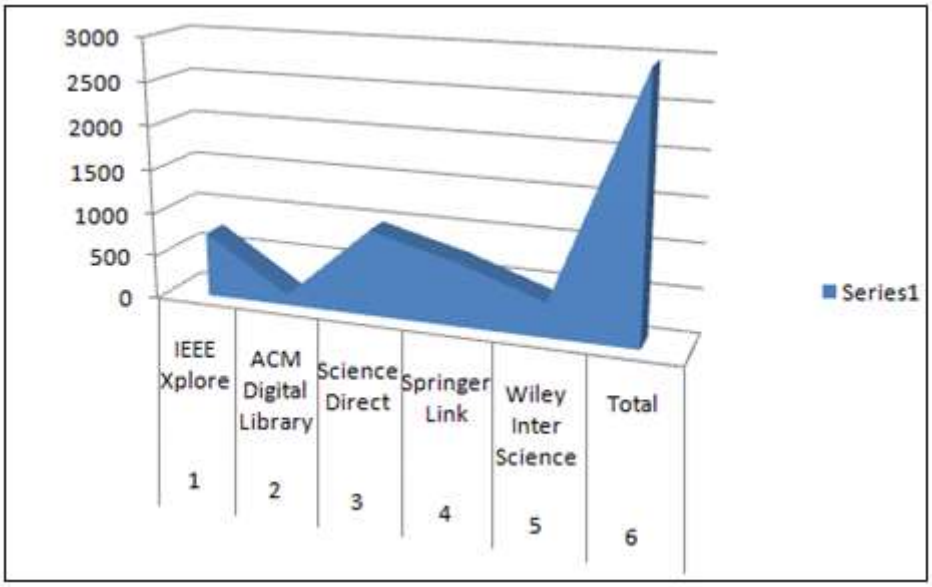

Figure 4.2. Increasing the Accessibility of Publication

5. CONCLUSIONS

Network safety is critical in Internet of Things. This strength in the position is particularly apparent urgent given how the potential consequences grew widely publicized following and the effect of attacks has become more radical. It could because of IoT encompass a diverse set of applications. Some one of the most significant IoT challenges are currently Safety, privacy, and confidentiality are all major concerns heterogeneity conduct, network capacity restriction and the massive data management and processing amounts of data in providing useful information. We investigated various to date, the preferences that have impacted data security in IoT in this paper. We based our findings on the findings of a thorough examination of chapter analyzed materials and articles that addressed our research concerns. Our discoveries suggest that the quantity of significant contribution to ensure IoT device security has increased in recent times and that is distinct levels of safety is being considered. The application of proper procedures in the Internet of Things allows for communication that is interoperable between limited Internet of Things devices and services.

There are some limitations to the study must be considered. The publications included with the review of the literature can still be relevant called into question. The method by which the databases and conference proceedings were chosen for our systematic review still needs to be refined. Because of the specific objectives and goals, a bias analysis as a result of article or text material selection it is still possible. There is also a chance that the results

obtained by searching for 'IoT As well as NETWORK SECURITY' in specific channels will be insufficient. There could be articles that are not found in the search because the terms the terms "IoT" as well as "NETWORK SECURITY" really aren't signifiers or components of the retrieval. Further research may be conducted with an emphasis on the potential increase in external consideration network security concerns the reality that there's been a greater emphasis on different levels of safety could be the driving principle. Furthermore, A few of the outside factors to consider when considering IoT security is attention to business considerations, which is also an excellent context for further research. All of these alternatives should entice researchers to participate in this area of questioning and research.

6. REFERENCES

[1] Naz, Sumera, Muhammad Akram, Mohammed M. Ali Al-Shamiri, and Muhammad Ramzan Saeed. "Evaluation of network security service provider using 2-tuple linguistic complex-rung orthopair fuzzy COPRAS method." Complexity 2022 (2022).

[2] Yu, Jing, Xiaojun Ye, and Hongbo Li. "A high precision intrusion detection system for network security communication based on multi-scale convolutional neural network." Future Generation Computer Systems 129 (2022): 399-406.

[3] Zhao, Mengwei, Hui Gao, Guiwu Wei, Cun Wei, and Yanfeng Guo. "Model for Network Security Service Provider Selection with probabilistic uncertain linguistic TODIM method based on prospect theory." Technological and Economic Development of Economy 28, no. 3 (2022): 638-654.

[4] Shin, Gun-Yoon, Sung-Sam Hong, Jung-Sik Lee, In-Sung Han, Hwa-Kyung Kim, and Haeng-Rok Oh. "Network Security Node-Edge Scoring System Using Attack Graph Based on Vulnerability Correlation." Applied Sciences 12, no. 14 (2022): 6852.

[5] Russell, James Stanley, Paul Scott, and Ahmad Attarha. "Stochastic shaping of aggregator energy and reserve bids to ensure network security." Electric Power Systems Research 212 (2022): 108418.

[6] Du, Meiyan. "Application of information communication network security management and control based on big data technology." International Journal of Communication Systems 35, no. 5 (2022): e4643.

[7] Afzal, Rafia, and Raja Kumar Murugesan. "Rule-based anomaly detection model with stateful correlation enhancing mobile network security." Intell. Autom. Soft Comput 31, no. 3 (2022): 1825-1841.

[8] Vinoth, S., Hari Leela Vemula, Bhadrappa Haralayya, Pradeep Mamgain, Mohammed Faez Hasan, and Mohd Naved. "Application of cloud computing in banking and e-commerce and related security threats." Materials Today: Proceedings 51 (2022): 2172-2175.

[9] Kryshtanovych, Myroslav, Ivan Dragan, Nataliia Chubinska, Natalia Arkhireiska, and Roman Storozhev. "Personnel Security System in the Context of Public Administration." IJCSNS International Journal of Computer Science and Network Security 22, no. 1 (2022): 248-254.

[10] Iyappan, Perumal, Jayakumar Loganathan, Manoj Kumar Verma, Ankur Dumka, Rajesh Singh, Anita Gehlot, Shaik Vaseem Akram, Sukhdeep Kaur, and Kapil Joshi. "A generic and smart automation system for home using internet of things." Bulletin of Electrical Engineering and Informatics 11, no. 5 (2022): 2727-2736.

[11] Diwakar, Manoj, Kanika Sharma, Ravi Dhaundiyal, Sheetal Bawane, Kapil Joshi, and Prabhishek Singh. "A review on autonomous remote security and mobile surveillance using internet of things." In Journal of Physics: Conference Series, vol. 1854, no. 1, p. 012034. IOP Publishing, 2021.

[12] Lakshmi, P. Sree, Monika Saxena, Sakshi Koli, Kapil Joshi, Khairul Hafezad Abdullah, and Durgaprasad Gangodkar. "Traffic Response System Based on Data Mining and Internet of Things (Iot) For Preventing Accidents." In 2022 2nd International Conference on Advance Computing and Innovative Technologies in Engineering (ICACITE), pp. 1092-1096. IEEE, 2022.

[13] Heidari, Arash, Nima Jafari Navimipour, and Mehmet Unal. "Applications of ML/DL in the management of smart cities and societies based on new trends in information technologies: A systematic literature review." Sustainable Cities and Society (2022): 104089.

[14] Hassan, Wan Haslina. "Current research on Internet of Things (IoT) security: A survey." Computer networks 148 (2019): 283-294.

[15] Lee, Jee Young, and Jungwoo Lee. "Current research trends in IoT security: a systematic mapping study." Mobile Information Systems 2021 (2021).

[16] Ruan, Junhu, Hua Jiang, Chunsheng Zhu, Xiangpei Hu, Yan Shi, Tianjun Liu, Weizhen Rao, and Felix Tung Sun Chan. "Agriculture IoT: Emerging trends, cooperation networks, and outlook." IEEE Wireless Communications 26, no. 6 (2019): 56-63.

[17] Sezer, Sakir. "T1C: IoT Security:-Threats, security challenges and IoT security research and technology trends." In 2018 31st IEEE International System-on-Chip Conference (SOCC), pp. 1-2. IEEE, 2018.

[18] Saheb, Tahereh, and Leila Izadi. "Paradigm of IoT big data analytics in the healthcare industry: A review of scientific literature and mapping of research trends." Telematics and informatics 41 (2019): 70-85.

[19] Kotha, Harika Devi, and V. Mnssvkr Gupta. "IoT application: a survey." Int. J. Eng. Technol 7, no. 2.7 (2018): 891-896.

[20] Kumar, Adarsh, Carlo Ottaviani, Sukhpal Singh Gill, and Rajkumar Buyya. "Securing the future internet of things with post-quantum cryptography." Security and Privacy 5, no. 2 (2022): e200.

[21] Kumar, Adarsh, and Deepak Kumar Sharma. "An optimized multilayer outlier detection for internet of things (IoT) network as industry 4.0 automation and data exchange." In International Conference on Innovative Computing and Communications, pp. 571-584. Springer, Singapore, 2021.

[22] Kumar, Adarsh, and Saurabh Jain. "Drone-based monitoring and redirecting system." In Development and Future of Internet of Drones (IoD): Insights, Trends and Road Ahead, pp. 163-183. Springer, Cham, 2021.

[23] Kumar, A. "Augusto de Jesus Pacheco D." Kaushik K., Rodrigues JJPC Futuristic View of the Internet of Quantum Drones: Review, Challenges and Research Agenda. Veh. Commun 36 (2022): 100487.

Concept and Design of a Deep-Functioning Robotic Arm Driven by an Android App to Transport Hazardous Goods

Praful Ranjan[1], Vaibhav Saini[2], Prasanthi Kumari Nunna[3]

[1]*Department of Electronics Engineering, GGP Varanasi*
[2]*Department of Electronics and Tele-communication Engineering, SIT Pune*
[3]*Department of Electronics and Communication Engineering, UPES Dehradoon*
prf98354@rediffmail.com[1], vaibhav46rnsaini@gmail.com[2], prasanti@ddn.upes.ac.in[3]

Abstract.

This research paper is based on robotic arm and its expansion and enlargement. Basically, it tells us about the technical aspects to some of the recent investigation in this area of activity. In this analysis of investigation there are numerous of exclusive questionable problems and field of exploration. Currently, various types of robotic arm are economically accessible. Many of the robotic arms are outstanding in precision and remarkable. In this paper, we will know about advancement of robotic arm, servo motors and mark out various specification of a robotic arm. A mobile robot that's effective to do pick and place behavior and can be controlled by Smartphone via Bluetooth. In android application, data packets are sent to Bluetooth module. It can be widely used in the automobile industries. Finally, this illustration of the robot is anticipated to get over of the problems like picking and placing the hazardous substances without touching it and this robot prototype is supposed to solve problems such as placing or choosing objects as well as picking and placing dangerous objects in the quickest and easiest method possible.

Keywords: *Robotic arm, Accuracy, Bluetooth, Data packets, Servo motors, Arduino, Automobile Industry.*

1 INTRODUCTION

These days there is an increase demand of robotic into working tasks to make work easier for tomorrow. Specially the work that have repetitive task. Basically, robotics is of two types industrial and service robot. According to IFR, an automatically controlled, multipurpose manipulator, reprogrammable which can be either fixed in place or movable. it does not include inventing operations. Movable robots are being used in variety of fields such as hospital operations, military tasks, office, hotels and agriculture. Depending on the application, it can be constructed to accomplish necessary functions like grabbing, moving, and even more.[1] Apart from worker who must pick and place something must be difficult for example, in chemistry the chemicals cannot be picked by bare hands of humans as well as in case of military such as to defuse bomb that requires a robot to pick and place it to the required space. Consequently, the work of human can be replaced by a locomotor's robot.

[2] The robot is a wirelessly operated that can ensures that the work from a long distance as well. Bluetooth is also a platform other than wireless controller that control robot without the use of any type of cables. The robotic motion and movement can be controlled by smart phone via Bluetooth. As per this project we will be able to move the arm of robot in all directions (left, right upward and downward) as per requirement. There are more than thousands of robotic arms which are made by different companies. Bluetooth, in addition to being wirelessly operated, is also a platform for controlling robots without the use of a cable. The robot's motions are controlled remotely through Bluetooth technology. The actuation of robotic arm is operated by producing PWM from a pin on the Arduino Mega board. Robotic arm may be operated autonomously or by human intervention and can be utilized to conduct a range of jobs with high precision. Analytical prediction of the behaviour of physical systems in many critical situations is either exceedingly difficult or impossible. Motivated by the limits of prototyping a physical system, modelling discovers significant reasons to analyse and investigate a system's performance. The robotic arm can be stationary or movable (wheeled), and it can be built for industrial or domestic use. The most often used robotic arm for the application i.e. pick and place is segmented. Wireless mobile robots have also been evolving in recent years. The robotic arm is currently used all around the world is more in industries rather than the domestic as robots are not much used for normal purpose. Robotic arm is also very useful in places that requires high accuracy, where there is no place for errors. Industrial arm may differ in size, types of joint, the joint sequence that are connected and motion range accepted at each joint. There are various parameters to manufacture and develops a robotic arm. The parameters are number of axis, freedom degree, working envelops, speed and acceleration, motion control and iterative.[3]

2. DESIGNING OF ROBOTIC ARM

In this section, we will talk about robotic arm this include the basic components like types of robots, servo motor, HC05BT module, Arduino uno etc. these have also covered kinematics in the development of robotic arm.

2.1 ***Types of Robotic Arm:*** It is of many types depends on the parameters and kinematics properties. Based on parameters, robotic arm is defined by multiple parameters i.e., no. of axis, degree of freedom, drive system, speed and acceleration of actuators, accuracy & repeatability and motion control. The research is focused on the creation and construction of a robotic arm control for a 5 Degree of Freedom movable robot arm for pick and place applications, allowing the robotic arm to be utilized as a lab-based model for learning and education as well as an autonomous model as needed.

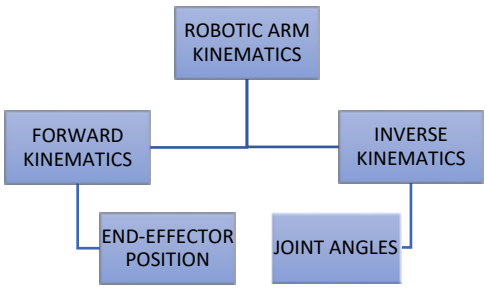

Figure 1: Types of robotic kinematics

2.2 Need for Robot Kinematics: Kinematics is the research of the movement of bodies without regard for the cause. Similarly, Robot kinematics is a relationship between position,

velocity and acceleration of links and joints. Kinematics is a need from robotic arm to do required work. Robot kinematic modelling enhances industrial automation processes by allowing them to be semi-autonomous or even completely autonomous. Because of the nature of the work and the operating environment, industrial robots are often made up of a series of stiff links set on a base. By kinematics robotic arm can pick and place objects like pick any object from location A and drop or place to the second location B accurately. Forward kinematics is simple and straightforward whereas inverse kinematics is very complex and much more difficult. [4] 3D based animated software that is Robo-analyser is used to study kinematics, DH (Denavit–Hartenberg) parameters and robot dynamics and it authorize animation and graph as an outcome.

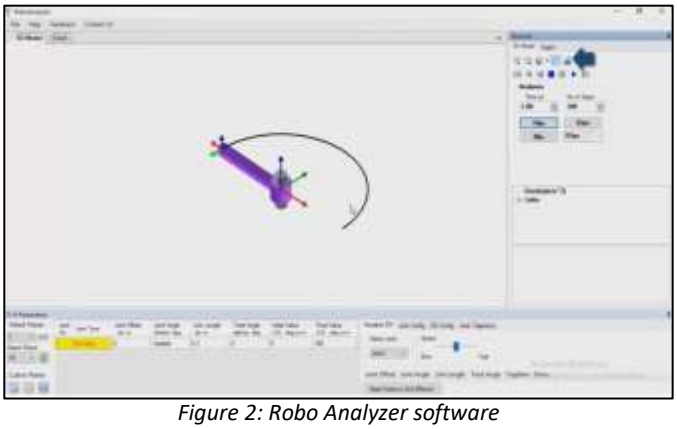

Figure 2: Robo Analyzer software

2.3 Hardware and software Implementation

2.3.1 Servo Motor: A servo motor, which functions as a rotary actuator, allows for accurate regulation of angular and linear position. The functions of the servomotor are to turn over a sequence of speed and to perform the control speed of the motor given by the instruction through PWM pulse width modulation pin in Arduino uno. Servo motor can control speed, position and torque of the motor simultaneously. [5]

2.3.2 Bluetooth Module (HC05 BT): Bluetooth is required to make our robotic arm more advanced and can be controlled wirelessly by smartphone through Bluetooth. Bluetooth is a standard short-range wireless interconnected tool; its repeating range is 1 to 100 meter and frequency of communication is 2.45 GHz. It can send 1600 data packs per second; each packet of data is sent on different channel. Speed of data transfer of transceiver is 3Mbps. [6]

2*.3.3 Servo Control App* This application is designed for IoT which can control the hardware remotely. In android application, data packets are send to Bluetooth module (HC05 BT). The Arduino uno receives the data from Bluetooth module through serial communication. Control signals are generated by Arduino uno for servo motor based on the value of the data packets [7]. Figure 4 represents the flowchart for better understanding. It has easy to use widgets which can be set with no additional training required. There is no need of any code required for the implementation. [8]

2*.3.4 Arduino uno Microcontroller* The ATmega328P-based Arduino Uno is a microcontroller board. It contains 14 digital I/O pins (six of which are PWM outputs),

analogue inputs, a 16 MHz quartz crystal, a USB connection, a power connector, and a reset button. It comes with everything you need to support the microcontroller; simply link it to a computer via USB or power it using an AC-to-DC connector or battery to get started.

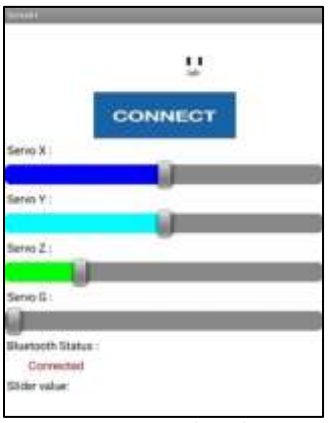

Figure 3: Servo control application

2.3.5 End Effector of the Robot The end effector is one feature that enables the robot to deliver adaptive solutions. This device is designed to interact with its environment, and the end effector's functionality is fully reliant on the robotics research. Essentially, an end effector is nothing more than a gripper or a device that functions according to the many applications generated in it and when it comes to robotic awareness. They are classified as Impactive, Ingressive, Astrictive, and Constitutive. Different end effectors respond differently to these.

- **Impactive:** This functions as a jaw or fingernail that physically grasps by colliding with the thing to be operated upon.
- **Ingressive:** The use of pins and needles to physically penetrate the surface of an item.
- **Astrictive:** It is just the suction established on the item's surface, which is generated by vacuum cups as an outsourced and by electromagnetic devices if applied.
- **Contiguous:** Close communication is necessary for the object's holding mechanism, such as surface tension produced at a precise point.

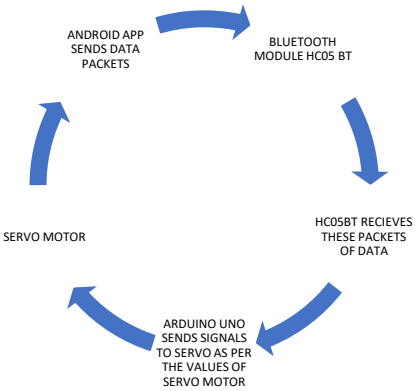

Figure 4: Servo control application flowchart

3. APPLICATION OF WORK

There are many applications of Robotic Arm in different industries i.e. Medical industry, Automotive industry, Agriculture industry, Education Industry, Chemical industry, and Food industry. When we talk about Medical industry, these autonomously robotic arms aid surgeons in the performance of less invasive surgeries. Healthcare mobility robots bring supplies, drugs, and food to patients and personnel, allows experts, hospital workers, and patients to communicate more effectively. For the oil and gas business, there are inspection robots that can move through a pipeline, as well as undersea robots for checking oil sites and rescue operations.

4. RESULTS AND DISCUSSION

Robotic arm using IOT, all servo motors and modules are working properly.[9] It is able pick any object less than 100 gm from location A and place it to location B with high accuracy.

3.1 General Homogeneous Transformation: In robotic arm, HTM is known as Homogeneous Transformation Matrices. It is used as a tool for exploring both the position and orientation. General homogeneous transformation equation used for this robotic arm is as follows: [10].

$$T=\begin{bmatrix} \cos\emptyset i & -sin\theta i cos\alpha i & sin\theta i sin\alpha i & a i cos\theta i \\ sin\emptyset i & cos\theta i cos\alpha i & -cos\theta i sin\alpha i & a i sin\theta i \\ 0 & sin\alpha i & cos\alpha i & ai \\ 0 & 0 & 0 & 1 \end{bmatrix}$$

3.2 Robotic Arm Gripper for Picking And Placing Constructs: Gripper is the component of robotic arm which is used to hold the object. Below is the snapshot of the gripper position one is in closed state and another is in open state. It is used for grabbing any object to pick and place. It is also called the head of the robotic arm. [11][12] The great variety of gripper types is owing to the broad range of objects that robots may grasp, which includes textiles, electronics, and automobile parts. A tiny, soft gripper, for example, is likely to be the ideal choice for direct handling of sensitive goods.[13]

Figure 5: Robotic arm, gripper

Figure 6: Robotic arm, gripper

3.3 Sideview of Robotic Arm: This is the picture of the whole robotic arm connected via jumper wire, Arduino uno, HC05 BT, 5V DC supply, and Arduino uno is programmed by Arduino IDE.[14]

Figure 7: Side view 1

Figure 8: Side view 2

5. CONCLUSION

This paper is illustrated a robotic arm and its components using IOT based services. The proposed design or the development is easily configurable and maintainable. These types of solution or machinery can be used in various industries where humans cannot operate or it is too dangerous for human beings on these sites. For this application embedded technologies like Bluetooth, Arduino MCU, advanced servo motors. Unique and homogeneous transformation matrices are computed, providing information on the location and direction of a robotic arm side. By comparing it to a human arm, the number of parts in this specific robotic arm is calculated. This is how the number of parts is calculated. In this article, we

evaluated the robotic arm in every way imaginable, including core strength capabilities, motion ranges, joints, and so on. The figures depict the robot's kinematic test. The proposed improvement is reusable, cost effective, and accurate. Overall, the goals of designing the software and hardware components for a wireless mobile robotic arm, establishing the pick and place system operation, and testing the robot that fulfils the requirements of purpose research have been met. Based on the examination, it is obvious that its action is exact, accurate, easy to regulate, and user pleasant.

5. REFERENCES

1. Virendra Patidar, "Survey of Robotic Arm and Parameters", 2016 International Conference on Computer Communication and Informatics (ICCCI -2016), Jan. 07 – 09, 2016, Coimbatore, INDIA
2. Md. Anisur Rahman, Alimul Haque Khan, Dr. Tofayel Ahmed, Md. Mohsin Sajjad, "Design, Analysis and Implementation of a Robotic Arm- The Animator", International Journal of Engineering Research · October 2013.
3. Rahul Mohadikar1, Amit Bokade2, Kalyani Barapatre3, Sanjana Bagde4, Dr. J. S. Gawai5, "Wireless Movable Robotic ARM", May 2021| IJIRT | Volume 7 Issue 12 | ISSN: 2349-6002.
4. Mohd Ashiq Kamaril Yusoffa , Reza Ezuan Saminb , Babul Salam Kader Ibrahimc, "Wireless Mobile Robotic Arm", International Symposium on Robotics and Intelligent Sensors 2012 (IRIS 2012).
5. Abdul Wali Abdul Ali, Fatin Asmida Abdul Razak and Nasri Hayima, "A Review on the AC Servomotor Control Systems", ELEKTRIKA- Journal of Electrical Engineering · August 2020.
6. 6 Agus Wibowo, "Communication Concept Between Bluetooth As a Master and Slave To Exchange Digital Information", International Journal of Engineering and Advanced Technology (IJEAT) ISSN: 2249 – 8958, Volume-9 Issue-2, December, 2019.
7. Moyeed Abrar, "Interfacing a servomotor with arduino uno microcontroller", International Journal of Recent Scientific Research Vol. 10, Issue, 02(E), pp. 31010-31014, February, 2019.
8. Leo Louis, "working principle of Arduino and using it as a tool for study and research", International Journal of Control, Automation, Communication and Systems (IJCACS), Vol.1, No.2, April 2016
9. Damir Žarko, Drago Ban, Davor Goriþki, "Improvement of a Servo Motor Design Including Optimization and Cost Analysis" , October 2006 DOI: 10.1109/EPEPEMC.2006.4778417 · Source: IEEE Xplore.
10. Shanta Pandey and Charlotte Lyn Bright, "What Are Degrees of Freedom?", Social Work Research · June 2008.
11. Zhang Ruishu, Zhang Chang, Zheng Weigang, "The status and development of industrial robots", IOP Conf. Series: Materials Science and Engineering 423 (2018) 012051 doi:10.1088/1757-899X/423/1/012051
12. Epenetus, A.B., Meera, C.S., Mohan, S. and Gupta, M.K., 2019. Development and motion control of spatial serial robotic manipulator under varying disturbances. *World Journal of Engineering*.
13. Meera, C.S., Sairam, P.S. and Gupta, M.K., 2016, December. Path planning and motion control for a 3 DOF massaging robot. In *2016 International Conference on Robotics and Automation for Humanitarian Applications (RAHA)* (pp. 1-6). IEEE.
14. Veeramalla, V., Mishra, J., Meera, C.S., Verma, V. and Gupta, M.K., 2020. Development and Gesture Control of Virtual Robotic Arm. In *Intelligent Communication, Control and Devices* (pp. 531-537). Springer, Singapore.